

**Computational Statistical Mechanics**  
by  
**William Graham Hoover**

**Computational Statistical Mechanics**  
by  
**William Graham Hoover**

**Business Address:**

**Department of Applied Science, University of California at Davis/Livermore and  
Lawrence Livermore National Laboratory, Livermore, California 94550 USA .**

**Telephone 415-422-9787; FAX 415-422-8681.**

**Born in Boston, Massachusetts, 18 April 1936.**

## Table of Contents

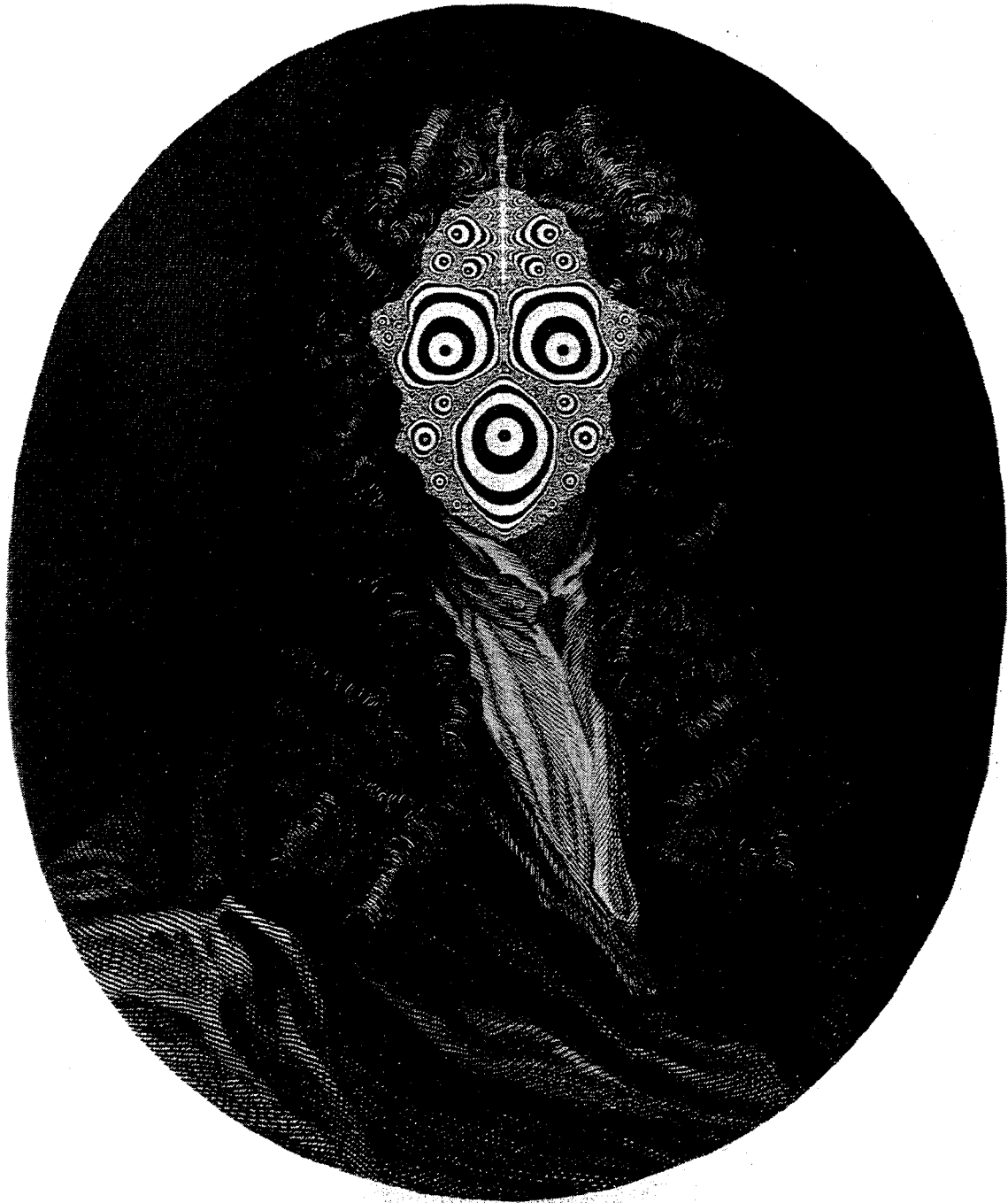
<u>1. Mechanics</u> .....	1
1.1 Introduction.....	1
1.2 Mechanical States.....	2
1.3 Newtonian Mechanics.....	3
1.4 Trajectory Stability.....	6
1.5 Trajectory Reversibility.....	8
1.6 Stoermer and Runge-Kutta Integration.....	10
1.7 Lagrangian Mechanics.....	16
1.8 Least Action Principle.....	19
1.9 Gauss' Principle and Nonholonomic Constraints.....	21
1.10 Hamiltonian Mechanics.....	24
1.11 Liouville's Theorem.....	26
1.12 Mechanics of Ideal-Gas Temperature.....	29
1.13 Thermostats and Nosé-Hoover Mechanics.....	31
1.14 Summary and References.....	34
<u>2. Thermodynamics</u> .....	35
2.1 Introduction.....	35
2.2 Thermodynamic States of Matter and The Zeroth Law.....	37
2.3 Heat Reservoirs.....	40
2.4 First Law of Thermodynamics.....	41
2.5 Second Law of Thermodynamics.....	45
2.6 Third Law of Thermodynamics.....	50
2.7 Thermodynamics of Ideal-Gas Compression.....	51
2.8 van der Waals' Equation of State.....	56
2.9 Thermodynamic Potential Functions.....	59
2.10 Summary and References.....	63
<u>3. Principles of Statistical Mechanics</u> .....	64
3.1 Introduction.....	64
3.2 Statistical Mechanical States.....	66
3.3 Volume of an N-Dimensional Sphere.....	70
3.4 Gibbs' Microcanonical Ensemble.....	70
3.5 Gibbs' Canonical Ensemble.....	73
3.6 Lagrange-Multiplier Derivation of the Canonical Ensemble.....	73
3.7 Heat-Reservoir Derivation of the Canonical Ensemble.....	75
3.8 Thermodynamics from the Canonical Ensemble.....	77
3.9 Maxwell-Boltzmann Velocity Distribution.....	79
3.10 Equilibrium Monte Carlo Method.....	80
3.11 Nosé Mechanics.....	83
3.12 Nosé-Hoover Mechanics.....	84
3.13 Grand Canonical Ensemble.....	86
3.14 Summary and References.....	86
<u>4. Applications of Equilibrium Statistical Mechanics</u> .....	88
4.1 Introduction.....	88
4.2 Tonks' One-Dimensional Hard-Rod Gas.....	88
4.3 One-, Two-, and Three-Dimensional Ideal Gases.....	93
4.4 Two- and Three-Dimensional Rigid Rotors.....	96
4.5 One-Dimensional Vibrator.....	100

4.6	One-Dimensional Harmonic Chain.....	103
4.7	Two- and Three-Dimensional Quasiharmonic Crystals.....	106
4.8	Einstein and Debye Models.....	110
4.9	Three-Dimensional Polyatomic Molecules.....	113
4.10	Chemical Reactions.....	115
4.11	Phonons and Photons.....	117
4.12	Electrons in Metals.....	120
4.13	Mayers' Virial Expansion of Thermodynamic Properties.....	121
4.14	Thermodynamic Perturbation Theory.....	126
4.15	Summary and References.....	128
<b>5.</b>	<b><u>Principles of Equilibrium Molecular Dynamics</u></b> .....	<b>130</b>
5.1	Introduction.....	130
5.2	Relation to Statistical Mechanics.....	131
5.3	Initial and Boundary Conditions.....	134
5.4	Interparticle Forces.....	136
5.5	Virial Theorem and Heat Theorem.....	140
5.6	Isoenergetic Molecular Dynamics.....	142
5.7	Gaussian Isokinetic Molecular Dynamics.....	145
5.8	Nosé-Hoover Isothermal Molecular Dynamics.....	146
5.9	Isothermal-Isobaric Molecular Dynamics.....	147
5.10	Numerical Techniques.....	150
5.11	Stability.....	155
5.12	Parallel Computation.....	156
5.13	Hard-Sphere Dynamics.....	157
5.14	Summary and References.....	158
<b>6.</b>	<b><u>Applications of Equilibrium Molecular Dynamics</u></b> .....	<b>160</b>
6.1	Introduction.....	160
6.2	Number-Dependence, Ensemble-Dependence, and Time-Dependence.....	162
6.3	Pair Distribution Functions.....	164
6.4	Free Energy and Phase Equilibria.....	166
6.5	One-Parameter Equations of State.....	171
6.6	Two-Parameter Equations of State.....	176
6.7	Many-Parameter Equations of State.....	177
6.8	Elastic Solids.....	178
6.9	Defects and Surfaces.....	179
6.10	Summary and References.....	180
<b>7.</b>	<b><u>Principles of Hydrodynamics</u></b> .....	<b>181</b>
7.1	Introduction.....	181
7.2	Hydrodynamic States.....	182
7.3	Eulerian and Lagrangian Coordinates.....	183
7.4	Continuity Equation.....	184
7.5	Pressure Tensor.....	186
7.6	Equation of Motion.....	191
7.7	Navier-Stokes Equations.....	192
7.8	Elasticity Equations.....	195
7.9	Heat Flux Vector.....	196
7.10	Energy Equation.....	197
7.11	Summary and References.....	199

<u>8. Applications of Hydrodynamics</u> .....	200
8.1 Introduction.....	200
8.2 Plane Couette flow.....	201
8.3 Poiseuille flow.....	203
8.4 Stokes' Flow Past a Sphere or Disk.....	205
8.5 More-General Analytic Solutions.....	207
8.6 Turbulence.....	208
8.7 Rayleigh-Bénard Problem.....	210
8.8 Numerical Methods.....	213
8.9 Summary and References.....	221
<u>9. Kinetic Theory</u> .....	222
9.1 Introduction.....	222
9.2 Kinetic-Theory States.....	224
9.3 Hard-Sphere Collision Rate and Free-Path Distribution.....	225
9.4 Free-Path Theory.....	232
9.5 Boltzmann's Equation.....	235
9.6 Maxwell-Boltzmann Distribution from the Boltzmann Equation.....	238
9.7 H Theorem and Irreversibility.....	238
9.8 Numerical Solutions of the Boltzmann Equation.....	240
9.9 Approximate Boltzmann Equation.....	243
9.10 Diffusion.....	244
9.11 Viscosity.....	247
9.12 Heat Conduction.....	248
9.13 Enskog Model.....	249
9.14 Green-Kubo Theory.....	250
9.15 Summary and References.....	253
<u>10. Introduction to Nonequilibrium Molecular Dynamics</u> .....	255
10.1 Introduction.....	255
10.2 Forces in Nonequilibrium Molecular Dynamics.....	257
10.3 Nonequilibrium Thermostats.....	261
10.4 Liouville's Theorem Far from Equilibrium.....	262
10.5 Divergence of the Nonequilibrium Steady-State Probability Density.....	264
10.6 Fractal Distributions.....	267
10.7 Irreversibility and the Second Law of Thermodynamics.....	269
10.8 Summary and References.....	273
<u>11. Applications of Nonequilibrium Molecular Dynamics</u> .....	274
11.1 Introduction.....	274
11.2 Diffusion.....	274
11.3 Shear Viscosity and Yield Strength.....	280
11.4 Heat Conduction.....	288
11.5 Shockwave Structure.....	293
11.6 Vibrational Relaxation.....	298
11.7 Lyapunov Spectra.....	301
11.8 Phase-Space Dimensionality Loss.....	304
11.9 Summary and References.....	306
<u>12. Summary</u> .....	308
<u>13. Useful Information</u> .....	310

## Acknowledgment

My intellectual debts are many. My main sources of inspiration were Peter Debye, Andy De Rocco, George Duvall, Joe Ford, Toshio Kawai, Ed Saibel, George Uhlenbeck, and Billy Waid. My research efforts have been generously supported and encouraged by Taisuke Boku, Tony De Groot, Jean-Pierre Hansen, Gianni Iacucci, Marvin Ross, Shuichi Nosé, Irv Stowers, Bob Watts, and Fred Wooten. I shared many discoveries with Bill Ashurst, Brad Holian, Tony Ladd, Bill Moran, Harald Posch, and Francis Ree. Besides furnishing the conventional wifely support Carol also read the book and worked through the problems. Without her, and my parents, Mary Wolfe Hoover and Edgar Malone Hoover, this work could not have been. It is dedicated to them.



### Frontispiece

"Newton's Face" succinctly suggests the qualitative changes wrought in mechanics by high-speed computation. The changing substance and style of statistical mechanics reflect our ability to study chaos and multifractal objects. I sincerely thank Murray Batchelor and Bruce Henry, of the Australian National University in Canberra, for furnishing this reproduction of their prize-winning photograph. Errol Craig provided diligent and creative help with many of the other illustrations.

# Computational Statistical Mechanics

## Preface:

The fundamental goal of Statistical Mechanics is to link the detailed determinism of many-body microscopic dynamics to the phenomenological averaged description of macroscopic behavior. During my own 30-year study of statistical mechanics computers have completely transformed the field, substantially widening the scope of this goal by making it possible to follow the motion of *millions*, soon to be *billions*, of particles. The corresponding coupled nonlinear differential equations of motion can be solved, numerically, for time intervals including millions of discrete time steps.

By now computers are readily available instructional tools for learning by doing. Computers are now firmly established in our high schools and low-cost transputers have made the speed of a CRAY available at the cost of an automobile. One can hope that this continuing growth of computational power will play a role in promoting a healthy diffusion of knowledge throughout the world.

But with our relatively newfound ability to compute comes a challenging responsibility. The challenge today is not so much generating results, as it is discovering imaginative ways to display results in comprehensible forms designed to promote understanding. Because the subject of this book, computational statistical mechanics, is now feasible, the goal of statistical mechanics has had to grow from the days when experiment and theory were the complementary alternative approaches to understanding. Our goal now is to achieve correspondence among three alternative descriptions of natural phenomena: theory, experiment, and computer simulation.

This wider goal has led to new methods providing a more intimate degree of understanding than was accessible to Boltzmann 100 years ago when he linked reversible mechanics to irreversible thermodynamics with his H Theorem. This new understanding is fundamentally related to another classical subject reinvigorated by computation, chaos, the exponentially sensitive dependence of the future on the past. This sensitive dependence has made a qualitative change in what it means to "solve" a problem. Chaos forces us to take a "statistical" approach. In a real sense chaos now provides not only an understanding of the fundamental origin of macroscopic irreversibility, but also a conceptually useful microscopic framework showing that our approach *must* be both computational *and* statistical. Long-time solutions for individual chaotic systems are out of the question, inaccessible to any approach, analytic or numerical. Chaos requires ensemble averages.

Most real macroscopic systems are nonequilibrium systems. In them, flows of mass, momentum, or energy respond to differences in composition, velocity, and temperature. Fast computers make it practical to generate for study "simulations," the computational analogs of these nonequilibrium flows. To predict accurate future states

from the present state of a system by computer simulation requires new combinations of microscopic dynamics with macroscopic thermodynamics, in which equilibrium equations of motion are augmented to deal with nonequilibrium constitutive relations, while still retaining their deterministic, time-reversible character. With these new dynamic equations, and with initial and boundary conditions specified, the simulated time development generally follows from approximate solutions of ordinary differential equations. This approach has proved to be useful and educational, for both small and large systems.

Our view of such nonequilibrium systems has been profoundly changed by computer simulation. Computers make it possible now to study nonequilibrium systems in their own right, not just as linear perturbations or equilibrium fluctuations. Accordingly, the nonequilibrium systems which are all around us make up more of today's computational statistical mechanics than was possible in the older statistical mechanics of Tolman, the Mayers, and Hill.

We can still formulate and understand the bases of both equilibrium and nonequilibrium many-body behavior by computing the solutions of systems of classical ordinary differential equations, using the old techniques of Gauss, Euler, and Newton on modern computing machines. But the cumbersome analytic approaches of a generation ago have either changed or been discarded. New ways, particularly the direct simulation methods, are much broader in scope, richer in the detail they provide, and more definite in their predictions. The new have replaced the old.

To keep pace with the continuing improvements in computer capacity and speed requires the continuous development of new methods and viewpoints. The interaction of computation, experiment, and theory has led to rapid qualitative gains in our ability to predict the future reliably and to resolve the classical paradox that reversible motion equations lead to patently irreversible solutions.

This book aims to use the tools of computation and simulation and the useful concepts from nonlinear dynamics to link the basis of statistical mechanics established by Maxwell, Boltzmann, and Gibbs to the concepts and computational tools available, and still being developed, a century later. Despite the antiquity of the foundations and the numerical techniques new discoveries are commonplace, so that computational statistical mechanics promises to be a fertile research area as it is applied to increasingly complicated problems. The present work describes the fundamentals underlying numerical simulation of nonequilibrium systems as well as the numerical techniques needed to apply these principles. I believe that physics can only be learned by first-hand exploration. Most physicists learn inductively, by example, rather than deductively. This book is for them. It consciously avoids vague formalism and whenever possible substitutes restricted particular examples for general propositions and theorems. It is necessary to measure, calculate, or compute in order to understand. With this in mind

I have included a selection of problems intended to encourage learning and understanding.

This book began in 1972, shortly after I began teaching in the University of California's Graduate Department of Applied Science at Davis and Livermore. This Department was conceived by Edward Teller in order to make available to students the Livermore Laboratory's unparalleled experimental, computational, and theoretical facilities. In the Department of Applied Science we teach the skills required to describe equilibrium and nonequilibrium systems, microscopic and macroscopic, from a fundamental viewpoint. The year-long graduate course described in the present book evolved over a 20-year period. I was first exposed to statistical mechanics in graduate courses at the University of Michigan, taught by De Rocco and Uhlenbeck, and built from this base through texts I have used in teaching, the Physical Chemistry of Moore and Adamson and the Statistical Mechanics of Reif and McQuarrie. Recently my teaching has more closely followed my current research interest in nonequilibrium statistical mechanics. This book reflects my own interests in achieving an understanding of macroscopic processes, particularly nonequilibrium processes, from a computational basis. I have included an account of equilibrium simulations and simulation techniques too, despite my feeling that this area is by now farther from the frontier and therefore of less interest in research.

This rewarding work has been generously supported by Universities in Canberra, Davis, Vienna, and Yokohama, as well as by the Livermore National Laboratory. It has been stimulated and encouraged by a host of friends around the world. Though such research is never finished it appears to me that now is a good time to pass on some of our accumulated present-day knowledge in order to speed future advances by those people privileged to enjoy the pleasures of solving puzzles in physics.

Livermore and Yokohama  
October 1987 – June 1990.



W. G. Hoover

# 1. Mechanics

*1 Introduction; 2 Mechanical States; 3 Newtonian Mechanics; 4 Trajectory Stability; 5 Trajectory Reversibility; 6 Stoermer and Runge-Kutta Integration; 7 Lagrangian Mechanics; 8 Least Action Principle; 9 Gauss' Principle and Nonholonomic Constraints; 10 Hamiltonian Mechanics; 11 Liouville's Theorem; 12 Mechanics of Ideal-Gas Temperature; 13 Thermostats and Nosé-Hoover Mechanics; 14 Summary and References*

## 1.1 Introduction

Because the basis of macroscopic behavior lies in the reproducible microscopic motion of particles governed by the simple reversible deterministic laws of mechanics, we begin our study by exploring classical mechanics. Our fundamental motivating desire is to find a microscopic mechanical basis for macroscopic phenomena. So we must start with mechanics. We will illustrate all the basic concepts with simple examples free of the obscuring shroud of mathematics.

Although Schroedinger's quantum mechanics is apparently more fundamental than Newton's classical mechanics, quantum mechanics has not yet been developed into a useful tool for dealing with nonequilibrium systems. We deal with quantum systems only in those few cases where classical mechanics is useless (phonons at low temperature, photons, electrons).

Classical mechanics has come far since Newton's 300-year-old formulation of the basic laws. Newton's work was based on gravitational forces because Kepler's analysis of planetary data had led to precise conclusions. But gravity is negligibly weak on the microscopic scale. It affects atomic trajectories only at the double-precision level.

On the atomic level, a variety of short-ranged few-body force laws containing a few adjustable parameters have been introduced to replicate the behavior of simple gases, liquids, and solids. And statistical mechanics has been developed to link these microscopic forces to macroscopic thermodynamic quantities, temperature, energy, and entropy. Numerical techniques can explore and characterize the link with high accuracy, and the stability and predictability of the solutions can be described in the relatively new language of nonlinear dynamics and chaos.

We begin by reviewing Newton's laws of motion first and commenting on the reversibility and stability of Newtonian trajectories. Numerical integration of the motion equations is emphasized because it is fundamental to our subject. We then describe Lagrange's and Gauss' formulations of the mechanics of constrained systems, and discuss also Hamilton's mechanics, which is a necessary prerequisite to the treatment of quantum systems and is as well useful in understanding Nosé's recent (1984) work. This last development makes it possible to incorporate temperature and pressure into microscopic reversible equations of motion.

Nosé's dynamical link between the microscopic and macroscopic points of view recurs repeatedly, in discussing both equilibrium and nonequilibrium systems. This work has made it possible to advance beyond Boltzmann in understanding the connection between microscopic reversibility and macroscopic irreversibility.

## 1.2 Mechanical States

Mechanics treats the time development of mechanical systems and furnishes the rules from which the future motion can be computed for any mechanical state. By the term "mechanical state" of a *microscopic* system we mean the list of present coordinates  $\{r\}$  and velocities  $\{\dot{r} = v\}$  of the degrees of freedom. The number of such pairs required depends on the complexity of the system described, and is called the *number of degrees of freedom*.

For instance, the number of coordinates required to locate a rigid tetrahedron in three-dimensional space is six, so that the tetrahedron has six degrees of freedom. Notice that a "tetrahedron" made up by joining together four point masses with six stiff springs would require 12 coordinates to locate it in three-dimensional space and 12 more velocities to completely specify its mechanical state. The constraint of making the tetrahedron rigid removes six degrees of freedom.

For this state information to be useful we must have equations of motion capable of predicting the future. We must know the *accelerations*, that is, the change of the velocities with time. Typically the accelerations and the underlying forces present in the equations of motion depend upon the types of the particles being described. Thus the composition of the system, the corresponding equations of motion, as well as any necessary boundary conditions must be given too before any calculations can be performed. The analog of such a microscopic "mechanical state" for a macroscopic system is the macroscopic "hydrodynamic state," in which the thermodynamic state and velocities are specified, and from which the future behavior can be determined.

Given equations of motion, accelerations or forces, and boundary conditions, knowing the current mechanical state makes it possible to simulate future behavior. Mathematicians call this an "initial value problem." The initial value is the current mechanical state. Consider a simple example. The mechanical state of a one-dimensional harmonic oscillator is specified by giving its coordinate  $x$ , and velocity  $v = \dot{x}$ . The *type* of oscillator must further be specified by giving the mass  $m$  and the force constant  $\kappa$ . Finally either Newtonian or Lagrangian mechanics leads to the same second-order differential equation of motion for the acceleration,

$$\ddot{x} = -(\kappa/m)x,$$

for which the solution satisfying the initial values of  $x$  and  $\dot{x}$  is unique.

At a particular time  $t$  the state of a quantum mechanical system can likewise be characterized by the real and imaginary parts of its wave function. The Schroedinger equation then provides two first-order partial differential equations for the time-development of the real and imaginary parts of the wave function.

Likewise the state of a macroscopic hydrodynamic system, given by local values of density, velocity, and energy, can be propagated by solving the corresponding five partial differential equations (one each for density, the three components of velocity, and energy). In principle the partial differential equations of quantum mechanics and continuum mechanics are superficially more complicated than the ordinary differential equations of classical mechanics. But by averaging these partial differential equations over spatial zones or by representing the solutions as sums of orthogonal functions, both quantum systems and hydrodynamic systems can likewise be converted into sets of ordinary differential equations.

The mechanical state of a system can be followed in time either by following a trajectory  $x(t)$  in coordinate space or in *phase space*, where both the coordinates  $\{q\}$  and the momenta  $\{p\}$  are simultaneously specified. Individual coordinate-momenta points in phase space give the complete dynamical state. In coordinate space the dynamical state requires also velocity, the *rate* at which the trajectory is traced out.

It is worthwhile to emphasize that the accuracy of any numerical solution is strictly limited, so that all of our computer-generated solutions are necessarily approximate. We will see that the typical Lyapunov instability of the equations of motion rapidly and relentlessly destroys computational accuracy, so that the expense of high accuracy is not feasible for long calculations. Generally eight-digit or twelve-digit single-precision accuracy is sufficient. So long as we are interested in reproducing averaged macroscopic behavior there is no evidence that this limited accuracy has practical consequences. If such evidence were to be found it would indicate a new and interesting underlying law of physics.

### 1.3 Newtonian Mechanics

Newton's mechanics furnishes a second-order differential-equation description of the time development of particle coordinates through the coordinate-dependent Forces  $\{F(r)\}$ . The forces depend upon the locations  $\{r\}$  of the masses  $\{m\}$  and the boundary conditions, with the boundary contribution to the forces usually specified as a time-varying function of the coordinates:

$$m\ddot{r} = F(r) + F_{\text{Boundary}}(r,t).$$

The velocity-dependent Lorentz Forces which prescribe the motion of charged particles in magnetic fields depend



upon  $\dot{r}$  as well as  $r$ . For us a more common origin for velocity-dependent forces will lie in the thermostats we will come to use to connect the microscopic and macroscopic descriptions of matter associated with Nosé's and Gauss' mechanics.

In most applications we consider locally neutral matter in which the interactions of the particles are relatively short-ranged, on a nanometer scale. Coulomb forces are longer-ranged, with an interaction energy equal to the room-temperature thermal energy,  $kT$ , at a separation of 50 nanometers.

To treat an N-Body problem in Newtonian mechanics requires three things: (i) initial conditions (the mechanical state, usually  $3N$  coordinates  $\{r\}$  and  $3N$  velocities  $\{v\}$  for an otherwise unconstrained three-dimensional system), (ii) a recipe for the forces, including boundary forces, and (iii) an *algorithm* for solving the equations. We explicitly emphasize the computational and approximate nature of mechanics by using the word algorithm. *Numerical* techniques are generally required because a typical system of three or more nonlinear equations can *only* be solved numerically. There are many exceptions, and these exceptions make up the so-called integrable systems which are exhaustively treated in most mechanics textbooks. Even for such exceptional integrable cases it is often much faster, and more informative, to follow the dynamics numerically than first to evaluate the corresponding analytic expression and then to enter that more complex description into a computer in order to visualize the trajectory.

But it was some of these exceptional integrable cases, with accurately tabulated trajectories, that provided the evidence leading Newton to invent mechanics. The motions of the individual planets can be understood very well on the basis of strong interactions between each planet and the much-more-massive sun and weak perturbations due to the mutual interactions of the planets. This separation is due to the thousandfold difference in mass between the sun and the planets. Kepler's laws describe the idealized motion of individual planets about a motionless sun. The three laws are all illustrated by the orbits appearing in Figure 1.1:

- (i) the bound periodic orbits are ellipses with the sun at a focus, rather than the center, of each such ellipse.
- (ii) these orbits sweep out area at a uniform rate.
- (iii) the mean radius of such an orbit varies as the  $3/2$  power of the period.

Kepler's First Law is a direct consequence of the inverse-square central (that is, no angular dependence) gravitational force. Kepler's Second Law is more general, and applies to any central force law. Today it would be called conservation of angular momentum ( $mr^2\dot{\theta}$ ) and so should apply for any radial potential. Kepler's Third Law is like the first in that it is specific for inverse-square forces. It is interesting to demonstrate the Third Law using dimensional analysis, a simple but powerful technique. Thus, if we assume that the mean potential energy is proportional to the

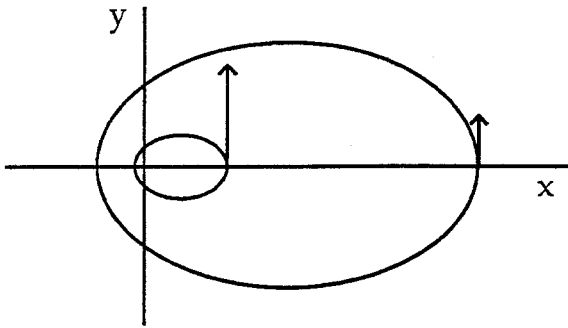


**Figure 1.1** Unit mass, unit field Kepler orbits with initial  $x$  coordinates  $1/16$  and  $1/4$ . The corresponding initial  $y$  velocity components are 2 and 1. The *maximum* speeds of 14 and 7 correspond to the *minimum* separations,  $1/112$  and  $1/28$ . Stoermer integration with  $dt = 0.001$ .

mean kinetic energy, with units  $M(L/T)^2$ , dimensional analysis and Kepler's Third Law establish that the potential energy varies as  $1/L$ .

To see this same result in a more detailed way, consider a radial power-law potential,  $\Phi \propto r^{-n}$ . The resulting central force,  $-\nabla\Phi$ , varies as  $r^{-n-1}$ . Then the dot product of the radius vector and the force, when averaged over time, gives a relation, often called the "Virial Theorem," between the potential and kinetic energies:

$$\langle n\Phi \rangle = \langle \mathbf{r} \cdot \mathbf{F} \rangle = \langle \mathbf{r} \cdot (m\ddot{\mathbf{r}}) \rangle .$$

For sufficiently long times the averaged time derivative of any bounded differentiable quantity vanishes. Thus,

$$\langle n\Phi \rangle = \langle \mathbf{r} \cdot \mathbf{F} \rangle = \langle (d/dt)(m\mathbf{r} \cdot \dot{\mathbf{r}}) \rangle - \langle m\dot{\mathbf{r}}^2 \rangle = 0 - 2K .$$

This isolated-system version of the virial theorem establishes that the ratio of the kinetic energy to the potential energy is  $-n/2$ . The kinetic energy depends on the orbit size and time as  $(r/t)^2$  while the potential energy varies as  $r^{-n}$ . The two energies can only be proportional to one another if the *time* of the orbit varies as the  $(n+2)/2$  power of the *size*. Thus, Kepler's Third Law implies  $n = 1$  for the gravitational potential.

The Kepler problem just discussed can be made much more complicated. We could include tidal forces and deformation as well as the corrections to the orbit which depend on the ratio of planet mass to solar mass. It is a famous problem of Laplace to understand whether or not the latter simplification is qualitatively important. That is, does the inclusion of three-body interactions lead to a qualitative change in the motion?

### Problem:

Discuss the dependence of the "escape velocity" on the mass ratio  $m/M$  for two bodies with a gravitational attraction  $\Phi \propto mM/r$ .

### 1.4 Trajectory Stability

It seems likely that the motion of the planets in our solar system is stable, although this is only certain on the time scale relevant to men. Our own goal is to understand many-body systems, both at and away from equilibrium. Such systems are generally unstable, so that trajectory stability deserves discussion. We say that a solution is *stable* if nearby solutions separate from one another less rapidly than exponentially in time. A solution is *unstable* if a nearby trajectory can separate from it exponentially fast in time. Because configuration space is a subspace of phase space the separation can be measured in either one.



The criterion of exponential separation should not come as a surprise. A *linear* analysis of the effect of a trajectory perturbation  $\delta$  has to predict a *linear* relation, of the form  $\dot{\delta} \propto \delta$ , leading to instability or stability, depending on the sign of the proportionality constant. The exponential instability of a perturbation, varying as  $\exp(\lambda t)$ , is important for two reasons. First, it is the typical situation, and limits the time for which an accurate numerical solution can be found. Second, it is the type of motion which requires as much information in the initial conditions as is available in the trajectories. That is, to follow the trajectories with given accuracy for a time  $t$  requires  $\lambda t / \ln 10$  decimal digits in the initial conditions. A solution is said to be *Lyapunov unstable*, exhibiting "Lyapunov Instability," if two neighboring trajectories do separate exponentially fast. Generic behavior in the alternative "stable" situation typically involves trajectory separations varying only linearly with time. Joseph Ford of Georgia Tech has aptly expressed exponential Lyapunov instability as the point at which our computers resemble "elaborate xerox machines." He means by this that the computers simply reproduce, as output, the same amount of information as was contained in the input, as initial conditions.

Figures 1.2 and 1.3 show examples of stable and unstable orbits, both involving a classical particle bouncing on a surface in a constant gravitational field. If the surface is flat the orbit is stable. A perturbed solution, with a slightly different velocity parallel to the plane deviates only linearly in time (because the displacement difference is the integral of the velocity difference). If, on the other hand, the surface is curved, differences can be amplified, and the bouncing of a ball can be Lyapunov unstable, with an exponential increase of trajectory separation with time. Let us carry out an approximate calculation of this instability. To avoid complexity we will restrict our attention to a single mass moving in an external field.

Consider a mass point dropped vertically in a unit gravitational field onto a fixed elastic ball of unit radius. The time between bounces is  $\tau$ , which varies as the

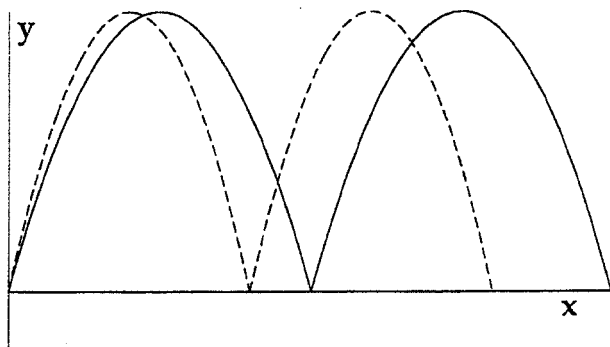


**Figure 1.2** Stable trajectories with initial y velocity component = 1 and  $\Delta\dot{x} = 0.1$ . Mass and gravitational field strength = 1.

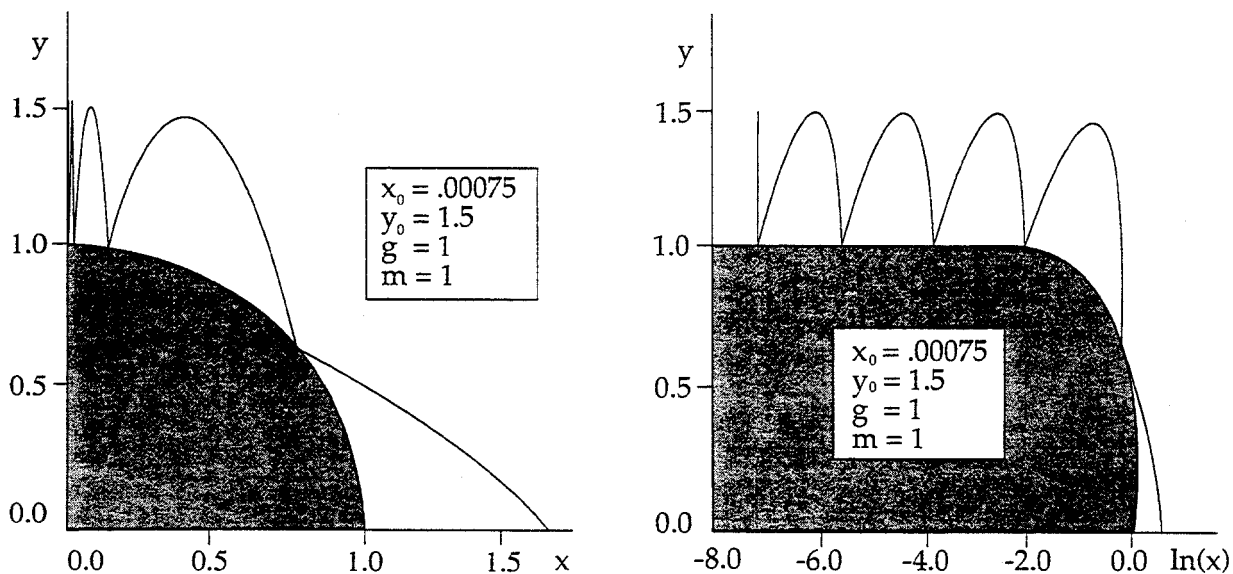


**Figure 1.3** Unstable trajectory with an initial offset of  $\Delta x = 0.00075$ .

square-root of the bounce height if the height is small. To begin, the mass point is offset slightly from the straight up position directly over the fixed ball. Provided that the offset is small, the problem can be solved analytically by relating the velocity after the  $n$ th bounce,  $v_n$ , to the offset at the  $n$ th bounce,  $x_n$ .

$$v_n = v_{n-1} + x_n \tau ;$$

$$x_n = [v_{n-1} + v_{n-2} + v_{n-3} + \dots] \tau = v_{n-1} \tau [R / (R - 1)] .$$

where we use  $R$  to denote the ratio  $x_n / x_{n-1} = v_n / v_{n-1} = R$ . If we divide these equations by  $v_{n-1}$  we find the following relations for  $R$ :

$$R = 1 + (x_n \tau / v_{n-1}) = 1 + R \tau^2 / (R - 1) ,$$

leading to two solutions:

$$R_{\pm} = (1/2)[2 + \tau^2 \pm (4\tau^2 + \tau^4)^{1/2}].$$

The plus sign, which corresponds to offsets increasing with time, and instability, gives the results  $R_+ = 9.90$  and  $3.73$  for  $\tau^2$  equal to  $8$  and  $2$ . The minus sign, corresponding to the reversed trajectory with decreasing offsets, gives the reciprocals of these values for  $R_-$ . The logarithm of the ratio of successive offsets,  $R$ , divided by the time between bounces, gives the rate of exponential divergence and is called the "Lyapunov exponent." In the two cases just considered the Lyapunov exponents have the values  $\pm \ln 9.90/8^{1/2} = \pm 0.810$  and  $\pm \ln 3.73/2^{1/2} = \pm 0.931$ . In the small bounce, small  $\tau$  limit, the Lyapunov exponent approaches  $1.000$ .

### 1.5 Trajectory Reversibility

Time-reversibility, or just "reversibility" for short, is characteristic of properly formulated microscopic motion equations in both classical and quantum mechanics. When we call a motion *reversible* we mean that a reversed movie of that motion, a solution of the complete set of equations, run backward through a movie projector, would still satisfy the same motion equations. This definition often, but not always, coincides with the formal mathematical operation of reversing the solution of a set of first-order differential equations by changing the signs of all the time derivatives.

Newtonian mechanics is patently reversible because changing the sign of the time has no effect on the accelerations,  $\{\ddot{r}\}$ . More general forms of mechanics, with constraints and frictional forces, make the reversibility question interesting. We will come back to these in discussing Gauss', Lagrange's, and Nosé's contributions to constrained mechanics later in this Chapter.

Let us now look at a simple integrable Newtonian mechanics problem with a known analytic solution, the one-dimensional harmonic oscillator, with unit force constant and unit mass. We use this example to introduce the simple Stoermer version of the second-order time-reversible Newtonian equation of motion:

$$x(t + dt) - 2x(t) + x(t - dt) = dt^2 F = - dt^2 x(t).$$

In this centered second-difference form the time-symmetry is apparent. Changing  $dt$  to  $-dt$  leaves the motion equation, and its solution, unchanged. (Of course the sign of the initial value of  $\dot{x}$  would be reversed in the reversed trajectory, but the equations of motion are unchanged).

In contrast to the reversible motions of systems governed by Newtonian mechanics, motions involving macroscopic hydrodynamic dissipation, diffusion, viscosity, or heat conduction are intrinsically irreversible. When diffusion, viscosity, or heat conduction play a role, the reversed motions are unnatural. Imagine reversing

a movie of breaking surf or a waterfall. These motions make no sense when run backward in time. On the other hand the equally-irreversible motions of clouds might appear quite reasonable when reversed, simply because the motion is slow, on a human time scale.

The “phenomenological” (meaning based on experience) laws governing macroscopic hydrodynamic equations are generally irreversible. The simplest example is the “Diffusion Equation,” Fick’s Second Law:

$$\partial\rho/\partial t = D\nabla^2\rho,$$

which has also a centered finite-difference representation:

$$\rho(t + dt) - \rho(t) = +D(dt/2)[\nabla^2\rho(t + dt) + \nabla^2\rho(t)],$$

where the plus sign preceding the diffusion coefficient  $D$  serves to emphasize the difference from the time-reversed version to follow. The time-reversed version of this equation,

$$\rho(t) - \rho(t - dt) = -D(dt/2)[\nabla^2\rho(t) + \nabla^2\rho(t - dt)],$$

is not only different, it is also very poorly behaved from the mathematical standpoint, having solutions growing in time as  $\exp[Dt(2\pi/\lambda)^2]$ , for arbitrarily small wavelengths  $\lambda$ .

For positive  $dt$  the diffusion equation can be solved by a variety of methods: Fourier series, Green’s functions, or the straightforward finite-difference approximation suggested above. For any of these approaches the left-hand side changes sign, with time reversal, while the right-hand side does not. Thus the diffusion equation is *irreversible*.

To understand the irreversibility in more detail consider the examples shown in the Figures. The reversible harmonic oscillator follows the trajectory  $x = \sin t$ , shown in Figure 1.4, equally well for positive and negative times. The diffusing density  $\rho(x,t)$  follows the irreversible diffusion equation. See Figure 1.5. In the laboratory a Gaussian distribution of the density spreading in time would continue to spread if time could be reversed. Of course, on a microscopic scale, if we could reverse all particle velocities (not easy!), the spreading *could* be reversed. This property of the diffusion equation, irreversibility, an “Arrow of Time,” is not an obvious property of Newton’s equations of motion. At the same time there is no doubt at all that Newtonian systems do diffuse. An understanding of this apparent paradox is one of the main goals of the statistical mechanics of nonequilibrium processes. Recent developments rooted in the

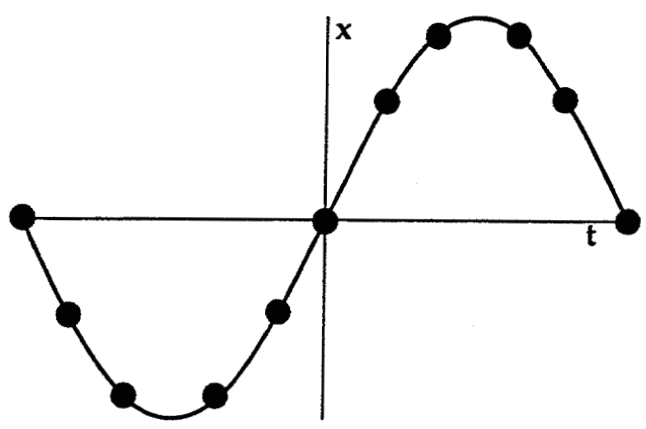
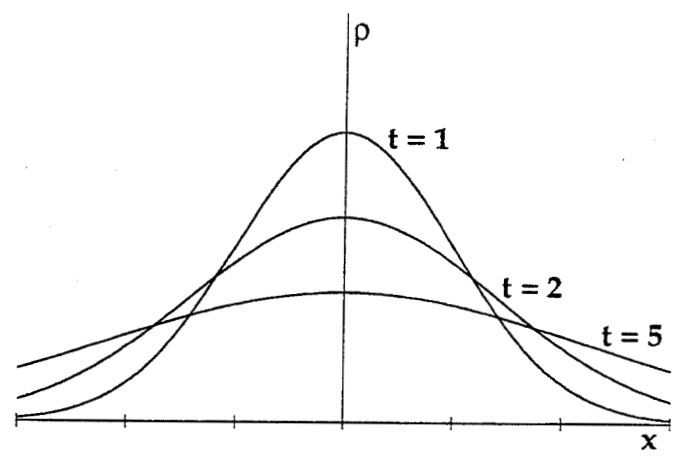


Figure 1.4 Reversible harmonic oscillator trajectory,  $x = \sin t$ . Stoermer integration with time step  $dt = \pi/5$ .

Figure 1.5 Irreversible solution of Fick's Second Law:  $\rho = \exp(-x^2/4t)$ . From top to bottom the density curves correspond to times +1, +2, and +5.



constrained mechanics of Lagrange, Gauss, and Nosé have made it possible to attain this understanding.

**Problems:**

1. Show that the prototypical Fourier-Series Solution  $\rho = \rho_k \exp(-t/\tau) \sin kx$  is a solution of the diffusion equation provided that the decay time  $\tau$  is related to the wavelength  $2\pi/k$  by  $\tau = 1/(k^2D)$ .
2. Show that the Gaussian function  $\rho = \delta\rho(4\pi Dt)^{-1/2} \exp(-x^2/4Dt)$  is a solution of the one-dimensional diffusion equation and that the halfwidth of the solution  $\langle x^2 \rangle^{1/2}$  varies as the square root of the time.
3. Consider a periodic ring of 5 sites in which the state of the  $j$ th site at time  $n$  is the weighted average of the previous state and the second difference of the coordinates,  $x_{j-1} - 2x_j + x_{j+1}$ . "Periodic" implies that  $x_6 = x_1$  and that  $x_0 = x_5$ . Comment on the relation of this problem to the Newtonian equations of motion and to the diffusion equation.

1.6 Stoermer and Runge-Kutta Integration

To illustrate algorithms for solving Newton's equations of motion we consider in more detail the stable and reversible harmonic oscillator, with unit mass and force constant, so that the equation of motion is

$$\ddot{x} = -x.$$

We choose the particular initial condition,  $x = 1$  at  $t = 0$ , and  $\dot{x} = 0$ , for which the solution is

$$x = \cos(t).$$

First consider the Stoermer algorithm with time step  $\delta$  :

$$[x_+ - 2x_0 + x_-]/\delta^2 = -x_0.$$

This algorithm gives the future coordinate,  $x_+$ , in terms of the present and past coordinates,  $x_0$  and  $x_-$ , and the current acceleration,  $-x_0$ . At a time  $n\delta$  the equation has a solution:

$$x = x_0 e^{in\alpha} \text{ with } \cos(\alpha) = 1 - (1/2)\delta^2 = 1 - (1/2)\alpha^2 + (1/24)\alpha^4 - \dots$$

If we solve this relation for the series expansion of  $\alpha$ ,

$$\alpha^2 = \delta^2 + (1/12)\delta^4 + \dots,$$

we find that for  $t\delta^2 \ll 1$  the approximate coordinate  $x(n\delta=t)$  is in error by  $(1/24)\delta^2 t \sin(t)$ . This "global error" characterizes the deviation of the approximate difference-equation solution from the exact differential-equation solution at a fixed time  $t$  as the time step  $\delta$  approaches zero. An alternative characterization of error is the local error. If we choose two adjacent coordinate values from an *exact* trajectory:  $x_-$ , at time  $t - \delta$ , and  $x_0$ , at time  $t$ :

$$x_- = \cos(t - \delta); x_0 = \cos(t),$$

for instance, then the difference  $\Delta x$  between the exact solution,  $\cos(t + \delta)$ , and the Stoermer approximation,  $[2 - \delta^2]\cos(t) - \cos(t - \delta)$ , gives the "local" single-time step error:

$$\Delta x = \cos(t + \delta) - [2 - \delta^2]\cos(t) + \cos(t - \delta) = C - \delta S - (\delta^2/2)C + (\delta^3/6)S + (\delta^4/24)C - \dots$$

$$- [2 - \delta^2]C + C + \delta S - (\delta^2/2)C - (\delta^3/6)S + (\delta^4/24)C + \dots \approx (\delta^4/12)C = (\delta^4/12)\cos(t),$$

where we have abbreviated  $\cos(t)$  and  $\sin(t)$  by  $C$  and  $S$ . Because the single-time step error is fourth-order in  $\delta$ , we refer to the Stoermer method as "third order," reflecting

the accuracy of a single integration step. The many-time step "global" error, giving the deviation from the true trajectory, is of order  $\delta^2$ , much larger than the single-time step "local" error, which is proportional to  $\delta^4$ . The difference,  $\delta^4$  versus  $\delta^2$ , has two sources: first, the difference equation is second order in time, requiring two integration steps to find  $x(t+dt)$ ; second, the number of time steps which contribute to the global error at time  $t$  varies as  $t/\delta$ . These two effects each contribute equally to the error. A simple computer program implementing the Stoermer algorithm for the one-dimensional oscillator appears at the end of this Section.

To improve upon the third-order accuracy of the Stoermer method it is convenient to use one of the "fourth-order" Runge-Kutta methods. The local error in the fourth-order Runge-Kutta method is *fifth* order in  $\delta$ . Because the method applies to *first-order* equations only a single power of  $\delta$  is lost in the integration step. The global error is thus of order  $\delta^4$  ( $t/\delta$  steps with errors of order  $\delta^5$ ) rather than  $\delta^2$ . As a concrete demonstration of the Runge-Kutta method we include a computer program at the end of this Section. The program integrates the coupled set of three first-order differential equations describing the Nosé-Hoover oscillator shown in the Figure 1.6.

Exactly the same fourth-order Runge-Kutta method can also be applied to ordinary quadrature, and then becomes equivalent to Simpson's Rule. It is only necessary to include the integrand's time-dependence in the RHS function called by Runge-Kutta. Simpson's Rule describes the integration of a cubic function exactly over a range  $dt$  and so is also a fourth-order method. As an example we integrate the exponential function  $e^t$  from 0 to 1 in a single integration step. If we define the indefinite integral  $I(t)$ :

$$I(t) = \int e^s ds ,$$

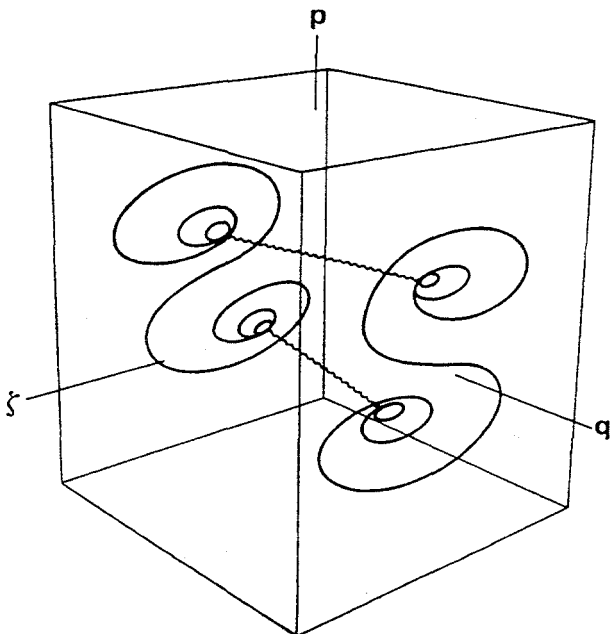


Figure 1.6 Nosé-Hoover oscillator described by the three first-order differential equations:

$$\dot{x} = p ; \dot{p} = -x - \zeta p ; \dot{\zeta} = 100(p^2 - 1) .$$

The initial conditions are:

$$x_0 = 0.0 ; p_0 = 1.0085 ; \zeta_0 = 0.0 .$$

then the first derivatives of I at the set of Runge-Kutta time values

{0, 0.5, 0.5, 1.0}

are

{ $e^{0.0} = 1.00000$ ;  $e^{0.5} = 1.64872$ ;  $e^{0.5} = 1.64872$ ;  $e^{1.0} = 2.71828$ }

leading to an average value of  $\dot{I}$  equal to 1.71886, close to the exact value,  $e - 1 = 1.71828$ .

#### STOERMER METHOD

CALCULATION OF A REGULAR HARMONIC OSCILLATOR TRAJECTORY.  
CALCULATION USES THE CLASSIC 3RD-ORDER STOERMER METHOD.

```

    DIMENSION YNEW(1), YNOW(1), YOLD(1), FORCE(1)
    T = 0.0
    YNOW(1) = 1.0
    YNEW(1) = 1.0
    DT = 3.14159265358979/30.0
    DO 30 LOOP = 1, 60
    DO 20 I = 1, 1
    YOLD(I) = YNOW(I)
20  YNOW(I) = YNEW(I)
    CALL STORM(DT, YNEW, YNOW, YOLD, FORCE)
    T = T + DT
    WRITE(3, 10) T, YNEW(1), YNOW(1), YOLD(1)
10  FORMAT("T, X, OLDX:", 3F12.7)
30  CONTINUE
    CALL EXIT
    END

    SUBROUTINE STORM(DT, YNEW, YNOW, YOLD, FORCE)
    DIMENSION YNEW(1), YNOW(1), YOLD(1), FORCE(1)

    CALL RHS(YNOW, FORCE)

    DO 1 I = 1, 1
1  YNEW(I) = 2.0*YNOW(I) - YOLD(I) + FORCE(I)*DT*DT

    RETURN
    END

    SUBROUTINE RHS(YNOW, FORCE)
    DIMENSION YNOW(1), FORCE(1), X(1)

    DO 10 I = 1, 1
    X(I) = YNOW(I)
1  FORCE(I) = - X(I)
    RETURN
    END

```

RUNGE-KUTTA METHOD

CALCULATION OF A REGULAR NOSE-HOOVER OSCILLATOR TRAJECTORY.  
CALCULATION USES THE CLASSIC 4TH-ORDER RUNGE-KUTTA METHOD.

```

DIMENSION YNOW(3),YDOT(3)
T = 0.0
YNOW(1) = 0.0
YNOW(2) = 1.0085
YNOW(3) = 0.0
DT = 0.01
DO 30 LOOP = 1,1702
CALL RK(DT,YNOW,YDOT)
T = T + DT
WRITE(3,10) T, YNOW(1),YNOW(2),YNOW(3)
10  FORMAT("T,Q,P,Z:",4F12.7)
30  CONTINUE
CALL EXIT
END

SUBROUTINE RK(DT,YNOW,YDOT)
DIMENSION YNOW(3),YDOT(3),YNEW(3)
DIMENSION DOT1(3),DOT2(3),DOT3(3),DOT4(3)

CALL RHS(YNOW,YDOT)

DO 1 I = 1,3
1  DOT1(I) = YDOT(I)

DO 2 I = 1,3
2  YNEW(I) = YNOW(I) + DT*DOT1(I)/2.0
   CALL RHS(YNEW,YDOT)

DO 3 I = 1,3
3  DOT2(I) = YDOT(I)

DO 4 I = 1,3
4  YNEW(I) = YNOW(I) + DT*DOT2(I)/2.0
   CALL RHS(YNEW,YDOT)

DO 5 I = 1,3
5  DOT3(I) = YDOT(I)

DO 6 I = 1,3
6  YNEW(I) = YNOW(I) + DT*DOT3(I)
   CALL RHS(YNEW,YDOT)

DO 7 I = 1,3
7  DOT4(I) = YDOT(I)

DO 8 I = 1,3
8  YNOW(I) = YNOW(I)
   & + DT*(DOT1(I)+2.0*(DOT2(I)+DOT3(I))+DOT4(I))/6.0

RETURN
END

```

```

SUBROUTINE RHS (YNEW, YDOT)
DIMENSION YNEW (3), YDOT (3)
Q = YNEW (1)
P = YNEW (2)
Z = YNEW (3)
YDOT (1) = P
YDOT (2) = -Q - Z*P
YDOT (3) = 100.0*(P*P - 1.0)
RETURN
END

```

### Problems:

1. Modify the Nosé-Hoover oscillator fourth-order Runge-Kutta computer program just displayed so as to solve the one-dimensional harmonic oscillator problem for time steps  $\delta = (2\pi/15)$ ,  $(2\pi/30)$ , and  $(2\pi/60)$ , carrying the solution from the initial values,  $\{x = 1.0, \dot{x} = 0.0\}$ , through one oscillator period of  $2\pi$ . Estimate the local and global errors from your numerical results. The fourth-order Runge-Kutta approximation for this oscillator problem has the analytic solution:

$$x_n = [1 - (\delta^6/72) + (\delta^8/576)]^{n/2} \cos(n\delta\lambda),$$

where  $\lambda$  can be obtained from the equation,

$$\tan(\delta\lambda) = [\delta - (\delta^3/6)] / [1 - (\delta^2/2) + (\delta^4/24)].$$

Compare computer evaluations of this analytic solution with your Runge-Kutta results to determine the accuracy of your computer.

2. Show numerically that exactly this same solution holds if the Runge-Kutta statements

```

2      YNEW(I) = YNOW(I) + DT*DOT1(I)/2.0
4      YNEW(I) = YNOW(I) + DT*DOT2(I)/2.0
6      YNEW(I) = YNOW(I) + DT*DOT3(I)
8      YNOW(I) = YNOW(I)
      & + DT*(DOT1(I)+2.0*(DOT2(I)+DOT3(I))+DOT4(I))/6.0

```

are changed to

```

2      YNEW(I) = YNOW(I) + DT*DOT1(I)/3.0
4      YNEW(I) = YNOW(I) - DT*DOT1(I)/3.0 + DT*DOT2(I)
6      YNEW(I) = YNOW(I) + DT*(DOT1(I)-DOT2(I)+DOT3(I))
8      YNOW(I) = YNOW(I)
      & + DT*(DOT1(I)+3.0*(DOT2(I)+DOT3(I))+DOT4(I))/8.0

```

3. Show that it is possible to reduce the storage used in implementing the fourth-order Runge-Kutta method to four locations per differential equation.
4. Show that it is possible to reduce the storage used in implementing the second-order Stoermer method to three locations per second-order differential equation, a nearly-threefold savings over the Runge-Kutta approach.
5. What are the largest time steps  $dt$  for which the Stoermer and the Fourth-Order Runge-Kutta equations for the one-dimensional harmonic oscillator have convergent solutions?
6. Introduce *time dependence* into subroutine RHS in order to integrate the function  $\exp(r)$ , where  $r$  is  $(x^2 + y^2)^{1/2}$ , over the unit square using  $dx = dy = 1/3$ .

### 1.7 Lagrangian Mechanics

In general, the Lagrangian motion equations describe the time evolution of a mechanical system characterized by a set of "generalized coordinates"  $\{q\}$ . The time variation of the coordinates defines the generalized velocities  $\{v = \dot{q}\}$ . The evolution follows from the Lagrangian,  $L = K - \Phi$ . It is assumed that the kinetic energy  $K$  and potential energy  $\Phi$  can be expressed in terms of the variables  $q$  and  $v$ . For each of the generalized coordinates  $q$  the Lagrange equation of motion is

$$(d/dt)(\partial L/\partial v)_q = (\partial L/\partial q)_v,$$

or, alternatively,

$$\dot{p} = (\partial L/\partial q),$$

where  $p$  is said to be the generalized momentum conjugate to  $q$ :

$$p \equiv (\partial L/\partial v)_q.$$

In the simple case that  $K$  depends just on the Cartesian velocities and  $\Phi$  just on the Cartesian coordinates then Lagrange's equations of motion are identical to Newton's and offer no obvious advantages. But the Lagrangian formalism is applicable in any coordinate system. A good choice of coordinates can furnish new information.

For example, an unconstrained two-dimensional harmonic oscillator, with unit mass and force constant, could be described with either Cartesian coordinates or polar coordinates, with either of the corresponding Lagrangians,

$$L_{xy} = (v_x^2 + v_y^2 - x^2 - y^2)/2;$$

$$L_{r\theta} = (r^2 v_\theta^2 + v_r^2 - r^2)/2.$$

From the Cartesian coordinate form we would just obtain the familiar Newtonian equations of motion. But the polar-coordinate case provides more information. The polar-coordinate equations of motion express directly the conservation of angular momentum:

$$\dot{v}_r = rv_\theta^2 - r ; d(r^2v_\theta)/dt = 0 .$$

Lagrangian mechanics is particularly useful in treating constrained systems. Two types of treatment are possible: we can either choose coordinates in which the constraint is implicit or we can impose the constraint explicitly by using a Lagrange multiplier. In this Section we will illustrate the first approach, solving a double-pendulum problem with two degrees of freedom. In Section 1.8 we will illustrate the second approach, eliminating a degree of freedom from the motion by imposing an explicit constraint.

Using these two approaches, Lagrangian mechanics provides two useful methods for treating constrained systems for which Cartesian coordinates are inconvenient. Models of this kind arise in computational statistical mechanical simulations of molecules with a rigid structure. A sulfur hexafluoride molecule, for instance, could be treated by fixing six fluorine centers at octahedral sites equidistant from a central sulfur atom. To simplify the illustration we consider here a simpler constrained system with just two degrees of freedom. The same ideas can easily be extended to more complex situations.

Consider now the double pendulum illustrated in the Figure 1.7. In the absence of constraints this system would have four degrees of freedom, the  $x$  and  $y$  coordinates of both masses. But we eliminate two degrees of freedom by using *generalized coordinates*, here angles which implicitly satisfy constraints on the pendulum lengths. For simplicity we constrain both pendula to have fixed lengths of unity supporting masses of unity. It is most natural to describe the constrained motion of the pendula in terms of the angles, defined relative to the field direction,  $\alpha$  and  $\beta$ . In Lagrangian Mechanics the motion calculation then follows from the Lagrangian function  $L(\alpha, \beta, v_\alpha, v_\beta)$ , which in this case has the usual form  $L = K - \Phi$ , where  $K$  and  $\Phi$  are the kinetic and potential energies. For the pendulum problem the potential energy is just the sum of the vertical coordinates,  $-\cos(\alpha)$  for the upper mass, and  $-\cos(\alpha) - \cos(\beta)$  for the lower one, multiplied by the gravitational field strength, which we will also choose equal to unity. Thus

$$\Phi = -2\cos(\alpha) - \cos(\beta) .$$

The kinetic energy,

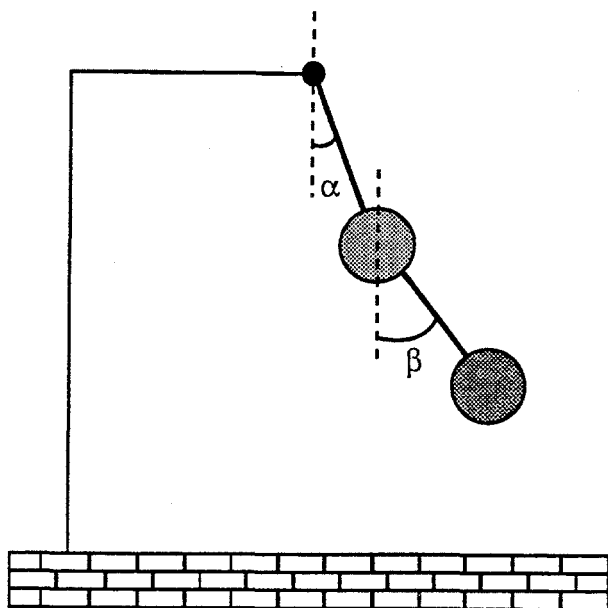


Figure 1.7 Double pendulum with Lagrangian  $L = \dot{\alpha}^2 + (1/2)\dot{\beta}^2 + \dot{\alpha}\dot{\beta}\cos(\alpha-\beta) + 2\cos\alpha + \cos\beta$ . The lengths, masses, and gravitational field strength are all set equal to unity.

$$K = \dot{\alpha}^2 + (1/2)\dot{\beta}^2 + \dot{\alpha}\dot{\beta}\cos(\alpha-\beta),$$

follows directly from the squares of the time derivatives of the two vectors  $(\sin(\alpha), \cos(\alpha))$  and  $(\sin(\alpha)+\sin(\beta), \cos(\alpha)+\cos(\beta))$ , which locate the masses relative to the support point at the origin. The four equations of motion from the Lagrangian:

$$p_{\alpha} = 2\dot{\alpha} + \dot{\beta}\cos(\alpha - \beta);$$

$$p_{\beta} = \dot{\beta} + \dot{\alpha}\cos(\alpha - \beta);$$

$$\dot{p}_{\alpha} = -2\sin\alpha - \dot{\alpha}\dot{\beta}\sin(\alpha - \beta);$$

$$\dot{p}_{\beta} = -\sin\beta + \dot{\alpha}\dot{\beta}\sin(\alpha - \beta),$$

can then be solved by expressing  $\dot{\alpha}$  and  $\dot{\beta}$  in terms of  $p_{\alpha}$  and  $p_{\beta}$  and solving the resulting four coupled equations of motion using the Runge-Kutta method illustrated in the previous Section.

### Problems:

1. Show that the double-pendulum problem just described is Lyapunov unstable for the initial conditions  $\alpha = \beta = \pi/2$  with  $\dot{\alpha}$  and  $\dot{\beta} = 0$ . The correct Lyapunov exponent is 0.30. To reproduce this result it is necessary to follow the motion of two nearby trajectories, a "reference" trajectory and a "satellite" trajectory, periodically rescaling the phase-space offset  $(\delta\alpha^2 + \delta\beta^2 + \delta p_{\alpha}^2 + \delta p_{\beta}^2)^{1/2}$  separating the satellite from the reference.

2. Discuss the dependence of the global error on the time  $t$  and the time step  $dt$  for a Lyapunov-unstable set of differential equations. For a Lyapunov exponent of 1.00 estimate the maximum time for which an accurate numerical solution can be obtained using 8-digit, 14-digit, and 33-digit arithmetic and a time step of 0.001. In the 33-digit case what must the order of the local integration error be to achieve this accuracy?

### 1.8 Least Action Principle

Here we continue our investigation of the Lagrangian equations of motion by first deriving them from Hamilton's variational Principle of Least Action and then proceeding to apply the equations to deal explicitly with a constraint. As a source of the equations of motion, the Principle is more basic than the equations themselves. We therefore begin with the Principle of Least Action, which states that the variation in the "action integral"  $\int L(q,v)dt$ , between two fixed points at two fixed times, must be an extremum, usually a minimum.

Let us illustrate the meaning of the Principle with a simple example, finding the least-action parabolic path for a particle in a gravitational field. See Figure 1.8. We choose the mass and the field strength equal to unity. If we specify both an initial point,  $(x,y)_0 = (0,0)$ , and a final point, at  $t = 1$ ,  $(x,y)_1 = (1,0)$ , the motion depends on a single variational parameter,  $\alpha$ :

$$x = t; y = \alpha t(1 - t).$$

The corresponding "action integral," the integral of the Lagrangian,

$$\int L dt = \int dt (1/2)[1 + \alpha^2(1 - 2t)^2 - 2\alpha t(1 - t)] = (3 - \alpha + \alpha^2)/6,$$

has its minimum value,  $11/24$ , for the Least-Action trajectory with  $\alpha = 1/2$ .

The general variational statement of the Principle:

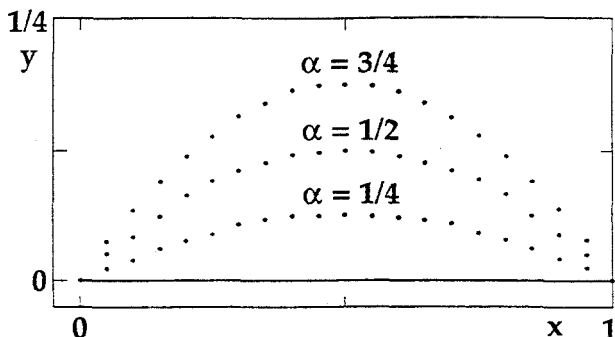


Figure 1.8 Parabolic trajectories in a unit gravitational field with  $\alpha$  values  $1/4$ ,  $1/2$ , and  $3/4$ .

$$\delta \int L(q,v) dt = 0 ,$$

can be made more explicit by considering the variations of both arguments of the Lagrangian,  $\delta q$  and  $\delta v$ :

$$\int [(\partial L(q,v)/\partial q)\delta q + (\partial L(q,v)/\partial v)\delta v] dt = 0 .$$

If the second term is integrated by parts, integrating  $\delta v = \delta \dot{q}$  with respect to time, then, because  $\delta q$  vanishes at the end points, a simpler form results:

$$\int [(\partial L(q,v)/\partial q) - (d/dt)(\partial L(q,v)/\partial v)] \delta q dt = 0 .$$

Aside from the two endpoint restrictions, the variation  $\delta q$  is an arbitrary function of time. It could, for instance, be chosen to vanish everywhere except in the neighborhood of a particular time. Thus, because the integral must vanish, the coefficient multiplying the arbitrary  $\delta q$  must vanish also. This requirement gives the Lagrangian equations of motion:

$$(d/dt)(\partial L(q,v)/\partial v)_q = (\partial L(q,v)/\partial q)_v .$$

In this form Lagrangian mechanics is specially easy to use in implementing implicit constraints by choosing appropriate generalized coordinates. An alternative form, which implements constraints using Lagrange multipliers is useful too in more complicated cases. This idea can be applied to constraints, or restrictions, involving both the coordinates and the momenta. To illustrate the application of Lagrangian mechanics to the simpler of these cases, an explicit holonomic constraint involving just coordinates, consider the motion of a mass constrained to lie on the unit circle by the constraint

$$C(x,y) = (x^2 + y^2 - 1)/2 = 0 .$$

The rotation of a rigid diatomic molecule could be treated in this way. Begin by considering the modified Lagrangian

$$L = (m/2)(v_x^2 + v_y^2) + \lambda C(x,y) ,$$

in which  $\lambda$  is to be selected in such a way that the product  $\lambda C$  always vanishes while satisfying the constraint  $C(x,y) = 0$ . No matter how complicated the dependence of  $\lambda$  on  $\{x,y,v_x,v_y\}$  the resulting dynamics will necessarily obey Lagrange's equations of motion. To find  $\lambda$  we combine the equations of motion from the Lagrangian:

$$m \dot{v}_x = \lambda x ; m \dot{v}_y = \lambda y ,$$

with the second time derivative of the constraint,

$$v_x^2 + v_y^2 + x \dot{v}_x + y \dot{v}_y = 0 ,$$

giving

$$v_x^2 + v_y^2 + (\lambda/m)(x^2 + y^2) = 0 .$$

for the Lagrange multiplier and  $-mv^2/r$  for the corresponding centripetal force.

In linking mechanics to macroscopic thermodynamics and hydrodynamics through many-body simulations, more complex many-body constraints involving particle velocities are often involved. Pressure, temperature, and heat flux all involve particle velocities. For these nonholonomic constraints, particularly in situations involving nonequilibrium systems, other forms of mechanics, building on old ideas of Gauss and newer ideas of Nosé are sometimes more useful than Lagrange's. In the next Section we describe Gauss' contribution.

### Problem:

A path travelling *through*, rather than *around*, a potential barrier, evidently has a lower action integral because the potential contribution to the integral is large and negative. Does this observation invalidate the Principle of Least Action?



### 1.9 Gauss' Principle and Nonholonomic Constraints

Gauss developed the mathematical least squares technique to minimize the statistical error in fitting approximate data. In 1829, Gauss applied his least squares technique to mechanics. Gauss suggested that nature and mathematics both follow analogous rules so that mechanical constraints should likewise best be satisfied by using the smallest possible constraint force. This is, whenever constrained equations of motion,

$$\{ m \dot{v} = F + F_c \} ,$$

are used the constraint forces  $\{F_c\}$  should be made as small as possible. Gauss' least-squares-based "Principle of Least Constraint" is

$$\Sigma F_c^2/(2m) \text{ is a minimum .}$$

To analyze or apply the Principle it is convenient to imagine modifying the constraint forces  $\{F_c\}$  slightly, adding variations  $\{\delta F_c\}$  which still satisfy the constraint:

$$\Sigma F_c^2/(2m) = \Sigma (F_c + \delta F_c)^2/(2m) .$$

Evidently the linear variation must vanish:

$$\Sigma F_c \cdot \delta F_c / m = 0 .$$

This restriction on the constraint force applies to any problem. We immediately illustrate this idea by applying it, choosing again the simplest interesting application, a rigid symmetric diatomic molecule, with zero center-of-mass velocity. We consider the problem from the standpoint of a single mass constrained to lie at a point  $(x,y)$  unit distance from the origin. In this case there are no forces other than the constraint force, so that the equation of motion, including a variation in the constraint force, is

$$m \dot{v} = F_c + \delta F_c .$$

Just as before, we differentiate the constraint,

$$C(x,y) = (x^2 + y^2 - 1)/2 = 0 ,$$

twice with respect to time to get a restriction on the acceleration, or equivalently, the constraint force:

$$r \cdot \dot{v} + v^2 = (r/m) \cdot (F_c + \delta F_c) + v^2 = 0 .$$

In the *absence* of the variation  $\delta F_c$  the constraint force must *itself* satisfy this equation,  $(r/m) \cdot F_c + v^2 = 0$ , so that *any* acceptable variation  $\delta F_c$  can have no radial component:

$$(r/m) \cdot \delta F_c = 0 ; (x/m) \delta F_c^x + (y/m) \delta F_c^y = 0 .$$

This equation and the variational form of Gauss' Principle,  $F_c \cdot \delta F_c / m = 0$ , can then be combined using an arbitrary Lagrange multiplier  $\lambda$ :

$$(F_c^x + \lambda x)\delta F_c^x + (F_c^y + \lambda y)\delta F_c^y = 0 .$$

If we then choose the Lagrange multiplier in such a way that the coefficient of  $\delta F_c^y$  vanishes, we have

$$(F_c^x + \lambda x)\delta F_c^x = 0 .$$

Because the variation  $\delta F_c^x$  is now arbitrary, the coefficient must vanish, giving explicit expressions for the constraint forces:

$$F_c^x = -\lambda x ; F_c^y = -\lambda y .$$

Substituting these into the conservation equation,  $(r/m) \cdot F_c + v^2 = 0$ , leads to the usual expression for the centripetal force,

$$-\lambda r = -(mv^2/r^2)r ,$$

in agreement with our calculation based on Lagrangian mechanics.

Next we use Gauss' Principle to enforce an isokinetic (constant kinetic energy) nonholonomic (involving velocities) constraint on the dynamics of a many-body system:

$$C(v_x, v_y, v_z) = (1/2)[\sum mv^2 - 2K] = 0 .$$

The sum is carried out over all degrees of freedom. Gauss' Principle,

$$\Sigma[F_c^x \delta F_c^x + F_c^y \delta F_c^y] / m = 0 ,$$

combined with the time derivative of the kinetic-energy constraint,

$$\Sigma[mv \cdot \dot{v}] = \Sigma[mv \cdot (F + F_c + \delta F_c)] = 0 ,$$

gives the Lagrange multiplier result  $F_c = -\zeta mv$ , with the Lagrange multiplier  $\zeta = \Sigma r \cdot F / 2K = -\dot{\Phi} / (2K)$ , where  $\Phi$  is the total potential energy. Thus, according to Gauss' Principle of Least Constraint, the isokinetic equation of motion is

$$m\dot{v} = F - \zeta mv ; \zeta = -\dot{\Phi} / 2K .$$

After introducing the ideal-gas thermometer of macroscopic thermodynamics, in Section 12, we will return to these same Gaussian equations of motion and use them to simulate macroscopic thermodynamic heat reservoirs.

### 1.10 Hamiltonian Mechanics

Hamiltonian mechanics is specially useful in statistical mechanics and in quantum mechanics. The generalized coordinates  $q$  and conjugate momenta  $p = (\partial L / \partial v)_q$  are treated as independent variables in the Hamiltonian.

$$H(q,p) = K(q,p) + \Phi(q,p) .$$

The corresponding equations of motion are

$$\dot{q} = (\partial H / \partial p)_q ; \dot{p} = - (\partial H / \partial q)_p .$$



Yoshida has shown that the approximate Stoermer integration method described in Section 1.6 has a very interesting connection with exact Hamiltonian mechanics. The *approximate* method for integrating Hamilton's equations of motion can be written in the form:

$$\{ q_+ = q_0 + dt(\partial H / \partial p)_+ ; p_+ = p_0 - dt(\partial H / \partial q)_0 \} ,$$

where  $dt$  is the integration time step. For a Hamiltonian with the form  $H(p,q) = \Sigma(p^2/2m) + \Phi(q)$  the momenta  $\{p\}$  can be eliminated from these difference equations by calculating the second differences,  $\{ q_+ - 2q_0 + q_- \}$ . The result is the set of Stoermer equations:

$$\{ q_+ - 2q_0 + q_- = dt^2(F_0/m) \equiv (dt/m)[p_+ - p_0] \} .$$

Apart from computer roundoff, the coordinate values generated by these difference equations correspond exactly to configurations observed at equally-spaced times  $\{0, dt, 2dt, 3dt, \dots\}$  along an exact continuous trajectory, for a Hamiltonian which differs from the specified Hamiltonian  $H$  by terms of order the time step  $dt$ . To illustrate this correspondence for the simplest interesting case, consider a one-dimensional harmonic oscillator with the ratio  $(\kappa/m)$  chosen so that Stoermer solution is:

$$q(t) = \cos(\omega t) ; p(t) = -\omega \sin(\omega t) + (dt/2)\cos(\omega t) ; (\kappa/m)(dt^2) \equiv 2 - 2\cos(\omega dt) ; \omega^2 \equiv 1 - (dt/2)^2 .$$

This approximate solution approaches the exact one for the Hamiltonian  $H_{\text{Oscillator}} = (1/2)(q^2 + p^2)$ ,  $q = \cos(t)$ , as the time step  $dt$  approaches zero. The finite-time-step difference-equation solution just given is also an *exact* solution of the *differential* equations of motion:

$$\dot{q} = p - (dt/2)q; \dot{p} = -q + (dt/2)p,$$

which follow from the "Stoermer Hamiltonian":

$$H_{\text{Stoermer}} = H_{\text{Oscillator}} - (dt/2)qp = (1/2)(q^2 + p^2 - dtqp).$$

Yoshida has shown that such a correspondence *always* occurs and has outlined a systematic procedure for finding higher-order approximate Hamiltonians with correspondingly more-accurate time-reversible difference equations. The finite-difference Stoermer solution for a specified Hamiltonian *always* corresponds to the exact differential solution of a related problem in Hamiltonian mechanics.

**Problem:**

1. Show that the harmonic-oscillator solution [  $q = \cos(\omega t)$ ;  $\omega^2 \equiv 1 - (dt/2)^2$  ] given above follows from the Stoermer Hamiltonian.
2. A straightforward attempt to improve the Stoermer integration method can be based on a higher-order centered-difference expression for the acceleration:

$$a_0 = [-q_{++} + 16q_+ - 30q_0 + 16q_- - q_{--}]/(12dt^2).$$

Find the order of this "method" and show that it is *unstable* for the one-dimensional harmonic oscillator. Then show that the alternative method,

$$q_{++} \approx q_+ + q_- - q_{--} + (dt^2/4)[5a_+ + 2a_0 + 5a_-],$$

is stable for an oscillator. Compare the "computational efficiency" [accuracy at a *fixed* time with a fixed *number* of force evaluations] of this latter method to that of the fourth-order Runge-Kutta method.

In the simplest cases the kinetic energy depends only on the momenta and the potential depends only on the coordinates. For the polar-coordinate version of the rigid rotator the Hamiltonian,

$$H = p\dot{q} - L(q, \dot{q}) = p_\theta \dot{\theta} - L(\theta, \dot{\theta}),$$

where  $p_\theta$  is  $mr^2\dot{\theta}$ , becomes

$$H = p_\theta\dot{\theta} - (p_\theta/r)^2/2m = (p_\theta/r)^2/2m ,$$

from which the expected equations of motion follow:

$$\dot{\theta} = p_\theta; \dot{p}_\theta = 0.$$

A recent application of Hamilton's mechanics to the treatment of macroscopic systems was first announced in 1984 by Shuichi Nosé. This development, which forges a strong link between microscopic mechanics and macroscopic computational statistical mechanics will be treated in Section 1.13.

In the next Section we will describe the flow of probability density through phase space using Hamilton's equations of motion, and show that these lead directly to Liouville's Theorem, which is of fundamental importance for statistical mechanics.

**Problem:**

Work out the Lagrangian and the Hamiltonian in spherical polar coordinates for a rigid rotor in three-dimensional space.

**1.11 Liouville's Theorem**

Hamilton's first-order equations make it possible to prove "Liouville's Theorem," an interesting and useful continuity equation for the comoving flow of phase-space probability,

$$df(q,p,t)/dt = \dot{f} = 0 .$$

The probability density  $f(q,p,t)$  gives the density of points in a region of phase space, with  $f dq dp = f dq_1 \dots dq_N dp_1 \dots dp_N$  giving the number of points in a region  $dq dp$  about the phase-space point  $(q,p)$ . The rate of change, with time, of  $f$  can be expressed in terms of either the "Eulerian" derivative  $\partial f / \partial t$ , which measures the variation at a fixed point in space, or with the "Lagrangian" derivative  $\dot{f}$ , which gives the comoving variation of  $f$  following the motion. It is simplest to calculate the Eulerian derivative first and then to express the Lagrangian derivative in terms of it. To do this we consider the net flow of probability in the  $q$  direction,

$$- [(f\dot{q})_{q+dq/2} - (f\dot{q})_{q-dq/2}] dp dt ,$$

and add to this the corresponding flow in the  $p$  direction,

$$-[(\dot{f}p)_{p+dp/2} - (\dot{f}p)_{p-dp/2}]dqdt .$$

Using the time derivative of Hamilton's equations of motion,

$$(\partial\dot{q}/\partial q) + (\partial\dot{p}/\partial p) = \partial(\partial H/\partial p)/\partial q - \partial(\partial H/\partial q)/\partial p = 0 ,$$

gives *Liouville's Theorem*:

$$(\partial f/\partial t) + \dot{q}(\partial f/\partial q) + \dot{p}(\partial f/\partial p) \equiv \dot{f} = -f[(\partial\dot{q}/\partial q) + (\partial\dot{p}/\partial p)] \equiv 0 .$$

In this derivation we have explicitly considered the flow in only two phase-space directions, the direction associated with  $q$  and the direction corresponding to the conjugate momentum  $p$ . But summing such a calculation over all the phase-space coordinates and momenta ( $3N$  of each for a three-dimensional unconstrained  $N$ -body system) establishes the same result in general. Thus *the probability density flows through phase space like an incompressible fluid*, with a constant density  $f$ , if Hamilton's equations are followed.

To make the concept of phase-space flow clearer let us consider the similar continuity equation of fluid mechanics where the space in question is three-dimensional physical space rather than a many-dimensional phase space. In this case we consider a fluid with continuously varying, and differentiable, mass density  $\rho(\mathbf{r})$  and velocity  $\mathbf{u}(\mathbf{r})$ . Velocity is measured relative to a three-dimensional inertial frame. If we consider the density within a fixed Eulerian cube  $dxdydz = \Delta^3$  centered on the point  $\mathbf{r} = (x,y,z)$ , then for a sufficiently short time interval  $dt \ll \Delta/|\mathbf{u}|$ , the flow of mass into the cube is a sum, over the six cube faces, of the flows normal to those faces. In the  $x$  direction these are:

$$[(\rho u)_{x-dx/2} - (\rho u)_{x+dx/2}]dydzdt \Rightarrow [-\rho(\partial u/\partial x) - u_x(\partial\rho/\partial x)]dxdydzdt .$$

Adding the analogous contributions from the  $y$  and  $z$  faces and dividing the sum by  $dxdydzdt$  gives the continuity equation:

$$\dot{\rho} = -\rho\nabla\cdot\mathbf{u} .$$

For a fluid the meaning of this equation is transparent. The fluid changes density, expanding or contracting according to the divergence of the velocity field. In phase space the Hamiltonian equations of motion guarantee that any spreading or contracting associated with a generalized coordinate,  $(\partial\dot{q}/\partial q)$ , is exactly offset by a corresponding contraction or spreading in the conjugate momentum,  $(\partial\dot{p}/\partial p)$ . The two derivatives sum to zero as a consequence of the Hamiltonian equations of motion.

The constant-density phase-space flow established by Liouville's Theorem is not affected by external forces. We will demonstrate that here for an interesting example. Consider a critically-damped one-dimensional harmonic oscillator with the equations of motion

$$\dot{x} = v ; a \equiv \dot{v} = -x - 2v ,$$

and initial values of  $(x,v) = (1,1)$ . The resulting trajectory, and its first two time derivatives are:

$$x = (2t + 1)e^{-t} ; v = (1 - 2t)e^{-t} ; a = (2t - 3)e^{-t} .$$

For this damped oscillator the probability density diverges as  $e^{+2t}$  and Liouville's Theorem is not satisfied. Consider however an undamped oscillator subject to an external force  $F(t) = a + x$  chosen so that the externally-forced trajectory will be *identical* to the damped trajectory above:

$$x = (2t + 1)e^{-t} ; \dot{x} = v = (1 - 2t)e^{-t} ;$$

$$\dot{v} \equiv a = (2t - 3)e^{-t} = -x + F(t) ; F(t) = (4t - 2)e^{-t} .$$

In this latter case, where the "damping" is the result of a velocity-independent but time-dependent external force,  $F(t) = (4t - 2)e^{-t}$ , Liouville's Theorem *does* apply, with

$$(\partial \dot{q} / \partial q) + (\partial \dot{p} / \partial p) = 0 + 0 ,$$

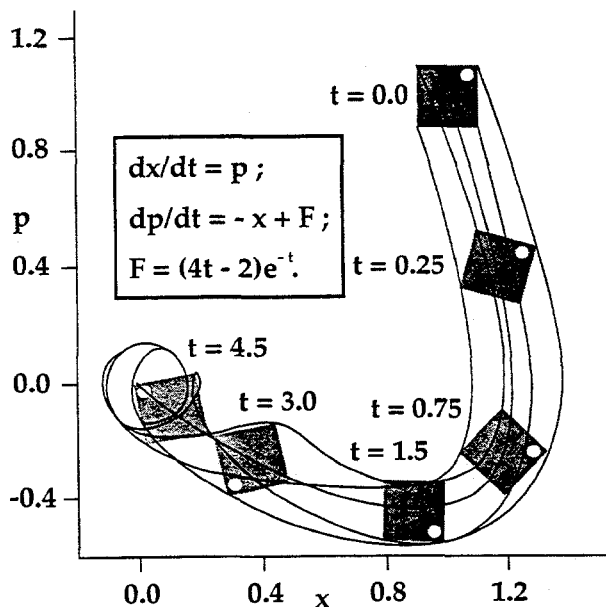


Figure 1.9 Forced harmonic oscillator obeying Liouville's Theorem. Only the central trajectory of this ensemble of oscillators is critically damped by the specified external force  $F(t)$ . The oscillator mass and force constant are both equal to unity.

so that phase-space area is conserved by the motion. In particular, a small element of area centered on the damped trajectory must likewise move through the phase space with fixed area. Figure 1.9 shows how this happens. The slightly different initial conditions at the corners of the initial phase-space square are not perfectly damped by the external force appropriate to the square's center. The area is indeed constant, and ends up rotating about the origin at the natural oscillator frequency.

Liouville's Theorem and its nonequilibrium analog are fundamental to statistical mechanics, both at equilibrium and away from it. We will see that the essential difference between equilibrium and nonequilibrium systems is the possibility for expansion and contraction in nonequilibrium phase-space flows.

### Problems:

1. Plot the trajectories of unit mass particles in a vertical gravitational field of unit strength with the initial values of  $z$  and  $p_z$  as follows:  $(0.0, 1.0)$ ,  $(0.0, 1.1)$ ,  $(0.1, 1.0)$ , and  $(0.1, 1.1)$  at times 0.2, 0.4, 0.6, and 0.8; comment on the validity of Liouville's Theorem in this case.
2. Consider a system with two springs and a dashpot. The lefthand mass obeys the equations  $\dot{x} = p_x$ ;  $\dot{p}_x = y - 2x$ ; the righthand mass obeys the equations  $\dot{y} = p_y$ ;  $\dot{p}_y = x - y - (5/3)\dot{y}$ . Note that an analytic solution of this problem is  $x = (\dot{y}/3) = \exp(-t)$ . Consider a grid of four points with initial values of  $x$  and  $p_x$  as follows  $(0.9, -0.9)$ ,  $(0.9, -1.1)$ ,  $(1.1, -0.9)$ ,  $(1.1, -1.1)$  and with  $y = 3.0$  and  $p_y = -3.0$ . Plot the locations reached by these points at times 0.5, 1.0, 2.0, and 3.0. Is Liouville's Theorem valid for this system? Suppose that the initial states had been a small four-dimensional hypercube in  $(x, p_x, y, p_y)$  space, initially centered on the point  $(1, -1, 3, -3)$ . How would the volume of this hypercube vary with time?

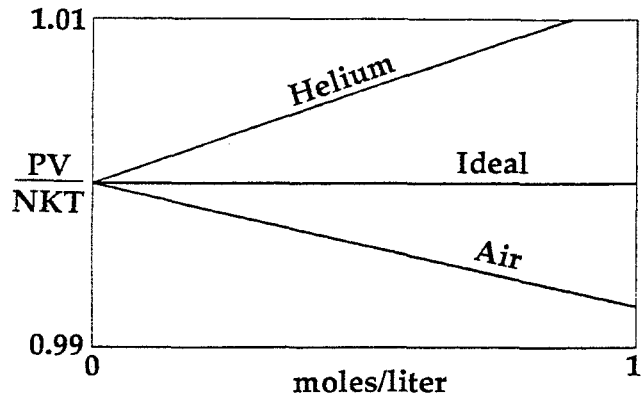
### 1.12 Mechanics of Ideal-Gas Temperature

Macroscopic *thermodynamics* differs from macroscopic mechanics in that *temperature* is included as a state variable. Temperature has both an experimental and a conceptual basis. It forms a vital link between the reversible world of microscopic mechanics and macroscopic irreversible thermodynamics.

Figure 1.10 illustrates the room-temperature low-density behavior of the pressure-volume product,  $PV/N$ , for two real gases, helium and air, as well as the hypothetical ideal gas. The limiting zero-density behavior of *any* real gas is ideal, independent of composition. This is "Boyle's Law." Because the limiting value varies with temperature, increasing as the gases are heated, the material-independent behavior of an ideal gas can be used to define the "ideal-gas temperature scale."

The ideal gas is a useful concept in mechanics, and sufficiently simple that we can relate the macroscopic temperature scale thus defined to a simple microscopic kinetic-

Figure 1.10 Density dependence of the PV product for Helium and Air. The ideal gas law is also indicated.



theory calculation of pressure. We will show how the definition of temperature is directly related to kinetic energy.

We here treat the limiting low-density case of an “ideal gas,” a gas so dilute that the interactions between its constituents can be ignored apart from their role in establishing equilibrium. This lack of internal interactions makes it possible to estimate the interaction between such an ideal gas and its surroundings from the collision rate at the walls of the container. We simplify the treatment by assuming the gas is composed of structureless mass points, all with the same mass,  $m$ .

From a macroscopic mechanical point of view the pressure of a homogeneous system is a second-rank tensor, with components  $\{P_{ij}\}$ , with the two indices indicating two space directions. These are first, the direction *perpendicular* to the interface at which the force is measured and second, the direction of the force exerted *by* the macroscopic system on its surroundings. Thus the force exerted by the system on a unit area of a confining wall perpendicular to the  $x$  axis has components  $P_{xx}$ ,  $P_{xy}$ , and  $P_{xz}$ . By symmetry, the pressure tensor of a field-free fluid, such as the ideal gas of interest here, is “isotropic,” independent of direction:

$$P = \begin{pmatrix} P & 0 & 0 \\ 0 & P & 0 \\ 0 & 0 & P \end{pmatrix} .$$

The nonzero elements represent the force per unit area perpendicular to the  $x$ ,  $y$ , and  $z$  axes,  $P_{xx}$ ,  $P_{yy}$ , and  $P_{zz}$ .

Let us work out the  $xx$  ideal-gas pressure-tensor component  $P_{xx}$  by relating the force on a small element of area  $da = \Delta^2$  on a wall perpendicular to the  $x$  axis to the momentum transferred at the container wall by the molecules colliding with the wall. During a time interval  $dt$  sufficiently short that motion in the  $y$  and  $z$  directions is much less than  $\Delta$ , the number of particles hitting  $da = \Delta^2$  with a positive  $x$  velocity component  $v_x$  is  $v_x f(v_x) dt da$ , where  $f(v_x) dv_x$  is the number of molecules per unit volume with a velocity component in the range of width  $dv_x$  about  $v_x$ . From the definition the integral of  $f$ , over all velocities,  $\int f(v_x) dv_x$ , is the “number density”

$(N/V) = \rho/m$ , assumed constant throughout the gas. The total x momentum transferred to unit area of the wall in unit time is the number of such collisions, divided by  $dt da$ , and multiplied by the momentum transferred by a single collision  $2mv_x$ , summed up over all positive values of  $v_x$ :

$$\langle P_{xx} \rangle = P = \int [(2mv_x)v_x f(v_x)] dv_x = (N/V) \langle mv_x^2 \rangle = \rho \langle v_x^2 \rangle = (2/3)E/V.$$

The integration is carried out over all positive values of  $v_x$ , and, again by symmetry, the total energy  $E$  is divided equally among the three directions in space:  $E = \rho \langle v^2 \rangle / 2 = (Nm/2) \langle v_x^2 + v_y^2 + v_z^2 \rangle$ . Thus the ideal-gas pressure-volume product is a measure of the gas energy and can be used directly to define the ideal-gas temperature scale. In the following Section we use this definition together with both the Gaussian mechanics of Section 1.9 and the Nosé-Hoover version of Hamiltonian mechanics to construct microscopic mechanical analogs for macroscopic thermostats.

### 1.13 Thermostats and Nosé-Hoover Mechanics

The idea of temperature just introduced through the ideal-gas thermometer can be implemented by using any of several extensions of Newtonian mechanics. We have already seen, in Section 1.9, that using Gauss' Principle of Least Constraint to impose the constraint of fixed kinetic energy leads to additional frictional forces:

$$m\dot{v} = F - \zeta mv ; \zeta = -\dot{\Phi}/2K.$$

It should be emphasized that, unlike a hydrodynamic drag force, with a frictional force  $-\zeta mv$  proportional to the particle size, speed, and the viscosity of the surrounding medium, *the Gauss'-Principle friction coefficient  $\zeta$  can be either positive or negative.* By contrast, negative friction coefficients cannot occur in hydrodynamics. In hydrodynamic flows dominated by viscosity the viscous "drag force"  $-\zeta mv$  continuously converts the kinetic energy of the flow into heat. The hydrodynamic "friction coefficient"  $\zeta$  in that situation is intrinsically positive. Gauss' "friction" is different. If the potential energy  $\Phi$  is increasing, then the corresponding tendency of the kinetic energy to decrease is offset by a negative friction. When the potential energy decreases, so that an unconstrained kinetic energy would increase, then  $\zeta$  becomes more positive.

Gauss' equations of motion can be applied away from equilibrium too, maintaining the temperature of a system on which work is being performed by external forces. In such a case the frictional forces play the role of thermostats. Because such thermostats are fundamental to both equilibrium and nonequilibrium statistical mechanics, we consider two other approaches to temperature control, Lagrangian and Nosé-Hoover mechanics.

To impose constant temperature using Lagrangian mechanics we augment the many-body Lagrangian function,

$$L = \Sigma(mv^2/2) - \Phi(r) ,$$

where  $\Phi(r)$  represents the potential of interaction of the bodies, by a Lagrange multiplier imposing constant kinetic energy:

$$L = \Sigma(mv^2/2) - \Phi(r) + \lambda[\Sigma(mv^2/2) - K_0] .$$

The momenta  $p = (\partial L/\partial v) = mv(1+\lambda)$  obey the Lagrangian equations of motion:

$$\dot{p} = F = -\nabla\Phi ,$$

and must simultaneously satisfy the constraint:

$$\Sigma(mv^2/2K_0) = \Sigma(p^2/2mK_0)(1+\lambda)^{-2} = 1 ,$$

where  $K_0$  is the specified constant value of the kinetic energy. Thus the equations of motion become:

$$m\dot{v} = [\dot{p}/(1+\lambda)] - [mv\dot{\lambda}/(1+\lambda)] = [F - \zeta mv]/(1+\lambda) ; \zeta = -\dot{\Phi}/2K_0 .$$

Unfortunately in this nonholonomic application of Lagrange's equations of motion the motion depends upon the initial choice of  $\lambda$ . If we make the simplest choice, zero, then initially Lagrange's and Gauss' equations of motion are exactly alike and the constraint force is minimized. The ambiguity in Lagrangian mechanics can be resolved by arbitrarily applying Gauss' Principle, setting  $\lambda$  equal to the minimum-force value, 0, at all times.

Gauss' thermostat is an example of "differential control," in which time-reversible forces  $\{-\zeta mv\}$  react to *differential* changes in potential energy,  $\dot{\Phi}$ , to *control* the kinetic energy. A more-useful alternative is *integral* control. Integral control can be applied to the kinetic energy and its fluctuations, and provides a more-flexible form of thermostat than Gauss'. The corresponding Nosé-Hoover equations of motion are exactly the same as Gauss' or Lagrange's:

$$m\dot{v} = F - \zeta mv ;$$

but the friction coefficient  $\zeta$  depends on the time-averaged temperature, increasing if the average is too high relative to  $K_0$ , and decreasing if the average is too low:

$$\zeta = (1/\tau^2) \int dt [(K(t)/K_0) - 1] \Leftrightarrow \dot{\zeta} = (1/\tau^2) [(K/K_0) - 1].$$

The arbitrary time scale  $\tau$  which appears in this "integral-control" thermostat is the timescale of the fluctuations in  $K(t)$  about the stationary average  $K_0$ .

We will come back to Nosé-Hoover mechanics in discussing Gibbs' canonical ensemble, in Chapter 3. Before leaving the general subject of mechanics let us take up one application of this idea in order to illustrate the difference between mathematical reversibility and time reversibility.

To illustrate the idea of *mathematical* reversibility consider the simplest application of Nosé's mechanics, a one-dimensional harmonic oscillator with mass, force constant, and thermostat relaxation time all chosen equal to unity. The three first-order equations describing the motion of such a "Nosé-Hoover oscillator" are:

$$\dot{x} = +p; \dot{p} = -x - \zeta p; \dot{\zeta} = +p^2 - 1.$$

where the frictional force,  $-\zeta p$ , differs from the usual macroscopic friction in that  $\zeta$  varies with time. To reverse the solution of these equations mathematically simply means to back up along the same  $\{x, p, \zeta\}$  trajectory, solving the reversed system of equations:

$$\dot{x} = -p; \dot{p} = +x + \zeta p; \dot{\zeta} = -p^2 + 1.$$

From the mathematical standpoint nothing has changed but the sign of  $dt$ . But these equations are different from the physical point of view because both  $p$  and  $\zeta$  have changed sign.

If we, as physicists, happen to know that both  $p$  and  $\zeta$  have a basis in Hamiltonian mechanics, where they represent momenta, then we recognize that both variables must change sign in a time-reversed motion. We can recognize that the forward and backward versions of the motion equations both describe the same physical system. We can alternatively see that  $\zeta$  must change sign from either Gauss' or Nosé and Hoover's feedback equations. In fact, if the motion is expressed entirely in terms of the time-variation of the physical coordinate  $x$  both the backward and the forward trajectories are equivalent to the same second-order integro-differential equation,

$$\ddot{x} = -x - \dot{x} \int dt' [\dot{x}'^2 - 1].$$

This equation resembles that for a damped oscillator,

$$\ddot{x} = -x - \zeta \dot{x},$$

with the friction coefficient  $\zeta$ , but differs from it in a qualitative way because the Nosé-Hoover oscillator friction coefficient varies with time and the dynamics is time-reversible.

We will come back to Gauss and Nosé-Hoover mechanics repeatedly in establishing connections between microscopic reversible dynamics and macroscopic thermodynamics and hydrodynamics. It is to macroscopic thermodynamics that we devote the following Chapter.

#### 1.14 Summary and References

The time development of isolated mechanical systems can be described by Newtonian, Lagrangian, or Hamiltonian mechanics. Of these, Lagrangian mechanics is best-suited to the imposition of holonomic (coordinate-dependent) constraints. Gauss' Principle of Least Constraint is more general and can be used to formulate some *nonholonomic* constraint problems for which Lagrangian mechanics is ineffective. Despite the underlying *exponentially* unstable "Lyapunov Instability" of the equations of motion any of these problems can readily be solved numerically until the accuracy is degraded by the instability. The third-order Stoermer and fourth-order Runge-Kutta methods are particularly useful.

Liouville's Theorem states that the *comoving* probability density is constant. This result holds for *Hamiltonian* phase-space flows. More general equations of motion incorporate temperature and lead to comoving probability densities that can vary with time through thermal interactions. *Temperature* is defined by the kinetic-theory pressure exerted by an ideal gas. An ideal-gas temperature can be imposed on a reversible deterministic mechanical system by applying Gauss' Principle or by adopting a more-flexible form of mechanics developed by Nosé and Hoover.

The mechanics texts I have found to be most useful are Landau and Lifshitz' *Mechanics*, Pars' *Treatise on Analytical Dynamics* (Oxbow Press, Woodbridge, Connecticut, 1979), and Sommerfeld's *Mechanics*. For a more detailed introduction to Nosé-Hoover mechanics see Sections 3.11 and 3.12, as well as two of Shuichi Nosé's 1984 papers, "A Unified Formulation of the Constant-Temperature Molecular Dynamics Methods," *Journal of Chemical Physics* 81, 511, and "A Molecular Dynamics Method for Simulations in the Canonical Ensemble," *Molecular Physics* 52, 255, and my 1985 paper, "Canonical Dynamics: Equilibrium Phase-Space Distributions," *Physical Review A* 31, 1695.

## 2. Thermodynamics

*1 Introduction; 2 Thermodynamic States of Matter and The Zeroth Law; 3 Heat Reservoirs; 4 First Law of Thermodynamics; 5 Second Law of Thermodynamics; 6 Third Law of Thermodynamics; 7 Thermodynamics of Ideal-Gas Compression; 8 van der Waals' Equation of State; 9 Thermodynamic Potential Functions; 10 Summary and References*

### 2.1 Introduction

Thermodynamics and macroscopic mechanics both deal with continua capable of undergoing changes in state. But they emphasize different aspects of macroscopic matter. Traditional macroscopic thermodynamics describes processes involving thermal energy transfers, through the flow of "heat," and mechanical energy transfers, through performing "work." Mechanics focuses on the details of flow and deformation processes such as bending, stretching, and rolling.

The macroscopic *thermodynamic* description of matter is the subject of this Chapter. Thermodynamics includes temperature in the list of variables required to describe the state of a material. Heat reservoirs are also introduced as abstract sources and sinks for the heat flows making changes in temperature possible. These new thermal variables make it possible to establish a link between macroscopic thermodynamics and microscopic statistical mechanics. Here we study macroscopic thermodynamics. We will explore the more-detailed microscopic view of this link when we introduce Statistical Mechanics in Chapter 3. Thermodynamics reflects reality and is the result of experience. An important part of that experience is the irreversibility associated with real processes and described by the Second Law of Thermodynamics. From the conceptual standpoint of mechanics thermodynamics can appear to be paradoxical because the matter it describes is governed by time-reversible microscopic equations of motion. We will return to this question in detail in Chapter 10, and show there that a proper introduction of *temperature* into mechanics, as outlined in Section 1.13, provides a direct mechanical prediction of the irreversible macroscopic behavior described by thermodynamics.

Two concepts are fundamental to a thermodynamic description of matter, the ideas of "system" and "thermodynamic state." First, we must separate conceptually the *system* being observed and described from its *surroundings*, on which it may perform work and from which it may extract heat. The system of interest can be as small as a single molecule or as large as the universe. Thermodynamics is sufficiently general to describe either. Second, we must specify the *state* of the observed and described system. This can be done in comprehensive detail for a molecule, giving its complete mechanical (quantum) state, but becomes impractical as the number of degrees of freedom is increased. The alternative description of "state" is classical, and includes the complete list of mechanical system variables, including all particle coordinates and velocities. Such a detailed cumbersome description can be avoided by introducing, at least conceptually, an averaging process. Averaging is appropriate for dealing with equilibrium states, which do not change at all on a macroscopic level, because the

macroscopic consequences of microscopic fluctuations in macroscopic properties are generally negligibly small. Even if fluctuations are noticeable *time* averaging can be justified as a reasonable description of a system with fluctuating properties.

From the physical standpoint we expect that localized properties sufficiently widely separated in time or space are statistically uncorrelated in their fluctuations. Averages computed by summing over  $N$  such quantities  $\{x_1, x_2, \dots, x_N\}$  (properties of  $N$  weakly-coupled molecules or  $N$  successive values of a dynamical variable) have expected rms fluctuations  $\Delta$  of order  $N^{-1/2}$  according to *the* fundamental result from statistics called the Central Limit Theorem:

$$\langle \Delta^2 \rangle^{1/2} = \langle [\sum \delta / N]^2 \rangle^{1/2} = \langle [\sum \delta_i \sum \delta_j] / N^2 \rangle^{1/2} = \langle \sum \delta^2 / N^2 \rangle^{1/2} = N^{-1/2} \langle \delta^2 \rangle^{1/2},$$

where  $\delta$  is a localized fluctuation:  $\delta \equiv x - \langle x \rangle$  and  $\delta_i$  is assumed not to be correlated with  $\delta_j$  unless  $i$  and  $j$  are equal.

In a typical situation the fluctuations of globally-summed “extensive quantities,” such as the total system energy or the volume occupied by the system, obey this Central Limit Theorem and are negligibly small, varying as the square root of the number of degrees of freedom. Even for small systems, systems with only a few degrees of freedom, a cumbersome complete description can often be usefully replaced by a statistical time average. In that case the Central Limit Theorem guarantees that the long-time fluctuations in time averages of stationary processes vary as the inverse square root of the sampling time.

In mechanics it is usual to consider energy changes caused by displacement and deformation. Energy changes involving heat transfer are ignored, except in special problems. Thermodynamics includes both. In thermodynamics mechanical deformation and heat flow enter on an equal basis. Emphasis is placed on the ways in which energy is stored in and transferred among systems and their surroundings through work and heat. The concept of *state* is widened in thermodynamics to include not only mechanical state variables, but also temperature. In thermodynamic investigations systems are generally imagined to interact with their surroundings in an idealized way. The surroundings can generally resist mechanical motion by exerting forces or stresses (components of the force per unit area) at the system-surroundings interface. Such forces can be modeled by applying microscopic external forces on selected boundary particles. The surroundings can also promote heat transfer or heat fluxes (energy per unit area and time) between the system and external sources or sinks of energy. Such flows of heat can likewise be modeled by using the Gauss or Nosé-Hoover thermostats discussed in Sections 1.9 and 1.13.

Like mechanics, thermodynamics is a logical structure built on a foundation of basic principles, called “Laws.” The Laws of thermodynamics sum up the results of phenomenological experience. The Zeroth Law defines thermometry, the process of measuring temperature, the property which distinguishes thermodynamics from

mechanics. The First Law is a statement of energy conservation and the Second Law is a statement of entropy increase. The Third Law affirms the validity of a statistical approach to the entropy, with particular emphasis on the limiting behavior of entropy near zero temperature. The *Second* Law is that thermodynamic law which uniquely separates classical reversible Newtonian behavior from macroscopic experience and which makes necessary the introduction of temperature into mechanics.

The arbitrarily empirical foundation of thermodynamics is apparent right at the start. Why just a single new variable, temperature? Why just work and heat? *That the state of a fixed quantity of fluid requires only two state variables, one mechanical and one thermal, rather than three, or four, or more, is empirical, and not something that can be proved.*

That the number of state variables is only two can be made plausible on the microscopic basis of statistical mechanics, but cannot generally be proved except in very special circumstances. In this Chapter we will discuss and illustrate the laws of thermodynamics and their application to some idealized macroscopic fluid systems. In the following Chapter we will develop the microscopic statistical-mechanical view of matter in order better to understand the basis of the macroscopic description.

## 2.2 Thermodynamic States of Matter and The Zeroth Law

In thermodynamics, as distinguished from mechanics, *thermal* properties play a vital role. "State" in macroscopic continuum mechanics is usually given by specifying the positions and velocities of a system's component parts. The stress state which results, and which influences or drives further motion, is related to deformation and flow by a "constitutive relation." Fluids *flow* in response to stress. For fluids, flow velocity is emphasized. Solids have mechanical strength and *strain*, rather than flow, deforming in response to stress. For solids, displacement and deformation make up the basic description. Thus the mechanical state of an elastic bar could include the mechanical displacement  $u(r)$ , away from the stress-free position, for all locations in the bar.

In mechanics the constitutive relation or "equation of state" for such a deformed bar would be the linear Hooke's-Law relation linking the stress tensor (the negative of the pressure tensor) in the bar to the deformation gradient  $\nabla u$ , or equivalently, to the (dimensionless) elastic strain tensor,  $\epsilon = [\nabla u + \nabla u^t]$ , where the superscript  $t$  indicates transpose. For a fluid the viscous stresses are instead related to the strain-rate tensor (units of inverse time), which has exactly the same form,  $\dot{\epsilon} = [\nabla u + \nabla u^t]$ , but with the variable  $u$  interpreted as flow velocity rather than as an elastic displacement. The use of symmetrized strain and strain-rate tensors is dictated by the symmetry of the pressure tensor, as is discussed in Section 7.5. In thermodynamics velocity is generally not relevant to state so that the thermodynamic description is simpler. The space variation of  $u(r)$  is replaced by global equilibrium values of a few state variables. Temperature and heat flow are emphasized and the materials described are most often

fluids, reducing the description of the mechanical state to a temperature-dependent scalar relation linking the hydrostatic pressure to the density.

The “mechanical equation of state” in thermodynamics is a specification of the pressure-volume relation while the “thermal equation of state” specifies the dependence of energy upon temperature. Thus the complete thermodynamic “equation of state” or constitutive equation consists of two parts, not just one.

To embark on a thermodynamic description we need an operational definition of temperature. In Section 1.12 we introduced the ideal-gas temperature scale. We adopt exactly this same scale in our thermodynamic description. Thus in thermodynamics “temperature” means the PV product for a standard sample of ideal gas. If the resulting temperature is to be measured in kelvins and the pressure-volume product in joules, the MKS unit of energy, then the “standard sample” of ideal gas would need to contain  $8 \times 10^{22}$  molecules. But because the conventional counting unit for molecules is the cgs mole,  $6.023 \times 10^{23}$  molecules, the conventional way of defining ideal-gas temperature is through the ideal-gas mechanical equation of state:

$$T \equiv PV/Nk ,$$

where N is the number of molecules and k is Boltzmann’s constant,  $1.38054 \times 10^{-23}$  joules/(molecule kelvin). At sufficiently low density all materials vaporize and obey this relationship because the occasional brief interactions of pairs of particles are a negligible perturbation. Thus, any gas can serve as an ideal gas provided that it is sufficiently dilute. But a gas like tungsten vapor, with a completely-negligible room-temperature vapor pressure, would not be a useful choice.

An ideal gas is described by its pressure-volume equation of state,

$$PV = NkT ,$$

where T is the temperature. In any real gas the number of particles, N, can vary with temperature. When heated well above room temperature a hydrogen molecule dissociates into two atoms, each of which can, with further heating, in turn ionize to yield an electron and a proton, producing a high-temperature pressure four times as large as the ideal molecular value. Likewise, at low temperatures where clustering is appreciable the number of moving bodies N contributing to the ideal-gas pressure is reduced well below the number of molecules.

The ideal gas is an excellent fundamental basis for thermodynamics because it combines operational significance with properties which are simple and easy to calculate. The ideal-gas concept forms a sturdy bridge between the macroscopic discipline of thermodynamics and the more detailed models of statistical mechanics and kinetic theory. Real gases require a more-complicated description. The energy depends upon volume as well as temperature, and in a nonlinear way. The most

obvious qualitative shortcoming of the ideal gas as a general thermodynamic gas-phase model is its failure to form liquid and solid condensed phases at low temperatures and high pressures. Such condensed phases require both attractive and repulsive forces between atoms. Such interatomic forces can be taken qualitatively into account through van der Waals' approximate equation of state, as is discussed in Section 2.8.

A fairly realistic phase diagram is shown in Figure 2.1 and is based on a molecular model, the "Lennard-Jones potential," with simple repulsive and attractive forces. This simple central-force model is enough to generate the gas, liquid, and solid phases. With more complex microscopic interactions the qualitative macroscopic behavior can become correspondingly more complex. See Figure 2.2, which shows a part of the phase diagram for water. Water molecules lie near, but slightly beyond, the current state-of-the-art in molecular description. Each molecule has nine degrees of freedom, is polarizable, and has long-range dipolar and quadrupolar forces. The structure of its phase diagram is a challenge to any microscopic model.

A complete thermodynamic description of the ideal gas requires also the *thermal* equation of state, which links energy and temperature. It is possible to estimate the

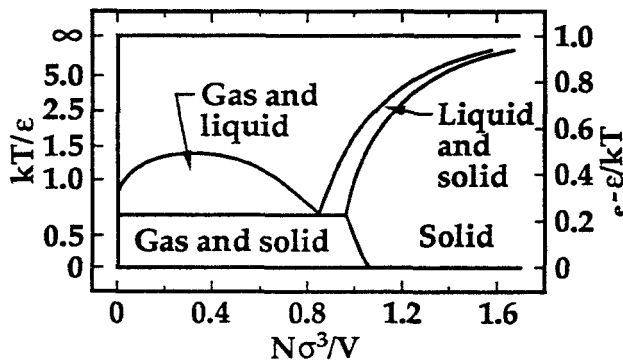
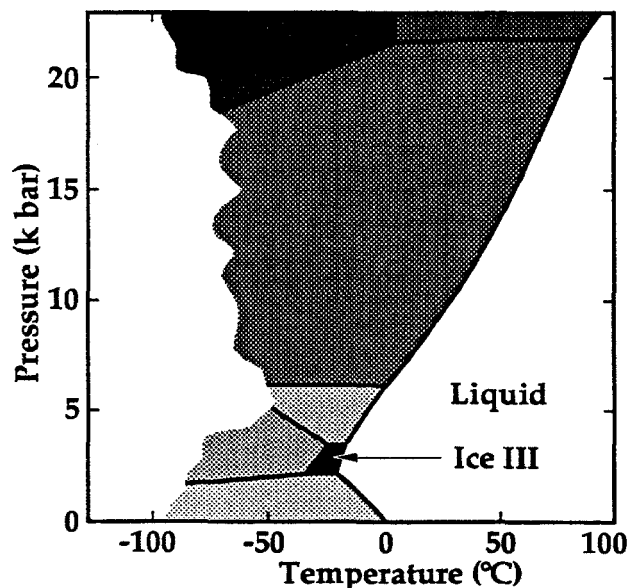


Figure 2.1 Density-temperature phase diagram for the Lennard-Jones potential,

$$\phi(r) = 4\epsilon[(\sigma/r)^{12} - (\sigma/r)^6],$$

determined by computer simulation. All three phases, gas, liquid, and solid, are shown.

Figure 2.2 Pressure-temperature phase diagram for water. The various solid phases are shaded and ice III is indicated.



thermal equation of state using statistical mechanics, as we shall see, but the estimate is relatively simple only in the case of electrically-neutral monatomic materials, the rare gases. In other cases the thermal equation of state is more complicated. The thermal equation of state for gases with any structure, even diatomic molecules, requires a phenomenological quantum-mechanical treatment of the vibrational and rotational states. For a gas of structureless molecules in three-dimensional space the kinetic-theory calculation establishes that the pressure-volume product  $NkT$  is two-thirds the kinetic energy of the molecules,

$$PV = NkT = (2E/3).$$

Despite its purely phenomenological historical basis thermodynamics is sufficiently general that it can equally-well describe the purely-theoretical properties of simple idealizations of matter amenable to theoretical calculations and computer simulation. In computational statistical mechanics we often introduce one-dimensional or two-dimensional model systems to simplify calculations. Two-dimensional problems are particularly useful in understanding simple flow and deformation problems. Thermodynamics applies also to the description and interpretation of the properties of such idealized systems.

### **Problem:**

Show that the thermal equation of state for a gas of  $N$  structureless molecules is  $PV = NkT = E$  in two dimensions and  $PV = NkT = 2E$  in one dimension.

Why doesn't the pressure depend upon the molecular mass?

### **2.3 Heat Reservoirs**

In discussing heat transfer in thermodynamics it is usual to introduce the idealization of a "heat reservoir," sometimes imagined to be a system with so many degrees of freedom that its temperature remains constant, even if heat is added or subtracted. The heat reservoir idea originated in the masses of air or water surrounding components of engines. Today the kinetic details of thermodynamic reservoirs are not usually spelled out. This is because thermodynamics is generally applied to idealized quasistatic processes in which rates are not important. Reservoirs need not have many degrees of freedom. A finite rather than an infinite reservoir mass can be used so long as there is an explicit provision for controlling the reservoir temperature. In any serious calculations of nonequilibrium processes, the details of the reservoirs need to be made explicit. In atomistic computer simulations thermostats with only a few degrees of freedom can play the role of heat reservoirs for microscopic systems. In such detailed microscopic thermostats a nonequilibrium definition of temperature is essential. We continue to define it in terms of the mean squared

thermal velocity. The temperature is then either maintained constant, by using Gaussian thermostats, or allowed to undergo well-behaved fluctuations around a specified mean value, with the mean controlled by using Nosé-Hoover thermostats.

To specify such an atomistic thermostat it is only necessary to identify one or more degrees of freedom which obey the thermostatted equations of motion introduced in Sections 9 and 13 of Chapter 1:

$$m \dot{v} = F - \zeta m v ; \zeta = \zeta_{\text{Gauss}} \text{ or } \zeta_{\text{Nosé-Hoover}} .$$

With the statistical mechanics introduced in Chapter 3 we will establish that the relation between mean-squared velocity and temperature is general for *all* equilibrium systems obeying classical mechanics, not just a special result for ideal gases. We adopt herewith exactly this same definition of temperature for nonequilibrium systems.

With the definition of temperature and the construction of thermometers it is possible to develop thermodynamics. The beginning is summarized in the empirical *Zeroth Law of Thermodynamics*: "If two bodies are in thermal equilibrium with a third body, then the two are in thermal equilibrium with each other." If the Zeroth Law did not hold then thermometry would be impossible. The Zeroth Law is based on the observation that temperature can be defined and measured for all materials in a consistent way.

Thermodynamics applies to any system with a reproducible equation of state. In the next three Sections we introduce the First, Second, and Third Laws of Thermodynamics. In each of these the ideal-gas model plays a fundamental role. In Section 2.8 we describe an extension of the ideal-gas model, introduced by van der Waals, which provides an approximate but highly-useful account of the properties of liquids, including vaporization, condensation, and the properties of mixtures.

## 2.4 First Law of Thermodynamics

Both the First and the Second Laws of Thermodynamics can be expressed negatively, as statements forbidding perpetual motion machines. But both Laws have positive predictive value. In this Section we will discuss the First Law of Thermodynamics and demonstrate its usefulness in predicting the outcome of irreversible processes.

The First Law presumes the empirical notion of stable thermodynamic equilibrium states. The simplest systems to which it can be applied are fluids. For a given mass of equilibrium fluid two independent variables, volume and temperature, or pressure and volume, for instance, implicitly specify all other equilibrium fluid properties. Regardless of its past history, a pound of equilibrated room-temperature room-pressure water always has the same mechanical, thermal, electric, and chemical properties. *All* of the "state functions" of equilibrium water can depend only on the water's two-parameter thermodynamic state.

It is presumed that during mechanical or thermal processing operations any of these state functions can deviate from the equilibrium equation-of-state properties for short times. The time required for the decay of processing transients can generally be estimated from appropriate transport coefficients. Measured in seconds, this decay time typically varies as the square of the system size measured in centimeters. Thus the mechanical and thermal equilibration of a swimming pool requires days.

In order for equilibrium thermodynamics to apply, it is necessary that the states of interest be relatively stable, persisting long enough to display steady properties. For most systems stability is not a problem on the timescale of laboratory measurements. Only relative stability is a requirement. On a long enough time scale nuclei other than iron are all unstable relative to nuclear transformations. Diamond is unstable relative to graphite under room conditions, but its properties are reproducible and accurately known. But composition changes can be very much faster, and times very much shorter, than the times required for spontaneous nuclear or chemical reactions. On a relatively short time scale, it is useful to think of liquid water, supercooled tens of degrees below its freezing point, as being in a reproducible thermodynamic state. Sufficiently small samples of supercooled water can exhibit well-defined thermodynamic properties (including negative pressure) on a time scale long enough for transients to decay and for measurements to be made.

The First Law of Thermodynamics applies to the transformations of materials of any composition among their thermodynamic states over times long enough for transients to decay but short enough to allow reproducible macroscopic measurements. The *First Law of Thermodynamics* asserts that energy, loosely defined as the power to do work, is a state function. If this were not the case then a cyclic process returning over and over to the same initial state, could act as a source or sink of energy. Such a source would be a perpetual motion machine "of the first kind." The First Law of thermodynamics implies that no such machines can be built.

The First Law can be expressed in more analytic terms by introducing the mutually-exclusive concepts of work and heat to describe energy changes. Work is any energy change caused by manipulation of an external system coordinate, typically the volume. For such a coordinate change the induced energy change  $dE$  is by definition equal to the work done on the system  $-dW$ . There are many kinds of energy change corresponding to thermodynamic work: the deformation of a fluid or solid, described by the product of the pressure tensor and the strain tensor:

$$dW = -V[P_{xx}d\epsilon_{xx} + P_{yy}d\epsilon_{yy} + P_{zz}d\epsilon_{zz} + P_{xy}d\epsilon_{xy} + P_{xz}d\epsilon_{xz} + P_{yz}d\epsilon_{yz}] ,$$

the motion of mass or charge in a gravitational or electric field; the increase of surface area against surface tension; the rotation of an electric or magnetic dipole in an electromagnetic field. All of these examples of energy changes controlled by coordinate values are work. On the other hand only a single type of energy change is called heat,

one which increases the energy by  $dQ$  while leaving coordinates unchanged. On a microscopic basis heat corresponds to *momentum* changes, with the center-of-mass momentum fixed, while work corresponds to *coordinate* changes. The analytic form of the First Law of Thermodynamics incorporates this division of energy changes into two types, stating that any system energy change  $dE$  is the result of heat taken into the system of interest less any work done by the system:

$$dE = dQ - dW .$$

Often a special symbol is used for the differential changes  $dQ$  and  $dW$  as a reminder that heat and work, unlike energy, are not thermodynamic state functions. Rumford's experimental demonstration that a virtually limitless quantity of heat could be obtained from a cannon blank (by boring the blank with a dull bit) is the usual evidence cited to show that of the three energies, only  $E$ , not  $Q$  and  $W$ , is a state function.

Some interesting initial-value problems can be solved by using the energy-conservation form of the First Law of Thermodynamics. Figure 2.3 illustrates such a problem.

Consider a three-dimensional monatomic ideal gas confined to a volume  $V_0$  by a piston of mass  $m$ , with the gravitational force  $mg$  on the area of the piston,  $A$ , exactly compensating for the upward pressure force  $P_0A$ :

$$mg = P_0A .$$

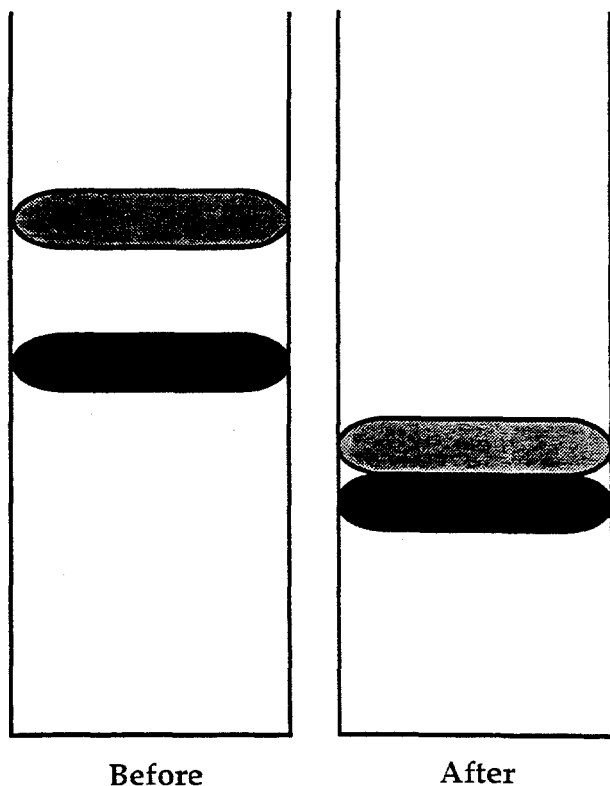


**Figure 2.3.** Three-dimensional monatomic ideal gas confined by a piston of mass  $m$ . The First Law of Thermodynamics predicts the final equilibrium state after a second such piston is dropped from above, doubling the equilibrium pressure.

A second piston, just like the first, is suspended a distance  $\Delta z = \Delta V/A$  above. Suppose that this second piston is dropped. What is the final state of the gas? It is assumed that the pistons have no thermal energy, only gravitational energy. The thermodynamic equation of state for the pistons is simply  $E = mgh$ . The thermodynamic equation of state for the three-dimensional ideal gas follows from the definition of an ideal-gas thermometer:

$$P_0 V_0 = NkT_0 = (2/3)E_0,$$

where the subscripts indicate initial-state conditions. The nonequilibrium process proceeds by converting the mechanical energy of the falling piston to thermal energy of the gas. The process is complicated. Analyzing its details would require knowing the viscosity and heat conductivity of the gas.

We can avoid this analysis and find the final state of the gas without such transport information by applying mechanical force balance and the thermal energy balance dictated by the First Law of Thermodynamics. For logical consistency it would be reasonable to start with a *Zeroth* Law of Mechanics stating that forces balance at equilibrium in the same way that the Zeroth Law of Thermodynamics describes temperature equilibration. This basic principle of mechanics is equivalent to Newton's *Third* Law of Motion. To apply it here notice that the mass supported by the gas doubles. Thus force balance requires

$$P_1 = 2P_0,$$

where the original piston pressure times its area  $P_0 A$  just balances the gravitational force  $mg$ . If we choose the coordinate origin at the base of the container the piston gravitational energy  $mgz$  is proportional to the gas' volume, and the energy balance becomes:

$$(3/2)P_0 V_0 + (mg/A)(V_0 + [V_0 + \Delta V]) = (3/2)P_1 V_1 + 2(mg/A)V_1 =$$

$$(3/2)P_0 V_0 + P_0 V_0 + P_0 [V_0 + \Delta V] = (3/2)P_1 V_1 + 2P_0 V_1 = 5P_0 V_1.$$

Thus the ratio of the final to the initial volume is

$$R = V_1/V_0 = (1/5)[(7/2) + (\Delta V/V_0)],$$

and the final volume can have any value greater than 7/10 the initial volume. Thus the First Law allows us to find the final equilibrium state without exploring the complex mechanism through which the state is achieved. Any other final state would be a violation of the First Law corresponding to the creation or annihilation of energy.

## 2.5 Second Law of Thermodynamics

The Second Law of Thermodynamics implies that perpetual motion machines "of the second kind" cannot be built. Such a machine would be capable of converting heat into work through a cyclic process conserving energy, and satisfying the First Law. Such a conversion is prohibited. Figure 2.4 shows a violation. An ocean-going liner taking sea water in and excreting sea-ice blocks, powered by the energy extracted from the water in the process of making ice blocks, would exemplify perpetual motion of the second kind.

An analytic approach to the Second Law of Thermodynamics can be based on the notion of efficiency of conversion of heat into work. The analysis is possible to carry out only because all reversible mechanical processes obeying the First Law while operating between two reservoir temperatures  $T_H$  and  $T_L$  must have exactly the same thermodynamic efficiency.

This equivalence is most easily established and understood by introducing a standard device to measure thermodynamic efficiency, the ideal-gas Carnot cycle. The Carnot-cycle analysis provides practice in First-Law calculations distinguishing work and heat. The Carnot cycle carries a fixed quantity of ideal gas isothermally from states 1 to 2 and 3 to 4, and adiabatically from states 2 to 3 and 4 to 1. A two-dimensional version, with  $PV = NkT = E$ , is shown in Figure 2.5. It is imagined that the gas can be placed in contact with reservoirs at  $T_H$  and  $T_L$  and can also do work by interacting with a spring or displacing a weight in a gravitational field. The Table shows the division of energy changes  $\Delta E$  in the cycle into heat and work for a  $D$ -dimensional ideal gas, with  $PV = NkT = (2/D)E$ :

Step:	$\Delta E/Nk$ :	$\Delta Q/Nk$ :	$\Delta W/Nk$ :
1→2:	0	$+T_H \ln(V_2/V_1)$	$+T_H \ln(V_2/V_1)$
2→3:	$-(D/2)(T_H - T_L)$	0	$+(D/2)(T_H - T_L)$
3→4:	0	$-T_L \ln(V_3/V_4)$	$-T_L \ln(V_3/V_4)$
4→1:	$+(D/2)(T_H - T_L)$	0	$-(D/2)(T_H - T_L)$
Total:	0	$(T_H - T_L) \ln(V_2/V_1)$	$(T_H - T_L) \ln(V_2/V_1)$

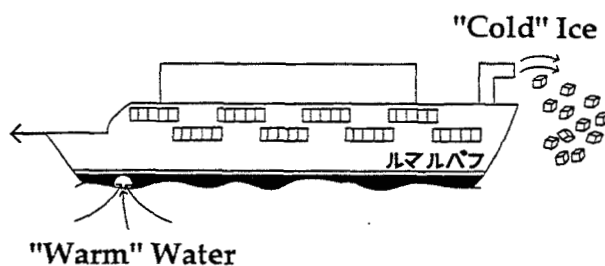


**Figure 2.4.** Violation of the Second Law of Thermodynamics by the cyclic conversion of heat into work.

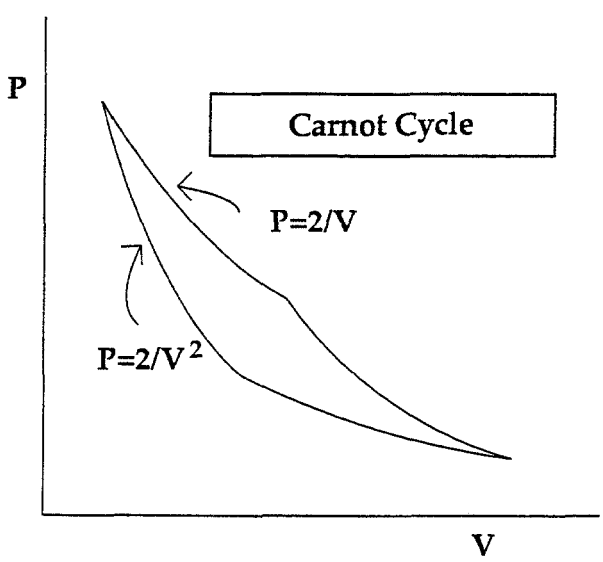


**Figure 2.5.** Two-dimensional ideal-gas Carnot cycle which converts heat into work with an efficiency  $(T_H - T_L)/T_H$ . For this gas  $PV = NkT = E$ . The cycle is bounded by two isotherms and two (steeper) adiabats.

The *isothermal* sections of the cycle 1→2 and 3→4 correspond to *constant-energy* processes because ideal-gas energy depends only on temperature. Thus, for the isothermal sections:

$$\Delta E_T = 0 = \Delta Q - \Delta W = \Delta Q - NkT \ln(V_{\text{Final}}/V_{\text{Initial}}),$$

so that the heat taken in and the work done must exactly balance. For the *adiabatic* sections 2→3 and 4→1  $\Delta Q$  vanishes so that the energy change comes only from the work done:

$$\Delta E = (D/2)Nk\Delta T = \Delta Q - \Delta W = -\Delta W.$$

From the corresponding *differential* relation along an adiabat:

$$dE = (D/2)NkdT = (D/2)PdV + (D/2)VdP = -PdV,$$

it is easy to show that the products  $P^D V^{D+2}$ ,  $T^D V^2$ , and  $T^{D+2} P^{-2}$  are all constant. The second of these relationships then establishes a further relation linking the four volumes in the Carnot cycle:  $V_1 V_3 = V_2 V_4$ . This equality has been used in constructing the Table. It can also be used to simplify the expression for the efficiency of the cycle:

$$(\Delta W_{12} + \Delta W_{23} + \Delta W_{34} + \Delta W_{41})/\Delta Q_{12} = (T_H - T_L)/T_H.$$

If we imagine coupling the ideal gas to any other material capable of complementary reversible transformations then the Second Law of Thermodynamics states that the efficiency must be exactly the same for that material. Otherwise the cycle, or its time-reversed version, could convert heat into work.

A second conclusion follows from our tabulated Carnot-cycle data: the cyclic integral of  $dQ/T$  vanishes for an ideal gas. The integral must therefore vanish for any other material with which the gas exchanges heat  $dQ$  at temperature  $T$  during a reversible cycle. Thus the integral of  $dQ/T$  is a new state function, called *entropy* and denoted by  $S$ , with  $dS$  given by  $dQ/T$ . Using this new state function as a measure of past heat transfers, the First and Second Laws of Thermodynamics can be combined, written entirely in terms of path-independent state functions for all reversible near-equilibrium processes:

$$dE = TdS - PdV .$$

Our conclusions would be of little interest if they applied only to ideal-gas Carnot cycles. But they actually apply to general cycles for any "thermodynamic material," that is, any material that has reproducible reversible state functions and is capable of exchanging heat and performing work. The summed heat transfers, each divided by the temperature corresponding to the transfer, for any such material are equal to the same sum for an ideal gas. This is because a general thermodynamic cycle can always be divided up into infinitesimal Carnot cycles. To see this, consider a geometric analog, dividing an arbitrary area in the  $xy$  plane into differential elements of area  $dx dy$ . In thermodynamics the adiabats and isotherms furnish a curvilinear coordinate system suitable for the subdivision of any pressure-volume-temperature equation-of-state surface.

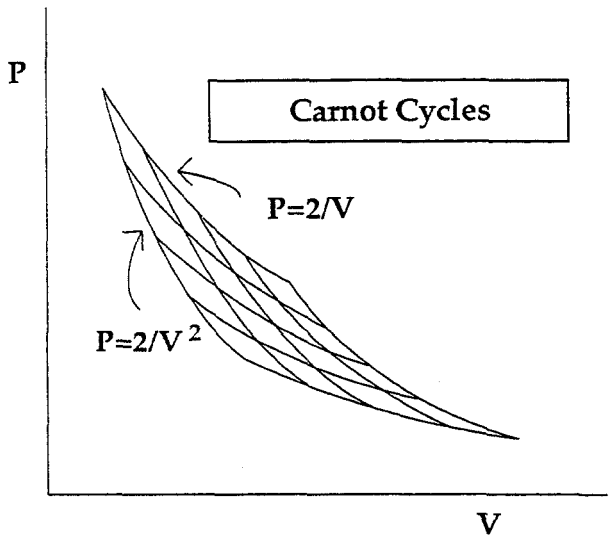


Figure 2.6. Subdivision of a Carnot cycle into subcycles. This same subdivision can be applied to any general thermodynamic cycle.

Figure 2.6 indicates such a reduction of a general cycle to small Carnot cycles, all of which are imagined to be traced out in a clockwise sense, converting heat into work. Because the internal heat and work transfers along the joint boundaries of adjacent infinitesimal cycles all cancel, the only remaining contribution for a general cycle is the perimeter integral of  $dQ/T$ . This holds true for any thermodynamic material capable of exchanging heat with ideal-gas reservoirs. Thus, for a general cycle and for a general material the cyclic reversible entropy change is equal to the sum of the corresponding differential ideal gas sum, and vanishes:

$$\oint dS = \oint dQ/T = \sum \oint (dQ_{\text{Subcycle}}/T) = 0.$$

It might be thought that the Carnot-cycle derivation is unnecessarily complex, and that a simpler cycle, with isothermal and isochoric sections could be used instead. But in that case it is not so easy to show that the heat taken in is proportional to the temperature.

**Problem:**

Discuss the applicability of the Carnot-cycle construction to water below its maximum-density temperature (roughly 4° centigrade) so that  $(\partial V/\partial T)_P$  is negative.

The *Second Law of Thermodynamics* can be phrased in terms of the entropy. For any *reversible* thermodynamic process the heat transfers balance so that the total entropy change is zero. For any *irreversible* cyclic process the First Law still guarantees that the heat taken in and the work done balance, but these must both be less than the corresponding entropy change:

$$dE + dW \equiv dQ \leq TdS.$$

This inequality gives another form for the Second Law of Thermodynamics: “*The entropy of the Universe can only increase.*”

To demonstrate the usefulness of this form of The Second Law of Thermodynamics consider a “thought-experiment” involving the conversion of work into heat. For variety as well as analytic simplicity we choose two-dimensional monatomic ideal gases in this example. The corresponding mechanical and thermal equations of state are

$$PV = NkT = E.$$

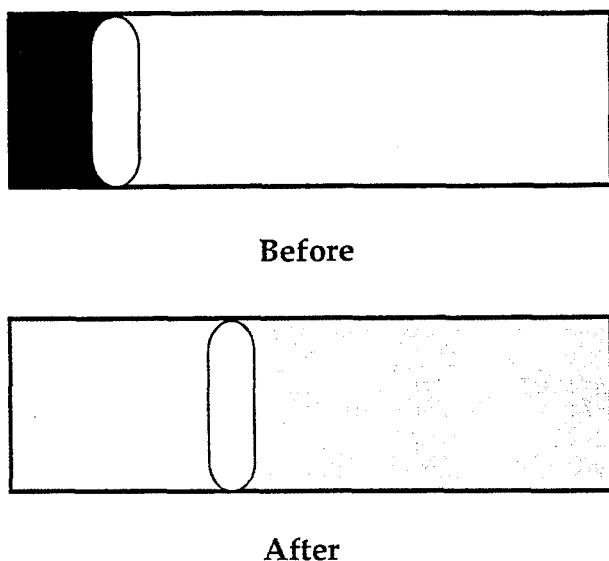


**Figure 2.7.** Ideal-gas chambers separated by an adiabatic frictionless piston. Initially the pressure in the left chamber is 9 times that in the right. The piston is then released. At equilibrium the Second Law of Thermodynamics requires

$$1.732 < \{V_{\text{Left}}, V_{\text{Right}}\} < 2.268.$$

Consider a vessel partitioned into two chambers by an adiabatic frictionless piston as shown in Figure 2.7. The chambers contain equal amounts of a two-dimensional ideal gas. In the lefthand chamber, with volume 1 and energy 3, the pressure is 9 times that of the righthand chamber, which has volume 3 and energy 1. Releasing the piston sets off a complex chaotic nonequilibrium flow, with shockwaves and rarefaction waves eventually being converted to thermal energy by the viscous and thermal dissipation of the gases. At the end of this process the two chambers must be in a state of mechanical equilibrium. Mechanical equilibrium implies that the final pressure must be equal to the energy density, 1, because the energy density,

$$P = E/V = (E_L + E_R)/(V_L + V_R) = (3 + 1)/(1 + 3) = 1,$$

must be uniform at mechanical equilibrium. But this mechanical-equilibrium condition places *no constraints whatever* on the position of the piston. For *any* division of the volume a corresponding division of the energy gives mechanical equilibrium. The piston can lie *anywhere* within the vessel. The First Law provides no information on the final location of the piston.

To predict the equilibrium position of the piston it is necessary to apply the Second Law of Thermodynamics. For this we need to express the entropy in terms of volume and energy. In two dimensions the heat transfer in a reversible process is given by the First Law of Thermodynamics:

$$dQ/T = (dE + dW)/T = Nkd\ln T + Nkd\ln V = dQ/T = dS.$$

Thus the ideal-gas entropy has the form:

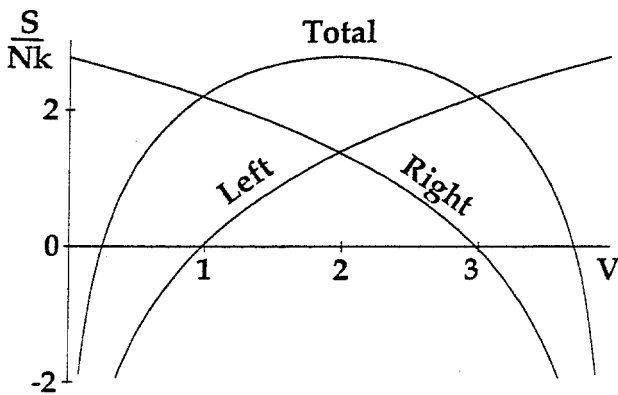


**Figure 2.8.** Local and Global entropies, relative to the initial state, for the two-chamber ideal-gas system shown in Figure 2.7.

$$S/Nk = \ln E + \ln V + \text{constant} .$$

In this example we will let the arbitrary integration constant vanish. Then, applying the uniform-pressure mechanical-equilibrium condition,  $E = V$ , the total entropy is

$$S/Nk = \ln[VV(4 - V)(4 - V)] .$$

As Figure 2.8 shows, this value exceeds the initial entropy,

$$S_0/Nk = \ln[1 \times 3 \times 3 \times 1] ,$$

for any volume between 1 and 3. So the Second Law of Thermodynamics definitely restricts the piston to occupy the middle half of the container. But a *much stronger* result can be obtained by applying a *local* version of the Second Law. Because *both* chambers are adiabatically insulated the entropy in each of them must increase:

$$S_L/Nk \equiv \ln[VV] > \ln[1 \times 3] ; S_R/Nk \equiv \ln[(4 - V)(4 - V)] > \ln[3 \times 1] .$$

Thus both the volume  $V = V_L$  and its complement  $4 - V = V_R$  must exceed  $3^{1/2} = 1.732$ . The fraction of the volume available to the piston,  $2 \times 0.268/4 = 0.134$  is reduced nearly fourfold from the weaker bounds provided by the global version of the Second Law.

## 2.6 Third Law of Thermodynamics

The equation  $S = k \ln W$  appears on Boltzmann's gravestone in Vienna's Central Cemetery. It relates the thermodynamic entropy to the number of available microstates  $W$ . The microstates are quantum states, solutions of the Schroedinger equation, although that equation was unknown until about 20 years after Boltzmann's death. The *Third Law of Thermodynamics* states that Boltzmann's entropy  $k \ln W$  is the same as the thermodynamic entropy,  $\int dQ_{\text{Rev}}/T$ .

Consider an example. The energy states for a quantum ideal gas in a one-dimensional box of length  $L$  are

$$E_{\text{Periodic}} = n^2 h^2 / 2mL^2 ; E_{\text{Rigid}} = n^2 h^2 / 8mL^2 ,$$

where  $h$  is Planck's constant,  $6.626 \times 10^{-34}$  jouleseconds, and the allowed values of  $n$  include either the complete set of integers or else just the positive ones, depending upon the choice of boundary conditions, periodic or rigid. For a system with many degrees of freedom,  $N$ , each characterized by a quantum number  $n$ , the number of states consistent with the total energy  $E = \sum E_n$  increases as  $\exp(N)$ , as we will show in detail in the next Chapter.

On the other hand, for a perfect quantum crystal the number of states is of order unity. The few degrees of freedom remaining at low temperatures, which specify the orientation of a crystal, for instance, provide a completely negligible contribution to the entropy. Thus the change in the thermodynamic entropy between a cold crystal and a warm gas can be calculated in advance, using Boltzmann's formula. Long before quantum mechanics had been discovered it was well known that the results of such calculations agree with experiment. This particular example can be worked out in detail using the integrated heat capacity data  $\{C_i\}$  together with the heats of the melting and vaporization transitions  $\{\Delta H_M, \Delta H_V\}$  to calculate entropy changes in the solid, liquid, and gas phases:

$$S_G(T) - S_S(T=0) = \Delta S_S + \Delta S_{S \Rightarrow L} + \Delta S_L + \Delta S_{L \Rightarrow G} + \Delta S_G .$$

$$\Delta S = \int dQ/T = \int (\partial Q / \partial T)_i d \ln T = \int C_i d \ln T ; \Delta S = \Delta H_M / T_M \text{ or } \Delta H_V / T_V ;$$

For nitrogen, for instance, the heat capacity contributions to the gas-phase entropy are approximately 13.6 for the solid and 2.7 for the liquid. Adding on the melting and vaporization contributions of 2.7 and 17.2 reproduces the experimental entropy for the gas at 77 kelvins and atmospheric pressure within 0.1. All of these numerical values are expressed in calories/mole.

The fundamental properties of thermodynamic entropy are, first, that it is a state function; second, that it increases in spontaneous processes; and third, that it follows Boltzmann's statistical connection to the number of microstates. We will come back to Boltzmann's microscopic interpretation of the macroscopic entropy in Chapter 3.

## 2.7 Thermodynamics of Ideal-Gas Compression

We illustrate macroscopic thermodynamic entropy calculations by considering in turn four different thermodynamic processes, each of which involves compressing an ideal gas. In each of these compression examples (isothermal, isentropic, isenthalpic, and shock) we consider a two-dimensional ideal gas with the equation of state:

$$PV = E = NkT, \quad S/Nk = \ln(VT).$$

The entropy and the energy could both contain arbitrary additive constants. For simplicity we set these equal to zero. This simple choice for the equation of state is made only to simplify these illustrative calculations. With numerical rather than analytic integration analogous calculations could be made with any thermodynamic equation of state.

We first review the isothermal and adiabatic compressions already included in our Carnot Cycle calculations which introduced the idea of efficiency and the Second Law of Thermodynamics. We then consider two other nonequilibrium adiabatic flow processes, the Joule-Thomson flow, which is both adiabatic and isenthalpic, and shockwave compression.

In an *isothermal* compression the energy change  $\Delta E = \int dE = \int dQ - \int dW$  vanishes because ideal-gas energy depends only on temperature. Thus, if the compression is carried out reversibly, the work done,

$$\Delta W = \int dW = \int (NkT/V)dV = NkT \ln(V_F/V_I),$$

must also be equal to the heat taken in. The corresponding entropy change,  $\Delta S = \Delta Q/T$ , is

$$dS = \int (1/T)dQ_{\text{rev}} = Nk \ln(V_F/V_I).$$

In a reversible *adiabatic* compression, well approximated by the relatively sudden small-amplitude compression induced by a sound wave, the entropy change vanishes (because  $\delta Q$  vanishes) so that the work done is equal to the decrease in system energy:

$$\Delta S = 0; \quad \Delta E = -\Delta W = Nk(T_F - T_I).$$

In the irreversible Joule-Thomson adiabatic flow experiment a gas is steadily "throttled" adiabatically, by pushing it through a porous plug. See Figure 2.9. The energy change  $\Delta E$  is given by the work done on the gas at the inlet,  $(PV)_{\text{in}}$  for a volume  $V$ , less the work done by the gas at the outlet  $(PV)_{\text{out}}$ , so that the energy change is equal to the work done on the system  $\Delta E = E_{\text{out}} - E_{\text{in}} = (PV)_{\text{in}} - (PV)_{\text{out}}$ . Such a process takes place at constant *enthalpy*, where the enthalpy is generally  $H \equiv E + PV$ . In our two-dimensional problem  $H$  is  $E + PV = 2PV = 2NkT$ . The entropy *change* for our ideal gas is positive and nonzero, indicating the irreversible nature of the "throttling" process:

$$\Delta S_{\text{T}}/Nk = \Delta \ln(VT) = \Delta \ln(H^2/P) = \ln(P_{\text{in}}/P_{\text{out}}) \geq 0.$$

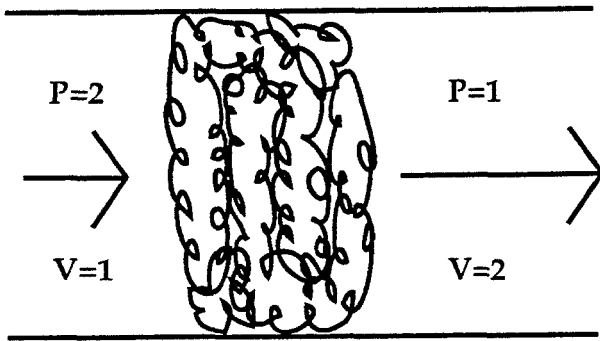


**Figure 2.9.** Adiabatic Joule-Thomson flow through a porous plug. The energy change of the flowing gas reflects the work done on the gas. For this process the enthalpy is unchanged while the entropy increases.

In an ideal gas enthalpy is a direct measure of temperature so that the gas neither heats nor cools in this process. In a real gas the "Joule-Thomson coefficient,"  $(\partial T/\partial V)_H$ , can be either negative or positive, vanishing at the "inversion" temperature. Below the inversion temperature this throttling process can be used to construct a refrigerator.

In this conventional description of the Joule-Thomson experiment a small error was made in the energy balance. We completely ignored the kinetic energy of the flow. This is of course reasonable in the usual case with the flow velocity of the order of cm/sec, because the neglected energy correction is of order  $(v/c)^2$ , where  $c$  is the sound speed, of the order of kilometers/sec. The correction becomes important at high speeds. In a shockwave experiment even an ideal gas will heat up. The neglected kinetic energy has to be taken into account.

Before specializing to the ideal gas, let us first consider the shock compression of a general fluid. In a shockwave, a "cold" fluid at a relatively low temperature, energy, and density, is suddenly compressed to a "hot" high-temperature, high-energy compressed state. The process generating such a shockwave can be considered from many points of view. The simplest of these, from the standpoint of thermodynamics and the First Law, is illustrated in Figure 2.10. In this prototypical thought experiment we begin with an equilibrium fluid initially moving to the left at speed  $v_{\text{piston}} = u_p/2$ . The fluid moves at the velocity of the righthand piston so that no disturbance occurs at the righthand boundary. There is an initial velocity discontinuity at the left boundary of the fluid where the fluid and the piston move in opposite directions. The left boundary of the fluid must move to the right, also at speed  $u_p/2$ . Immediately a shockwave is launched into the cold fluid, converting it to a hot shocked high-density state and changing the fluid velocity from  $-u_p/2$  to  $+u_p/2$ . At the moment the resulting shockwave has passed completely through the fluid, the work done by the two pistons is exactly equal to the internal energy change of the fluid, because we constructed our thought experiment to make the net change in kinetic energy zero. Just as in the Joule-Thomson experiment, the energy change is  $E_F - E_I$ , and this is equal to the work done  $(P_F + P_I)(V_I - V_F)/2$ . This energy-conservation relation is a finite-difference form of the First Law for an adiabatic process;  $dE = -PdV$ . The shock process is *adiabatic*, with no heat flow, but also *irreversible*. The entropy produced is

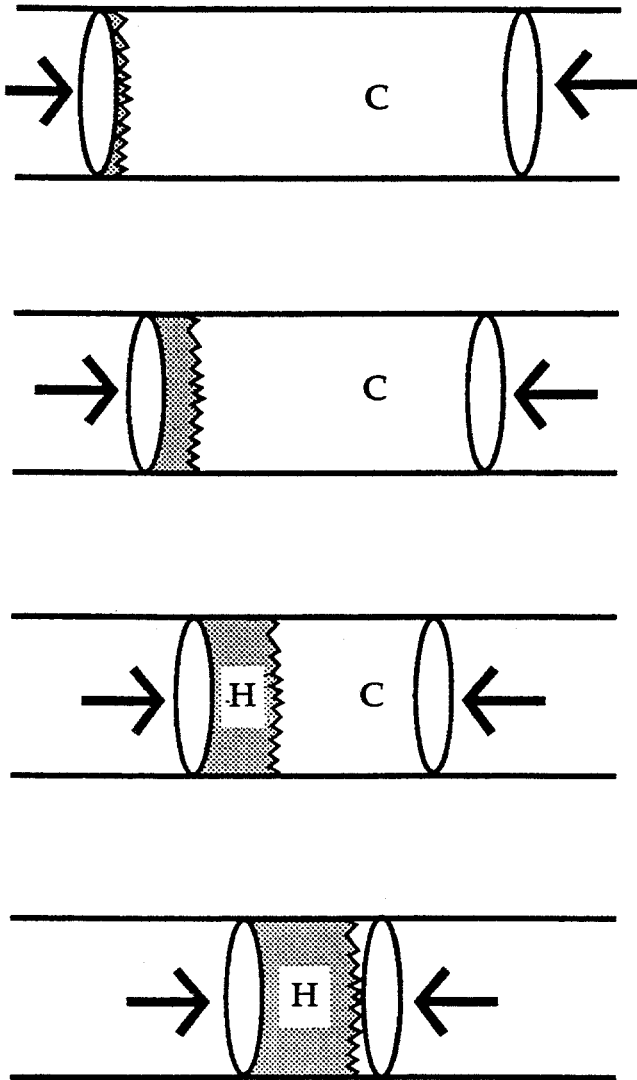


**Figure 2.10.** Adiabatic shockwave compression of a fluid. In the top view the fluid moves to the left, at a laboratory-frame speed  $u_p/2$ . The shockwave formed at the left boundary propagates across the system at a laboratory-frame speed of  $u_s - (1/2)u_p$ . Because both boundaries move symmetrically at velocities  $\pm u_p/2$ , the center-of-mass kinetic energy is unchanged in the frame shown here.

equivalent to an irreversible conversion of work into heat, leading to an entropy change which is third order in the compression  $dV$ .

Let us use the twofold compression of a two-dimensional ideal gas,  $V_I = 2V_F$ , to illustrate these results:

$$\Delta E = (PV)_F - (PV)_I = (P_F - 2P_I)V_F = (1/2)(P_F + P_I)(V_I - V_F) \equiv [(P_F V_F) + (P_I V_F)]/2 .$$

These energy-conservation equations are satisfied by a fivefold increase in pressure. The energy has likewise increased,  $E_F/E_I = 5/2$ , with an entropy change:

$$\Delta S/Nk = \ln[(EV)_F/(EV)_I] = \ln(5/4) = 0.224 .$$

**Problem:**

Calculate the two-dimensional ideal-gas entropy change as a function of the shock compression,  $\delta = \Delta V/V_I$ , and show that  $\Delta S/Nk$  varies as  $\ln[(2 - 3\delta + \delta^3)/(2 - 3\delta)] \approx \delta^3/(2 - 3\delta) \approx (1/2)\delta^3$ , so that the entropy change is third-order in the compression. Show also that the maximum compression for this gas is threefold.

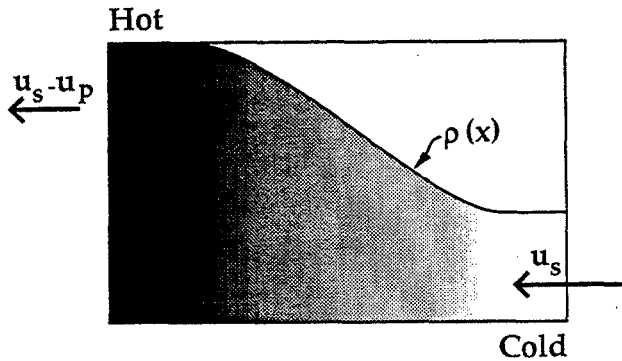


**Figure 2.11.** Adiabatic shockwave compression of a fluid. In this frame, fixed on the wave, cold fluid enters from the right, at speed  $u_s$ , while hot fluid exits to the left, at speed  $u_s - u_p$ .

Starting with samples of heavy metals instead of gases shockwave experiments can be used to reach highly-compressed thermodynamic states at pressures approaching 100 megabars, perhaps 50 times greater than those available in static presses. By using the conservation relations for steady flow, accurate *equilibrium* equation-of-state information can be obtained from these rapid explosively-driven experiments. These conservation relations lead once again to the result which we derived above for shockwave compression,  $\Delta E = -\langle P \rangle \Delta V = (P_C + P_H)(V_C - V_H)/2 \equiv (P_I + P_F)(V_I - V_F)/2$ .

The complete set of conservation relations is most easily derived by considering a coordinate system moving with the shockwave. In this coordinate frame, fixed on the wave and shown in Figure 2.11, cold fluid enters from the right, at velocity  $-u_s$ , and hot fluid exits at the left, with velocity  $-u_s + u_p$ . The mass flux (flow of mass per unit area and time) flowing in must balance the mass flux flowing out:

$$\rho_I u_s = \rho_F (u_s - u_p) \equiv \rho u .$$

Likewise, the momentum increase,  $\rho u u_p$ , per unit time and area within the Lagrangian volume element shown in the Figure must result from and be equal to the difference in pressure forces exerted at the left and right boundaries:

$$P_F - P_I = -\rho_F (u_s - u_p)^2 + \rho_I u_s^2 = \rho u u_p .$$

For slow compressions, with the density change  $\delta\rho = \rho_F - \rho_I$  small, these two conservation relations simplify to the usual result for the propagation of sound waves:  $\delta P / \delta\rho = (\partial P / \partial\rho)_S = c^2$  with  $u_p / u_s = \delta\rho / \rho$ . Notice that the derivative  $(\delta P / \delta\rho)$  is the *adiabatic* (isentropic) derivative.

The two conservation relations for mass and momentum, along with the corresponding energy-conservation relation we derived on page 54 are called the "Hugoniot relations." By using these general conservation principles we can determine equilibrium thermodynamic properties directly from measured shockwave data. By measuring the piston and shock velocities the pressure along the "Hugoniot"

pressure-volume curve can be determined as a function of volume. The energy measurements can be compared to independent estimates based on measuring the energy radiated from the shocked material.

If the two conservation relations for mass and momentum are applied *within the shockwave*, where the longitudinal force per unit area  $P_{xx}$  has a nonequilibrium value, a stress-volume relation called the "Rayleigh line" results, describing the surprising result that the *nonequilibrium* pressure-tensor component  $P_{xx}$  increases *linearly* with volume as the shockwave is traversed:

$$P_{xx}(x) = P_I + \rho_I u_s^2 - (\rho_I u_s)^2 / \rho(x) .$$

Similarly the total comoving flux of energy,  $e(x)(\rho_I u_s) + Q_x$ , where  $e(x)$  is the energy per unit mass, varies *quadratically* in the volume through the shockwave.

### Problem:

Calculate the entropy change for the twofold shockwave compression of a *three-dimensional* ideal gas with equation of state  $PV = NkT = (2/3)E$ .

### 2.8 van der Waals' Equation of State

In introducing the Laws of Thermodynamics we have so far emphasized ideal gases. They play a key role in defining temperature and thermodynamic efficiency. To avoid the impression that thermodynamics treats only such gases and to indicate how phase equilibria arise from the Second Law, we consider here van der Waals' equation of state, a simple analytic relation linking pressure, volume, and temperature together in a way that nicely correlates experimental data for real fluids, including mixtures.

In his thesis on the coexistence of gases and liquids, van der Waals extended the simple ideal-gas equation of state by including the effects of attraction and repulsion between pairs of interacting molecules. The two effects were taken into account, approximately, through two adjustable parameters, van der Waals' constants  $a$  (units  $ML^5/T^2$ ) and  $b$  (units  $L^3$ ). The effect of *attractive* forces, corresponding to  $a$ , is to reduce the *pressure* by an amount proportional to the cohesive energy divided by the volume  $V$ . For a dilute gas the cohesive energy should vary linearly with density, with the reduction in pressure varying as the square of the gas number density  $N/V$ .

The effect of *repulsive* forces, corresponding to  $b$ , is to reduce the available *volume* by an amount proportional to the number of molecules present  $N$ . Van der Waals incorporated both effects in his approximate equation of state:

$$[P + (N^2a/V^2)][V - Nb] = NkT ,$$

At low density both non-ideal pressure effects become negligibly small, as  $(N/V)^2$  and  $(N/V)$ , respectively. In this limit van der Waals' mechanical equation of state

reproduces the ideal gas law,  $PV = NkT$ . At high density van der Waals' pressure always exceeds the ideal value, and diverges at the volume  $Nb$  rather than at zero volume. Choosing water as an example, with a molar volume of  $18 \text{ cm}^3$  for  $6 \times 10^{23}$  molecules,  $b$  is about  $3 \times 10^{-23} \text{ cm}^3$ . The parameter  $a$  can likewise be estimated from the heat of vaporization or from the critical temperature.

Because van der Waals' equation of state describes materials in terms of only two parameters,  $a$  and  $b$ , the equation of state has a useful corresponding-states form. By introducing dimensionless ratios, a "reduced volume"  $V/(Nb)$  and a "reduced temperature"  $kTb/a$ , the dimensionless "compressibility factor"  $PV/NkT$  can be expressed as a universal function of these two dimensionless reduced variables:

$$PV/(NkT) = [(V/Nb)(kTb/a)]^{-1} + [1 - (Nb/V)]^{-1}.$$

Figure 2.12 shows three "isotherms" (mechanical pressure-volume relations with temperature held fixed): passing above, through, and below the "critical point." The critical point is a unique pressure-volume-temperature state. At higher temperatures it is impossible to distinguish the low-density gas phase from the higher-density liquid phase. Above the critical temperature there is only a single fluid phase. At and above that temperature no gas-liquid interface can be observed. The critical pressure and volume are those at which such an interface can form at temperatures just below the critical value.

Any subcritical isotherm, such as the lowest isotherm shown in the Figure, contains a "van der Waals' loop" section which makes no sense thermodynamically, and on two separate grounds. First, *all* of the loop is *thermodynamically* unstable. Second, the central part is *mechanically* unstable too.

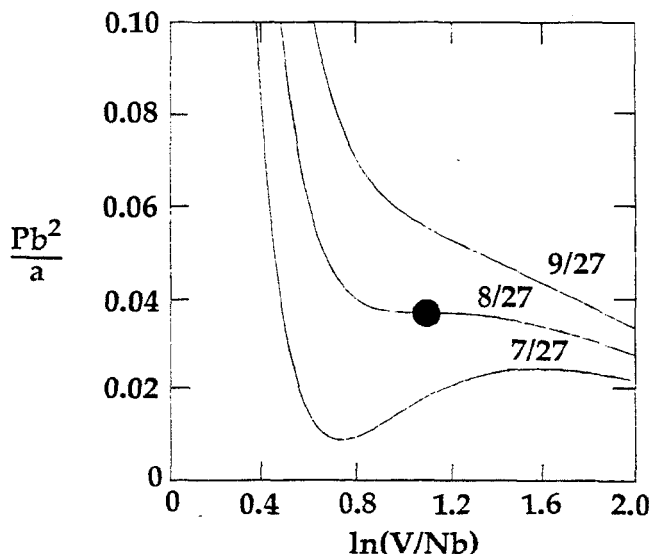


**Figure 2.12.** Isotherms, with labels giving  $kTb/a$ , according to van der Waals' Equation of State. The lowest isotherm exhibits both mechanical and thermodynamic instability. The critical point is indicated.

The mechanical instability is easy to see. In the central region, inside the "spinodal" curve along which the isotherms have zero slope, the derivative of pressure with respect to volume is positive. In such a system any fluctuation in density would continue to grow (because the lower-density part would have the higher pressure) so that a homogeneous system is impossible. Thus, for mechanical stability, it is necessary that the pressure not increase with volume.

Recognizing *thermodynamic* instability requires using the Second Law of Thermodynamics. We can imagine joining high-density "liquid" states to lower-density "gas" states by any of several horizontal tie lines. From the standpoint of mechanics any such combination is stable. But only one of them satisfies the Second Law of Thermodynamics and matches the efficiency of a corresponding ideal-gas Carnot cycle. This is the tieline obeying Maxwell's "equal area" rule:

$$\int P_{vdW}(T)dV = \int P_{eq}(T)dV = P_{eq}(T)(V_{gas} - V_{liquid}) .$$

A higher tie line would produce less work, and a lower one more work. In either case the entropy computed from such a cycle would not be a state function. Thus the Second Law of Thermodynamics is more useful than the First Law in distinguishing possible from impossible thermodynamic processes. The Second Law shows that the straight-line states are more stable thermodynamically than those following other paths such as the van der Waals loops.

The disappearance of the gas-liquid interface above the "critical" temperature defines that temperature and is common to all liquids. By relating the critical temperature to van der Waals'  $a$  and the critical volume to van der Waals'  $b$ , the critical properties of real materials can be used to predict the remainder of the fluid equation of state, including both the the gas and the liquid phases.

We identify this critical temperature by requiring that the relative-maximum pressure and the relative-minimum pressure along an isotherm, the spinodal boundaries of mechanical stability for which  $(\partial P/\partial V)_T$  is zero, coincide, so that  $(\partial^2 P/\partial V^2)_T$  vanishes as well:

$$(\partial P/\partial V)_T = +2Na/(V^3) - NkT/(V - Nb)^2 = 0 ;$$

$$(\partial^2 P/\partial V^2)_T = -6Na/(V^4) + 2NkT/(V - Nb)^3 = 0 .$$

Dividing the first of these equations by the second leads to the critical temperature and volume, from which the critical pressure follows:

$$V_c/Nb = 3 ; kT_c b/a = 8/27 ; P_c b^2/a = 1/27 .$$

These predictions are only semiquantitative, for real materials, but are very useful for rough calculations. Detailed predictions from the van der Waals equation are least accurate near the critical point. The constant-volume heat capacity for the van der Waals fluid exhibits a maximum, with a discontinuity, at the critical point.

Experiments on the rare gases suggest much more than a maximum, a logarithmic divergence instead. Consider water, with a critical volume of  $57\text{cm}^3/\text{mole}$ , a critical temperature of 647 kelvins, and a critical pressure of 221 atmospheres. Using these critical parameters to identify van der Waals'  $a$  and  $b$  leads to a predicted condensed-phase volume that is 6% high and a vaporization energy which is 40% low.

For *all* materials van der Waals' equation makes the prediction that the critical compressibility factor is constant,  $(PV/NkT)_c = 3/8$ . In most cases this value is too high. The data for water give  $(PV/NkT)_c = 0.24$ . The rare-gas values are closer, but still about 20% lower than van der Waals' prediction. A qualitative success of van der Waals' equation of state is the prediction that supercooled liquids can support negative pressures of order kilobars. The predicted temperature dependence of these tensile pressures is in rough accord with experiment.

### Problems:

1. Plot the temperature-density region within which van der Waals' equation predicts negative pressures.
2. Experimental data suggest that the absolute value of the pressure change,  $P - P_c$ , varies as the 4.2 power of the volume change,  $V - V_c$ , on the critical isotherm near the critical point. How well does this agree with the predictions of the van der Waals' equation?
3. Develop a numerical method to evaluate the analytic variation of the pressure, density, and temperature in the vicinity of the van der Waals critical point. That is, find  $(\partial \ln \Delta P / \partial \ln \Delta \rho)_T$  at  $T = T_c$ ,  $(\partial \ln \Delta \rho / \partial \ln \Delta T)_P$  at  $P = P_c$ , and  $(\partial \ln \Delta T / \partial \ln \Delta P)_\rho$  at  $\rho = \rho_c$  in the immediate vicinity of the critical point.

## 2.9 Thermodynamic Potential Functions

It is usual in thermodynamics to consider a system which can do work on, or extract heat from, its surroundings. If we choose to include a part of these surroundings in our "system," we can still apply the same reasoning, based on the laws of thermodynamics, and find potential functions describing the resulting composite system.

For the usual thermodynamic system the potential function is the internal energy  $E$ , which can vary in response to heat flowing in and work being done, and can, for reversible processes, be expressed in terms of state functions:

$$dE = dQ - dW = TdS - PdV .$$

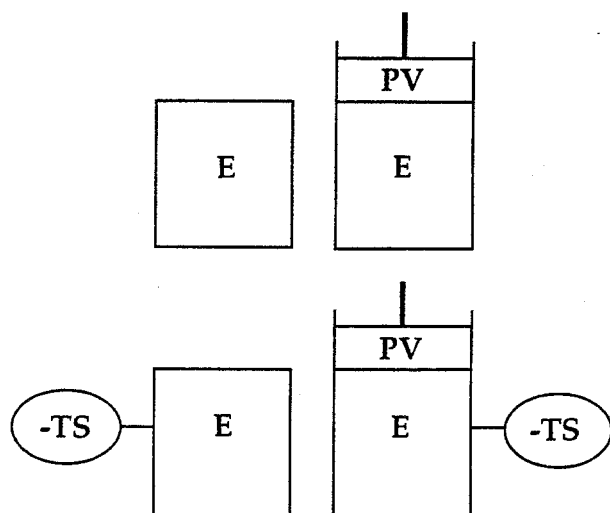


**Figure 2.13.** Systems described by the internal energy  $E$  (upper left), enthalpy  $H = E + PV$  (upper right), Helmholtz free energy  $A = E - TS$  (lower left), and Gibbs' free energy  $G = E + PV - TS$  (lower right).

Consider now the system shown at the upper right corner of Figure 2.13, composed of a subsystem with internal energy  $E$  in mechanical equilibrium with a confining piston, with energy  $PV = mgV/A$ , where  $A$  is the piston area. The total energy of this composite system, for which pressure replaces volume as a natural variable, is called the *enthalpy*, and is denoted by the symbol  $H$ :  $E_{\text{Total}} = H \equiv E + PV$ , the function we found useful in analyzing the Joule-Thomson flow. For a differential process,

$$dH = dE + PdV + VdP = TdS + VdP ,$$

it is evident that the variational statement of the Second Law,

$$dE \leq TdS + PdV ,$$

becomes, for the composite {system + piston}:

$$dE_{\text{Total}} = dH \leq TdS + VdP .$$

Thus the enthalpy acts as a thermodynamic potential for systems which are thermally isolated but exposed to a constant pressure  $P$ .

A different potential function is appropriate for systems in equilibrium with a thermal heat bath, as is shown in the lower lefthand portion of Figure 2.13. So long as this heat bath can give up energy  $dQ$  to the system without changing the bath temperature  $T$ , the total energy of the system can be written

$$A = E_{\text{Total}} \equiv E - TS ,$$

where the energy of the heat bath is set equal to zero, at zero temperature, so that  $TS$  is a measure of the bath's energy loss in providing the system energy  $E$ .  $A$  is called Helmholtz' free energy or the Helmholtz free energy.

The corresponding differential relation for the Helmholtz free energy is

$$dE_{\text{Total}} = dA = dE - TdS - SdT \leq -PdV - SdT ,$$

showing that it reaches a minimum value for fixed volume and temperature. For the statistical mechanics which we develop in Chapter 3 Helmholtz' Free Energy, in which volume and temperature are the natural variables, will be the thermodynamic potential function we most often use.

Finally Gibbs' Free Energy, or the Gibbs Free Energy,  $G$ , can be defined as the total energy of a three-part composite system including subsystem, confining piston, and heat reservoir:  $E_{\text{Total}} = G \equiv E + PV - TS$ . The differential form:

$$dE_{\text{Total}} = dG = dE + PdV + VdP - TdS - SdT \leq VdP - SdT ,$$

shows that Gibbs' Free Energy reaches a minimum under conditions of constant pressure and temperature. Because these conditions are those of mechanical and thermal equilibrium Gibbs' Free Energy is the most fundamental of the four potentials.

Each of the thermodynamic potentials,  $E$ ,  $H$ ,  $A$ , and  $G$ , is a state function satisfying a Second-Law variational principle at equilibrium. Because the potentials are state functions the mixed second partial derivatives of the potential functions are independent of the order of differentiation. This is readily apparent if the finite-difference form of the second derivatives is considered. For example,  $(\partial^2 E / \partial S \partial V)$  can be calculated from the finite-difference representation:

$$(\partial^2 E / \partial S \partial V)(\delta S \delta V) =$$

$$E[S - (\delta S/2), V + (\delta V/2)] + E[S + (\delta S/2), V + (\delta V/2)] +$$

$$E[S - (\delta S/2), V - (\delta V/2)] + E[S + (\delta S/2), V - (\delta V/2)] ,$$

in the limit that  $\delta S$  and  $\delta V$  approach zero. From the differential  $dE = TdS - PdV$  the derivative can be evaluated in either of two different ways:

$$(\partial^2 E / \partial S \partial V) = (\partial / \partial V)_S (\partial E / \partial S)_V = (\partial / \partial S)_V (\partial E / \partial V)_S = (\partial T / \partial V)_S = -(\partial P / \partial S)_V .$$

The final relation  $(\partial T / \partial V)_S = -(\partial P / \partial S)_V$  is a "Maxwell Relation." Three more such Maxwell relations can be derived, one each for the enthalpy, Helmholtz, and

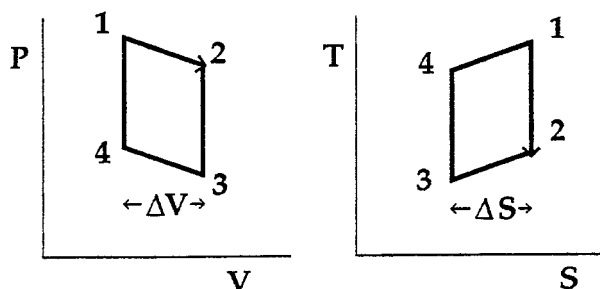


**Figure 2.14.** Pressure-volume and temperature-entropy views of a thermodynamic cycle described by the Maxwell relation  $(\partial T/\partial V)_S = -(\partial P/\partial S)_V$ .

Gibbs free energies. It is interesting to note that each has the form  $dPdV = dSdT$  and represents the First-Law statement that, for an infinitesimal cycle, the work done is equal to the heat taken in for any reversible thermodynamic cycle. Figure 2.14 illustrates the cycle appropriate to the variables  $S$  and  $V$ .

Before leaving macroscopic thermodynamics to explore the foundations of microscopic statistical mechanics it is worthwhile to point out one more family of identities which follows from the two-variable state-function form of thermodynamics. The general relationship for any *three* variables linked together functionally is

$$(\partial x/\partial y)_z (\partial y/\partial z)_x (\partial z/\partial x)_y = -1.$$

If we consider, for example, pressure as a function of volume and temperature, we find the relation

$$(\partial P/\partial T)_V (\partial T/\partial V)_P (\partial V/\partial P)_T = -1.$$

For an ideal gas the derivatives can all be evaluated, and confirm the general result:

$$(Nk/V)(P/Nk)(-NkT/P^2) = -NkT/PV = -1.$$

### Problems:

1. Demonstrate that  $(\partial x/\partial y)_z (\partial y/\partial z)_x (\partial z/\partial x)_y = -1$  by first considering a differential variation in  $x(y,z)$  and then requiring that the independent variations  $dy$  and  $dz$  be chosen such that  $dx$  vanishes. This corresponds to examining the variation, perpendicular to the  $x$  axis, of the surface  $z = z(x,y)$ .
2. Show that the ratio of the constant-pressure heat capacity to the constant volume heat capacity is the same as that of the constant-entropy "adiabatic bulk modulus"  $B_S$  to the constant-temperature "isothermal bulk modulus"  $B_T$ :  $C_P/C_V = (\partial Q/\partial T)_P / (\partial Q/\partial T)_V = (\partial H/\partial T)_P / (\partial E/\partial T)_V = B_S/B_T = [-V(\partial P/\partial V)_S] / [-V(\partial P/\partial V)_T]$ .

## 2.10 Summary and References

Thermodynamics is distinguished from classical mechanics by the inclusion of the ideal-gas temperature in the list of state variables. The ideal gas is an integral part of all the Laws of Thermodynamics. The *Zeroth Law of Thermodynamics* states that two bodies in thermal equilibrium with a third body are in thermal equilibrium with each other. The *First Law of Thermodynamics* identifies *energy* as a state function, declaring that cyclic processes can neither create nor destroy energy. By considering reversible Carnot cycles, *entropy* can also be identified as a state function associated with the reversible flow of heat,  $dS = dQ_{\text{rev}}/T$ . The *Second Law of Thermodynamics* declares that cyclic processes cannot convert heat into work, implying that entropy cannot decrease in a thermally-isolated system. The *Third Law of Thermodynamics* affirms that *statistical calculations* of entropy, based on counting microscopic states and applying Boltzmann's  $S = k \ln W$ , agree with macroscopic *thermodynamic measurements* of entropy, based on integrating reversible heat transfers.

van der Waals' equation of state approximates the effects of attractive and repulsive forces on fluid behavior. The model provides a useful semiquantitative corresponding-states description of the gas phase, the liquid phase, the two-phase region, and the fluid region which exists above the critical temperature.

The enthalpy  $H = E + PV$ , Helmholtz free energy  $A = E - TS$ , and Gibbs free energy  $G = H - TS = A + PV = E + PV - TS$  are convenient thermodynamic potentials. These potentials represent the total energy of *composite* thermodynamic systems linked to mechanical pistons with energy  $PV$  or to heat reservoirs with energy  $-TS$ , or both.

Zemansky's *Heat and Thermodynamics* and (O. K.) Rice's *Statistical Thermodynamics* contain stimulating ideas. For more exhaustive treatments see Partington's Five-Volume classic *Treatise on Physical Chemistry* and *Physical Chemistry* by Moelwyn-Hughes. For detailed numerical solutions of the piston problems see B. Moran and W. G. Hoover, "Pressure-Volume Work Exercises Illustrating the First and Second Laws," *American Journal of Physics* 47, 851 (1979). High-pressure shockwave experiments are described by C. E. Ragan, "Ultrahigh-Pressure Shockwave Experiments," *Physical Review A* 21, 458 (1980).

### 3. Principles of Statistical Mechanics

*1 Introduction; 2 Statistical Mechanical States; 3 Volume of an N-Dimensional Sphere; 4 Gibbs' Microcanonical Ensemble; 5 Gibbs' Canonical Ensemble; 6 Lagrange-Multiplier Derivation of the Canonical Ensemble; 7 Heat-Reservoir Derivation of the Canonical Ensemble; 8 Thermodynamics from the Canonical Ensemble; 9 Maxwell-Boltzmann Velocity Distribution; 10 Equilibrium Monte Carlo Method; 11 Nosé Mechanics; 12 Nosé-Hoover Mechanics; 13 Grand Canonical Ensemble; 14 Summary and References*

#### 3.1 Introduction

The goal of Statistical Mechanics is to relate averaged macroscopic processes and properties, such as the mechanical and thermal equations of state, to underlying Hamiltonian trajectories and mechanisms. We wish to replace the detailed dynamical evolution of many degrees of freedom with equivalent phase-space averages depending upon only a few independent variables, two in the case of an equilibrium fluid with fixed composition. The idea is an appealing one. Specifying temperature and pressure, for instance, seems much simpler than following the time development of the coordinates and momenta. Statistical mechanics sets out to find the macroscopic equilibrium and nonequilibrium properties by appropriate averaging over microscopic statistical mechanical states. The weights of these states are all that is required, and these follow from the Liouville Theorem. Gibbs created the formal structure of statistical mechanics, building on the foundation laid by Maxwell and Boltzmann.

When statistical mechanics was developed by Maxwell, Boltzmann, and Gibbs there was no real alternative to statistical averaging. Because the basis of 19th and early 20th-century theories was necessarily analytic rather than computational, mechanical time averages could only be calculated for systems with independent or weakly coupled degrees of freedom. Today's computers are not only more nearly accurate, but also ten orders of magnitude faster than humans. With these machines we can follow nonlinearly coupled trajectories for millions, or even billions of time steps. No longer is time averaging difficult. Equilibrium and nonequilibrium mechanical time averages can now be as easily calculated as are the alternative statistical averages of Maxwell, Boltzmann, and Gibbs.

Away from equilibrium, linear transport theory is a well-established useful computational tool. Fick's diffusivity, Newton's viscosities, and Fourier's heat conductivity all originated as phenomenological descriptions of real materials. These nonequilibrium macroscopic models were successfully linked to Gibbs' equilibrium statistical mechanics by Green and Kubo's linear response theory, as described in Section 9.14. Nonlinear transport theory is still being developed and is not yet a reliable predictive tool. Our knowledge of nonlinear nonequilibrium problems will continue to rely on direct simulation until a workable theory is developed. For this reason the principles and applications of nonequilibrium statistical mechanics cannot be separated from the principles and applications of direct dynamic simulation. These subjects are treated in Chapters 10 and 11. In this Chapter we concentrate on Gibbs'

equilibrium statistical mechanics and an introduction to its computational implementation.

We begin with traditional derivations for the two most useful links between microscopic states and the macroscopic thermodynamic equation of state. These links are Gibbs' microcanonical and canonical ensembles. The "microcanonical ensemble" expresses the thermodynamic entropy for an isolated Hamiltonian system in terms of the number of its microstates. The formulation is summarized in Boltzmann's legacy,  $S = k \ln W$ . The fixed independent variables are composition, volume, and energy so that the end product is an expression for  $S(N, V, E)$ . This relation furnishes a complete description of the equation of state. Pressure, temperature, heat capacity, and compressibility all follow from the entropy by differentiation. Gibbs' "canonical ensemble" is an alternative approach and expresses the macroscopic Helmholtz Free Energy for any Hamiltonian system in terms of the energies of its microstates. Here the independent variables are composition, volume, and temperature. From the Helmholtz Free Energy,  $A(N, V, T)$  the remaining properties follow by differentiation.

The link between microscopic Hamiltonian mechanics and thermodynamics using Gibbs' ideas involves two steps: first, the microstates to be used in averaging and their relative weights need to be determined; second, the appropriate macroscopic thermodynamic potential, either  $S(N, V, E)$  or  $A(N, V, T)$ , needs to be expressed in terms of a weighted sum over these microscopic states. This two-step process gives a complete formal solution to the problem of expressing thermodynamic properties in terms of microscopic quantities. Because Gibbs' statistical mechanics treats only equilibrium states this picture does not resolve the paradoxical dependence of the Second Law of Thermodynamics on microscopically reversible mechanics. But statistical mechanics does provide a key connection linking *temperature* to the microscopic kinetic energy. This link, together with the Nosé-Hoover mechanics developed in Section 12, makes possible a direct derivation of the Second Law from reversible microscopic equations of motion.

It became possible to compute microscopic averages for specified Hamiltonian functions shortly after the Second World War, using the computer techniques of Monte Carlo and Molecular Dynamics simulation developed at Los Alamos and at Livermore. Except for some pathological one-dimensional problems, these first computer results were generally in quantitative agreement with Gibbs' theory.

The fundamental structure of equilibrium statistical mechanics has not changed. Gibbs' theory appears to be complete. The theory has been uniformly successful in correlating the results of experiment and computation. The basic equations have been known and used successfully for nearly a century. But it is equally true that before fast computers were available applications had to be limited to relatively simple models with uncoupled or weakly coupled degrees of freedom. Computers have made it possible to extend Gibbs' statistical treatment to large numbers of strongly-coupled degrees of freedom.

Equilibrium statistical mechanics is an unusual scientific discipline in that the basic equations are known. The main problem today, at equilibrium, lies in finding more realistic models for interatomic and intermolecular forces. This is, and will remain, an active research field, combining new computational techniques with novel experiments. Progress in models for forces draws on quantum chemistry, which deals with isolated atoms or molecules, as well as condensed matter physics, which emphasizes the collective effects inherent in bulk matter. With recipes for the forces in hand the machinery of statistical mechanics can be used to calculate equilibrium properties. But because the calculations based on Gibbs' and Boltzmann's equations are difficult, much remains to be done, both in understanding the properties of idealized Hamiltonian systems and in reproducing experimental data for real materials.

### 3.2 Statistical Mechanical States

From the conceptual standpoint the simplest equilibrium systems are "isolated systems," constant-energy systems with fixed composition and definite boundaries. Perfect isolation can best be idealized in theory or computation by eliminating altogether boundary interactions with physical container walls by considering the *periodic* boundaries shown in Figure 3.1. In such a periodic system, linear momentum, as well as mass and energy, is conserved. Angular momentum is not. Given the boundary conditions and the energy the first two tasks of equilibrium statistical mechanics are (1) to identify the available microstates, and (2) to specify state probabilities which provide phase-space averages corresponding to time averages. We begin by assuming that the system of interest is described by a Hamiltonian  $H(q,p)$ .

For such a Hamiltonian system, Liouville's Theorem provides the state weights. We saw in Section 1.11 that Hamilton's equations of motion produce an *incompressible* phase-space flow of probability density  $f(q,p,t)$ :

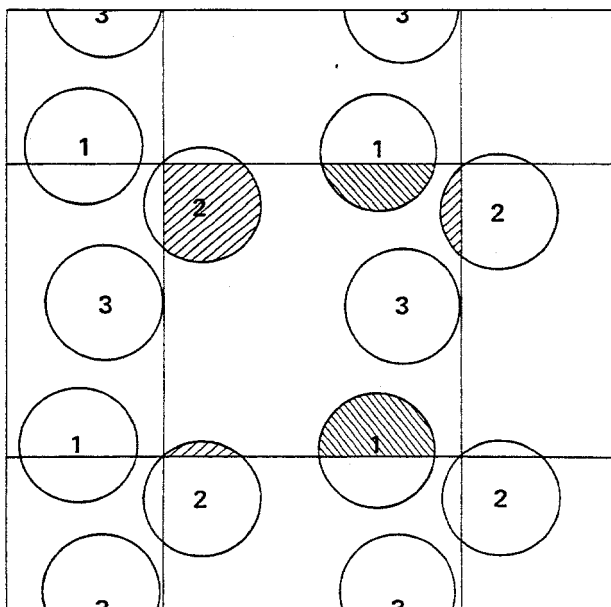


**Figure 3.1.** Two-dimensional spatially "periodic" system.

$$df(q,p,t)/dt \equiv \dot{f} \equiv (\partial f/\partial t) + \dot{q}(\partial f/\partial q) + \dot{p}(\partial f/\partial p) =$$

$$(\partial f/\partial t) + \dot{q}(\partial f/\partial q) + \dot{p}(\partial f/\partial p) + f[(\partial \dot{q}/\partial q) + (\partial \dot{p}/\partial p)] \equiv 0.$$

The probability density flows through phase space without changing, just like the density of an incompressible fluid. Because a classical isolated system provides a probability flow in phase space which conserves phase volume, *equal volumes in phase space must be assigned equal weights* in stationary equilibrium statistical averages. Thus all accessible states in the space must have equal weights.

The state weights are likewise very simple for isolated systems in quantum mechanics. In quantum systems it is generally true that equal classical phase-space volumes correspond to equal numbers of quantum states, where a quantum state is a solution of Schroedinger's Equation. Thus the analogous choice for quantum systems is to include, with equal weights, *all* the solutions of Schroedinger's time-independent Equation:

$$H\psi_i(q) = E_i\psi_i(q),$$

where  $H$  is the Hamiltonian operator, and the  $\{E_i\}$  are the energy eigenvalues, corresponding to the eigenfunctions  $\{\psi_i(q)\}$ . Bohr's Correspondence Principle states that in the "Classical Limit" (that is, when the energy levels are very closely spaced relative to the product of Boltzmann's constant and the temperature,  $kT$ ) quantum and classical calculations must agree. In this limit it is possible to show generally that a single quantum state "corresponds" to a phase volume  $h^\#$ , where  $\#$  is the number of degrees of freedom. Thus the quantum and classical recipes are consistent.

Let us consider this correspondence in more detail for a harmonic oscillator with Hamiltonian  $H = (p^2 + q^2)/2$ . In quantum mechanics the coordinate representation of the energy eigenfunctions gives a state dependent probability density for the coordinate  $q$ . Let us choose  $(h/2\pi)$ , as well as the force constant and mass, equal to unity. The oscillator energy eigenvalues are  $[n + (1/2)](h/2\pi)\omega = n + (1/2)$ . For the energy  $E_{10} = 10.5$  Figure 3.2 shows the quantum probability density  $\text{Prob}(q) = \psi^*\psi$ . In the corresponding classical case the time spent between  $q - (dq/2)$  and  $q + (dq/2)$  is proportional to  $dt = dq/\dot{q}$ . With proper normalization the classical probability density is:

$$\text{Prob}(q) = (1/\pi)[21 - q^2]^{-1/2},$$

which diverges integrably at the turning points while otherwise closely resembling a coarse-grained average of the quantum probability density.

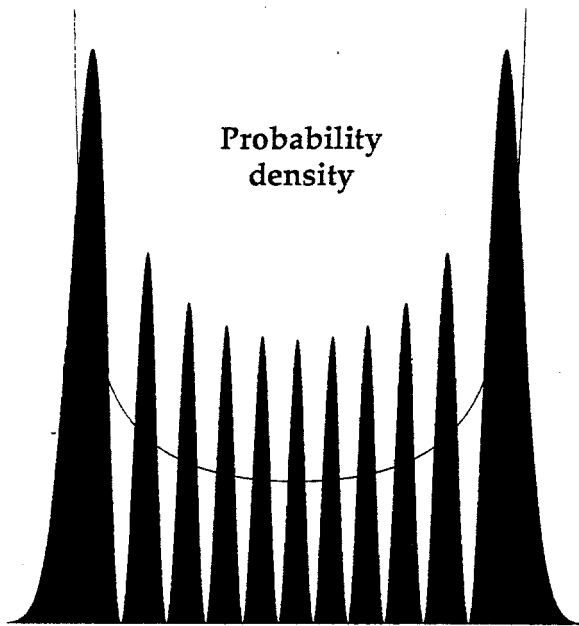


**Figure 3.2.** The quantum probability density and the classical probability density are shown for a harmonic oscillator with energy  $10.5h\nu$ .

With the classical and quantum states identified, the basic premise of statistical mechanics is that all states are to be included with equal weights. In classical equilibrium statistical mechanics the states correspond to that region of phase space which is consistent with our knowledge of the system. In quantum equilibrium statistical mechanics the states to be included are the solutions of the Schrodinger equation consistent with our knowledge of composition, volume, and energy.

It is by no means possible to prove, or even to imagine, that an isolated system could actually visit all such states. In equilibrium statistical mechanics we will make no effort to study this problem. It lacks physical relevance. Because the number of states generally increases exponentially with the number of degrees of freedom the time required for exhaustive sampling reaches the age of the universe for very small systems of from ten to a hundred particles. The possibility that a statistical mechanics based on including *all* states can make acceptable predictions relies on the smallness of fluctuations in the *available* states rather than on the certain knowledge that *all* such states are actually visited. Of course both laboratory and computer experiments are subject to similar limitations of finite observation time and finite accuracy.

The conservation of phase-space volume is responsible for the emphasis, in statistical mechanics, on Hamiltonian mechanics. The usual beginning of a statistical-mechanical problem is a statement of the governing Hamiltonian. To simplify the present Chapter we consider explicitly only atomistic systems with the simplest possible interesting Hamiltonian, a kinetic energy  $K(p)$ , coupled with a pairwise-additive potential energy  $\Phi(q)$  that depends only upon the pair separations  $\{r_{ij}\}$  :

$$H = K + \Phi ; K = \sum p_i^2 / (2m) ; \Phi = \sum \phi(r_{ij}) .$$

Such a model can provide a very accurate description of rare-gas behavior and a qualitative description of metals. Three-body potentials and the collective embedded-atom energies used to make semi-quantitative calculations for metals can be added. Simple pairwise-additive models for which complete thermodynamic information is available include the inverse power potentials  $\phi = \epsilon(\sigma/r)^n$  (ranging from the Coulomb case,  $n = 1$ , to the hard-sphere case,  $n = \infty$ ) and the Lennard-Jones potential

$$\phi = 4\epsilon[(\sigma/r)^{12} - (\sigma/r)^6],$$

as well as more specialized potentials with roughly similar shapes but with many additional parameters selected to reproduce all relevant experimental data for particular rare-gas atoms. It should be pointed out that the infinite range of the inverse power potentials is inconvenient for computer calculations, particularly for nonequilibrium simulations involving thousands or even millions of particles. The range is generally drastically reduced by using finite-range cutoff functions bringing the potential and force to zero at a distance only somewhat greater than the particle diameter  $\sigma$ . It is desirable that the force vary continuously with distance. Unless the cutoff is very smooth, so that the force varies continuously as a function of distance, the accuracy of the numerical integration can be badly degraded.

**Problem:**

Investigate the sensitivity of trajectory accuracy to force truncation and smoothness by comparing energy conservation for four potentials:  $\phi(x) = |x|$ ,  $\phi(x) = \sin(|x|)$ ,  $\phi(x) = (1/2)x^2$ , and  $\phi(x) = (1/8)(3x - |x|)^2$ . In each case begin the simulation at a turning point with  $\phi = 0.50$  and compare fourth-order Runge-Kutta solutions with 800 time steps of 0.1, 400 time steps of 0.2, and 200 time steps of 0.4 to solutions generated with the Stoermer method using 3200 time steps of 0.025, 1600 time steps of 0.050, and 800 time steps of 0.100.

To describe molecules, semiconductors, and metals more complicated interactions are required. For these the basic formalism of statistical mechanics is unchanged, but the details are complex. There are a variety of statistical ensembles, each corresponding to a particular choice of macroscopic independent variables. We will discuss the two most fundamental and useful of these ensembles, Gibbs' microcanonical and canonical ensembles, in Sections 3.4 and 3.5. But first we wish to derive a formula for the volume of a many-dimensional hypersphere. This formula, which shows that the number of microstates depends exponentially on the number of degrees of freedom, is an integral component of Gibbsian ensemble studies.

### 3.3 Volume of an N-Dimensional Unit Sphere

Consider the N-dimensional integral, over all space, of the Gaussian function  $\exp(-r^2)$ :

$$\int \dots \int \exp(-r^2) dr^N = [\int \exp(-x^2) dx]^N = \pi^{N/2} .$$

This same integral can be evaluated in polar, rather than Cartesian coordinates. Denote the hypervolume of an N-dimensional hypersphere of radius R by  $C_N R^N$ . Then the surface area of an N-1-dimensional hypersphere of radius r is  $N C_N r^{N-1}$ . Thus an alternative representation of the same integral is

$$\pi^{N/2} = \int \dots \int \exp(-r^2) dr^N = \int N C_N r^{N-1} \exp(-r^2) dr = (N C_N / 2) \Gamma(N/2) ,$$

where  $\Gamma$  is the gamma function,  $\Gamma(n+1) \equiv n!$ . We can use this result for  $C_N$ :

$$C_N = 2\pi^{N/2} / [N\Gamma(N/2)] ,$$

to work out the hypervolume of an N-dimensional hypersphere:

$$V_N = C_N R^N = 2(\pi R^2)^{N/2} / [N\Gamma(N/2)] .$$

### 3.4 Gibbs' Microcanonical Ensemble

The succinct equation on Boltzmann's gravestone,

$$S = k \ln W ;$$

where both the entropy and the number of quantum states depend on composition, volume, and energy:

$$S(N, V, E) = k \ln W(N, V, E) ,$$

is amazing. Fundamentally it relates thermodynamics to quantum mechanics, and quantum mechanics was not developed until about 20 years after Boltzmann's death. But the classical meaning of "state" as a many-dimensional phase-space volume was already well-established experimentally and had been embodied in the statistical Third Law of Thermodynamics. In the remainder of this Section we verify that Boltzmann's equation  $S = k \ln W$  provides a unique microscopic foundation for macroscopic thermodynamics. Boltzmann's entropy clearly satisfies the properties of Second-Law entropy too. The logarithm of the number of microstates  $\ln W(N, V, E)$  is certainly an extensive state function which can only increase as constraints are relaxed.

Just as in our approach to macroscopic thermodynamics the ideal gas plays a special role in microscopic statistical mechanics. We begin by calculating the number of states  $W(N,V,E)$  available for such a gas. In a three-dimensional gas of  $N$  identical mass-point particles with coordinates confined to a box of volume  $V$  and with momenta restricted to a kinetic energy  $K = E = \sum p_i^2 / (2m)$ , the number of states is given by the corresponding phase-space integral:

$$W_{\text{ideal}} = (1/h^3)^N (1/N!) \int dq^N \int dp^N = (V/h^3)^N (1/N!) \int dp^N .$$

The coordinate integration over the box of volume  $V$  is easy. The  $N!$  accounts for the permutations of  $N$  particles among  $N$  separate locations  $\{q\}$  in configuration space. If the particles are all of the same type, "indistinguishable particles," then every set of distinct coordinate values occurs  $N!$  times in the integration. The factor  $h^3$  converting phase-space volume to quantum states was established through Bohr's Correspondence Principle.

The momentum calculation is simplest if all states  $\{p\}$  with energies *below*  $E$  are included. If  $N$  is small enough for the difference to be important the result can be differentiated with respect to energy to find the number of states in an energy range  $\Delta E$ . The integral up to the energy  $E$  is the volume of a  $3N$ -dimensional hypersphere of radius  $(2mE)^{1/2}$ . This is

$$V_{3N} = C_{3N} R^{3N} = 2(2\pi m E)^{3N/2} / [3N \Gamma(3N/2)] .$$

as we established in Section 3.3.

With the ideal-gas phase-space integration worked out, all of thermodynamics can be derived by coupling such an ideal gas to other, more general systems. By imagining various reservoirs coupled mechanically to the system of interest solids under anisotropic loads can be treated just as easily as fluids. To establish the general connection between this ideal-gas phase-space volume and thermodynamics requires coupling a general system to the gas. The coupling should be weak, so as not to change the microstates available from those of a truly isolated system. Weak coupling can be imagined as a spring or thin wire infrequently linking system and gas together. For simplicity, we will here consider a fluid coupled to the gas. If the fluid-gas coupling is weak in this sense, then the total number of states  $W_T$  for the composite system, ideal gas plus fluid, can be made to approximate the product  $W_T = W_I W_F$ . If we ask for the most probable distribution of energy between the gas and the fluid it is only necessary to maximize  $W_T$  with respect to a variation in the fluid energy  $\delta E_F$ . The argument is simplest using the logarithm of  $W_T$ :

$$\delta \ln W_T = 0 = \delta E_F [(\partial \ln W_I / \partial E_F)_V + (\partial \ln W_F / \partial E_F)_V] ;$$

$$0 = \delta E_F [-(\partial \ln W_I / \partial E_I)_V + (\partial \ln W_F / \partial E_F)_V] .$$

For the most likely distribution of energy between fluid and ideal gas we find

$$(\partial \ln W_F / \partial E_F)_V = (\partial \ln W_I / \partial E_I)_V = (3/2)(N_I / E_I) \equiv 1 / (kT) ,$$

where the definition of ideal-gas temperature introduced in Chapter 1 has been used. Thus the equilibrium condition with respect to energy flow is that the fluid temperature and ideal gas temperature be equal. By including the second-derivative terms in the expansion about equilibrium it is possible to show that the fluctuations about the mean are small, of order  $N^{1/2}$ , as the Central Limit Theorem would suggest.

Suppose that we next consider the more-general possibility of an additional *mechanical* coupling between a general fluid and an ideal gas with a fixed total volume. We regard  $\ln W$  as a function of both  $V$  and  $E$ . Just as before the temperatures must be equal. The additional volume variation leads to an analogous result for the pressures:

$$(\partial \ln W_F / \partial V_F)_E = (\partial \ln W_I / \partial V_I)_E = (N/V)_I = P / (kT) .$$

Thus both temperature and pressure are equal under the conditions of thermal and mechanical equilibrium. We have determined the equilibrium properties, temperature and pressure, from the ideal-gas states, not those of the fluid with which it is in equilibrium. Thus, for a general fluid, the differential expansion of  $\ln W(V,E)$  has the same form as does the expansion of  $S(N,V,E)/k$  from thermodynamics:

$$d \ln W_F = d(S/k) = (1/kT)[dE + PdV] .$$

The additional observation that Boltzmann's entropy  $S = k \ln W$  vanishes for a nondegenerate ground state establishes that Boltzmann's entropy and the thermodynamic entropy are one and the same.

In summary, the thermodynamic entropy,  $S(N,V,E)$ , from which other properties can be obtained by differentiation, has Boltzmann's form,

$$S_{\text{Quantum}}/k = \ln W .$$

In the quantum case  $W$  is the number of quantum states with energy less than or equal to  $E$ . In the classical case,  $W$  corresponds to an integral:

$$S_{\text{Classical}}/k = \ln(1/h)^{3N} (1/N!) \int dq^N \int dp^N ; H \leq E .$$

The classical phase-space integral,

$$e^{S/k} = W(N,V,E) = (1/h)^{3N} (1/N!) \int dq^N dp^N ; H \leq E ,$$

is traditionally referred to as Gibbs' microcanonical partition function. Often it is given the special symbol  $\Omega$  rather than the  $W$  from Boltzmann's grave monument. No matter what the notation the result achieved is most remarkable. For any Hamiltonian system *all* of thermodynamics can be developed by working out the number of quantum microstates, or the corresponding classical phase-space volume,  $W$ , corresponding to the number of particles  $N$ , in the volume  $V$ , with the energy  $E$ .

### 3.5 Gibbs' Canonical Ensemble.

The word "canonical" means simplest or prototypical. Statistical calculations are indeed simplest using the canonical ensemble. Gibbs' "canonical ensemble" corresponds to a conceptual picture. It represents a thermodynamic system in equilibrium with a heat reservoir. The word "ensemble" is used in the sense of collection. Gibbs' ensemble is made up of many similar copies of the system in question, all with the same composition, volume, and reservoir temperature, but otherwise allowed to fluctuate over their accessible microstates by exchanging energy with other ensemble members. In Gibbs' picture the ensemble has so many members that fluctuations in the ensemble-averaged properties can be ignored.

In writing his two-volume text, Gibbs justified his canonical distribution, with state probabilities proportional to  $\exp(-E/kT)$ , with the observation that this distribution is uniquely appropriate to composite systems made up of independent parts with additive energies and with the same form of distribution. For independent subsystems only the exponential form, additive in the energy, will do:

$$\exp(-E_{\text{Total}}/kT) = \prod \exp(-E_{\text{System}}/kT) = \exp(-\sum E_{\text{System}}/kT) .$$

Of course, Gibbs was right. But it is educational to see in more detail how the exponential canonical form arises. We will therefore consider two alternative ways of "deriving" Gibbs' distribution of ensemble members over their states by considering a composite constant-energy system. Satisfied that the distribution is correct we then will discuss two very different types of numerical methods for simulating the properties of the ensemble. Chapter 4 is devoted to applications of Gibbs' microcanonical and canonical ensembles.

### 3.6 Lagrange-Multiplier Derivation of the Canonical Ensemble

Let us first take the conceptual picture underlying Gibbs' Ensemble literally and link together many replicas of the system of interest, all with the same composition and volume, but with individual energies free to fluctuate in such a way that the total energy  $E_{\text{Total}}$  is fixed. See Figure 3.3. If the number of ensemble members  $N_{\text{Total}}$  is large enough, it is plausible that a steady state will be reached. In such a steady state

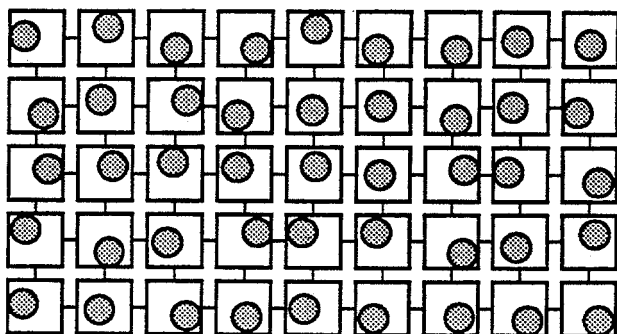


**Figure 3.3.** Gibbs “Canonical Ensemble” of weakly-coupled systems. This artificial coupling can be avoided by using Nosé-Hoover mechanics.

we denote the number of ensemble members in a particular energy state  $i$ , with energy  $E_i$ , by  $N_i$ . We imagine that the ensemble contains so many members  $N_{\text{Total}}$  that the fluctuations in the  $\{N_i\}$ , which are of order  $N_i^{1/2}$ , can be neglected. Such a steady state must correspond to an equilibrium condition because the ensemble is an isolated system. By symmetry the time-averaged properties of all members of such an ensemble are identical to the equilibrium properties. We will next find the  $\{N_i\}$ .

A mathematical treatment of this problem can be based on Lagrange multipliers, where the multipliers are used to impose the two constraints of fixed ensemble membership and fixed total energy:

$$\sum N_i = N_{\text{Total}} ; \sum N_i E_i = E_{\text{Total}} .$$

For convenience in notation we use the energy-state sums. These would be exactly correct for quantum systems. The corresponding classical integrals can be viewed as the limit of a sequence of approximate phase-space sums in which the phase-space hypervolume corresponding to a microstate with  $\#$  degrees of freedom,  $(dqdp)^\# = h^\#$  approaches zero.

Consider a particular distribution  $\{N_i\}$  of the ensemble members among the energy states  $\{E_i\}$ . The  $N_{\text{Total}}$  members can be distributed over these states in

$$W(\{N_i\}) = N_{\text{Total}}! / \prod N_i!$$

ways, provided that the  $\{N_i\}$  satisfy the total membership and energy constraints. The maximum and the most probable states coincide as  $N_{\text{Total}}$  is increased. At the optimum equilibrium composition any variation of  $W$ , and hence  $\ln W$  must vanish:

$$\delta \ln W(\{N_i\}) = 0 = -\delta \sum \ln N_i! \rightarrow -\delta \sum N_i \ln(N_i/e) = -\sum \ln N_i \delta N_i = 0 ,$$

where we have used the approximation  $\ln N_i! \rightarrow \int \ln x dx \rightarrow N_i \ln(N_i/e)$ , ignoring corrections with variations that vanish for large  $N$ . Again the variation is subject to the two constraints,

$$\Sigma \delta N_i = 0 ; \Sigma E_i \delta N_i = 0 .$$

To solve this variational problem the constraints on the  $\{\delta N_i\}$  are first multiplied by arbitrary Lagrange "multipliers"  $\alpha$  and  $\beta$  and then combined with the variational equation. The result is

$$\Sigma [-\ln(N_i) - \alpha - \beta E_i] \delta N_i = 0 .$$

The reason for this operation is to remove the two inconvenient restrictions that the  $\{\delta N_i\}$  must satisfy. We can select values of the two multipliers  $\alpha$  and  $\beta$  which force the *first two* terms in the sums to vanish (the terms involving  $\delta N_1$  and  $\delta N_2$ ) at the equilibrium composition:

$$\ln N_1 + \alpha + \beta E_1 = \ln N_2 + \alpha + \beta E_2 = 0 .$$

The variational problem then becomes simpler because the variations of the remaining  $\{\delta N_i\}'' = \{\delta N_3, \delta N_4, \delta N_5, \dots\}$ , where the double prime indicates that the first two terms are missing, are no longer restricted:

$$\Sigma'' [\ln N_i + \alpha + \beta E_i] \delta N_i = 0 ,$$

Thus the remaining variations  $\{\delta N_{i \geq 3}\}$  are completely arbitrary. We could choose, for instance, to have all of the  $\delta N_i$  but one equal to zero. Because the one nonzero  $\delta N_i$  could be any of them, the sum over the complete set can vanish only if every one of the variational coefficients multiplying the  $\{\delta N_i\}$  vanishes:

$$\{\ln N_i + \alpha + \beta E_i\} = 0 ,$$

so that the most likely distribution satisfies this equality for all  $i$ , not just  $i = 1$  and  $2$ . Choosing  $\alpha$  to fix the total number of members at  $N_{\text{Total}}$  we compute the probability of finding a particular member in state  $i$ . The solution of this variational problem is

$$\text{prob}_i = N_i / N_{\text{Total}} = \exp[-\beta E_i] ,$$

agreeing with Gibbs' statement that the distribution among the energy microstates is exponential.

### 3.7 Heat-Reservoir Derivation of the Canonical Ensemble

An alternative derivation of this same exponential result for the distribution of members among microstates can be based on a thought experiment equilibrating a

single system with a reservoir. The reservoir could be composed of many replicas of the system of interest and would then be equivalent to the ensemble just treated. To emphasize the generality of the result we instead consider an ideal-gas heat reservoir. We indicate the total energy, reservoir energy plus system energy, by  $E_T = E_R + E_S$ . We imagine the reservoir has many degrees of freedom  $N$  so that  $N!$  can again be replaced by  $(N/e)^N$  with negligible error. Then the number of reservoir microstates approaches

$$W_R = (Ve/Nh^3)^N (4\pi m E_R / 3N)^{3N/2}.$$

For large  $N$  the reservoir can have arbitrarily many states with such a large energy  $E_R = 3NkT/2$  that the Taylor's series expansion,

$$\begin{aligned} \ln W_R(E_T - E_S) &= \\ \ln W_R(E_T) - (d \ln W_R / dE) E_S + (1/2) (d^2 \ln W_R / dE^2) E_S^2 + \dots \\ &= \ln W_R(E_T) - (3N/2E_R) E_S + (3N/4E_R^2) E_S^2 + \dots, \end{aligned}$$

can be truncated after the term linear in  $E_S$ . The quadratic terms shown above vanish as  $1/N$ . Thus the number of states available to the composite system when the single system is in a definite state  $i$ , with energy  $E_S = E_i$ , is

$$W_T = W_R(E_T) \exp[-E_i/kT],$$

and the normalized probability of observing the  $i$ th state is again

$$\text{prob}_i = \exp[-E_i/kT] / \sum \exp[-E_j/kT].$$

This result can be generalized to include "degenerate states," states with the same energy, which taken together compose an energy "level." An example would be the  $(2L + 1)$  equal-energy states of a rigid rotor with angular momentum quantum number  $L$ . If  $g_j$  such "degenerate" states all have the same energy  $E_j$  then the "level probability"  $\text{prob}_j$  has the form:

$$\text{prob}_j = g_j \exp[-E_j/kT] / \sum g_i \exp[-E_i/kT].$$

In the next Section we use this exponential canonical distribution over energy states to derive all of macroscopic thermodynamics.

### 3.8 Thermodynamics from the Canonical Ensemble

Just as the microcanonical distribution relates the number of microstates to the entropy, Gibbs' canonical distribution relates an exponential energy sum over these states,  $\sum \exp(-E_i/kT)$ , to the Helmholtz free energy of thermodynamics. This sum is the canonical "Partition Function" or "Zustandsumme"  $Z(N,V,T)$ :

$$Z(N,V,T) = \sum \exp(-E_i/kT) .$$

The sum over states describes the way in which systems are partitioned among their states. It is the normalization for the state probabilities,

$$\text{prob}_i = \exp(-E_i/kT) / \sum \exp(-E_j/kT).$$

This sum is useful because its logarithmic derivatives with respect to temperature and volume have the form of ensemble averages with probabilities  $\{\text{prob}_i\}$ . The temperature derivative of  $\ln Z$  gives directly the mean value of the internal energy:

$$(\partial \ln Z / \partial \ln T)_{N,V} = \sum (E_i/kT) \exp(-E_i/kT) / \sum \exp(-E_i/kT) = \langle (E_i/kT) \rangle .$$

Differentiating once more, we can find the derivative of the average energy with respect to temperature, the constant-volume heat capacity,  $C_V$ :

$$\begin{aligned} (1/k)(\partial \langle E \rangle / \partial T)_V &= C_V/k = (\partial / \partial T)(T \partial \ln Z / \partial \ln T)_{N,V} = \\ &= \frac{[\sum \exp(-E_j/kT)] \{ \sum (E_i/kT)^2 \exp(-E_i/kT) \} - \{ \sum (E_i/kT) \exp(-E_i/kT) \}^2}{[\sum \exp(-E_i/kT)]^2} \\ &= C_V/k = \langle (E/kT)^2 \rangle - \langle (E/kT) \rangle^2 = \langle [(E/kT) - \langle E/kT \rangle]^2 \rangle . \end{aligned}$$

We see that the heat capacity is an intrinsically positive measure of energy fluctuations. A negative heat capacity would signal thermal instability. If colder materials would grow cooler still in the presence of hotter ones a homogeneous temperature field would be impossible and thermal equilibrium could not be established.

#### Problems:

1. Calculate the canonical-ensemble temperature dependence of the heat capacity for a single pendulum using the fourth-order Runge-Kutta method. Set the pendulum length and mass, Boltzmann's constant, and the gravitational field strength all equal to unity and study the temperature range from 0 to 4. The heat capacity can be calculated in either of two ways: by working out values of the energy for two temperatures separated by  $dT$  or by evaluating both  $\langle E \rangle$  and  $\langle E^2 \rangle$  and applying the conventional fluctuation formula,  $C_V/k = \langle (\Delta E/kT)^2 \rangle$ .

Compare the *first* of these to the microcanonical heat capacity obtained by time-averaging  $mv^2/2$  for two complete orbits corresponding to closely-spaced values of the energy.

2. Molecular dynamics simulations show that the constant-volume heat capacity of a dense cool periodic system with attractive *Gaussian* interactions [ $\Phi = \sum \phi = -\sum \exp(-r^2)$ ] is negative. That is, increasing the energy  $E = K + \Phi$ , results in a *decreased* kinetic energy  $K$ . Does this result contradict the energy-fluctuation formulation of the constant-volume heat capacity,  $C_V/k = \langle (\Delta E/kT)^2 \rangle$ ?
3. Consider the isoenergetic classical one-dimensional motion of a single particle in the potential  $\phi(x)$  with  $\phi(|x| < L/4) = -|\epsilon|$ ;  $\phi(L/4 < |x| < L/2) = 0$ ;  $\phi(L/2 < |x|) = \infty$ . Discuss the behavior of the ideal gas temperature  $\langle mv^2/k \rangle$  in the energy range near  $E = \phi + K = 0$ .

The derivative of the canonical partition function with respect to volume also has a simple physical significance. Because the energy states depend on volume through the boundary conditions, the volume derivative gives directly the ensemble average of the energy response to an infinitesimal volume change:

$$\begin{aligned} (\partial \ln Z / \partial \ln V)_{N,T} &= \langle -(V/kT)(dE_i/dV) \rangle = \\ &= \frac{\sum -(V/kT)(dE_i/dV) \exp(-E_i/kT)}{\sum \exp(-E_i/kT)} \end{aligned}$$

This volume derivative gives the pressure:

$$(\partial \ln Z / \partial \ln V)_{N,T} = \langle PV/kT \rangle .$$

The “Virial Theorem” provides a detailed mechanical force-based description of this link between the microscopic energy and the macroscopic pressure. This link is discussed in detail in Section 5.5. The volume deformation process can be elaborated to the case of an elastic solid and the *second* derivatives of the partition function with respect to the elastic strains can then be calculated, giving the elastic constants in terms of fluctuations in the pressure tensor. We describe a simpler and more direct approach to the elastic constants in Chapter 5.

These temperature and volume derivatives make it possible to relate the canonical partition function to the Helmholtz free energy,  $A = E - TS$ , for which the corresponding derivatives of  $A/T$  are

$$\begin{aligned} d(A/T) &= [(\partial(A/T)/\partial V)_T]dV + [(\partial(A/T)/\partial T)_V]dT \\ &= -(P/T)dV - (A/T^2)dT - (S/T)dT = -(P/T)dV - (E/T^2)dT . \end{aligned}$$

Thus the canonical partition function is the exponential of  $-A/kT$ . This relation is arguably the most useful link between the microscopic and macroscopic descriptions of equilibrium properties.

This same result becomes obvious from the definition of the partition function  $Z(N,V,T)$  if we write it as a sum over finite energy intervals, with  $E - (\Delta E/2) < E_i < E + (\Delta E/2)$ :

$$Z \approx \sum W(N,V,E,\Delta E)e^{-E/kT},$$

with the energy in the exponent an appropriate average for the range  $\Delta E$  about  $E$ . If we use Boltzmann's relation for the number of states  $W = \exp(S/k)$  and keep only the maximum term in the sum, the resulting approximate partition function becomes

$$Z(N,V,T) \approx \exp(S/k)\exp(-E/kT) \equiv \exp(-A/kT).$$

The classical form corresponding to the quantum sum is

$$Z(N,V,T) = (1/N!h^{\#}) \int \dots \int dq^{\#} dp^{\#} \exp[-H(q,p)/kT] = \exp(-A/kT).$$

We conclude that the Helmholtz free energy  $A = E - TS$  can be calculated from a knowledge of the Hamiltonian by working out either the sum over quantum states or the corresponding classical phase integral. This "working out" is not so easy. In fact accurate quantum states are not available for systems containing more than a few electrons and it is impractical to work out classical phase integrals involving more than perhaps  $10^{10}$  sampling points. In order to use the canonical-ensemble expression for thermodynamic properties special numerical methods need to be developed.

We will outline three useful numerical schemes, one static and two dynamic in this Chapter. All three of these schemes rely on the separability of the Hamiltonian into kinetic and potential parts. The separation implies that the velocity distribution always has the universal Maxwell-Boltzmann distribution. This useful distribution is the subject of the next Section.

3.9 Maxwell-Boltzmann Velocity Distribution

For a separable Hamiltonian  $H = K + \Phi$  with a kinetic energy  $K(p)$  depending solely on the momenta and a potential energy  $\Phi(q)$  depending solely on coordinates, the momentum probability distribution is independent of configuration and its contribution to the Helmholtz free energy has the ideal-gas form. This simplifies numerical work. To determine the configurational part of the Helmholtz free energy sampling can be carried out in configuration space with a probability proportional to the configuration dependent part of the Boltzmann probability,  $\exp[-\Phi(q)/kT]$ . In the

microcanonical case the weighting function is different, and is proportional to the momentum-space hypersphere volume,  $(E - \Phi)^{3N/2}$ .

The canonical distribution for the momenta,

$$\text{Prob}(\{p\}) = \prod (2\pi mkT)^{-1/2} \exp(-p^2/2mkT),$$

can be used to work out all the moments of the distribution. Let us consider two different ways to work out the average value of  $p^4$  for a single two-dimensional ideal-gas molecule. In ordinary Cartesian coordinates the product becomes

$$\langle p^4 \rangle = \langle p_x^4 + 2p_x^2 p_y^2 + p_y^4 \rangle = (mkT)^2 [3 + 2 + 3].$$

In polar coordinates the same average can be written as the ratio of two integrals:

$$\langle p^4 \rangle = \int p^5 dp \exp(-p^2/2mkT) / \int p dp \exp(-p^2/2mkT) = 8(mkT)^3 / (mkT).$$

### Problem:

Use the hypersphere volume formula from Section 3.3 to find the microcanonical probability density for a single momentum to lie in the range  $dp$  about  $p$  in a system with  $N$  degrees of freedom and kinetic energy  $E$ . Show that the large- $N$  form of this microcanonical probability density is proportional to the corresponding canonical one, with  $\langle K \rangle_{\text{Canonical}} = K_{\text{Microcanonical}}$ , and hence must coincide with it.

### 3.10 Equilibrium Monte Carlo Method

The goal of equilibrium statistical mechanics is to express any observable quantity as the average of a corresponding microstate function. In quantum mechanics observables correspond to operators and the expectation value of such an observable is computed by averaging the corresponding operator over the quantum probability density. In classical statistical mechanics the phase-space function corresponding to the observable  $\text{Obs}(q,p)$  has to be averaged over properly-weighted microstates. In the canonical ensemble, with the state weights known,  $\{\exp(-E_i/kT)\}$ , it is a relatively easy matter to generate microstates with frequencies proportional to these weights. If such states were generated by making random "Monte-Carlo" trials and weighted averages were computed the averages would eventually converge to the canonical-ensemble average:

$$\langle \text{Obs}(q,p) \rangle = \frac{\sum \text{Obs}_i \exp(-E_i/kT)}{\sum \exp(-E_i/kT)}.$$

This straightforward form of averaging is impractical for most interesting systems with more than a few degrees of freedom because most parts of phase space have

negligible probability. An example illustrates this point: we will see that the ratio of the occupied to the unoccupied parts of configuration space  $\{r^N\}$  is about  $(1/400)^N$  for a dense three-dimensional fluid, so that a billion Monte-Carlo trial configurations are unlikely to result in even a single acceptable configuration for as few as half a dozen such particles. Random sampling is hopelessly inefficient. A *modified* Monte Carlo sampling method was invented at Los Alamos and applied to the hard-disk equation of state by Metropolis, the Rosenbluths, and the Tellers. It is a simple workable scheme based on sampling relatively small energy changes ( $\Delta\Phi \approx kT$ ) in configuration space with relative probabilities proportional to  $\exp(-\Phi_i/kT)$  so that explicit weights are not needed:

$$\langle \text{Obs} \rangle_{\text{MRT}} = \sum \text{Obs}_i / \sum 1 .$$

Provided that the chain of samples generated is not sensitive to the initial conditions, the statistical uncertainties should obey the Central Limit Theorem of Section 2.1, varying as the inverse square root of the number of configurations sampled. The uncertainty is most conveniently estimated by breaking up the calculation into a small number of batches, 5 or 10, and using these as independent estimates of the mean value. The mean squared fluctuations, divided by the number of batches minus one, can then be used to estimate the square of the statistical errors. The chain of Monte Carlo configurations is generated through a sequence of biased moves. Any move *decreasing* the potential energy is accepted. Those moves which would *increase* the potential energy are accepted with a probability  $\exp(-\Delta\Phi/kT)$ . This scheme guarantees long time convergence to a probability density proportional to  $\exp(-\Phi/kT)$ .

Let us demonstrate the Monte Carlo scheme with a thought experiment in which we follow the progress of an ensemble of systems able to occupy two states with corresponding weights  $(2/3)$  and  $(1/3)$ . If we begin with all systems in the ground state all systems attempt the transition to the upper level, and half are successful, leaving state populations after the first trial of  $(0.5, 0.5)$ ; after two trials the populations are  $(0.75, 0.25)$ ; and after three  $(0.625, 0.375)$ . These are enough data for us to guess, correctly, that the lower state population after  $n$  trials is  $(2/3) + (1/3)(-1/2)^n$ , so that the state populations converge exponentially to their equilibrium values.

The Monte Carlo method requires "random" numbers. A simple function generating these on the interval from 0 to 1 is the following:

```

FUNCTION RANDOM(IX, IY)
  I = 1029*IX + 1731
  J = I + 1029*IY + 507*IX - 1731
  IX = MOD(I, 2048)
  J = J + (I-IX)/2048
  IY = MOD(J, 2048)
  RANDOM = (IX+2048*IY)/4194304.0
  RETURN
END

```

The first time, and *only* the first time, this function is called the two arguments IX and IY should be set equal to zero. A Monte Carlo program to implement the Metropolis-Rosenbluths-Tellers procedure proceeds according to the following plan:

- (1) CHOOSE INITIAL N-PARTICLE CONFIGURATION, MAXIMUM MOVE SIZE, AND SET IX AND IY EQUAL TO 0.
- (2) GENERATE A RANDOM NUMBER  $R = \text{RANDOM}(IX, IY)$  AND CHOOSE PARTICLE  $(N \cdot R + 1)$  FOR A TRIAL MOVE.
- (3) TENTATIVELY MOVE THIS PARTICLE FROM ITS "OLD" LOCATION TO A NEW ONE AND COMPUTE THE RESULTING CHANGE IN CONFIGURATIONAL PROBABILITY  $\text{EXP}(-\Delta\Phi/KT)$ .
- (4) GENERATE ANOTHER RANDOM NUMBER  $R = \text{RANDOM}(IX, IY)$  AND ACCEPT THE TENTATIVE MOVE IF R IS LESS THAN  $\text{EXP}(-\Delta\Phi/KT)$ ; OTHERWISE REJECT THE MOVE.
- (5) UPDATE AVERAGES, USING THE "OLD" LOCATION AGAIN IF THE TENTATIVE MOVE WAS REJECTED, AND THE "NEW" LOCATION OTHERWISE.
- (6) GO TO 2 UNTIL RESULTS FROM SUFFICIENTLY MANY MOVES ARE ACCUMULATED.

### Problems:

1. Test the random-number generator  $\text{RANDOM}(IX, IY)$  by computing the moments  $\langle R_i \rangle$ ,  $\langle R_i^2 \rangle$ , and  $\langle R_i^3 \rangle$ . Also check the "serial correlation" by computing the averages  $\langle R_i R_{i+1} \rangle$  and  $\langle R_i R_{i+2} \rangle$ . Generate sufficiently many "random" numbers  $\{R_i\}$  that these averages have an expected error of no more than 1%. Show, numerically, that the generator repeats after  $2^{22} = 4,194,304$  calls.
2. Construct two Metropolis-Rosenbluth<sup>2</sup>-Teller<sup>2</sup> canonical-ensemble Monte-Carlo programs for the harmonic oscillator Hamiltonian  $H = (q^2 + p^2)/2$ , one in the full phase space and the second only in coordinate space. Use jump lengths of  $\{0.5, 1.0, 2.0, 4.0, 8.0\}(R - 0.5)$ , where R is randomly distributed between 0 and 1 for the trial moves. Verify that  $\langle p^2 \rangle = 1$  in both cases and discuss the possibility of using  $\langle p^4 \rangle$  to decide which jump length is "best."
3. Check the single-pendulum canonical-ensemble heat-capacity at temperatures of 0.25, 1, 2, 3, and 4 by working out  $\langle E \rangle$  and  $\langle E^2 \rangle$  by Monte Carlo sampling. Choose the pendulum length and mass as well as the gravitational field strength and Boltzmann's constant all equal to unity. The values should be close to the values calculated in Problem 1 of Section 3.8 using the Runge-Kutta method:  $\{C_V/k\} = \{0.615, 0.354, 0.114, 0.053, 0.031\}$ .

Soon after fast computers were developed both Monte Carlo and molecular dynamics were applied to the same relatively difficult thermodynamic problem, the

equation of state of hard disks. The Monte Carlo method is an effective computational statistical-mechanical technique for simulating *equilibrium* thermodynamic properties. In the absence of constraints the equilibrium velocity distribution is the Maxwell-Boltzmann distribution. As a consequence, the equilibrium Monte Carlo approach is marginally simpler to program because velocities are unnecessary. Until 1974, when useful thermodynamic perturbation theories began to be developed, as described in Section 4.14, computational statistical mechanics focussed on equilibrium simulations for which the Monte Carlo method is particularly useful.

As computers became more powerful and as the ability to predict equilibrium properties improved, researchers' interest turned toward nonequilibrium problems and transport theory. Away from equilibrium the velocity distribution and the phase-space weights are not known. There is no perturbation theory away from equilibrium. For nonequilibrium applications a dynamical approach is essential. Such an approach can be based on Nosé-Hoover mechanics, as is discussed in the next two Sections. The more limited but straightforward method of Newtonian simulation is described in Chapters 5 and 6.

### 3.11 Nosé Mechanics

Newtonian mechanics is tied to the initial energy. To introduce temperature either Gauss', Lagrange's, or Nosé and Hoover's ideas need to be followed. Of these three approaches only Gauss' and Nosé and Hoover's appear to be useful for nonequilibrium systems. Because Gauss' mechanics can be viewed as a special case of Nosé-Hoover mechanics, we will emphasize that mechanics in exploring the link between Gibbs' ensemble theory and dynamical simulation.

In 1984 Nosé introduced a special Hamiltonian,

$$H_{\text{Nosé}} = K(p)/s^2 + \Phi(q) + (\# + 1)kT \ln s + (p_s^2/2Q),$$

in which the usual phase-space variables  $\{q, p\}$  are augmented by a new [dimensionless] variable  $s$  and its conjugate momentum [with units of action,  $ML^2/T$ ]  $p_s$ . Here we again use  $\#$  to indicate the number of degrees of freedom.  $Q$  is a parameter [with units  $ML^2$ ] determining the coupling strength between the phase-space variables and  $s$ . Nosé showed that *microcanonical* ensemble averages for his new Hamiltonian are equivalent to *canonical* ensemble averages over the coordinates  $q$  and the "scaled" momenta  $p/s$ . In this Section we reproduce Nosé's derivation, writing the integral of the microcanonical phase-space probability over the new pair of conjugate variables  $s$  and  $p_s$ ,

$$\Delta W(N, V, E, q, p) = (1/N! h^\#) dq^\# dp^\# \int ds dp_s \delta(H(q, p, s, p_s) - E),$$

first in terms of new momenta,  $p' = p/s$ . This introduces a factor  $s^\#$  into the integral. Then the delta function restricting the Nosé Hamiltonian to the value  $E$  is written in terms of the variable  $s$ :

$$\delta(H(q,p',s,p_s) - E) \equiv (\partial s / \partial H) \delta(s - \exp[E - K' - \Phi - (p_s^2/2Q)] / [\# + 1]kT).$$

When the  $s$  integration is carried out and followed by integration over  $p_s$ , the resulting probability density for the coordinates  $\{q\}$  and scaled momenta  $\{p'\}$  is exactly the canonical distribution. The idea of introducing a new variable so that the microcanonical distribution becomes canonical is a clever one. Unfortunately the "time scaling," or equivalently "mass scaling," required to carry out the momentum integration complicates the interpretation of the corresponding Hamiltonian dynamics. But Nosé's time scaling is computationally cumbersome, unsuited to nonequilibrium simulations, and can be avoided entirely by using the modification described in the next Section.

### 3.12 Nosé-Hoover Mechanics

Working in Canada, with Mike Klein, Nosé invented, or discovered, a new form of mechanics which can generate Gibbs' canonical phase-space distribution. A simpler, more direct approach is to start out with *new equations of motion* rather than a new Hamiltonian:

$$\dot{q} = p/m; \dot{p} = F(q) - \zeta(q,p)p; \dot{\zeta} = ?,$$

and to ask the question "What must the *time development* of the friction coefficient  $\zeta$  be in order to generate the canonical distribution when these equations of motion are solved?" It is straightforward to answer that question by studying the flow of probability density in an extended phase space in which the new variable  $\zeta$  defines one of the axes. The continuity equation in this extended  $(2\# + 1)$ -dimensional phase space is the analog of Liouville's flow equation:

$$(\partial f / \partial t) + \partial(f\dot{q}) / \partial q + \partial(f\dot{p}) / \partial p + \partial(f\dot{\zeta}) / \partial \zeta = 0,$$

where  $f(q,p,\zeta)$  is the product of the usual canonical probability density and an unknown function  $g(\zeta)$  depending on  $\zeta$  alone. For the canonical distribution to be steady  $(\partial f / \partial t)$  must vanish. The three remaining terms must therefore sum to zero:

$$\partial(f\dot{q}) / \partial q + \partial(f\dot{p}) / \partial p + \partial(f\dot{\zeta}) / \partial \zeta =$$

$$\{(p/m)[F(q)/kT]f\} + \{[F(q) - \zeta p](-p/mkT)f - \zeta f\} + \{\dot{\zeta}(d \ln g / d \zeta)f\} = 0.$$

The terms involving the interparticle forces cancel. In order for the resulting equation to have a steady solution  $g$  must be a Gaussian,

$$g = C \exp(-\zeta^2 \tau^2 / 2),$$

so that the complete steady-state distribution function is Gibbs' canonical distribution augmented by a Gaussian distribution in the friction coefficient:

$$f(q,p,\zeta) = \exp[-H(q,p)/kT] \exp[-\zeta^2 \tau^2 / 2].$$

The relaxation time  $\tau$  can be chosen arbitrarily, and  $\zeta$  must itself be determined by the feedback equation:

$$\dot{\zeta} = (1/\tau^2) \Sigma[(p^2/mkT) - 1].$$

This last equation is an example of "integral feedback," with a "control variable," the friction coefficient  $\zeta$ , given by the time integral of the discrepancy between the actual and the average kinetic energy. The system of differential equations is time reversible, due to its Hamiltonian basis, and preserves the canonical distribution in the phase space. Notice that in the time-reversed trajectory  $\zeta$ , which originated as the momentum conjugate to  $s$ , changes sign in the same way as do the other momenta  $\{p\}$ .

### Problems:

1. Show that the augmented canonical Gibbs distribution  $f(q,p,\zeta)$  is a steady solution if the Nosé-Hoover friction coefficient  $\zeta$  applies to only a *subset* of the equations of motion,  $\{\dot{p} = F(q) - \zeta p\}_s$ , while the *rest* obey the Hamiltonian motion equations,  $\{\dot{p} = F(q)\}_r$ . Assume that only the kinetic energy of the subset is used in computing  $\zeta$ :  $\dot{\zeta} = (1/\tau^2) \Sigma_s[(p^2/mkT) - 1]$ .
2. Show that the augmented canonical Gibbs distribution  $f(q,p,\zeta)$  is a steady solution of the equations of motion if the *weighted* Nosé-Hoover friction coefficient  $\zeta w(q)$  applies to *all* degrees of freedom,  $\{\dot{p} = F(q) - \zeta w(q)p\}$ , even if the weight function is nonzero in only a small region. Assume that the *weighted* kinetic energy is used in computing  $\zeta$ :  $\dot{\zeta} = (1/\tau^2) \Sigma w(q)[(p^2/mkT) - 1]$ .

Notice that in *both* these problems it is possible to prove that the canonical distribution is *a* steady solution, but not necessarily *the* steady solution of the Nosé-Hoover equations of motion. If a system is not sufficiently mixing in phase space (one-dimensional problems often lack mixing; the harmonic oscillator is an example) regular periodic orbits can exist, even in a thermostatted system. For mixing systems no such orbits are stable.

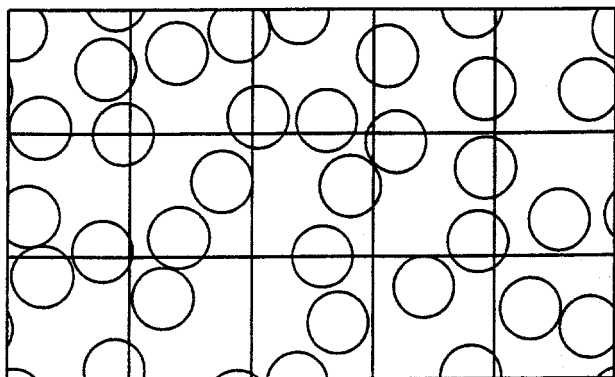


**Figure 3.4.** Gibbs' "Grand Canonical Ensemble" can be viewed as a set of weakly-coupled systems which exchange mass, momentum, and energy. The illustration shows 15 such systems with an average of two particles each.

### 3.13 Grand Canonical Ensemble

The Grand Canonical ensemble is an extension of the canonical ensemble and is useful for problems in which the composition of the system is variable. Typical applications include the dissociation and recombination of polyatomic molecules linked by chemical equilibria involving two or more reacting species. The grand canonical ensemble then resembles a canonical ensemble except that the coupled systems can exchange particles. See Figure 3.4. If we consider the most likely state of a composite system composed of two parts which can exchange *particles*, so that  $N$  varies, the usual Lagrange-multiplier derivation leads to the result:

$$\exp(PV/kT) = \sum Z(N,V,T)z^N,$$

which allows us to compute the pressure as a function of  $V$ ,  $T$ , and the thermodynamic activity,  $z$ , by summing over the number of particles,  $N$ . The "activity"  $z_i$  describes the work of changing the composition of a system by adding a particle of type  $i$ . The "chemical potential,"  $\mu_i$ , can be formally defined as the partial derivative of the Helmholtz free energy with respect to  $N_i$ ,  $\mu = (\partial A / \partial N)_{V,T}$ , and  $z_i = \exp(\mu_i/kT)$ . We consider examples using the Grand Canonical Ensemble in Sections 4.10–4.12.

### 3.14 Summary and References

Liouville's Theorem states that the comoving phase-space probability density is unchanged in Hamiltonian flows. For an isolated system this result implies that all accessible phase space *volumes* are equally likely. Thus equal phase-space volumes represent equally-likely mechanical states. In Bohr's *Correspondence Limit* a quantum state corresponds to a classical phase-space hypervolume  $h^\#$ , where  $\#$  is the number of degrees of freedom. Boltzmann's exact link between mechanics and thermodynamics,  $S(N,E,V) = k \ln W$ , is formalized in Gibbs' microcanonical ensemble. By considering a small weakly-coupled part of a larger isolated system, Gibbs constructed the canonical ensemble, with energy states  $\{E_i\}$  and state weights  $(1/Z)\exp(-E_i/kT)$ . Nosé discovered a

deterministic time-reversible version of Hamiltonian mechanics, incorporating integral feedback, which reproduces these canonical-ensemble state weights. The simpler and more-efficient Nosé-Hoover approach avoids cumbersome "time-scaling" and likewise reproduces the canonical distribution. The normalization  $Z$  of the canonical-ensemble state probabilities is the canonical partition function ("Zustandsumme")  $Z(N,V,T) = \sum \exp(-E_i/kT) = \exp(S/k) \exp(-E/kT) \equiv \exp(-A/kT)$ .

The most useful statistical mechanics texts are the Mayers' *Statistical Mechanics*, McQuarrie's *Statistical Thermodynamics*, and Reif's *Statistical and Thermal Physics*. The many-body molecular-dynamics simulations resulting in a negative heat capacity are discussed in H. A. Posch, H. Narnhofer, and W. Thirring, "Computer Simulation of Collapsing Systems" in *Simulation of Complex Flows*, Proceedings of the 1989 Brussels NATO Advanced Study Institute (M. Mareschal, Editor, Plenum Press, New York).

## 4. Applications of Equilibrium Statistical Mechanics

*1 Introduction; 2 Tonks' One-Dimensional Hard-Rod Gas; 3 One-, Two-, and Three-Dimensional Ideal Gases; 4 Two- and Three-Dimensional Rigid Rotors; 5 One-Dimensional Vibrator; 6 One-Dimensional Harmonic Chain; 7 Two- and Three-Dimensional Quasiharmonic Crystals; 8 Einstein and Debye Models; 9 Three-Dimensional Polyatomic Molecules; 10 Chemical Reactions; 11 Phonons and Photons; 12 Electrons in Metals; 13 Mayers' Virial Expansion of Thermodynamic Properties; 14 Thermodynamic Perturbation Theory; 15 Summary and References*

### 4.1 Introduction

From the standpoint of mechanics, equilibrium properties are simply time averages, with microscopic dynamics providing the mechanism underlying macroscopic averaged observable quantities. Gibbs' statistical mechanics provides an alternative to time averages: exact ensemble formulae linking microstates and their energies to macroscopic observable properties including the thermodynamic equation of state. In this Chapter we consider a range of idealized problems suited to analytic work based on Gibbs' ideas. These problems can successfully correlate a wide range of experimental and computational data and suggest useful computational approaches for less tractable situations. Our examples include gases and solids together with an approximate treatment of liquids.

We also discuss quantum ideal gases. These systems are simple enough for analytic study and shed light on the difference between classical and quantum behavior for light particles, not only photons, but also phonons and electrons. In all but one of the problems treated in this Chapter Gibbs' partition function, either microcanonical or canonical, can be reduced to a product of one-dimensional partition functions.

As the density is increased and the effect of interparticle interactions begins to play an important role, corrections to the product approach become necessary. Strongly-coupled systems usually require computer simulation. But if the interactions are sufficiently weak, a systematic diagrammatic approach considering two-body, three-body, four-body, ... correlations can be effective. In this Chapter we consider an example of this approach, developing the Mayers' expansion of the fluid free energy as a density series, the "virial expansion." This approach provided the first quantitative test of many-body computer simulations and a basis for a very successful approach to liquid thermodynamic properties: the perturbation theory based on a combination of Gibbs' ideas with results from computer simulation. Very strongly coupled systems still require computer simulation, as is discussed in Chapters 5, 6, 10, and 11.

### 4.2 Tonks' One-Dimensional Hard-Rod Gas

We begin our exploration of the applications of Gibbs' statistical mechanics by studying what *appears* to be a many-body system with simple properties, the one-dimensional hard-rod system. We first issue a warning that one-dimensional dynamical systems are not at all typical in their dynamical behavior. We will see, for instance, that in one-dimensional systems, either fluid or solid, particle positions fluctuate with increasing amplitude as the system size is increased. Position

fluctuations of order  $N^{1/2}$  are required to satisfy the Central Limit Theorem described in Section 2.1. The Theorem implies that sufficiently large regions containing an *average* number of particles  $N$  must have *fluctuations* of order  $N^{1/2}$ . To generate these fluctuations in one dimension, individual particles must move cooperatively over a range of length proportional to  $N^{1/2}$ . In three-dimensional solids the situation is simpler. The Central Limit Theorem can be satisfied with finite displacements and the large- $N$  rms displacement in three-dimensional solids approaches a constant independent of  $N$ . In two dimensions the same problem gives rise to a more subtle logarithmic dependence of position fluctuations on system size.

But mechanical and thermodynamic properties, such as energy and pressure, which depend primarily on local interactions of neighboring particles, can be accurately represented by one- and two-dimensional models. Despite the pathological dynamics underlying fluctuations in one and two dimensions, one-dimensional equilibrium phase-space averages are well-defined and can be useful models of real behavior. Phase-space averages for one-dimensional systems can be used to develop and test new theoretical and computational techniques. At the same time irreversibility and the approach to equilibrium are poorly represented by one-dimensional systems. These systems usually, but not always, lack a feature fundamentally-important for irreversibility, Lyapunov instability. That exponential separation of trajectories is an essential part of the phase-space mixing typical of interesting two- and three-dimensional systems. The one-dimensional hard-rod system and *all* of the harmonic crystals studied in this Chapter are examples of systems with smooth *non-mixing* phase-space flows. In the equal-mass hard-rod system, for instance, the velocity distribution never changes. Colliding particles simply exchange velocities.

Hard impenetrable particles cannot exchange positions in one dimension. Consider  $N$  hard rods on a one-dimensional line segment. The one-dimensional nature of the hard-rod problem imposes a left-to-right ordering on the particles and this ordering leads to a simple method of solution. The  $N$  individual particles in this system all have the same mass,  $m$ , and a single degree of freedom. They all have the same "length"  $\sigma$  which prevents any two neighboring rods from a closer approach. The "volume"  $V > N\sigma$  to which the particles are confined by a boundary potential  $\Phi_{\text{Box}}$  is a one-dimensional line segment. We will work out Gibbs' canonical partition function for this system, starting with the Hamiltonian,

$$H = K + \Phi_{\text{Box}} + \Sigma\phi ,$$

and the corresponding canonical partition function,

$$\exp(-A/kT) = (1/h^N N!) \int dx^N \int dp^N \exp[-H(x,p)/kT] .$$

The  $N!$  accounts for the indistinguishability of the  $N$  particles. The multiplicative factor  $h^{-N}$ , where  $h$  has units of action  $[ML^2/T]$ , is required to make the partition function dimensionless. We saw in Chapter 3 that applying the Third Law of Thermodynamics and Bohr's Correspondence Principle to ideal gases, requiring that the classical and quantum partition functions agree in the classical limit, requires that  $h$  be chosen equal to Planck's constant,  $6.626 \times 10^{-34}$  jouleseconds. The basis for this choice in the symmetry of ideal-gas wave functions is discussed in Section 4.3.

The hard-rod momentum integrals here have the same form as they do in all the unconstrained classical canonical partition functions treated in this Chapter. The  $N$ -variable momentum integral can be evaluated by first writing it as the  $N$ th power of a one-dimensional integral:

$$\int dp^N \exp[-\sum p^2/2mkT] = [\int dp \exp(-p^2/2mkT)]^N = (2\pi mkT)^{N/2}.$$

To evaluate the configurational contribution to the partition function,

$$(1/N!) \int dx^N \exp[-(\Phi_{\text{Box}} + \sum \phi)/kT],$$

the integral over all the coordinates, we must identify the boundary potential  $\Phi_{\text{Box}}$ , or, equivalently, specify boundary conditions limiting the coordinate integrations. There are two simple cases shown in Figure 4.1, periodic boundaries, in which case the wall potential  $\Phi_{\text{Box}}$  vanishes, and rigid boundaries. For this one-dimensional hard-rod problem the two are simply related. Consider periodic boundary conditions, with the particles arranged on a ring of circumference  $V > N\sigma$ . If we hold any one of the  $N$  particles fixed, say Particle 1, then the integral over the others is just a rigid-boundary

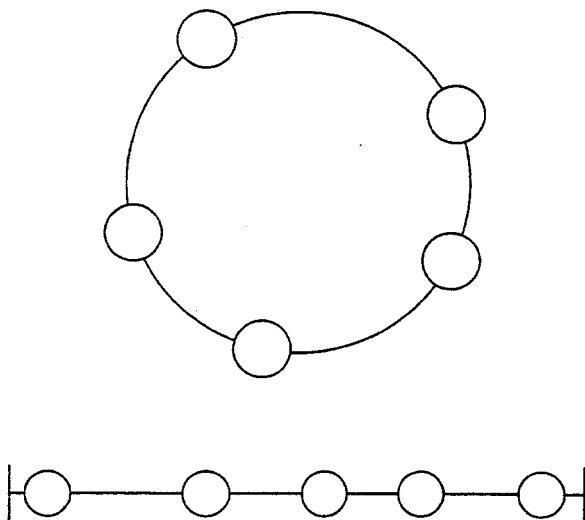


**Figure 4.1.** Periodic-Boundary and Rigid-Boundary one-dimensional systems.

integral inside a box of length  $V - \sigma$ . Because the rigid-boundary case has a particularly simple form we consider that one here.

For the rigid case we consider a line segment bounded by rigid walls at  $x = 0$  and  $x = V > N\sigma$ . The set of  $N$  particle coordinates  $\{x\}$  describes the locations of the centers of the particles and these coordinates are restricted by  $\Phi_{\text{Box}}$  to lie between  $x = (\sigma/2)$  and  $x = V - (\sigma/2)$ . Notice that once the  $N$  particles have been successfully placed in the box, without overlapping, they remain permanently ordered, from left to right, in one of  $N!$  equivalent ways. We can work out the configuration integral for the natural ordering,  $x_1 < x_2 < x_3 < \dots$ . Choosing just this one ordering out of the  $N!$  equivalent possibilities exactly compensates for the  $(1/N!)$  appearing in the canonical partition function. The complete partition function then becomes

$$\exp(-A/kT) = (1/\lambda^N) \int dx_1 \int dx_2 \dots \int dx_N ;$$

$$(\sigma/2) < x_1 < x_2 < \dots < x_N < V - (\sigma/2) ,$$

where we have introduced the conventional abbreviation  $\lambda = h/(2\pi mkT)^{1/2}$  for the de Broglie wavelength, a length equal to the rigid box length at which the quantum ground-state energy becomes  $\pi kT/4$ ,  $\pi/2$  times the classical kinetic energy.

The coordinate integration can then be carried out in a variety of ways. The simplest is to switch to new coordinates  $\{x\} \Rightarrow \{y\}$ :

$$y_1 = x_1 - (\sigma/2) ; y_2 = x_2 - (3\sigma/2) ; y_3 = x_3 - (5\sigma/2) \dots .$$

The  $\{y\}$  coordinates measure the particle displacements from their leftmost possible location. For these new variables the integration limits run from 0 to  $V - N\sigma$  with the set of  $N - 1$  restrictions  $\{y_1 < y_2 < \dots < y_N\}$ . See Figure 4.2.

The configurational integral over these new coordinates is simply one of  $N!$  equal parts of an  $N$ -dimensional hypercube of sidelength  $V - N\sigma$ , and so corresponds to the *hypervolume*  $(V - N\sigma)^N / N!$ . Thus the complete exact partition function is:

$$\exp(-A/kT) = Z(N, V, T) = (V - N\sigma)^N / (N! \lambda^N) .$$

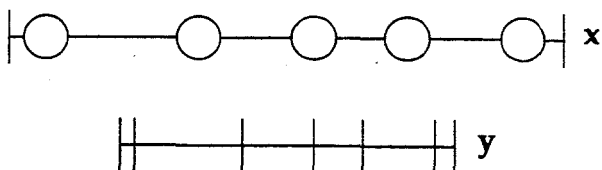


**Figure 4.2.** Transformation to relative coordinates  $\{y_n = x_n - [n - (1/2)]\sigma\}$ .

We can then apply Gibbs' canonical-ensemble formulae from Section 3.8 to get the thermal and mechanical equations of state:

$$E/kT = (\partial \ln Z / \partial \ln T)_V = N/2 ; PV/kT = (\partial \ln Z / \partial \ln V)_T = NV/(V - N\sigma) ;$$

The internal energy  $E = NkT/2$  illustrates the general rule, sometimes called the "equipartition" theorem, that any separable Cartesian degree of freedom with a kinetic energy  $p^2/2m$  has a canonical-ensemble average kinetic energy of  $kT/2$ . The corresponding kinetic contribution to the partition function is a multiplicative factor,  $[\int dp \exp(-p^2/2mkT)] = (2\pi mkT)^{1/2}$ , which contributes  $1/2$  to the derivative  $(\partial \ln Z / \partial \ln T)_V = E/kT$ . The same rule likewise applies to separable quadratic potential energies. Each degree of freedom in the potential energies of the harmonic crystals treated in Sections 4.6 and 4.7 likewise contributes  $kT/2$  to the canonical-ensemble average energy.

The mechanical equation of state of the hard-rod gas is more interesting. The hard-rod pressure is the same as that exerted by an ideal gas confined to a volume of reduced size. The size is reduced by exactly the volume  $N\sigma$  occupied by the particles. The resulting equation of state,  $P/kT = N/(V - N\sigma)$ , is identical to the repulsive part of van der Waals' equation, discussed in Section 2.8.

If the hard-rod partition function were multiplied by  $\exp(N^2a/VkT)$ , as if each particle interacted weakly and attractively with a large number of others, with that number proportional to the "number density"  $N/V$ , then the *complete* van der Waals equation would result, including the unphysical van der Waals loops we studied in Section 2.8. These loops correspond to mechanical instability, with negative compressibility as well as to thermodynamic instability, with both free energies,  $A(N,V,T)$  and  $G(N,P,T)$ , exceeding the equilibrium two-phase values. These instabilities reflect the qualitative complexity of the order imposed by attractive forces at low temperatures. This cooperative effect cannot be treated as a perturbation. Nevertheless the hard-rod system does illustrate the fundamental excluded-volume effect underlying the usefulness of van der Waals' equation of state and as well as the perturbation theory of liquids we review in Section 4.14.

The hard-rod partition function can also be used to illustrate one of the pathological properties of one-dimensional systems, the linear divergence, with  $N$ , of the mean-squared displacement  $\langle \delta^2 \rangle$ . We will just work out the simplest case here, using rigid boundaries and determining the probability for finding the central particle at a displacement  $\delta$  away from its most likely position at  $\langle x \rangle = V/2$ . The calculation proceeds in three steps: first, express the probability density for  $\delta$  as the normalized product of two  $(N - 1)/2$  particle partition functions, one with a volume  $[(V - \sigma)/2] + \delta$ , the other with a volume  $[(V - \sigma)/2] - \delta$ ; next, use the large- $n$  form of Stirling's approximation,  $\ln n! \approx n \ln n - n + (1/2) \ln(2\pi n)$ , to show that the large- $N$  probability density is proportional to  $\exp[-2N\delta^2/(V - N\sigma)^2]$ ; finally, compute the second moment from the resulting normalized Gaussian distribution, finding  $\langle \delta^2 \rangle = (V - N\sigma)^2/4N$ ,

showing that the mean-squared displacement diverges linearly with  $N$  at any fixed density  $N\sigma/V$ .

The one-dimensional hard-rod gas furnishes an interesting illustration of the reduction of an apparently complicated problem to a product of simple ones. The hard-rod partition function also provides us with a useful exact mechanical equation of state which we will later use to illustrate and test the Mayers' theory of dense fluids treated in Section 4.13.

### Problem:

Work out the periodic-boundary canonical partition functions for one, two, and three hard-rod particles and show that they are related to the corresponding rigid-boundary canonical partition functions by the rule  $Z_P = N[V/(V - N\sigma)]Z_R$ .

### 4.3 One-, Two-, and Three-dimensional Ideal Gases

The prototypical ideal-gas problems are fundamentally important in connecting classical and quantum statistical mechanics to macroscopic thermodynamics. These problems yield a wide range of results useful in both equilibrium and nonequilibrium problems. We begin with the simplest case, the canonical-ensemble treatment of the classical ideal gas. In the classical case there is no analog of the quantum uncertainty principle to couple the momentum and coordinate probabilities. In the classical case the momentum distribution,

$$\text{prob}(p)dp = \exp(-p^2/2mkT)dp / \int \exp(-p^2/2mkT)dp = (2\pi mkT)^{-1/2} \exp(-p^2/2mkT)dp ,$$

depends only on temperature, not on coordinates. This normalized probability density  $\text{prob}(p)$  is defined to be the limiting probability of finding a momentum in the interval  $dp$  centered at  $p$  as  $dp$  becomes small. "Normalized" means that the integral of  $\text{prob}(p)$  over its range is 1.

The probability density can be used to calculate all of the moments  $\langle |p|^n \rangle$  in terms of the gamma functions,  $\Gamma((n+1)/2)$  :

$$\begin{aligned} \int |p|^n \text{prob}(p)dp &= \int |p|^n \exp(-p^2/2mkT)dp / \int \exp(-p^2/2mkT)dp = \\ &= (2\pi mkT)^{-1/2} \int |p|^n \exp(-p^2/2mkT)dp = (1/\pi)^{1/2} (2mkT)^{n/2} \Gamma((n+1)/2) . \end{aligned}$$

From the special results,  $\Gamma(1/2) = \pi^{1/2}$  and  $\Gamma(1) = 1$ , and the general recursion relation,  $\Gamma(n+1) = n\Gamma(n)$ , all of the moments follow easily. These results will prove to be useful in studying the properties of nonequilibrium low-density gases.

The classical momentum integration is always the same for independent degrees of freedom, giving a factor of  $(2\pi mkT)^{1/2}$  for each one. If the interaction potential is

zero then the only role played by the potential function  $\Phi = \Phi_{\text{Box}}$  is to keep the particles in the volume  $V$ . In this case the coordinate integration likewise includes an independent factor of  $V$  for each particle. The product of the momentum integration and the coordinate integration, divided by  $N!$  to account for the indistinguishability of the particles, and by  $h^{DN}$  to convert phase-space volume to the equivalent number of quantum states, is the classical canonical partition function for a monatomic ideal gas in any number  $D$  of dimensions:

$$Z_N(V,T) = V^N / (N! \lambda^{DN}).$$

The thermal equation of state is  $E = DNkT/2$  and the mechanical equation of state is  $PV = NkT$ .

**Problem:**

Consider a classical one-dimensional particle of mass  $m$  confined to the positive part of the  $x$  axis by a hard wall at  $x = 0$  and interacting with a gravitational field,  $F_{\text{field}} = -mg$ . Work out the canonical partition function, the internal energy, and the heat capacity. Is the heat capacity  $C_v$  or  $C_p$ ?

The entropy from the three-dimensional ideal-gas canonical partition function is given by the "Sackuer-Tetrode formula,"

$$S/Nk = (E - A)/NkT = 5/2 + \ln(V/N\lambda^3).$$

Apart from negligible corrections of order  $1/N$  exactly the same entropy follows from Gibbs' microcanonical ensemble,

$$W(N,V,E) = e^{S/k} = V^N V_{3N} / (N! h^{3N}),$$

if we use the formula from Section 3.3 for the volume of a  $3N$ -dimensional hypersphere of radius  $(2mE)^{1/2}$ :

$$V_{3N} = 2(2\pi mE)^{3N/2} / [3N\Gamma(3N/2)],$$

to work out  $S/Nk$  from  $(1/N)\ln W(N,V,E)$ . Because the number of quantum states can never be less than one it is evident that quantum effects, ignored in our classical ideal-gas calculation, prevent  $V/N$  from falling below  $\lambda^3 e^{-5/2}$ , where  $\lambda$  is the de Broglie wavelength.

The quantum ideal-gas partition function is fundamentally a sum rather than an integral. To work it out we need to sum over all sets of occupation numbers  $\{N_j\}$  for the single-particle energy states:

$$Z_Q = \sum \exp(-N_i E_i / kT) ; \sum N_i = N ;$$

with no restriction on the  $\{N_i\}$  for "Bose statistics" and with all the  $\{N_i\}$  equal to 0 or 1 for "Fermi statistics." It is cumbersome to deal with these restrictions in the canonical ensemble. A simpler approach is the grand canonical ensemble used in Sections 4.11 and 4.12 to discuss photons, phonons, and electrons. Here we only observe that if the minimum spacing between the single-particle states,  $h^2/2mL^2$ , is sufficiently small, the sets of  $\{N_i\}$  will have negligible degeneracy, as if all  $N$  values were distinct. In the absence of degeneracy there is exactly one symmetric many-particle wave function and one antisymmetric many-particle wave function. Consider for instance the description of a three-body system of identical particles occupying three one-particle states with wave functions  $\alpha(x)$ ,  $\beta(x)$ , and  $\chi(x)$ . If the particles are bosons the corresponding three-particle wave function is the symmetric combination combination of  $3!$  terms:  $(1/3!)^{1/2}[\alpha_1\beta_2\chi_3 + \alpha_2\beta_3\chi_1 + \alpha_3\beta_1\chi_2 + \alpha_1\beta_3\chi_2 + \alpha_2\beta_1\chi_3 + \alpha_3\beta_2\chi_1]$ . If the particles are fermions the corresponding three-particle wave function is the antisymmetric combination of these same terms:  $(1/3!)^{1/2}[\alpha_1\beta_2\chi_3 + \alpha_2\beta_3\chi_1 + \alpha_3\beta_1\chi_2 - \alpha_1\beta_3\chi_2 - \alpha_2\beta_1\chi_3 - \alpha_3\beta_2\chi_1]$ . The  $N!$  different permutations of distinct particles among states obtained by expanding the product overcount, by a factor  $N!$ , the number of symmetric (Bose) or anti-symmetric (Fermi) many-particle states. Thus quantum mechanics gives exactly the same multiplicative factor of  $N!$  as does Gibbs' classical statistical mechanics. In this limit, the "classical limit," the many-particle partition function becomes  $1/N!$  times the  $N$ th power of the one-particle partition function:

$$Z_Q = \sum \exp(-N_i E_i / kT) \Rightarrow (1/N!) [\sum \exp(-E_i / kT)]^N \Rightarrow$$

$$(1/N!) [(1/h)^D \int dx^D \int dp^D e^{-H/kT}]^N = Z_C .$$

In the classical limit the sum over states approaches a Gaussian integral over independent quantum numbers  $n$ , with the result:

$$Z_Q = \sum \exp(-n^2 h^2 / 2mL^2 kT) \Rightarrow Z_C = (1/N!) (2\pi mL^2 kT / h^2)^{DN/2} .$$

The classical  $(1/N!)$  corrects for the indistinguishability of the particles in this limit. It is important to recognize that the quantum and classical partition functions would be different, by exactly a factor of  $h^{-DN}$ , unless the classical "phase integral,"

$$(1/N!) \int dx^{DN} \int dp^{DN} \exp[-H/kT] ,$$

included this same multiplicative factor. The comparison shows that for dilute gases individual quantum states must correspond to a classical phase-space volume  $(dqdp)^\#$ .

In principle *any* material could be vaporized and converted into an ideal gas. Thus this result linking the number of quantum states and the classical phase-space volume is generally valid in the classical limit. We will see it again in comparing the quantum and classical partition functions for constrained rotors and vibrators.

**Problem:**

Planck's constant  $h$  is  $6.626 \times 10^{-34}$  jouleseconds. Show that the room-temperature de Broglie wavelength  $h(2\pi mkT)^{-1/2}$  of an electron is 4 nanometers and that the room-temperature de Broglie wavelength for an argon atom is less than 10% of the atom's diameter (estimated from the interatomic spacing in the triple-point solid, 0.40 nanometers).

**4.4 Two- and Three-Dimensional Rigid Rotors**

The spacing of the quantum-mechanical molecular rotational and vibrational energy levels depends on the atomic masses and is largely unaffected by density changes. We follow tradition here and express the level spacings in terms of characteristic temperatures,  $\theta_{\text{rot}} \equiv h^2/4\pi^2mr^2k$  and  $\theta_{\text{vib}} \equiv hv/k$ . For diatomic hydrogen, nitrogen, and iodine gases the rotational temperatures are respectively 88, 3, and 0.05 kelvins, orders of magnitude less than the corresponding vibrational temperatures, 6300, 3400, and 310 kelvins. In most cases the vibrational temperatures are so high that it is reasonable to treat diatomic molecules as rigid rotors over a restricted range of temperature. In this approximation the molecular center-of-mass degrees of freedom have the exactly the same translational states as do those of a point particle with the same mass. The rotational partition functions, on the other hand, have some interesting properties. We explore the simplest cases here.

To begin, consider a homonuclear diatomic molecule in which two identical masses,  $m$ , are separated by a distance  $r$ , as is shown in Figure 4.3. In two dimensions the motion is restricted to the plane and the rotational Lagrangian is:

$$L_{2D} = m(r\dot{\theta})^2/4 ;$$

The corresponding two-dimensional Hamiltonian,

$$H_{2D} = p_{\theta}^2/mr^2 ,$$

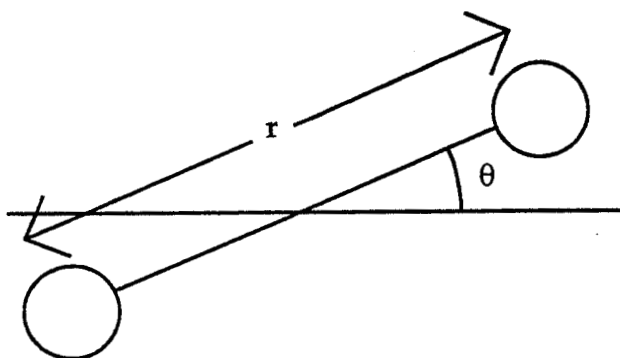


Figure 4.3. Two-dimensional rigid-rotor diatomic molecule with Lagrangian  $m(r\dot{\theta})^2/4$ .

is identical to the Hamiltonian for a particle with “mass” or “moment of inertia” ( $mr^2/2$ ) in a periodic box of “length”  $2\pi$ , and so the two-dimensional rotor has the same eigenvalues,  $n^2h^2/2mL^2 = n^2h^2/4\pi^2mr^2$ , and likewise must obey Bohr’s Correspondence Principle at high temperature.

**Problem:**

Compute and compare the canonical-ensemble heat capacities for the odd and even quantum numbers for the two-dimensional rotor.

The phase-space description of the rigid-rotor Hamiltonian becomes more interesting in three dimensions. In spherical polar coordinates the corresponding three-dimensional Lagrangian and Hamiltonian functions are:

$$L_{3D} = (mr^2/4)[(\dot{\theta}\sin\phi)^2 + \dot{\phi}^2];$$

$$H_{3D} = [(p_\theta/\sin\phi)^2 + p_\phi^2]/mr^2.$$

The quantum eigenvalues are  $n(n+1)h^2/4\pi^2mr^2$ , with degeneracies of  $(2n+1)$ , corresponding to the discrete set of allowed values of the angular-momentum projection. Replacing the sum over states by an integral gives the high-temperature limit of the quantum canonical partition function:

$$Z_{Q3D} = \sum(2n+1)\exp[-n(n+1)h^2/4\pi^2mr^2kT]$$

$$\Rightarrow (1/2)\int dx(2x+1)\exp[-x(x+1)h^2/4\pi^2mr^2kT] = 2\pi^2mr^2kT/h^2,$$

where the prefactor of  $1/2$  corresponds to selecting either odd or even quantum numbers  $n$  so as to satisfy the Pauli exclusion principle.

The classical partition function for this same Hamiltonian is an integral over both  $\theta$  and  $\phi$ , as well as their conjugate momenta. It is important to notice that the phase-space integration contains no Jacobian corresponding to a transformation from Cartesian to polar coordinates. This illustrates the general rule that *the phase-space*

volume element is simply  $dqdp$  for the generalized coordinate  $q$  corresponding to any degree of freedom:

$$Z_{C3D} = (1/2)h^{-2} \int d\theta \int d\phi \int dp_\theta \int dp_\phi \exp[-(p_\theta/\sin\phi)^2 - p_\phi^2] / mr^2kT .$$

$$[0 < \theta < 2\pi; 0 < \phi < \pi]$$

The  $h^{-2}$  is justified by applying the Bohr's Correspondence Principle and the prefactor of  $1/2$  preceding the integral corrects for overcounting indistinguishable configurations in the same way as does the  $(1/N!)$  introduced in the translational configurational integral. Any orientation of a homonuclear diatomic molecule described by the angles  $\theta$  and  $\phi$  is *indistinguishable* from the rotated (inverted) orientation with angles  $\theta \pm \pi$  and  $\pi - \phi$ . The  $(1/2)$  is the reciprocal of the "symmetry number" and accounts for the indistinguishability of the two ends of the rigid rotor. Because all six permutations of the three carbon atoms can result from rotations, the symmetry number for the triangular molecule "cyclopropane" is 6 rather than 3, as is discussed in more detail in Section 4.9. The symmetry number for the aptly-named cubic organic molecule "cubane,"  $C_8H_8$ , is 24 because each of the eight carbon atoms can be chosen to define a positive three-fold axis of symmetry through the molecule. See Figure 4.4.

The integration over  $p_\theta$  and  $p_\phi$  gives  $\pi mr^2kT \sin\phi$ . Thus the classical partition function for a rigid rotor is

$$Z_{C3D} = 2\pi^2 mr^2 kT / h^2 .$$

Again the apparently arbitrary division by  $h^2$  in the classical partition function is justified by the resulting exact agreement with the quantum partition function calculated above.

The dynamics of general *three-dimensional* rigid bodies requires *three* angular degrees of freedom, not just one. One angle describes the rotation of the body about an axis defined by the other two angles; these last can be chosen to be the usual spherical polar coordinates. See Figure 4.5. In an inertial Cartesian frame the *instantaneous* kinetic energy has the usual form:

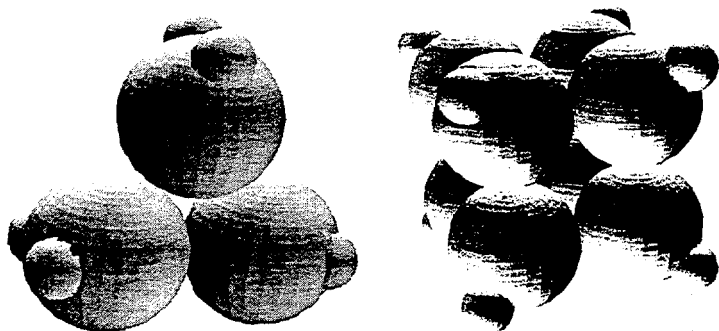


Figure 4.4. Cyclopropane and Cubane. The symmetry numbers, 6 and 24, correspond to the number of equivalent configurations of the molecules which can be obtained by rotation.

$$L = (1/2)\Sigma[m(y^2 + z^2)\omega_x^2 + m(z^2 + x^2)\omega_y^2 + m(x^2 + y^2)\omega_z^2] \equiv$$

$$(1/2)[\omega_x^2 I_{xx} + \omega_y^2 I_{yy} + \omega_z^2 I_{zz}],$$

where the sum is to be carried out over all masses in the body and the axes are chosen so that the *moment of inertia tensor* has only the diagonal elements  $I_{xx}$ ,  $I_{yy}$ , and  $I_{zz}$ . The Hamiltonian corresponding to this Lagrangian is:

$$H = L = (1/2)[(p_x^2/I_{xx}) + (p_y^2/I_{yy}) + (p_z^2/I_{zz})].$$

This formulation suggests the correct form for the canonical partition function, including an angle integration of  $8\pi^2$  and a momentum contribution of  $(2\pi I kT)^{1/2}$  from each of the three principal moments of inertia:

$$Z_R = (8\pi^2/h^3)(2\pi I_{xx} kT)^{1/2}(2\pi I_{yy} kT)^{1/2}(2\pi I_{zz} kT)^{1/2}.$$

To generate the rigid-body dynamics it is simplest to consider *Cartesian*, rather than spherical polar, angular velocities  $\{\omega_x, \omega_y, \omega_z\}$  measured in a comoving frame *fixed in the body*. To illustrate we choose the right-handed Cartesian frame for the brick shown in Figure 4.5, with the three moments of inertia  $\{I_{xx} = \Sigma m(y^2 + z^2), I_{yy} = \Sigma m(z^2 + x^2), I_{zz} = \Sigma m(x^2 + y^2)\}$  chosen equal to 4, 3, and 2, respectively. At any instant of time Euler's equations of motion (for derivations see Pars' or Landau and Lifshitz' texts) for the angular velocities  $\omega_x$ ,  $\omega_y$ , and  $\omega_z$  are:

$$\dot{\omega}_x = \omega_y \omega_z (I_{yy} - I_{zz}) / I_{xx}; \quad \dot{\omega}_y = \omega_z \omega_x (I_{zz} - I_{xx}) / I_{yy}; \quad \dot{\omega}_z = \omega_x \omega_y (I_{xx} - I_{yy}) / I_{zz}.$$

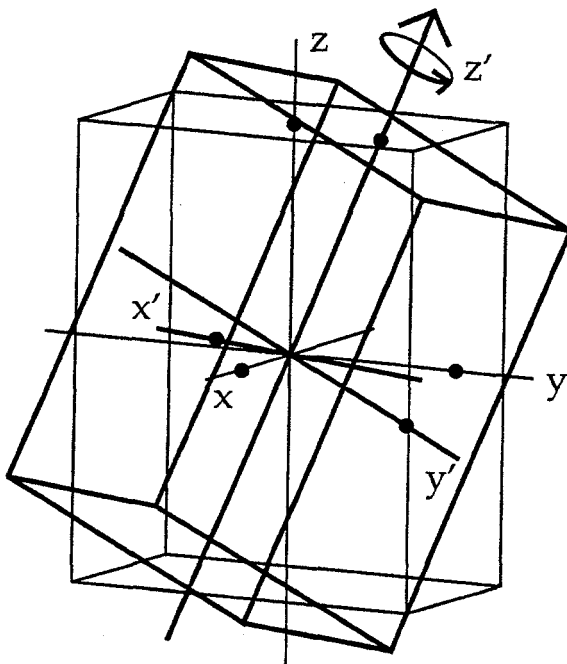


**Figure 4.5.** Rigid right rectangular parallelepiped with principal moments of inertia 4, 3, and 2. Two orientations of the rigid body are shown here. Three "Euler angles," including the usual two spherical polar coordinates, can be used to describe the orientation of the body but it is somewhat simpler to use cartesian coordinates.

If we begin by choosing orthonormal basis vectors  $\{x,y,z\}$  initially coinciding with the laboratory frame, we can keep track of the subsequent motion of the vectors in terms of the body-fixed instantaneous rotation rates:

$$\dot{x} = y\omega_z - z\omega_y; \dot{y} = z\omega_x - x\omega_z; \dot{z} = x\omega_y - y\omega_x.$$

**Problem:**

Follow the motion of a brick with  $\{I_{xx}, I_{yy}, I_{zz}\} = \{4, 3, 2\}$ , as shown in Figure 4.5, with initial angular velocity  $\omega = \{\omega_x, \omega_y, \omega_z\} = \{0, 1, 0\}$  for 1000 time steps of length 0.10 using the fourth-order Runge-Kutta method and determine whether or not the resulting motion is exponentially unstable to small changes in  $\omega$ . The brick *cannot* exhibit Lyapunov instability (*long-time exponential instability*) because conservation of energy and angular momentum restrict its state of motion to an intrinsically-nonchaotic two-dimensional state space.

4.5 One-Dimensional Vibrator

The one-dimensional harmonic oscillator is the epitome of stability. It is also the basic building block from which models of polyatomic molecules and crystalline solids are constructed. This same model also provides us with another chance to see that the quantum canonical partition function and the classical phase integrals agree within a factor of exactly  $h^\#$  where  $\#$  is the number of degrees of freedom.

The oscillator Hamiltonian is

$$H = [(p^2/m) + \kappa q^2]/2,$$

where  $m$  is the mass and  $\kappa$  is the force constant. The classical partition function, including the multiplicative factor  $1/h$  required to convert from phase-space volume to quantum states, is the product of two Gaussian functions:

$$\begin{aligned} Z_C &= (1/h) \int dq \int dp \exp[-H/kT] = \\ &= (1/h) \int dq \exp(-\kappa q^2/2kT) \int dp \exp(-p^2/2mkT) = \\ &= (1/h) (2\pi kT/\kappa)^{1/2} (2\pi mkT)^{1/2} = kT/h\nu, \end{aligned}$$

where  $\nu$  is the oscillator frequency in hertz,  $2\pi\nu = \omega = (\kappa/m)^{1/2}$  and  $\omega$  is the "angular frequency" in radians/second.

To compute the quantum mechanical canonical partition function, we begin with the energy eigenvalues  $\{E_n = (n + 1/2)h\nu\}$  for a one-dimensional harmonic oscillator. The sum over these energy states is a geometric series, with successive terms differing by a factor of  $e^{-h\nu/kT} \equiv e^{-x}$ :

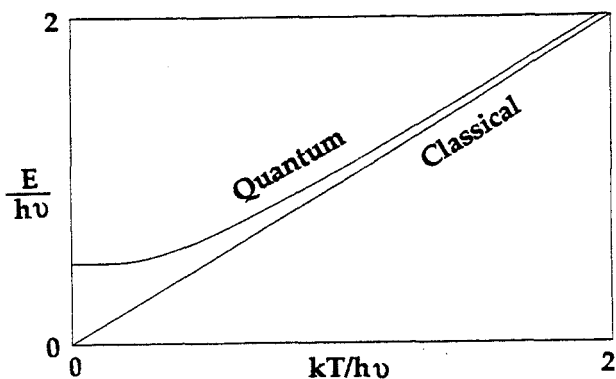


Figure 4.6. Variation of Quantum and Classical oscillator energies with temperature. The difference at low temperature is the "zero-point energy" of  $h\nu/2$ .

$$Z_Q = \exp[-A_Q/kT] = \sum \exp[-E_n/kT] = e^{-x/2} + e^{-3x/2} + e^{-5x/2} + \dots = e^{-x/2}/(1 - e^{-x}),$$

where  $x$  is the reduced energy  $h\nu/kT$ . From the quantum Helmholtz free energy  $A_Q$  the internal energy  $E$  can be calculated as a function of temperature. See Figure 4.6. At low temperatures, where the reduced energy  $x$  is large, the energy-state series

$$Z_Q = e^{-x/2}/(1 - e^{-x}) = e^{-x/2} + e^{-3x/2} + e^{-5x/2} + \dots,$$

converges rapidly. Differentiation confirms that the low-temperature limiting zero-point energy  $E(0) = kT(\partial \ln Z / \partial \ln T)_0$ , coming from the first term of the series, is equal to the ground state energy,  $h\nu/2$ , and that the low-temperature large- $x$  heat capacity vanishes as  $x^2 e^{-x}$ .

The opposite high-temperature limit offers yet another confirmation of Bohr's Correspondence Principle. The quantum partition function can be expanded for small  $x = h\nu/kT$  by working out the ratio of the series for  $e^{-x/2}$  and  $1 - e^{-x}$ :

$$\begin{aligned} Z_Q &= e^{-x/2}/(1 - e^{-x}) = \\ &= [1 - (x/2) + (x^2/8) - (x^3/48) + (x^4/384) - \dots] / [x - (x^2/2) + (x^3/6) - (x^4/24) + (x^5/120) - \dots] = \\ &= (1/x) \exp[-(x^2/24) + (x^4/2880) - \dots], \end{aligned}$$

where  $(1/x) = kT/h\nu$  reproduces the high-temperature classical result and the sum of the series in  $x$  in the exponent is proportional to the "Wigner-Kirkwood series," which expresses quantum corrections to the classical Helmholtz free energy as a power series in Planck's constant  $h$ .

The harmonic oscillator provides an interesting application for the canonical-ensemble expression for the constant-volume heat capacity,

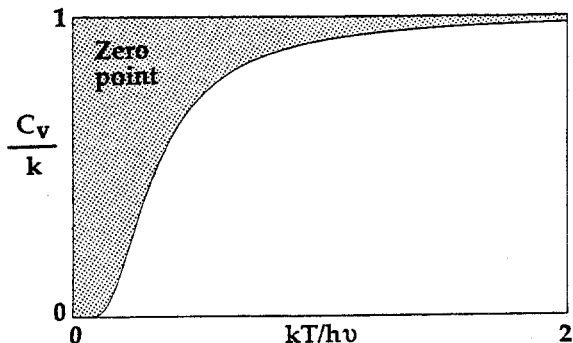


**Figure 4.7.** Heat capacity for quantum and classical oscillators. The area of the shaded region is  $1/2$ , corresponding to the zero-point energy,  $h\nu/2$ .

$$C_v = (\partial E / \partial T)_v = [\langle E^2 \rangle - \langle E \rangle^2] / kT^2 .$$

In the classical case  $\langle E^2 \rangle = \langle K^2 + 2K\Phi + \Phi^2 \rangle = (3 + 2 + 3)(kT)^2/4$  is  $2(kT)^2$  and  $\langle E \rangle^2$  is  $(kT)^2$ , leading to the constant single-oscillator heat capacity  $k$ . For a harmonic oscillator the quantum energy always exceeds the classical value and the quantum heat capacity is always less, lying below the classical value by  $k$  at low temperature and approaching the classical value from below at high temperature. The excess energy in the quantum case can be calculated by integrating the heat capacity:

$$E_Q(T) - E_C(T) = E_Q(0) - E_C(0) + \int (C_Q - C_C) dT' .$$

Then, from Bohr's observation that the two energies must agree at high temperature, we see that the zero-point energy,  $E_Q(0) - E_C(0)$ , must be equal to the integrated area between the classical and quantum heat capacity curves. See Figure 4.7. This example is a good illustration of the way in which Gibbs' statistical mechanics makes it possible to obtain information about microscopic Hamiltonians directly from macroscopic data.

### Problem:

Show that the probability density for finding a classical one-dimensional oscillator with Hamiltonian  $H = (1/2)(q^2 + p^2)$  in the coordinate range  $dq$  about  $q$  diverges at the turning points, with  $\text{prob}(q) = (1/\pi)[2H - q^2]^{-1/2}$ , in agreement with the calculation in Section 3.2. Show that for a *two*-dimensional oscillator the probability for finding an oscillator in the range  $dx dy$  is a constant for all accessible values of  $x$  and  $y$ :

$$\iint dp_x dp_y \delta(2H - p_x^2 - p_y^2 - x^2 - y^2) = 1/(2\pi H) .$$

Show that a *three*-dimensional oscillator has maximum configurational probability density at the origin. Hint: For a function  $f(x)$  which vanishes at  $x_0$  the relation  $\delta(f(x)) = \delta(x_0)/(df/dx)$  holds.

#### 4.6 One-Dimensional Harmonic Chain

By using Hooke's-Law oscillator springs to couple arrays of masses together, with the resulting frequencies chosen to match experimental frequency spectra, we can construct simple microscopic models for solids, glasses, and polyatomic molecules. In this Section we determine the properties of a *one-dimensional* chain of identical masses coupled by Hooke's-Law springs. I repeat the warning that most one-dimensional systems, including these oscillator systems, are atypical because their phase-space trajectories are *stable*. The one-dimensional chain also displays the same diverging particle displacements, with increasing system size, as does the hard-rod system. Nevertheless both the hard-rod and the harmonic-chain models are extremely useful idealizations of real behavior.

In most cases the oscillator frequencies are relatively high. Typical crystal vibration frequencies of  $\nu = 10^{13}$  hertz correspond to characteristic temperatures  $T = h\nu/k$  of nearly a thousand kelvins, so that quantitative room-temperature calculations require a quantum treatment. Nevertheless, the corrections to the classical partition functions are often small. Note the small coefficients in the Wigner-Kirkwood series given in Section 4.5 for a single oscillator. The classical canonical partition function for a many-body chain can be evaluated either by working out the classical phase integral or by separating the Hamiltonian into independent contributions from the normal-mode vibrations. We consider both methods for the one-dimensional harmonic chain and show explicitly that they lead to identical results.

Consider a nearest-neighbor Hooke's-law chain, such as the one shown in Figure 4.8, in which  $N$  identical masses interact with each other and with two confining walls with Hooke's-Law springs, all with the same force constant  $\kappa$ . The corresponding Hamiltonian is a simple quadratic form leading to a canonical partition function which can be integrated by completing the square. To show the power of inductive reasoning we first work out examples for  $N = 1, 2$ , and 3 masses coupled to one another and to the two boundaries, by  $N + 1$  springs:

$$Z_N = (1/\lambda)^N \int dx^N \exp[-\Phi_N/kT],$$

$$\Phi_1 = (\kappa/2)[x_1^2 + x_1^2];$$



Figure 4.8. Five-Particle One-Dimensional Hooke's-Law Chain.

$$\Phi_2 = (\kappa/2)[x_1^2 + (x_1 - x_2)^2 + x_2^2];$$

$$\Phi_3 = (\kappa/2)[x_1^2 + (x_1 - x_2)^2 + (x_2 - x_3)^2 + x_3^2].$$

The corresponding integrals can be converted into products of iterated Gaussian integrals by repeatedly "completing the square." For example,

$$\Phi_3 = \kappa[(x_1 - (1/2)x_2)^2 + (3/4)(x_2 - (2/3)x_3)^2 + (2/3)x_3^2].$$

The one-, two-, and three-body partition functions obtained in this way have the following forms:

$$Z_1 = (1/h)^1(2\pi mkT)^{1/2}(2\pi kT/\kappa)^{1/2}(2)^{-1/2};$$

$$Z_2 = (1/h)^2(2\pi mkT)^{2/2}(2\pi kT/\kappa)^{2/2}(3)^{-1/2};$$

$$Z_3 = (1/h)^3(2\pi mkT)^{3/2}(2\pi kT/\kappa)^{3/2}(4)^{-1/2},$$

from which it is easy to guess the form of the general case.

To derive the general case directly, notice that the configurational integral for any one-dimensional chain can be written in terms of the set of reduced coordinates  $\{y = x(\kappa/mkT)^{1/2}\}$ , leaving a dimensionless integral over the  $\{y\}$  to work out. The integral can then be calculated directly by using a general result for Gaussian integrals:

$$\int \dots \int \exp[-x \cdot \kappa \cdot x] dx^N = \pi^{N/2} / \text{Det}^{1/2},$$

where Det is the Determinant of the symmetric force-constant array  $\kappa$ . For an N-particle chain, the corresponding determinant has a diagonal filled with ones and adjacent off-diagonal elements of  $-1/2$ . The final result for the set of canonical partition functions is

$$Z_C = (1/h)^N(2\pi mkT)^{N/2}(2\pi kT/\kappa)^{N/2}(N+1)^{-1/2},$$

in agreement with the special cases worked out above.

### Problem:

Derive a recursion relation linking the determinant of the N-particle symmetrized  $N \times N$  force-constant matrix to the analogous determinants for  $N - 1$  and  $N - 2$  particles. Show that this result is consistent with the partition function just given.

There is yet another elegant alternative to computing the partition function by completing the square or by using Gaussian integration. This alternative uses the normal-mode solutions of the equations of motion. The equations of motion for a one-dimensional chain can be written in terms of the particle coordinates  $\{x_j\}$ :

$$m\ddot{x}_j = \kappa[x_{j+1} - 2x_j + x_{j-1}],$$

or in terms of the displacements  $\{\delta_j\}$  of these coordinates relative to the rest positions  $\langle x_j \rangle = jd$ :

$$m\ddot{\delta}_j = \kappa[\delta_{j+1} - 2\delta_j + \delta_{j-1}],$$

where the subscripts indicate contiguous positions along the chain. Any solution of these equations of motion can be expanded in a Fourier time series. The unusual feature for a chain is that the Fourier coefficients are constant. The initial conditions determine the solution for all time. From the standpoint of equilibrium statistical mechanics all we need do is to select those solutions which satisfy our desired boundary conditions. If we assume that the motion of the  $i$ th coordinate is a superposition of waves with wavelengths  $\{\lambda_n\} = \{2\pi/k_n\}$ , which oscillate with frequencies  $\{\omega_n\}$ , we must find the  $N$  independent "normal-mode" solutions:

$$\delta_j(n) = C(n)\exp[i(\omega_n t - jdk_n)],$$

where  $\delta_j$  is the displacement of the  $j$ th atom from its equilibrium position  $jd$ . We find that the solutions satisfying the equations of motion all yield the same "dispersion relation" for the dependence of frequency on wavelength:

$$(m/\kappa)\omega_n^2 = 2 - 2\cos(k_n d) = 4\sin^2(k_n d/2).$$

By separating the  $N$ -particle chain Hamiltonian into separate Hamiltonians, one for each "mode" of vibration,  $n = 1, 2, \dots, N$ , the partition function can again be written as a product. For our rigid-wall boundary conditions the solutions are sine waves that vanish for artificial motionless boundary particles corresponding to  $j = 0$  and  $j = N + 1$ .

To illustrate let us use the general solution to find the five vibrational modes for the 5-particle chain. In this case the particle amplitudes are proportional to sines of angles which are multiples of  $(\pi/6)$ . The corresponding frequencies,

$$\{(m/\kappa)\omega_n^2\} = \{2 - 3^{1/2}, 1, 2, 3, 2 + 3^{1/2}\},$$

follow easily from the dispersion relation with  $k_n = (2\pi n/6d)$ .

The corresponding canonical partition function for the five-particle crystal is the product of normal mode partition functions:

$$Z_C = \prod(kT/h\nu) = (2\pi kT/h)^5(m/\kappa)^{5/2}(6)^{-1/2},$$

where the 6 comes from the product of normal mode frequencies. Notice that the partition function agrees with our calculations based on completing the square or evaluating the force-constant determinant. *Periodic* one-dimensional chains can be treated in the same way. The same dispersion relation describes also the vibrational modes of a six-atom *periodic* crystal, with  $n = 0, \pm 1, \pm 2, 3$ .

Because the linear transformation to normal-mode coordinates can be viewed as a rotation of the phase-space coordinate system, the *determinant* of the force constant matrix is unchanged, giving a simple derivation of the Gaussian-integral approach to the partition function. Likewise the *trace* of the matrix, proportional to the second moment of the frequency distribution, is unchanged. For either boundary condition the mean squared frequency is always  $2(\kappa/m)$ .

The *inverse* second moment has intrinsic physical interest. It is proportional to the mean squared displacement of the particles about their equilibrium locations. The corresponding "thermal cross section" is responsible for the scattering of xrays, neutrons, and sound waves. Again, the phase-space rotation to normal-mode coordinates makes it possible to show that the modes make additive contributions to the total mean-squared displacement:

$$\langle \delta^2 \rangle = \sum \langle E_n / m\omega_n^2 \rangle,$$

where  $E_n$  is the energy in the  $n$ th normal mode. From the analytic form of the dispersion relation it is easy to show that the pathological linear divergence of  $\langle \delta^2 \rangle$  in one dimension has the form  $\langle \delta^2 \rangle = (N+1)(kT/\kappa)/12$  for periodic boundaries. The wavelengths with rigid boundaries are effectively twice as large. The mean value, over the chain, of  $\langle \delta^2 \rangle$  diverges as  $(N+2)(kT/\kappa)/6$  for rigid boundaries.

#### Problem:

Integrate the probability density for the particle displacements in a one-dimensional rigid-boundary chain,  $\exp(-\Phi_N/kT) / \int \dots \int \exp(-\Phi_N/kT) dx^N$  over all but one of the displacement coordinates. In this way show that the mean-squared displacement for the  $j$ th particle in a chain with rigid boundaries is given by  $\langle \delta^2 \rangle_j = (kT/\kappa)j(N+1-j)/(N+1)$ .

#### 4.7 Two- and Three-Dimensional Quasiharmonic Crystals

The one-dimensional crystal is a special case yielding a simple sinewave dispersion relation  $\omega = 2(\kappa/m)^{1/2}\sin(kd/2) = 2(\kappa/m)^{1/2}\sin(\pi d/\lambda)$  linking the crystal

vibration frequencies to the allowed wavelengths  $\{\lambda\}$ . For the one-dimensional chain and the two-dimensional close-packed triangular lattices the corresponding dispersion relations lead to known analytic forms for the partition functions. The three-dimensional close-packed lattices, face-centered cubic and hexagonal close-packed, are both sufficiently complicated that their free energies have only been determined numerically.

Although the situation in real crystals may seem even more complicated than these simple models because numerical evaluation is absolutely required, the underlying mathematics is unchanged. In fact a numerical calculation of the free energy is relatively straightforward and easy to check. The calculation is simplest for *periodic* crystals with only a single atom in the spatially-periodic repeating structural unit, the "unit cell." In such a case the three-dimensional problem reduces to the solution of three simultaneous equations and the two-dimensional problem to two simultaneous equations. See Figure 4.9.

We will work out the simplest nontrivial example here, complicated enough to illustrate the geometric difficulties but simple enough that some analytic results can still be obtained. The two-dimensional square lattice is not mechanically stable to shear with nearest-neighbor forces. Parallel displacements of neighboring rows of particles induce no linear restoring forces. Accordingly we consider the close-packed triangular lattice, in which each particle has six neighbors. We choose the rest position of one particle at the origin  $(0,0)$  and indicate its six neighbors by subscripts illustrated in Figure 4.10 and corresponding to displacements paralleling the oblique coordinate directions shown in Figure 4.9. If we choose a nearest-neighbor potential energy function  $(\kappa/2)(r - d)^2$ , where  $d$  is the rest length of the Hooke's-Law springs, we can calculate the forces on the origin particle as a function of small displacements from equilibrium. The linearized equations of motion for the particle located at the origin ( $x_{00} = y_{00} = 0$ ) become:

$$m\ddot{x}_{00} = \kappa(3/16)^{1/2}(\delta y_{0+} + \delta y_{0-} - \delta y_{-+} - \delta y_{+-}) + \kappa[\delta x_{+0} + \delta x_{-0} + (1/4)(\delta x_{0+} + \delta x_{-+} + \delta x_{0-} + \delta x_{+-}) - 3\delta x_{00}];$$

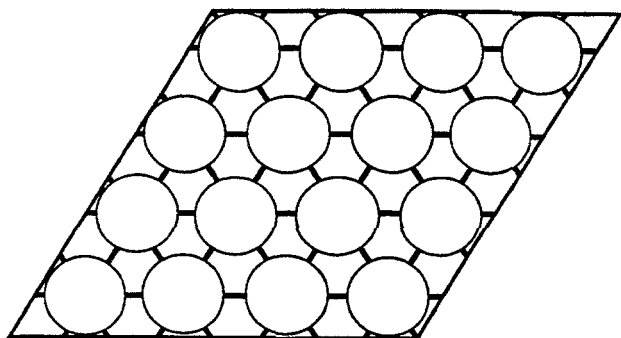
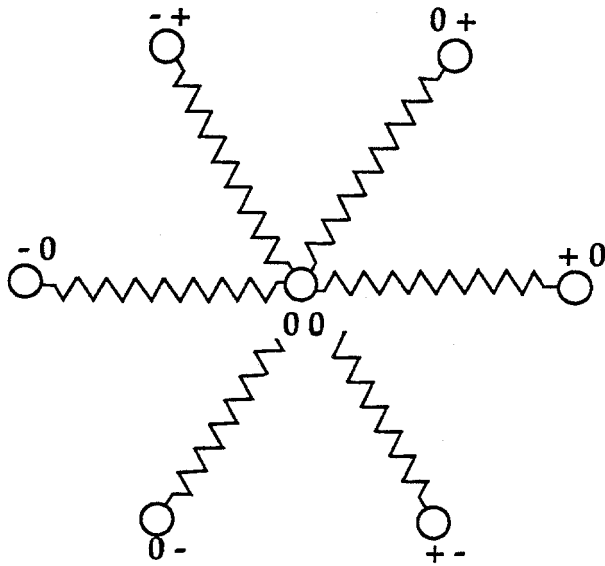


Figure 4.9. Sixteen-particle two-dimensional harmonic crystal. Stable triangular-lattice structure.



**Figure 4.10.** Nomenclature for the six nearest neighbors in the triangular-lattice structure illustrated in Figure 4.9.

$$m\delta\ddot{y}_{00} = \kappa[(3/16)^{1/2}(\delta x_{0+} + \delta x_{0-} - \delta x_{-+} - \delta x_{+-})] + \kappa(3/4)(\delta y_{0+} + \delta y_{-+} + \delta y_{0-} + \delta y_{+-} - 4\delta y_{00}).$$

Just as in one dimension, the solutions of these coupled linear equations are sine waves, of the form  $(X, Y)\exp[ik \cdot r - i\omega t]$ , where the  $\{r\}$  are the fixed lattice coordinates about which the particles vibrate. The spatial part of the phase,  $\exp[ik \cdot r]$ , vanishes at the origin particle. If we substitute this complex solution into the equations of motion we obtain a purely-real dispersion relation linking the angular frequency of vibration,  $\omega$ , to the interatomic force constants and the atomic masses. By evaluating the solution for each value of  $k$  consistent with the periodic boundary conditions, the thermodynamic properties can be calculated.

A three-dimensional crystal, with  $X$ ,  $Y$ , and  $Z$  displacement amplitudes, would have three solutions for every  $k$ . In the two-dimensional crystal considered here there are only two. We illustrate them in the simplest case. If the wave propagation direction coincides with the  $x$  axis, so that  $k = (k_x, 0)$ , the coupling between the  $x$  and  $y$  displacements vanishes, producing a longitudinal mode, with motion parallel to the  $x$  axis, and a transverse mode, with motion *perpendicular* to that axis. In this special case, after dividing out a common factor of  $e^{-i\omega t}$  from both sides, the equations of motion simplify to

$$-m\omega^2 X = \kappa[2\cos(k_x d) + \cos(k_x d/2) - 3]X;$$

$$-m\omega^2 Y = \kappa[3\cos(k_x d/2) - 3]Y.$$

In the long wavelength limit, corresponding to small  $k$ , these two equations give the longitudinal and transverse sound velocities:

$$c_L = (\omega_x/k_x) = (9\kappa d^2/8m)^{1/2}; c_T = (\omega_y/k_x) = (3\kappa d^2/8m)^{1/2}.$$

As a consequence of the linear-elastic isotropy of the triangular lattice, these *same* longitudinal and transverse sound velocities result, in the long wavelength limit, for *any* propagation direction.

In order to calculate the free energy for a crystal following this approach it is necessary to average over all of the crystal's normal modes of vibration. There are exactly  $2N$  such modes corresponding to  $N$  periodically repeating  $k$ -space (often called "reciprocal-space") points. The modes depend on the shape of the repeating unit chosen, but with fixed shape and increasing size, the resulting frequency distribution and free energy per particle approach limits independent of crystal shape. For the simplest situation, with one particle per unit cell, the natural cell shape is a parallelogram. Then the corresponding fundamental sampling region in  $k$  space is also a parallelogram, but it is more conventional to use an equivalent region, the "First Brillouin Zone," as shown in Figure 4.11 for the triangular lattice. This choice corresponds to choosing the *longest wavelengths possible* for each lattice vibration, by sampling a region as close as possible to the  $k$  space origin. The sampling of points representing lattice vibrations in this hexagonal region only achieves hexagonal symmetry in the limit that the crystal becomes infinite in size.

This triangular-lattice nearest-neighbor crystal is particularly well-suited to analytic study. Huckaby obtained an exact expression for the infinite-crystal free energy per particle. The periodic bulk-crystal calculations described here can be generalized to describe surface modes of vibration, "Rayleigh Waves." See Figure 4.12. By using *complex*  $k$ -space vectors to damp the motion within the crystal, surface Rayleigh-wave vibrations appear as linear combinations of longitudinal and transverse waves chosen to satisfy a boundary condition of vanishing normal stress at the crystal boundary.

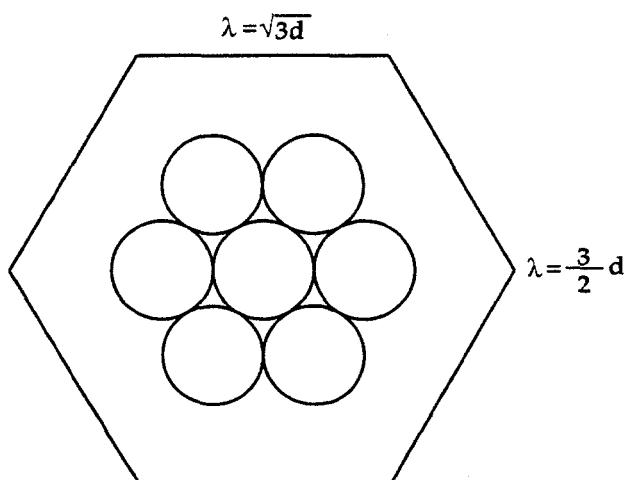


**Figure 4.11.** "Reciprocal space" first Brillouin zone, containing those  $k$  vectors describing periodic lattice waves which lie closest to the origin. The shortest wavelengths which can be propagated parallel and perpendicular to the close-packed planes are indicated. The hexagonal portion of a triangular lattice indicates the relative orientation of the lattice planes and the Brillouin zone.

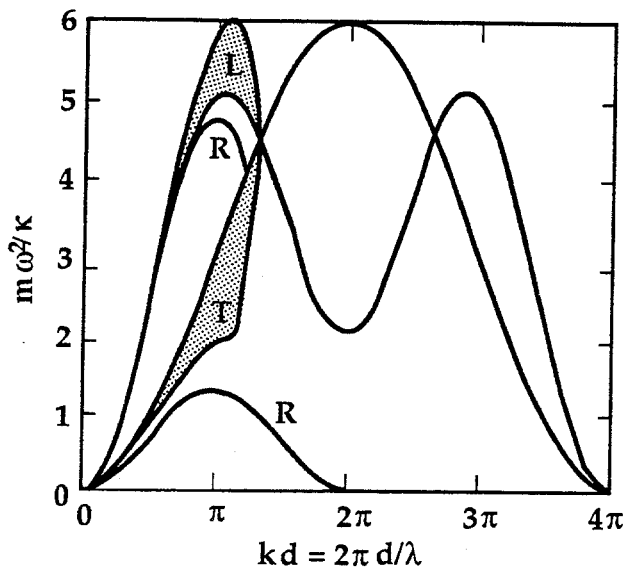


**Figure 4.12.** Bulk and surface wave frequencies in the Triangular Lattice. Bulk modes, longitudinal and transverse, propagating parallel to the close-packed directions are described by the curves extending from  $kd = 0$  to  $kd = 4\pi$ . The two shaded regions indicate *all* bulk-mode frequencies, independent of direction. Surface "Rayleigh" waves, parallel to the close-packed directions, are described by the two dispersion relations R.

The lower branch of surface vibrations turns out to have exactly the same sinusoidal dispersion relation as does the one-dimensional chain, but with a long wave limiting velocity, called the Rayleigh velocity, somewhat less than the transverse sound speed.

### Problem:

1. Show that the same sound speeds,  $c_L$  and  $c_T$ , are obtained in the long wavelength limit for a wave propagating *perpendicular* to the  $x$  axis, with  $\mathbf{k} = (0, k_y)$ .
2. Work out the classical canonical partition function for three two-dimensional particles with equal masses  $m$  linked together in the shape of an equilateral triangle by three identical Hooke's-Law springs, each with force constant  $\kappa$ . Include all of the translational, rotational, and vibrational degrees of freedom. Choose the zero of energy to correspond to the least-energy state of the "molecule."

### 4.8 Einstein and Debye models

Because it is tedious to compute the exact frequency distribution it is natural to try simple approximate models. Figure 4.13 compares the simplest two such models with the exact distribution for the triangular lattice. The simpler of the two approximate models for the vibrations of a crystal lattice is called the Einstein model or the "cell model" and corresponds to letting each particle vibrate in the "cell" imposed by the potential field of its fixed neighbors. With a nearest-neighbor Hooke's-Law potential the restoring force for a small displacement  $\delta$ , is  $-2\kappa\delta$  in one dimension, because there are two interacting neighbors. In two or three dimensions the restoring force exerted by a neighboring particle is  $-\kappa\delta\cos^2\alpha$  where  $\alpha$  is the angle between the displacement direction and the interacting Hooke's-Law neighbor. Summing these contributions

over all nearest neighbors, six in two dimensions and twelve in three, gives Einstein-model restoring forces of  $-3\kappa\delta$  in two dimensions, for the triangular lattice, and  $-4\kappa\delta$  in

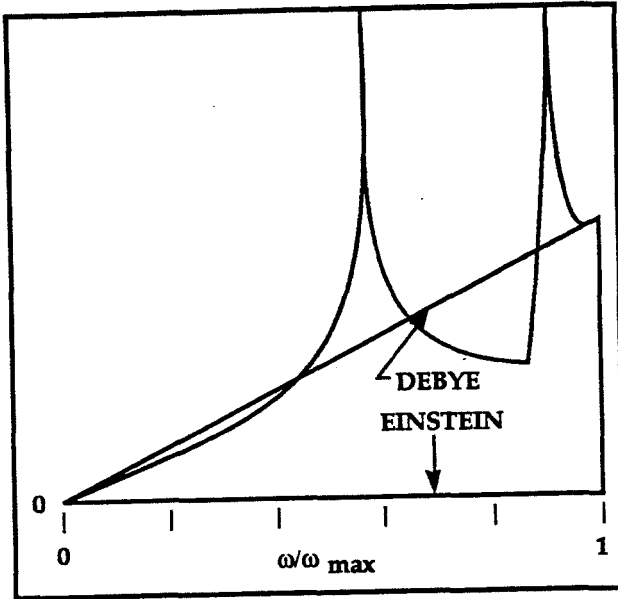


**Figure 4.13.** Exact frequency distribution for the Triangular Lattice. The distribution has two integrable singularities. The linear Debye distribution and the Einstein frequency are indicated.

three dimensions, for either close-packed arrangement, face-centered cubic or hexagonal. Although neither of these last two crystals is elastically isotropic a Taylor's series expansion of the linear restoring force for a single-particle motion is isotropic for the first nonvanishing term linear in the displacements. Thus the Einstein frequencies for the one-, two-, and three-dimensional close-packed crystals are  $(2\kappa/m)^{1/2}$ ,  $(3\kappa/m)^{1/2}$ , and  $(4\kappa/m)^{1/2}$ , respectively.

The second moment from this one-frequency Einstein model is exactly correct for harmonic systems. This is because the trace of the force-constant matrix is invariant to a phase-space rotation such as the rotation diagonalizing the Hamiltonian. But the inverse second moment is qualitatively wrong in one dimension, where the Central Limit Theorem establishes that the mean squared displacement, and hence this moment, must diverge. The inverse second moment according to the Einstein model,

$$\langle \delta^2 \rangle = \{ \langle \delta_x^2 \rangle \text{ or } \langle \delta_x^2 \rangle + \langle \delta_y^2 \rangle \text{ or } \langle \delta_x^2 \rangle + \langle \delta_z^2 \rangle \} = (DkT)/(m\omega_{\text{Einstein}}^2),$$

is qualitatively wrong in both one and in two dimensions. The Einstein-model prediction is always finite while both one- and two-dimensional crystals have mean-square displacements which diverge as the number of particles increases. Because these results follow from the Central Limit Theorem they apply in both the classical and the quantum cases. The divergence is linear in one dimension and logarithmic in two. The quantum Einstein model also predicts too low a heat capacity, at low temperature, as we saw in Section 4.5.

To go beyond the Einstein model it is necessary to consider a distribution of waves with lengths varying in scale from the interatomic spacing up to the size of the crystal. The Debye model gives a qualitatively correct description of the long wavelength

crystal vibrations and qualitatively improved predictions for the mean-squared displacement and heat capacity.

The Debye model begins by ignoring atomistic details and picturing the crystal as an isotropic continuum. In three dimensions the possible "plane-wave" excitations of a continuum ( $\exp(2\pi i \mathbf{n} \cdot \mathbf{r}/L)$ ) can be labelled by triples of integers  $\{n_x, n_y, n_z\}$ . For isotropy, waves with the same value of  $n = (n_x^2 + n_y^2 + n_z^2)^{1/2}$  must have also the same vibrational frequency,  $\omega = 2\pi v = (2\pi c n/L)$ , where  $c$  is the sound speed and  $\lambda = L/n$  is the wavelength. Thus in  $D$  dimensions the number of plane-wave modes with frequencies less than  $\omega$  [corresponding to sets of integers less than  $(vL/c)$ ] varies as  $\omega^D$ . The number of modes in a real system with # degrees of freedom is exactly # while the number of modes available in a continuum is infinite. To correct this deficiency of the continuum description, the frequency distribution is arbitrarily cut off at a maximum frequency  $\omega_{\text{Debye}}$ , such that the total number of modes is  $DN$ . For all of the included vibrations the wavelength  $\lambda$  and frequency  $\omega$  are assumed to be related by the exact long-wavelength dispersion relation:

$$\omega = 2\pi v = ck = 2\pi c/\lambda .$$

The averaged sound velocity  $c$  can be chosen by fitting the second moment of the frequency distribution or by fitting the long wavelength sound velocity. Because these two slightly different ideas are qualitatively similar we will adopt the simpler first approach, avoiding the necessity for averaging the longitudinal and transverse sound velocities, and setting the ratio of the Debye and Einstein frequencies to force agreement of the second moments:

$$\langle \omega^2 \rangle_{\text{Debye}} \equiv \int (\omega^{D+1}/\omega^{D-1}) d\omega = D\omega_{\text{Debye}}^2/(D+2) = \omega_{\text{Einstein}}^2 \Rightarrow$$

$$\omega_{\text{Debye}}/\omega_{\text{Einstein}} = [(D+2)/D]^{1/2} ,$$

in  $D$  dimensions.

From either of the Debye or the Einstein model approximations the free energy and the mean squared displacement can be calculated and compared to the corresponding exact results from the equations of motion. In one dimension for instance the exact Helmholtz free energy per particle, obtained by averaging  $kT \ln(hv/kT)$  over the distribution of frequencies, lies below the Einstein-model prediction,  $kT \ln(hv_{\text{Einstein}}/kT)$ , by  $kT \ln(2^{1/2})$ . Analytic work in two dimensions, using Huckaby's result, and numerical work in three dimensions completes the series of results for one-, two-, and three-dimensional close-packed crystals:

$$(A - A_{\text{Einstein}})/NkT = -0.347 ; -0.273 ; -0.247(\text{FCC}) ; -0.245(\text{HCP}) .$$

Because the Einstein cell model predicts the correct value for the classical internal energy,  $E = NDkT$  in  $D$  dimensions, these same results can equally well be expressed in terms of the excess entropy:

$$(S - S_{\text{Einstein}})/Nk = +0.347 ; +0.273 ; +0.247(\text{FCC}) ; +0.245(\text{HCP}) .$$

The Debye model is qualitatively correct in predicting linear and logarithmic divergence of the mean-squared displacement in one and two dimensions. The predicted three-dimensional result,

$$\langle \delta^2 \rangle_{\text{Debye}} = (DkT/m) \langle \omega^{-2} \rangle_{\text{Debye}} \Rightarrow (9kT/m\omega_{\text{Debye}}^2) = (27kT/5m\omega_{\text{Einstein}}^2) ,$$

is high by about 7% for face-centered cubic close-packed crystals with nearest-neighbor Hooke's-Law forces. The free energy and entropy errors due to the Debye model:

$$(S - S_{\text{Debye}})/Nk = -0.203 ; -0.073 ; -0.008(\text{FCC}) ; -0.010(\text{HCP}) ,$$

are modest improvements over the Einstein model.

### Problem:

Calculate the Einstein frequency numerically for a nearest-neighbor Lennard-Jones potential  $\phi(r) = 4(r^{-12} - r^{-6})$  in a two-dimensional triangular lattice with nearest-neighbor spacing equal to  $2^{1/6}$ . Do this by moving one particle a small distance  $\delta$  and computing the change in energy,  $\delta\phi = (1/2)\kappa_{\text{Einstein}}\delta^2$ . Show that the energy change becomes independent of direction for small  $\delta$ .

### 4.9 Three-Dimensional Polyatomic Molecules

If the atoms in a polyatomic molecule are all linked together by stiff Hooke's-Law springs (including noncentral angular forces proportional to small conformational changes), then the resulting Hamiltonian can be written,

$$H = H_T + H_R + H_V ,$$

where the translational, rotational, and vibrational Hamiltonians have the quadratic forms we have already studied in this Chapter. The canonical partition function, from which the Helmholtz free energy and thermodynamic properties can be derived, follows directly from the assumed Hamiltonian.

Let us illustrate the general approach with a single simple example, the triangular organic molecule cyclopropane,  $C_3H_6$ . The geometry of the molecule appears in Figure 4.14. A description of the locations of all 9 atoms requires 27 Cartesian coordinates so

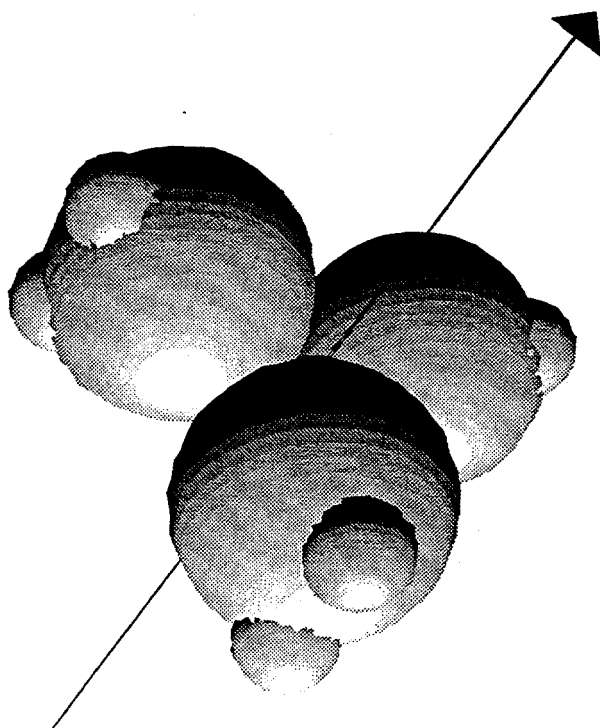


**Figure 4.14.** Geometry of  $C_3H_6$ , cyclopropane. The z axis, about which the molecule has threefold rotational symmetry, is indicated. The basic structure is an equilateral triangle of carbon atoms. The carbon-carbon bond length is 0.1515 nm; the carbon-hydrogen bond length 0.108 nm, and the hydrogen-carbon-hydrogen angle 115.5 degrees.

that the cyclopropane molecule has  $\# = 27$  degrees of freedom. Of these, three locate the center of mass and make a multiplicative contribution to the partition function:

$$Z_T = (V/h^3)(2\pi mkT)^{3/2},$$

where  $m$  is the molecular mass,  $(3 \times 12 + 6 \times 1)/(6.023 \times 10^{23})$  grams for cyclopropane.

To evaluate the rotational partition function for cyclopropane we begin by constructing the moment-of-inertia tensor, adding up the components of the dyadic array  $\sum m_i r_i r_i$ , with the  $\{r_i\}$  measured from the center of mass. Evidently the Lagrangian for rotational motion is a quadratic form including these sums and corresponding angular velocities. For cyclopropane we choose a coordinate system with the z axis perpendicular to the plane of the carbon atoms so that the tensor is diagonal, with  $I_{xx} = I_{yy} = (1/2)I_{zz}$ . See Figure 4.14.

**Problem:**

Use the data quoted in Figure 4.14 to compute the moments of inertia for cyclopropane.

The rotational partition function is:

$$Z_R = (8\pi^2/6h^3)(2\pi kT)^{3/2} I_{xx}(I_{zz})^{1/2}.$$

where the symmetry number of six corresponds to the six equivalent orientations of the cyclopropane molecule. The remaining 21 degrees of freedom are vibrational and

these can be determined by fitting a microscopic force-constant model to experimental data. For each of these vibrations the contribution to the partition function has the same form:

$$Z_V = \prod Z_i ; Z_i = \exp(-hv_i/2kT) / [1 - \exp(-hv_i/kT)] .$$

The single-molecule partition function,  $Z = Z_T Z_R Z_V$ , or equivalently the Helmholtz free energy,  $-kT(\ln Z_T + \ln Z_R + \ln Z_V)$ , can be calculated in this way for any polyatomic molecule for which the required structural and vibrational information is available. In the next Section we indicate how such properties of individual molecules can be used to predict the result of chemical equilibria.

#### 4.10 Chemical Reactions

We can illustrate the usefulness of molecular partition functions by considering a simplified chemical-equilibrium calculation. Real calculations involve the determination of moments of inertia and vibrational frequencies from experimental data. The symmetry of nuclear spin states imposes requirements on the rotational quantum numbers. To avoid intricate details we illustrate the idea by considering a purely-classical three-dimensional equilibrium system in which homonuclear  $A_2$  molecules can dissociate to form pairs of  $A$  atoms of atomic mass  $m$ . First, for simplicity, we consider the calculation as if all the particles were distinguishable. Then the distinguishable-particle partition function  $Z_D$  for  $N_1$  atoms and  $N_2$  molecules, with the total number of atoms  $N = N_1 + 2N_2$  fixed, can be written as a simple product:

$$\begin{aligned} Z_D &= [N! / (N_1! 2N_2!)] [2N_2! / N_2!] (1/2)^{N_2} (Z_1)^{N-2N_2} (Z_2)^{N_2} \\ &= [N! / (N_1! N_2!)] (1/2)^{N_2} (Z_1)^{N_1} (Z_2)^{N_2} , \end{aligned}$$

$$(Z_1) = V(1/\lambda)^3 ;$$

$$(Z_2) = V(2^{1/2}/\lambda)^3 \exp(\epsilon/kT) (kT/hv) (4\pi^2 m r^2 kT/h^2) .$$

The numerical factors in the first expression for the  $N$ -atom partition function arise as follows. The first factor, in brackets, is the binomial coefficient describing the number of ways to divide  $N$  distinguishable particles into two groups, an "atomic" group with  $N_1$  members, and a "molecular" group, with  $2N_2$  members. The next two terms,  $[2N_2! / N_2!] (1/2)^{N_2}$ , give the number of ways in which the  $2N_2$  members of the "molecular" group can be linked in pairs to form  $N_2$  diatomic molecules. The factor of  $1/2$  arises for each molecule because the order in which the two atoms forming the molecule are chosen is immaterial. The rotational partition function is twice as large as it would be were the particles indistinguishable. Finally, the energy  $\epsilon$  is the static

zero-temperature binding energy of the diatomic molecule relative to two isolated atoms and the vibrational frequency of the molecule is  $\nu$ .

Now consider the more-physical situation in which the atoms *are* indistinguishable. The partition function for indistinguishable atoms is less, by exactly a factor of  $N!$ , than that for distinguishable particles. This can be seen in detail by writing the partition function as a product of partition functions for indistinguishable atoms and molecules:

$$Z_I = [(Z_1)^{N_1}(Z_2)^{N_2}/(N_1!N_2!)] .$$

Because the atoms are indistinguishable the molecular partition function  $Z_2$  is only half that calculated above:

$$(Z_2) = V(2^{1/2}/\lambda)^3 \exp(\epsilon/kT)(kT/h\nu)(2\pi^2 m r^2 kT/h^2) .$$

The two partition functions differ by exactly a factor of  $Z_D/Z_I = N!$ , in accord with the notion that distinguishability cannot affect the composition of the equilibrium state.

To find the equilibrium composition for either system, distinguishable or indistinguishable, with the volume and temperature fixed, we find the composition which *maximizes* the partition function  $Z$ , equivalent to *minimizing* the Helmholtz Free Energy. The partition-function maximum must occur when the reaction induced by a further dissociation  $N_1 \rightarrow N_1 + 2$  and  $N_2 \rightarrow N_2 - 1$  makes no change in the partition function:

$$(Z_2/N_2) = (Z_1/(N_1 + 1))(Z_1/(N_1 + 2)) .$$

Thus, for large  $N_1$ , the equilibrium constant  $K_p$  giving the ratio of diatomic-molecule concentration to the square of the atom concentration becomes,

$$K_p(T) = [N_2/V]/[N_1/V]^2 = [Z_2/V]/[Z_1/V]^2 = e^{\epsilon/kT}(4\pi kT/m)^{1/2}(r^2/\nu) .$$

The calculation of chemical equilibria from spectroscopic information is one of the most useful applications of equilibrium statistical mechanics.

If the constraint of fixed total mass were imposed by using a Lagrange multiplier then a variational calculation minimizing the Helmholtz free energy would show that the Lagrange multiplier is the thermodynamic "chemical potential"  $\mu_i$  divided by  $kT$ :

$$\mu_i/kT = -(\partial \ln Z / \partial N_i)_{N_j, V, T} .$$

In thermodynamics, the equilibrium condition, corresponding to maximizing the partition function, is that the total chemical potential change  $\sum \mu_i \Delta N_i$  vanishes.

### 4.11 Phonons and Photons

Analysis of quantum systems is complicated by the requirements of the Pauli Principle. The Pauli Principle makes quantum calculations in the microcanonical and canonical ensembles unduly cumbersome. Instead it is much more convenient to sum over  $N$  and treat quantum ideal gases using Gibbs' grand partition function:

$$\Xi(z, V, T) = \sum_N Z_N z^N.$$

The grand partition function can be related to thermodynamic properties just as we did the microcanonical and canonical ensembles. The connections with thermodynamics are as follows:

$$\langle E/kT \rangle = (\partial \ln \Xi / \partial \ln T)_{z, V}; \quad \langle N \rangle = (\partial \ln \Xi / \partial \ln z)_{V, T}; \quad PV/kT = \ln \Xi.$$

In the ideal-gas case energy states are products of independent single-particle states so that the canonical partition functions occurring in the sum over  $N$  are products of Boltzmann factors for each occupied state:

$$Z\{N_i\} = \prod \exp(-N_i E_i / kT).$$

Particles obeying Fermi statistics are restricted to  $N_i$  values of either 0 or 1. All such combinations result if the product over all single-particle states  $\prod [1 + z \exp(-E_s/kT)]^{+1}$ , is expanded. Particles obeying Bose statistics are not so restricted. Any level of occupancy is acceptable, so that the corresponding Bose product, over all single-particle states, is  $\prod \sum z^n \exp(-nE_s/kT) = \prod [1 - z \exp(-E_s/kT)]^{-1}$ . Both the Fermi and the Bose results can be summarized in a single expression for the Grand Partition Function,

$$\Xi(z, V, T) = \prod [1 \pm z \exp(-E_s/kT)]^{\pm 1},$$

with the plus sign corresponding to Fermi statistics and the minus sign to Bose statistics.

For small systems the type of boundary influences the allowed energies  $\{E_s\}$ . For sufficiently large systems the resulting boundary-dependent partition function becomes independent of the boundary conditions to order  $N^{-1/D}$  so that either rigid or periodic boundaries can be used. For a *periodic* ideal gas composed of particles with mass  $m$  and energies  $E_n = (n^2 h^2 / 2mL^2)$  these one-particle states are plane-wave states. The single-particle stationary states satisfying *rigid* boundary conditions  $E_{n>0} = (n^2 h^2 / 8mL^2)$  lead to equivalent results in the large-system limit.

In this Section we consider the behavior of two kinds of boson systems which require quantum mechanics for their accurate treatment, radiation, "photons," and lattice vibrations, "phonons." Both types of excitations have no mass and are usually

pictured as waves. Both types of waves are bosons and can therefore occupy the same quantum state repeatedly. Such a situation cannot arise in classical statistical mechanics because the classical energy is continuously variable so that there is no probability that particles share the same energy. The phonons resemble photons only at sufficiently low temperatures. When the density of states falls below the ideal value due to dispersion the phonon energy falls below that which we calculate below and saturates at  $kT$  per lattice mode.

The mathematics of photons and phonons at low temperature is similar, but with the energy, frequency, and inverse wavelength proportional to the speed of light for photons and the speed of sound for phonons, respectively:

$$E_{\text{Photon}} = hv = hc_{\text{Light}}/\lambda ; E_{\text{Phonon}} = hv = hc_{\text{Sound}}/\lambda .$$

The grand partition function for either type of boson is

$$\Xi(z, V, T) = \prod [1 - z \exp(-E_s/kT)]^{-1} ,$$

where the product includes all single-boson states. It is convenient to classify these single-particle energy states according to the set of quantum numbers  $n = (n_x, n_y, n_z)$ , where the magnitude of the quantum number  $n$  is related to the wavelength  $\lambda$ , and energy  $E_s = E_n$ :

$$E = hv = hc/\lambda = nch/V^{1/3} .$$

Because the total number of photons and phonons is unrestricted, as is also the number occupying each energy state, the partition function can be automatically maximized by setting  $(\partial \ln Z / \partial N)_{V, T}$  equal to zero, or, equivalently,  $z = \exp(\mu/kT)$  to 1. Thus the low-temperature chemical potential vanishes for photons and phonons.

The degeneracies of these two kinds of excitations are different. For every quantum-number choice  $n$  there are two separate photon states, corresponding to the two transverse polarization directions of light, and three separate phonon states, corresponding to the longitudinal and two transverse branches of the dispersion relation. Accordingly the grand partition function at equilibrium, explicitly taking degeneracy into account, has the form:

$$\Xi(V, T) = \prod [1 - \exp(-E_n/kT)]^{-\otimes} ,$$

where the degeneracy coefficient,  $\otimes$ , is equal to two for photons, corresponding to the two possible polarizations for transverse waves. For phonons with a given wave vector the longitudinal and transverse vibrational frequencies generally differ. In that case the degeneracy coefficient of three represents a product over the three separate

phonon modes. With this simplified notation the logarithm of  $\Xi(z=1,V,T)$  can then be written as an integral over the quantum number  $n$ ,

$$\ln \Xi(V,T) = -\otimes \int 4\pi n^2 dn \ln[1 - \exp(-E_n/kT)] = PV/kT.$$

The derivative of the integral with respect to temperature then completes the thermodynamic information by providing the internal energy:

$$\begin{aligned} \langle E/kT \rangle &= (\partial \ln \Xi / \partial \ln T)_V; \\ &= \otimes \int 4\pi n^2 dn [E_n/kT] [\exp(-E_n/kT)] / [1 - \exp(-E_n/kT)], \\ &= \otimes [4\pi V / (ch)^3] \int E^2 dE [E/kT] / [e^{+E/kT} - 1]. \end{aligned}$$

In the case of radiation, with degeneracy  $\otimes = 2$ , it is usual to express the energy in terms of the Stefan-Boltzmann constant  $\sigma$ :

$$\langle E/kT \rangle_{\text{Photons}} = (8\pi^5/15)(kT/hc)^3 V \equiv (4V/ckT)\sigma T^4.$$

This expression defines that constant and results from an evaluation of the definite integral  $\int x^3 dx / [e^{+x} - 1] = \pi^4/15 = 6.4939$ .

**Problem:**

Either rewrite the integral as a sum and evaluate the sum, or use Runge-Kutta integration to verify the numerical result just given.

From the dependence of the photon and phonon energies on temperature and volume it is easy to show that Gibbs' free energies for these systems vanish. In either case differentiation of the energy to find the constant-volume heat capacity gives  $C_V = 4E/T$ . Then, integrating  $(C_V/T)$  with respect to temperature gives for the entropy  $S/k = (4/3)E$ . Finally, the Helmholtz Free energy is  $-E/3$  and  $E - TS + PV = G = 0$ . Gibbs' free energy vanishes whenever the Helmholtz free energy is linear in the volume,  $G = A + PV = A - (\partial A / \partial \ln V)_T$ , and in this case reflects the physical fact that photons can be created automatically in such a way as to minimize the Gibbs free energy.

The different values of the sound and light speeds entering into the photon and phonon energies make these systems interesting in very different regimes. For photons a temperature exceeding 50,000 kelvins is required before the photon pressure reaches atmospheric pressure. Thus radiation pressure is mainly of interest to astrophysicists and bomb designers. On the other hand the phonon heat capacity obeys the simple  $T^3$  behavior only so long as the thermal energy is much less than the maximum energy,  $kT \ll h\nu_{\text{Einstein}}$ .

#### 4.12 Electrons in Metals

It seems peculiar that electrons could be treated as ideal in any sense, because two electrons separated by one atomic diameter have an interaction energy of a few electron volts, equivalent to a temperature exceeding 50,000 kelvins. At the same time the localization energy of the electrons,  $h^2/(2mL^2)$  is nearly ten times larger.

But qualitatively convincing experimental evidence for this electron-gas view is indicated in the Figure 4.15. The heat capacity for lithium definitely becomes linear in

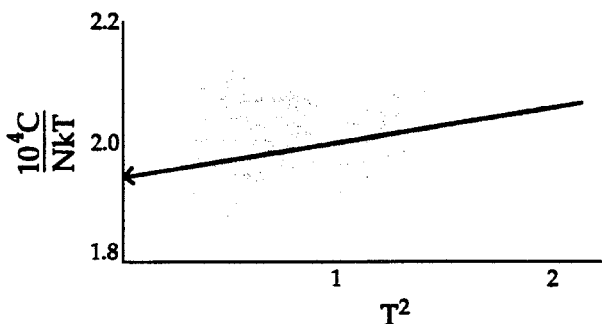


**Figure 4.15.** Low-temperature heat capacity of lithium. The grey area indicates the range of data, plotted so as to separate the linear  $T^1$  electronic contribution from the cubic  $T^3$  lattice heat capacity. The intercept, which gives the coefficient of the linear contribution exceeds the calculated ideal electron-gas value by about a factor of two.

temperature in the regime below about 2 kelvins where the phonon heat capacity of the lattice, proportional to  $T^3$ , can be ignored. Electrons in metals show quantum effects because their mass is relatively small. Let us calculate the heat capacity for an ideal Fermi gas for comparison with the experimental electronic heat capacity.

Electrons have a twofold spin degeneracy so that the grand partition function, expressed as a sum over single-particle states,

$$\Xi(z, V, T) = \prod [1 + z \exp(-E_s/kT)]^{+2},$$

where the plus signs identify the electrons as fermions, gives for the electron energy and the number of electrons:

$$\langle E/kT \rangle = (\partial \ln \Xi / \partial \ln T)_V; \quad \langle N \rangle = (\partial \ln \Xi / \partial \ln z)_V;$$

$$\langle E/kT \rangle = \otimes \int 4\pi n^2 dn [E_n/kT] [z \exp(-E_n/kT)] / [1 + z \exp(-E_n/kT)] =$$

$$\otimes [4\pi V / (ch)^3] \int E^2 dE [E/kT] / [e^{+(E-\mu)/kT} + 1];$$

$$\langle N \rangle = \otimes \int 4\pi n^2 dn [z \exp(-E_n/kT)] / [1 + z \exp(-E_n/kT)] =$$

$$\otimes [4\pi V / (ch)^3] \int E^2 dE / [e^{+(E-\mu)/kT} + 1],$$

where  $\otimes$  is the spin degeneracy of 2. The chemical potential needs to be selected to reproduce the correct number of electrons. For lithium at  $13 \text{ cm}^3/\text{mole}$   $\mu$  is 5 electron

volts. A numerical evaluation of the integral leads to a predicted heat capacity half that shown in the Figure, reflecting the inhomogeneity in the "electron gas" induced by the lattice of positive ions.

**Problem:**

Use numerical integration to determine the chemical potential for the conduction electrons in lithium metal, one per nucleus, in order to reproduce the molar volume of the metal, 13 cm<sup>3</sup>.

**4.13 Mayers' Virial Expansion of Thermodynamic Properties**

All of the applications we have so far discussed have been simplified by separating the energy into one-dimensional problems, either by considering effectively noninteracting particles, such as the one-dimensional hard-rod gas, or by considering noninteracting elastic wave modes, as in the one-dimensional chain and the quantum ideal gases. To go beyond such problems generally involves numerical work, but there is one important exception to this rule, the systematic "virial" expansion of the thermodynamic properties in powers of the number density developed by the Mayers. This approach makes it possible to deduce the general aspects of condensation and was particularly important for the progress of statistical mechanics before computer simulation superseded cumbersome analytic approaches.

The Mayers' treatment can be carried out in other ensembles, but for clarity and simplicity we use the canonical ensemble. Likewise, quantum polyatomic mixtures can be treated but we choose instead to consider a classical system of particles which interact with a central pairwise-additive potential function  $\phi(r)$ . If this function could be treated as a small perturbation then the partition function would approach that of an ideal gas. The Mayers' idea was to expand the Boltzmann factor in the partition function,

$$Z = (1/N!)(\lambda^3)^{-N} \int \dots \int dr^N \exp[-\sum \phi/kT] ,$$

as a power series in the deviation from ideality. The sum in the exponent is to be taken over all  $N(N-1)/2$  pairs of particles. The Mayers' expansion introduces the "f-function"  $f(r)$ , and results in a product of  $N(N-1)/2$  terms, one for each pair:

$$\exp[-\Phi/kT] = \exp[-\sum \phi/kT] = \prod \exp[-\phi/kT] \equiv \prod [1 + f] ;$$

$$f(r) \equiv \exp[-\phi(r)/kT] - 1 .$$

The effect of introducing the f-function expansion is to generate a power series number-density expansion of the free energy around the low-density limit. We illustrate how the density series arises by writing out the full expansion for three particles:

$$Z_3 = (1/3!)(\lambda^3)^{-3} \int \dots \int dr^3 [1 + f_{12} + f_{13} + f_{23} + f_{12}f_{13} + f_{12}f_{23} + f_{13}f_{23} + f_{12}f_{23}f_{13}]$$

The first term in brackets integrates to  $V^3$ . Provided that the container is larger than the range of the potential  $\phi$ , the next three integrals are proportional to  $V^2$ , and become negligible relative to the first term at large  $V$ . The four remaining terms all vanish unless all three particles can interact as a "cluster." All such contributions are proportional to the volume  $V$ . Thus in the general case the Mayer's' idea generates a polynomial in the volume  $V$  which can formally be expressed as a power series in the number density,  $N/V$ . In the process of extracting the  $N$ th root of the partition function, to calculate the free energy per particle, the apparently divergent series becomes convergent, and, for low enough number density, useful.

In the general case it is only necessary to collect together terms with the same topological structure and to evaluate the corresponding integrals. For instance the integrals of  $f_{12}$ ,  $f_{23}$ , and  $f_{13}$  over configuration space are clearly equal, by symmetry. In the three-particle partition function there are three topologically different types of clusters, so that the integral could equally well be written:

$$Z_3 = (1/3!)(\lambda^3)^{-3} \int \dots \int dr^3 [1 + 3f_{12} + 3f_{12}f_{13} + f_{12}f_{23}f_{13}] .$$

In a many-body system there is one more type of integral which contributes to the nonideal free energy to the same order as those shown,  $\int \dots \int dr^4 f_{12}f_{34}$ . If we now write in the correct many-body combinatorial factors, and calculate the ratio of the partition function to the corresponding ideal-gas form, we get:

$$\begin{aligned} Z_N/Z_{\text{Ideal}} = \\ V^{-N} \int \dots \int dr^N [1 + [N(N-1)/2]f_{12} + [N(N-1)(N-2)/2]f_{12}f_{13} + \\ [N(N-1)(N-2)(N-3)/8]f_{12}f_{34} + [N(N-1)(N-2)/6]f_{12}f_{13}f_{23}] + \dots \end{aligned}$$

Each integral is a product of volume integrations:

$$\begin{aligned} V^{-N} \int \dots \int dr^N [1] &= 1; \\ V^{-N} \int \dots \int dr^N [f_{12}] &= \int dr_{12} f_{12} / V ; \\ V^{-N} \int \dots \int dr^N [f_{12}f_{13}] &= V^{-N} \int \dots \int dr^N [f_{12}f_{34}] = [\int dr_{12} f_{12} / V]^2 ; \\ V^{-N} \int \dots \int dr^N [f_{12}f_{13}f_{23}] &= \iint dr_{12} dr_{13} f_{12} f_{13} f_{23} / V \end{aligned}$$

with only a few of the coordinates constrained by the Mayer  $f$  functions and all of the rest, including one of the members of each cluster, here taken to be Particle 1, contributing a factor of  $V$ .

The final step in converting this series in the inverse volume to a useful expression for the Helmholtz free energy is to express the  $N$ th root of the partition function as an exponential function, thereby generating a density series expansion of the nonideal Helmholtz free energy. In this step a remarkable cancellation occurs. All disconnected clusters of  $f$  functions as well as all clusters which could be made disconnected by removing a single point, disappear in the large- $N$  limit. See Figure 4.16. Apart from a correction of order  $1/N$  the final expression for the free energy is

$$(A_{\text{ideal}} - A)/NkT = (1/N)\ln[Z/Z_{\text{ideal}}] = -\sum(N/V)^{n-1}B_n(T)/(n-1).$$

Differentiation with respect to temperature and volume gives the virial-expansion expressions for the energy and the pressure:

$$E/NkT = (3/2) - \sum(dB_n(T)/d\ln T)(N/V)^{n-1}/(n-1); \quad PV/NkT = 1 + \sum B_n(T)(N/V)^{n-1}.$$

$$B_2(T) = -(1/2)\int dr_{12}f_{12};$$

$$B_3(T) = -(1/3)\int\int dr_{12}dr_{13}f_{12}f_{13}f_{23};$$

$$B_4(T) = -(1/8)\int\int\int dr_{12}dr_{13}dr_{14}f_{12}f_{23}f_{34}f_{41}[3 + 6f_{13} + f_{13}f_{24}];$$

....

The Mayer's result for the general virial coefficient,  $B_n(T)$ , can be written as a sum, over all  $n$ -point "star graphs," with the points labelled and distinguishable, of products of the corresponding  $f$  functions linking these points:

$$B_n(T) = [(1-n)/n!]\int\int\dots\int dr^{n-1}\prod f_{ij}.$$

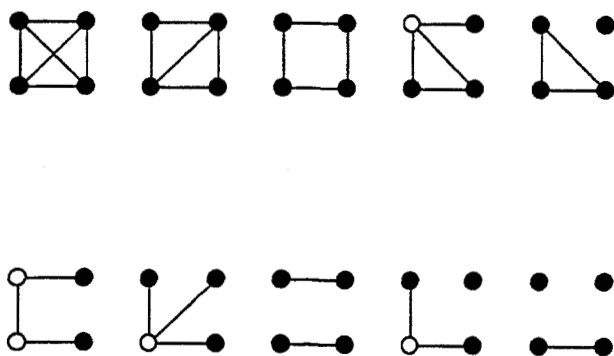


**Figure 4.16.** The ten topologically distinct four-particle products of Mayer  $f$  functions. The diagrams reflect the Mayer's notation, with the  $f$  functions indicated by lines connecting the corresponding points. Cut points, sometimes called "articulation points," are shown here as open circles.

Star graphs are connected graphs linking together  $n$  points in such a way that removal of any point *fails* to separate the resulting  $n-1$  point graph into disconnected graphs. All star graphs are included in this sum for  $B_n(T)$ . The number of topologically-distinct types of star graphs increases rapidly with the number of points  $n$ . About 30 years ago Ford and Uhlenbeck compiled a list of all star graph types of up to seven points. There are 10 types of 5-point stars, 56 types of six-point stars and 468 types of seven-point stars. Extending Ford and Uhlenbeck's tabulation to the eight-point stars by hand was not an appealing task. In 1990 Foidl and Kasperkovitz programmed a work station so as to list the 7123 types of eight-point stars.

In most cases the integrals corresponding to the graphs need to be worked out numerically. The hard-rod gas studied in Section 4.2 is an exception and furnishes a useful check of the Mayer's expansion. It is easy to see, because the  $f$ -function is  $-1$  for  $-\sigma < x < +\sigma$ , that the integral  $\int f dr$  is  $-2\sigma$ . The evaluation of the integral contributing to the third virial coefficient,  $\iint dr_{12} dr_{13} f_{12} f_{13} f_{23} = -3\sigma^2$ , is shown in Figure 4.17. These integrals give second and third virial coefficients of  $\sigma$  and  $\sigma^2$ , respectively, in agreement with Tonk's analytic equation of state derived in Section 4.2.

In the one-dimensional hard-rod case the integrals contributing to  $B_4$  have values  $3(+16/3) + 6(-14/3) + 1(+12/3) = (60 - 84)/3$ . As this simple example suggests, near cancellation of the positive and negative terms complicates numerical evaluation of the higher virial coefficients. The integrals need to be worked out with high accuracy. Only for fairly simple force laws is it possible to generate more than a few accurate terms in the series. For hard spheres the first seven terms are accurately known. Nevertheless the error in the seven-term expansion of the hard-sphere pressure reaches 10% at the freezing density.

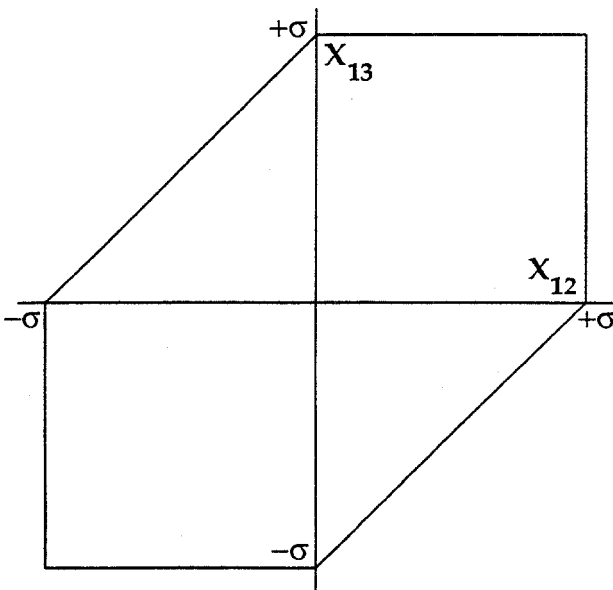


Figure 4.17. Integrand for the hard-rod third virial coefficient. The hexagonal region, in which each rod overlaps the other two has an area  $3\sigma^2$ . Because the product  $f_{12}f_{13}f_{23}$  is  $-1$  in that region the corresponding integral is  $-3\sigma^2$ .

**Problems:**

1. Explain why the number of *types* of  $n$ -point star graphs is about  $2^{n(n-1)}/2/n!$
2. Express the second virial coefficient  $B_2(T)$  for three-dimensional soft spheres, with the potential function  $\phi(r) = \epsilon(\sigma/r)^n$ , in terms of the gamma function and determine the logarithmic derivative  $d \ln B_2(n)/d \ln T$ .
3. For the "Gaussian Model," with the Mayer  $f$ -function  $f(r) \equiv -\exp(-r^2/2)$ , the star integrals in  $D$  dimensions are simple powers of the corresponding one-dimensional integrals. Compute  $B_2$ ,  $B_3$ , and  $B_4$  for this soft repulsive potential in one, two, and three dimensions.
4. Find the closed form for the "Carnahan-Starling" approximation to the hard-sphere equation of state:

$$PV/NkT = 1 + 4x + 10x^2 + 18x^3 + 28x^4 + \dots,$$

where  $x$  is  $(\pi\sigma^3/6)(N/V)$ . Use this closed-form expression to evaluate the ratio of the corresponding  $N$ -sphere canonical partition function to the ideal-gas partition function at the freezing density. The hard-sphere freezing density is about two-thirds the maximum close-packed value.

Except at very low densities, where a few terms give an accurate representation of the energy and the pressure, it is considerably simpler to obtain the thermodynamic properties by direct simulation rather than evaluating the Mayer's virial coefficients. Nevertheless a numerical evaluation of the five-term approximation to the virial series is feasible for simple force laws and leads to semiquantitative agreement for gas-phase isotherms quite close to the critical point. See Figure 4.18 for a comparison of the truncated virial series with the results of direct computer simulation using the Lennard-Jones pair potential.

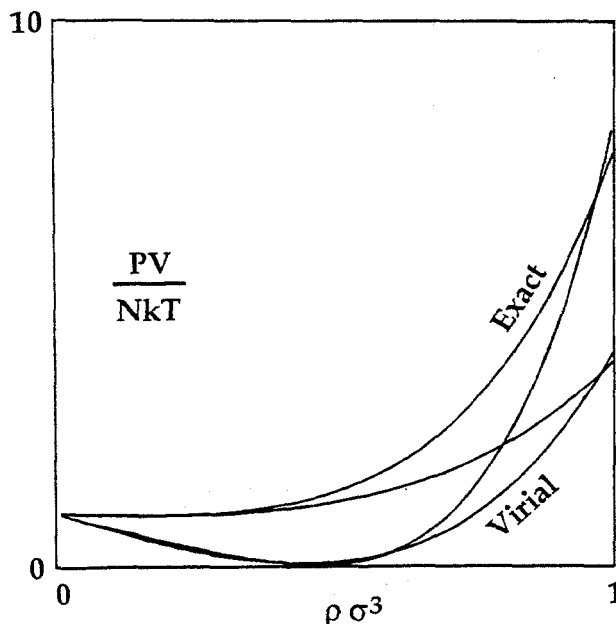


**Figure 4.18.** The five-term virial approximation to the Lennard-Jones mechanical equation of state is compared with computer simulation data. The virial series is low by approximately a factor of two at the highest density shown. The isotherms correspond to the temperatures  $kT/\epsilon = 1.35$  and  $2.74$ .

#### 4.14 Thermodynamic Perturbation Theory

Perturbation theory offers a method of using known properties of a reference system to approximate the properties of a system with a somewhat different Hamiltonian. This idea can be applied to statistical calculations by taking the phase-space probability density for one Hamiltonian as a basis, calculating the effects of the difference  $\delta H = H - H_0$  as a perturbation. Typically the kinetic energy is unaffected by the perturbation so that the change in the Hamiltonian is only a change in the potential energy,  $\delta H = \delta \Phi$ . If we indicate the reference system with a subscript  $0$ , then the partition function ratio gives directly the difference in free energy as the averaged exponential of the perturbation energy over the reference probability distribution:

$$\begin{aligned} \exp(-A/kT)/\exp(-A_0/kT) &= \frac{\sum \exp[-(H_0 + \delta H)/kT]}{\sum \exp[-H_0/kT]} \\ &= \langle \exp(-\delta H/kT) \rangle_0 = \langle \exp(-\delta \Phi/kT) \rangle_0 \end{aligned}$$

where the angular brackets with the subscripted angular brackets  $\langle \dots \rangle_0$  indicating an average over the reference distribution function. To first order in  $\delta \Phi$ , the averaged perturbation free energy is given by:

$$\begin{aligned} A - A_0 &\equiv -kT \ln[\langle \exp(-\delta \Phi/kT) \rangle_0] \approx \\ &kT \ln[\exp(\langle \delta \Phi \rangle_0/kT)] \approx \frac{\sum \delta \Phi \exp(-H_0/kT)}{\sum \exp(-H_0/kT)}. \end{aligned}$$

Using an inequality of which Gibbs was very fond,  $e^x > 1 + x$ , where  $x$  is  $-\delta \Phi/kT$ , establishes that this first-order approximation to the free energy is also a rigorous upper bound:

$$Z > Z_0 \exp(-\langle \delta \Phi \rangle_0/kT); \quad \delta A < \langle \delta \Phi \rangle_0.$$

Thus the actual partition function *always* exceeds the approximate one constructed using first-order perturbation theory.

If the potential energy is a sum of pair terms the perturbation energy can be expressed in terms of the pair distribution  $g_0(r)$  for the reference system:

$$\langle \delta \Phi/kT \rangle_0 = (N^2/2V) \int dr 4\pi r^2 g_0(r) (\phi - \phi_0).$$

In the reference system  $g_0(r)$  is defined as the probability of finding a second particle at a distance in the range  $r$  to  $r+dr$  divided by the corresponding probability in an ideal gas with the same number density,  $(N4\pi r^2 dr/V)$ . One commonly-used reference system is the hard-sphere fluid because the two-body distribution function for this system is known accurately. For details see Mansoori and Canfield's 1969 papers in the Journal of

Chemical Physics. A simple and useful approximation to the hard-sphere Helmholtz Free Energy function is:

$$(A - A_{\text{Ideal}})/NkT = 4x + 5x^2 + 6x^3 + 7x^4 + \dots = \sum(n + 3)x^n,$$

where  $x$  represents a reduced density,  $\pi\sigma^3N/6V$ , for hard spheres of diameter  $\sigma$ . The pair distribution function  $g_o(r)$  can be used to calculate approximate thermodynamic properties for any pair potential. The agreement obtained for the Lennard-Jones potential is quite satisfactory, as is indicated in Figure 4.19.

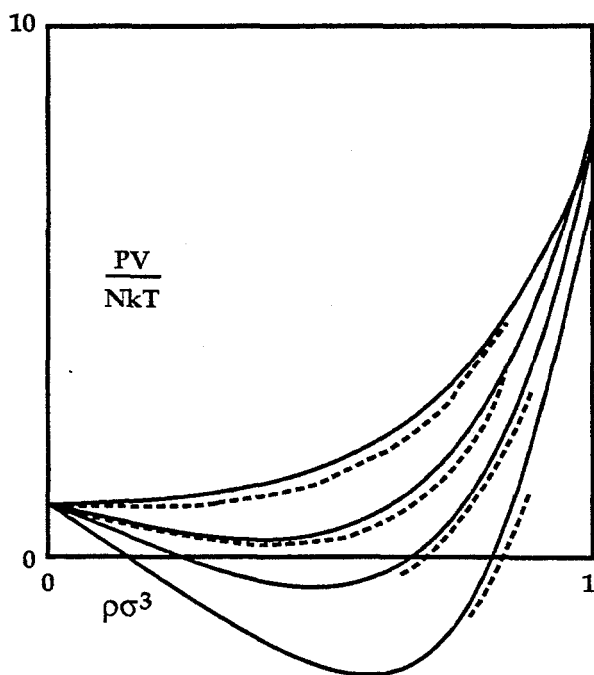


Figure 4.19. Comparison of the Lennard-Jones mechanical equation of state with the prediction of Mansoori and Canfield's Perturbation Theory. Each of the four approximate isotherms, for the set:

$$\{kT/\epsilon\} = \{0.72, 1.00, 1.35, 2.74\},$$

shown as solid lines, lies slightly above the corresponding data obtained from computer simulations.

Only a few systems are simple enough to treat analytically. To illustrate the perturbation-theory process consider one of these simple cases, a one-dimensional harmonic chain. The Hamiltonian contains Hooke's-Law nearest-neighbor springs and the usual kinetic energy:

$$H = H_0 + \delta H = \sum p^2/2m + \sum(\kappa/2)(x_i - x_{i+1})^2.$$

In Section 6 we found that the large- $N$  exact Helmholtz free energy for this system is  $A/NkT = \ln(hv/kT)$  where  $(2\pi v)^2 \equiv \omega^2 = \kappa/m$ . For an even simpler reference system let us consider the simple independent-oscillator Einstein-model Hamiltonian:

$$H_0 = \sum p^2/2m + \sum(\kappa_0/2)(\delta x_i)^2.$$

The first-order perturbation evaluation of the exact potential energy function is,

$$\langle \delta\Phi \rangle_0 = \langle \sum (\kappa/2)(x_i - x_{i+1})^2 \rangle_0 = \langle \sum \kappa x_i^2 \rangle_0 = (\kappa/\kappa_0)kT,$$

corresponding to an upper bound on the free energy:

$$A/NkT < \ln[h(\kappa_0/m)^{1/2}/(2\pi kT)] + \langle \delta\Phi/NkT \rangle_0 = (1/2)\ln\kappa_0 + (\kappa/\kappa_0) + \text{constant}.$$

The value of  $\kappa_0$  which minimizes the approximate free energy is exactly equal to the Einstein value,

$$\kappa_0 = 2\kappa \equiv \kappa_{\text{Einstein}}.$$

This result, that the perturbation-theory estimate of  $\kappa_0$  agrees with the Einstein frequency is generally valid, not just in one dimension, but also in two and three. The general result that the perturbation-theory free energy is too high establishes that the Einstein-model partition function is *always* an underestimate of the true partition function.

#### 4.15. Summary and References

The one-dimensional hard-rod and harmonic-chain models give useful caricatures of many-body systems. The corresponding N-body partition functions reduce to Nth powers of 1-body partition functions. In both cases the individual-particle rms displacements are proportional to the square root of the number of particles.

These one-dimensional translational and vibrational problems, along with two- and three-dimensional rigid rotors, all illustrate the general rule, required by Bohr's Correspondence Principle, that *a single quantum state corresponds to a classical phase-space hypervolume  $h^\#$ .*

The vibrational frequencies for any periodic harmonic crystal follow from the motion within a single periodic unit cell. The low-frequency probability density, proportional to the Debye-model distribution  $\omega^{D-1}$ , governs both the low-temperature quantum heat capacity and the size-dependence of the atomic rms displacement.

By combining the *translational, rotational, and vibrational* contributions to molecular partition functions, low-density chemical equilibria between reacting polyatomic molecules can be predicted.

In appropriate ranges of temperature and density the conduction electrons in metals, the photons in the radiation field, and lattice vibrations, phonons, can all be usefully approximated as quantum ideal gases, by using Gibbs' Grand Canonical Partition Function.

The Mayers' systematic density expansion of the dense-fluid partition function—the virial series—provides a semiquantitative description of condensation. Another systematic approach, perturbation theory, uses reference system distribution functions to estimate the contribution of Hamiltonian perturbations to the free energy. Perturbation theory provides a relatively simple and more-nearly accurate approximation to the properties of real fluids.

Tonks' 1936 paper in *Physical Review* is a classic. The Mayers' readable text *Statistical Mechanics* contains a wealth of analysis devoted to the virial series as well as a comprehensive treatment of the partition functions of polyatomic molecules. Additional discussion of number dependence can be found in my 1985 Springer-Verlag book, *Molecular Dynamics*. A method for enumerating star graphs appears in C. Foidl and P. Kasperkovitz, "Systematic Generation of Linear Graphs-Check and Extension of the List of Uhlenbeck and Ford," *Journal of Computational Physics* 89, 246(1990). For details of two-dimensional triangular lattice calculations see D. A. Huckaby, "Exact Classical Harmonic Free Energy of the Triangular Lattice," *Journal of Chemical Physics* 54, 2910 (1971) and W. G. Hoover, A. J. C. Ladd, D. Friesen, and B. Moran, "Analytic and Numerical Surface Dynamics of the Triangular Lattice," *Journal of Chemical Physics* 76, 3744 (1982). The liquid perturbation theory pioneered by G. A. Mansoori and F. B. Canfield, "Variational Approach to Melting and the Equilibrium Properties of Simple Liquids," *Journal of Chemical Physics* 51, 4958 and 4967 (1969) has reached a high degree of sophistication. See for instance D. Boercker and D. A. Young, "Variational Limits on the Helmholtz Free Energy of Simple Fluids," *Physical Review A* 40, 6379 (1989). Data for testing such phenomenological approaches can be found in F. H. Ree's "Analytic Representation of Thermodynamic Data for the Lennard-Jones Fluid," *Journal of Chemical Physics* 73, 5401 (1980) and "Thermodynamic Properties of the Fluid and Solid Phases for Inverse Power Potentials," by W. G. Hoover, S. G. Gray, and K. W. Johnson, *Journal of Chemical Physics* 55, 1128 (1970).

## 5. Principles of Equilibrium Molecular Dynamics

*1 Introduction; 2 Relation to Statistical Mechanics; 3 Initial and Boundary Conditions; 4 Interparticle Forces; 5 Virial Theorem and Heat Theorem; 6 Isoenergetic Molecular Dynamics; 7 Gaussian Isokinetic Molecular Dynamics; 8 Nosé-Hoover Isothermal Molecular Dynamics; 9 Isothermal-Isobaric Molecular Dynamics; 10 Numerical Techniques; 11 Stability ; 12 Parallel Computation; 13 Hard-Sphere Dynamics; 14 Summary and References*

### 5.1 Introduction

Scientists were first exposed to the possibility of large-scale computing during the Second World War when numerical simulations began to play a leading role in weapons design. After the War Molecular Dynamics was among the first challenging scientific applications for the fast computers. Fermi, at Los Alamos, and then Alder and Wainwright, at Livermore, took on the classical N-body problem of molecular dynamics, realizing that the only barrier to success was speed, because the principles, laid down by Newton, were straightforward. In conventional isoenergetic molecular dynamics Newton's equations of motion are solved numerically, beginning with assumed initial conditions and subject to fixed boundary conditions. At Los Alamos and Livermore the early exploratory calculations dealt with isolated periodic systems and systems confined by rigid boundaries. At Brookhaven Vineyard's simulations of solid-phase radiation-damage cascades used viscoelastic boundaries to absorb elastic wave energy.

Computer speed was then, and still is now, the limiting factor in computer simulation. In the 1950's Newton's equations were straightforward to solve so long as the total number of operations involved was no more than  $10^9$  or so. A typical 40-hour computation could follow the motion of a few hundred particles for a few thousand time steps.

The early molecular-dynamics calculations were vital to the growth and development of statistical mechanics. In the 1950's computers were still too slow to permit quantitative simulations of data gathered for real materials. At that time the goals were more modest: first, to attain semi-quantitative agreement with laboratory experiments; second, to test the predictions of approximate statistical-mechanical theories against results from computer simulation. Molecular dynamics was particularly useful in evaluating the accuracy of approximate many-body theories for model systems with simple pairwise-additive interatomic interactions. Theoretical approximations were usually based on judicious combinations of intuition and truncated series expansions. Such approximations were plentiful in the days before straightforward simulation supplanted them.

During the past half-century computers have become steadily faster, with larger capacities, and computation has become much cheaper. Today the main bottleneck is dealing with vast quantities of computed "information." Today it would be possible to calculate the progress of a billion particle coordinates for a million time steps. Such a calculation would take a month and generate  $10^{15}$  coordinate values. But at present it

is not at all practical to display, process, or store such a large quantity of "information." Current rates of data transmission are typically less than a billion per day and this places a firm limit on the useful size of present-day simulations.

We will begin this Chapter by relating molecular dynamics simulations to the traditional ensemble theory of statistical mechanics, as developed by Gibbs. We then describe the boundary conditions and the interparticle forces necessary to any simulation. We next discuss four different types of molecular dynamics, each equivalent to a particular Gibbs ensemble. After outlining these four approaches we then illustrate and discuss some of the computational details required to implement these ideas on today's computers.

## 5.2 Relation to Statistical Mechanics

Classical mechanics is the basis of Gibbs' statistical ensemble theory. The formalisms of Newtonian, Lagrangian, and Hamiltonian mechanics are well-suited to *posing* the N-Body problem, but none of these theories offers an operational plan for *solving* the equations of motion, except in very simple circumstances. Gibbs replaced the mechanically well-posed but physically inconceivably-difficult task of integrating the classical many-body equations of motion by the somewhat more manageable task of averaging over static phase-space states. For systems simple enough to make calculations feasible, Gibbs' replacement was a real step forward. There is no doubt that the partition function for a rotating rigid body or a double pendulum can more easily be calculated than can an exact long-time orbit.

The logical foundation for Gibbs' simplification is Liouville's Theorem, which describes the flow of phase-space probability density  $f(q,p,t)$ . Liouville's Theorem guarantees that a homogeneous statistical ensemble, obeying Hamilton's equations of motion and uniformly filling a classical phase-space energy shell, with  $E - (dE/2) < H(q,p) < E + (dE/2)$ , is "stationary." That is, the density function  $f(q,p,t)$  does not change with time,  $(\partial f/\partial t)_{q,p} = 0$ . Only such a time-independent stationary ensemble, with  $f(q,p,t) = f(q,p)$ , can serve as a model for stationary equilibrium properties.

Figure 5.1 illustrates Liouville's flow theorem for an ensemble of harmonic oscillators with a uniform distribution in energy between the limits  $E - (dE/2)$  and  $E + (dE/2)$ . The representative points simply rotate about the origin at the fixed oscillator frequency  $\omega$ . For the circular orbits shown in the Figure there is no tendency for the distribution to change with time. In the general case of a transient nonequilibrium Hamiltonian phase-space flow shape changes can occur, but only with constant comoving volume and density.

Most interesting phase-space flows are chaotic and incredibly complicated, exhibiting a mixing in the phase space more thorough than the mixing of paint. This mixing is promoted by Lyapunov instability, which carries initially neighboring points away from one another exponentially fast. Because interesting flows occur in *bounded* regions of space, exponential divergence typically leads to bending and folding, leading

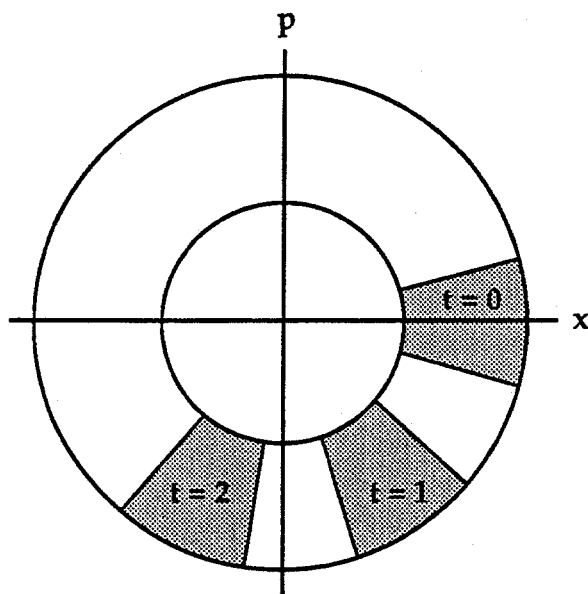


**Figure 5.1.** Constant-Volume phase-space flow of harmonic-oscillator probability density. An ensemble of oscillators, shown shaded, circles the origin at constant energy and angular velocity.

to phase-space mixing. We considered a simple example of this Lyapunov instability in Chapter 1, where we followed the motion of a ball bouncing on a curved surface. We will extend our study of Lyapunov instability to many-body systems in Chapter 11.

Despite the underlying mixing and instability of Lyapunov-unstable phase-space flows, Liouville's Theorem shows that, whatever the motion, simple and regular like the oscillators, or wildly mixing and chaotic, like a fluid of hard spheres, so long as the dynamics is described by Hamilton's equations, the comoving phase-space density cannot change:

$$\{\dot{q} = +(\partial H/\partial p) ; \dot{p} = -(\partial H/\partial q)\} \Rightarrow df(q,p,t)/dt = \dot{f} = 0,$$

Thus, for a uniform energy-shell ensemble, a model of Gibbs' microcanonical ensemble, it is clear that the time and phase averages are identical. Of course such a microcanonical ensemble of noninteracting systems bears scant resemblance to single-system laboratory or computer experiments.

Because statistical ensemble theory and molecular dynamics seem so different, it is natural to view their equivalence with suspicion. The first extensive two- and three-dimensional computer simulations were carried out in parallel. Wood and Parker, at Los Alamos, compared their "Monte Carlo" microcanonical-ensemble simulations to corresponding molecular dynamics simulations of Alder and Wainwright, at Livermore. At first the agreement seemed to be less than perfect, but as the runs became longer and the relatively subtle effects of constraining the center-of-mass motion were included in the analysis, the agreement became perfectly satisfactory, even for the smallest systems, consistent with exact agreement between Gibbs' statistical mechanics and Newtonian dynamics.

Today explicit ensemble calculations can be performed dynamically. Simple computer experiments can be carried out for ensembles with one million members. But it remains much simpler, and is therefore more usual, to follow the phase-space trajectory for a single system, just as in a laboratory experiment. Computational and laboratory experiments usually study single systems, not ensembles.

Is the apparent agreement exact? Is the motion of a single system really related to that of an ensemble? This is still a hard question. It is only in very simple circumstances that a definite answer can be given. In a few simple cases the answer is "yes." An example is a periodic system of two hard disks with zero center-of-mass velocity. The phase-space flow for such a system eventually comes arbitrarily near all phase-space points consistent with the initial total momentum and (kinetic) energy. Such a flow is said to be "quasi-ergodic."

The simpler term "ergodic" was originally used to describe trajectories passing through, rather than just near, all accessible states. Because the number of points on a phase-space surface perpendicular to the flow direction is "uncountable," only strictly periodic flows can be ergodic in this sense. On the other hand the number of points in any computational surface is certainly countable but likewise completely inaccessible. Some systems never leave the immediate neighborhood of stable phase-space "fixed points." An idealized linear system, with independent oscillatory modes, for instance, evolves without any mixing among its modes. It is therefore clear to a physicist that a similar nonmixing motion should prevail if any nonlinear terms perturbing such a linear system are sufficiently small. The corresponding mathematical result is called the Kolmogorov-Arnold-Moser theorem. Fermi's work at Los Alamos showed that the perturbations can be rather large without destroying the nearly-periodic nature of one-dimensional harmonic chains.

A homogeneous phase-space ensemble, filling an energy shell at constant density, is representative of the time-averaged behavior of some dynamical systems, such as a Lyapunov-unstable single pair of two hard disks, but such a homogeneous phase-space-filling ensemble has no relevance to quasiperiodic nearly-linear motions, such as those of a ball rolling in the vicinity of a potential-energy surface minimum.

What about the general case? In most cases the question is irrelevant because the physical time or computer simulation time required to pass even reasonably close to all states is impossibly long. Thus *the utility and validity of statistical mechanics cannot reasonably be based on ergodic theory*. Statistical mechanics must instead be justified on the slightly paradoxical basis that the results are *insensitive* to the initial conditions because the underlying chaotic dynamics is *sensitive* to the initial conditions. In this Chapter we shall therefore consider equations of motion which are consistent with Gibbs' ensemble theory. We rely on Lyapunov instability to induce phase-space mixing, to destroy any dependence on initial conditions, and to provide time averages in statistical agreement with phase-space averages.

In fact the two approaches are very nearly alike. Neither the static phase-space average nor the dynamical time average can be carried out exhaustively. There is not enough time. But there is also no reason at all to expect that increasing the sampling time would ever reveal any discrepancy between the two approaches. Jaynes has forcefully pointed out that any such discrepancy would signal a new and interesting underlying law of physics.

**Problem:**

Show that the accessible phase space for the periodic two-disk problem outlined above can be reduced to a three-dimensional space  $\{x,y,\theta\}$ . Estimate the order of magnitude of the computer time required to come within a (generalized) distance  $d = (dx^2 + dy^2 + d\theta^2)^{1/2}$  of a given accessible phase-space point assuming that the disks occupy a rectangular periodic box with  $L_y/L_x = 3^{1/2}$  at four-fifths the close-packed density. How small would  $d$  have to be to make the time required exceed  $10^{17}$  seconds? How does this  $d$  compare to the limit of numerical precision imposed by 32-bit arithmetic?

**5.3 Initial and Boundary Conditions**

Prerequisite to any numerical solution of differential equations are the initial and boundary conditions. The initial coordinates are typically lattice sites of a regular lattice. Otherwise it is difficult to fit the required density of particles into the container. The initial velocities are typically chosen from a Maxwell-Boltzmann distribution. For an example see the illustration in Section 10.

The boundary conditions for equilibrium calculations are usually taken to be periodic (with zero center-of-mass velocity) because this choice minimizes the dependence of the results on system size. To simulate the properties of matter with *gradients* of mass, momentum, or energy requires the more complicated boundaries treated later.

The earliest molecular dynamics calculations were carried out on relatively small systems, usually only a few atomic diameters wide and with up to a few hundred degrees of freedom. If such a simulation were carried out with real boundaries most particles would be surface particles. Consider cubes of 32, 108, 256, 500, ...  $4n^3$  particles selected from a face-centered cubic crystal. The number of surface particles for this same series is 28, 76, 148, 244, ...  $12n^2 - 12n + 4$ . To eliminate the surface effects which would otherwise dominate the properties of such small systems, periodic boundaries are most commonly used. See Figure 5.2. In an isolated system with periodic boundary conditions, mass, momentum, and energy are all conserved. When any particle "leaves" the system by passing through a "boundary" an identical "image particle" enters through the opposite boundary.

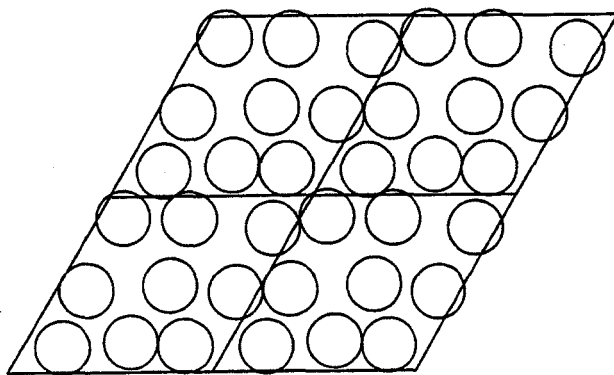


Figure 5.2. A nine-atom two-dimensional periodic system. Four periodic cells are shown.

### Problems:

1. Find the Cartesian coordinates for four particles arranged in a regular tetrahedron within a basic cubic cell of the face-centered cubic structure. The sidelength of such a cubic cell is  $2^{1/2}$  times the interparticle spacing.
2. Find the number and distance of the first-, second-, third-, ... seventh-nearest neighbors of a particle at the origin in a face-centered-cubic crystal. Use an interparticle nearest-neighbor spacing of unity.

Early molecular dynamics simulations at Livermore, using 870 hard disks, showed that the melting transition was lowered by about 10% in density and in pressure if the periodic boundaries were replaced by rigid ones. On the other hand, except near phase transitions, small-system boundary effects in fluid  $N$ -particle periodic systems were generally of order  $1/N$ . Accordingly, most equilibrium simulations have used periodic boundaries.

With the gains in computer speed, size, and economy it is now possible to study million-particle *driven* nonequilibrium systems with relatively complex boundary conditions. One of the earliest successful boundary types was Ashurst's "fluid wall," a set of particles separated from the bulk by a reflecting barrier. See Figure 5.3. The mean velocity and temperature of this set of boundary particles can be controlled so as to induce a shear flow or a heat flux at a system boundary.

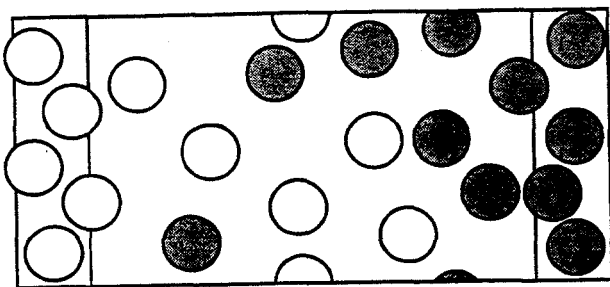
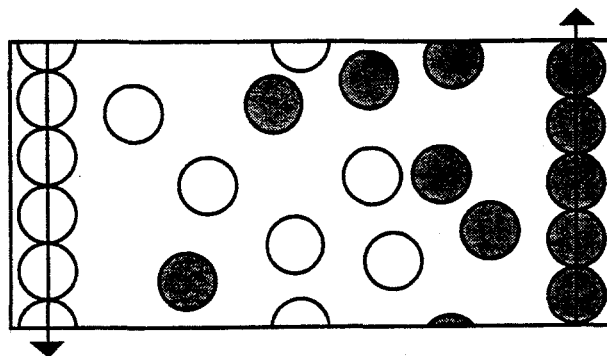


Figure 5.3. Viscous flow driven by the motion of Ashurst's globally-constrained "fluid walls." Upward-moving particles have been shaded. Both the total momentum and the kinetic energy of the four-particle wall regions are fixed by Gaussian thermostats described in Section 7.

**Figure 5.4.** Viscous flow driven by the motion of rigidly-moving corrugated walls. Upward-moving particles have been shaded. The walls move as units with their thermal motion controlled by Nosé-Hoover thermostats as is described in Section 8.



Shockwaves were generated by balancing entering and leaving streams of particles. For a steadily moving wave the balance of the mass, momentum, and energy current in such streams must satisfy the Hugoniot conditions discussed in Section 2.7. Moving and oscillating boundaries were likewise used to induce viscous flows. See Figure 5.4. Vineyard pioneered the use of boundary springs and dashpots to mock up the properties of a larger surrounding medium. These varied boundary types gradually led to new forms of equilibrium and nonequilibrium mechanics, specially suited to highspeed computer simulation. In this Chapter we consider the connection of these methods to Gibbs' statistical mechanics. We will return to nonequilibrium mechanics in Chapter 10.

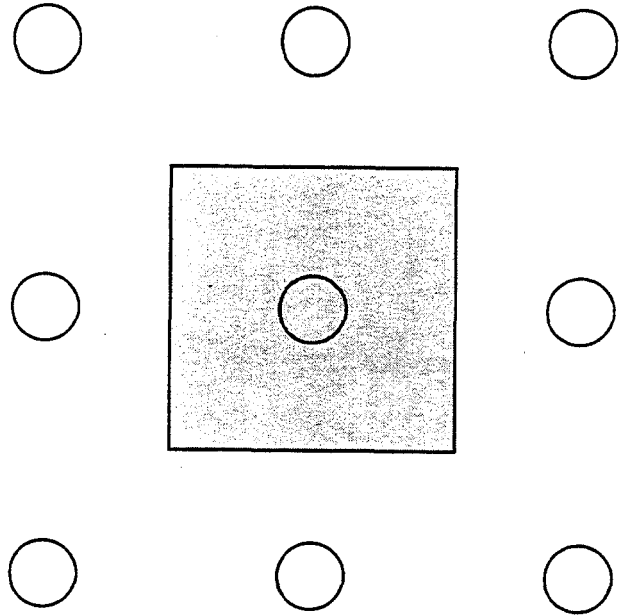
#### 5.4 Interparticle Forces

Before undertaking any molecular dynamics simulation the forces must be specified. The earliest calculations used the simplest possible forces, hard-sphere and square-well interactions. Because these forces generate piecewise-linear trajectories with isolated impulsive momentum transfers the calculations can be faster than those using continuously variable forces. The simplest differentiable extension of the singular hard-sphere potential is the family of inverse-power "soft-sphere" or "soft-disk" potentials:

$$\phi(r) = \epsilon(\sigma/r)^n,$$

all of which satisfy a scaling relation discussed in detail in Chapter 6, with an excess Helmholtz Free Energy depending on the ratio of the characteristic potential energy to the thermal kinetic energy. This nice scaling property still holds with a finite interaction range and periodic boundary conditions if the interactions are restricted to nearest-image pairs. See Figure 5.5. In practice the energy and pressure calculations are slow to converge from  $n = 4$  ("Maxwell molecules") up to  $n = 6$ . In approaching the hard-sphere limit,  $n = \infty$ , trajectory convergence would probably be difficult. But intermediate values of  $n$  are well-behaved and exhibit both fluid and solid phases with very reasonable equilibrium and nonequilibrium properties.

Figure 5.5. A particle located at the center of the Figure is shown, along with eight of its periodic images. Any other particle within the shaded "nearest-image" region interacts with that central particle rather than with one of the images.



The Lennard-Jones 12-6 potential,

$$\phi(r) = 4\epsilon[(\sigma/r)^{12} - (\sigma/r)^6],$$

originally with variables  $n$  and  $m$  rather than 12 and 6 provides a semi-quantitative description of rare-gas thermodynamic and transport properties. The attractive forces lead to the separate existence of two fluid phases, a gas and a liquid, with a phase diagram resembling that of argon. See Figure 5.6.

The binding energy of a face-centered-cubic crystal, using this potential, is a little more than  $6\epsilon$  per particle, and can be used to fit the well-depth of the interaction to experimental sublimation energies. The static-lattice equilibrium interparticle spacing can likewise be fitted to experimental density data to obtain the collision diameter  $\sigma$ . For gas-phase simulations the second virial coefficient  $B(T)$  is an alternative source of potential parameters. Start with the Mayer's formulation of the second virial coefficient:

$$B(T) = (-1/2) \int 4\pi r^2 dr [\exp(-\phi/kT) - 1].$$

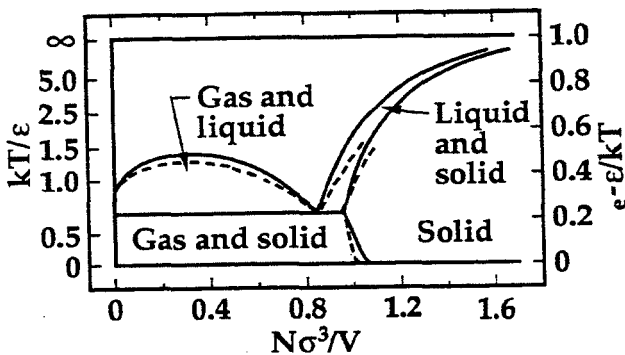


Figure 5.6. Comparison of Lennard-Jones phase diagram with that of argon. The heavy phase lines were determined by computer simulation. The dashes correspond to experimental phase lines for argon.

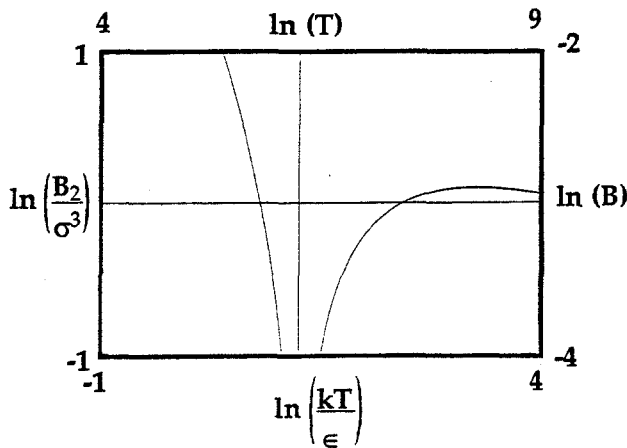


Figure 5.7. Determination of Lennard-Jones potential parameters from second virial coefficient data. The horizontal scale difference is the logarithm of  $\epsilon/k$ . The vertical scale difference is the logarithm of  $\sigma^3$ . The numerical values shown correspond to  $\epsilon/k = e^5$  (kelvins) and  $\sigma = 1/e$  (nm).

If we then introduce a dimensionless integration variable,  $x = r/\sigma$ , we find directly that the “reduced” (dimensionless) second virial coefficient for the Lennard-Jones potential,  $B_{LJ}/\sigma^3$ , is given by a definite integral depending only on the reduced temperature  $kT/\epsilon$ . A logarithmic plot of the experimental data  $\ln B(\ln T)$  can then be compared to the universal theoretical plot giving  $\ln(B/\sigma^3)$  as a function of  $\ln(kT/\epsilon)$ , as is shown in Figure 5.7. The differences in the abscissa and ordinate values give the potential parameters  $\sigma$  and  $\epsilon$  directly:

$$\ln T = \ln(kT/\epsilon) + \ln(\epsilon/k) ; \ln B = \ln(B/\sigma^3) + \ln(\sigma^3) .$$

### Problems:

1. Show that the static-lattice zero-pressure condition for the Lennard-Jones potential implies that the lattice sums  $\Sigma(\sigma/r)^{12}$  and  $\Sigma(\sigma/r)^6$  differ by exactly a factor of two. Use this criterion to find the three-dimensional static-lattice zero-pressure binding energy per particle.
2. Use Runge-Kutta (Simpson’s Rule) quadrature to evaluate the second virial coefficient for the Lennard-Jones potential. Show that the coefficient vanishes at a temperature, the “Boyle temperature” near  $kT/\epsilon = 3.42$ .

Because the Lennard-Jones potential has an inconvenient and unphysical infinite range, it is usual to “truncate” the potential so that the interaction energy and force vanish beyond a specified cutoff distance. It is clear that the truncation should be made smoothly, so as to avoid unnecessary numerical integration errors in the trajectories. For that reason the Lennard-Jones-spline potential described in Section 10 should be used in numerical work. More sophisticated potentials for the rare gases have been fitted to a wide range of physical properties. The most extensive calculations are Barker’s. His results for argon are shown in Figure 5.8. Diatomic and polyatomic molecules can be approximated by rigid arrays of Lennard-Jones force centers.

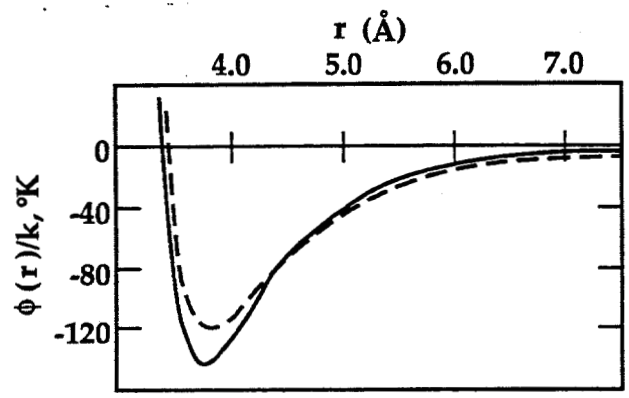


Figure 5.8. Comparison of Barker's accurate potential for argon with the Lennard-Jones potential. The bowl of the accurate potential is about 15% deeper. The accurate high-energy repulsive potential is considerably less steep than the Lennard-Jones inverse twelfth power potential.

Ionic materials require special treatment because Coulomb interactions have notoriously poor convergence properties unless the periodic boundary condition is implemented with care. Remember that the interaction energy of two charges,  $\pm e^2/r$ , is equal to  $kT$  at a separation of 50 nanometers, close to the limiting size of feasible three-dimensional simulations. Thus a strong repulsive force between positive and negative ions is required to stabilize any simulation involving Coulomb attractions. Even a qualitative simulation of a relatively simple material like table salt, crystalline sodium chloride, requires, in addition, forces depending upon the polarizability of the ions. Water is even more complicated and the literature contains several models which describe a selection of water's properties. Fitting the phase diagram of water with such a potential lies well beyond the current state of the art.

Typical metals have complex properties too. Iron has a relatively strong body-centered-cubic structure while that structure is typically mechanically unstable to shear deformation, or nearly so, when pair potentials are used to estimate the shear moduli. For a static lattice a pair potential leads to the prediction that the energy required to insert a vacancy in the crystal is the same as the "binding energy" required to remove an atom. For pair potentials, even taking thermal motion into account, these two energies are nearly equal. A simple face-centered-cubic metal, gold, has a vacancy energy roughly *four times smaller* than its atomic binding energy. The ratio is close to three for the other two coinage metals, copper and silver. In studying the mechanics of cubic crystals it is usual to define three independent elastic constants  $C_{11}$ ,  $C_{12}$ , and  $C_{44}$  which give the dependence of the stress tensor on the strain tensor in an adiabatic deformation. Pairs of the subscripts {1, 2, 3, 4, 5, 6} are conventional abbreviations for the pairs of tensor components, {xx, yy, zz, xy, xz, yz} linked by the elastic constants. For example, the response of  $\sigma_{xx}$  to a strain in the y direction  $\epsilon_{yy}$  is  $C_{12}\epsilon_{yy}$  and defines that elastic constant. Likewise, the response of the shear stress  $\sigma_{xy}$  to a shear strain  $\epsilon_{xy}$  is  $C_{44}\epsilon_{xy}$ . For a pair potential in *any* cubic static lattice the two elastic constants  $C_{12}$  and  $C_{44}$  are equal. But metals do not generally obey this symmetry requirement. Gold has elastic constants  $C_{12}$  and  $C_{44}$  which differ by more than a factor of three. Thus the evidence is clear that even semiquantitative simulations of metals, like those of ionic and covalent materials, require a many-body potential.

For metals, the “embedded-atom” model suggested by Daw and Baskes is a useful phenomenological approach, hardly more expensive to implement than a simple pair potential. The additional part of the energy, the embedded-atom energy  $\Phi_{ea}$ , is based on a density function  $\rho(\mathbf{r})$ , centered on each atom. The embedded-atom contribution to the energy of any atom  $\phi_{ea}$ , say atom  $i$ , is then expressed as an additional nonlinear “embedding” function of the effective density at that atom  $\rho_i = \sum \rho(r_{ij})$ . A simple choice of these density and embedding functions, suitable for describing simple metals like copper and nickel, has the form:

$$\Phi_{ea} = \sum \phi_{ea}(\rho) = \epsilon \epsilon \sum (\rho_i \ln \rho_i) ; \rho_i = \sum \rho_{ij} ; \rho_{ij} = (1/ze) [(R_m^2 - r^2)/(R_m^2 - d^2)]^2 .$$

The quartic density functions vanish beyond the maximum distance  $R_m$ , and provide a binding energy  $\epsilon$  at the rest separation  $d$ , for a coordination number  $z$ . If the embedded-atom interaction involves only the  $z$  nearest neighbors of each atom then  $\rho_i \ln \rho_i$  has its minimum value,  $-1/e$ , for each atom. Such an approach makes it possible to fit the vacancy and surface energies for metals and to account for the difference between two elastic moduli,  $C_{44}$  and  $C_{12}$ , which are identical for any cubic-symmetry arrangement of particles with pairwise-additive forces. The calculations are only slightly more time-consuming than those using purely pairwise-additive forces. This form of the embedded-atom approach does *not* satisfactorily account for the high strength of body-centered metals like iron or for the disordered structures of glasses.

With this introduction to the simple models for treating the interatomic forces in spherical rare-gas atoms, simple diatomic and polyatomic molecules, ionic systems, and metals, we next turn to the formulation of the pressure tensor and the heat flux vector in forms suitable for numerical evaluations.

### 5.5 Virial Theorem and Heat Theorem

In comparing results from many-body molecular dynamics simulations to theoretical predictions or to experimental data microscopic expressions for the mechanical variables, energy, temperature, pressure, and heat flux are required. We wish to emphasize here that the mechanical forms of the pressure and heat flux follow directly from the equations of motion. Microscopic expressions for the flows of mass, momentum, and energy can all be derived directly from mechanics, without using Gibbs’ statistical ensemble averages. The “virial theorem” and “heat theorem” express the pressure tensor and heat flux vector in terms of the microscopic coordinates  $\{\mathbf{r}\}$  and momenta  $\{\mathbf{p}\}$ . To derive the virial theorem start with the time-averaged sum, over all particles, of the tensor product of the particle coordinates and forces  $\{\mathbf{r}\mathbf{F}_i\}$ :

$$\langle \sum \mathbf{r} \mathbf{F}_i \rangle = \langle \sum \mathbf{r} \ddot{\mathbf{m}} \rangle = (d/dt) \langle \sum \mathbf{r} \mathbf{p} \rangle - \langle \sum \mathbf{p} \mathbf{p} / m \rangle ,$$

where the "total" forces  $F_t$  include not only interatomic forces but also interactions with the container walls. Observe next that, because  $\Sigma\langle rp \rangle$  is bounded, the average value of its time derivative must vanish:  $(d/dt)\Sigma\langle rp \rangle = 0$ . For a *stationary* system to which boundary forces with time-averaged values  $P_{xx}$ ,  $P_{yy}$ ,  $P_{zz}$ ,  $P_{xy}$ ,  $P_{xz}$ , and  $P_{yz}$  per unit area are applied at the walls, the forces  $\{F_t\}$  can be separated into internal interatomic contributions and external boundary contributions. Thus the  $xx$  and  $xy$  elements of the tensor  $\Sigma\langle rF_t \rangle$  are  $-P_{xx}V + \Sigma\langle xF_{int}^x \rangle = -\Sigma\langle p_x p_x / m \rangle$  and  $-P_{xy}V + \Sigma\langle xF_{int}^y \rangle = -\Sigma\langle p_x p_y / m \rangle$ , respectively. To simplify the derivation consider the case in which the internal forces are pairwise-additive, with the force on Particle  $i$  due to Particle  $j$ ,  $F_{ij}$ , equal to minus the force on Particle  $j$  due to Particle  $i$ ; then the internal force contributions can be combined and written as sums over pairs:

$$P_{xx}V = \Sigma\langle (xxF/r)_{ij} \rangle + \Sigma\langle p_x p_x / m \rangle ; P_{xy}V = \Sigma\langle (xyF/r)_{ij} \rangle + \Sigma\langle p_x p_y / m \rangle .$$

These expressions for the pressure tensor components are *identical* to those following from explicit volume averages derived in the next Section. Their equilibrium analogs can alternatively be derived directly from Gibbs' canonical partition function. The present derivation is more general. It applies equally well to nonequilibrium and equilibrium states of both solids and fluids.

Because it is straightforward to derive an analogous theorem relating the heat flux vector to a time-averaged sum of atomistic quantities we do so here. To simplify the notation we again consider explicitly the case of pairwise-additive forces. Begin with the time rates of change of the individual-particle energies  $\{\dot{E}_i\}$ , where the individual particle energies include *half* the interaction of each particle with its neighbors,  $E_i \equiv K_i + \Phi_i = p_i^2/2m + \Sigma(\phi_{ij}/2)$ :

$$\begin{aligned} \dot{E}_i &= \dot{K}_i + \dot{\Phi}_i + \dot{E}_i^{wall} = (1/m)[\Sigma p_i \cdot (F_{ij}) + \Sigma(F_{ij}/2) \cdot (p_j - p_i)] + \dot{E}_i^{wall} \equiv \\ &(1/m)\Sigma(F_{ij}/2) \cdot (p_j + p_i) + \dot{E}_i^{wall} . \end{aligned}$$

Multiply by  $r_i$ , sum over all particles, symmetrize, and time average:

$$\begin{aligned} \Sigma\langle r_i \dot{E}_i \rangle &\equiv (d/dt)\Sigma\langle r_i E_i \rangle - \Sigma\langle (p_i/m) E_i \rangle = \\ &(1/m)\Sigma\langle r_{ij}(F_{ij}/2) \cdot (p_j + p_i) \rangle + \Sigma\langle r_i \dot{E}_i^{wall} \rangle = -\Sigma\langle (p_i/m) E_i \rangle , \end{aligned}$$

where we have again used the fact that the averaged time derivative of a bounded quantity,  $(d/dt)\Sigma\langle rE \rangle$ , vanishes. Now imagine that the system is enclosed by boundary walls which can exchange energy with the individual particles. The stationary wall contributions of these boundary forces are the products of the heat flux vector and the

corresponding wall areas. For the  $x$  contribution of this flux we find the final expression:

$$Q_x V = \sum \langle (p_x/m) E_i \rangle + (1/m) \sum \langle x_{ij} (F_{ij}/2) \cdot (p_j + p_i) \rangle .$$

We will consider an alternative derivation of this same heat-flux expression in Chapter 7 and apply it to nonequilibrium flows in Chapter 11.

### 5.6 Isoenergetic Molecular Dynamics

Newtonian mechanics was developed to explain the orbital regularities of the planets. The most fundamental form of molecular dynamics is the straightforward application of this idea on an atomic scale, following the constant-energy development of an isolated system. *Isoenergetic* molecular dynamics is the solution of Newton's classic equations of motion:

$$\{m\ddot{x} = F(x)\} ,$$

for all the degrees of freedom making up the system of interest.

Stoermer's centered second-difference form of Newton's equations of motion,

$$m(x_+ - 2x_0 + x_-) / dt^2 = F_0(x_0) ,$$

is particularly well suited to computer simulation because it is easy to program, has minimum storage requirements, and is remarkably stable. This same simple Stoermer form can readily be generalized to describe isothermal and isobaric forms of dynamics. These more general approaches are discussed in the next three Sections. The extraordinary stability of these Stoermer equations is apparently related to their time reversibility. So long as the underlying difference scheme contains no extraneous exponentially-unstable errors, the symmetry of such time-reversible equations rules out any tendency for the energy to increase or decrease with time.

To implement the Stoermer solution of Newton's isoenergetic equations of motion begin by choosing both current and previous values, one time step earlier, for all the particle coordinates. The difference between these initial values gives an approximate kinetic energy,

$$K_{-1/2} = \sum (m/2) (x_0 - x_-) dt^{-2} ,$$

which can be chosen so as to match the desired initial energy. To continue, simply solve for the new coordinates  $\{x_+\}$  in terms of the current and previous values  $\{x_0\}$  and  $\{x_-\}$ . The subscripts  $\{-,0,+\}$  indicate three successive times, separated by a time step  $dt$ . A conservative choice for the time step separating successive force evaluations is one twentieth of a typical vibrational period. Because this time is much less than a

picosecond, total simulation times for real materials seldom exceed a microsecond of real time.

The same Stoermer algorithm, iterated repeatedly, with the set of three successive times  $\{t-dt, t, t+dt\}$  replacing the set  $\{-, 0, +\}$ , produces a discrete approximation to the hypothetical continuous solution of Newton's equations of motion. Like the original idealized Newtonian equations the Stoermer finite-difference solutions are deterministic and time-reversible.

If geometric constraints are present in the equations of motion these can be included in the numerical solution by using Lagrange multipliers. In addition to the interatomic forces discussed in Section 4, the forces  $F(x)$  can include electromagnetic or gravitational external fields. Angle-dependent forces, such as those stabilizing the covalent bond angles in water or the ionic crystal structure in sodium chloride, require potential functions depending on the coordinates of at least three masses. The simplest such many-body potential is quadratic in the angular distortion,  $\phi(\alpha) = (1/2)\delta\alpha^2$ .

With the forces specified, the resulting motions are followed until the initial conditions have been forgotten and the time averages have stabilized. What are these averages and what is a reasonable sampling time? In the absence of external time-dependent forces the volume and the energy do not change with time. These are the independent state variables of Newtonian mechanics. On the other hand the pressure and temperature fluctuate on the timescale of collisions. These fluctuations establish a minimum timescale for trajectory time averages. A more conservative and realistic estimate can be based on the time required for diffusion across the system. Constancy of the energy furnishes a crude check on the accuracy of the trajectory calculations.

The dependence of pressure on the state variables gives a form of the mechanical equation of state  $P(V, E)$ . Pressure could be determined by averaging momentum transfer at the container wall, but such a pressure is undefined for periodic boundaries and has unreasonably large fluctuations for rigid boundaries. A simpler picture emerges if we view pressure as a spatially-averaged momentum flux. Thus a sampling plane with a particular orientation and area  $da$  will intersect particle momenta or particle-pair line-of-force interactions with a probability proportional to the pressure-tensor component  $P_{ij}$ , the sampling time  $dt$ , and the area  $da$ . See Figure 5.9. The

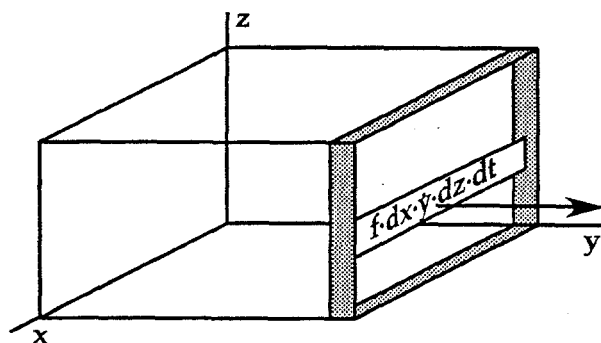


Figure 5.9. Sampling plane for measuring flux of mass, momentum, or energy. Here the kinetic flow of the density "f" in the y direction, during a time  $dt$  and through an area  $dx dz$ , is indicated.

volume-averaged value of the pressure tensor at any time is obtained by computing the flux through such an oriented sampling plane and averaging the location of that plane over the entire volume. If we take this mechanical view of the pressure tensor as the spatially-averaged flux of momentum, there are two contributions, one kinetic and one potential, for systems described by pair potentials:

$$PV = \Sigma(pp/m) + \Sigma r_{ij} F_{ij} .$$

In a fluid, with an "isotropic" pressure tensor,  $P_{xx} = P_{yy} = P_{zz} = P$  in three dimensions, it is usual to average the diagonal elements of the pressure tensor to calculate the scalar hydrostatic pressure:

$$PV = (1/D)[\Sigma(p^2/m) + \Sigma r_{ij} \cdot F_{ij}] .$$

The time-averaged value of this instantaneous pressure provides the mechanical equation of state  $P(V,E)$ . This is exactly the same result derived from the virial theorem in Section 5.

To evaluate the *thermal* equation of state  $T(V,E)$  we need a microscopic definition of temperature. We have already seen that temperature corresponds to the second moment of the ideal-gas velocity distribution. We can adopt this same definition for *any* classical system because Gibbs' statistical mechanics shows that the Maxwell-Boltzmann form of the velocity distribution is the most-probable form for any smooth potential function. Though the energy is fixed, the temperature defined in this way fluctuates, and the fluctuations help determine a reasonable sampling time. In a three-dimensional system the sum of potential and kinetic energies is fixed, with the kinetic part related to the temperature:

$$(3/2)NkT = \langle K \rangle .$$

The kinetic energy contains no contribution from the center-of-mass velocity. Because no forces oppose this motion and because thermodynamic properties are independent of such motion it is most reasonable to exclude it in periodic isoenergetic calculations.

**Problem:**

Show that the classical canonical partition function for the center-of-mass coordinate in a periodic  $D$ -dimensional system of  $N$  identical particles, each with mass  $m$ , is  $(V/Nh^D)(2\pi Nm kT)^{D/2}$ .

The thermal energy can thus be determined as a function of temperature. Then, assuming that the Sackuer-Tetrode ideal-gas entropy applies at low density, the Helmholtz free energy can be found by integrating:

$$d(A/T) = -(E/T^2)dT - (P/T)dV .$$

Thus Newtonian isoenergetic dynamics provides a straightforward route to the complete equation of state. Microscopic analogs of the macroscopic pressure and temperature are first measured as functions of volume and energy. These thermodynamic data,  $P(V,T)$  and  $E(V,T)$ , can then be integrated to obtain the fundamental statistical quantity, the canonical partition function corresponding to the underlying Hamiltonian. It is also feasible to evaluate *second* derivatives of the free energy, such as the compressibility and the heat capacity, by measuring pressure and temperature fluctuations, but better accuracy results if the higher derivatives are evaluated instead by differentiating analytic fits to measured values of pressure and energy.

In extending Newtonian mechanics to microscopic simulations volume and energy are the most natural independent variables. These constants of the motion are fixed by the initial conditions. In real laboratory experiments pressure and temperature are more natural choices. For this reason molecular dynamics methods based on these independent variables have been developed too. We discuss them in the next three Sections.

### 5.7 Gaussian Isokinetic Molecular Dynamics

There are two different, but plausible ways to introduce thermodynamic temperature into molecular dynamics. Both ways are based on the ideal-gas temperature scale. We discuss the simpler isokinetic or "Gaussian" molecular dynamics in this Section and the more elegant canonical isothermal "Nosé-Hoover" molecular dynamics in Section 5.8. In the simpler Gaussian approach to the motion the kinetic energy is kept constant, "isokinetic," by using constraint forces to offset the natural temperature fluctuations. If a globally-averaged ideal-gas thermometer were applied to such an isokinetic system it would always record the same kinetic temperature. We have already seen how to impose such an isokinetic constant-temperature constraint on a many-body dynamical system. Gauss' Principle of Least Constraint suggests using time-reversible constraint forces  $F_c = -\zeta p$ :

$$m\ddot{r} = F(r) - \zeta m\dot{r} ; \zeta = -\dot{\Phi} / 2K = \Sigma(F \cdot p / m) / (2K).$$

This Gaussian "isokinetic" dynamics cannot be applied to a system with only a single degree of freedom, such as a harmonic oscillator, because the velocity would then be a constant of the motion. Two degrees of freedom can be enough. The system of two hard disks with periodic boundaries, discussed in Section 2, for instance, is equivalent to a two-dimensional one-body problem. This problem provides a simple and well-defined example of isokinetic dynamics. Notice that Gaussian dynamics is *time*

*reversible*, with the friction coefficient  $\zeta$  changing sign in the reversed trajectory so that the "frictional" force  $-\zeta p = -(-\zeta)(-p)$  is in fact exactly the same whether a trajectory is traced out forward or backward in time. The fact that the time-reversed trajectory satisfies exactly the same equations of motion establishes the time-reversibility of Gaussian dynamics.

The link between Gaussian isokinetic dynamics and thermodynamics is no different from the Newtonian link. In the isokinetic case both the total energy and the pressure fluctuate in response to Gauss' frictional forces. The time-averaged energy  $\langle E \rangle$  and pressure,  $\langle P \rangle = (1/3)\langle P_{xx} + P_{yy} + P_{zz} \rangle$  in three dimensions, with the tensor components defined as in Section 5, are measured as functions of the kinetic temperature and volume.

$$\langle E \rangle = (1/t) \int ds E(s) ; \langle P \rangle = (1/t) \int ds P(s) .$$

For sufficiently long simulation times  $t$  the Central Limit Theorem suggests expected sampling errors of order  $t^{-1/2}$ . Just as in the Newtonian case, the Helmholtz Free Energy, from which the other thermodynamic functions all follow, can be determined by integration:

$$d(A/T) = -(E/T^2)dT - (P/T)dV .$$

This possibility of controlling the temperature with time-reversible feedback, rather than allowing it to fluctuate, is a relatively-new idea which was stimulated by the availability of fast computers. The details of such schemes vary, but Gauss' formulation is without doubt the simplest of them. The same equations apply if the kinetic energy has a specified time variation,  $K = K(t)$ .

Liouville's phase-space flow equation can be used to show that Gauss' equations of motion apply to a special isokinetic ensemble for which  $\partial f / \partial t$  vanishes. In that ensemble the stationary configurational probability density is canonical, proportional to  $\exp(-\Phi/kT)$  while the momentum probability is microcanonical, proportional to the product of two delta functions,  $\delta[K - (\#kT/2)]\delta[\Sigma p]$ , where  $\#$  is the number of degrees of freedom. Because the mathematics is less cumbersome we will derive the corresponding result only for the isothermal-isobaric ensemble discussed in Section 5.9. Both the Gaussian isokinetic and the Nosé-Hoover isothermal ensembles are special cases of that more general approach.

### 5.8 Nosé-Hoover Isothermal Dynamics

In Gibbs' canonical ensemble the thermal-equilibrium kinetic energy is *not* constant, but instead fluctuates about its average value, with the mean-squared fluctuations proportional to the kinetic part of the heat capacity:

$$\langle \Delta K^2 \rangle / \langle kT^2 \rangle = DNk .$$

It required a really new idea, due to Keio University's Nosé Shuichi, to invent a deterministic time-reversible dynamics reproducing these fluctuations and generating the complete canonical phase-space distribution. We described the simplest derivation of Nosé's equations in Chapter 2. That derivation was based on two assumptions: (1) a constraint force,  $-\zeta p$ , with the *form* of the force suggested by Gauss' Principle; (2) the *requirement* that the canonical distribution be a steady solution of the equations of motion. With these two assumptions, the Nosé-Hoover equations of motion result:

$$\dot{\zeta} = [(K(t)/K_0) - 1]/\tau^2; K_0 = (D/2)NkT .$$

It is interesting that the response time  $\tau$  associated with the heat exchange does not affect the equilibrium coordinate and momentum distributions at all. Of course, time correlations *are* affected for times of order  $\tau$  or larger. If  $\tau$  is chosen on the order of the sound traversal time of the system then the "artificial" nature of the thermostat is unimportant. These same correlations would also be affected by boundary interactions. The Nosé-Hoover equations can easily be integrated using the Runge-Kutta method. As an alternative, a simple modification of Stoermer's numerical method is also effective for solving the Nosé-Hoover equations of motion:

$$(x_+ - 2x_0 + x_-)/dt^2 = (F_0/m) - (\zeta_0)(x_+ - x_-)/(2dt) .$$

The friction coefficient can itself be integrated in time by using either of two time-reversible schemes:

$$(\zeta_+ - \zeta_0)/dt = [\Delta K_{1/2}/\langle K \rangle]/\tau^2; K_{1/2} = \sum m(x_+ - x_0)^2/(2dt^2) .$$

$$(\zeta_+ - \zeta_-)/(2dt) = [\Delta K_0/\langle K \rangle]/\tau^2; K_0 = \sum m(x_+ - x_-)^2/(8dt^2) .$$

Either of these approaches reduces the required storage by roughly a factor of three relative to that required for the fourth-order Runge-Kutta method. The constancy of Nosé's generalized Hamiltonian, as described in Sections 10 and 11, provides a welcome check of the numerical work.

Just as in the Gaussian isokinetic case, Nosé-Hoover dynamics is time-reversible. In the time-reversed trajectory the friction coefficient changes sign so that the "frictional" thermostat force is independent of the direction of increasing time.

### 5.9 Isothermal-Isobaric Molecular Dynamics

Gibbs' isothermal-isobaric ensemble has appeal and utility because temperature and pressure are the fundamental variables describing thermal and mechanical

equilibria. The connection of the isothermal-isobaric ensemble to thermodynamics is a natural extension of the canonical ensemble. To produce an ensemble with a specified pressure  $P_0$  the phase-space weighting function  $\exp[-(E+P_0V)/kT]$  should be used, where the external pressure  $P_0$  and temperature  $T$  are specified independent variables while volume and energy vary. We saw in Section 2.9 that a combined system, including a confining piston with gravitational energy  $P_0V$ , is isenthalpic and isobaric. The corresponding Gibbs ensemble can be described by adding a piston coordinate to the list of dynamical state variables in an otherwise canonical ensemble. Adding a thermostat as well as a piston produces an isothermal-isobaric ensemble. For such a *stationary* ensemble the specified pressure  $P_0$ , determined by the piston mass and area as well as the gravitational field strength, exactly offsets the appropriately-averaged value of  $-(dE/dV)$ . If we retain the notation of a sum over quantum states the isothermal-isobaric partition function becomes

$$\exp(-G/kT) = \sum \exp(-E/kT) \exp(-P_0V/kT) .$$

The connection with Gibbs' free energy can be established in the usual way, differentiating with respect to  $P_0$  and  $T$ , and recognizing the thermodynamic relation  $d(G/T) = (V/T)dP - (H/T^2)dT$ , where  $H$  is the enthalpy,  $H = E + PV$ .

The same ideas can be generalized to the case that the pressure is a tensor function without difficulty.  $P_0V$  is then replaced by the volume integral of  $V_0P_0:\epsilon$ , where  $P_0$  is the pressure tensor and  $\epsilon$  is the strain tensor. The components of the strain tensor become functions of time, obeying feedback equations based on corresponding elements of the pressure tensor.

The isothermal-isobaric ensemble is primarily useful for determining the properties of pure phases. It might be thought that phase equilibria could be treated too, with the volume automatically adjusting to match that of the phase with least Gibbs free energy. This idea has been applied to both solid-fluid and solid-solid phase transformations. In both cases it was found that near equilibrium the rate of transformation becomes too slow to observe. In an early attempt to locate the hard-sphere phase transformation Wood, at Los Alamos, followed two separate constant-pressure calculations, one solid and one fluid, for 40 hours of machine time, hoping to see the less-stable phase disappear. Instead *neither* phase changed. Probably the simplest method for determining the coexistence pressure and temperature for two or more coexisting phases is to equilibrate a system in which *all* phases initially coexist. More accurate results can be obtained, but with more labor, by determining the free energies separately for each coexisting phase.

Let us work out the details of the phase-space flow for the isotropic case appropriate to a fluid, with the pressure a scalar function of volume. We wish to generate the phase-space probability density corresponding to Gibbs' isothermal-isobaric ensemble:

$$\exp(-G/kT) = \Sigma \exp(-E/kT) \exp(-P_0 V/kT);$$

where both pressure and temperature are specified constants, while the volume and energy can vary. Throughout this Section we have added a subscript  $_0$  to emphasize that the pressure  $P_0$ , on which the distribution function depends, is constant and generally differs from the time-varying virial pressure described in Section 5.5, which has a long-time-average value of  $P_0$ . In order to vary the volume it is convenient to introduce special reduced particle coordinates, which we will indicate by  $\{x\}$ . In the simplest possible case, in which the volume  $V$  is a  $D$ -dimensional cube, the scaled Cartesian coordinates  $\{x\}$  represent the usual laboratory-frame coordinates  $\{q\}$  divided by the boxlength,  $V^{1/D}$ . By introducing not only a Nosé-Hoover thermostating friction coefficient  $\zeta$ , but also a variable strain rate  $\dot{\epsilon}$ , a set of differential equations of motion producing the isothermal-isobaric probability density can be worked out. We denote the relaxation times for the temperature and volume by  $\tau_T$  and  $\tau_V$ , respectively. For  $\#$  degrees of freedom, the generalized probability density is:

$$f(x,p,V,\zeta,\dot{\epsilon}) = V^{N-1} \exp[-(1/kT)(E + P_0 V) - (\#/2)(\tau_T \zeta)^2 - (D/2)(\tau_V \dot{\epsilon})^2];$$

$$E(x,p,V) = \Phi(xV^{1/D}) + K(p).$$

The multiplicative factor of  $V^{N-1}$  serves as a Jacobian from the dimensionless variables  $d \ln V \prod dx$  to the laboratory-frame variables. The equations of motion which preserve this distribution are the set:

$$\dot{x} = p/mV^{1/D}; \quad \dot{p} = F(xV^{1/D}) - (\zeta + \dot{\epsilon})p;$$

$$\dot{V} = DV\dot{\epsilon}; \quad \dot{\zeta} = (\Delta K/K_0)(1/\tau_T^2); \quad d\dot{\epsilon}/dt = V\Delta P/(kT\tau_V^2).$$

To see that this is true we need to consider the analog of Liouville's flow equation for the probability density,  $f(x,p,V,\zeta,\dot{\epsilon})$ , in a generalized phase space with coordinate axes  $\{x\}$ ,  $\{p\}$ ,  $V$ ,  $\zeta$ , and  $\dot{\epsilon}$ :

$$\begin{aligned} (\partial f/\partial t) = & -f[(\partial \dot{x}/\partial x) + (\partial \dot{p}/\partial p) + (\partial \dot{V}/\partial V) + (\partial \dot{\zeta}/\partial \zeta) + (\partial/\partial \dot{\epsilon})(d\dot{\epsilon}/dt)] \\ & - [\dot{x}(\partial f/\partial x) + \dot{p}(\partial f/\partial p) + \dot{V}(\partial f/\partial V) + \dot{\zeta}(\partial f/\partial \zeta) + (d\dot{\epsilon}/dt)(\partial f/\partial \dot{\epsilon})]. \end{aligned}$$

Only two of the first five terms on the righthand side are nonzero. Their sum is:

$$-f[(\partial/\partial p)\dot{p} + (\partial \dot{V}/\partial V)] = +f[\#\zeta + (\#-D)\dot{\epsilon}],$$

where # is the number of degrees of freedom. The remaining five terms are as follows:

$$\begin{aligned}
 -\dot{x}(\partial f/\partial x) &= -(f/kT)\Sigma(p/m)\cdot F; \\
 -\dot{p}(\partial f/\partial p) &= +(f/kT)\Sigma(p/m)\cdot [F - (\zeta + \dot{\epsilon})p]; \\
 -\dot{V}(\partial f/\partial V) &= +(f/kT)\dot{\epsilon}[DP_0V - \Sigma(p/m)\cdot F - D(N-1)kT]; \\
 -(\dot{\zeta})(\partial f/\partial \zeta) &= +(f/kT)2(\Delta K)\zeta; \Delta K = K - \#(kT/2); \\
 -(\dot{\epsilon})(\partial f/\partial \dot{\epsilon}) &= +(f/kT)D(V\Delta P)\dot{\epsilon}; \Delta P = P - P_0.
 \end{aligned}$$

Diligent attention to detail reveals that all these terms sum up to zero, verifying that the distribution is stationary,  $(\partial f/\partial t) = 0$ . Thus the equations of motion preserve the isothermal-isobaric phase-space distribution.

In numerical applications it is convenient to eliminate the momentum variables, by differentiating the reduced velocities with respect to time. This shows that the coupled first-order equations of motion:

$$\dot{x} = p/mV^{1/D}; \dot{p} = F(xV^{1/D}) - (\zeta + \dot{\epsilon})p,$$

can be replaced by the equivalent second-order equations:

$$\ddot{x} = (F/m)V^{-1/D} - (\zeta + 2\dot{\epsilon})\dot{x};$$

Special cases of all of these equations apply to the isokinetic ensemble of Section 5.7 and the canonical ensemble of Section 5.8. In both cases the strain rate variable  $\dot{\epsilon}$  is zero. The isokinetic equations correspond to the additional limit  $\tau_T \rightarrow 0$ . Because the equations of motion just described include the necessary features for equilibrium molecular dynamics simulations we describe next a simple numerical method for solving these isothermal-isobaric equations in the following Section on Numerical Techniques.

### 5.10 Numerical Techniques

The first molecular dynamics calculations were carried out by Fermi and his coworkers at Los Alamos. Initially their goal was to characterize the approach to equilibrium of many-body one-dimensional anharmonic chains, using either cubic or quartic anharmonicities. Most of the calculations were carried out with 16 and 32 particles. The results of that work surprised Fermi. The chains failed to equilibrate. Instead the initial condition recurred, relatively accurately, long before the expected Poincaré recurrence time. This failure of the one-dimensional chain to forget its initial

conditions is an example of a system for which Gibbs' statistical mechanics is not a particularly useful theory. For such a pathological system the only way to identify the accessible part of phase space is to carry out a molecular dynamics simulation.

In a more typical situation, with Lyapunov-unstable phase-space mixing, the phase-space average and molecular dynamics simulations can be expected to agree. A typical molecular dynamics simulation proceeds according to the following plan:

- (1) Generate initial configuration and velocities.
- (2) Advance coordinates and velocities by one time step  $dt$ .
- (3) Update averages by summing or integrating.
- (4) Unless enough time has been sampled GO TO (2).

If the basic computer program is to be used for a variety of problems it is convenient to impose the periodic boundaries and to calculate the forces in separate subroutines.

For large systems it would be time-consuming and unrealistic to include interactions between all of the  $N(N-1)/2$  pairs of particles in the system. Generally we would expect shielding to make interactions beyond the first few neighbors of limited physical interest. For this reason the force calculation is usually cut off at a distance only somewhat larger than the expected nearest-neighbor separation. Thus the interaction of two particles is typically zero, except when the two are within the relatively-short range of the forces. In a periodic system it is usual to restrict all the particle coordinates to lie between 0 and  $L$ , or, alternatively, between  $-L/2$  and  $+L/2$ . Then the difference in any two coordinate values,  $x_{ij} = x_i - x_j$  say, lies between  $-L$  and  $L$ . The "nearest-image distance" which gives the coordinate difference between Particle  $i$  and the closest version of the periodic Particle  $j$ , is then computed with the *smallest* (in magnitude) of three possible values,  $\{x_{ij} - L, x_{ij}, x_{ij} + L\}$ . See again the nearest-image convention as illustrated in Figure 5.5. It is convenient at the end of each time step to replace coordinates in a fixed interval, either that from 0 to  $L$  or that from  $-L/2$  to  $+L/2$ . For an integration technique such as Stoermer's, which computes  $x(t+dt)$  from  $x(t)$  and  $x(t-dt)$ , both  $x(t+dt)$  and  $x(t)$  need to be shifted simultaneously.

The Lennard-Jones pair potential,

$$\phi = 4\epsilon[(\sigma/r)^{12} - (\sigma/r)^6],$$

has infinite range, so that the time required to calculate the force for  $N$  atoms varies as  $N(N-1)$ . To avoid this expense Holian and Evans suggested using an interpolating cubic spline between the inflection point  $r_I$  and the cutoff radius  $r_M$ :

$$\phi = 3.2920028(\epsilon/\sigma^3)(r_M - r)^3 - 4.86489008(\epsilon/\sigma^2)(r_M - r)^2$$

$$(r_I/\sigma) = (26/7)^{1/6} = 1.24445506; (r_M/\sigma) = 1.737051787.$$

Such a smooth cutoff is vital to reproducibility of results.

Let us apply the ideas just discussed to an isothermal-isobaric computer simulation. For simplicity we consider a two-dimensional solid system at zero pressure. But the calculations can be generalized easily. From the solution of the equations of motion we will obtain time-averaged values for the energy and volume at the specified temperature and pressure. We choose to study 36 Lennard-Jones-spline particles at a temperature of  $0.20\epsilon/k$ , roughly half the melting temperature. Under these conditions the triangular lattice solid phase shown in Figure 5.10 is mechanically and thermodynamically stable. The lattice coordinates and initial velocities can be generated as follows:

```

INDEX = 0
TEMP = 0.20
IX = 0
IY = 0
DO 10 IROW = 1,6
DO 10 JCOL = 1,6
INDEX = INDEX + 1
8 VX(INDEX) = 10.0*(RANDOM(IX, IY) - 0.5)
IF (RANDOM(IX, IY) .GE. EXP(-VX(INDEX)*VX(INDEX)/(2.0*TEMP)) GO TO 8
9 VY(INDEX) = 10.0*(RANDOM(IX, IY) - 0.5)
IF (RANDOM(IX, IY) .GE. EXP(-VY(INDEX)*VY(INDEX)/(2.0*TEMP)) GO TO 9
IF (INDEX.EQ. (INDEX/2)*2) XNOW(INDEX) = IROW - 0.75
IF (INDEX.NE. (INDEX/2)*2) XNOW(INDEX) = IROW - 0.25
YNOW(INDEX) = (JCOL - 0.5)*SQRT(0.75)
10 CONTINUE

```

where  $\text{RANDOM}(IX, IY)$ , described in Section 3.10, generates suitably random numbers between zero and one and changes the random-number "seeds"  $IX$  and  $IY$  each time it is called. To convert the lattice coordinates, with a nearest-neighbor separation of unity, to "reduced" coordinates corresponding to a total volume of unity, divide both  $x$  and  $y$  values by the square root of  $18.0 \cdot \text{SQRT}(3.0)$ . At the end of each time step it is

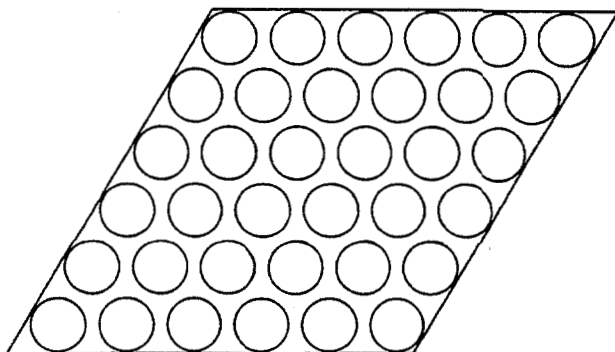


Figure 5.10. 36-particle section of a periodic triangular lattice with interparticle spacing  $d$  and area  $18(3^{1/2}d)$ .

convenient to store the self-explanatory variables {XNEW, XNOW, XOLD} and to replace the variables XOLD and XNOW by XNOW and XNEW. Initially, set XOLD (INDEX) = XNOW (INDEX) - VX (INDEX) \* DT.

In our 36-body two-dimensional example the dynamics is described by  $2N + 3 = 75$  differential equations of four types:

$$\{m\ddot{x} = F/V^{1/2} - (\zeta + 2\dot{\epsilon})m\dot{x}\};$$

$$\dot{\epsilon} = (1/2)d\ln V/dt; d\dot{\epsilon}/dt = V\Delta P/(kT\tau_V^2); \dot{\zeta} = \Delta K/(K_0\tau_T^2).$$

The first of these represents a set of 72 second-order equations of motion, equivalent to 144 first-order equations, written in terms of reduced variables scaled by the square root of the volume  $V$ . In each the force  $F_{ij}$  is a function of the distance  $x_{ij}V^{1/2}$ . The three remaining (first-order) equations determine the controlled variables: strain  $\epsilon$ , strain rate  $\dot{\epsilon}$ , and friction coefficient  $\zeta$ . The one-dimensional strain is half the two-dimensional volume strain,  $d\ln x + d\ln y = d\ln V$ . The last two control equations describe the response of the strain rate  $\dot{\epsilon}$  and the friction coefficient  $\zeta$  to the instantaneous pressure and temperature fluctuations  $\Delta P$  and  $\Delta K$ , which are calculated using the instantaneous mechanical definitions:

$$PV = (1/2)\sum r_{ij}F_{ij} + (1/2)\sum p^2/m;$$

$$K = (1/2)\sum p^2/m.$$

The  $ij$  sum is carried out over all pairs of particles and the kinetic-energy sum includes each particle once.

As in the illustration above, the initial coordinates generally are chosen from a close-packed periodic crystal arrangement. The initial velocities are usually chosen from a Maxwell-Boltzmann distribution; the velocities can subsequently be made to sum to zero by subtracting  $(1/N)\sum v$  from each one. Then the equations of motion are converted to corresponding difference equations:

$$m(x_+ - 2x_0 + x_-)/dt^2 = F_0/V_0^{1/2} - (\zeta_0 + 2\dot{\epsilon}_0)m(x_+ - x_-)/(2dt);$$

$$\dot{\epsilon}_0 = (V_+ - V_-)/(V_0 4dt);$$

$$(\dot{\epsilon}_+ - \dot{\epsilon}_-)/2dt = V_0\Delta P/(kT\tau_V^2);$$

$$(\zeta_+ - \zeta_-)/2dt = \Delta K/(K_0\tau_T^2).$$

Provided that values of the strain rate  $\dot{\epsilon} = d\epsilon/dt$ , the friction coefficient  $\zeta$ , and the set of reduced coordinates  $\{x\}$  are saved from the previous time step this set of  $2N + 3 = 75$  equations can be solved in an explicit four-step process:

1. Compute the set of new coordinates  $\{x_+\}$  from the first equation.
2. Compute the "volume" (here actually an area)  $V_+$  from the second equation.
3. Compute the new one-dimensional strain rate,  $\dot{\epsilon}_+$  from the third equation.
4. Compute the new friction coefficient  $\zeta_+$  from the fourth equation.

There are a variety of interesting features in the solution. To test the computer program for reversibility at time  $t$  (although the underlying equations are obviously reversible) exchange the "now" and "new" coordinates and change the signs of  $\dot{\epsilon}$  and  $\zeta$ ; then take up the calculation again. The trajectory will be retraced, limited in accuracy only by computer roundoff.

To test the computer program for numerical stability try increasing the time step from a conservative value of  $0.0025(m\sigma^2/\epsilon)^{1/2}$ . The equations are still numerically stable for a considerably larger time step, perhaps eight times larger, but become unstable, for larger values.

### Problems:

1. For the one-dimensional Nosé-Hoover oscillator problem,

$$\ddot{x} = -x - \zeta\dot{x}; \dot{\zeta} = \dot{x}^2 - 1,$$

find the maximum time step for which the generalized Stoermer equations of motion just described and the Runge-Kutta equations of motion have solutions and comment on the nature of both solutions for a slightly smaller time step.

2. Consider a single Lennard-Jones particle oscillating between two fixed neighbors in one dimension. Study a canonical isothermal trajectory, using a characteristic energy-transfer time of  $(m\sigma^2/\epsilon)^{1/2}$  and show that the Stoermer dynamics of this problem is stable, over a calculation of several vibration times, using a time step of  $dt = 0.09(m\sigma^2/\epsilon)^{1/2}$  at a temperature of  $kT/\epsilon = 0.35$  and, using a time step of  $0.16(m\sigma^2/\epsilon)^{1/2}$ , at a temperature of  $kT/\epsilon = 0.05$ .

If the temperature is defined by the equation  $NkT = K$  then the total energies and the densities, relative to the zero-temperature zero-pressure density  $\rho_0$ , should be within a percent of the following values, obtained with relatively short runs,  $t_{\max} = 100(m\sigma^2/\epsilon)^{1/2}$ , using time steps of  $0.005(m\sigma^2/\epsilon)^{1/2}$  or  $0.01(m\sigma^2/\epsilon)^{1/2}$ :

Temperature $kT/\epsilon$ :	0.20	0.25	0.30
Energy $E/N\epsilon$ :	-2.56	-2.44	-2.30
Density $\rho/\rho_0$ :	0.955	0.941	0.925

The relaxation times  $\tau_V$  and  $\tau_T$  were arbitrarily chosen equal to  $36(m\sigma^2/\epsilon)^{1/2}$  and  $(m\sigma^2/\epsilon)^{1/2}$ , respectively. The same computer program used to generate these results can also be used for isoenergetic or purely isothermal simulations by removing the extraneous non-Newtonian forces. Because numerical integration is approximate, it is convenient to check the work by examining the constancy of energy and momentum and the reversibility of the trajectories. It might be thought that introducing fluctuations in energy and volume would destroy any constants of the motion, but this is wrong. For periodic boundaries the quantity,

$$C = \Phi + K + P_0 V + (DkT/2)(\tau_V \dot{\epsilon})^2 + K_0(\tau_T \zeta)^2 + 2K_0 \int \zeta dt',$$

where the current time  $t$  is the upper limit on the friction-coefficient integral, is a constant of the motion.

### Problem:

Show that the time derivative of the function  $C$  defined above, evaluated by applying the chain rule to derivatives with respect to  $x$ ,  $V$ , and  $\dot{\epsilon}$ , is identically equal to zero so that the constancy of  $C$  can be used as a numerical check of the computation.

### 5.11 Stability

Before Lyapunov instability was recognized as a nearly universal feature of coupled differential equations, stability was easy to define. A numerical technique was said to be "stable" if two initially close solutions remained close together. This definition is not useful in dealing with Lyapunov-unstable equations. For these systems it is not easy to separate intrinsic instability of the equations from additional numerical instability. A logical requirement is that any additional instability added by the solution algorithm should be small relative to the intrinsic instability in the equations being solved.

In our Chapter 1 example of the Lyapunov-unstable bouncing ball we saw that the information loss rate was about one decimal digit in two bounces. This is typical also for a dense fluid, and means that the initial conditions no longer determine the details of the solution after about a dozen collisions per particle. Despite this "sensitivity to initial conditions" there is no evidence that the trajectory so generated differs in any way from the "better" trajectory which could be generated by using double-precision arithmetic.

Numerically-time-reversible algorithms, like the Stoermer algorithm, are specially well-behaved. The underlying reason for this can be seen in analyzing the linear harmonic-oscillator problem  $\ddot{x} = -x$  with the initial condition  $\dot{x} = 0$ . For a time-reversible method the solution of this problem cannot gain or lose energy because such a hypothetical gain or loss would need to be reversed in the reversed trajectory. Thus

the linear oscillator problem undergoes a *phase error* rather than an *amplitude error*. The rate at which a time-reversible trajectory propagates is slightly too fast or too slow. From an intuitive standpoint phase errors seems less serious than amplitude errors, and for two different reasons. First, in a many-body problem, phase errors tend to cancel to a large extent, making the time-reversible algorithms unreasonably good. Second, amplitude errors tend to amplify through Lyapunov instability, while phase errors do not.

Lyapunov instability is itself a more-subtle nonlinear phenomenon which needs investigation on a case-by-case basis. Its presence can readily be detected by following the phase-space separation of two neighboring trajectories. If the separation is amplified exponentially, as  $\exp(\lambda t)$ , the underlying motion is Lyapunov unstable. In Chapter 11 we will discuss numerical methods for the accurate determination of the Lyapunov exponent  $\lambda$ .

The presence of Lyapunov instability rules out the generation of trajectories which are accurate at long times. Nevertheless these trajectories need to satisfy some basic criteria for acceptability. The main criteria are the preservation of constants of the motion. In isoenergetic Newtonian mechanics with a fixed number of particles and with forces occurring in pairs, with  $F_{ij} + F_{ji} = 0$ , mass and momentum conservation are nearly automatic. Conservation of energy remains as a useful criterion for acceptability.

In Nosé-Hoover mechanics, where energy is no longer conserved, there are analogs of energy conservation which serve as useful checks of the numerical work. For the Nosé-Hoover harmonic oscillator, with a frictional force  $-\zeta p$  maintaining a temperature of unity and following the equation of motion  $\dot{\zeta} = (p^2 - 1)/\tau^2$ , Nosé's generalized Hamiltonian,

$$H_{\text{Nosé}} = (1/2)(q^2 + p^2 + \tau^2 \zeta^2) + \int dt' \zeta(t'),$$

is a constant of the motion. Because Nosé's equations satisfy integral feedback they are absolutely stable from the standpoint of this constant of the motion. For other methods, such as the fourth-order Runge-Kutta method, a rescaling of the velocities:

$$(v'/v)^2 = T_{\text{new}}/T_{\text{old}},$$

can correct for longtime algorithmic amplitude errors.

## 5.12 Parallel Computation

The scale and complexity of molecular dynamics simulations keeps pace with improvements in computer speed and storage capacity. Computer speed is limited by the speed of transmitting data and is currently doubling every ten years. Computer size doubles in three years. In 1990 low-cost transputers are available which make it

possible to carry out CRAY-size CRAY-speed computations at about one-thousandth the cost of a CRAY computer. By linking transputers together in a checkerboard or cube arrangement a calculation can be divided into roughly equal nearly-independent parts which exchange boundary and global average information at the completion of each time step. For efficiency the problem treated needs to be large enough that the data exchange time is small relative to the computational time within each processor. For the 64-transputer SPRINT at Livermore it is relatively inefficient to study problems with fewer than a few thousand particles.

In continuum mechanics each zone interacts only with its contiguous neighbors. Thus distributing parts of a problem to an array of processors is natural for continuum problems in which space can be divided into cells. Atomistic fluid simulations require that particles can change neighbors. To take advantage of this subdividing for molecular dynamics requires additional programming. The simplest approach is to classify particles' locations within a regular gridwork of cells, with a cell width or grid spacing equal to the range of the interparticle forces. By storing the grid coordinates of each particle as well as the coordinates relative to its gridpoint those particles with which it interacts can be readily identified. The required information can be stored more efficiently by using a "linked list."

The gridwork or cell approach reduces the loss of significant figures which would otherwise occur in systems hundreds or thousands of atomic diameters in size. At present an investment of the cost of an automobile in 64 commercially-available megabyte transputers makes it possible to follow the dynamics of one million two-dimensional Lennard-Jones particles in about 30 seconds per Stoermer time step.

### 5.13 Hard-Sphere Dynamics

When molecular dynamics was new it was necessary to test theoretical predictions for the simplest possible interesting system, a classical fluid of three-dimensional hard spheres. Alder and Wainwright at Livermore developed efficient methods for solving the equations of motion for the (discontinuous) hard-sphere potential. The solution method is very different from the Runge-Kutta or Stoermer approaches useful for continuous potentials. Because the hard spheres travel along straight lines between collisions, and at collision simply exchange relative velocity, a hard-sphere molecular dynamics program can be based on a tabulation of times to collision for all pairs of spheres which might reasonably collide.

For hard spheres the molecular dynamics follows this plan:

- (1) Choose initial coordinates and velocities.
- (2) Compute the times  $\{t_{ij}\}$  which must pass before  $i$  and  $j$  collide.
- (3) Select the shortest time and advance all particles.
- (4) Change the velocities of the colliding particles  $i$  and  $j$ .
- (5) Recompute the  $t_{ik}$  and  $t_{jk}$  for the colliding particles.

(6) Update averages.

(7) Unless sufficient collisions have occurred GO TO (3) or GO TO (2).

The collision-time table is occasionally refreshed completely and is modified for the two colliding particles at every collision.

**Problem:**

Integrate the equations of motion for a periodic four-particle chain of Hooke's Law particles, choosing conditions that propagate a rightmoving sinusoidal wave through the system. Find  $dt$  such that the energy is conserved to four figures throughout one wave traversal time. You should find that both the kinetic and potential energies are constants of the motion.

**5.14 Summary and References**

The generalized Stoermer method, which is highly-stable and minimizes storage requirements, is particularly well-suited to large-scale computations of all kinds. The same general scheme can be applied to isoenergetic, isokinetic, isothermal, and isobaric simulations. With such methods simulations involving billions of particles are now technically feasible. But smaller systems of perhaps 100 atoms often provide sufficiently useful results. For *mixing* systems the results of small-system simulations appear to be in exact agreement with Gibbs' statistical mechanics. Computational efficiency is best with periodic boundaries and very smooth potential functions with continuous forces. The many-body embedded-atom approach provides an efficient model for simulating simple metals.

The explosive growth of the computer industry is reflected in the research literature on molecular dynamics. A sceptical attitude is a specially useful prerequisite to research in this area. The Proceedings of the Enrico Fermi Summer School Course 97, "Molecular-Dynamics Simulation of Statistical-Mechanical Systems" as well as D. Frenkel, I. R. MacDonald, and G. Ciccotti's reprint volume *Simulation of Liquids and Solids* (North-Holland, Amsterdam, 1986) give condensed summaries. See also D. C. Rapoport's "Large-Scale Molecular Dynamics Simulation Using Vector and Parallel computers," *Computer Physics Reports* 9, 1 (1988). An admirable comprehensive collection of references and techniques has been provided by M. P. Allen and D. J. Tildesley, *Computer Simulation of Liquids* (Clarendon Press, Oxford, 1987).

For a review of Fermi, Pasta, and Ulam's calculations at Los Alamos see J. L. Tuck and M. T. Menzel, "The Superperiod of the Nonlinear Weighted String Problem," *Advances in Mathematics* 9, 399 (1972). The series "Studies in Molecular Dynamics," mostly by B. J. Alder and T. E. Wainwright, chronicles the early days of hard-disk and hard-sphere dynamics. See for instance the fourth paper in the series, "The Pressure, Collision Rate, and Their Number-Dependence for Hard Disks," *Journal of Chemical Physics* 46, 686 (1967). *Soft-sphere* thermodynamic properties are discussed in a paper by W. G. Hoover, M. Ross, K. W. Johnson, D. Henderson, J. A. Barker, and B. C. Brown, "Soft-Sphere Equation of State," *Journal of Chemical Physics* 52, 4931 (1970). In addition to the papers on Nosé-Hoover mechanics cited in Chapter 1 see also H. A. Posch, W. G. Hoover, and F. J. Vesely, "Dynamics of the Nosé-Hoover Oscillator: Chaos, Order, and Stability," *Physical Review A* 33, 4253 (1986).

The use of Stoermer-based algorithms in recent million-atom simulations is discussed in B. L. Holian, A. J. De Groot, W. G. Hoover and C. G. Hoover, "Time-Reversible Equilibrium and Nonequilibrium Isothermal-Isobaric Simulations with Centered-Difference Stoermer Algorithms," *Physical Review A* 41, 4552 (1990). The SPRINT computer is described by A. J. De Groot, S. R. Parker, and E. M. Johansson, in *SVD and Signal Processing; Algorithms, Applications and Architectures*, E. F. Deprettere, Editor (North-Holland, Amsterdam, 1988).

John Barker's accurate determination of the rare-gas force laws is summarized in "Many-Body Interactions in Rare Gases: Krypton and Xenon," *Physical Review Letters* 57, 230 (1986) and in earlier work referred to there. The very smooth Lennard-Jones spline potential was invented by B. L. Holian and D. J. Evans, "Shear Viscosities away from the Melting Line: Comparison of Equilibrium and Nonequilibrium Molecular Dynamics," *Journal of Chemical Physics* 78, 5147 (1983). The embedded-atom potential model for metals is described in S. M. Foiles, M. I. Baskes, and M. S. Daw, "Embedded-Atom-Method Functions for the Face-Centered-Cubic Metals, Cu, Ag, Au, Ni, Pd, Pt, and Their Alloys," *Physical Review B* 33, 7983 (1986). The plnp form of the embedded-atom metal potential discussed in Section 4 was developed at Los Alamos by Art Voter, Brad Holian, and the Hoovers. For a recent application see "Large-Scale Elastic-Plastic Indentation Simulations *via* Nonequilibrium Molecular Dynamics," W. G. Hoover, A. J. De Groot, C. G. Hoover, I. Stowers, T. Kawai, B. L. Holian, T. Boku, S. Ihara, and J. Belak, *Physical Review A* (December, 1990).

## 6. Applications of Equilibrium Molecular Dynamics

*1 Introduction; 2 Number-Dependence, Ensemble-Dependence, and Time-Dependence; 3 Pair Distribution Functions; 4 Free Energy and Phase Equilibria; 5 One-Parameter Equations of State; 6 Two-Parameter Equations of State; 7 Many-Parameter Equations of State; 8 Elastic Solids; 9 Defects and Surfaces; 10 Summary and References*

### 6.1 Introduction

The first molecular dynamics simulations were designed to test and extend theoretical calculations based on Gibbs' ensemble approach to equilibrium thermodynamic properties and on Boltzmann's kinetic-theory approach to irreversibility and transport properties. Low-density series calculations based on these microscopic theories could be compared directly to the corresponding measured results of computer simulation. This direct comparison of theoretical calculations with computer experiments avoided the force law uncertainties which inevitably cloud the interpretation of laboratory experiments. Molecular dynamics simulations make it possible to base both theoretical predictions and computer experiments on exactly the same force laws.

At first, the force laws used were the simplest possible, corresponding to two-dimensional hard disks and three-dimensional hard spheres. For such hard particles the thermodynamic equation of state links pressure to the only one relevant thermodynamic state variable, density. Two fundamental hard-sphere properties, the collision rate and the two-body probability distribution, are directly related to the pressure. The magnitude of the kinetic temperature is irrelevant and only sets the time scale, with the motion proceeding at a rate proportional to the square root of the temperature. Thus, at any density only a single temperature needs to be studied. If all the particle velocities were multiplied by  $(T'/T)^{1/2}$ , corresponding to a change in temperature from  $T$  to  $T'$ , the resulting particle trajectories would be unchanged. Only the *rate* at which the trajectories are traced out would vary.

Given a fixed thermodynamic state one can still vary both the boundary conditions and the number of particles. At Livermore, Alder and Wainwright simulated the Newtonian dynamics of periodic equilibrium hard-sphere systems including from 4 to 500 particles and compared time averages of their measured properties with the predictions of approximate models. Figure 6.1 shows the Alder-Wainwright equation-of-state results for relatively-small systems of hard disks and spheres. Until these data were generated, the pressure for the high-density fluid was uncertain within a factor of two and even the existence of the hard-disk and hard-sphere solid phases was uncertain and controversial.

For moderately dense fluids it was generally expected that the Mayers' virial expansion would correctly describe the pressure. The low density simulations confirmed this expected agreement. What would happen at high density was controversial. Would the strongly-compressed fluid form an ordered crystalline

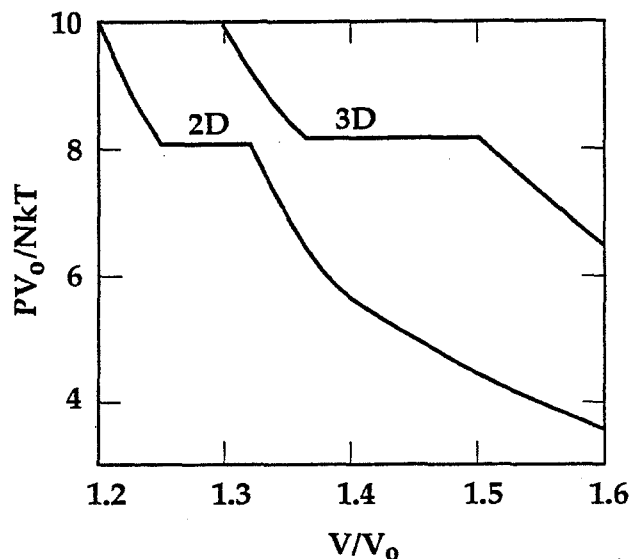


**Figure 6.1.** Computed mechanical equations of state for hard disks (lower curve) and hard spheres (upper curve). In both cases the high-density solid phase can coexist with a lower-density fluid phase. The close-packed volume is  $V_0$ .

solid or a disordered glass? Because the harmonic approximation is *never* valid for the hard-sphere solid phase the relative stability of the fluid and solid phases could only be guessed at. Alder and Wainwright's dynamic simulations indicated a stable solid phase at high density linked to the lower-density fluid phase by a van-der-Waals-like loop, as is shown in Figure 6.2. These hard-disk and hard-sphere calculations established the ability of computer simulation to locate phase transitions and to furnish reliable equations of state for dense fluids and anharmonic solids. Of the many theoretical approaches which preceded computer simulation only the exact theories, the Mayer's gas-phase virial theory and the quasiharmonic solid-phase theory, have turned out to have lasting value. The other approaches were all approximations, and became defunct as computer simulations began to take on the role of experiments, determining which of the many approximate models was best.

As the surviving models became more sophisticated and more nearly accurate the goal of computation became more ambitious: quantitative agreement with laboratory

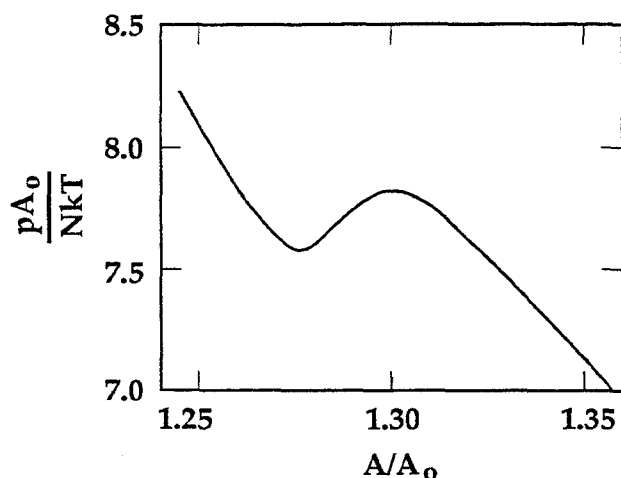


**Figure 6.2.** Van der Waals loop for periodic systems of 870 Hard Disks. The smooth curve indicates the averaged result of dozens of high-speed computations requiring hundreds of hours of computer time. Typical uncertainties in the measured pressures for a single computation were as much as 10%.

experiments on real materials. That is the primary goal of equilibrium molecular dynamics today. This work is limited primarily by difficulties in determining useful models for the interatomic forces, as was outlined in Chapter 5.

Here we begin by discussing the dependence of the simulated results on variables other than thermodynamic state. The results of the simulations depend upon the number of particles, the boundary conditions, the choice of ensemble, and the timescales describing the rates of heat and work exchange between system and surroundings. We discuss the use of computational results in thermodynamic phase-stability calculations. This application makes it possible to generate phase diagrams from the results of molecular dynamics simulations.

Here we emphasize the simplest prototypical equilibrium applications of molecular dynamics, for one- and two-parameter two-body force laws, designed to measure average properties from Gibbs' ensemble theory. In addition to thermodynamic properties, the two-body distribution function, which is useful in applying thermodynamic perturbation theory, is discussed. We indicate how the elastic and defect properties of solids can be obtained from the equilibrium simulations. Non-equilibrium applications of molecular dynamics are discussed in Chapters 10 and 11.

## 6.2 Number-Dependence, Ensemble-Dependence, and Time-Dependence

Simulations designed to characterize the equation of state can best minimize number dependence by using *periodic* boundaries. This choice avoids surface effects of order  $N^{-1/D}$ . Choosing the *number* of particles to be studied is more difficult, and depends on the property being studied as well as the available computer time. Hard and fast rules have exceptions, but the concepts involved in planning computer simulations are simple. In order best to approximate the large-system limit the residual influences of transients from the initial conditions, uncertainties due to the finite sampling time, as well as the intrinsic errors resulting from number-dependence, should all be roughly equal. In a typical situation, with each of these errors varying as a power of the number of particles and the time period of the simulation, it is both cost-effective and educational to study a series of small calculations, *extrapolating* to the large-system limit, rather than spending the same amount of computer time on the largest feasible calculation.

*How many particles should be used?* For periodic systems the Mayers' virial series, described in Section 4.13, makes it possible to estimate the number-dependence of the pressure and specific energy. Both should show variations of order  $1/N$  and, except near phase transitions Alder and Wainwright's hard-particle simulations have verified this expected behavior. In addition to these known systematic size-dependent errors the sampling time interval is significant. Data from early times, before transient inhomogeneities decay, must be discarded. We can guess that the time required should correspond to the time required for mass, momentum, and energy to diffuse across the system. System size varies as  $N^{1/D}$  in  $D$  dimensions. The Central Limit Theorem

suggests, and kinetic theory confirms, that the time required to *diffuse* such a length varies as the square of the length, requiring a time of the order of  $N^{2/D}$  times the collision time.

For single-particle intensive properties, such as the kinetic temperature, in which nearly-independent single-particle contributions fluctuate on the time scale of a collision, the Central Limit Theorem suggests that  $N^2$  independent one-particle samples, corresponding to the order of  $N$  collisions for each of the  $N$  particles making up the system, would bring the expected uncertainties in one-particle averaged quantities down to the same level, of order  $1/N$ . For collective many-particle relaxation properties, such as stress-tensor fluctuations, the number of collisions per particle might rather need to vary as  $N^2$  to generate  $N^2$  independent samples. Thus, for a fixed level of accuracy in a two-dimensional system, a linear doubling of system size means an increase in computing of factors of 8 or 64 as well as a fourfold increase in the number of particles and in computer storage capacity.

Choice of ensemble is mainly determined by convenience. The generalized forms of mechanics which control pressure and temperature by integral feedback make such simulations hardly more complicated than those carried out at constant energy and density. But the ensemble choice does affect the *fluctuations* in the results, which are usually of order  $1/N$  or  $(\ln N)/N$ . Stirling's approximation to  $N!$  indicates that the finite-system free energy and entropy per particle deviate from the large-system limiting value by terms of order  $(\ln N)/N$ :

$$\exp(-A_{\text{Ideal}}/NkT) = (V^N/N!\lambda^{3N})^{1/N} \approx (Ve/N\lambda^3)e^{-[\ln(2\pi N)/(2N)]}.$$

The effect of these corrections can largely be eliminated by computing the free energy and entropy *relative* to ideal gases with the same number of particles. With the ability to manipulate *billions* of degrees of freedom on the near horizon the typical number-dependence of computer experiments with errors of order  $N^{-1}$ ,  $N^{-1}(\ln N)$ ,  $N^{-1/2}$ , or even  $N^{-1/3}$  no longer prevents accurate computation, but an understanding of these effects can save considerable time and effort.

The numerical quality of results in molecular dynamics can always be improved by longer calculations. The Central Limit Theorem suggests that uncertainties due to sampling time can be cut in half by quadrupling the sampling time. But the calculations themselves are imperfect models of reality so that sampling time errors are usually not the main cause of disagreement with experiment. Selecting the proper physical model is still more an art than a science.

Thermodynamic properties are thought of as characterizing "bulk" matter, enough material so that surface effects and fluctuations can be ignored but not *so* much that diffusion times exceed reasonable observation times. For real materials, periodic boundaries are not a possibility. Real materials exhibit size-dependence too, with surface effects, decays of transients, and sampling fluctuations. In order that the

fraction of surface particles be below 0.1% in three dimensions a micron-sized sample of about  $10^{12}$  molecules is required. The diffusion time for such a sample is a reasonable value, about a millisecond. The diffusion time for a cubic centimeter of water is still reasonable, about a day, but the diffusion time for a cubic meter of water is unreasonable, about 30 years. The scales of computer experiments and laboratory experiments began to overlap at the micron level in 1984, with the simulation of a krypton film on graphite at the same scale as the corresponding physical experiment. By using periodic boundaries the computer experiments can reach micron accuracy with only 100 atoms.

The bulk entropy and free energy deviations of order  $\ln N/N$  are always negligible relative to surface effects, and are of order  $20/N$  for a cubic micron of water. These deviations are of the same order as the shifts in average values incurred by changing from one Gibbs ensemble to another. Fluctuations and ensemble shifts are completely negligible from a thermodynamic standpoint.

A variety of calculations have been carried out to check the number-dependence of thermodynamic phase equilibria. With periodic boundary conditions the primary effect follows from the  $\ln N/N$  dependence of the free energy. The fluid phase is stabilized by density fluctuations, and so encroaches on the region of solid-phase stability as the number of particles is increased.

In the case of the Lennard-Jones potential,

$$\phi(r) = 4\epsilon[(\sigma/r)^{12} - (\sigma/r)^6],$$

if the nearest-image convention is used in calculating the energy, then the truncation error, which is proportional to  $1/N$ , is about the same as the  $1/N$  errors in the energy and pressure, still exceeding 1% of the binding energy for a cutoff radius of  $4\sigma$ . Generally the deterioration of numerical integration accuracy caused by discontinuous forces makes such forces undesirable.

### 6.3 Pair Distribution Functions

For the simplest model of the many-body potential energy, a sum of pair terms,  $\Phi = \sum\phi$ , both the internal energy  $E = K + \Phi$  and the pressure tensor  $P = P_K + P_\Phi$  can be expressed in terms of one-particle and two-particle sums:

$$E = \sum(p^2/2m) + \sum\phi; PV = \sum(pp/m) + \sum rF.$$

The time-averaged values of the pair sums  $\sum\phi$  and  $\sum rF$  can both be expressed in terms of the probability  $\text{prob}(r)dr$  for finding the distance separating a particular pair of particles in the range from  $r - (dr/2)$  to  $r + (dr/2)$ . The potential energy sum  $\Phi = \sum\phi$  includes  $(N/2)(N-1)$  terms, one for each pair of particles in the system. For a homogeneous fluid state these all have identical time-averaged values:

$$\langle \Phi \rangle = (N/2)(N-1)\langle \phi \rangle = (N/2)(N-1) \int \phi(r) \text{prob}(r) dr ;$$

For a fluid in hydrostatic equilibrium the diagonal elements of the PV tensor are equal, making it possible to express the scalar compressibility factor  $PV/NkT$  in terms of the angle-averaged force between particles a distance  $r$  apart:

$$PV/NkT = 1 + [(N-1)/(2DkT)] \langle r \cdot F \rangle = 1 - [(N-1)/(2DkT)] \int r(d\phi/dr) \text{prob}(r) dr .$$

Both the total energy  $E$  and total compressibility factor  $PV$  include  $N(N-1)/2$  single-pair contributions.

The pair distribution function for real liquids and solids can be reconstructed from its Fourier Transform, measured by neutron or xray scattering. The pair function provides direct structural information, the number density of particle pairs a distance  $r$  apart. It is usual to define the "radial distribution function"  $g(r)$  as the ratio of this pair probability to the ideal-gas pair probability at the same density. Thus the number of pairs of particles in the range  $dr$  about  $r$ , divided by  $[(N(N-1)/2]2\pi r dr/V$  in two dimensions, or  $[(N(N-1)/2]4\pi r^2 dr/V$  in three dimensions, defines the radial distribution function. The radial distribution function is unity for sufficiently "large," but not *too* large, values of  $r$ . The distance  $r$  must be large relative to the range of correlations and simultaneously small relative to the box size. Despite the influence of the periodic boundary conditions on  $g(r)$  typical small-system effects on thermodynamic properties are of order  $1/N$ . In an  $N$  particle system confined to a volume  $V$  the pair distribution function  $g(r)$  can be measured and used to evaluate the integral forms for the time-averaged potential energy and the compressibility factor,  $PV/NkT$ . Both thermodynamic quantities can be expressed as spatial integrals weighted by  $g(r)$ . In three dimensions these are:

$$\langle \Phi \rangle = (N/2)(N-1)\langle \phi \rangle = (N-1)(N/2V) \int \phi(r) 4\pi r^2 g(r) dr ;$$

$$PV/NkT = 1 + [(N-1)/(6kTV)] \int 4\pi r^2 g(r) (-rd\phi/dr) dr .$$

The pair or "radial" distribution function  $g(r)$  is an essential part of thermodynamic perturbation theory. The theory expresses the Helmholtz free energy for a perturbed Hamiltonian in terms of the Helmholtz free energy and the pair distribution for a reference Hamiltonian. This approach was discussed in Section 4.14. In principle, *any* of Gibbs' ensembles can be used to calculate the probability of finding two particles a distance  $r$  apart by integrating over the coordinates of the remaining  $N-2$  particles. In the canonical ensemble this probability has the form:

$$\text{prob}(r_1, r_2) dr_1 dr_2 = \text{prob}(r_1 - r_2) dr_1 dr_2 = dr_1 dr_2 \int \dots \int \exp(-H/kT) dr^{N-2} / \int \dots \int \exp(-H/kT) dr^N ,$$

and the Mayer's' approach of Section 4.13 can be applied, giving a number density expansion for the radial distribution function:

$$g(r_{12}) = \exp(-\phi(r_{12})/kT)[1 + (N/V)\int f_{13}f_{23}dr_3 + \dots]$$

The exact expression, given by the full expansion, is as difficult to evaluate as is the partition function itself. On the other hand molecular dynamics lends itself easily to measurement of the pair and triplet distribution functions. In the pair case simply construct a histogram in which the coordinate separations of pairs of interacting atoms are collected during the force calculation. Pair probability results beyond the periodic-boundary nearest-image separation are not reliable.

### Problems:

1. Work out the explicit form of the integral just given,  $\int f_{13}f_{23}dr_{13}$ , for one-dimensional hard rods of length  $\sigma$ .
2. Determine the probability distribution  $\text{prob}(|q|)$  from a Runge-Kutta solution of the motion of a one-dimensional classical harmonic oscillator with Hamiltonian  $H = (1/2)(q^2 + p^2) = 1/2$  using 10, 20, 40, and 80 divisions of the interval from  $|q| = 0$  to  $|q| = 1$ . Compare these data with the analytic result,  $(2/\pi)(1 - q^2)^{-1/2}$  and discuss the use of extrapolation techniques to minimize the errors.

### 6.4 Free Energy and Phase Equilibria

Ice water is a prototypical two-phase system. At pressures below two kilobars ordinary ice, "Ice I," and liquid water can coexist, with the same temperature and pressure but with different energies and densities. All pure substances display such phase equilibria in characteristic reproducible temperature and pressure ranges with phase boundaries across which two physically distinct phases can coexist at thermal and mechanical equilibrium. The coexisting phases generally differ in *all* of their properties with the exceptions of pressure, temperature, and composition. There is no limit to the number of phases which a particular material can exhibit, but the number of *coexisting* phases, at a particular temperature and pressure, is limited. Gibbs' "Phase Rule," based on equating the chemical potentials, the pressure, and the temperature, for a system with  $C$  distinct components, gives the limit,  $C + 2$ . Thus a pure single-component material, like water, can exhibit at most three *coexisting* phases.

In Section 2.2 we discussed a portion of the water phase diagram containing eight different phases. For a single simple material like water the coexistence of any *two* such phases can be described by a thermodynamic "phase line" along which the two phases coexist at equal pressure and temperature,  $P_{12}(T) = P_1(T) = P_2(T)$ . The intersection of two such lines gives a triple point, at which *three* phases coexist, with

$P_{123}(T) = P_1(T) = P_2(T) = P_3(T)$  equal to the same "triple-point" pressure for all three phases. Refer to the phase diagram of water in Section 2.2 for several examples. For pure water the temperature and pressure are 273 kelvins and 592 pascals at the {ice I + liquid water + water vapor} triple point. This easily-reproduced point is used as a primary temperature standard.

As a sample phase-line calculation, let us estimate the dependence of the "sublimation pressure" on temperature for a solid in equilibrium with its vapor. For simplicity, we describe the solid as a harmonic crystal, with canonical partition function,

$$Z_{\text{Solid}} = [\exp(-\Phi_0/NkT)(kT/hv)^D]^N,$$

and we consider its equilibrium with such a low-density vapor that the vapor can be treated as ideal, with canonical partition function,

$$Z_{\text{Gas}} = (Ve/N\lambda^D)^N.$$

We then apply Gibbs' idea and maximize the partition function for a system containing both phases. The condition of "chemical equilibrium," here a sublimation equilibrium, corresponds to maximizing the partition function in the same way as do the thermal and mechanical conditions of equilibrium. The chemical analog of temperature and pressure is called "chemical potential," and is equal to the equilibrium derivative of free energy with respect to  $N_i$ . In a closed system with fixed volume, temperature, and number of particles, phase equilibrium occurs when the vaporization of one additional particle causes no change in the canonical partition function,

$$\delta \ln Z \equiv 0 = \delta \ln Z_{\text{Solid}} + \delta \ln Z_{\text{Gas}} = -(\partial \ln Z_{\text{Solid}} / \partial N) + (\partial \ln Z_{\text{Gas}} / \partial N);$$

$$-(\partial \ln Z_{\text{Gas}} / \partial N) \equiv (\mu/kT)_{\text{Gas}} = \ln(N\lambda^D/V) = \ln(P\lambda^D/kT)$$

$$-(\partial \ln Z_{\text{Solid}} / \partial N) \equiv (\mu/kT)_{\text{Solid}} = (+\Phi_0/NkT) + D \ln(hv/kT).$$

Thus the equilibrium vapor pressure of a solid has a very strong *exponential* dependence on the inverse temperature:

$$P/kT = (2\pi mv^2/kT)^{D/2} \exp(+\Phi_0/NkT).$$

In this sublimation example the chemical potentials of the solid and gas phases are equal for phase equilibrium. This condition defines the "sublimation line,"  $P_{\text{SG}}(T_{\text{SG}})$ . A calculation with liquid included would similarly predict the unique pressure-

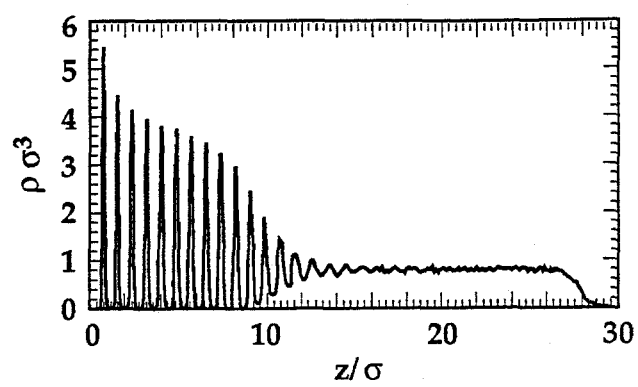


Figure 6.3. Time-averaged density profile for the three-dimensional Lennard-Jones triple point.

temperature point at which the solid, liquid, and gas phases *all* have the same chemical potential. This is the “triple point,” ( $P_{SLG}, T_{SLG}$ ).

Typically a change in the pressure or temperature of two interacting phases causes the thermodynamic properties, density and energy, for instance, to change continuously. Molecular dynamics makes it possible to study and to simulate such phase equilibria by both direct and indirect methods. The *direct* approach requires simulating the two-phase interface in a sufficiently large system that the resulting equilibrium reflects that of bulk matter. Ladd and Woodcock carried out a direct simulation of the *triple point* of argon in this way, with a 1500-atom isochoric and isoenergetic system in which all *three* phases simultaneously coexisted. Figure 6.3 shows a density profile taken during their simulation. The profile shows coexisting solid, liquid, and vapor regions. Such a three-phase equilibrium is *stable* to small changes in the volume or energy but would be *unstable* to *any* change in pressure or temperature. This is because all three phases are simultaneously stable for only a single value of pressure and temperature but over wide and continuous ranges of volume and energy, corresponding to any point in the triangular composition diagram shown in Figure 6.4. Because the chemical potentials of the three phases have different dependences on pressure and temperature the coincidence of all three phases fixes a definite thermodynamic pressure-temperature point, the “triple point.”

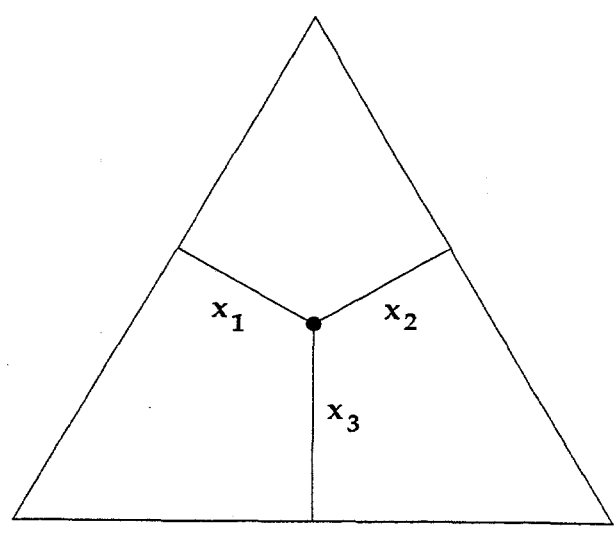


Figure 6.4. Triangular three-phase diagram. The “mole fraction” of the three components is proportional to the length of the perpendicular to the opposite side of the triangle. The sum of the three lines is constant, unity, for any composition.

**Problem:**

Discuss the possibility of studying two-phase and three-phase equilibria with independent variable sets (V,T) and (P,E).

The fundamental microscopic criterion for phase equilibrium is the balance of chemical potential,  $\mu = -kT(\partial \ln Z / \partial N)$ , so that the partition function is unchanged by the transfer of matter between any pair of coexisting phases. Indirect approaches to phase equilibria can be based on the measurement, or calculation, of any one of the thermodynamic potential functions,  $\{E(S,V), H(S,P), A(T,V), G(T,P)\}$ , for the coexisting phases. In that way the composition of a two-phase system can be computed without the need for the kind of direct simulation carried out by Ladd and Woodcock. Many methods have been developed for this purpose. For fluid phases the most straightforward approach is to calculate the excess Helmholtz free energy (relative to an ideal gas with the same N, V, and T) by combining temperature and volume integrations:

$$d(A_{\text{Excess}}/NkT) = (-\Phi/NkT)d\ln T - [(PV/NkT)-1]d\ln V .$$

The solid-phase free energy can be roughly estimated, with errors usually no greater than  $0.2NkT$ , from either the Einstein model or from the quadratic-form "quasiharmonic" approximation to the Hamiltonian. If desired, either approximate model for the free energy can then be corrected by a constant-volume energy integration:

$$d(A_{\text{Excess}}/NkT) = (-E_{\text{Excess}}/NkT)d\ln T ,$$

where the excesses are defined relative to the model's free and internal energies.

In free energy calculations it is sometimes convenient to simulate the properties of phases outside their natural ranges of stability by introducing artificial constraint fields. Such an extension is a requirement for a phase with an equation-of-state surface  $P(V,T)$  surrounded by neighboring phases' surfaces. Ice III is such an example. The hard-sphere solid presents a similar difficulty because there is no thermodynamically-stable limiting hard-sphere solid state for which the entropy can be calculated analytically by applying Third-Law statistical calculations. For hard spheres the harmonic approximation never applies. At high density the hard-sphere free energy diverges to infinity. Computer simulations show that the hard-sphere solid phase becomes *thermodynamically* unstable at about 36% expansion from close-packing and *mechanically* unstable at about 60% expansion. The hard-sphere solid entropy can nevertheless be evaluated in numerical simulations by artificially stabilizing the phase with a potential which favors it over the competing phases. For example, the solid phase can be reversibly extended all the way to the low-density limit by forcing each

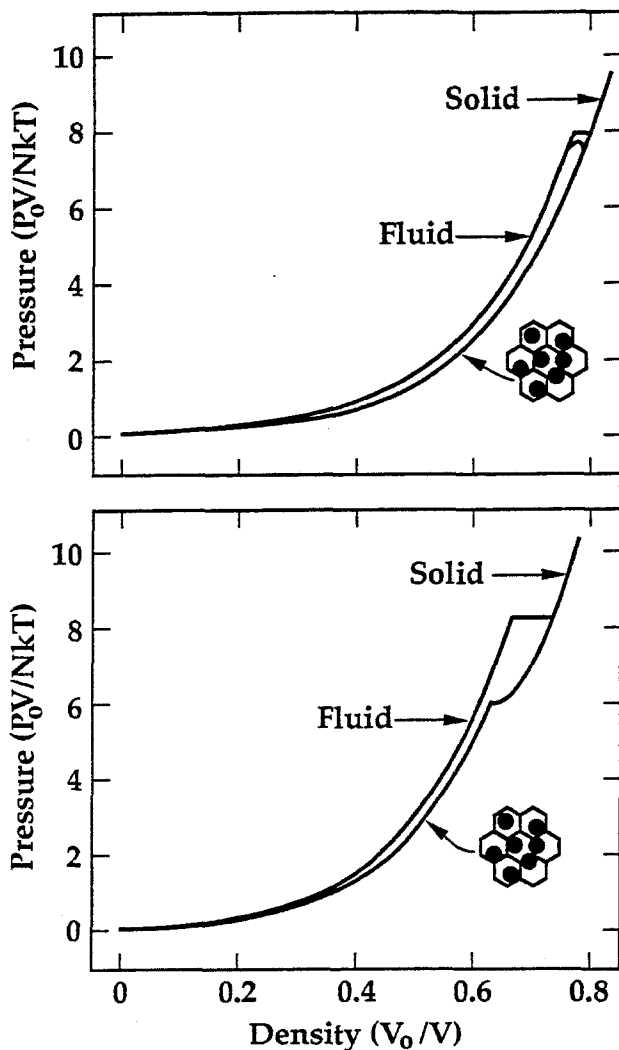


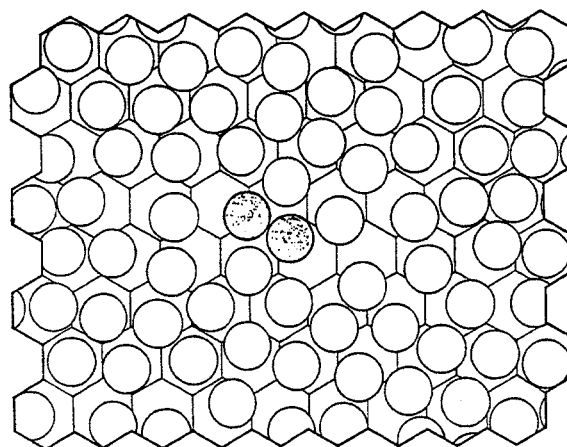
**Figure 6.5.** The fluid and solid mechanical equations of state are shown for hard disks (above) and hard spheres (below). In both cases the solid-phase equations of state can be extended to low densities by imposing the single-occupancy restriction on the simulation. The corresponding calculations provided the first accurate determination of the transition densities of the coexisting phases.

particle to occupy an individual cell. See Figure 6.5 for both the hard-sphere and the analogous hard-disk case. Each disk is artificially confined by walls to the region closer to its own equilibrium lattice location than to any other. But interactions with neighboring disks, crossing the confining wall potentials, are still possible, as indicated in the Figure 6.6. The perturbation to the thermodynamic properties induced by the cell walls is negligible in the range where the solid is stable. Outside that range the spatial ordering imposed by the cell walls prevents the melting of the solid and makes it possible to compute the solid-phase free energy by integrating the thermodynamic equation of state for the artificially stabilized phase. Figure 6.5 shows the hard-sphere equation of state for the fluid and solid phases, including the artificially-stabilized extension of the solid phase to low density.

### **Problem:**

If the probability for a deviation  $r$ , within  $dx dy dz$ , from a particle's most-likely position is Gaussian,  $(2\pi\sigma^2)^{-3/2} \exp(-r^2/2\sigma^2) dx dy dz$ , find the probability that this particle lies *outside* a spherical volume  $V/N$  when the root-mean-squared average value of  $r$  is one-eighth the nearest-neighbor separation  $d$ . Use the spacing appropriate for a face-centered-cubic crystal,  $(V/N) = d^3/2^{1/2}$ .

**Figure 6.6.** Single-occupancy cells for hard disks. The *center* of each disk is required to remain within that disk's private cell. Because the *edges* of these particles can project beyond the cell boundaries third-neighbor disks can interact. Two such disks are lightly shaded. The pressure of this single-occupancy system lies within 10% of the fluid pressure.



### 6.5 One-Parameter Equations of State

The thermodynamic states of real materials depend upon two independent variables in addition to composition, a thermal variable as well as a mechanical variable, so that a complete thermodynamic description of a system with fixed composition requires that a two-dimensional state space be mapped out. An accurate study of a typical fluid phase, for instance, would require perhaps 100 separate points. With today's inexpensive work stations such a project is feasible, but still daunting. For most applications a simpler phase diagram with only a single independent variable can be adequate and the number of phase points studied can be reduced tenfold. The family of inverse-power "soft-disk" or "soft-sphere" potentials,

$$\phi(r) = \epsilon(\sigma/r)^n,$$

provides a simple prototypical thermodynamics and hydrodynamics, with both fluid and solid phases, as well as intermediate unstable "glassy phases," with all these phases described by a single independent variable which serves to combine together density and temperature. These single-component glassy phases are interesting disordered solids which are typically less stable than crystalline solids. That glasses are less stable than crystalline solids is empirical, the result of experience as well as calculation. It is not even obvious that the lowest-energy arrangement of atoms is a regular lattice. At finite temperatures when both entropy and energy contribute to stability, the relative stability of glassy phases it is even harder to judge. The fact that the rare gases and simple metals generally crystallize into regular lattice forms suggests that covalent bonds or a mixture of different particle sizes are required to stabilize the glasses observed in nature. Nevertheless, because the *thermodynamically* unstable but *mechanically* stable glasses are prevented by their relatively long diffusion times from crystallizing, they can exhibit reproducible thermodynamic properties—energy,

pressure, temperature, density, entropy—which depend upon *cooling rate* in addition to the usual thermodynamic state variables.

For the purely-repulsive inverse-power potentials,  $\{\phi(r) = \epsilon(\sigma/r)^n\}$ , the gas-liquid equilibrium is absent, due to the absence of attractive forces. Crude models of real materials, particularly at high pressure where the contributions of attractive forces are small, can be readily constructed by choosing an appropriate repulsive exponent  $n$ . The effects of attractions can be treated as a perturbation, as in van der Waals' equation, and simply be added on to the repulsive soft-sphere properties.

There are two ways to see that the thermodynamics of inverse-power potentials can be described in terms of a single independent variable combining temperature and volume. The more straightforward demonstration begins with Gibbs' canonical partition function, written in terms of the reduced coordinates used in discussing isobaric dynamics in Section 5.9. We again choose a  $D$ -dimensional volume, cubic for  $D = 3$ , and define variables  $0 < \{x_i\} < 1$  spanning the volume. For statistical mechanics, this is enough. Gibbs' canonical partition function takes the form

$$\exp[-(A/kT)] = Z = (1/N!)(V/\lambda^D)^N \int \dots \int dx^D \exp[-(\epsilon/kT)(\sigma^D/V)^{n/D} \sum(x_{ij})^{-n}].$$

Because the limits of integration are volume independent it is clear that the excess (relative to an ideal gas with the same  $\{N, V, T\}$ ) Helmholtz free energy, computed from the ratio  $\ln[Z/Z_{\text{Ideal}}]$ , can only depend on the temperature and volume in the combination  $TV^{(n/D)}$  which appears in the integral. Likewise the nonideal parts of the pressure and energy,  $(PV/NkT) - 1$  and  $(\Phi/NkT) = (E/NkT) - (D/2)$ , can depend only on the combination  $(N\sigma^D/V)^{n/D}(\epsilon/kT)$  and, because both are derivatives of the excess Helmholtz free energy with respect to the same argument, they are related to each other:

$$-(\partial[A_{\text{Excess}}/NkT]/\partial \ln V) = -(n/D)(\partial[A_{\text{Excess}}/NkT]/\partial \ln T) =$$

$$(PV/NkT) - 1 = (n/D)(\Phi/NkT).$$

This relation between energy and pressure is again the virial theorem, a special case of which led to the establishment of Newtonian mechanics from Kepler's Laws.

The same corresponding-states relation between the temperature variation and the density variation can alternatively be derived directly from the equations of motion by introducing a reduced time,  $t^* = t(kT/m)^{1/2}V^{-1/D}$ , as well as the reduced coordinates  $\{x_i\}$ , scaled in terms of the interparticle spacing  $(V/N)^{1/D}$ . With corresponding initial conditions the solution of the equations of motion  $\{x(t^*)\}$  depends on temperature and volume only through the combination:

$$(\epsilon/kT)(N\sigma^D/V)^{n/D}.$$

For a system with hard-sphere interactions ( $n = \infty$ ) it is obvious that particle trajectories traced out at the same density but at two different temperatures differ only in the relative *rates* of motion. The sequence of configurations is exactly the same at any temperature for corresponding initial and boundary conditions. For soft spheres a less obvious, but similar, result holds. The number density can be increased with temperature so as to keep the sequence of collisional scattering angles unchanged so that the time history of the scaled configuration,  $(r/V^{1/D})$  is independent of temperature. This condition corresponds to keeping the ratio of kinetic and potential energies fixed.

**Problem:**

Show that the scaled dynamics for the inverse-power potentials depends only on the scaled initial conditions and the parameter  $(\epsilon/kT)(N\sigma^D/V)^{n/D}$ .

The special case  $n = \infty$ , corresponding to hard spheres in three dimensions and hard disks in two, was the first to be extensively investigated by molecular dynamics and established the ability of dynamical simulations to characterize phase transformations. It is qualitatively different from the smaller values used to describe real materials. The limiting hard-sphere potential has neither a harmonic expansion nor a nonideal constant-volume heat capacity. For hard spheres the constant-volume heat capacity always has the ideal-gas value,  $3Nk/2$ .

The equation of state for an inverse-power soft-disk or soft-sphere system is most easily visualized at constant volume. At sufficiently low temperatures the harmonic approximation applies. In this case the kinetic and potential energies contribute equally to the total heat capacity of  $DNk$ . When the particle displacements becomes sufficiently large (about one-seventh of the interparticle spacing in the three-dimensional case) the face-centered cubic close packed crystal melts to a fluid with a somewhat higher heat capacity. The heat capacity then falls, approximately as  $1/T$ , to the ideal-gas value as the system becomes progressively more ideal through heating.

The variation of the equation of state in three dimensions with  $n$  can be seen in Figure 6.7. Both the static lattice energy,  $\Phi_0$ , and the thermal kinetic energy,  $3NkT/2$ , have been subtracted from the energies shown. Lindemann's rough melting criterion, described below,

$$\langle \delta^2 \rangle^{1/2}/d)_{\text{Melt}} = (\langle \delta_x^2 + \delta_y^2 + \delta_z^2 \rangle^{1/2}/d)_{\text{Melt}} \approx 1/7 \approx (3kT/m\omega^2 d^2)^{1/2},$$

where  $d$  is the interparticle spacing and  $\langle \delta^2 \rangle^{1/2}$  is the (three-dimensional) rms vibrational amplitude, suggests that a reduced temperature scale based on the Einstein frequency would bring the data for different  $n$  into correspondence. The data show that this *corresponding states relation* is a useful approximation.

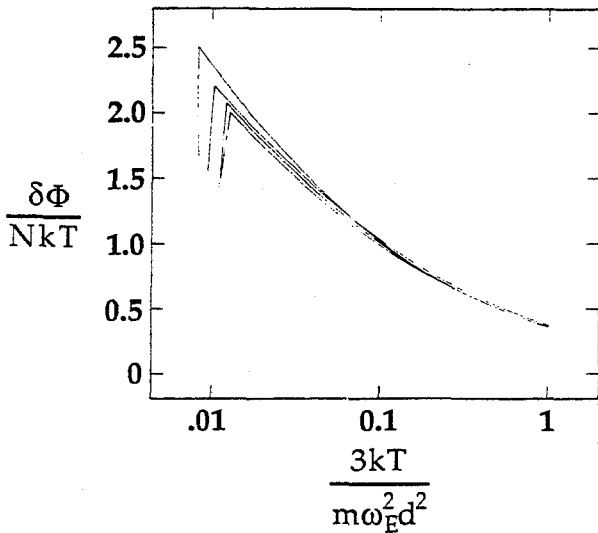


**Figure 6.7.** Thermal equations of state for three-dimensional inverse-power potentials. From top to bottom the curves shown correspond to the four  $n$  values {4,6,9,12}. The temperature-dependence of the potential-energy increase, starting from the cold face-centered lattice, is shown. The Einstein frequency is  $\omega_E$ .

**Problems:**

1. For the soft-sphere potential functions  $\phi = \epsilon(\sigma/r)^n$  use Lindemann's melting criterion to estimate the maximum value of  $n$  for which the harmonic approximation gives a useful description of the solid phase.
2. Use an Einstein-like model of the hard-sphere face-centered-cubic solid to estimate a "vibrational amplitude" for hard spheres. That is, with all spheres but one fixed at their perfect-lattice positions, estimate the maximum displacement possible for the one moving particle. If the partition function is proportional to the  $3N$ th power of this amplitude, show that the mechanical equation of state has the "free-volume" form given below.

At low density the extrapolated large- $N$  limits of the two- and three-dimensional hard-disk and hard-sphere equations of state  $PV/NkT$  agree perfectly with the corresponding limiting values from the Mayers' virial expansions:

$$P_2V/NkT = 1 + B\rho + 0.7812(B\rho)^2 + 0.5327(B\rho)^3 + \dots ; B = (1/2)\pi\sigma^2 ;$$

$$P_3V/NkT = 1 + B\rho + 0.625(B\rho)^2 + 0.28695(B\rho)^3 + \dots ; B = (2/3)\pi\sigma^3 .$$

Here  $\rho$  is the number density  $N/V$  rather than the mass density. At high, solid-phase densities the measured pressure is more closely described by the "free-volume" form derived from the cell model:

$$PV/NkT = [1 - (\rho/\rho_{\text{Max}})^{1/D}]^{-D} .$$

In an intermediate density interval, beginning about 2/3 the maximum density in three dimensions and 3/4 in two dimensions, in what Wood once called the "interval of confusion," pressure fluctuations are relatively large. Hundreds of hours of computer simulation were required for the accurate averages establishing a van der Waals-like loop joining the fluid and solid phases.

Despite the lack of attractive forces hard disks and hard spheres both exhibit stable crystalline phases at sufficiently high pressure. The difficulty in packing spheres randomly so as to achieve the close-packed density makes the existence of two distinct phases seem obvious today. But in the days before computer simulation the possibility of a first-order (discontinuous) transition between the phases was hotly debated.

"Theories" of melting were then, as they still are, just models. The Lindemann model of melting, for instance, declares that melting occurs when the root-mean-squared displacement reaches a characteristic fraction of the interparticle spacing. The model is a useful rule of thumb. Figure 6.8 shows that this relation is satisfied, approximately, by three-dimensional solids and that the fraction is about 1/7. On the other hand two-dimensional solids have a mean-squared displacement which varies as the logarithm of the crystal size, so that the "Lagrangian" fluctuation in the spacing between neighboring particles is more significant than the "Eulerian" position fluctuation relative to a fixed location in space. All approximate models of melting or freezing based on the properties of a single phase wrongly ignore the fact that phase equilibria depend on the properties of two or more competing phases rather than on the mechanical instability of one phase.

**Problem:**

Work out the canonical partition function for two hard disks in a two-dimensional rectangular periodic "volume" with sidelengths  $L$  and  $3^{1/2}L$ . Show that this system has a melting transition at a density near 3/4 the maximum density. At what density could the cooperative motion of three-dimensional hard-sphere atoms in parallel close-packed planes lead to a corresponding melting transition?

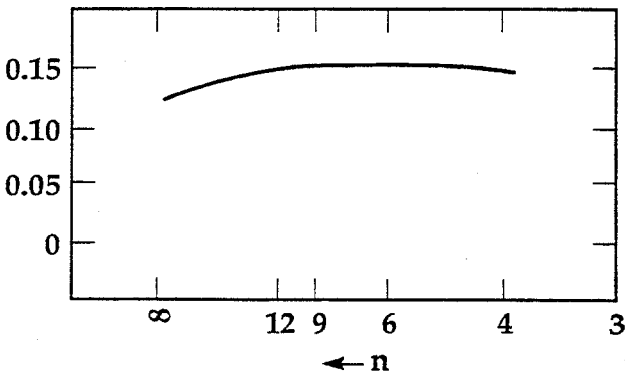


Figure 6.8. Estimates for the root-mean-squared displacement, divided by the nearest-neighbor spacing, for face-centered-cubic inverse-power solids at their melting points. The entry  $n = \infty$  corresponds to hard spheres.

## 6.6 Two-Parameter Equations of State

More-complicated two-parameter force laws such as the Lennard-Jones-spline detailed in Section 5.10 are still sufficiently simple for a Corresponding States Principle to apply. Whenever the pair potential function  $\phi(r)$  is the product of a characteristic energy  $\epsilon$  and a function involving a single characteristic length  $\sigma$  the thermodynamic properties can be expressed in terms of a corresponding scaled volume,  $V/N\sigma^D$  and a scaled temperature  $kT/\epsilon$ . An example is the Lennard-Jones potential:

$$\phi(r) = 4\epsilon[(\sigma/r)^{12} - (\sigma/r)^6];$$

which was investigated intensively beginning with Rahman and Verlet's investigations. The Lennard-Jones-spline potential is much better suited to numerical work because the higher-neighbor interactions are absent and the potential and its derivatives are continuous.

The phase diagram for the Lennard-Jones potential is compared to that for argon and to the predictions of van der Waals' equation in Figure 6.9. For any given state point the isoenergetic Newtonian equations of motion are solved, giving pressure and temperature as functions of volume and energy. Even though later work by John Barker showed that the true shape of the interatomic potential for argon is significantly different from the Lennard-Jones form, with a less-steep repulsion and a deeper narrower well, the semi-quantitative agreement leaves no doubt that computer simulation can reproduce the details of macroscopic thermodynamic behavior by using simple atomistic models for the interactions.

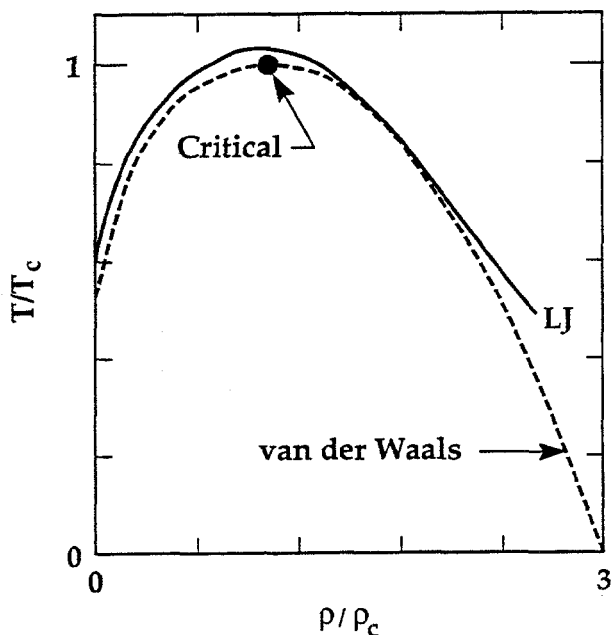


Figure 6.9. Comparison of the Lennard-Jones, van der Waals, and Argon gas-liquid coexistence regions. The Lennard-Jones critical point is slightly too high relative to the experimental point for argon (indicated by an arrow). The Lennard-Jones coexistence curve terminates at the triple-point temperature while the van der Waals coexistence curve continues on to  $T = 0$ .

6.7 Many-Parameter Equations of State

Calculations can be made more flexible, and more complicated, in a variety of ways. To represent a polar molecule, water, for instance, a rigid framework of charges can be arranged to reproduce the dipole and quadrupole moments of the molecule. The dipole moment can be made to depend on the local electric field at the molecule, computed by adding contributions from other molecules, so as to reproduce the macroscopic polarizability. There is no logical end to the complex process of adding parameters in order to fit experimental data.

The number of published simulations using molecular dynamics now numbers in the thousands. The complete list of materials investigated with computer simulation is correspondingly vast, including mixtures of polar and nonpolar liquids, alkali halides, alkali metals, salts, unsaturated and saturated hydrocarbons, superionic conductors, semiconductors, metals, as well as molecules and membranes of biological interest. As an example of a conceptually simple and interesting model consider Sumnesh Gupta's recent simulations of propane and benzene. In both these cases the molecules were represented as rigid frameworks of Lennard-Jones interaction sites, with the sites chosen to occupy three of the four vertices of a square for propane, C<sub>3</sub>H<sub>8</sub>, and the six vertices of a regular hexagon for benzene, C<sub>6</sub>H<sub>6</sub>. With a CRAY computer 500 such molecules could be followed for 10<sup>4</sup> time steps, allowing the pressure and energy to be determined with an accuracy of better than one percent. Gupta carried out a parallel set of calculations leaving out the attractive forces, with the goal of evaluating perturbation theory for noncentral forces. The pair distribution function for the propane model is compared to that calculated with a purely-repulsive reference fluid in Figure 6.10.

Problem:

What should the limiting low-temperature and high-temperature heat capacities, C<sub>V</sub>, for Gupta's models of propane and benzene be?

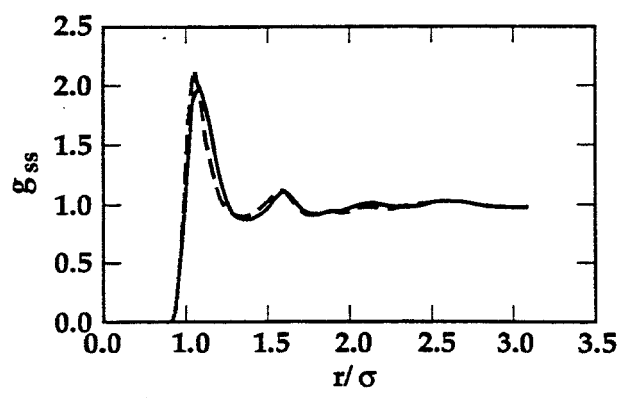


Figure 6.10. Pair distribution functions for Gupta's model of liquid propane. The solid line gives the carbon-carbon pair distribution for the complete model. The dashes show the effect of ignoring the attractive forces.

## 6.8 Elastic Solids

Both slow isothermal deformations and the relatively-fast adiabatic deformations induced by sound waves can be measured experimentally by a variety of methods and compared to corresponding theoretical calculations using models for the interatomic forces. These models aim to calculate the elastic constants  $\{C\}$  in the linear Hooke's-Law relation linking the stress and strain tensors:

$$\sigma \propto \varepsilon.$$

The proportionality coefficients, which have units of stress, are the "elastic constants." The *adiabatic* elastic constants  $\{C^S\}$  determine the speed of propagating sound waves. The *isothermal* elastic constants  $\{C^T\}$  describe the stresses required for isothermal deformations of these solids. To take advantage of the correspondence between microscopic calculations and macroscopic experiments the elastic properties of crystals have been investigated in considerable detail. The use of periodic boundaries makes contact with the usual plane-wave approach of solid state physics in which phonons periodic in space and time are investigated. Free-boundary simulations would be complicated by the presence of a vapor phase, surface relaxation and reconstruction, as well as the possibility of a liquid surface film.

Let us consider the simplest three-dimensional case, a periodic cubic crystal subject to small deformations from the stress-free state. For a general stress-free crystal each of the six stress components  $\{\sigma_{xx}, \sigma_{yy}, \sigma_{zz}, \sigma_{xy}, \sigma_{yz}, \sigma_{zx}\}$  can respond to changes in each of the six elastic strains  $\{\varepsilon_{xx}, \varepsilon_{yy}, \varepsilon_{zz}, \varepsilon_{xy}, \varepsilon_{yz}, \varepsilon_{zx}\}$ , requiring an array of 36 elastic constants to describe the linear response. For a *cubic* crystal symmetry reduces the number of nonzero constants to just 12, among which there are only three distinct stress-strain coefficients,  $C_{11}$ ,  $C_{12}$ , and  $C_{44}$ :

$$\sigma_{xx} = C_{11}\varepsilon_{xx}; \sigma_{yy} = C_{12}\varepsilon_{xx}; \sigma_{xy} = C_{44}\varepsilon_{xy}; \varepsilon_{xx} = du_x/dx; \varepsilon_{xy} = [(du_x/dy) + (du_y/dx)].$$

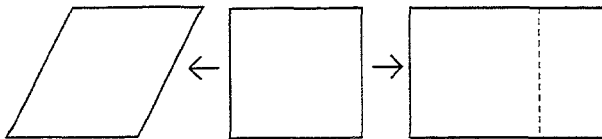


Figure 6.11. Deformations from which the elastic constants  $C_{11}$ ,  $C_{12}$ , (right) and  $C_{44}$  (left) can be determined.

See Figure 6.11 for a pictorial representation of these definitions. The conventional usage of the subscript  $44$  to indicate the coupling of shear stress to shear strain in cubic crystals is strange, but too well-established to ignore. The coefficients  $C_{ij}$  can be calculated indirectly from Gibbs' canonical partition function by working out the Taylor series expansions of the internal energy and the Helmholtz free energy as power series in the strains. The coefficients in the strain series are then obtained as equilibrium

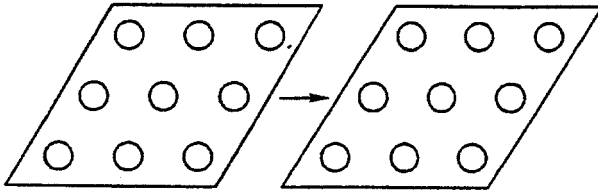


Figure 6.12. The scarcely-perceptible 5% shear deformation of a 9-particle crystal.

ensemble averages in the unstrained state. The required ensemble averages include slowly-convergent fluctuations of pressure-tensor or strain-tensor components.

A more direct purely-computational approach more closely resembling the conditions of real experiments illustrates the simplifications possible with a regular repeating structure. If a periodic crystal is simply constructed with a built-in strain, imposed by applying properly-chosen oblique boundary conditions, then the mean stress-tensor components give directly the elastic constants without the need for evaluating fluctuations. This is a simple and effective method for determining the elastic response of solids. The deformation shown in Figure 6.12 illustrates this idea. It shows a 9-atom periodic Hooke's-Law crystal which has undergone a shear strain of  $0.05 = du_x/dy$  from its stress-free state. In Figure 6.12 the nearest neighbors interact with Hooke's-Law springs with force constant  $\kappa$  and rest length  $d$ . The corresponding potential energy increase is  $0.0004686\kappa d^2$  per particle. The virial-theorem value of the shear stress:

$$\sigma_{xy} = -(1/V)\sum_{xy} F/r = 0.02163\kappa,$$

gives a corresponding shear modulus of  $0.4326\kappa$ , not far from the analytic value for an infinitesimal strain,  $(3/16)^{1/2}\kappa = 0.4330\kappa$ .

### 6.9 Defects and Surfaces

Perfect crystals are rare. Entropy encourages vacancies. The classical canonical partition function for a stress-free crystal containing a single vacancy differs from that of a perfect crystal by a multiplicative factor of  $N \exp(-E_V/kT) \Pi(v/v')$ , where  $N$  is the number of sites available for occupation by a vacancy,  $E_V$  is the corresponding increase in energy due to the presence of the defect, and the perfect-lattice vibrational frequencies  $\{v\}$  shift to the set  $\{v'\}$  in the presence of a vacancy. Quantitative calculations are simplest using periodic boundaries. With periodic boundaries it is evident that every configuration of a perfect  $N$ -atom crystal corresponds to  $N$  different configurations of an  $(N-1)$ -atom crystal with a single vacant site. In the absence of lattice relaxation around the vacant site it can likewise be seen that the "missing" interactions due to a vacancy are identical to those which bind a particle to the lattice. Thus in a perfect crystal, with pairwise additive forces, the vacancy energy  $E_V$  and the binding energy are identical. For copper the vacancy energy of 1.3 electron volts is about 50 times  $kT$  at room temperature. Thus an equilibrium room-temperature

copper crystal with  $\exp(50)$  atoms should contain on the order of a single vacancy. For triple-point argon the vacancy energy is much less, roughly 10 times  $kT_{TP}$ . At the melting point the density of vacancies in solid argon is roughly one part per million. Thus vacancies play a nearly negligible role in the equilibrium thermodynamic properties of solids. Their role in promoting diffusion is an interesting nonequilibrium problem.

Surfaces are a much more interesting equilibrium phenomenon because they can be avoided only in computer experiments. Surface atoms have a much higher energy than do bulk atoms, so it is thought that they may nucleate a liquid film at temperatures below the bulk melting temperature. Ladd and Woodcock's density profile certainly suggests a gradual transition from solid to liquid. This area appears to be a promising one for future research.

### 6.10 Summary and References

A carefully-designed molecular dynamics simulation simultaneously minimizes the effects of size dependence, statistical fluctuations, and the residual influence of initial conditions. With proper care phase equilibria can be reliably characterized by direct simulation, or by indirect thermodynamic calculations. Phase diagrams for a variety of simple force laws have been so generated and serve as model descriptions for real materials. Many such data can be successfully correlated with semiempirical corresponding-states approaches related to Lindemann's melting model. Special simulation techniques can be used to study the properties of vacancies and other crystal defects.

The hard-sphere transition was characterized accurately in 1968. See "Melting Transition and Communal Entropy for Hard Spheres," W. G. Hoover and F. H. Ree, *Journal of Chemical Physics* **49**, 3609 (1968) and "Studies in Molecular Dynamics. V. High-Density Equation of State and Entropy for Hard Disks and Spheres," by B. J. Alder, W. G. Hoover, and D. A. Young. For a Lennard-Jones triple-point study see A. J. C. Ladd and L. V. Woodcock, "Interfacial and Co-existence Properties of the Lennard-Jones System at the Triple Point," *Molecular Physics* **36**, 611 (1978). "Surface Melting," J. G. Dash, *Contemporary Physics* **30**, 89 (1989) reviews the evidence for the existence of thick liquid films on solids just below the melting point.

The indirect route to phase equilibria through thermodynamic perturbation theory is described by G. A. Mansoori and F. B. Canfield, "Variational Approach to the Equilibrium Thermodynamic Properties of Simple Liquids," *Journal of Chemical Physics* **51**, 4958 (1971). S. Gupta's polyatomic simulations are summarized in "Computer Simulation and Perturbation Theory of Fluids Modelled Using Three- and Six-Site Lennard-Jones Potentials," *Molecular Physics* **68**, 699 (1989). For the first large-scale atomistic simulation see "Molecular-Dynamic Simulations of the Incommensurate Phase of Krypton on Graphite Using More Than 100,000 Atoms," F. F. Abraham, W. E. Rudge, D. J. Auerbach, and S. W. Koch, *Physical Review Letters* **52**, 445 (1984) as well as Farid Abraham's stimulating review, "Computational Statistical Mechanics, Methodology, Applications, and Supercomputing," *Advances in Physics* **35**, 1 (1986).

# 7. Principles of Hydrodynamics

1 Introduction; 2 Hydrodynamic States; 3 Eulerian and Lagrangian Coordinate Systems; 4 Continuity Equation; 5 Pressure Tensor; 6 Equation of Motion; 7 Navier-Stokes Equations; 8 Elasticity Equations; 9 Heat Flux Vector; 10 Energy Equation; 11 Summary and References

## 7.1 Introduction

Hydrodynamics once meant the dynamics of water. But the breadth of the subject has come to include general flows of continuous matter, solids as well as fluids, as well as related problems in static stress analysis in which there is no flow at all. Thus another classical body of knowledge, elasticity theory, is included in hydrodynamics. The fundamentals of hydrodynamics parallel those of molecular dynamics: conservation of mass and energy, together with Newton's equations of motion for the flow of momentum. In hydrodynamics continuum constitutive equations are the analog of atomistic forces, and serve to distinguish one material from another. But the hydrodynamic equations of motion have to be developed for continua rather than particles. The forces causing flows are either *external* forces, from fields or moving boundaries, or *internal* forces, described in terms of the hydrodynamic pressure tensor P. Thus the hydrodynamic analog of interatomic forces is the "constitutive relation" describing the response of individual materials to sources of momentum and energy. The mechanical constitutive relation or "equation of state" for each material gives the pressure tensor as a function of the geometric flow variables, *strains* in the case of elastic solids and *strain rates* in the case of viscous fluids.

Because the macroscopic thermodynamic view includes an additional thermal variable, temperature or internal energy, the constitutive equations needed to specify a well-posed hydrodynamic problem must describe also the flow of energy in response to temperature gradients. Energy flows are usually assumed to follow Fourier's law of heat conduction,  $Q = -\kappa \cdot \nabla T$ . Once both the mechanical and thermal constitutive relations are given, the remaining task is to solve Newton's equations for the motion together with Fourier's heat flow equation for the energy.

There are a variety of analytic and numerical methods for solving problems in hydrodynamics, many more than in molecular dynamics because the underlying equations are *partial* differential equations rather than ordinary ones. The hydrodynamic equations are typically *irreversible*, rather than reversible, and absolutely unstable when reversed, so that it is only possible to predict the future. The past is inaccessible. The chief simplifying feature of the continuum approach, relative to the atomistic one, is that the flows take place in one-, two-, or three-dimensional geometrical spaces rather than in the abstract many-dimensional phase space of statistical mechanics.

The numerical limitations are similar to those governing molecular dynamics simulations. The system of interest has to be described by fewer than a billion degrees of freedom, and followed in time for no more than a million time steps. The computational work involves the evaluation of *spatial* derivatives, usually evaluated

with centered-difference approximations, as well as *time* derivatives, which can also be evaluated with difference methods or by using the same Runge-Kutta methods suitable for the ordinary differential equations of particle mechanics. The usual approach to continuum problems is to "discretize" the continuum, using finite-difference or finite-element methods to describe the solution in terms of nodal or cell variables. An attractive alternative for linear problems is to represent the field variables by truncated Fourier series. The numerical simulation of mass, momentum, and energy flows based on the equations of hydrodynamics is an active area of research which influences and profits from developments in computation. We will discuss elementary analytic and numerical approaches to specific continuum problems in Chapter 8.

Just as in molecular dynamics most hydrodynamic flows are driven by the interaction of initial conditions with specified boundary conditions. Unlike the time-reversible mechanical equations governing molecular dynamics the hydrodynamic flow equations are irreversible and would therefore generally decay to a state of uniform motion in the absence of external driving forces.

The fundamental picture on which the hydrodynamic approach is based is the continuum approximation. It is assumed that matter can be treated as continuously variable, with properties that change continuously and differentially in space and time. The fundamental equations are derived by considering flows within infinitesimal volume elements. The derivations indicate that the solutions of the fundamental equations will be useful provided they describe material properties which vary slowly on an atomistic scale. The generation and motion of shockwaves and dislocations as well as the failure of materials through fracture or flow are examples of problems for which the usual continuum approach can fail. The underlying continuity assumption is responsible for disagreement with experiment whenever the discontinuous properties of real matter are important.

## 7.2 Hydrodynamic States

Hydrodynamic systems require the specification of a thermodynamic state at every point, possibly as a function of time, though often the goal of a hydrodynamic simulation is the characterization of a nonequilibrium steady state in which time plays no essential role. Composition and mass density are the usual mechanical state variables, and these can be augmented by temperature or energy density whenever thermal properties are important. A constitutive description of the material is then required to express the momentum and energy flows in terms of the state variables. In addition to these material properties of thermodynamics, information describing the flow itself must be given. The *boundary* separating the hydrodynamic system from its surroundings can act as a source or a sink of mass, momentum, and energy. These boundary conditions are generally idealizations taken to represent experience. The underlying atomistic behavior responsible for these observed boundary conditions is an active area of research.

From the material and boundary information the flows of mass, momentum, and energy are to be calculated. The plan of a typical time-dependent hydrodynamic calculation is as follows:

- 1a. Describe the constitutive properties.
- 1b. Specify the initial conditions.
- 1c. Describe the boundary conditions.
- 2. Calculate new coordinates from the velocities.
- 3. Calculate new stresses, including viscous contributions.
- 4. Calculate accelerations from the stress gradients.
- 5. Calculate new temperatures from the energy and composition.
- 6. Calculate heat flows from the temperature gradients.
- 7. Calculate new velocities from accelerations.
- 8. Unless the calculation is complete, GO TO 2.

None of these steps can be carried out until a coordinate system describing the system of interest has been developed and used to generate a finite-element or finite-difference mesh upon which the solution is to be followed. The two most useful types of coordinate systems are described in the next Section.

7.3 Eulerian and Lagrangian Coordinate Systems

In a numerical solution of the hydrodynamic equations two specially simple coordinate systems can be used. "Eulerian" coordinates are fixed in space. In the Eulerian description matter flows through a fixed grid, as in Figure 7.1. Such a coordinate system is ideal for studying the approach to a stationary nonequilibrium state. The changing mass, momentum, and energy in each hydrodynamic zone is computed by summing up the corresponding flux contributions across the zone boundaries.

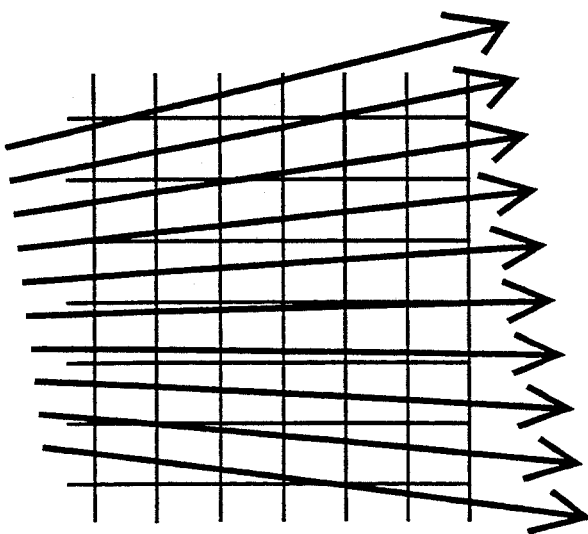


Figure 7.1. Eulerian zones, fixed in space, through which material streams.

Transient problems, particularly those involving large deformations or the tracking of interfaces separating different materials, are not so easily treated with a fixed coordinate frame. For them Lagrangian coordinates are a better choice. In the Lagrangian description coordinates are measured in a fixed laboratory frame, but refer to particular elements of the moving fluid or solid and follow the flow. There are no comoving mass fluxes in a Lagrangian problem unless the system contains interdiffusing species.

#### 7.4 Continuity Equation

The continuity equation is the macroscopic analog of conservation of mass. Because the material being studied is a continuum it is assumed that the flow properties are continuous differentiable functions of their arguments, except at boundaries. We begin with a fixed laboratory frame in which a gridwork of cell boundaries divides the continuum into Eulerian zones, as shown in Figure 7.1. We focus on one of these zones in order to formulate the continuum analogs of atomistic mass, momentum, and energy conservation.

The mass flowing into an Eulerian zone extending from  $x - (\delta x/2)$  to  $x + (\delta x/2)$  and with fixed boundaries  $\delta a$  normal to the  $x$  axis, is given by the difference between the mass loss rate  $(-\rho \delta a \dot{x})$  on the right and the mass gain rate  $(+\rho \delta a \dot{x})$  on the left. These rates can be visualized as dot products of the "mass flux"  $\rho v$ , and a vector normal to the area  $\delta a$ . If the flow velocity and mass density are both continuous variables then the time rate of change of mass, or equivalently, density, can be expressed as a power series in  $dx$ . Dividing by the zone volume, the first nonvanishing term is:

$$(\partial \rho / \partial t) = -\partial(\rho v) / \partial x.$$

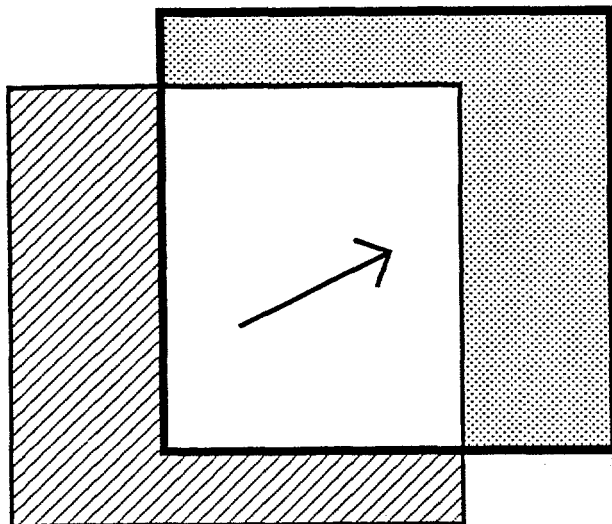


Figure 7.2. Flows entering and leaving a fixed Eulerian zone. During a short time interval  $dt$  the striped material enters the fixed Eulerian zone. Simultaneously the dotted material in the zone flows out. The continuity equation furnishes an exact description of such a flow.

The density derivative  $(\partial\rho/\partial t)$  is a *partial* derivative because it is calculated at a fixed spatial location. The space derivative  $-\partial(\rho v)/\partial x$  is likewise a *partial* derivative because the contributing flows are measured at the same time. By analyzing a series expansion, assuming sufficient differentiability, we can show that the deviations from the first nonvanishing terms shown above vanish as  $(\delta x)^2$  so that the differential equation is valid for sufficiently small zone widths  $\delta x$ .

By choosing a small square or cubic Eulerian zone the derivation just outlined for a one-dimensional flow can readily be generalized to two- and three-dimensional flows. See Figure 7.2. Adding up all the contributions for flow into and out of the area element in a *two*-dimensional continuum gives, for instance

$$(\partial\rho/\partial t) = -\partial(\rho v_x)/\partial x - \partial(\rho v_y)/\partial y = -\nabla \cdot (\rho \mathbf{v}) .$$

The last dot-product form of the *continuity equation*,  $(\partial\rho/\partial t) = -\nabla \cdot (\rho \mathbf{v})$ , uses the "del" operator  $\nabla$  to represent  $(d/dx, d/dy)$  in two dimensions or  $(d/dx, d/dy, d/dz)$  in three.

Let us derive the same result using the comoving Lagrangian coordinate system. Notice that the variation in density for a *moving* fluid is fundamentally different from that of a fixed Eulerian zone. The density change experienced by a moving element includes not only the fixed-space derivative  $(\partial\rho/\partial t)$  but also the change in density encountered as a consequence of motion,  $\mathbf{v} \cdot (\partial\rho/\partial \mathbf{x})$ . It is simplest to calculate the complete density change for an initially-square two-dimensional Lagrangian comoving volume element. The mass of any such element,  $\rho \delta x \delta y$ , is constant. As the element moves, with the flow velocity  $\mathbf{v}(x, y)$ , both the density  $\rho$  and the size  $\delta x \delta y$  can vary but their product is fixed. The comoving Lagrangian time derivative of the logarithm must therefore vanish:

$$0 = (d/dt) \ln(\rho \delta x \delta y) = (d \ln \rho / dt) + (d \ln \delta x / dt) + (d \ln \delta y / dt) = d \ln \rho / dt + \nabla \cdot \mathbf{v} = 0 ,$$

giving the usual *Lagrangian form of the continuity equation*,  $d \ln \rho / dt + \nabla \cdot \mathbf{v} = 0$ , valid for one-, two-, and three-dimensional continua. To see that this form is equivalent to the Eulerian version of the continuity equation it is necessary to expand the Lagrangian derivative of density, explicitly indicating the changes of density with time and with space. In two dimensions the expansion is:

$$d \ln \rho / dt = [(\partial\rho/\partial t) + v_x(\partial\rho/\partial x) + v_y(\partial\rho/\partial y)] / \rho = [(\partial\rho/\partial t) + \mathbf{v} \cdot \nabla \rho] / \rho .$$

In combination with the form  $d \ln \rho / dt + \nabla \cdot \mathbf{v} = 0$  we find

$$(\partial\rho/\partial t) + \mathbf{v} \cdot \nabla \rho = -\rho \nabla \cdot \mathbf{v} ,$$

equivalent to the Eulerian form above. Just as before the derivation requires only that the flow velocity be sufficiently differentiable. The neglected terms are of order  $\delta x^2$ ,  $\delta x \delta y$ , and  $\delta y^2$  and can be made arbitrarily small. The continuity equation also follows from the identity that the volume strain rate is given by the divergence of the velocity.

The flow equation relating the density change to the velocity through conservation of mass is called the *continuity equation*. The Eulerian and Lagrangian coordinates are not the only possible choices for expressing the continuity equation. Evidently the density change could just as well be calculated in an *arbitrarily* moving frame, by adding an appropriate convective derivative to the Eulerian derivative. One situation in which another coordinate frame is the simplest choice is the shockwave problem. Then the flow equations are simplest when described in a frame moving with the shockwave so that *all* the time derivatives, such as  $(\partial \rho / \partial t)$  and  $(\partial v / \partial t)$ , vanish.

### Problem:

Consider the one-dimensional motion of a longitudinal sinusoidal wave, with wavelength 1, which obeys the "wave equation"  $(\partial^2 u / \partial t^2) = c^2 (\partial^2 u / \partial x^2)$  where  $u$  is the "displacement" of the medium from its undisturbed rest state. Let the mass density  $\rho$  and sound velocity  $c$  of the medium also be unity. Work out the analytic variation with time of the coordinates, velocities, and pressure, in both the Eulerian and Lagrangian coordinate systems. Assume that the constitutive relation is a *linear* one, with  $P_{xx} = -\rho c^2 \epsilon_{xx}$  where the strain  $\epsilon_{xx}$  is the  $x$  derivative of  $u$ . Estimate the error that would be incurred in a numerical propagation of the wave for a distance of one wavelength if the second spatial derivative is replaced by a centered-difference approximation. Let the system be periodic, with a length equal to the wavelength, and divided into 10 equal zones. Check your analysis with a Runge-Kutta simulation.

## 7.5 Pressure Tensor

The flow of *momentum* can also be described in either Eulerian or Lagrangian coordinates. From the Eulerian standpoint it is most natural to think of momentum as flowing into and out of a fixed zone. From the alternative viewpoint of a comoving Lagrangian zone it is more natural to focus on the forces exerted on a moving zone by neighboring zones. A momentum flux is required in either case. When this flux is measured in the comoving frame it is called the *pressure tensor*, and the components are the force/area ratios. The pressure tensor, or "Pressure" for short, describes the force per unit area exerted by a Lagrangian fluid element on the surrounding fluid. Pressure is a second rank (two-subscript) tensor because two directions are required to describe the force/area ratios. These two are the direction normal to the area and the direction of the force. The force per unit area exerted on the positive side of a surface perpendicular to the  $x$  axis has components  $-P_{xx}$ ,  $-P_{xy}$ , and  $-P_{xz}$ . Thus *the fundamental definition of  $P_{ij}$  is the flux of  $j$  momentum in the  $i$  direction.*

**Problem:**

Show that the hydrostatic pressure in a fluid with variable mass density  $\rho(z)$  and in mechanical equilibrium under the influence of a gravitational field  $g$ , which accelerates mass in the negative  $z$  direction, satisfies the equation

$$dP/dz = dP_{zz}/dz = -\rho g .$$

In solid mechanics it is usual to discuss the *stress tensor*, or *stress*, rather than pressure. The word "tensor" was originally developed to describe the *tension* in solids under load. The stress tensor  $\sigma$  is just the negative of the pressure tensor,

$$\sigma = \begin{pmatrix} -P_{xx} & -P_{xy} & -P_{xz} \\ -P_{yx} & -P_{yy} & -P_{yz} \\ -P_{zx} & -P_{zy} & -P_{zz} \end{pmatrix} .$$

For the simplest isotropic elastic solids it is usual to neglect the distinction between isothermal and adiabatic deformation and to describe the response of stress to strain in terms of two material properties. Only two are required because only two modes of deformation are possible for an isotropic material, volume change and shape change. Thus the pair of material properties describing a general elastic response can be the bulk and shear moduli,  $B$  and  $G$ . Equivalently the two Lamé constants,  $\eta$  and  $\lambda$ , can be used. The definitions of  $B$  and  $G$  are:

$$B = dP/d\ln\rho = -(1/3)(P_{xx} + P_{yy} + P_{zz})/(\epsilon_{xx} + \epsilon_{yy} + \epsilon_{zz}) ; G = -P_{xy}/\epsilon_{xy} .$$

while the Lamé constants are defined by the phenomenological Hooke's-Law description of the stress tensor as a linear function of the strains:

$$\sigma = \lambda(\nabla \cdot \mathbf{u})\mathbf{I} + \eta(\nabla \mathbf{u} + \nabla \mathbf{u}^t) .$$

In this definition of  $\lambda$  and  $\eta$   $\mathbf{I}$  is the unit tensor and  $\mathbf{u}$  is the vector displacement from the stress-free reference state. Because the study of tensors and tension began with experiments on the deformation of rods an alternative description of elastic behavior is often adopted. The alternative is based on the simplest experiment, the extension of a uniform test cylinder. An isotropic cylindrical rod of rest length  $L$ , which has been extended in length by  $\delta L$  parallel to the  $x$  axis, is said to have been *strained*, undergoing a *strain*  $\epsilon_{xx} = \delta L/L$ ; unless special precautions prevent it the stretching will induce accompanying strains  $\epsilon_{yy} = \epsilon_{zz} = \epsilon$  in the radial direction. The resulting components of the pressure tensor and stress tensor are:

$$-P_{xx} = \sigma_{xx} = \lambda(\epsilon_{xx} + \epsilon_{yy} + \epsilon_{zz}) + 2\eta\epsilon_{xx} = \lambda(\epsilon_{xx} + 2\epsilon) + 2\eta\epsilon_{xx} ;$$

$$-P_{yy} = \sigma_{yy} = -P_{zz} = \lambda(\epsilon_{xx} + 2\epsilon) + 2\eta\epsilon.$$

Using again the shorthand notation  $\nabla$  to represent  $(\partial/\partial x, \partial/\partial y)$  in two dimensions or  $(\partial/\partial x, \partial/\partial y, \partial/\partial z)$  in three gives a form valid for either two- or three-dimensional isotropic continua:

$$P = -\lambda(\nabla \cdot \mathbf{u})\mathbf{I} - \eta(\nabla \mathbf{u} + \nabla \mathbf{u}^t),$$

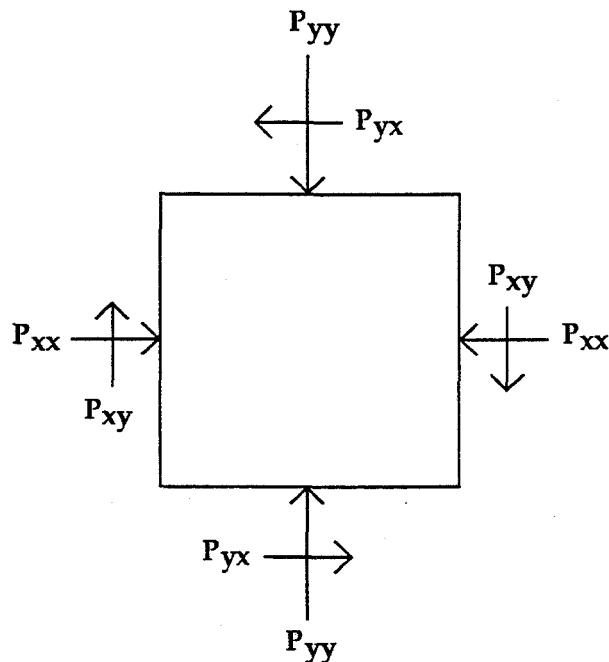
where  $\mathbf{I}$  is the unit tensor. In *one* dimension  $\nabla \cdot \mathbf{u}$  and  $\nabla \mathbf{u}$  are identical and there is only a single elastic modulus. If the sides of a three-dimensional elastic rod are maintained stress free then the ratio of the contraction of the bar to the extension,  $-\epsilon/\epsilon_{xx}$ , is called *Poisson's ratio*,  $\nu$ , and given by the expression  $\nu = \lambda/(2\eta + 2\lambda)$ . The ratio of the longitudinal stress to the strain in this experiment is called *Young's modulus*, usually denoted by  $E$ :

$$E = (2\eta + \lambda) + 2\lambda(\epsilon/\epsilon_{xx}) = (3\lambda\eta + 2\eta^2)/(\lambda + \eta).$$

### Problems:

1. Show that the one-dimensional analog of Young's modulus  $E$ ,  $\sigma_{xx}/\epsilon_{xx}$ , for a one-dimensional chain of particles linked by Hooke's-Law springs is equal to the spring constant  $\kappa$ . For a two-dimensional strip of nearest-neighbor triangular-lattice particles linked by Hooke's-Law springs show that Young's modulus,  $\sigma_{xx}/\epsilon_{xx}$ , is  $8\eta/3 = (2/3)\sqrt{3}\kappa$ .
2. Estimate Young's modulus for diamond, assuming a typical vibrational frequency of  $10^{13}$  hertz.

**Figure 7.3.** Forces on a comoving Lagrangian zone are described by the *pressure tensor*. The element  $P_{ij}$  gives the force in the  $j$ th direction on the face perpendicular to the  $i$ th direction.



An important, but far from obvious, property of the pressure tensor is its symmetry. The off-diagonal elements are equal in pairs:

$$P_{xy} = P_{yx}; P_{yz} = P_{zy}; P_{zx} = P_{xz},$$

for instance. This symmetry is required for mechanical stability. If *any* pair  $\{P_{i \neq j}, P_{j \neq i}\}$  of off-diagonal elements were not precisely equal then the resulting torque would vanish less strongly than the mass as the volume element became smaller, causing infinite angular accelerations. Thus the symmetry of the pressure tensor follows from the requirement that the continuum must have well-defined accelerations. To see this, consider the two-dimensional element of area shown in Figure 7.4 and imagine that  $P_{yx}$  exceeds  $P_{xy}$  by  $\delta P$ . The effect would be a counterclockwise rotation increasing  $\theta$ . The resulting surface forces do work  $\delta P L^2 d\theta$  during a positive rotation  $d\theta$  which is converted into kinetic energy of the area element  $(1/2)\langle \rho v^2 \rangle L^2 = (1/2)\langle \rho (r\dot{\theta})^2 \rangle L^2 = (\rho L^4 \dot{\theta}^2 / 12) = \delta P L^2 d\theta$ . Setting the time derivatives of these two equal energies equal to each other gives an ordinary differential equation for the rotation:

$$d(\delta P L^2 d\theta) / dt = (d/dt)[(\rho L^4 / 12) \dot{\theta}^2] = \dot{\theta} \ddot{\theta} \rho L^4 / 6.$$

Thus the angular acceleration diverges as  $L^{-2}$  if the pressure tensor is not symmetric.

### Problem:

Show that the same result for the angular acceleration is obtained in three dimensions if again  $P_{yx}$  exceeds  $P_{xy}$  by  $\delta P$ .

The symmetry of the pressure tensor can also be seen directly from the atomistic point of view in a system composed of particles which exert central forces on one another. To see this, remember the virial theorem expression for the pressure tensor:

$$PV = \sum r_{ij} F_{ij} + \sum (pp/m).$$

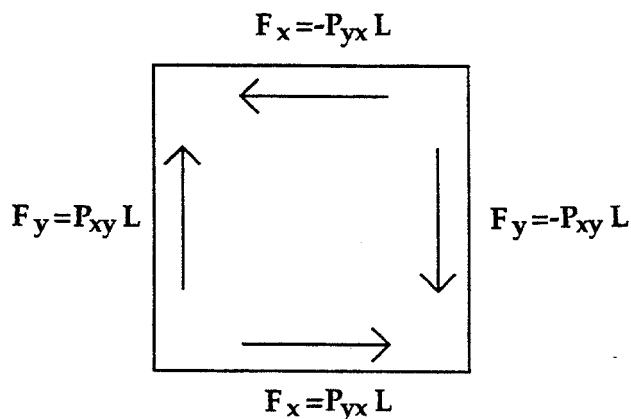


Figure 7.4. Rotational forces corresponding to  $P_{xy}$  and  $P_{yx}$ . Unless the pressure tensor is symmetric the angular acceleration from these forces diverges as  $L$  approaches zero.

The two contributions to the PV tensor product,  $r_{ij}F_{ij}$  from each interacting pair of particles and  $(pp/m)$  from each mass, both have this symmetry. It is possible to define nonsymmetric pressure tensors for molecules interacting with noncentral forces but we shall not do so.

To develop more familiarity with the pressure tensor we will work out the relations linking the Cartesian and polar-coordinate representations of  $P$ . Given the flux of  $x$  momentum in the  $x$  direction  $P_{xx}$  and the flux of  $x$  momentum in the  $y$  direction  $P_{yx}$ , it is clear that the flux of  $x$  momentum across a sampling plane normal to the *radial* direction is

$$P_{xx}\cos\theta + P_{yx}\sin\theta .$$

Similarly, the flux of  $y$  momentum, across the same sampling plane, normal to the radial direction is

$$P_{xy}\cos\theta + P_{yy}\sin\theta .$$

The radial components of these two contributions make up the total *radial* flux of radial momentum.  $P_{rr}$  is the radial part of these two momentum fluxes:

$$P_{rr} = [P_{xx}\cos\theta + P_{yx}\sin\theta]\cos\theta + [P_{xy}\cos\theta + P_{yy}\sin\theta]\sin\theta ;$$

$$P_{rr} = [P_{xx}\cos^2\theta + (P_{xy} + P_{yx})\sin\theta\cos\theta + P_{yy}\sin^2\theta] .$$

The combination  $(P_{xy} + P_{yx})$  is of course  $2P_{xy} = 2P_{yx}$ , but has been written as is for clarity.

The corresponding shear flux contributions of these  $x$  and  $y$  momenta *in the  $\theta$  direction* is the pressure-tensor component  $P_{r\theta}$ :

$$P_{r\theta} = -[P_{xx}\cos\theta + P_{yx}\sin\theta]\sin\theta + [P_{xy}\cos\theta + P_{yy}\sin\theta]\cos\theta .$$

Finally, considering the flow of  $\theta$  momentum across a sampling plane perpendicular to the direction of increasing  $\theta$  leads to the result:

$$P_{\theta\theta} = [P_{xx}\sin^2\theta - (P_{xy} + P_{yx})\sin\theta\cos\theta + P_{yy}\cos^2\theta] .$$

Exactly these same results follow automatically from the mathematical operation of tensor rotation from the original Cartesian  $xy$  frame through an angle  $\theta$  to the local Cartesian version of the polar-coordinate frame:

$$P(r,\theta) = R \cdot P(x,y) \cdot R^t; \quad R = \begin{matrix} \cos(\theta) & \sin(\theta) \\ -\sin(\theta) & \cos(\theta) \end{matrix} .$$

**Problem:**

Consider a two-dimensional particle with mass  $m$ , moving in a box with area  $V$  and with momentum  $p = (p_x, p_y)$ . What are the instantaneous contributions of this particle to the Cartesian pressure tensor components  $P_{xx}$ ,  $P_{xy}$ , and  $P_{yy}$ ? Express the momentum of this same particle in polar coordinates,  $p = (p_r, p_\theta)$ . Then also compute the contribution to the polar-coordinate momentum fluxes  $P_{rr}$ ,  $P_{r\theta}$ , and  $P_{\theta\theta}$ , all in terms of the original momentum components  $p_x$  and  $p_y$ .

7.6 Equation of Motion

Assume a continuous differentiable form for the pressure tensor  $P(r)$  at every point in space. The vector divergence of this tensor, together with any external gravitational or electromagnetic forces, can then be used to calculate accelerations. To establish this result we again consider a Lagrangian cube  $\delta x \delta y \delta z$  of material moving with the flow velocity  $u(r) = u(x, y, z)$ . The acceleration of this comoving cube in the  $x$  direction, for instance, has three independent contributions  $-(\partial P_{xx} / \partial x) \delta x \delta y \delta z$  from the difference of the pressure forces applied at the  $x$  faces,  $-(\partial P_{yx} / \partial y) \delta y \delta z \delta x$  from those at the  $y$  faces, and  $-(\partial P_{zx} / \partial z) \delta z \delta x \delta y$  from the  $z$  faces. If the pressure tensor is sufficiently differentiable, the errors in the resulting differential equation of motion will vanish as the square of the cube's sidelength. In the absence of external fields the  $x$  component of the equation of motion is

$$\rho \dot{u}_x = -(\nabla \cdot P)_x .$$

The generalization, valid in any number of dimensions, is

$$\rho \dot{u} = -\nabla \cdot P = +\nabla \cdot \sigma ,$$

where the ordinary time derivative signifies the comoving Lagrangian derivative following the motion.

It is sometimes convenient to use curvilinear coordinates rather than Cartesian coordinates. In such a case the stress and strain tensors can be transformed by standard mathematical techniques, or by physical reasoning, as illustrated in the last Section, or the new equations can alternatively be derived by force balance. To illustrate the latter approach, consider the radial forces on the two-dimensional area element  $r dr d\theta$  shown in Figure 7.5. The product of the mass and the radial acceleration  $(\rho r dr d\theta) \dot{u}_r$  is given by the sum of two terms. The radial components of the forces on the two curved surfaces are:

$$(r P_{rr} d\theta)_{r-(dr/2)} - (r P_{rr} d\theta)_{r+(dr/2)} .$$

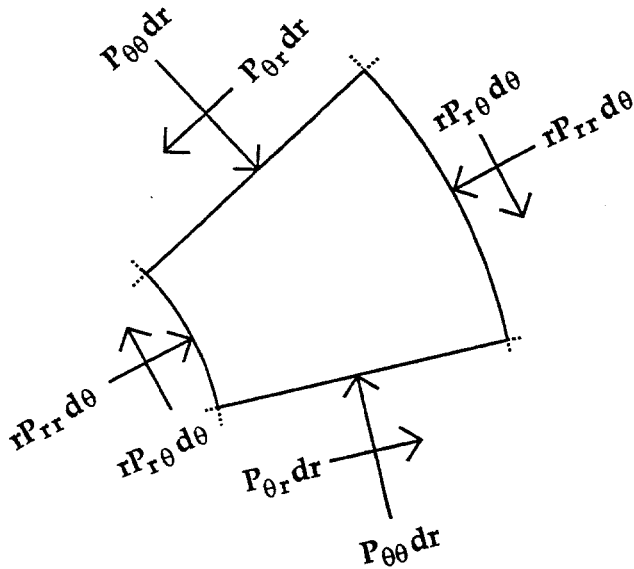


Figure 7.5. Force balance calculation using polar coordinates. Notice particularly that the forces on the straight sides of the polar volume element have resultants in the radial direction.

The radial components of the forces on the two flat boundaries are of two kinds; the shear components,

$$[(P_{\theta r})_{(-d\theta/2)} - (P_{\theta r})_{(+d\theta/2)}] dr ,$$

and the radial resultants of the "hoop stresses," both of which have the same sign:

$$[(dr P_{\theta\theta})_{(-d\theta/2)} + (dr P_{\theta\theta})_{(+d\theta/2)}](d\theta/2).$$

From the sum of these three contributions the radial equation of motion is:

$$\rho \dot{u}_r = -(\partial P_{rr}/\partial r) - (1/r)(\partial P_{\theta r}/\partial \theta) - (1/r)(P_{rr} - P_{\theta\theta}) .$$

Similarly, the equation of motion in the  $\theta$  direction is:

$$\rho \dot{u}_\theta = -(\partial P_{r\theta}/\partial r) - (1/r)(\partial P_{\theta\theta}/\partial \theta) - (1/r)(P_{r\theta} + P_{\theta r}) .$$

### 7.7 Navier-Stokes Equations

It is the result of experience that the more rapidly a fluid is deformed the greater is the work required to accomplish the deformation. The hypothetical reversible process of thermodynamics requires the least work and the greatest amount of time. It is reasonable, and in accord with considerable experimental data, to suppose that the pressure tensor, for a simple fluid away from equilibrium, can be expanded as a power series in the strain rate. Because typical strain rates seldom exceed a megahertz while one could expect stress to relax at gigahertz or terahertz rates it is likewise "reasonable," because it is likewise supported experimentally, to truncate the presumed expansion

after the first nonvanishing term. The additional nonequilibrium term, proportional to the strain rate, introduces Newton's phenomenological "viscosity" into the constitutive relation. For isotropic fluids there can be only two viscosities, a "shear" viscosity which resists changes in shape and a "bulk" viscosity which resists changes in volume. It is advantageous in formulating hydrodynamics to express the bulk viscosity in terms of a hybrid viscosity  $\lambda = \eta_v - (2\eta/D)$ , where  $\eta$  is the shear viscosity. The motivation for this queer choice is the simple form taken by the stress tensor. We will see that this form is analogous to the equations describing elastic deformation in a homogeneous isotropic medium.

**Problem:**

Calculate the time required for an iron atom to move one interatomic spacing, 0.25 nanometers, at the room-temperature thermal velocity  $(3kT/m)^{1/2}$  and discuss why it is that the longitudinal sound velocity in iron, nearly 6 km/sec, is about fifteen times faster than the corresponding thermal speed.

The pressure tensor  $P$  (the negative of the stress tensor  $\sigma$ ) for a Newtonian fluid has the form

$$P = (P_{eq} - \lambda \nabla \cdot \mathbf{u}) \mathbf{I} - \eta (\nabla \mathbf{u} + \nabla \mathbf{u}^t),$$

where the equilibrium pressure  $P_{eq}$  and the two viscosity coefficients  $\eta$  and  $\lambda$  all depend upon the local thermodynamic state and the superscript  $t$  indicates the *transpose* of the velocity gradient tensor  $\nabla \mathbf{u}$ . This equation is the constitutive relation for a "Newtonian fluid." To understand the significance of this tensor form it is useful to consider the three special cases shown in Figure 7.6. If a fluid expands isotropically with a *volume* strain rate  $\dot{\epsilon} = (\partial u_x / \partial x) + (\partial u_y / \partial y) + (\partial u_z / \partial z) = \nabla \cdot \mathbf{u} = d \ln V / dt$ , then the pressure must also be isotropic and the tensor must be diagonal, with all three diagonal elements equal to  $P_{eq} - [\lambda + (2/3)\eta] \dot{\epsilon}$ . Thus the "bulk" viscosity, which gives the excess pressure in compression and the excess tension in expansion is

$$\eta_v = \lambda + (2/3)\eta.$$

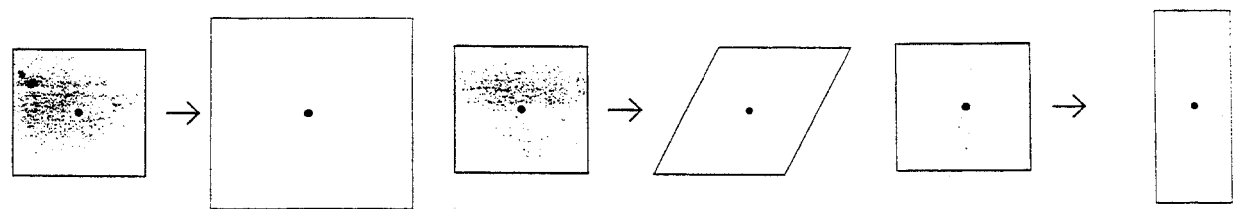


**Figure 7.6.** Deformations of a shaded volume element illustrating isotropic expansion (left) as well as two shear deformations (center and right).

**Problem:**

Show that the bulk viscosity is  $\eta_v = \lambda + \eta$  in a two-dimensional Newtonian viscous fluid.

Next consider the steady shear of a fluid, with  $u_x = \dot{\epsilon}y$ , where  $\dot{\epsilon}$  is the shear strain rate. Then the only nonvanishing element of  $\nabla u$  is  $(\partial u_x / \partial y) = \dot{\epsilon}$ . Because this element of  $\nabla u$  contributes to the viscous pressure tensor element  $P_{yx}$  as well, through the transpose of  $\nabla u$ , the corresponding (symmetric) pressure tensor for this simple shear flow is

$$P = \begin{pmatrix} P_{eq} & -\eta\dot{\epsilon} & 0 \\ -\eta\dot{\epsilon} & P_{eq} & 0 \\ 0 & 0 & P_{eq} \end{pmatrix} .$$

The typical hydrodynamic fluid, water, has a room temperature shear viscosity of 0.01 poise = 0.001 pascal seconds. If we describe the viscosity in terms of a relaxation time, the "Maxwell relaxation time," by dividing the viscosity by the shear modulus (here we can use the shear modulus for ice as an estimate because the zero-frequency shear modulus for water is zero), a value of order one picosecond results, correctly suggesting that the mechanism for viscous flow is atomic rearrangement. By way of contrast, the typical gas, air, has a room temperature shear viscosity one thousand times less and a modulus perhaps one hundred thousand times less than that of water. Thus the Maxwell relaxation time for air is about a nanosecond, and corresponds to the time between collisions.

Last, consider a fluid which is being squeezed in the  $x$  direction and stretched in the  $y$  direction, so that  $\nabla \cdot u$  vanishes and the deformation takes place at constant volume. The pressure tensor for that flow, described by two elements of the velocity-gradient tensor,  $du_x/dx = +\dot{\epsilon}/2 < 0$  and  $du_y/dy = -\dot{\epsilon}/2 > 0$ , is

$$P = \begin{pmatrix} P_{eq} - \eta\dot{\epsilon} & 0 & 0 \\ 0 & P_{eq} + \eta\dot{\epsilon} & 0 \\ 0 & 0 & P_{eq} \end{pmatrix} .$$

Because this flow is identical to the previous example, in a coordinate frame which has been rotated  $45^\circ$ , we see that shear need not involve off-diagonal pressure tensor components. These are fully equivalent to differences in diagonal elements in a rotated coordinate system.

The equation of motion for a viscous fluid is called the Navier-Stokes equation:

$$\rho \dot{u} = -\nabla \cdot P = -\nabla \cdot [(P_{eq} - \lambda \nabla \cdot u)I - \eta(\nabla u + \nabla u^t)] .$$

It is often assumed that the fluid flow is incompressible, with  $\nabla \cdot \mathbf{u} = 0$ , so that the bulk viscosity does not influence the flow, but we use the term Navier-Stokes equation to mean the equation of motion for a fluid with Newtonian viscosities, both shear and bulk. If the material properties have no dependence on energy then the Navier-Stokes equation together with the continuity equation is enough to formulate a well-posed problem. In the more usual case that energy plays a role then the flow of energy, as discussed in Sections 9 and 10, must be included also.

### 7.8 Elasticity Equations

Although all materials have a directionally-ordered structure on the atomistic level that structure is often irregular enough on a larger scale, perhaps a micron, so that the material can be treated as macroscopically homogeneous and isotropic. In analyzing the small deformations associated with stresses that are small relative to the moduli, that is, stresses of order a few atmospheres for typical solids, it is useful to imagine expanding the stress tensor as a series in the strains and to keep only the first nonvanishing term. Displacement is not the same as deformation. Deformation requires a *symmetric* displacement gradient. Strain is related to the displacement gradient. Strain is fundamentally a second-rank (two-index) tensor because the *direction* of displacement varies with *location*. Antisymmetric combinations of displacement gradients correspond to rotations irrelevant in the linear theory of a symmetric pressure tensor.

In hydrodynamics the symmetrized velocity gradient leads to linear stress deviations from equilibrium. In elasticity theory, displacements replace the velocities and the symmetrized displacement gradient,  $\nabla \mathbf{u} + \nabla \mathbf{u}^t$ , likewise describes deviations from the unstrained stress-free state. For the simplest possible idealized elastic continuum, assumed to be both homogeneous and isotropic, the linear equation of state has the same form as that for a viscous fluid:

$$\boldsymbol{\sigma} \equiv \lambda \nabla \cdot \mathbf{u} \mathbf{I} + \eta (\nabla \mathbf{u} + \nabla \mathbf{u}^t),$$

where again  $\mathbf{I}$  is the unit tensor. The equilibrium stress is not written explicitly because, in elasticity theory, the stress expansion is ordinarily carried out about the state of zero stress. Otherwise it is necessary to define and use nonlinear strains.

The elastic moduli  $\eta$  and  $\lambda$  are called the Lamé constants. Their numerical values range from about an atmosphere in very soft materials, such as rubber, to several megabars for hard materials, such as diamond. The ratio of the viscosity coefficients, with units of [pressure  $\times$  time], to the moduli are again "Maxwell relaxation times" with typical numerical values on the order of an atomic collision time, about a picosecond.

### 7.9 Heat Flux Vector

The heat flux vector completes the formal list of ingredients required for a continuum description of the flow of mass, momentum, and energy. Heat flux describes the comoving flow of energy, with units [energy/area  $\times$  time] = [power/area]. The "area" becomes a length in two-dimensional problems. Like the pressure tensor the heat flux vector requires definition in the comoving Lagrangian frame. If we imagine inserting a thin insulating comoving area in an otherwise unchanged continuum, the tendency of opposite sides of the insulator to heat and cool would reveal the presence of a heat flux. If the temperature gradients are sufficiently small it is reasonable to imagine expanding the heat flux as a power series in the gradient and to keep only the first nonvanishing term. The result is Fourier's Law:

$$Q = -\kappa \cdot \nabla T.$$

The dot product is used here as a reminder that the heat conductivity  $\kappa$  can be a tensor if the medium is anisotropic, as is graphite for instance. The anisotropy can be induced in an isotropic medium by external fields or by rotations. For example, in a rapidly rotating cylinder of fluid, hot in the center and cold on the boundary, the flow of heat is not entirely radial, even in the comoving frame.

#### Problem:

The steady comoving (corotating) heat flow in a rapidly-rotating annulus of fluid or solid, heated at the inner radius and cooled at the outer radius, can be described by an *antisymmetric* heat conductivity tensor with  $\kappa_{xy} = -\kappa_{yx}$ . Sketch the flux lines in the corotating frame and describe the mechanism responsible for the nonsymmetric contribution to the heat flux.

Just as is the case for the pressure tensor it is possible to write down microscopic expressions relating the heat flux vector directly to the underlying particle coordinates and momenta. To do so imagine sampling the kinetic part of the heat flux component  $Q_x^k$  by considering the flow across an infinitesimal sampling plane perpendicular to the  $x$  axis. Average the position of this plane over all locations in the volume  $V$ . The quantity sampled, the rate at which energy crosses the sampling plane due to *kinetic* particle motion, is proportional to the normal velocity  $v_x$  of crossing particles and to the energy transported:

$$Q_x^k = (1/V) \sum v_x [(p^2/2m) + \phi],$$

where the potential energy flow associated with each particle includes half of its interactions with other particles.

The rate at which energy is transported across a sampling plane through the action of interparticle forces gives the remaining *potential* part of the heat flux:

$$Q_x^\phi = (1/V) \sum_{ij} x_{ij} [F_{ij} \cdot (p_i + p_j) / 2] ; Q_x = Q_x^k + Q_x^\phi .$$

Exactly these same relations for the heat flux vector were derived in Section 5.5 by time averaging a microscopic expression involving the single-particle energy changes,  $\{\dot{E}_i\}$ .

7.10 Energy Equation

With microscopic expressions for the pressure tensor P and heat flux vector Q we can express the rate of change of specific energy e (that is, energy per unit mass) for a deforming and conducting volume element  $\delta x \delta y \delta z$ . Such a volume element can do work on, and exchange heat with, its surroundings. These energy transfers obey the time-dependent version of the First Law of Thermodynamics,

$$\dot{E} = \dot{Q} - \dot{W}:$$

$$\rho \delta x \delta y \delta z \dot{e} = -\delta x \delta y \delta z \nabla \cdot Q - \delta x \delta y \delta z P : \nabla u .$$

Dividing by the volume completes the set of equations describing the flows of mass, momentum, and energy in a continuum.

In using the double-dot notation  $-P : \nabla u$  to represent the density of mechanical work done by a deforming Lagrangian volume element we mean to include nine similar contributions in three dimensions. In two dimensions there are four:

$$-P_{xx}(\partial u_x / \partial x) - P_{xy}(\partial u_y / \partial x) - P_{yx}(\partial u_x / \partial y) - P_{yy}(\partial u_y / \partial y) = -P_{xx} \dot{\epsilon}_{xx} - P_{xy} \dot{\epsilon}_{xy} - P_{yy} \dot{\epsilon}_{yy} .$$

In the last form we have used the symmetry of the pressure tensor to combine together the two contributions to the shear strain rate  $\dot{\epsilon}_{xy} = (du_x / dy) + (du_y / dx)$ .

Although it is tempting, and even correct, to write the energy equation,

$$\rho \dot{e} = -\nabla \cdot Q - P : \nabla u ,$$

by direct appeal to the First Law of Thermodynamics, such an argument cannot be made with confidence unless one has carried out the painful algebra required for a "rigorous" derivation. We indicate the steps here for the one-dimensional case, leaving the two- or three-dimensional analogs to the conscience of the student. Suppose density  $\rho(x,t) \equiv \rho$ , velocity  $v(x,t) \equiv v$ , pressure  $P_{xx}(x,t) \equiv P$ , heat flux  $Q_x(x,t) \equiv Q$ ,

and energy density per unit mass,  $e(x,t) \equiv e$ , are *all* differentiable functions of the laboratory frame coordinate  $x$ , and the time  $t$ ; then the rate at which the energy in a fixed Eulerian zone of length  $dx$  changes with time,  $(\partial/\partial t)[\rho e + (1/2)\rho v^2]dx$  is given by summing up the convective flow of energy  $-(\partial/\partial x)[\rho v e + (1/2)\rho v^3]dx$ , the work done  $-(\partial/\partial x)(Pv)dx$ , and the heat flux  $-(\partial Q/\partial x)dx$ . The fixed zone length is common to all these contributions so that energy balance requires:

$$(\partial/\partial t)[\rho e + (1/2)\rho v^2] = -(\partial/\partial x)[\rho v e + (1/2)\rho v^3] - (\partial/\partial x)(Pv) - (\partial Q/\partial x).$$

The left-hand side can be written:

$$\rho(\partial e/\partial t) + (\partial\rho/\partial t)[e + (1/2)v^2] + \rho v(\partial v/\partial t).$$

The right-hand side has the form:

$$-[e + (1/2)v^2][\partial(\rho v)/\partial x] - \rho v[\partial[e + (1/2)v^2]/\partial x] - v(\partial P/\partial x) - P(\partial v/\partial x) - (\partial Q/\partial x).$$

The time derivatives of the density and velocity can then be eliminated by straightforward substitution, using the Eulerian forms of the continuity equation and the equation of motion:

$$(\partial\rho/\partial t) = -\partial(\rho v)/\partial x; \partial(\rho v)/\partial t = -\partial[P + \rho v^2]/\partial x \Leftrightarrow \rho(\partial v/\partial t) = -(\partial P/\partial x) - \rho v(\partial v/\partial x).$$

The result is the much simpler Lagrangian form of the (one-dimensional) energy equation:

$$\dot{\rho e} = \rho[(\partial e/\partial t) + v(\partial e/\partial x)] = -P(\partial v/\partial x) - (\partial Q/\partial x).$$

With this derivation of the energy equation we have obtained the complete set of Lagrangian equations for hydrodynamic flows:

$$d \ln \rho / dt = -\nabla \cdot \mathbf{u}; \quad \rho \dot{\mathbf{u}} = -\nabla \cdot \mathbf{P}; \quad \dot{\rho e} = -\nabla \cdot \mathbf{Q} - \mathbf{P} : \nabla \mathbf{u}.$$

These equations, when supplemented by the constitutive equations for the pressure tensor and the heat flux vector are a closed set of equations, making it possible to simulate the dynamics of a continuum numerically.

### 7.11 Summary and References

Continuum flows of mass, momentum, and energy can be described in a space-fixed "Eulerian" frame or in a material-fixed "Lagrangian" frame. The comoving fluxes of momentum and energy are the "pressure tensor" and the "heat flux vector." Once the material-dependent "constitutive equations" describing the response of these comoving fluxes to velocity and temperature gradients are specified the conservation relations for mass, momentum, and energy lead to a well-posed problem.

The conservation relations take their simplest form in the Lagrangian comoving frame:

$$d \ln \rho / dt = -\nabla \cdot \mathbf{u} ; \rho \dot{\mathbf{u}} = -\nabla \cdot \mathbf{P} ; \rho \dot{e} = -\nabla \cdot \mathbf{Q} - \mathbf{P} : \nabla \mathbf{u} .$$

These partial differential equations can be solved with numerical techniques resembling those applied to problems in molecular dynamics.

The most useful references are Landau and Lifshitz' *Theory of Elasticity and Fluid Mechanics*. The classic reference for solids is the text *Elasticity* by Horace Lamb. It is surprisingly hard to find a good treatment of stress in curvilinear coordinate systems. But see *Computational Fluid Mechanics and Heat Transfer* by D. A. Anderson, J. C. Tannehill, and R. H. Pletcher (McGraw-Hill, New York, 1984).

## 8. Applications of Hydrodynamics

*1 Introduction; 2 Plane Couette Flow; 3 Poiseuille Flow; 4 Stokes' Flow Past a Sphere or Disk; 5 More-General Analytic Solutions; 6 Turbulence; 7 Rayleigh-Bénard Problem; 8 Numerical Methods; 9 Summary and References*

### 8.1 Introduction

Microscopic many-body mechanics and macroscopic continuum hydrodynamics are equally complex. Just as in mechanics, real problems in hydrodynamics generally require numerical work. Only a few textbook examples can be solved analytically. The deceptively-simple structure of the Navier-Stokes equations, when combined with equally simple constitutive equations and stationary boundary conditions, conceals the ability to generate the wildly chaotic behavior of a waterfall. It might well be thought that this capability for chaos comes about because a continuum description requires an infinite number of degrees of freedom, not just a finite number. But this view is wrong. A large number of degrees of freedom is not at all necessary for unpredictable chaotic behavior. Three quadratic ordinary differential equations can produce chaos. Lorenz' caricature of the Navier-Stokes equations, truncated to only three degrees of freedom with quadratic interactions, the simplest possible form of nonlinearity, is fully enough for chaos. Further, the number of *effective* degrees of freedom in a continuum is actually *not* infinite because short wavelengths are inactive. Features with short wavelengths (small  $\lambda$ ) have even shorter lifetimes, of order  $\lambda^2$ , because they are strongly damped by viscous forces of order  $1/\lambda$ . This damping is a fortunate circumstance. The numerical simulation of hydrodynamic flows would be impossible were it not for this loss of high-frequency modes.

Stationary solutions of the Navier-Stokes equations can represent interesting steady nonequilibrium fluid flows, with constant mass, momentum, and energy currents fed by boundary fluxes and external forces. In contrast, the only stationary solutions of the atomistic equations of motion represent cold motionless solids. The stationary Navier-Stokes solutions representing nonequilibrium dissipative irreversible flows are either stable or unstable to small perturbations. Close enough to equilibrium these flows must certainly be stable. Stability far from equilibrium is often hard to judge.

Because the viscosity and conductivity in the Navier-Stokes equations are dissipative, continuously converting work into heat until only uniform motion remains, well-behaved steady-state solutions can certainly be found sufficiently close to equilibrium by reducing the strength of the nonequilibrium driving terms. In this Chapter we focus on plane Couette flow, Poiseuille flow, and the Stokes flow around a slowly-moving sphere, three of the most elementary illustrative problems, for three reasons. First, these simple stationary flows, and the analogs of the first two for heat flow, provide operational methods for measuring the viscosity and heat conductivity required in analyzing more complex situations. Second, these simple flows share many physical and mathematical features with their more complex chaotic relatives. Finally,

these stable stationary flows provide much-needed checks for the numerical approaches which are necessary for most real applied problems. After describing these elementary examples we outline numerical techniques which can be applied to more complex and more realistic hydrodynamic problems.

8.2 Plane Couette Flow

A viscous fluid confined between two coaxial rotating cylinders can exhibit a variety of unstable unsteady size-and-shape-dependent two- and three-dimensional flows as the relative rotation rate is increased, but if the sample size and rotation rates are both sufficiently small a stable laminar two-dimensional flow can result in which fluid viscosity smoothly dissipates the momentum imparted to the fluid by the moving cylinders. If both cylinder radii greatly exceed the size of the gap between the cylinders, then the simplest special case, "plane Couette flow" results, with the angular velocity increasing linearly with radius. See Figure 8.1. In a Cartesian coordinate system, with the radial direction replaced by y and the tangential direction by x, this prototypical flow has the form

u\_x = \dot{\epsilon} y ,

where \dot{\epsilon} is the strain rate and the x velocity component u\_x matches the wall velocity at limiting values of y, here chosen equal to \pm L/2. We wish to consider only the laminar-flow case in which there is no motion in the z direction. We therefore describe the motion in the xy plane.

The two-dimensional Navier-Stokes equations of motion \rho \dot{u} = \rho(\partial u/\partial t) + \rho u \cdot \nabla u = \nabla \cdot \sigma are satisfied within the flow with the stream velocity u = (u\_x, 0), with u\_x proportional to y, and a constant stress tensor \sigma, which includes the viscous contribution \sigma\_{xy} = \sigma\_{yx} = \dot{\epsilon}:

\rho(\partial u\_x/\partial t) = -\rho u\_x(\partial u\_x/\partial x) - \rho u\_y(\partial u\_x/\partial y) + (\partial \sigma\_{xx}/\partial x) + (\partial \sigma\_{yx}/\partial y) = -0 - 0 + 0 + 0 = 0 ;

\rho(\partial u\_y/\partial t) = -\rho u\_x(\partial u\_y/\partial x) - \rho u\_y(\partial u\_y/\partial y) + (\partial \sigma\_{xy}/\partial x) + (\partial \sigma\_{yy}/\partial y) = -0 - 0 + 0 + 0 = 0 .

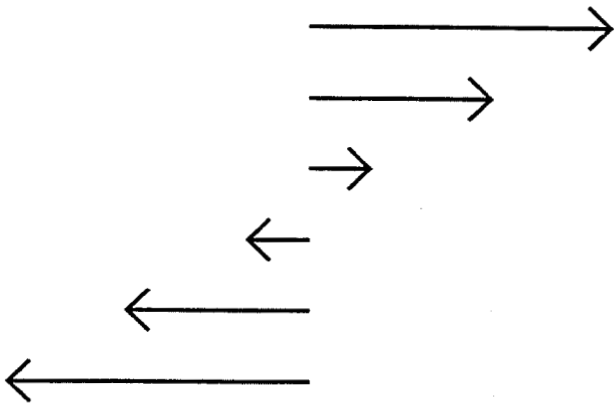


Figure 8.1. Plane Couette Flow. The horizontal velocity component u\_x is a linear function of the vertical coordinate y:

u\_x = \dot{\epsilon} y.

The two Navier-Stokes equations of motion are also satisfied *at the boundaries*,  $y = \pm L/2$ , provided that these boundaries exert forces matching the viscous force per unit area  $P_{xy} = P_{yx} = -\eta \dot{\epsilon}$  exerted by the shearing fluid. At high rates of strain, viscous heating, proportional to  $\dot{\epsilon}^2$ , can complicate the analysis of this problem, by causing the fluid temperature, density, viscosity, and heat conductivity to vary in space and time. These nonlinearities can be ignored if, as is the usual case, the heating rate is sufficiently small. For water, with a strain rate of 1 hertz, the rate at which mechanical energy is converted into heat is 0.01 ergs/(gram second). Thus, except on a time scale of years, the nonequilibrium state induced by plane Couette flow can be treated as stationary, isochoric, and isothermal.

Plane Couette flow is also stable to small perturbations. Consider, as an example, a velocity perturbation of the form,

$$\delta u_x = \delta s_n(t) \sin(k_n y); \quad k_n = 2\pi n/L.$$

The wave vector component  $k_n$  has been chosen so that the corresponding velocity perturbation vanishes on the boundaries at  $y = \pm L/2$  for  $n = 1, 2, 3, \dots$ . If such a perturbation is introduced into the constant-volume "linearized" (meaning: ignoring terms of order  $u^2$ , including heating) equation of motion:

$$\rho(\partial u/\partial t) \equiv \rho(\partial u/\partial t) + \rho u \cdot \nabla u \equiv \rho \dot{u} = \nabla \cdot \sigma \equiv \eta \nabla^2 u,$$

then the two-dimensional diffusion equation for velocity results, with the kinematic viscosity  $\nu = (\eta/\rho)$  replacing the usual diffusion coefficient:

$$\partial u_x/\partial t = (\eta/\rho)(\partial^2 u_x/\partial y^2).$$

The amplitude of the sinusoidal velocity perturbation  $\delta s(t)$  decays exponentially with time:

$$(d/dt)\delta s(t) = -(\eta/\rho)k_n^2 \delta s(t),$$

with a characteristic  $n$ -dependent decay time  $\tau_n = (\rho/\eta k_n^2) = (\rho/\eta)(L/2\pi n)^2$ .

To make the problem definite, consider room-temperature water, which has a kinematic viscosity  $\nu = (\eta/\rho)$  of about 0.02[cm<sup>2</sup>/sec]. For the maximum wavelength,  $L$ , the decay time, in seconds, is roughly  $L^2$ , where  $L$  is measured in centimeters. During the decay the walls perform extra work. The extra stress at the boundary due to the perturbation is  $\delta \sigma_{yx} = -\eta \delta s_n(t) k_n \cos(k_n y)$  corresponding to an extra work per unit wall area of

$$-\eta \delta s_n(0) k_n \cos(k_n y) \dot{\epsilon} L \tau_n = \pm \rho \delta s_n(0) \dot{\epsilon} L^2 / (2\pi n).$$

For centimeter lengths and hertz strain rates, corresponding to perturbation lifetimes of the order of seconds, the extra work is completely negligible compared to the thermal energy content of the fluid.

**Problem:**

Suppose that liquid water undergoes steady plane Couette flow in a channel 1 centimeter wide with a constant strain rate  $\dot{\epsilon}$  of 1 hertz. The boundaries of the channel are maintained at a constant temperature  $T$ . The resulting stationary temperature profile should satisfy the *steady* linearized heat-flow equation,

$$0 = (\partial T / \partial t) = D_T \nabla^2 T + (\partial T / \partial t)_{\text{Source}},$$

where the "source term"  $(\eta / \rho c_p) \dot{\epsilon}^2$  gives the rate of temperature increase due to viscous heating. The rate at which *kinetic* energy density is converted into *thermal* energy density is given by the product of the shear stress and the strain rate,  $\sigma \dot{\epsilon} = \eta \dot{\epsilon}^2$ . Dividing this power density by the heat capacity per unit volume  $\rho c_p$  gives the source term described above. For simplicity assume that the viscous heating is uniform throughout the fluid and further ignore the temperature dependence of  $D_T$ ,  $\eta$ , and  $\rho$ . Calculate the stationary temperature profile across the channel assuming that the thermal diffusivity of water,  $D_T = (\kappa / \rho c_p)$ , is  $1.23 \text{ cm}^2 / \text{sec}$ . What is the boundary heat flux required to maintain this stationary thermal state in the water?

**8.3 Poiseuille Flow**

Shear viscosity is conventionally measured by allowing fluid to flow through a vertical cylindrical tube of radius  $R$  under the influence of gravity  $g$ . Consider a fluid with shear viscosity  $\eta$  and mass density  $\rho$ , falling steadily through a cylindrical tube, driven by the gravitational acceleration  $g$ , as shown in Figure 8.2. For a sufficiently small radius  $R$  or a sufficiently large viscosity  $\eta$ , the flow is slow, so that the Navier-Stokes equations can safely be linearized. In this case the mass flux is inversely proportional to the viscosity, as we shall see. Just as in studying plane Couette flow we will ignore the small flow-induced changes in material properties, density, temperature, viscosity, and conductivity. The resulting linearized equation of motion can be applied to the viscous surface forces and the gravitational "body" (bulk) force acting on a small cylinder of fluid, coaxial with the tube, but with a smaller radius,  $r$ , and with length  $dz$ . The viscous upward force integrated over the curved surface,  $+2\pi r \eta (du_z / dr) dz$ , must exactly balance the net downward gravitational body force, integrated over the volume,  $+\pi r^2 \rho g dz = -\pi r^2 (dP / dz) dz$ . The linear differential equation which results from equating these forces can then be integrated to find the velocity profile  $u_z(r)$ , choosing the integration constant such that the velocity at  $r = R$  vanishes. The resulting velocity profile is a parabola, with maximum (downward) speed along the axis of the tube:

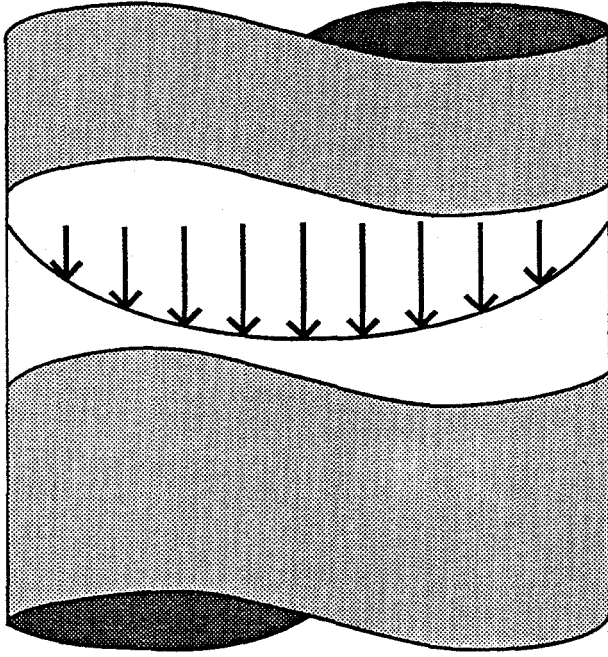


Figure 8.2. Steady gravity-driven Poiseuille flow field in a vertical cylindrical tube. The vertical velocity depends quadratically on the horizontal coordinate.

$$u_z = (g/4)[r^2 - R^2](\rho/\eta) .$$

Exactly the same profile results if the force balance on an infinitesimal cylindrical shell, of thickness  $dr$ , is analyzed. In this latter case the inner surface of the shell is accelerated downward and the outer surface upward, by viscous forces. For an infinitesimal shell the difference in the viscous forces is  $drdz(d/dr)[2\pi r\eta(du_z/dr)]$  and the integrated gravitational body force is  $2\pi r dr dz g$ . The resulting *second-order* ordinary differential equation:

$$(du_z/dr) + r(d^2u_z/dr^2) = (d/dr)[r(du_z/dr)] = r(\rho/\eta)g ,$$

can be integrated once, from 0 to  $r$ , yielding the same *first-order* differential equation as was obtained by considering the force balance on a cylinder rather than a shell:

$$(du_z/dr) = (1/2)r(\rho/\eta)g .$$

Just as in the linear analysis of plane Couette flow, linearized Poiseuille flow has to be sufficiently slow for the flow to remain laminar and with negligible heating. In practice there is no difficulty in meeting these conditions.

Given the flow profile,  $u_z(r) = (g/4)[r^2 - R^2](\rho/\eta)$ , an integration over the radius  $r$  gives the mass flow [mass/time]:

$$(g/4)\int 2\pi r dr [r^2 - R^2](\rho/\eta) = -(g/8)\pi R^4(\rho^2/\eta) ,$$

showing that the total flow of mass varies inversely with the viscosity and at a rate varying as the fourth power of the tube radius. The negative sign corresponds to downward flow.

**Problem:**

1. The flow just described should exhibit "turbulent instability" (described in Section 8.6) near a "Reynolds number" of 2000, where the (dimensionless) Reynolds number is the product of the tube radius and average speed, divided by the kinematic viscosity. Estimate the radius of a tube providing this Reynolds number for water in the earth's gravitational field.

**8.4 Stokes' Flow Past a Sphere or Disk**

If a sphere falls sufficiently slowly through a viscous fluid intuition suggests that the resistance should vary as the exposed area times the viscous stress (which varies as the velocity divided by the diameter of the moving body) and must balance the gravitational force. Thus, for a slowly falling sphere, the flow should vary linearly in the viscosity, velocity, and radius. This rough analysis is in fact correct for sufficiently slow motion, but fails when the flow is rapid, when many varieties of wild instabilities result.

The detailed analysis of the low-speed resistance, leading to a retarding force on a falling sphere proportional to the radius, shear viscosity, and velocity, can be found in Chapter XI of Lamb's Hydrodynamics. For a sphere of radius  $R$ , falling downward with speed  $V$ , the radial flow velocity  $v_r(r, \theta)$  of the surrounding fluid a distance  $r$  away from the center of the sphere is:

$$v_r = V \cos(\theta)(3r^2R - R^3)/2r^3,$$

where  $\theta$  is measured relative to the direction of motion. Notice that fluid just in front of the sphere moves radially with the radial velocity  $V$  while fluid at the rear of the sphere, moves radially with the radial velocity  $-V$ . Both of these locations as well as any other on the surface of the sphere have exactly the same Cartesian velocity,  $V$  in the direction of the accelerating field. The angular ( $\theta$ ) velocity  $v_\theta$  of fluid motion in the  $xy$  plane (setting  $z$  equal to zero) for this same problem is

$$v_\theta = V \sin(\theta)(R^3 - 5r^2R)/4r^3.$$

Thus the fluid velocity matches the sphere velocity at all points on the surface of the sphere. The flow field around the sphere is indicated in Figure 8.3. From the flow field the force exerted by the fluid on the sphere can be calculated:

$$F = -6\pi\eta RV.$$

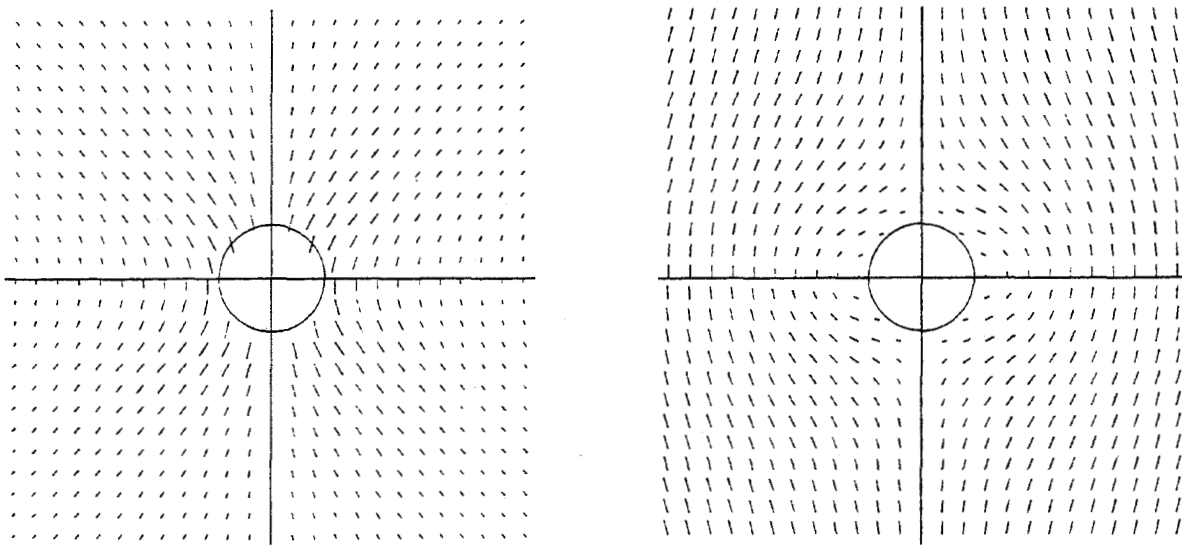


**Figure 8.3.** Steady “Stokes’ Flow” about a slowly-moving sphere immersed in a viscous fluid. At the left the laboratory-frame velocities are indicated by lines. At the right the flow of the fluid *relative* to the sphere is indicated. For clarity the horizontal component of the flow velocity has been increased by a factor of ten in this Figure.

If instead the fluid were allowed to “slip” around the sphere, so that the tangential velocity were not forced to match the sphere velocity on the surface, the resistance would be reduced to two thirds this value.

Apart from the numerical multiplier,  $6\pi$ , the “Stokes’ Drag” formula just given follows easily from dimensional analysis: if we consider the units of sphere radius  $R[L]$ , fluid viscosity  $\eta[M/LT]$ , and sphere velocity  $v[L/T]$ , it is apparent that a *force*, with units  $[ML/T^2]$  and depending only upon powers of these three physical quantities can result, if, and only if, each contributing factor is linear. We could just as easily apply the same reasoning in two dimensions, considering the fall of a planar disk through a viscous two-dimensional fluid. Only the units of viscosity are different. In two dimensions the units of viscosity are  $[M/T]$ . In two dimensions both the intuitive argument and dimensional analysis lead to the same result, that the frictional force on a falling disk is independent of the size of the disk. This paradoxical result, “Stokes’ Paradox,” can be understood by using the Navier-Stokes equations to analyze the way in which the boundary influences the two-dimensional flow. Experiments, carried out by timing the fall of horizontal wires in water, agree with the relatively-complicated analysis. Both approaches show that the resistance depends *logarithmically* on the distance to the boundary. Even in the simpler three-dimensional case the simple laminar flow around a moving sphere has also a paradoxical characteristic. The kinetic energy associated with the flow, the volume integral of  $(\rho/2)v^2$ , *diverges*.

At sufficiently high speeds the analysis can fail in three dimensions too when the retarding force proportional to the mass of fluid being disturbed must be included. To see this consider a 100 kilogram skydiver falling steadily through the earth’s

atmosphere. The gravitational force of 1000 newtons must be balanced by the atmospheric drag force. The viscous force exerted by the atmosphere is of order area  $\times$  velocity gradient  $\times$  viscosity, or, for air, 1 square meter  $\times$  (velocity/meter)  $\times$  0.001(kilogram/metersecond) , requiring a nearly-relativistic velocity of  $10^6$  meters/second to balance the gravitational force. But the terminal velocity for a man is actually *four orders of magnitude* smaller. The correct order of magnitude results if we take into account an additional energy-loss mechanism, quadratic rather than linear, noting that the falling body leaves behind a wake of meter-size vortices rotating at the body's velocity. The flow is unstable and turbulent.

**Problem:**

Carry out the estimate suggested above for the terminal velocity.

**8.5 More-General Analytic Solutions**

Consider a small-amplitude velocity flow field  $u(r,t)$  with the magnitude of  $u$  sufficiently small that quadratic terms in the equation of motion can be ignored:

$$\rho(\partial u/\partial t) \cong \rho(\partial u/\partial t) + \rho u \cdot \nabla u \cong \rho \dot{u} = \nabla \cdot \sigma \cong \eta \nabla^2 u .$$

In such a case any initial-value velocity field can be propagated forward in time using the *linearized* equation of motion for a viscous fluid:

$$(\partial u/\partial t) = (\eta/\rho) \nabla^2 u .$$

The linearized equation does not distinguish between Eulerian and Lagrangian derivatives. It is equivalent to a diffusion equation for velocity:

$$(\partial u/\partial t) = (\eta/\rho) \nabla^2 u .$$

Except at boundaries, where additional conditions may need to be imposed, any two solutions of such a linear equation can be superposed so that the progress of any initial condition, represented as a sum of orthogonal functions, continues to be represented by the sum as these functions are propagated forward in time. If the initial velocity distribution is represented by a Fourier series then the coefficient of  $\exp(ik \cdot r)$ ,  $A_k(t)$ , decays exponentially to zero with a characteristic time of  $\tau_k = (\rho/\eta k^2)$ .

Another useful analytic method is to represent the initial condition as a set of delta functions. These decay as Gaussian functions, with halfwidths increasing as the square root of the elapsed time:

$$u(x,t) = \delta u [4\pi t(\eta/\rho)]^{-1/2} \exp[-x^2/(4t\eta/\rho)] .$$

Both the Fourier and Gaussian solutions are irreversible and can only be propagated *forward* in time. The Gaussian function is obviously singular at the time origin, while the Fourier coefficient appears not to be. But notice that the exponential *growth* rate (as opposed to decay) of either an inverted Fourier series, or a series of delta functions, is limited only by the number of significant figures kept.

The solution of any small-amplitude problem in fluid dynamics corresponds to a related problem in elasticity theory because the underlying linearized equation of motion is the same:

$$\rho(\partial u/\partial t) \equiv \rho \dot{u} = \nabla \cdot \sigma ; \sigma = \lambda(\nabla \cdot u)I + \eta(\nabla u + \nabla u^t) .$$

For instance the Stokes-flow velocity field around a sphere of radius  $R$ , moving with a *velocity*  $u$  through a viscous "incompressible fluid" [meaning that  $\lambda + (2/3)\eta$  is infinite for the fluid] is identical to the corresponding elastic displacement field in an elastic continuum. In the corresponding elastic problem a rigid spherical inclusion of radius  $R$  is displaced by a *distance*  $u$ . The shear modulus of the elastic continuum  $\eta$  must have the same numerical value as does the shear viscosity of the corresponding fluid and the elastic bulk modulus,  $\lambda + (2/3)\eta$  in three dimensions, must be large enough to correspond to the motion of an incompressible fluid. We discuss this correspondence between elastic and viscous solutions of flow problems in Section 8.8, Numerical Methods.

## 8.6 Turbulence

Turbulence is a macroscopic manifestation of the chaos lurking in most nonlinear problems. The details depend upon the boundary conditions and cover a range of length scales from the minimum "Kolmogorov" length of about 1 millimeter, up to the size of the object in question, whether it is a submarine, jet airplane, continent, or galaxy. Numerical simulation will continue to make real contributions to turbulent problems for the foreseeable future because most such problems lie beyond the capability of any conceivable future computing machine.

What is turbulence? It is a complex fluctuating flow resulting when the Lyapunov instability of the hydrodynamic equations generates information more rapidly than it can be dissipated by viscosity, making the flow field unpredictable, except in a statistical sense.

When does turbulence occur? We can estimate this by comparing two significant times for a typical Lagrangian volume element, the time  $\tau_{\text{Shear}}$  required for it to change shape, and the time  $\tau_{\text{Decay}}$  in which viscosity can dissipate the velocity gradients causing the shape to change. If the decay time is too slow we can expect that the fluid will progress in a turbulent fashion. Let us estimate the two times for the deforming cube of sidelength  $L$  shown in Figure 8.4, with a velocity difference  $v$  between the top and the bottom surfaces:

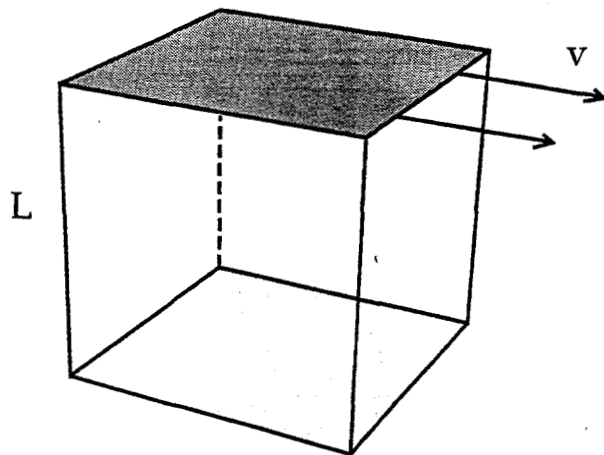


Figure 8.4. Deforming cube. The corresponding Reynolds Number is  $Lv/\nu$ , where  $\nu$  is the "kinematic viscosity,"  $\eta/\rho$ .

$$\tau_{\text{Shear}} = L/\nu ; \tau_{\text{Decay}} = L^2/(\eta/\rho).$$

Thus we expect the flow to be regular or chaotic depending on the (dimensionless) ratio of these times, called the *Reynolds Number*,  $Re$ :

$$Re = [L^2/(\eta/\rho)]/[L/\nu] = Lv/(\eta/\rho) = Lv/\nu ,$$

where  $\nu$  is the conventional symbol for the kinematic viscosity,  $\nu = (\eta/\rho)$ . The Reynolds number is a useful criterion for similarity in flows. For Reynolds numbers less than 1000 or so the flow is typically laminar. For larger Reynolds numbers the flow becomes turbulent. Why 1000 rather than one? The straightforward approach to this question is to Fourier-analyze the Navier-Stokes equations for a particular flow, such as the Poiseuille flow experiment described in Section 3. If this is done results agreeing with experiment for the instability threshold can be obtained. An oversimplified estimate can be based on the observation that the characteristic decay time for the linear problem involves a dimensionless factor of  $(2\pi)^2$ , about 40. The nonlinear instability can be characterized by the square of this same factor.

**Problem:**

Estimate the minimum length scale at which turbulent flow can occur, the "Kolmogorov length," for the atmosphere and for the ocean by finding the minimum length for which motion at the sound velocity can lead to a Reynolds number of 2000.

The transition from orderly laminar motion to chaos can be (and has been) followed in excruciating detail for sufficiently simple boundary conditions. In the next Section we discuss a simple prototypical problem, now nearly 100 years old, but still the subject of intensive investigations and still regularly yielding surprising results.

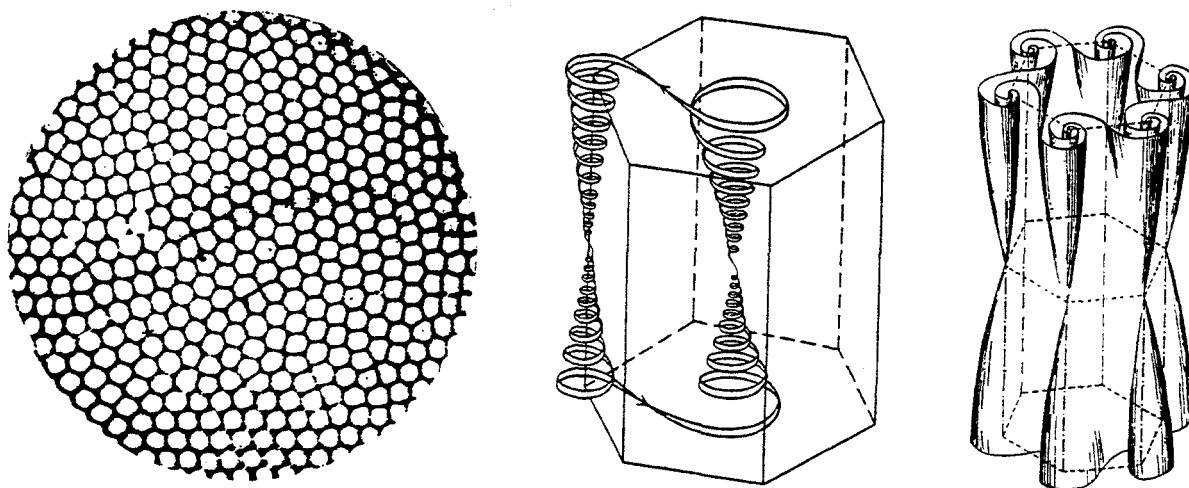


**Figure 8.5.** Top view (left) of Bénard's convection cells. The circulation within these cells and the deformation of a typical cell are indicated in the other two views. All three views are taken from Subrahmanyan Chandrasekhar's classic treatise, Hydrodynamic and Hydromagnetic Stability.

### 8.7 Rayleigh-Bénard Problem

The Rayleigh-Bénard problem originated in the study of the regular convection cell structures seen in fluid layers heated from below. A regular pattern of *hexagonal* convection cells is shown in Figure 8.5. In each hexagonal columnar cell hot fluid rises in the center and cooler fluid falls at the perimeter of the cell. Individual particle trajectories are indicated in the Figure. If the convecting layer is relatively shallow a simpler cylindrical flow can be observed. In the latter case neighboring rolls rotate in opposite directions and generally transport energy upward.

In both cases there is no overall mass transport. The upward and downward mass currents balance. But irreversible Fourier heat conduction, on the other hand, insures that the rising hot fluid transfers heat to the upper boundary while the falling cooler fluid picks up heat from the lower boundary. Thus the direction of heat transfer is the same for clockwise or counterclockwise roll motions. Neighboring cylindrical rolls rotate in opposite directions as they transport energy upward. Both the roll motion and the hexagonal circulation cells are driven by gravitationally-induced buoyant forces and are retarded by viscous forces, allowing steady states to develop. These flow patterns are among the simplest examples of nonequilibrium steady states, driven by boundary sources and sinks of heat. Such a problem depends upon the thermal expansion, heat capacity, heat conductivity, and shear viscosity of the conducting fluid. We will consider here a qualitative treatment of this problem and point out the connection, established by Lorenz, with chaotic mechanics.

To begin, we consider heat flow through a fluid layer of thickness  $L$ , heat conductivity  $\kappa$ , and shear viscosity  $\eta$  heated from below in the presence of a gravitational field  $g$ . If the temperature difference  $\Delta T$  driving the flow of heat is

sufficiently small then the fluid is *static* with velocity zero everywhere, and the rate at which energy travels from bottom to top is given by Fourier's Law:

$$(\text{Power/Area})_{\text{Static}} = \kappa \Delta T / L.$$

A potential competing mechanism for energy transfer is the *dynamic* rotation of convective rolls with a characteristic speed  $v$ , and a corresponding heat transfer time  $L/v$ . The rate at which such dynamic rolls transfer thermal energy depends upon the heat capacity per unit volume  $\rho c$ :

$$(\text{Power/Area})_{\text{Dynamic}} = \rho c \Delta T v.$$

Because the dynamic roll mechanism is damped by viscosity the rolls are dormant for small temperature differences. In the absence of a large temperature difference the viscous force per unit area retarding the roll motion:

$$F_{\text{Drag}}/\text{Area} = \eta(v/L),$$

exceeds the buoyant driving force of thermal expansion:

$$F_{\text{Lift}}/\text{Area} = (\partial\rho/\partial T)\Delta T g L.$$

But for large temperature differences the forces can balance. When they do, the dynamic roll velocity can be estimated by equating the magnitudes of the two forces:

$$v = (\partial\rho/\partial T)\Delta T g L^2 / \eta.$$

The resulting transition from conduction to convection has been exhaustively studied because it can be understood in part through Fourier analysis of the flow field. Further transitions, for greater temperature differences  $\Delta T$ , can be understood to a lesser extent. Quantitative agreement would require the rigid boundary walls and finite roll lengths of laboratory experiments rather than the periodic boundaries favored by numerical analysts. The observed fact that the roll patterns can change on a time scale of days is clear evidence that even apparently simple hydrodynamic problems can lie far beyond the possibility of comprehensive numerical simulation.

The "Rayleigh number"  $Ra$  is a dimensionless ratio describing the deviation of the Rayleigh-Bénard system from equilibrium. The Rayleigh number is just the ratio of our estimates for the two competing heat fluxes, using the roll velocity estimated from force balance:

$$Ra = \text{Power}_{\text{Dynamic}}/\text{Power}_{\text{Static}} = \rho c \Delta T v / (\kappa \Delta T / L) = \rho c v L / \kappa =$$

$$Ra = [\rho c L / \kappa][(\partial \rho / \partial T) \Delta T g L^2 / \eta] = [(\partial \rho / \partial T) \Delta T g \rho c L^3 / (\kappa \eta)].$$

Provided that the Rayleigh number is sufficiently small the problem is a simple one with a linear temperature profile and with heat being transmitted from bottom to top by conduction. If the temperature difference becomes large enough a more efficient mode of energy transport is the formation of turbulent rolls or convection cells.

To describe the motion of a fluid heated from below in the presence of a gravitational field from the standpoint of computational physics is difficult because the time scale of the changing patterns can be days of real time. But the Rayleigh-Bénard problem is of interest in demonstrating that the chaos which pervades atomistic equations of motion is present on the continuum level too.

A truncated Fourier analysis of this problem leads to three simultaneous equations, written down by Lorenz in 1963 and historically responsible for much of the current interest in chaos. The three equations describe the time evolution of the clockwise rotation rate of the rolls,  $x$ , and the horizontal and vertical heat transfer rates,  $y$  and  $z$ :

$$\dot{x} = -\sigma(x - y); \dot{y} = Ra x - y - xz; \dot{z} = xy - bz.$$

The parameters  $\sigma$ ,  $Ra$ , and  $b$  correspond to the Prandtl number  $\eta c_p / \kappa$ , the Rayleigh number, and a geometric variable describing the aspect ratio of the flow. A longtime trajectory in  $xyz$  space using the most popular combination of the three parameters  $\{\sigma = 10, Ra = 28, b = 8/3\}$  leads to the familiar chaotic attractor shown in Figure 8.6.

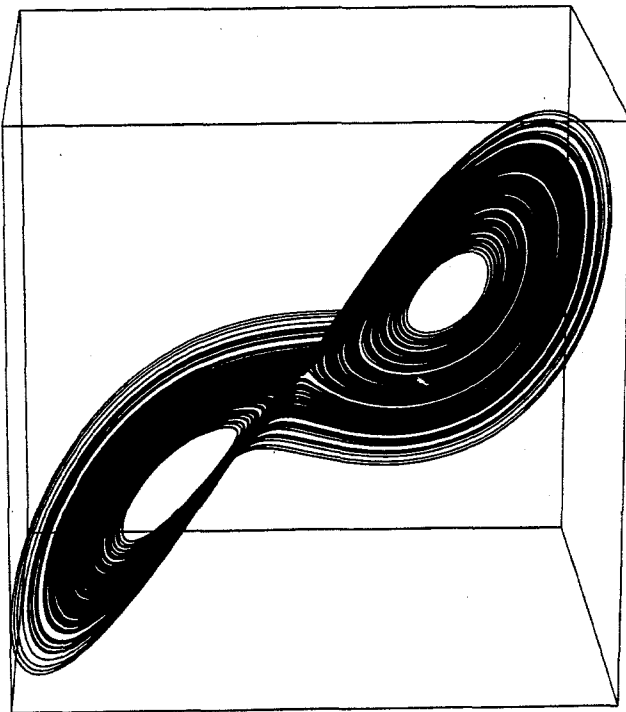


**Figure 8.6.** The "Lorenz attractor," for  $\{\sigma = 10, Ra = 28, b = 8/3\}$  has a dimensionality slightly greater than 2. The Figure was generated using the initial conditions  $\{x, y, z\} = \{-7, -11, +17\}$ .

This attractor is *almost* a two-dimensional object. In fact it is an example of a "fractal object," with "information dimension" of approximately 2.06. We will define the concepts of fractal objects and their fractal dimensionality in our study of nonequilibrium dynamics in Chapters 10 and 11.

### 8.8 Numerical Methods

Since the early days of computers the literature describing research in computational fluid dynamics has grown continuously more complex while the governing equations have remained remarkably simple in structure. Some of the many people working in this field, competing for limited resources, have found it useful to stress the new and abstruse to a degree seldom matched outside the medical and legal professions. As a result, much of the accumulated knowledge in the field is inaccessible to outsiders. For this reason it is plausible that in the upcoming post-teraflop age the automation of a few relatively simple but computationally-intensive methods may occasionally prevail over the proliferating more-efficient but less-accessible algorithms designed for special problems. In choosing to pursue simple approaches to complex phenomena we outline elementary methods for solving idealized two-dimensional problems in elasticity and fluid flow in this Section.

To begin we consider two-dimensional isotropic problems in linearly-elastic deformation. In this case the linearized (in displacement) equation of motion and the linear (in strain) stress tensor have the form:

$$\rho(\partial u/\partial t) = \nabla \cdot \sigma; \sigma = \lambda \nabla \cdot u \mathbf{I} + \eta(\nabla u + \nabla u^t) .$$

where  $u$  stands for elastic displacement and the constitutive properties  $\lambda$  and  $\eta$  are Lamé's elastic constants. For simplicity we will restrict our examples to stationary solutions for which the time derivatives all vanish.

In the elastic case we wish to minimize the total (integrated) potential energy  $\Phi$ , a quadratic form in the displacements:

$$\Phi = \iint [(\lambda/2)(\nabla \cdot u)^2 + (\eta/4)(\nabla u + \nabla u^t) : (\nabla u + \nabla u^t)] dr ,$$

where the double dot notation indicates a sum over all the  $D^2 = 4$  products of corresponding  $ij$  elements:  $A:B = \sum A_{ij}B_{ij}$ . Let us illustrate how this form for the elastic energy arises by working out the two-dimensional case in detail. In an isotropic compression, with  $\Delta V/V = \epsilon_{xx} + \epsilon_{yy} = 2\epsilon$ , the hydrostatic elastic stresses  $\sigma_{xx}$  and  $\sigma_{yy}$  are equal and the elastic energy of compression is proportional to the bulk modulus,  $B = (\lambda + \eta)$  in two dimensions:

$$\sigma_{xx} = \lambda(\nabla \cdot \mathbf{u}) + 2\eta\epsilon_{xx} = (\lambda + \eta)(2\epsilon) = \lambda(\nabla \cdot \mathbf{u}) + 2\eta\epsilon_{yy} = \sigma_{yy}; \Delta\Phi/V = (1/2)(\lambda + \eta)(\nabla \cdot \mathbf{u})^2.$$

In the *simple shear* of an isotropic medium the energy density,  $(1/2)\eta\epsilon^2$  for  $du_x/dy = \epsilon$ , must be independent of the direction of the coordinate axes. A counterclockwise coordinate rotation through an angle  $\theta$ , with  $(x', y') = (x\cos\theta + y\sin\theta, -x\sin\theta + y\cos\theta)$  shows that the simple  $(x, y)$  shear deformation is equivalent to the set of deformations  $\{\epsilon_{xx} = -\epsilon_{yy} = \epsilon\sin\theta\cos\theta; \epsilon_{xy} = \epsilon(\cos^2\theta - \sin^2\theta)\}$ . The corresponding deformation energy turns out to be, as it must, independent of  $\theta$ :

$$\begin{aligned} \Delta\Phi/V &= (\eta/2)[(\epsilon_{xx} - \epsilon_{yy})^2 + \epsilon_{xy}^2] = (\eta\epsilon^2/2)[4(\sin\theta\cos\theta)^2 + (\cos^2\theta - \sin^2\theta)^2] \\ &= (\eta\epsilon^2/2)(\cos^2\theta + \sin^2\theta)^2 = (\eta\epsilon^2/2). \end{aligned}$$

In the corresponding viscous case, where  $u$  is the *stream velocity*, we would minimize instead the volume-integrated rate of viscous dissipation. The two solutions, elastic and viscous, would be identical provided that we could choose elastic coefficients with  $\eta \ll \lambda$  corresponding to incompressible flow.

We can obtain numerical solutions of such elastic problems by using either Lagrangian or Eulerian coordinates. In the Lagrangian case we could begin by spanning the domain of the problem with a simple triangular lattice, as shown in Figure 8.7, with nearest-neighbor points of mass  $m$  joined by Hooke's-Law springs of rest length  $d$  and force constant  $\kappa$ . For illustrative purposes we can imagine a regular lattice of identical triangles, but, as the example problem in the Figure indicates, this restriction is by no means necessary.

A calculation of the energy required for a small shear or compression of a regular triangular lattice shows that the corresponding Lamé constants  $\eta$  and  $\lambda$  are simply related to the Hooke's-Law force constant  $\kappa$ :

$$\eta = \lambda = 3^{1/2}\kappa/4.$$

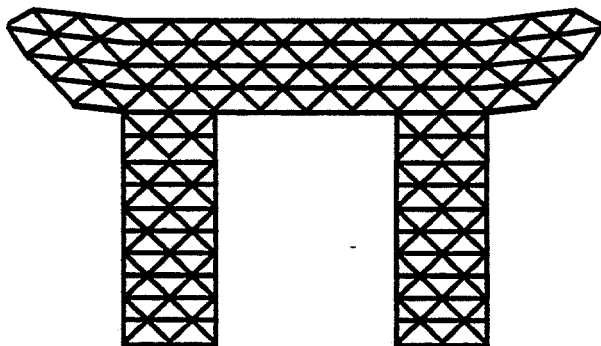


Figure 8.7. Representation of an elastic body as a set of contiguous "finite-element" Lagrangian zones.

**Problem:**

Consider the following three sets of small homogeneous deformations of a regular triangular lattice in which nearest-neighbor particles interact with a Hooke's-Law potential,  $\phi(r) = (\kappa/2)\delta r^2$ , and the rest length of the springs is  $d$ .

1. Uniform expansion:  $\epsilon_{xx} = +\epsilon$ ;  $\epsilon_{yy} = +\epsilon$ .
2. Uniform shear:  $\epsilon_{xy} = [(du_x/dy) + (du_y/dx)] = +\epsilon$ .
3. Uniform shear:  $\epsilon_{xx} = +\epsilon/2$ ;  $\epsilon_{yy} = -\epsilon/2$ .

Show that the bulk modulus,  $\lambda + \eta$ , from Case 1 and the shear modulus  $\eta$  from Case 2 imply that  $\eta = \lambda = 3^{1/2}\kappa/4$ . Show that Case 3 can also be described by exactly the same shear modulus  $\eta$  as was Case 2, establishing the fact that the triangular lattice is elastically isotropic for small displacements.

The triangular lattice with central forces implies a definite relation between the two Lamé constants,  $\eta = \lambda$ . To treat the general case the energy needs to be written as a sum of dilatational and shear contributions. This can be done without difficulty. If we consider a dilatational potential responding only to the dilation of each triangle:

$$\Phi_{\text{Volume}} = \Sigma(\alpha/2A_0)(A - A_0)^2,$$

the corresponding elastic constant resisting shear is zero and the corresponding contribution to the bulk modulus  $\lambda + \eta$  is proportional to  $\alpha$ . In carrying the calculations out it is convenient to write the area of a triangle  $A$  in terms of the three sidelengths,  $\{r,s,t\}$ :

$$A = (1/4)[2r^2s^2 + 2r^2t^2 + 2s^2t^2 - r^4 - s^4 - t^4]^{1/2}.$$

If we likewise consider a shear potential  $\Phi_{\text{Shear}}$  responding quadratically only to the *shear* of initially-identical equilateral triangles, with sidelengths  $r$ ,  $s$ , and  $t$  in a deformed state:

$$\Phi_{\text{Shear}} = \Sigma(\beta/2)[(r - s)^2 + (s - t)^2 + (t - r)^2],$$

the corresponding contribution to the bulk modulus  $B$  vanishes and the shear modulus  $G$  is proportional to  $\beta$ . Thus, by using a combination of the volume and shear potentials we can choose the force constants  $\alpha$  and  $\beta$  to match any desired ratio of the moduli,  $B/G = (\lambda + \eta)/\eta = (\lambda/\eta) + 1 \propto (\alpha/\beta)$ .

As computer hardware costs continue to decline relative to software costs simple algorithms will be more widely adopted. Figure 8.8 shows "SPRINT," a present day computer providing the high speed performance and reliability of a CRAY computer at 1/1000 the cost. The SPRINT computer, built by Tony De Groot as a Ph. D. thesis project in the University of California's Department of Applied Science at Livermore, contains

**Figure 8.8.** Tony De Groot and the SPRINT computer, built as a Ph. D. dissertation project in the Department of Applied Science, University of California at Davis/Livermore. In simulating the motion of more than one million atoms this machine outperforms the CRAY "supercomputers" at a fraction of the cost.

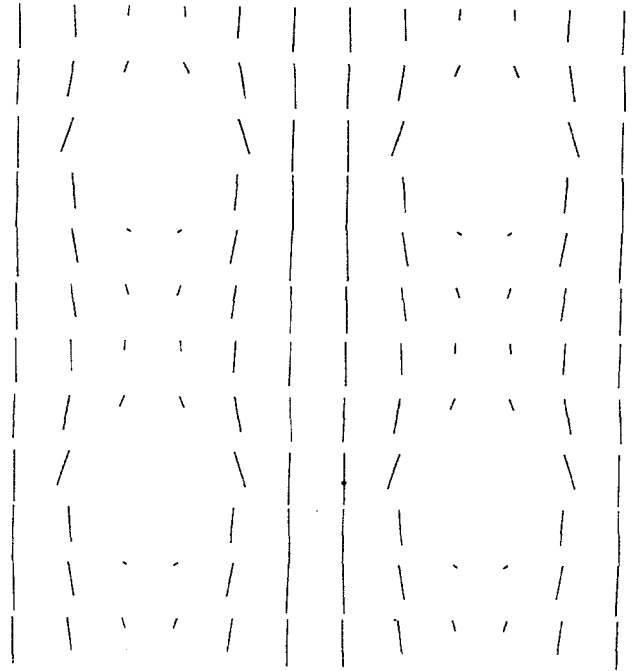


64 one-megabyte processors. There is no technological barrier to building a thousand-fold larger version of this same machine. The growing availability and increasing power of such low-cost parallel computers suggests that in the future relatively simple approaches to numerical solutions may prove generally more cost-effective than cumbersome specialized schemes designed primarily to reduce problem size with an increased time step.

A simple two-dimensional Eulerian finite-difference scheme can be based on a regular or irregular quadratic or triangular grid in which the space derivatives are evaluated by finite-difference approximations while the time derivatives are accurately integrated using a Runge-Kutta technique. At Keio University Makoto Kubota and Toshio Kawai have followed this approach, developing an automatic language *Distran* ("Translator for Distributed Systems") for the description of hydrodynamic problems specially for parallel processors. Let us formulate and solve a very simple such problem to illustrate some of the steps involved.

Our sample problem is shown in Figure 8.9. It represents the top-to-bottom steady flow of a fluid, driven by gravity through a regular periodic array of square obstructions. The "unit cell" for this problem is spanned by 36 equally-spaced points joined at the edges with the usual periodic boundaries. The hydrodynamic equations for this problem need to be written in Eulerian space-fixed coordinates rather than in Lagrangian material-fixed coordinates. Thus the two-dimensional continuity equation and equation of motion,  $d\rho/dt = -\nabla \cdot \mathbf{u}$ ;  $\rho \dot{\mathbf{u}} = -\nabla \cdot \mathbf{P}$ , can be used to calculate the time

**Figure 8.9.** Downward flow, driven by gravity, around a periodic array of square obstacles using periodic boundary conditions. The 36-node solution described in the text has been repeated four times and is shown in four periodic cells, covering 144 nodes in all. The obstacles span 4 nodes in each 36-node portion of the solution.



evolution of the equilibrium pressure  $P_{eq}(\rho)$  and velocity  $\mathbf{u} = (u, v)$  at fixed locations in space:

$$(\partial P_{eq}/\partial t) = (\partial P_{eq}/\partial \rho)_S (\partial \rho / \partial t) = -c^2 \nabla \cdot (\rho \mathbf{u}) \cong -c^2 \rho \nabla \cdot \mathbf{u} ;$$

$$(\partial \mathbf{u} / \partial t) = -u(\partial u / \partial x) - v(\partial u / \partial y) - (1/\rho)[(\partial P_{xx} / \partial x) + (\partial P_{yx} / \partial y)]$$

$$= -u(\partial u / \partial x) - v(\partial u / \partial y) - (1/\rho)(\partial P_{eq} / \partial x) + (\eta/\rho) \nabla^2 \mathbf{u} .$$

To simplify the calculation of the pressure derivative,  $(\partial P_{eq} / \partial t)$ , we have ignored the density gradient  $\nabla \rho$ . For relatively gentle flows this is a reasonable approximation, because the density is nearly constant and  $\mathbf{u} \cdot \nabla \rho$  is of second order in the volume strain while  $\rho \nabla \cdot \mathbf{u}$  is first order. We also have ignored the *bulk-viscosity* contribution to  $(\partial \mathbf{u} / \partial t)$ :  $-(\eta + \lambda)(\nabla \cdot \mathbf{u}) / \rho$ . In a flow where shear predominates over compression this too is a reasonable approximation.

The equation of motion in the *vertical* direction follows from the horizontal example by symmetry, except that the vertical gravitational acceleration  $-g$  must be added:

$$(\partial v / \partial t) = -g - u(\partial v / \partial x) - v(\partial v / \partial y) - (1/\rho)(\partial P_{eq} / \partial y) + (\eta/\rho) \nabla^2 v .$$

The unknowns describing the problem are just three in number at each Eulerian grid point, one each for the equilibrium pressure and the two components of velocity. The steady-state solution shown in the Figure 8.9 was achieved in 400 fourth-order Runge-Kutta time steps of 0.35, starting with the fluid at rest. The calculation is unstable with a time step of 0.40. Let us describe the solution of this problem based on the general

approach outlined in Chapter 7, but omitting heat flow, and the explicit calculation of the stresses:

1a. Description of the constitutive properties.

For convenience we choose the sound speed and the kinematic viscosity both equal to unity. The mechanical equation of state is taken to be isentropic, without any explicit dependence on energy.

1b. Specify the initial conditions.

The horizontal and vertical grid spacings are taken equal to unity. The initial velocity and pressure are zero everywhere. The gravitational field strength is arbitrarily chosen equal to 1.0 in this example problem.

1c. Describe the boundary conditions.

The velocity at the four central grid points is a fixed boundary condition and remains zero for all time. Periodic boundaries are applied in both the horizontal and the vertical directions.

2. Calculate the time derivative of the local-equilibrium pressure from the velocities.

The time-rate-of-change in the equilibrium pressure at each point, *including those points where the velocity vanishes*,  $(\partial P_{eq}/\partial t) = -c^2\rho\nabla\cdot\mathbf{u}$ , is calculated from the divergence of the velocity field,  $\nabla\cdot\mathbf{u} \equiv (1/2)[u_{+0} - u_{-0} + v_{0+} - v_{0-}]$ . In locating the four nearest neighbors indicated by the subscripts the periodic boundary conditions are used for all edge sites.

3. Calculate the time derivative of the velocity from the pressure-tensor gradient.

$(\partial u/\partial t)$  and  $(\partial v/\partial t)$  require only  $\nabla^2 u$  and  $\nabla^2 v$  in addition to the velocity and equilibrium pressure gradients.  $\nabla^2 u$ , for instance, is evaluated from the finite-difference approximation:

$$\nabla^2 u \equiv [u_{+0} + u_{-0} + u_{0+} + u_{0-} - 4u_{00}].$$

Just as before, the neighbors contributing to the derivatives for edge sites are located by using the periodic boundaries.

4. Advance the pressure and velocity components in time.

For the time integration the fourth-order Runge-Kutta method described in Section 6 of Chapter 1 with  $dt = 0.35$  is a good choice.

5. Unless the calculation is complete, GO TO 2.

The calculation converges quickly to the steady solution shown in the Figure.  
The subroutine "RHS (YNEW, YDOT)" used has the following form:

```

SUBROUTINE RHS (YNEW, YDOT)
DIMENSION YNEW (36), YDOT (36)
DIMENSION U (6, 6), V (6, 6), P (6, 6), UDOT (6, 6), VDOT (6, 6), PDOT (6, 6)

G = 1.0

INDEX = 0
DO 10 I = 1, 6
DO 10 J = 1, 6
INDEX = INDEX + 1
U (I, J) = YNEW (INDEX)
V (I, J) = YNEW (INDEX + 36)
P (I, J) = YNEW (INDEX + 72)
10 CONTINUE

DO 20 I = 1, 6
DO 20 J = 1, 6
IP = I + 1
IM = I - 1
JP = J + 1
JM = J - 1
IF (IP.EQ.7) IP = 1
IF (IM.EQ.0) IM = 6
IF (JP.EQ.7) JP = 1
IF (JM.EQ.0) JM = 6
UDOT (I, J) = U (IP, J) + U (IM, J) + U (I, JP) + U (I, JM) - 4.0 * U (I, J)
VDOT (I, J) = V (IP, J) + V (IM, J) + V (I, JP) + V (I, JM) - 4.0 * V (I, J)
UDOT (I, J) = UDOT (I, J) - 0.5 * (P (IP, J) - P (IM, J))
VDOT (I, J) = VDOT (I, J) - 0.5 * (P (I, JP) - P (I, JM)) - G
UDOT (I, J) = UDOT (I, J) - 0.5 * U (I, J) * (U (IP, J) - U (IM, J))
UDOT (I, J) = UDOT (I, J) - 0.5 * V (I, J) * (U (I, JP) - U (I, JM))
VDOT (I, J) = VDOT (I, J) - 0.5 * U (I, J) * (V (IP, J) - V (IM, J))
VDOT (I, J) = VDOT (I, J) - 0.5 * V (I, J) * (V (I, JP) - V (I, JM))
PDOT (I, J) = -0.5 * (U (IP, J) - U (IM, J) + V (I, JP) - V (I, JM))
20 CONTINUE

DO 30 I = 3, 4
DO 30 J = 3, 4
UDOT (I, J) = 0.0
VDOT (I, J) = 0.0
30 CONTINUE

INDEX = 0
DO 40 I = 1, 6
DO 40 J = 1, 6
INDEX = INDEX + 1
YDOT (INDEX) = UDOT (I, J)
YDOT (INDEX + 36) = VDOT (I, J)
YDOT (INDEX + 72) = PDOT (I, J)
40 CONTINUE

RETURN
END

```

In real applications the time step used in such a hydrodynamic simulation needs to satisfy two stability criteria. The time step  $dt$  must be sufficiently small that information travels no farther than one mesh point per time step. For information travelling at the sound speed this gives the "Courant condition":

$$dt < dx/c,$$

where  $dx$  is the spacing of the computational mesh and  $c$  is the speed of sound. The equivalent restriction for the diffusive flow of momentum, through the kinematic viscosity  $\nu$ , is

$$dt < (dx)^2/2\nu.$$

Other things being equal, this suggests that numerical convergence will be most efficient when both restrictions are equally effective, with  $dx = 2\nu/c$ . Except in studying boundary phenomena or shockwaves such a mesh size is unphysically small, of the order of the mean free path. In practical applications the viscosity can be made artificially large, or the sound speed artificially small, in order to enhance convergence.

### Problems:

1. Reproduce the velocity field shown in the Figure for the  $6 \times 6$  36-site periodic flow described in the text.
2. Enlarge the calculation described in the text to a  $32 \times 32$  1024-site square with a zero velocity obstacle occupying the central  $16 \times 16$  square of 256 sites. Use an offset form of periodic boundaries identifying the lattice of periodic points at  $\{(24 \pm 8)m, 32n\}$ , using the plus sign for  $n$  even and the minus sign for  $n$  odd. Solve for the motion with field strengths of 0.1, 0.2, 0.3, and 0.4. You should find a stationary solution, a stable fluctuating solution, and an unstable solution.
3. Consider the propagation of a sound wave in a one-dimensional Hooke's-Law chain. The displacement of the particle located at  $x$  in the unstrained chain is:

$$\delta x = \Delta \cos[kx - \omega t]; \quad \omega = 2(\kappa/m)^{1/2} \sin(kd/2); \quad k = (2\pi/\lambda).$$

Use the gradient of the strain,  $\epsilon = (\partial \delta x / \partial x)$ , to show that the difference between the Eulerian and Lagrangian strain rates,  $-\partial \ln \rho / \partial t$  and  $-d \ln \rho / dt$ , is of order  $(\Delta/\lambda)^2$ .

4. Consider a one-dimensional system satisfying the finite-difference version of the diffusion equation,

$$\partial \rho / \partial t \equiv [\rho_0(t + dt) - \rho_0(t)] / dt = [D / (dx)^2] [\rho_+ - 2\rho_0 + \rho_-] \equiv D \nabla^2 \rho,$$

and determine the maximum time step  $dt$  for which an initial condition with spatially alternating positive and negative values of the density perturbation  $\pm\delta\rho$  decays.

5. Consider a one-dimensional system satisfying a finite-difference version of the wave equation,  $\partial^2\rho/\partial t^2 = c^2\nabla^2\rho$ , and determine the maximum time step  $dt$  for which an initial condition with spatially alternating positive and negative values of the density perturbation  $\pm\delta\rho$  continues to propagate.

### 8.9 Summary and References

The stable field-induced velocities found in stationary hydrodynamic flows, including Couette flow, Poiseuille flow, and Stokes flow, can be used to measure viscosity. For such slow flows the distinction between Eulerian and Lagrangian derivatives can be ignored and a Fourier series or sum-of-Gaussians can represent the solution. The underlying equations of hydrodynamics can also produce turbulent flow fields if the relative strength of the driving forces is high enough. Lorenz' truncated three-term model of Rayleigh-Bénard flow is the simplest set of chaotic equations to emerge from the hydrodynamic equations.

A variety of numerical methods well-suited to the low-cost simulations of the future can be applied to special problems in hydrodynamics. The simplest approaches use finite-difference approximations for the spatial derivatives of the flow variables.

For applications of the hydrodynamic equations the *Physics of Fluids* and the *Journal of Fluid Mechanics* should be consulted. An idea of the thousands of approaches to numerical solutions can be found in the *Proceedings of the 11th International Conference in Fluid Dynamics* held at Williamsburg, Virginia in 1988, published as Volume 323 in the Springer-Verlag series *Lecture Notes in Physics*. The article "A Comparison of Numerical Schemes on Triangular and Quadrilateral Meshes," by D. R. Lindquist and M. B. Giles, emphasizes some of the interesting loose ends prevailing in the numerical work. E. N. Lorenz' original work, "Deterministic Nonperiodic Flow," in the *Journal of Atmospheric Science* 20, 130 (1963) is a model of clarity.

## 9. Kinetic Theory

1 Introduction; 2 Kinetic-Theory States; 3 Hard-Sphere Collision Rate and Free-Path Distribution; 4 Free-Path Theory; 5 Boltzmann's Equation; 6 Maxwell-Boltzmann Distribution from the Boltzmann Equation; 7 H Theorem and Irreversibility; 8 Numerical Solutions of the Boltzmann Equation; 9 Approximate Boltzmann Equation; 10 Diffusion; 11 Viscosity; 12 Heat Conduction; 13 Enskog Model; 14 Green-Kubo Theory; 15 Summary and References



### 9.1 Introduction

Kinetic Theory aims to relate nonequilibrium constitutive relations to underlying atomistic force laws and to explain and describe the nonequilibrium hydrodynamic states of gases. The nonequilibrium state description needs to account for the structure and evolution of the nonequilibrium states as well as their decay, "the approach to equilibrium." In kinetic theory this ambitious program is to be based on the statistical-mechanical analysis of isolated uncorrelated two-body collisions. The main analytical tool available for this work is the Boltzmann Equation, the subject of Section 9.5. The Boltzmann Equation provides a description, accurate for low-density gases, of the effect of two-body collisions on the one-body phase-space density  $f(r,p,t)$ . The binary molecular collisions on which the equation is based lie near the limit of analytic work. Force laws more complex than hard spheres typically require numerical work even in this simplest case. In summary, kinetic theory is the discipline developed to explain gas-phase properties, mainly the nonequilibrium properties ignored by Gibbs, by analyzing the uncorrelated binary collisions which dominate low-density gas dynamics.

Because most nonequilibrium systems are *close to* rather than *far from* equilibrium, their structure and evolution can be usefully and reproducibly characterized by local values and gradients of concentration, momentum, or energy, neglecting both higher-order derivatives and nonlinear terms. The gradients drive flows of mass, momentum, and energy which tend relentlessly toward equilibrium. To persist, the gradients must be maintained by nonequilibrium boundary conditions. They would otherwise die away. Most of kinetic theory has to do with the *linear* theory of these nonequilibrium gradient-induced flows. The linear flow properties are summarized in Fick's, Newton's, and Fourier's empirical rules, or "Laws," for the fluxes of mass, momentum, and energy:

$$J = -D\nabla\rho ; P = (P_{eq} - \lambda\nabla\cdot u)I - \eta(\nabla u + \nabla u^t) ; Q = -\kappa\nabla T .$$

For three-dimensional fluids, the fluxes  $J$ ,  $P$ , and  $Q$  have respectively units of [mass, momentum, and energy per unit area per unit time]. In many applications of elastic theory and hydrodynamics the equilibrium pressure  $P_{eq}$  is so close to zero as to be

negligible. In kinetic theory the situation is different and the equilibrium pressure must be included. Except in shock waves the nonequilibrium momentum flux is typically much smaller in magnitude than the background equilibrium pressure  $P_{eq} \equiv NkT/V$ . All the transport coefficients and the equilibrium pressure can depend on the local state. In the linear theory such dependence is generally ignored.

Kinetic theory, as summarized by the Boltzmann Equation, has succeeded in deriving these same linear relations linking the fluxes to the gradients from very reasonable assumptions. The theory further provides accurate estimates for the "transport coefficients,"  $D$ ,  $\lambda$ ,  $\eta$ , and  $\kappa$ , in terms of the interatomic forces. This direct link between microscopic models and macroscopic hydrodynamic properties is the analog of Gibbs' link between microscopic states and macroscopic thermodynamic properties. But, unlike Gibbs' theory, kinetic theory is restricted to gases.

For gases the Boltzmann-Equation theory provides much more than the three linear transport laws. First, it is possible to show that the Maxwell-Boltzmann velocity distribution is *the* stationary solution for an isolated system. This distribution then provides equilibrium properties consistent with the predictions of Gibbs' equilibrium statistical mechanics. Boltzmann was able to demonstrate that uncorrelated binary collisions will eventually establish this stationary equilibrium Maxwell-Boltzmann velocity distribution in *any* isolated system and that the approach to this equilibrium is monotonic, resembling the monotonic increase of entropy described by the Second Law of Thermodynamics. From the conceptual standpoint this is the most important result derived from the Boltzmann equation: the Second Law of Thermodynamics. Subject only to the assumption that successive collisions are uncorrelated Boltzmann was able to "explain" irreversible hydrodynamic behavior, consistent with the Second Law of Thermodynamics, for isolated systems obeying reversible Newtonian mechanics.

From the standpoint of applications to real gas-phase flows the quantitative prediction of transport properties is Boltzmann's most important contribution. Starting from the Boltzmann Equation, it is possible to show, in agreement with laboratory experiments, that there are shear viscosity and heat conductivity coefficients with definite nonzero limits at low density. The Boltzmann Equation also correctly predicts the temperature dependence of these transport coefficients on the basis of the interparticle forces and so provided one of the earliest ways for getting direct evidence characterizing these forces from macroscopic measurements.

A generation after Boltzmann's work, the Mayers were successful in accounting for the density expansion of gas-phase equilibrium thermodynamic properties on the basis of the cluster theory outlined in Section 4.13. It is natural to think that a similar expansion procedure would work for nonequilibrium systems, with the shear viscosity, for instance, having a density power-series expansion with temperature-dependent coefficients. But away from equilibrium there is so far no known high-probability partition function on which to base such an expansion. Kinetic theory makes use of Lyapunov-unstable particle trajectories which are highly sensitive to small

perturbations, making an expansion about the equilibrium state difficult. Recent work, both experimental and theoretical, makes it highly unlikely that a nonequilibrium density expansion exists. Despite this difficulty, there is a highly-useful approximate model for the nonequilibrium behavior of dense fluids, the Enskog model described in Section 13, which *does* have a density expansion.

Likewise it might be expected that beyond the linear transport theory of diffusion, viscosity, and heat conduction lies an even richer field of nonlinear phenomena. Although the nonlinearity is real enough it seems extremely difficult to reach general conclusions. Nonlinearity generally implies chaos and chaos generally implies the need for case-by-case analysis. Because most readily-observed phenomena occur at greatly subsonic speeds phenomenological nonlinear terms are of limited utility. It is fortunate that in many cases the deviations from linear behavior are extremely small and are even more difficult to measure than they are to calculate. For simple fluids the experimental evidence for series expansions of the transport coefficients in powers of the strain rate or the temperature gradient is meager or nonexistent because the required rates and gradients must be large which in turn implies that the spatial resolution scale must be very small. Shockwaves, with a scale governed by the microscopic mean free path, are the prototypical nonlinear problem with the best promise of producing useful results.

So the main goal of kinetic theory has remained the understanding of linear nonequilibrium phenomena for low-density gases. This restricted theory can be approached through the much simpler free-path theory, a straightforward intuitive approach yielding useful engineering estimates. This free-path theory can then be improved upon in a systematic way, at the expense of considerable analysis, by turning to the Boltzmann equation. In this Chapter we begin by outlining the approximate hard-sphere free-path theory and a useful intermediate approximation to the exact Boltzmann approach, the "Krook-Boltzmann" equation, which improves on the free-path theory by providing semiquantitative nonequilibrium distribution functions. We consciously avoid the study of *nonlinear* problems here, putting these off to the following two Chapters, because we believe that a direct numerical approach has so far been more profitable and illuminating than the existing relatively-cumbersome theoretical analyses.

## 9.2 Kinetic-Theory States

What are the state variables that need to be specified in order to develop and apply kinetic theory? The states of matter studied in gas-phase kinetic theory require the same general information as do hydrodynamic states. The initial spatial distribution of mass and composition must be specified, together with the thermodynamic state of gas under investigation, including a mechanical variable, such as density or pressure, and a thermal variable, such as temperature or energy. Finally, the constitutive flow properties, and the problem's boundary conditions, which can include time dependent

sources of mass, momentum, and energy must be given. The goal of gas-phase kinetic theory is then the same as the goal of hydrodynamic simulation, predicting the future state of such a system. Kinetic theory is in a way more basic than is hydrodynamics, through its link to interatomic forces, but its predictions are certainly less general, being restricted to gases.

The predictions of the linear theory are accurately known and are summarized in Chapman and Cowling's classic work, *The Mathematical Theory of Non-Uniform Gases*. They are identical to the phenomenological laws of Fick, Newton, and Fourier. Differences in concentration lead to particle currents. Differences in velocity lead to viscous drag and differences in temperature lead to heat flux. Beyond these three linear phenomena lies a chaotic nonlinear world where exploration is difficult and general understanding is meager.

The Navier-Stokes equations furnish a very general description of fluid flow, equally-correct for dense fluids, like water or mercury, and dilute ones, like air. Kinetic theory is much more restrictive. Kinetic theory treats nearly-ideal gases, in which molecules collide only occasionally. Air at room temperature and pressure is the prototypical kinetic-theory medium. The atmosphere has a density only about one thousandth that of liquid air so that the nonideal pressure correction to the ideal gas law is much less than a percent. For air the approximation of isolated binary collisions is a reasonable one.

In this Chapter our goal is limited. We use kinetic theory to discuss *linear* problems with nonequilibrium states so near to equilibrium that squares of the deviations can be ignored. By adopting this restriction we can avoid dealing with the details of nonequilibrium boundary conditions and thermostats. We will return to these important topics in discussing a method better suited to their study, nonequilibrium molecular dynamics, in Chapters 10 and 11.

### 9.3 Hard-Sphere Collision Rate and Free-Path Distribution

Collisions underlie transport theory. They are the basis of the Boltzmann Equation. Without collisions there could be no equilibration so that the linear transport laws could not hold. The relative simplicity of binary collisions, and their fundamental importance to transport theory suggests we begin with their study. The equilibrium collision rate for hard spheres is a relatively simple exact calculation and furnishes a good introduction to the details involved in the Boltzmann-Equation approach to kinetic theory. We will calculate this rate by choosing a particular type of collision for a particular pair of particles. By averaging over all such collision types and by noting that the long-time collision rate is the same for any pair of similar spheres we use this simple two-body calculation to calculate the many-body collision rate.

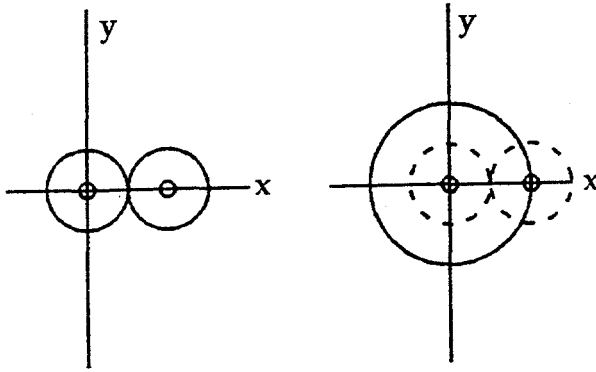


**Figure 9.1.** Collision geometry for two spheres colliding on the  $x$  axis, with  $v_{x1} > v_{x2}$ . The leftmost sphere, Particle 1, is shown at the origin. In the left view both spheres are shown. The right view shows also the equivalent collision of a large sphere, with a *radius* equal to the sphere diameter, and a point mass.

Let us begin by considering the probability that during the time interval  $dt$  two Hard Spheres labelled 1 and 2 undergo a collision such that Sphere 2 collides with Sphere 1 within the infinitesimal area  $da$  which defines the positive  $x$  axis indicated in Figure 9.1. Notice first that in the Figure the collision between two identical spheres with radii  $\sigma/2$  has been replaced by an equivalent collision between a large sphere of *radius*  $\sigma$  and a mass point. Both bodies have the same mass,  $m$ . This same replacement could be made for *any* interaction which depends only on the distance between the two colliding particles. The area  $da$  is not shown. It would be an infinitesimal two-dimensional area perpendicular to the  $x$  axis. In the analogous two-dimensional case  $da$  would be replaced by a one-dimensional length perpendicular to the  $x$  axis. This probability calculation generalizes more easily to hard rods and hard disks than does the usual equivalent textbook calculation using spherical polar coordinates. To get the total collision rate  $\Gamma_{12}$  the  $x$ -axis collision rate needs to be multiplied by the ratio of the total collision area to the infinitesimal area  $da$  considered here:  $(4\pi\sigma^2/da)$  for spheres,  $(2\pi\sigma/da)$  for disks, and  $(2/da)$  for rods, where each of these particle types has a collision diameter  $\sigma$ . Evidently a collision can occur only if  $v_{x1} > v_{x2}$ . In that case the probability for collision during a sufficiently-short time  $dt$  is just the ratio of the possible locations for Sphere 2 (relative to 1) to the total volume  $V$ . In three dimensions these spatial locations leading to collision occupy a squat cylinder of cross-sectional area  $da$  and infinitesimal height  $(v_{x1} - v_{x2})dt$ . Introducing the large-system equilibrium probabilities for the two velocity components completes the formulation of the average two-particle collision rate  $\Gamma_{12}$  as a definite integral:

$$\Gamma_{12} = (4\pi\sigma^2/da)(m/2\pi kTV) \int dv_{x1} \int dv_{x2} (v_{x1} - v_{x2}) da \exp[-(m/2kT)(v_{x1}^2 + v_{x2}^2)].$$

The two one-dimensional integrals can be evaluated by a 45 degree (clockwise) rotation of the velocity axes, switching to new velocities  $\alpha$  and  $\beta$  (the Jacobian of the transformation is unity):

$$\alpha = (v_{x1} - v_{x2})/2^{1/2} > 0; \beta = (v_{x1} + v_{x2})/2^{1/2};$$

$$\Gamma_{12} = (4\pi\sigma^2/da)(2\pi kTV/m)^{-1} \int d\alpha \int d\beta 2^{1/2} \alpha da \exp[-(m/2kT)(\alpha^2 + \beta^2)].$$

Working the two integrals out gives the exact collision rates for two spheres, with the results for disks and rods following by analogy:

$$\Gamma_{12} = (kT/\pi m)^{1/2}(4\pi\sigma^2/V) \text{ (spheres) ;}$$

$$\Gamma_{12} = (kT/\pi m)^{1/2}(2\pi\sigma/V) \text{ (disks) ;}$$

$$\Gamma_{12} = (kT/\pi m)^{1/2}(2/V) \text{ (rods) .}$$

All three results can be summarized in terms of the appropriate collision cross sections and the one-, two-, and three-dimensional mean speeds, computed from the first moments of the corresponding Maxwell-Boltzmann distributions:

$$\Gamma_{12} = 2^{1/2}v(cs/V) ;$$

$$v = (8kT/\pi m)^{1/2} ; cs = \pi\sigma^2 \text{ (spheres) ;}$$

$$v = (\pi kT/2m)^{1/2} ; cs = 2\sigma \text{ (disks) ;}$$

$$v = (2kT/\pi m)^{1/2} ; cs = 1 \text{ (rods) .}$$

An alternative derivation of the collision rate, equally exact, but perhaps less plausible, can be based on computing the mean value of the relative speed of the colliding particles and observing that the scattering cross section is velocity independent.

From the collision rate we can calculate "Maxwell's mean free path"  $\lambda_M$ , defined as the long-time average distance between a particle's successive collisions. The average is most easily visualized by considering an equilibrium many-body hard-sphere system. The calculation of the average outlined here is exactly correct in the low-density limit. The sphere diameter is  $\sigma$ , defining the distance of closest approach. The total distance traveled by  $N$  hard spheres in time  $t$  is  $Nvt$ , where  $v$  is the three-dimensional mean speed,  $(8kT/\pi m)^{1/2}$  and the number of collisions  $\Gamma_N t$  is  $N(N-1)(1/2)^{1/2}v\pi\sigma^2 t/V$ . The  $N$ -body collision rate  $\Gamma_N$ ,  $N(N-1)/2$  times the two-body rate  $\Gamma_{12}$ , is an equilibrium property which can be calculated from the Mayers' virial theory, by expressing the probability for finding pairs of spheres in contact as a power series in the number density  $N/V$ :

$$\Gamma_N t = [N(N-1)(1/2)^{1/2}v\pi\sigma^2 t/V][1 + 0.625(Nb/V) + 0.28695(Nb/V)^2 + 0.1103(Nb/V)^3 + \dots],$$

where the second virial coefficient  $b$  is  $2\pi\sigma^3/3$ . Because each two-body collision simultaneously terminates *two* free paths the average path length,  $\langle\lambda\rangle$ , approaches the "Maxwell" mean free path  $\lambda_M$  at low density, where spatial correlations can be ignored:

$$\langle\lambda\rangle \Rightarrow \lambda_M = \Sigma vt / (2\Gamma_N t) = V / (2^{1/2} N \pi \sigma^2).$$

What is the distribution of the paths' lengths around the mean? Visualize a dilute gas of atoms characterized by a velocity-independent collision probability  $1/\tau$ . We mean by this that any atom has a probability  $dt/\tau$  of undergoing a collision during the time interval  $dt$ . How many atoms,  $N(t)$ , have undergone no collisions up to the time  $t$ ? Evidently the set of uncollided atoms is depleted according to the linear relation:

$$N(t + dt) = N(t) - N(t + [dt/2])dt/\tau \Rightarrow d\ln N/dt = -1/\tau.$$

Thus the number of uncollided particles falls off with time as  $N(0)e^{-t/\tau}$ . Provided that the collision probability is velocity-independent the corresponding distribution of the paths travelled by the  $N$  particles is also exponential:

$$\text{Prob}(\lambda)d\lambda = e^{-\lambda/\langle\lambda\rangle} d\lambda/\langle\lambda\rangle.$$

But because the expected path length actually *increases* with speed, as shown in Figure 9.2, the exponential free-path probability density which holds for spheres of the same speed is, when averaged over all velocities, a fairly-complicated function. The resulting exact low-density distribution was compared to distributions measured with molecular dynamics at a variety of fluid and solid densities by Einwohner and Alder.

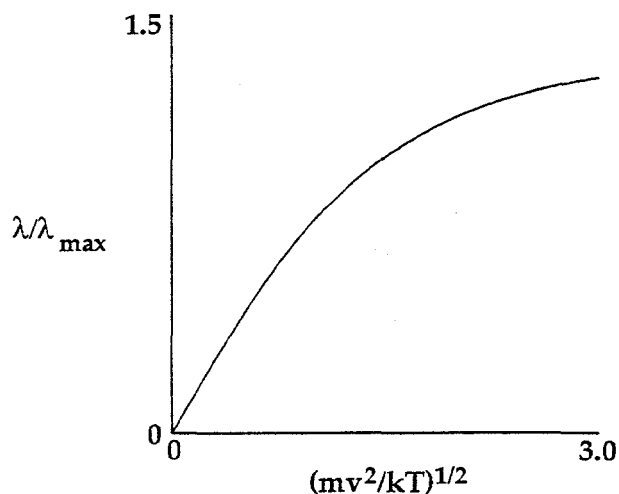
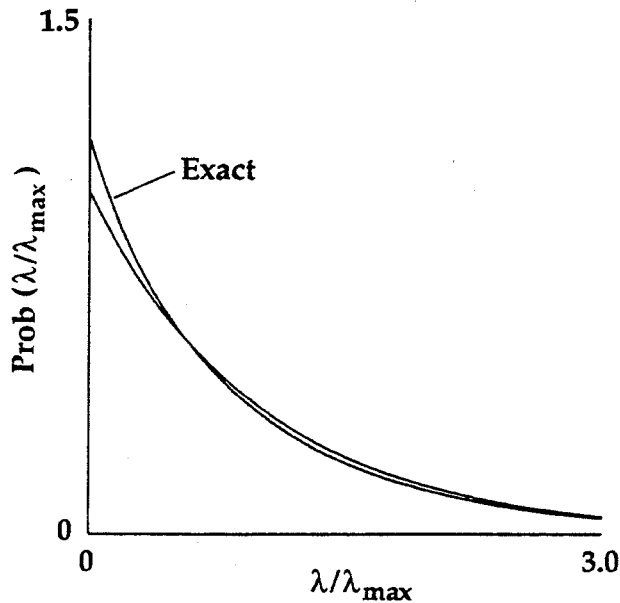


Figure 9.2. Equilibrium dependence of the low-density hard-sphere free path on speed. The high-speed limit is exactly  $2^{1/2}$  times the Maxwell mean free path.



**Figure 9.3.** Frequency distribution of free paths for low-density hard spheres. For short free paths the exact distribution lies above the single-speed exponential approximation. Such an exponential distribution is also approximately followed for *dense* hard disks and spheres, either fluid or solid.

The low-density calculated result, averaged over all velocities, is reproduced in Figure 9.3 and is compared there to the single-speed exponential free-path distribution. The measured distribution taken from the molecular dynamics calculations showed that the shape of the free-path distribution is changed only a little as the hard-sphere gas is compressed to become a dense fluid. *Even in the solid phase* the simple exponential approximation,

$$\text{Prob}(\lambda)d\lambda = \exp(-\lambda/\lambda_M)d\lambda/\lambda_M,$$

where  $\lambda_M$  is the Maxwell mean free path, is accurate within a few percent, for paths which are not too long.

### Problems:

1. Reproduce the low-density plot of path length as a function of speed for spheres, and calculate the corresponding relation for disks and rods.
2. What are the largest and smallest speeds possible *after* a collision of two hard disks with initially equal speeds? What geometric situation leads to such a collision?
3. Work out the Maxwell mean free path for a mixture of two hard-sphere gases with the same masses but with *unequal* diameters  $\sigma_1$  and  $\sigma_2$ . Assume that the mixture contains  $N/2$  spheres of both types.

Before leaving the subject of free paths we mention a subtle factor of approximately two. For an *exponential* distribution of times *to* collision the time *between* collisions is twice the time to the next collision. A gambling analogy should clarify this statement: by symmetry, the mean number of throws required to throw the

next six with a fair die is the same as the number of throws which would have to be repeated to reach the last six:

$$1(1/6) + 2(5/6)(1/6) + 3(5/6)(5/6)(1/6) + \dots = 6.$$

Consider now a long series of throws. Evidently the mean number of throws in the many segments beginning and ending with a six approaches 12 for a sufficiently large sample. It is equally evident that in a large sample of  $N$  throws there are  $N/6$  sixes partitioning the sample into  $N/6$  segments with mean length 7, if both endpoints are included in each segment's length. Both results, 12 and 7, for the "mean segment length" are correct! In the first case segments are weighted according to their length while in the second case all segments are weighted equally.

### Problems:

1. Consider sub-sequences of "heads" from a long sequence of  $N$  tosses of a fair coin. Estimate the number of subsequences containing  $n$  successive heads (of the forms THT, THHT, THHHT, ... for  $n = 1, 2, 3, \dots$ ) as a function of  $n$  and compute the total number of subsequences containing at least one head.
2. Consider a long sequence of  $N$  throws of a fair  $s$ -sided die with sides labelled 1, 2, ...  $s$ . (In the example discussed in the text  $s$  is 6;  $s$  is 2 for a fair coin.) What is the probable number of sub-sequences composed solely of 1's? Assume each such sub-sequence is preceded and succeeded by non 1's. Use a random-number generator, such as that appearing in Section 3.10, to check your estimate for  $s = 3$ . Choose  $N$  sufficiently large that the expected error in your "Monte-Carlo" result is less than a percent.

Thus, by analogy, if we examine a snapshot of an equilibrium hard-sphere system and ask for the mean value of all paths currently being traversed we expect to find a value approximately twice the Maxwell free path. To see this for a simple approximate model, consider modifying the exponential distribution of free paths,

$$\text{Prob}(\lambda)d\lambda = e^{-\lambda/\langle\lambda\rangle}d\lambda/\langle\lambda\rangle,$$

so as to obtain a new probability  $\text{Prob}'(\lambda)d\lambda$  weighting each path according to its length:

$$\text{Prob}'(\lambda)d\lambda = \lambda e^{-\lambda/\langle\lambda\rangle}d\lambda/\langle\lambda\rangle^2.$$

The mean value computed from this weighted distribution is  $2\langle\lambda\rangle$ . The analogous exact kinetic-theory calculation is complicated by the dependence of the free path on velocity. The precisely-calculated value is (twice) the so-called "Tait free path," with  $\lambda_T$

$\cong 0.96\lambda_M$ . Formally the Tait path is the average over an equilibrium path distribution in which each path is weighted according to the time required to trace it out.

Hard spheres are particularly suited to kinetic-theory calculations. Not only do the collisions occur at definite times and with scattering angles independent of the magnitude of the velocity, they also produce *isotropic* scattering in the center-of-mass frame. We now demonstrate this interesting and useful property by considering the collision of two spheres in the center-of-mass coordinate frame. See Figure 9.4.

For convenience we choose the initial velocities of the two spheres to be parallel to the x axis so that the collision is defined by two variables: the first is the "impact parameter"  $b < \sigma$  which gives the *distance* of closest approach in the absence of forces (or, equivalently, an angle  $\beta < \pi/2$ , with  $\sin(\beta) = b/\sigma$ ); the second collisional variable is the angle  $\alpha < 2\pi$ , which gives the *direction* of the point of collision from the origin in the yz plane. By symmetry *all values of  $\alpha$  are equally likely*. The probability of an impact parameter  $b$  in a range of width  $db$  about  $b$  is therefore  $2\pi b db / \pi\sigma^2$  with the directional probability, after collision, for the incoming particle independent of  $\alpha$ , over each cone of constant  $b$  or  $\beta$ . It is most convenient to describe the collision process in terms of yet another angle, the "scattering angle"  $\theta = \pi - 2\beta$ , which depends only on  $b$ , or  $\beta$ . See again the Figure. The chain of identities is as follows:

$$\text{Prob}(\theta)d\theta = \text{Prob}(\beta)d\beta = \text{Prob}(b)db = 2bdb/\sigma^2 = 2\sin(\beta)\cos(\beta)d\beta = \sin(\theta)d\theta ; (\text{spheres}) .$$

The calculated probability distribution, varying as the sine of the scattering angle  $\theta$  between the x axis and the direction of the post-collision trajectory, and augmented by the uniform probability density in the angle  $\alpha$  is  $\sin(\theta)d\theta d\alpha$ , exactly the same as the corresponding solid-angle volume element in spherical polar coordinates  $\sin(\phi)d\phi d\theta$ , establishing that the center-of-mass-frame scattering of two similar hard spheres is isotropic.

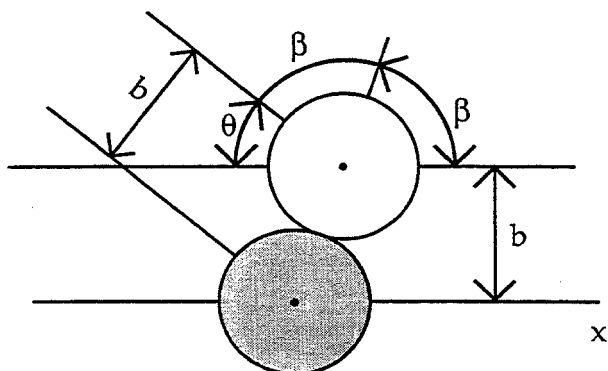


**Figure 9.4.** Hard-Sphere collision geometry in a frame fixed on the shaded particle. The scattering particle enters from the right, at the relative velocity and with the impact parameter  $b$ . The relative velocity is scattered through an angle

$$\theta \equiv \pi - 2\beta .$$

Following the same calculation for the collision of two hard disks gives a cosine law,

$$\text{Prob}(\theta)d\theta = \text{Prob}(\beta)d\beta = \text{Prob}(b)db = db/\sigma = \cos(\beta)d\beta = (1/2)\sin(\theta/2)d\theta ; (\text{disks}) ,$$

rather than the uniform distribution which would correspond to isotropy. The disk scattering is predominantly head-on. The geometry for other force laws is less-suited to analysis than to numerical evaluation. In particular the scattering no longer depends solely on direction so that the results must generally be tabulated as functions of the relative speed. Attractive forces add even more numerical complexity, at sufficiently low energy, by providing nearly-bound orbiting collisions.

### Problems:

1. Consider the inverse fourth power repulsive potential, often called the "Maxwell Model" potential. Use Runge-Kutta integration to confirm that simultaneously *increasing* the impact parameter  $b$  by a factor of 2, and *decreasing* the relative velocity  $v$  by a factor of 4 leaves the scattering angle unchanged. For a fixed relative velocity compare the dependence of scattering angle on impact parameter to that calculated for hard spheres.
2. Consider the balance of the attractive two-body Lennard-Jones force with the centrifugal force,  $\mu\omega^2r$ , where  $\mu$  is the reduced mass  $m/2$ , to find the highest center-of-mass temperature,

$$(3/2)kT_{\text{com}} \equiv (m/2)(v_1^2 + v_2^2) ; v_1 + v_2 \equiv 0 ,$$

for which the Lennard-Jones potential  $\phi = 4\epsilon[(\sigma/r)^{12} - (\sigma/r)^6]$  can provide an *infinite* scattering angle (that is, a long-lived binary molecule).

### 9.4 Free-Path Theory

The simplest possible kinetic model for understanding a *nonequilibrium* three-dimensional low-density gas is based on an *equilibrium* discrete-state single-speed model with one-sixth of the atoms traveling in each of the six Cartesian coordinate-axis directions at the mean thermal speed relative to the local stream velocity. We imagine that this caricature distribution is maintained at local equilibrium through the mechanism of collisions so that the fluxes arriving at any observation plane depend on the character of the distributions one mean free path away, from which the flowing particles originated. Because this theory is maximally approximate we will not point out the many places where refinements could be introduced. We will, for instance, use  $\lambda$  here to indicate both the free path and its average. Boltzmann's Equation, introduced in the next Section, makes piecemeal refinement of this crude picture unnecessary.

To begin, consider a binary mixture of mechanically identical black and white hard spheres at mechanical and thermal equilibrium with constant total mass density  $(Nm/V) = \rho = \rho_B + \rho_W$  and temperature  $T$ , but with locally *nonequilibrium* concentration gradients, with nonvanishing gradients  $d\rho_B/dx = -d\rho_W/dx$ . We can estimate the mass flux  $J_B$  [with units  $M/L^2T$ ] of black particles at  $x = 0$  by summing up the streaming contributions from such particles' last collisions at  $x = \pm\lambda$ :

$$J_B(x=0) = (v\rho_B/6)_{-\lambda} - (v\rho_B/6)_{+\lambda} = (-\lambda v/3)d\rho_B/dx + O(\lambda^3).$$

The error is of order  $\lambda^3$  owing to the cancellation of the quadratic terms in the two expansions of the density flows at the observation plane,  $\pm v\rho_B/6$ . The linearized result is exactly Fick's First Law, with a free-path diffusion coefficient  $D_{FP} = \lambda v/3$ . For air the value is roughly

$$D_{FP} = (1/3)[(V/N)/(2^{1/2}\pi\sigma^2)](8kT/\pi m)^{1/2} = 0.120(V/N\sigma^2)(kT/m)^{1/2} \cong 0.1\text{cm}^2/\text{sec}.$$

For liquid water the assumptions are much less good, and the estimated value,  $10^{-4}\text{cm}^2/\text{second}$ , is ten times too high when compared to the experimental value.

To estimate the *shear viscosity* of a gas using this free-path version of kinetic theory we imagine an isothermal homogeneous flow field with strain rate  $du_x/dy = \dot{\epsilon}$  in which the  $x$  velocity component varies linearly with  $y$  and vanishes at our Eulerian observation plane,  $y = 0$ :

$$\langle v_x \rangle = (du_x/dy)y = \dot{\epsilon}y.$$

The pressure-tensor component  $P_{yx}$  gives the flux of  $x$  momentum through the plane  $y = 0$ , given here by the difference of two currents originating below and above that plane and distant from it by one free path:

$$P_{yx}(y=0) = P_{xy} = (\rho v_x v_y/6)_{-\lambda} - (\rho v_x v_y/6)_{+\lambda} = (-\lambda\rho v/3)(du_x/dy) + O(\lambda^3).$$

The linearized result is exactly Newton's viscous flow law, from which we can identify the free-path coefficient of shear viscosity:

$$\eta_{FP} = (\lambda v/3)\rho = D_{FP}\rho = (2/3\pi\sigma^2)(mkT/\pi)^{1/2} = 0.120(mkT)^{1/2}/\sigma^2.$$

This density-independent result correctly predicts, or explains, the surprising fact that *the shear viscosity approaches a nonzero limit at low density*. Although fewer particles are available to carry the momentum at low density the distance each travels between collisions, of order the free path  $\lambda = V/(2^{1/2}N\pi\sigma^2)$ , exactly compensates for the decreased number of carriers.

The heat conductivity defined by Fourier's Law,  $Q = -\kappa \nabla T$ , can be calculated similarly, by imposing a temperature gradient. To avoid shock waves the concentration necessarily varies, in such a way that the *pressure* is constant:  $d \ln T / dx + d \ln \rho / dx = d \ln P / dx = 0$ . We compute the energy flow across an observation plane at  $x = 0$ . To avoid introducing the explicit dependence of concentration on  $x$  we replace the number density  $\rho / m = N / V$  by the ideal-gas value  $P / kT$  and we use the estimate  $C_p$  rather than  $C_v$  to estimate the dependence of the local energy on temperature. The resulting energy flux  $[M/T^3]$  is

$$Q_x(x=0) = [(N/V)vC_p T/6]_{-\lambda} - [(N/V)vC_p T/6]_{+\lambda} =$$

$$[(P/kT)vC_p T/6]_{-\lambda} - [(P/kT)vC_p T/6]_{+\lambda} = (-PC_p \lambda / 3k)(dv/dx) + O(\lambda^3).$$

Because the speed  $v = v_x$  varies as the square root of temperature the derivative  $(dv/dx) = (dv/dT)(dT/dx)$  can be replaced by  $(v/2T)(dT/dx)$  so that we can once again linearize the series expansion, and identify the free-path heat conductivity  $\kappa$ :

$$\kappa_{FP} = PC_p \lambda v / 6kT = (1/2)D_{FP} \rho c_p = 0.150k(mkT)^{1/2} / \sigma^2; c_p \equiv C_p / m.$$

A comparison of our free-path results with the corresponding exact results from the Boltzmann Equation shows that our free-path transport coefficients all have the correct functional dependence on density and temperature and are therefore qualitatively correct. But the numerical values are too small. In particular the numerical coefficients 0.120 and 0.150 given above for the viscosity and heat conductivity are instead 0.179 and 0.678 in the exact theory. This quantitative disagreement is in part due to "velocity persistence," the statistically-averaged tendency of two- or three-dimensional particles to continue moving in their original direction of motion after collision. The free-path numerical errors are in larger part due to the nonlinear dependence of momentum and energy transport on velocity, with our uncorrelated single-speed averages underestimating the contribution of the faster particles. Even for hard spheres, a near-exact three-figure version of these calculations requires days, as opposed to minutes, of work analyzing the solutions of the Boltzmann Equation, the subject of the next Section.

### **Problem:**

Extend the collision rate calculation to show that the average energy of colliding particles in  $D$  dimensions,  $(m/2)\langle v \cdot v \rangle_c$  is  $(D+1)kT/2$ . Then show that the equilibrium velocity persistence for  $D$ -dimensional hard spheres,  $\langle v' \cdot v \rangle_c / \langle v \cdot v \rangle_c$ , where  $v$  and  $v'$  indicate velocities before and after collision, is  $[D - (3/2)] / [D + (1/2)]$ .

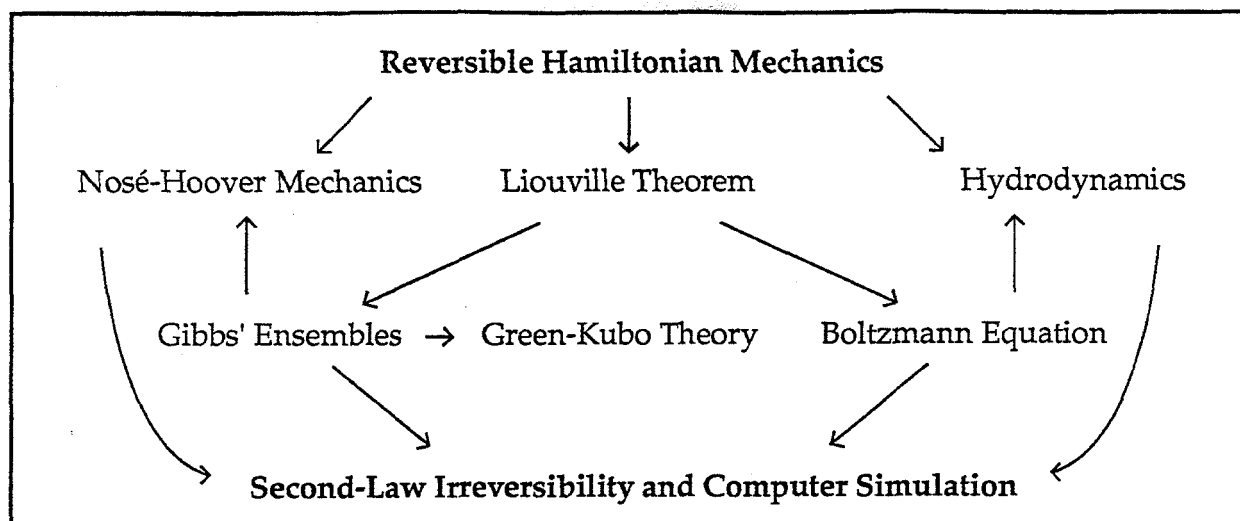


**Figure 9.5.** Logical interconnections linking reversible Hamiltonian mechanics to Computer Simulation and to the irreversible behavior described by the Second Law.

### 9.5 Boltzmann's Equation

There is an æsthetic pleasure in exploring the consequences of an exact theory based on simple assumptions, even though the details require painful algebra. Figure 9.5 is a sketch showing the logical connections linking Hamilton's Reversible Mechanics and macroscopic irreversibility. All of these connections rely on the concept of flow in a state space. Boltzmann's Equation provides an exact description for low-density gases near equilibrium. We derive the equation here, primarily because the most important consequence of the equation, the proof of Boltzmann's H Theorem, equivalent to a gas-phase Second Law of Thermodynamics, then requires very little additional algebra.

The goal of Boltzmann's Equation is to calculate the evolution of the one-particle probability density for those particles at  $r$  within  $dr$  and with momenta within  $dp$  of  $p$  at time  $t$ ,  $f(r,p,t)drdp$ , by analyzing the effect of collisions statistically. We call a particle representative of these particles a "Boltzmann Particle" to distinguish it from potential collision partners with other values of the momentum. In the absence of collisions the Boltzmann Equation and the Liouville Equation for Hamiltonian systems provide equivalent information, that particles stream through one-particle phase space with unchanged Lagrangian probability density,  $\dot{f} = 0$ . Collisions change the one-particle density. The Boltzmann equation describes the effect of collisions statistically:

$$\dot{f} = (\partial f / \partial t)_c = (\partial f / \partial t)_{\text{gain}} - (\partial f / \partial t)_{\text{loss}}.$$

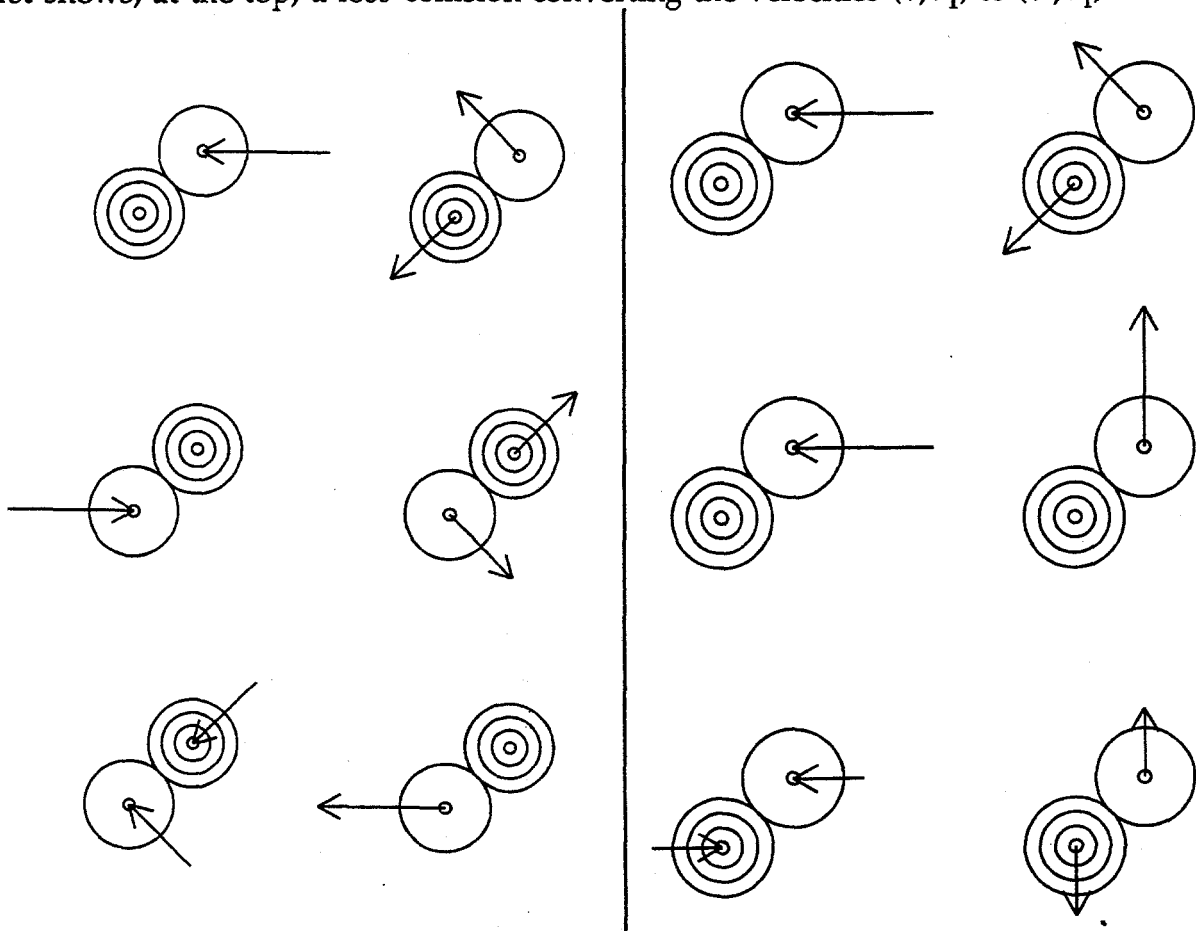
The "collision term" has been written here as the difference between a "gain" term and a "loss" term. The loss term is the simpler of the two:  $(\partial f / \partial t)_{\text{loss}}drdpdt$  includes losses from  $f(r,p,t)drdp$  due to collisions of a Boltzmann Particle during the time interval  $dt$  with Particles having momenta in the range  $dp_1$  about  $p_1 = mv_1$ , of which  $f_1 = f(r,p_1,t)drdp_1$  such particles are available for collision. Notice that in the Boltzmann

equation both the colliding particles are considered to come from the *same* location in space,  $r$ , not from locations one or two free paths distant. The construction of the "loss term" parallels the collision-rate calculation of Section 9.3:

$$(\partial f / \partial t)_{\text{loss}} = \iiint f_1 v_{\text{relative}} b db d\theta dp_1,$$

where each collision is conveniently described in a coordinate system moving with the Boltzmann Particle's velocity  $v$ , so that Particle 1 appears to approach the Boltzmann Particle with relative speed  $v_{\text{relative}} = (1/m)|p - p_1|$  with an impact parameter  $b$  and the angle  $\theta$ . The angle  $\theta$  describes the orientation of the collision plane. For disks it is simplest to replace the three-dimensional integration  $b db d\theta$  by an integral over  $b$  values ranging from  $-\sigma$  to  $+\sigma$ .

Next, the "gain term" is constructed from the loss term by following a two-step procedure: first, invert space, changing  $r$  to  $-r$ ; then, reverse time, running the spatially inverted collision backward in time. Because this two-part procedure is intricate we first illustrate it graphically for a particular numerical example. In Figure 9.6 each collision shown begins at the left and ends on the right. The Boltzmann Particle is shown with concentric circles. Particle 1 is shown as a single open circle. The Figure first shows, at the top, a loss collision converting the velocities  $(v, v_1)$  to  $(v', v'_1)$



Figures 9.6(left) and 9.7(right). Collision of a Boltzmann Particle, shown with concentric circles and initially at rest, with Particle 1, initially moving horizontally.

with the coordinate origin chosen midway between the Boltzmann Particle and Particle 1. This coordinate choice is convenient for visualizing the inversion operation. From the standpoint of the Boltzmann Equation, with the range of forces negligible relative to the mean free path, this coordinate origin *between* the two particles is negligibly different from one fixed *on* the Boltzmann Particle. Next the spatially-inverted collision is shown, in which the signs of both particles' Cartesian coordinates *and* velocities are reversed. At the bottom the *time reversed inverted* collision is displayed, with the spatially-inverted collision followed backward in time.

The net effect of simultaneously inverting in space and reversing in time is to convert the post-collision velocities  $v'$  and  $v'_1$  back to  $v$  and  $v_1$  by pairing up each conceivable loss collision with a corresponding gain collision. This collision-pairing process can be considered in any one of three coordinate frames. Figure 9.7 shows again the collision of Figure 9.6 in all three frames. Again the sequence of events follows from left to right. In the Laboratory Frame the velocity changes are:

Boltzmann-Particle:

$$(0,0) \leftrightarrow (-1,-1)$$

Particle 1:

$$(-2,0) \leftrightarrow (-1,1) .$$

Read the arrows to the right for the direct collision and to the left for the reversed inverse collision. In the Boltzmann-Particle Frame, a frame centered on the Boltzmann Particle, the velocity change of Particle 1 is

Particle 1

$$(-2,0) \leftrightarrow (0,2) .$$

Finally, in the Center-of-Mass Frame the velocity changes are:

Boltzmann-Particle:

$$(1,0) \leftrightarrow (0,-1)$$

Particle 1:

$$(-1,0) \leftrightarrow (0,1) .$$

The impact parameter for this collision is  $2^{-1/2}\sigma$ . In either the Boltzmann-Particle frame or the center-of-mass frame the scattering angle for this collision is  $\pi/2$ .

With only a slight increase in difficulty these same ideas can be applied to central-force collisions between Particles with different masses by introducing the reduced mass. Collisions between particles with shapes which lack inversion symmetry require special consideration which we are unwilling to provide. The interested reader is referred to Figure 2 of Tolman's *Statistical Mechanics*.

**Problem:**

Work out the lefthand side of the Boltzmann Equation in spherical polar coordinates.

### 9.6 Maxwell-Boltzmann Distribution from the Boltzmann Equation

It is easy to show that the *unique* stationary solution of the Boltzmann Equation for an isolated system is the Maxwell-Boltzmann distribution:

$$f(r,p,t)_{MB} = (N/V)(2\pi mkT)^{-D/2} \exp(-p^2/2mkT) .$$

This follows from the fact that the collisions treated on the righthand side of the Boltzmann Equation conserve only mass, momentum, and energy, the first three moments of the velocity distribution. Because the other moments are not conserved by collisions any *stationary* distribution can depend only on mass, momentum, and energy.

To simplify the derivation we consider the logarithm of  $f$ , which, like  $f$  itself, must also depend only on the conserved moments, and write it in terms of  $D+2$  unknown constants:

$$\ln f_0 = A + B \cdot p + Cp^2 ,$$

where the subscript indicates a stationary distribution. By insisting that  $f$  have moments  $\langle \rho/m \rangle$ ,  $\langle \rho v \rangle$ , and  $\langle \rho [(DkT) + \langle p^2 \rangle/m] \rangle$  the three constants can be identified uniquely, so that the *stationary* distribution must also be *the* equilibrium distribution. The resulting equilibrium distribution has the familiar Maxwell-Boltzmann form:

$$f_{MB} = (\rho/m)(2\pi mkT)^{-D/2} \exp[-(p - \langle p \rangle)^2/2mkT] .$$

The result that *any arbitrary distribution* describing an isolated system must change monotonically and irreversibly toward this Maxwell-Boltzmann form is the content of Boltzmann's H Theorem, a link between microscopic gas-phase mechanics and the Second Law of Thermodynamics, discussed in the following Section.

### 9.7 H Theorem and Irreversibility

For a three-dimensional monatomic equilibrium ideal gas the thermodynamic entropy is, apart from an additive constant, equal to the average value of  $-Nk \ln f$ :

$$S(N,E=[3NkT/2],V)/Nk \equiv -\langle \ln f_{eq} \rangle = -(1/N) \int_{eq} \ln f_{eq} dpdr =$$

$$\ln(V/N) + (3/2) \ln(2\pi mkT) + \text{constant} .$$

This correspondence strongly suggests that a gas-phase analog for the Second Law of Thermodynamics,  $\dot{S}_{isolated} > 0$ , be sought by using the Boltzmann Equation to compute the time dependence of a *nonequilibrium* entropy  $-Nk \langle \ln f_{neq} \rangle$ . This idea is a good one, at least for dilute gases. In an isolated system, or even in a system subject to time-

dependent but velocity-independent forces, the sign of the entropy change from the Boltzmann Equation cannot be negative. To see this it is simplest to compute the spatially-averaged Lagrangian (comoving) derivative of the local single-particle phase-space entropy density,  $-k \ln f$ :

$$\begin{aligned} \dot{S}/Nk &= -(1/N) \int (d/dt) [f \ln f] dp dr = -(1/N) \int f [1 + \ln f] dp dr \equiv -(1/N) \int f \ln f dp dr = \\ &-(1/N) \int dp dp_1 (f' f'_1 - f f_1) \ln (f' f'_1 / f f_1) v_b db d\theta dr . \end{aligned}$$

By using symmetry the righthand side can be written as the symmetrized sum of four integrals, one each for  $-(1/4) \ln f'$ ,  $-(1/4) \ln f'_1$ ,  $+(1/4) \ln f$ , and  $+(1/4) \ln f_1$ . The sum can then be written:

$$\dot{S}/Nk = (1/N) \int dp dp_1 (1/4) (f' f'_1 - f f_1) \ln (f' f'_1 / f f_1) v_b db d\theta dr > 0 ,$$

The final inequality, which demonstrates the inexorable increase of entropy, follows because both  $(f' f'_1 - f f_1)$  and the logarithm of  $(f' f'_1 / f f_1)$  necessarily have the same sign. This firm conclusion from the Boltzmann Equation is called the *H Theorem*. The Theorem shows that Boltzmann's approximate nonequilibrium entropy cannot decrease in an isolated gas-phase system. This is a gas-phase demonstration of the Second Law of Thermodynamics. It is certainly the most impressive result of Boltzmann's kinetic theory.

The H Theorem attracted the attention of many of Boltzmann's colleagues because it seemed too good to be true. Two objections to the H Theorem were raised, one by Loschmidt and one by Zermélo. Loschmidt objected to Boltzmann's H Theorem on the grounds that reversible mechanics cannot predict irreversible behavior. He reasoned that because any trajectory going forward in time can be reversed, *reversible* equations can contain no *unidirectional* behavior. We will see in Chapter 11 that Loschmidt was simply wrong. Reversible equations can and do predict irreversible results. Of course, Boltzmann's Equation is *not* time-reversible. Leaving aside the boundary conditions, if  $f$  were an even function of  $p$  then the righthand collisional side of the Boltzmann Equation would be independent of time while the lefthand side,  $\dot{f}$ , would change sign in a time-reversed trajectory.

Zermélo objected to the H Theorem on the basis of "Poincaré recurrence." Poincaré pointed out that Hamiltonian mechanics within a bounded region of phase space must *ultimately(!)* restore the initial conditions arbitrarily well. Thus any Hamiltonian trajectory along which entropy had increased would later necessarily have a compensating decreasing portion. For an isolated system Zermélo was right, but it is salient and sobering to remember that the Poincaré recurrence time on which his argument is based exceeds the age of the universe for systems of perhaps two dozen degrees of freedom. Remember also that the dynamics is Lyapunov unstable on the

time scale of the collision time, typically nanoseconds to picoseconds. For an accurate dynamical history occupying a second of real time the underlying calculations would need to be carried out with an accuracy of  $10^{12}$  decimal places. Just storing a single coordinate for such a calculation would completely fill the memory of today's largest computer.

The H Theorem's explanation of macroscopic irreversibility on the basis of microscopic dynamics and the two classical objections to it, Loschmidt's "Reversibility Paradox" and Zermélo's "Recurrence Paradox" continue to raise adrenalin levels to this day. But there is no doubt that the Theorem is correct. In a classic calculation Alder and Wainwright confirmed, for an initially nonequilibrium single-speed periodic system of 100 hard spheres that, within statistical fluctuations, the increase of Boltzmann's nonequilibrium entropy with time follows Boltzmann's Equation and satisfies the H Theorem. See Figure 9.8. The small fluctuations seen about the equilibrium value remind us to remember Zermélo and Poincaré. We will return to the fascinating topic of the dynamical origin of irreversible behavior in Chapter 11.

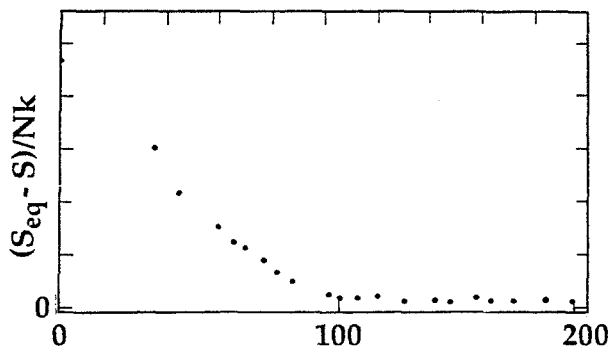


Figure 9.8. Measured increase in a 100-sphere low-density "Boltzmann entropy,"  $-\ln\langle f(v) \rangle$ , for 100 hard spheres with identical initial speeds. The tick marks indicate the times at which the 100th and 200th collisions occurred.

### 9.8 Numerical Solutions of the Boltzmann Equation

From the computational standpoint it is a challenging and demanding task to pose and solve interesting nonlinear problems in gas dynamics by solving the Boltzmann Equation. In the most general case the one-particle distribution function  $f(\mathbf{r}, \mathbf{p}, t)$  depends upon three space variables, three momentum variables, as well as time. Straightforward grid-based integration methods are not practical for such seven-dimensional problems. But the quantitative understanding of many such problems is crucial to applications in aerodynamics and plasma physics. There is no other reasonable approach when the molecular free path is comparable to the system dimensions. To solve the Boltzmann Equation the impractical six-dimensional phase-space grid can be replaced by a less-costly effective alternative closely resembling molecular dynamics simulation: numerical propagation of representative particles in a three-dimensional physical-space grid. The complete evolution of the distribution function can then be followed by describing its changes with time as the sum of two additive parts, a *streaming* collision-free part and a collisional part:  $\dot{f} \equiv (df/dt)_s + (\partial f/\partial t)_c$ .

Between collisions particles "stream" through physical space according to the one-particle ideal-gas equations of motion:

$$\dot{\mathbf{r}} = (\mathbf{p}/m) ; \dot{\mathbf{p}} = \mathbf{F}_{\text{Boundary}} + \mathbf{F}_{\text{Driving}} .$$

Generally the streaming trajectories between collisions can be evaluated analytically, so that there is no need for a time-consuming step-by-step Runge-Kutta or Stoermer integration. At intervals, as the particles are propagated, pairs of particles in each spatial bin are chosen for collision with a *Monte Carlo* sampling procedure based on the local collision rate. The two parameters describing a low-density collision, the impact parameter  $b$  and an angle  $\alpha$  defining the plane of the collision, are selected randomly. From these two parameters and the initial velocities the post-collision velocities can be determined.

The collision sequence which results, combined with the streaming motion between collisions, provides an approximate solution of the Boltzmann Equation. Errors can be estimated and reduced by *increasing* the number of particles followed in each bin while simultaneously *decreasing* the bin sizes. Let us illustrate the velocity sampling technique for the simplest interesting situation, a spatial bin containing three identical hard spheres with total energy  $E = (1/2m)(p_1^2 + p_2^2 + p_3^2)$  and zero center-of-mass velocity,  $v_1 + v_2 + v_3 \equiv 0$ . We will show how to determine the *equilibrium* velocity distribution for such a bin. The solution of the Boltzmann equation is a continuous distribution, obtained from discrete particle dynamics by averaging. In a stationary problem the "average" is a *time* average for a single long simulation. In a transient problem the average must instead be carried out over *many* similar simulations with slightly different initial conditions. The present simple equilibrium problem is stationary, and can therefore be solved by generating a single long series of collisions. In the absence of external forces, velocity, and concentration gradients this requires only a statistical analysis of collisions. The Boltzmann-Equation collision rate for such a three-particle system is the sum of the three pair collision rates, with each of these proportional to the magnitude of the corresponding relative momentum:

$$p_{12} \equiv p_1 - p_2 ; p_{13} \equiv p_1 - p_3 ; p_{23} \equiv p_2 - p_3 .$$

Thus the pair  $ij$  can be selected with relative probability  $v_{ij}/(v_{12} + v_{13} + v_{23})$  where the  $v_{ij}$  are the speeds corresponding to the relative momenta.

For simplicity we choose to describe hard-sphere particles. As emphasized in Section 3, hard-sphere scattering is particularly simple because it is isotropic in the center-of-mass frame. If we use a random number  $R_1$  to select, for instance, Spheres 2 and 3 for collision, the velocities *after* collision define the endpoints of a randomly-oriented diameter of a sphere of radius  $(v_{23})/2$  centered at  $(p_2 + p_3)/(2m) \equiv -p_1/(2m)$ .

The two spherical polar angles  $0 < \theta < 2\pi$  and  $0 < \phi < \pi$  defining one of the two relative velocities can then be constructed from two random numbers  $R_2$  and  $R_3$ :

$$\theta = 2\pi R_2 ; \phi = \cos^{-1}(2R_3 - 1) .$$

The resulting velocity distribution can then be time-averaged, if the problem is a stationary state, or simply repeated (with different random numbers) if the problem is transient. The following outline indicates the steps necessary in a computer program generating the properly weighted velocity distribution for three particles, as just described.

1. Set speed bin weights all equal to zero.
2. Choose colliding pair of spheres.
3. Calculate time since last collision and add to bin weights.
4. Choose angles  $\theta$  and  $\phi$ .
5. Compute post collision velocities and return to Step 2.

The bin weights referred to in Step 3 are simply the (properly normalized) times which the particles spend in the bins. These relative times can be updated at each collision for all three particles.

In the equilibrium situation the resulting velocity distribution can be checked by a direct analytic calculation. If we describe the three sphere velocities  $\{v_1, v_2, v_3\}$  with the variables  $v_1$ ,  $\theta$ , and  $\phi$ , where the last two angles describe the velocities  $v_2 + (1/2)v_1$  and  $v_3 + (1/2)v_1$  as two endpoints defining the diameter of a sphere, centered at  $-(1/2)v_1$ , and with a radius  $[(E/m) - (3/4)v_1^2]^{1/2}$ , then the velocity distribution can be obtained by working out the integral:

$$\text{prob}(v)dv \propto (v^2 dv)(v'^2 dv')(d\theta \sin\phi d\phi) \delta\{[(E/m) - (3/4)v^2 - v'^2]^{1/2}\} ,$$

where  $v$  is the speed of Sphere 1. The integral can be evaluated by using the identity:

$$\delta\{[(E/m) - (3/4)v^2 - v'^2]^{1/2}\} / \delta\{v' - [(E/m) - (3/4)v^2]^{1/2}\} =$$

$$\partial v' / \partial \{[(E/m) - (3/4)v^2 - v'^2]\} \propto 1/v' ,$$

with the result:

$$\text{prob}(v)dv \propto (v^2 dv)[(E/m) - (3/4)v^2]^{1/2} .$$

In a *nonequilibrium* case the same sampling procedure can be used for the post-collision velocities but the trajectories must also be advanced *between* collisions by solving the ideal-gas equations of motion.

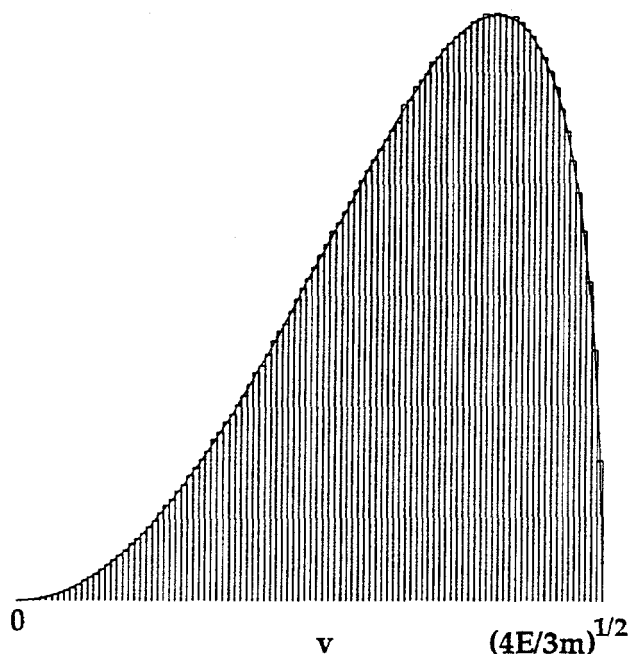


**Figure 9.9.** Velocity distribution for a three-sphere periodic system based on 10,000,000 equilibrium collisions.

**Problem:**

Use Monte Carlo sampling to generate a 10,000-collision histogram for the three-sphere equilibrium problem described in this section. Use 100 bins. Compare the resulting histogram of the distribution of sphere speeds  $\{\text{prob}(v)\Delta v\}$ , with the analytic result derived above,  $v^2[(E/m) - (3v^2/4)]^{1/2}$ . How should the errors compare to those shown in Figure 9.9, generated with ten million collisions? Show, analytically *and* numerically, that  $\langle v^2 \rangle = 2E/3m$ .

**9.9 Approximate Boltzmann Equation**

An accurate solution of the Boltzmann Equation for a real problem requires one of these integration or sampling techniques. But to understand the form of the equation's solution for linear problems of mass, momentum, and energy flow, a *linearized* Boltzmann Equation, called the "Krook-Boltzmann" Equation or the "Exponential-Relaxation" Equation, provides a useful labor-saving alternative:

$$\dot{f} = (\partial f / \partial t)_c = (\partial f / \partial t)_{\text{gain}} - (\partial f / \partial t)_{\text{loss}} \equiv (f_0 / \tau) - (f / \tau) = (f_0 - f) / \tau \equiv \dot{f}_{\text{KB}} .$$

Here the gain and loss terms are approximated by linear functions of  $f$  rather than the exact quadratic ones. The motivation for linearity is simplicity. At the same time it is "reasonable" to expect relaxation toward equilibrium to occur in a time of order the collision time  $\tau$ . Deviations from equilibrium are pictured as decaying due to interactions with a local-equilibrium bath described by  $f_0(\rho, \langle v \rangle, T)$ , where the density, stream velocity, and temperature are "local variables," functions of  $r$ . This simple picture is not far fetched. The rigorous Chapman-Enskog solution of the Boltzmann Equation proceeds by linearizing the deviations of  $f(r, p, t)$  about the local-equilibrium

distribution function  $f_0$  and computing the effect of collisions on the perturbation by using the equilibrium distribution of velocities.

The success of the Enskog approach shows that the relaxation process is linked to the collision time even in dense liquids. Such linear functions would by themselves provide exponential decay to the equilibrium distribution  $f_0$  in a collision time of order  $\tau$ . In any interesting problem the continuing influence of boundary conditions and the lingering effects of the initial spatial variation of  $f_0$  slow or prevent this decay. In solving the Krook-Boltzmann equation the equilibrium distribution  $f_0$  is to be worked out using the mean density, momentum, and energy at  $r$ . Likewise the collision time  $\tau$ , which governs the rate of approach to local equilibrium, can depend on these local variables as well as on the velocity. In our continuing pursuit of simplicity, we leave all of these refinements aside and assume that  $\tau$  is constant, equal to the time between collisions.

The same general thermodynamic and hydrodynamic conclusions follow from the Krook-Boltzmann equation as from the true Boltzmann Equation. If  $\dot{f}$  vanishes then  $f$  must have the equilibrium form,  $f_0$ . Furthermore, if we calculate the time derivative of  $\int \ln f$  in comoving Lagrangian coordinates, we can introduce the equilibrium entropy and find the Krook-Boltzmann analog of the H Theorem:

$$\begin{aligned} \dot{S}_{KB}/Nk &= -(1/N) \iint (d/dt)[\ln f] dp dr = -(1/N) \iint f[1 + \ln f] dp dr \equiv \\ &-(1/N) \iint \dot{f} \ln f dp dr = -(1/N) \iint (f_0 - f) \ln[f/f_0] dr dp / \tau > 0. \end{aligned}$$

The integral  $\iint (f_0 - f) \ln[f_0] dr dp$  vanishes because the moments of  $f$  are used to *define*  $f_0$ . The integral is included here to simplify the proof of the Krook-Boltzmann H Theorem.

In the following three Sections we apply this approximate Boltzmann equation to transport of mass, momentum, and energy in order to characterize the forms of the corresponding nonequilibrium distribution functions.

### 9.10 Diffusion

In a system at mechanical and thermal equilibrium, concentration gradients give rise to proportional currents described by two phenomenological relations called Fick's First and Second Laws of diffusion:

$$J = -D \nabla \rho ; \partial \rho / \partial t = D \nabla^2 \rho .$$

In the MKS system of units the mass current  $J$  is measured in kilograms per square meter per second. Notice that reversing the time changes the signs of  $J$  and  $\partial \rho / \partial t$  while leaving  $\nabla \rho$  and  $\nabla^2 \rho$  unchanged. Thus *both* of Fick's equations are irreversible. Fick's Second Law follows from the First provided that the *square* of the concentration

gradient is negligible. In that case the chain-rule concentration dependence of  $D$  can be ignored. To derive Fick's Second Law, it is sufficient to compute the time rate-of-change of the mass inside an Eulerian zone  $dx dy dz$ , by considering successively the flux differences across the  $x$ ,  $y$ , and  $z$  faces.

Fick's first law, that the mass flux  $J$ , is proportional to the density gradient, is an assumption. The reason for assuming a linear law, without including additional terms in  $\nabla^3 \rho$  for instance, can be seen by considering the equilibrium situation in which the concentration is uniform. Figure 9.10 shows a division of the distribution function for  $v_x$  into rightgoing and leftgoing parts. These two halves of the one-dimensional equilibrium Maxwell-Boltzmann distribution correspond to currents travelling at the one-dimensional distribution's mean speed,  $(2kT/\pi m)^{1/2}$ , about three-fifths the three-dimensional speed of sound  $(5kT/3m)^{1/2}$ . The fact that there is no noticeable mass flow at equilibrium is due to the balancing of these two huge currents. Away from equilibrium the situation is different. If the concentration varies slowly with  $x$  then the current flowing to the right past an Eulerian observation plane is slightly different from that flowing to the left, reflecting the difference in source concentrations.

Consider the Krook-Boltzmann Equation describing a time-independent concentration gradient, parallel to the  $x$  axis, in the absence of external fields:

$$\dot{f} = (\partial f / \partial t) + v \cdot \nabla f = (p_x / m)(\partial f / \partial x) = (f_0 - f) / \tau .$$

We imagine that locally  $f$  can be written as the equilibrium distribution,  $f_0$ , plus a first-order deviation  $\tau f_1$  where  $f_1$  is also a function of velocity:

$$f(r, p) = f_0(r, p) + \tau f_1(r, p) + \text{"higher-order terms"} .$$

This assumption is a reasonable one, even for a liquid, because  $\tau$  gives the timescale for the decay of nonequilibrium effects. As  $\tau$  approaches zero the Krook-Boltzmann form of the H Theorem guarantees that the equilibrium distribution,  $f_0(r, p)$  results. Close to

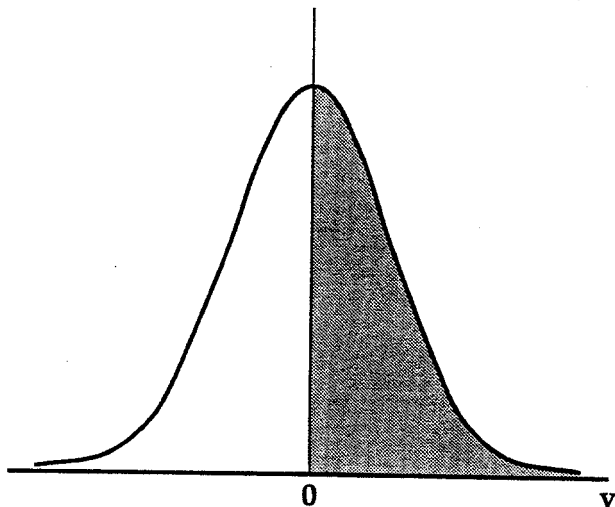


Figure 9.10. The average speed in each half of this one-dimensional velocity distribution is the mean speed,  $(2kT/\pi m)^{1/2}$ .

equilibrium the first nonvanishing term on the lefthand side of the Krook-Boltzmann Equation,

$$(p_x/m)(\partial f/\partial p)(dp/dx) \equiv (p_x/m)(f_0/p)(dp/dx),$$

must likewise approach the first nonvanishing term on the right,  $-f_1$ . Thus the *nonequilibrium* steady-state distribution function has the form

$$f = f_0[1 - \tau(p_x/m)d \ln p/dx + \dots].$$

We avoid estimating the higher-order terms because these would require a speculative discussion of boundary conditions. (It is evident, for instance, that a strictly constant gradient,  $dp/dx$ , leads either to nonsense or, to a boundary.) We come back to the question of well-posed nonequilibrium steady states in the next two Chapters.

But the linear deviation from the equilibrium distribution function already establishes most of the interesting results of linear transport theory. If we calculate the local mass current, by integrating  $fp$  over all  $p$  we find  $\langle J_x \rangle = -(\tau kT/m)(dp/dx)$  so that the Fick's-Law diffusion coefficient is:

$$D_{KB} = -J_x/(dp/dx) = (kT/m)\tau = (\pi/8)v^2\tau,$$

where  $v$  is again the mean speed  $(8kT/\pi m)^{1/2}$ . The Krook-Boltzmann diffusion coefficient can be compared to our free-path estimate  $D_{FP} = \lambda v/3$  by choosing  $v\tau = \lambda_M$ . The Krook-Boltzmann value then exceeds the Free-Path value by a numerical factor of  $3\pi/8$ . The true solution of the Boltzmann equation is somewhat higher. The analytic form of the true solution of the Boltzmann equation differs slightly from the Krook-Boltzmann form too. The perturbation  $\tau f_1(p)$  is the product of the equilibrium distribution and a *polynomial* in the velocity, rather than just a single linear term. But the terms beyond the first do not change the qualitative features at all. The main advantage of the Krook-Boltzmann equation is the relative ease with which qualitatively-correct nonequilibrium distribution functions can be found. Figure 9.11 illustrates the Krook-Boltzmann perturbation in two-dimensional velocity space.

Before going on to calculate the viscosity and heat conductivity from the Krook-Boltzmann equation we note that were we boldly to define a nonequilibrium entropy in terms of  $\langle \ln f_{neq} \rangle$  the first-order term in the expansion around  $f_0$  would vanish because entropy is a maximum at equilibrium. Because nonlinear terms require a discussion of boundary conditions and thermostats this means that we can draw no firm conclusions concerning a nonequilibrium entropy from the Krook-Boltzmann equation.

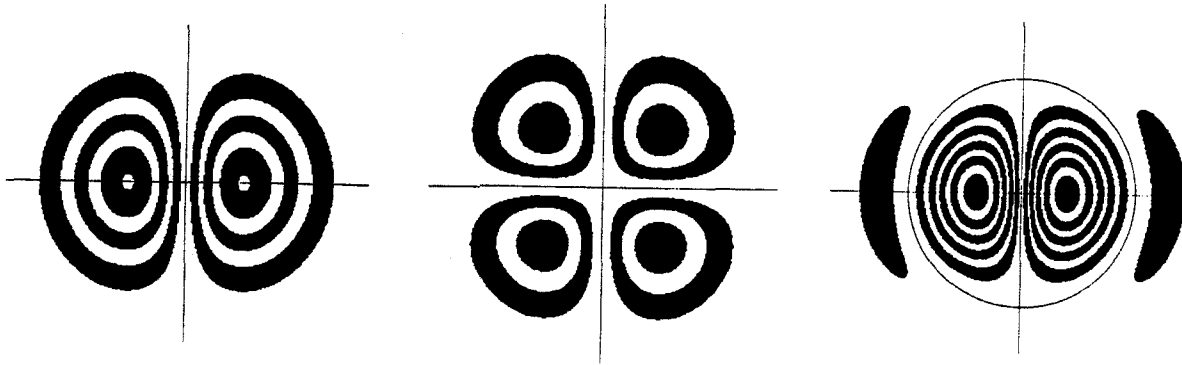


**Figure 9.11.** Velocity probability contours for the perturbation function  $f_1$ , from the nonequilibrium part of the Krook-Boltzmann equation. From left to right these represent diffusive, viscous, and heat-conducting flows. The functions displayed are  $x\exp(-r^2/2)$ ,  $xy\exp(-r^2/2)$ , and  $(x/2)(r^2 - 4)\exp(-r^2/2)$ . The width of the bands is 0.1. The data plotted span the range  $-4 < \{x,y\} < +4$ .

**Problem:**

Because concentration gradients in liquids relax toward equilibrium in much the same way as in gases it is reasonable to use the Krook-Boltzmann equation for analyzing liquid diffusion. But the collision time for the liquid is orders of magnitude shorter than that for a gas. Use the Debye frequency for ice, or an estimate based on the sound speed in water, to estimate an appropriate Krook-Boltzmann collision time  $\tau$  for liquid water. Compare the resulting self-diffusion coefficient to the room-temperature value,  $10^{-5}\text{cm}^2/\text{second}$ .

**9.11 Viscosity**

To find the Krook-Boltzmann distribution function for a viscous shear flow we consider the simplest steady flow field  $u_x = \dot{\epsilon}y$ . Near equilibrium the corresponding distribution function approximates the local-equilibrium form:

$$f_0(y,p) = (N/V)(2\pi mkT)^{-3/2} \exp(-[(p_x - my\dot{\epsilon})^2 - p_y^2 - p_z^2]/2mkT),$$

so that the lefthand side of the Krook-Boltzmann equation is

$$\dot{f} = (\partial f/\partial t) + (p_y/m)(\partial f/\partial y) \equiv 0 + (p_x p_y/mkT)\dot{\epsilon} f_0.$$

As usual close to equilibrium, the righthand side,  $(f_0 - f)/\tau$ , is just  $-f_1$ , establishing the result:

$$f_{KB} = f_0 + \tau f_1 + \dots = f_0 [1 - \tau \dot{\epsilon} (p_x p_y/mkT) + \dots].$$

The shear viscosity follows from the average of  $P_{yx} = P_{xy}$ :

$$-\dot{\eta}\dot{\epsilon} = P_{yx} = \int dp f_{KB}(p_x p_y / m) = -\dot{\tau} \int dp f_o(p_x p_y / mkT)(p_x p_y / m) = -\dot{\tau} \dot{\epsilon} p kT / m = -P \dot{\tau} \dot{\epsilon} ,$$

so that the shear viscosity is just the product of the pressure and the collisional relaxation time  $\tau$ :  $\eta_{KB} = P\tau$ . Again using the correspondence between Maxwell's Free Path and the collision time  $\tau$ ,  $v\tau = \lambda_M$  we find an increase over the free-path prediction,  $\eta_{FP}$ , of 18%. If we include the even larger viscosity from the Boltzmann Equation we find the values:

$$\eta = [0.120, 0.141, 0.179](mkT)^{1/2} / \sigma^2 ,$$

for the three approaches, free-path, Krook-Boltzmann, and Boltzmann.

The Krook-Boltzmann viscosity expression works well for air, where an atomic mass of 30 with a collision diameter of 0.3 nanometers results in a predicted room-temperature viscosity of 0.00022 poise, about 20% higher than the experimental value. For a liquid like water this gas-phase estimate would be much too low, by roughly a factor of 100. A much better estimate for water can be based on Andrade's idea that collisions transfer momentum a distance of one atomic diameter on a timescale of the Einstein vibrational period. For liquids this "collisional transport" is much more effective than the streaming mechanism described by the Boltzmann Equation and the Krook-Boltzmann approximation. Collisional transport is included, approximately, in Enskog's model for dense-fluid transport, discussed in Section 13.

### 9.12 Heat Conduction

The local-equilibrium distribution function for isobaric heat flow parallel to the x axis is,

$$f = [P/kT(x)][2\pi mkT(x)]^{-D/2} \exp[-p^2/2mkT(x)] ,$$

where  $P/kT(x)$  has replaced the number density  $\rho(x)/m$  to incorporate the constant-pressure condition required for mechanical equilibrium. Chain-rule evaluation of the lefthand side of the Krook-Boltzmann equation,  $\dot{f}$ , followed by linearization around the equilibrium distribution, yields the result:

$$\dot{f}_o = (\partial f / \partial T)(dT/dx)(p_x/m) = f_o(d \ln T / dx)(p_x/m)[(p^2/2mkT) - (D/2) - 1] ,$$

which is equal to the near-equilibrium righthand side,  $(f_o - f)/\tau \cong -f_1$ . The relatively intricate shape of the nonequilibrium part of the distribution function,  $\tau f_1$ , can be visualized from the contour plot shown in Figure 9.11 for the two-dimensional case. The heat current,  $Q_x = \int f(p_x/m)(p^2/2m)dp$ , can be worked out from corresponding fourth and sixth moments of the equilibrium velocity distribution function. This gives

$$\kappa = D(D + 2)\rho k(kT/m)\tau/6 = D\rho C_p(kT/m)\tau/3,$$

where  $C_p$  is the constant pressure heat capacity per particle,  $(D+2)k/2$ .

**Problem:**

Show the result just quoted for the heat conductivity.

Making the usual substitution for the collision time and including the exact hard-sphere conductivity in the three-dimensional comparison leads to the values,

$$\kappa = [0.150, 0.353, 0.678]k(mkT)^{1/2}/\sigma^2,$$

for the free-path, Krook-Boltzmann, and Boltzmann approaches.

**9.13 Enskog Model**

Enskog sought to modify the Boltzmann Equation to explain the transport properties of dense fluids. To a large extent he was successful. The Enskog "Model" provides transport properties lying within about a factor of two of the correct values for dense fluids. The model is a hard-sphere-based model incorporating two modifications of the low-density Boltzmann calculation of collisions. The modifications take into account two separate effects of high density. The first corrects the low-density N-particle equilibrium collision rate calculated from the Boltzmann Equation:

$$\Gamma_{BE} = [N(N - 1)(1/2)^{1/2}(8kT/\pi m)^{1/2}\pi\sigma^2/V],$$

increasing the collision rate by a multiplicative factor  $Y$  which follows from the Mayers' virial series:

$$Y = \Gamma(Nb/V)/\Gamma_{BE} = [1 + 0.625(Nb/V) + 0.28695(Nb/V)^2 + 0.1103(Nb/V)^3 + \dots].$$

The second equally-important modification depends on the finite size of colliding hard-sphere particles, "action at a distance." In the *dilute-gas* Boltzmann Equation the colliding particles with momenta  $p$  and  $p_1$  both represent the velocity distribution at  $r$ . In a *dense fluid* the density, stream velocity, and temperature can vary on the scale of an atomic diameter. When a Boltzmann-Enskog Particle at  $r$  undergoes a "loss collision" with a particle one diameter distant, at  $r_1 = r + \sigma$ , the corresponding "reversed-inverse" gain, collision described in Section 9.5, involves a particle with  $r'_1 = r - \sigma$ . We use the abbreviations  $+\sigma$  and  $-\sigma$  in the Enskog Equation to indicate these modifications:

$$\dot{f}_{\text{Enskog}} = \iiint dp_1 [Y(-\sigma/2) f' f'_1(-\sigma) - Y(+\sigma/2) f f_1(+\sigma)] v b d b d \theta .$$

$Y(r)$  is the ratio of the hard-sphere collision rate to the low-density rate calculated in Section 2. The collision rate is evaluated midway between the two colliding particles. In order to define this collision rate for a general force law, not just hard spheres, Enskog suggested matching the collisional part of the pressure for the fluid of interest, the "thermal pressure"  $P_{\text{Thermal}} \equiv T(dP/dT)_v$ , to the hard-sphere pressure. To do this an estimate for the effective hard-sphere diameter  $\sigma$  is required. An approximate diameter can be chosen by matching the high-temperature low-density second virial coefficient to the hard-sphere value,  $(2\pi\sigma^3/3)$ .

To solve Enskog's equation the remaining step is to expand both the relative collision rates  $Y$  and the  $f$ -functions in spatial Taylor's series by introducing the density and temperature gradients. When this is done the perturbed nonequilibrium distribution function  $f_1(r,p,t)$  turns out to be of exactly the same Boltzmann-Equation form as before, but multiplied by a linear function of the gradients. Likewise the nonequilibrium parts of the fluxes contain linear functions of the gradients. The net effect is to multiply the linear transport coefficients by explicit functions of the equilibrium collision rate ratio  $Y$ :

$$D/D_0 = 1/Y;$$

$$\eta/\eta_0 = [1 + 0.8bpY + 0.761(bpY)^2]/Y;$$

$$\kappa/\kappa_0 = [1 + 1.2bpY + 0.755(bpY)^2]/Y.$$

The quantitative importance of these corrections can be seen by considering the extreme case of a liquid at its freezing point. At the maximum density of the hard-sphere fluid, where freezing occurs,  $bp$  is 1.975 and  $Y$  is 5.8. The three contributions to the heat conductivity ratio  $\kappa/\kappa_0$  are respectively 0.17, 2.37, and 17.1. Half of the middle term is associated with kinetic contributions to the flux, and half with potential. Thus "collisional transport," the instantaneous transfer of momentum and energy from one colliding particle to another, accounts for almost all of the dense-fluid viscosity and thermal conductivity. Except in the case of diffusion, the streaming motion described by the Boltzmann Equation is relatively unimportant in dense fluids.

#### 9.14. Green-Kubo Theory

Only for dilute gases is the Boltzmann Equation correct. In dense fluids and solids an alternative approach to transport is required. Enskog's *model* lacks the potential for systematic improvement required of a theory. At present, there is no useful analytic theory of dense-fluid transport, so that computer simulation is required. An approach which makes use of *equilibrium* computer data to predict *nonequilibrium* properties is

the formal solution of linear transport theory obtained by Green and Kubo. The result of their approach is to express the linear nonequilibrium transport coefficients in terms of equilibrium correlation functions:

$$D = \int \langle v_x(0)v_x(t) \rangle_{\text{eq}} dt ;$$

$$\eta = (V/kT) \int \langle P_{xy}(0)P_{xy}(t) \rangle_{\text{eq}} dt = (V/4kT) \int \langle [P_{xx}(0) - P_{yy}(0)][P_{xx}(t) - P_{yy}(t)] \rangle_{\text{eq}} dt ;$$

$$\eta_V = (V/kT) \int \langle \delta P(0)\delta P(t) \rangle_{\text{eq}} dt ;$$

$$\kappa = (V/kT^2) \int \langle Q_x(0)Q_x(t) \rangle_{\text{eq}} dt .$$

All the time integrations range from 0 to  $\infty$ . The integrands are often called "autocorrelation" functions because they express the correlation of fluctuations of a single property at two different times. Because equilibrium correlations are stationary, these Green-Kubo correlations can depend only on the time *difference*,  $t$  in the integrals above. By saving velocity, pressure, and heat flux data from the recent past, perhaps ten collision times, and accumulating the correlation functions in bins, all four transport coefficients can be determined simultaneously.

The Green-Kubo results follow directly from the assumed linear forms of the underlying phenomenological laws. Fick's Law, for instance, establishes that the probability density for a group of particles in the range  $dx$  about  $x$  at time  $t$ , and initially at the origin at time zero, has a Gaussian distribution,

$$\text{Prob}(x)dx = (4\pi Dt)^{-1/2} \exp(-x^2/4Dt) ,$$

with a second moment  $\langle x^2 \rangle_{\text{eq}} = 2Dt$ . If we write the equilibrium average for  $\langle x^2 \rangle$  at time  $t$  as an integral over two dummy time variables,  $t_1$  and  $t_2$ , the result is an equilibrium correlation integral for the diffusion coefficient  $D$ :

$$D = (1/2t) \langle x^2 \rangle = (1/2t) \iint dt_1 dt_2 \langle v_x(t_1)v_x(t_2) \rangle_{\text{eq}} ,$$

where the maximum integration time  $t$  has to be long relative to the collision time. The double time integral can be reduced to the Green-Kubo form by carrying out the following three steps. First, notice that the *equilibrium* correlation between  $t_1$  and  $t_2$  can depend only upon the time *difference*,  $t_1 - t_2$  (equilibrium averages are stationary), so that the double integral can be replaced by a single integral over the *relative* time  $\Delta t = t_1 - t_2$ :

$$D = (1/2) \int d\Delta t \langle v_x(0)v_x(\Delta t) \rangle_{\text{eq}} = (1/2) \int dt \langle v_x(0)v_x(t) \rangle_{\text{eq}} .$$

Second, the finite time limits for the integration of the relative time variable  $\Delta t$  are formally replaced by  $\pm\infty$ . Finally, using the time-reversal symmetry of the equilibrium equations of motion reproduces the Green-Kubo final form, with integration limits of 0 and  $\infty$ :

$$D = \int \langle v_x(0)v_x(t) \rangle_{\text{eq}} dt .$$

This exact Green-Kubo form for the diffusion coefficient shows a close resemblance to the simpler inexact free-path and Krook-Boltzmann models. If we imagine that velocity correlations decay exponentially in time, with a characteristic collisional relaxation time  $\tau$  independent of the velocity, then the equilibrium autocorrelation integral can be worked out and the approximate diffusion coefficient evaluated:

$$D \approx \int \langle v_x(0)v_x(0)\exp(-t/\tau) \rangle_{\text{eq}} dt = (kT\tau/m) .$$

The result is the same as that derived from the Krook-Boltzmann equation.

Helfand showed that the shear-viscosity autocorrelation integral can be derived in an analogous way, by relating the shear viscosity to the long-time transverse diffusion of momentum:

$$\eta = (\rho/mkT) \langle x^2 p_y^2 \rangle / 2t .$$

To illustrate a different approach more closely related to the nonequilibrium methods discussed in Chapters 10 and 11 we begin instead with a many-body local-equilibrium distribution function, modelled on Gibbs' canonical distribution function:

$$f(\dot{\epsilon}, t=0) = \exp[-\{2m\Phi + \sum(p_x - my\dot{\epsilon})^2 + p_y^2 + p_z^2\} / 2mkT] / Z(N, V, T) N! h^{3N} .$$

If the boundary conditions include a steady shear flow, with  $\dot{\epsilon} \equiv du_x/dy$ , the *energy will increase*, with  $\Delta E(t) \equiv -\int P_{xy}(s)V\dot{\epsilon} ds$ , with the probability density  $f(t)$  unchanged, so that  $f_{\text{neq}}/f_{\text{eq}} \equiv \exp(\Delta E/kT)$ . If we then expand the distribution function about the equilibrium value, keeping no terms beyond the linear term of order  $\dot{\epsilon}$ , we find:

$$f(t) = f_{\text{eq}}[1 - (\dot{\epsilon}/kT) \int P_{xy}(s)V ds] .$$

In this way we can reproduce the remarkable result of Green and Kubo that the *nonequilibrium* pressure tensor component at time  $t$  can be written in terms of an *equilibrium* average:

$$\langle P_{xy}(t) \rangle_{\text{neq}} = -(\dot{\epsilon}/kT) \langle P_{xy}(t) \int V P_{xy}(s) ds \rangle_{\text{eq}} .$$

Then, by repeating the argument that equilibrium correlations can depend only on time *differences*,  $t-s$  in this case, the final form for the shear viscosity becomes the Green-Kubo result:

$$\eta = (V/kT) \int_0^\infty \langle P_{xy}(0)P_{xy}(t) \rangle_{eq} dt,$$

where the integration limits are 0 and  $\infty$ .

The corresponding calculation for *volume* deformation as opposed to *shape* deformation provides the equivalent formulation of the bulk viscosity. The bulk viscosity formula is obtained by replacing  $P_{xy}$  by  $\delta P$ , the deviation of the instantaneous pressure,  $(P_{xx} + P_{yy} + P_{zz})/3$ , from the long time average value. A relatively complicated argument establishes also the corresponding Green-Kubo link between the heat conductivity and the autocorrelation function of the heat flux.

In summary, even for dense fluids and solids, *all* the transport properties can be evaluated in terms of equilibrium time correlation functions. At present there is no technique for obtaining these correlation functions other than direct computer simulation. The transport coefficients can alternatively be evaluated by direct simulation of nonequilibrium flow processes. That approach is the subject of the next two Chapters.

### 9.15. Summary and References

Kinetic theory describes the effect of collisions on the flow properties of nonequilibrium dilute gases. The effect of collisions can be treated approximately, in terms of the mean free path, or exactly, by solving Boltzmann's Equation. These approaches establish that the shear viscosity and thermal conductivity have definite nonzero values for dilute gases. Enskog's approximate treatment of the increased collision rate in dense fluids provides semiquantitative estimates for the marked increases of viscosity and conductivity over the low-density values and the corresponding decrease of the diffusion coefficient.

The approximate Krook-Boltzmann equation, which assumes an exponential relaxation toward equilibrium, provides semiquantitative nonequilibrium distribution functions. Both this approximate approach and the Boltzmann Equation lead to H Theorems equivalent to the Second Law of Thermodynamics (but valid only for dilute gases). Despite the approximate nature of the Theorems' derivations they correctly identify collisions as the mechanism leading to chaos and irreversible behavior in nonequilibrium dilute gases. The Green-Kubo formulas express the *nonequilibrium* transport coefficients in terms of *equilibrium* autocorrelation functions. These expressions can be derived by considering the time evolution of small perturbations to the Maxwell-Boltzmann distribution function.

*Kinetic Theory*, by Present, supplements the standard works, Steve Brush's translation of Boltzmann's *Lectures on Gas Theory* (University of California, Berkeley, 1961), Chapman and Cowling's *Mathematical Theory of Nonuniform Gases*, and Hirschfelder, Curtiss, and Bird's *Molecular Theory of Gases and Liquids* (Wiley, New York, 1954). See Reif's *Statistical and Thermal Physics* for a good treatment of the approximate Boltzmann Equation. For the free-path calculations see T. Einwohner and B. J. Alder, "Free Path Distributions and Collision Rates for Hard-Sphere and Square-Well Molecules," *Journal of Chemical Physics* **49**, 1458 (1968). Alder and Wainwright's article describing the test of the H Theorem begins on page 97 of the 1956 Proceedings of the Brussels IUPAP Symposium on Transport Processes in Statistical Mechanics. Numerical solutions of the Boltzmann Equation have an extensive history. For an introduction see two recent papers in the *Physics of Fluids*: E. Meiburg, "Comparison of the Molecular Dynamics Method and the Direct Simulation Monte Carlo Technique for Flows around Simple Geometries," **29**, 3107 (1986), and G. A. Bird, "Direct Simulation of High-Vorticity Gas Flows," **30**, 364 (1987). Helfand's interesting derivation of the Green-Kubo expressions appears in "Transport Coefficients from Dissipation in a Canonical Ensemble," *Physical Review*, **119**, 1 (1960).

## 10. Introduction to Nonequilibrium Molecular Dynamics

*1 Introduction; 2 Forces in Nonequilibrium Molecular Dynamics; 3 Nonequilibrium Thermostats; 4 Liouville's Theorem Far From Equilibrium; 5 Divergence of the Nonequilibrium Steady-State Probability Density; 6 Fractal Distributions; 7 Irreversibility and the Second Law of Thermodynamics; 8 Summary and References*

### 10.1 Introduction

Gibbs developed equilibrium statistical mechanics, an exact microscopic prescription for analyzing the equilibrium thermodynamic properties of macroscopic systems. He showed that Boltzmann's Relation between thermodynamic entropy and the number of microscopic states,  $S = k \ln W$ , holds not just for dilute gases, but also for any conceivable equilibrium system. Gibbs' statistical mechanics is most easily applied to systems with independent or nearly-independent degrees of freedom, but numerical applications of his formulation can be extended to strongly-coupled degrees of freedom through systematic expansions such as the Mayers' density expansion and through ensemble-based perturbation theories developed to extend the usefulness of reference results from computer simulation.

Away from equilibrium no comprehensive logical foundation like Gibbs' exists to describe the states of nonequilibrium systems, even very small simple systems with only one or two degrees of freedom. To solve the dilute gas problem Boltzmann used a simplified version of dynamics in which correlations are ignored. His approach can be applied far from equilibrium, but only to gases. To solve the linear-response perturbation-theory problem Green and Kubo used equilibrium dynamics and equilibrium distribution functions as their basis. Green and Kubo's linear perturbation theory can be applied to any phase of matter, dilute or dense, but only close to equilibrium.

From the conceptual standpoint the *simplest* nonequilibrium system is a "steady state," a system driven away from equilibrium by stationary boundary conditions. Typical boundary conditions impose a specified mean velocity and a specified temperature on selected degrees of freedom. In order that these boundary conditions result in a *nonequilibrium steady state* the time-averaged values of chemical potential, velocity, or temperature must vary along the system boundary. Away from equilibrium these boundaries must provide at least one source and at least one sink of energy for a steady state to be achieved. All the simple classic problems of hydrodynamics, such as Couette flow, Poiseuille flow, and the Stokes Drag on a Sphere, are stationary nonequilibrium steady states. It is embarrassing that for this simplest kind of nonequilibrium problem, there is at present no applicable atomistic theory. In such a case there is no real alternative to solving the equations of motion, simulating nonequilibrium systems with nonequilibrium molecular dynamics. This is the simplest approach.

Why is it that a purely-theoretical treatment of nonequilibrium problems is so difficult? A clue is emerging from current research on chaotic systems. Chaotic

systems are characterized by the steady production of information called "sensitive dependence on initial conditions." The quantity of information so produced exceeds the content of any analytic theory. For this reason nonequilibrium studies necessarily focus on simulation as the simplest route to nonequilibrium behavior.

Nonequilibrium computer simulations have three useful roles to play: (1) providing the basic data through *computer experiments*, generally providing more details and greater accuracy than is available in laboratory experiments, (2) helping to identify and analyze causal mechanisms underlying the observed results of computer experiments and having analogs in laboratory experiments carried out far from equilibrium, and (3) suggesting conceptual approaches for developing necessarily-approximate theoretical treatments modelling these two kinds of experiments.

Unlike laboratory experiments, computer experiments are becoming steadily more elaborate without becoming more costly. The growth of transputer technology made it possible in 1989 to simulate nonequilibrium flows of as many as one million atoms. An enlarged portion of a single frame taken from a million-atom videotape appears in Figure 10.1. If the cost of a current "supercomputer" were invested in a machine based on SPRINT's design, it would make possible simulating systems with *billions* of particles using exactly this same technology. Along with such revolutionary advances in parallel computation, laboratory inventions such as the scanning-tunneling and atomic-force-balance microscopes are beginning to provide useful nonequilibrium flow information on the atomic level. The gap between the atomistic systems modelled in computer simulation and those being studied in current engineering practice is narrowing. Engineering processes by definition involve nonequilibrium systems. For this reason nonequilibrium molecular dynamics methods of simulation is playing a growing role in designing engineering materials processes. Because the simplest processes are steady ones, and because these lie well

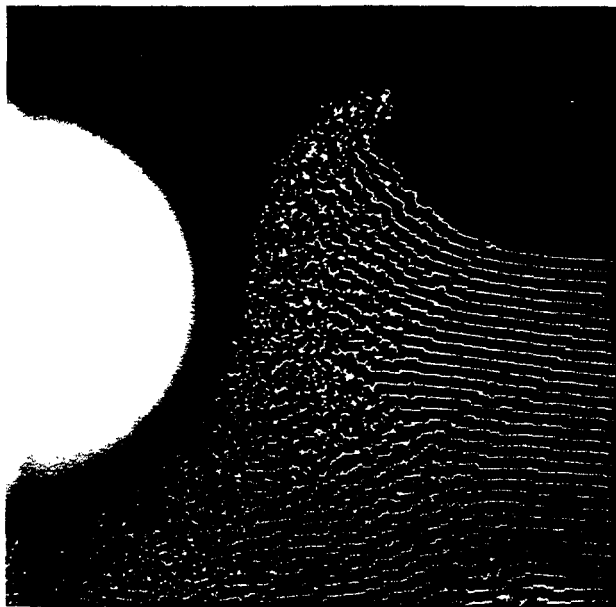


**Figure 10.1.** Portion of a six-day simulation, involving 1,036,800 atoms interacting with an embedded-atom potential typical of copper or nickel at half the melting temperature, carried out on Tony De Groot's SPRINT computer at the Livermore National Laboratory. Simulations of this kind are used to follow the rate-, force law-, and temperature-dependence of the plastic yield strength. Here a disk-shaped indenter is penetrating the surface of a crystal made up to 720 rows of 1440 atoms each.

beyond the capabilities of current theoretical understanding, we restrict our introductory study of nonequilibrium simulations to steady states.

Just formulating a nonlinear nonequilibrium problem requires new ideas. Heat needs to be treated explicitly. Boundary conditions, described by special equations of motion, are crucial, for it is these which make it possible to create and maintain a nonequilibrium state. Nonequilibrium molecular dynamics simulations require additional variables. In our kinetic-theory description of nonequilibrium systems we introduced gradients in concentration, velocity, and temperature and measured the resulting fluxes of mass, momentum, and energy, with neither the need nor the desire to identify their sources. In nonequilibrium simulations sources and boundary conditions must be specified explicitly.

The steady-state simulation techniques described in these two Chapters can readily be extended to spatially-varying time-dependent processes. In this Chapter we outline the ideas underlying simulations of nonequilibrium steady states. These simulations require a Nonequilibrium Molecular Dynamics, an extension of Newtonian mechanics incorporating driving and constraint forces, while also including the same deterministic reversible thermostats which we applied to equilibrium systems in Chapter 4. In this Chapter we describe the nonequilibrium techniques and point out their intimate connection to the Second Law of Thermodynamics. In Chapter 11 we provide detailed applications illustrating these ideas.

## 10.2 Forces in Nonequilibrium Molecular Dynamics

In discussing externally-driven nonequilibrium systems explicit mechanisms need to be introduced for performing mechanical work and transferring heat, the two fundamental energy-transfer mechanisms linking microscopic mechanics to thermodynamics. We seek a time-reversible deterministic description of nonequilibrium phenomena. Thus, away from equilibrium we expect that system variables necessarily include external coordinates, capable of doing work, and external heat reservoirs, capable of exchanging heat with selected system degrees of freedom. In such a nonequilibrium system the accelerations can be written in terms of the atomistic forces, boundary forces, constraint forces, and driving forces:

$$\dot{\mathbf{p}} = \mathbf{F}_A + \mathbf{F}_B + \mathbf{F}_C + \mathbf{F}_D.$$

The simplest system leading to interesting nonequilibrium steady states and involving all four types of forces is the Galton Board or Pachinko-Parlor Machine shown in Figure 10.2. For simplicity we use a two-dimensional Board with *periodic boundaries* so that the scattering particle cannot escape. A constant driving force  $F_D$  plays the role of gravity or an electric field, providing an energy source for the Board. A moderating constraint force  $F_C$  acts to keep the kinetic temperature of the system fixed so that the *direction*, but not the magnitude, of the velocity can vary. The scattering

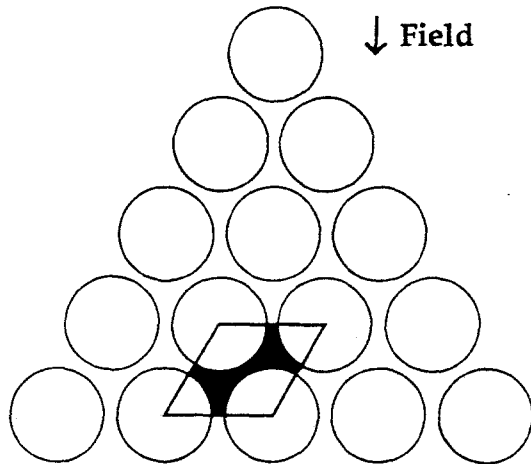


**Figure 10.2.** A portion of a periodic "Galton Board" in which a mass point scatters elastically from fixed scatterers in the presence of a vertical accelerating gravitational field. A parallelogram unit cell of the periodic structure is indicated. An alternative hexagonal cell is illustrated in Figure 11.3.

interaction can then be viewed either as a boundary force  $F_B$ , if we choose a coordinate frame fixed on one particle, or as an atomistic force  $F_A$  describing the collisional hard-disk interaction of the two particles in the alternative center-of-mass frame. We will return to this example system in Section 11.2. A snapshot of the steady-state Galton-Board phase-space distribution appears also in the present Chapter, in Section 10.5.

In many-body simulations "Atomistic" forces are derived from potential functions such as the hard sphere or Lennard-Jones-Spline pair potential or the many-body embedded-atom potential discussed in Section 5.4. The Boundary forces, Constraint, and Driving forces can be, but typically are not, explicitly time-dependent and typically change the number of independent variables in the dynamical description. Simple examples of driving forces include the external field inducing a current in the Galton Board and the external strain rate driving a homogeneous periodic shear flow. The same Nosé-Hoover or Gaussian friction coefficients used at equilibrium to simulate dynamics at a fixed temperature and pressure can just as easily be applied to nonequilibrium flows. Nosé-Hoover friction coefficients are additional system variables providing constraint forces. In driven constrained systems the phase space can be extended to include new variables such as  $\zeta_{NH}$  and  $\dot{\epsilon}$ , or can alternatively be contracted by imposing constraints on existing variables. Gaussian friction coefficients depend explicitly on phase-space coordinates and open no new regions in phase space. By choosing appropriate external forces together with boundary conditions describing imposed velocity or temperature gradients all of the classical flow situations described by Fick's Laws of Diffusion, Newtonian viscous flow, and Fourier's Laws of Heat Transfer can be, and have been, simulated.

By using special boundary regions, within which the velocity and temperature are specified, shear flow and heat flow can be simulated. The first extensive nonequilibrium steady-state simulations proceeded in this way in order to simulate laboratory experiments as closely as possible. Boundary regions separated from the system by walls were used, as shown in Figure 10.3. But the directional effects present at any wall impose an artificial geometric order, suggesting that *homogeneous* periodic

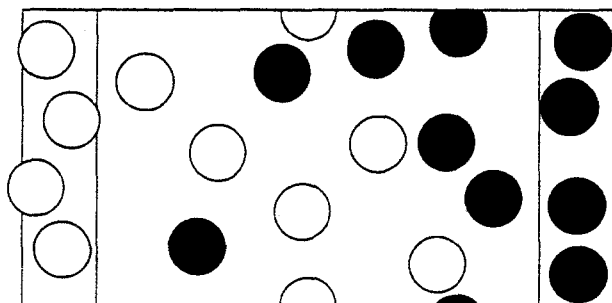


**Figure 10.3.** "Fluid Walls," as used by Ashurst to drive a shear flow. The mean velocity and thermal temperature in each fluid wall is maintained constant by Gaussian constraint forces. The black disks represent particles moving upward. The white disks represent particles moving downward.

flows should deviate less from the properties of macroscopic systems. With periodic boundaries it is easy to generate a particle current, or currents, using an external field. The simplest such field corresponds to a driving force  $F_D = \pm E_j$ , with half the particles accelerated in one direction and the remainder in the opposite direction.

It is likewise straightforward to implement periodically shearing boundary conditions, though care must be taken to keep the particle trajectories continuous as they cross the fictitious periodic boundary. The periodic dynamics must be independent of the location of this imaginary boundary. The simplest formulation of periodic shear flow proceeds by defining a "momentum"  $p$  based on a velocity measured relative to the local average stream velocity,  $\dot{\epsilon}y$ :

$$\dot{x} = (p_x/m) + \dot{\epsilon}y ; \dot{y} = (p_y/m) .$$

Provided that the strain rate  $\dot{\epsilon}$  is constant, the Newtonian equations of motion in the laboratory frame become:

$$m(d/dt)[\dot{x} - \dot{\epsilon}y] = \dot{p}_x = F_x - \dot{\epsilon}p_y ; \dot{p}_y = F_y .$$

The velocity-dependent force  $-\dot{\epsilon}p_y$  resembles a Coriolis force and describes the *apparent* horizontal acceleration, relative to the *local* stream velocity, resulting from vertical motion perpendicular to the streaming. These equations of motion simulate a nonequilibrium shear flow. We will see that an exact consequence of these nonequilibrium equations of motion is the Green-Kubo relation linking the nonequilibrium shear stress,  $-P_{xy}$ , to the corresponding autocorrelation function:

$$-\langle P_{xy}(t) \rangle_{\text{neq}} = (\dot{\epsilon}/kT) \langle P_{xy}(t) \int_0^t P_{xy}(s) ds \rangle_{\text{eq}} .$$

This relation is exact, even far from equilibrium, provided that the autocorrelation integral on the right hand side is integrated from time  $s = 0$  to time  $s = t$  using the *nonequilibrium* equations of motion given above. A cyclic homogeneous version of this approach, changing the *density* of the system, rather than the shape, as a function of time, with  $\dot{\rho} = \epsilon \rho \cos(\omega t)$ , provides the hysteretic response of bulk viscosity.

It is not so obvious how to induce a steady heat current in a periodic system. Gillan and Evans used an external field  $E_Q$  with a characteristic length  $\lambda$ :  $E_Q \equiv 1/\lambda$ . The field couples to individual-particle energy and pressure fluctuations and generates a heat current fully consistent with the exact linear-response theory of Green and Kubo:

$$\Delta \dot{p}_x = (1/\lambda)[\delta E + V\delta P_{xx}^\phi]; \Delta \dot{p}_y = (1/\lambda)[V\delta P_{xy}^\phi].$$

The  $\{V\delta P^\phi\}$  are the fluctuations of the individual particles' contributions to the potential part, indicated by a superscript  $\phi$ , of the pressure tensor. The  $\{\delta E\}$  are the fluctuating single-particle contributions to the internal energy:

$$\delta E_i = K_i - (K/N) + (1/2)\sum\phi(r_{ij}) - (\Phi/N); K_i = p_i^2/(2m); \sum\delta E_i \equiv 0.$$

If Gauss' Principle is applied to the heat-flow problem, by finding the least-constraint force which generates a heat flux  $Q$ , the resulting equations of motion wrongly include the complete pressure-tensor fluctuations,  $\delta P = \delta P^k + \delta P^\phi$ , not just the potential parts found in Gillan and Evans' correct prescription.

Close to equilibrium all of the nonequilibrium methods just discussed for generating diffusive, viscous, and conducting flows are fully consistent with the predictions of the Green-Kubo linear response theory. But these equations and the corresponding linear flows do not lead to nonequilibrium steady states. Instead the macroscopic irreversible increase in energy caused by the additional forces,

$$\dot{E} = +V(E_j/m)\langle J \rangle \text{ or } -\dot{\epsilon}VP_{xy} \text{ or } + (V/\lambda)\langle Q_x \rangle ,$$

causes each such nonequilibrium system to heat, so that the thermodynamic energy and temperature increase with time. For small deviations from equilibrium the heating rate is *quadratic* in the deviation from equilibrium, and typically very small for real flows. But in computer simulations the departure from equilibrium needs to be sufficiently large that the nonequilibrium fluxes can be distinguished from equilibrium thermal fluctuations. In computer simulations the resulting temperature increase serves to gradually reduce the influence of the driving field. The temperature increase would continue until the effect of the driving field became negligibly small relative to thermal fluctuations. If the temperature increase is slow enough, or can be made irrelevant by introducing appropriate scaled variables, then even such a nonsteady simulation can be used to generate correct transport coefficients. But an approach with the twin virtues of simplicity and elegance together with the additional promise of defining and treating nonlinear effects is to generate *nonequilibrium steady states* by using thermostats to stabilize a thermal variable such as internal energy or temperature. In the next Section we discuss the thermostats that make it possible to generate nonequilibrium steady-state flows of mass, momentum, and energy.

### 10.3 Nonequilibrium Thermostats

In the equilibrium simulations described in Chapter 6, temperature was controlled by imposing a Gaussian constraint on the kinetic energy of selected degrees of freedom or, alternatively, by using the Nosé-Hoover integral-feedback force to impose a canonical distribution. *Either* approach is effective provided that the system is sufficiently mixing to reach equilibrium. *Both* approaches provide phase-space distributions which can be analyzed with Gibbs' statistical mechanics. The time required to attain equilibrium is of considerable interest because there are cost advantages in speed. Unless it is specially desirable to follow the flow of heat through the system, the most efficient thermostat influences all of a system's degrees of freedom.

Thermalization could be accomplished by occasionally changing the velocity of one, or several, particles, choosing new velocities randomly from an appropriate Maxwell-Boltzmann distribution, or, alternatively, by applying a random force together with a corresponding fixed frictional drag force. In computation such "stochastic" probabilistic methods as these have drawbacks: the deterministic time-reversible character of the motion is destroyed, and with it, the constants of the motion crucial to checking numerical work; the stochastic irreversibility also complicates theoretical analyses based on the smooth phase-space flows satisfying Liouville's Theorem. Finally, the numerical reproducibility of reversible dynamics is a useful tool in comparing and validating computational results.

#### Problems:

1. Write and test a computer program to follow the motion of a particle in a periodic shear flow, with stream velocity  $u_x = \dot{\epsilon}y$ , and with horizontal "boundaries" at  $\{y_B\} = 0, \pm 1, \pm 2 \dots$ . Compute  $x$ ,  $y$ ,  $p_x$ , and  $p_y$  as functions of time and confirm that your numerical integration of the equations of motion provides a smooth continuous trajectory as the box boundaries are crossed.
2. Compare the period of the lowest vibrational frequency to the time required for heat flow across the system, both for system diameters of 10, 100, and 1000 atomic diameters. For the heat flow use Horrocks and McLaughlin's estimate for thermal diffusivity:  $\kappa / (\rho c_p) = v d^2$ , where  $v$  is the Einstein frequency,  $d$  is the interparticle spacing, and  $c_p$  is the heat capacity per unit mass.
3. Estimate the time required to reduce the kinetic energy of an  $N$ -particle harmonic chain by a factor of  $1/e$  by damping the motion of a single particle in the chain with a frictional force  $-\zeta p$ . Check this estimate by computer simulation for chains of 2, 4, 8, and 16 Hooke's-Law particles with initial velocities selected from a Maxwell-Boltzmann distribution. See page 152. What is the apparent number-dependence of the optimum value of  $\zeta$  for this specific damping force  $F(q,p) = -\zeta p$ ?

Gauss' Principle of Least Constraint provides a time-reversible method for maintaining a fixed kinetic temperature and the Nosé-Hoover thermostat similarly maintains, at equilibrium, a complete canonical distribution. Both these thermostat forces have time-reversible deterministic friction-coefficient forms:

$$F_C = -\zeta p; \zeta_{\text{Gauss}} = -\dot{\Phi}/(2K); \dot{\zeta}_{\text{NH}} = [(K/K_0) - 1]/\tau^2,$$

with the friction coefficients fluctuating with time.  $K$  is the kinetic energy of the degrees of freedom to which the Nosé-Hoover thermostat is applied and  $\Phi$  is the potential energy associated with these same degrees of freedom. The parameter  $\tau$  determines the timescale of the thermostat response. The frictional forces can be applied throughout a system, or solely within special boundary regions, such as those driving shear or heat flows. Frictional forces can be applied to individual particles or to individual degrees of freedom. By combining the driving forces described in Section 2 with these nonequilibrium thermostats we can simulate nonequilibrium steady states. In the following Section we analyze the corresponding phase-space structures.

### Problem:

In Section 3.12 we saw that the *extended* canonical distribution

$$f(q,p,\zeta) \propto \exp(-H/kT)\exp(-\zeta^2\tau^2/2)$$

is consistent with a *coordinate-weighted* thermostat applied to an arbitrary subset of the momenta  $\{p\}$ . Prove that this result can be further generalized to describe a thermostat which depends also on time:

$$\dot{p} = F(q) - \zeta p w(q,t); \dot{\zeta} = [(K/K_0) - 1]w(q,t)/\tau^2.$$

Notice that the distribution function is independent of the weight function  $w(q,t)$ .

### 10.4 Liouville's Theorem Far From Equilibrium

Because most of the state variables for nonequilibrium systems are the same as those used at equilibrium it is natural also to analyze nonequilibrium motions in a generalized phase space, extending or contracting the phase space, if need be, to include any strain rates, fields, or friction coefficients which vary with time and to satisfy any new constraints. In the corresponding extended or contracted phase space the continuous flow of probability density for any motion obeying differentiable equations of motion must still follow the phase-space continuity equation:

$$\dot{f} = -f(\partial\dot{\Gamma}/\partial\Gamma),$$

where  $\Gamma$  now represents *all* of the coordinates,  $\{q,p,\zeta,\dot{\epsilon},\dots\}$ , in the space. Phase-space flows following Hamilton's equations of motion must obey the equilibrium form of Liouville's Theorem,  $\dot{f} = 0$ , because the contributions to the righthand side cancel for

each coordinate and its conjugate momentum. Gauss', as well as Nosé and Hoover's, thermostat forces  $-\zeta p$  provide nonvanishing contributions to the righthand side because  $(\partial \dot{p} / \partial p)$  is minus the friction coefficient  $-\zeta$ . Thus for *either* of these forms of deterministic thermostatted mechanics the nonequilibrium analog of Liouville's Theorem is the instantaneous phase-space identity:

$$\dot{f} = \Sigma \zeta f \Rightarrow d \ln f / dt = \Sigma \zeta \equiv \Sigma -\dot{Q} / kT,$$

where the friction-coefficient sum is to be carried out over all thermostatted degrees of freedom;  $-\dot{Q}$  is a "power loss," the rate at which heat is extracted by the friction coefficient  $\zeta$  corresponding to the temperature  $T$ . As a corollary, the comoving probability density in the extended, or contracted, nonequilibrium phase space varies with time in accordance with the time-integrated total energy  $-\Delta Q$  extracted from the system by the thermostats:

$$f(t) = f_0 \exp(-\Delta Q / kT).$$

In the typical case, heat is extracted so that  $\Delta Q = \int \dot{Q} dt$  is negative and the probability density increases, indicating shrinkage of phase space volume. If heat were added the probability density would decrease, indicating expansion. This geometric identity relating phase volume and heat flow follows directly from the equations of motion for either form of thermostat.

To simulate any nonequilibrium steady state at least *two* links with the outside world are necessary. These can be sources or sinks of chemical energy, work, or heat. The last two of these possibilities have been thoroughly investigated, beginning with Ashurst's work on the simulation of viscous and heat conducting flows by introducing two "fluid walls" to exchange momentum and energy with a central Newtonian region. The constraints of fixed total momentum and energy in the wall regions were maintained by adjusting the velocities at the end of every time step in a way equivalent to applying Gauss' Principle of Least Constraint to the fluid-wall reservoir degrees of freedom.

A fixed external field, like gravity, can provide the necessary energy source to maintain a nonequilibrium flow. So long as the force  $F = F(q)$  depends only on coordinates, the corresponding contribution to the phase-space flow density,  $(\partial / \partial p)F(q)$ , is zero. Without a thermostat the equilibrium form of Liouville's Theorem:  $\dot{f} = 0$ , applies to such a flow.

Suppose the work-performing external field is time-dependent. Consider, for instance the corrugated moving wall shown in Figure 10.4, capable of doing work with a force  $F = F(q,t)$  depending upon both coordinates and the time. Even so  $(\partial / \partial p)F(q,t)$ , and hence  $\dot{f}$  are *still* both zero in the absence of heat reservoirs. By contrast, if heat is extracted by using *momentum*-dependent forces  $F = F(p)$ , then  $(\partial / \partial p)F(q,p,t)$ , and

likewise  $\dot{f}$  are both nonzero. Such a situation is typical of nonequilibrium molecular dynamics simulations of periodic systems with static coordinate-independent fields. An example is the Galton Board.

**Problem:**

Formulate Cartesian equations of motion for a mass point moving in the two-dimensional potential  $\phi(r,\theta) = (r^2/4)[2 + \cos(3\theta)]$ . Consider the nonequilibrium case in which the temperatures of the x and y motions differ.

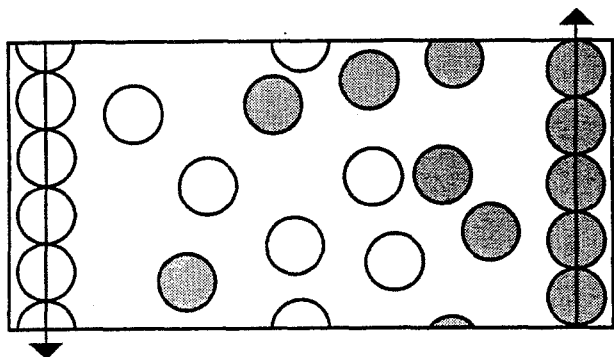


**Figure 10.4.** Shear flow induced by moving corrugated walls, equivalent to time-dependent boundary forces, generate a shear flow. The right (left) corrugations move up (down) at a fixed speed.

### 10.5 Divergence of the Nonequilibrium Steady-State Probability Density

What is a nonequilibrium steady state? A steady state can be characterized by properties which fluctuate about definite values, with the averages converging toward these values at long times. An isolated system, provided that its mechanics is sufficiently "mixing," eventually equilibrates and becomes an equilibrium system. A nonequilibrium system can be identified through its interactions with the external world. If the external world performs work upon and exchanges heat with such a system, or exchanges heat separately with distinct groups of degrees of freedom, then the system can achieve a nonequilibrium steady state distinguished from the time-independent equilibrium situation by nonequilibrium flows of mass, momentum, or energy. The flows can be described in either of two ways, in terms of the forces driving them, such as the external fields and external strain rates driving mass, momentum, and energy currents, or, alternatively, in terms of the steady values of these responding nonequilibrium currents. Thus a nonequilibrium steady state is characterized by a (time-averaged) stationary response to at least two fixed interactions with the outside world.

If such nonequilibrium steady states are achieved by using Gaussian or Nosé-Hoover thermostats then the phase-space probability density, according to the Liouville Theorem, *inevitably* behaves in a specific characteristic way, *diverging to infinity*. This divergence follows directly from the equations of motion:

$$\dot{f} = -f(\partial \dot{p} / \partial p) \equiv f \Sigma \zeta \Rightarrow d \ln f / dt = \Sigma \zeta ;$$

$$f(t) = f(0) + \int dt f(t) \Sigma \zeta(t) \Rightarrow \ln f(t) = \ln f(0) + \int dt \Sigma \zeta(t) \Leftrightarrow f(t) \equiv f(0) \exp[\langle \Sigma \zeta \rangle t] \Rightarrow \infty .$$

Provided that the friction coefficients have a time-averaged nonzero steady-state sum, both  $f$ , and its logarithm, necessarily diverge to infinity for long times. Because the product of phase-space volume and probability density is conserved, a negative time average for the friction-coefficient sum  $\langle \Sigma \zeta \rangle$  would imply an unacceptable infinite phase-space volume, and so would be incompatible with a bounded phase-space distribution. Thus, in steady states, nonzero friction implies overall positive friction,  $\langle \Sigma \zeta \rangle > 0$ . Both  $f$  and  $\ln f$  must diverge in any nonequilibrium steady-state flow.

This divergence of the distribution function corresponds to a breaking of Loschmidt's time-reversal symmetry: formally, any trajectory along which the probability density is increasing and the volume is contracting, could evidently be run backward in time. But because the backward motion would increase the occupied phase-space volume, such a reversed solution cannot be allowed in a nonequilibrium steady state.

### Problems:

1. Consider the one-dimensional motion of a point with unit mass in the potential  $\phi = -x - \cos x$  with a friction coefficient determined by the equation  $\dot{\zeta} = [p^2 - 1]$ . Determine the number of time steps for which this motion can be accurately reversed to the initial condition  $\{x, p, \zeta\} = \{0, 0, 0\}$  using the fourth-order Runge-Kutta method and time steps of 0.1, 0.01, and 0.001.
2. Use a centered-difference algorithm to solve the Stoermer analog of the problem described above. Notice that an extra value of the coordinate needs to be generated initially, as well as just prior to reversal, to guarantee the algorithm's mathematical reversibility.

This symmetry breaking exhibited by the nonequilibrium equations of motion is the "Arrow of Time" associated with the Second Law of Thermodynamics. For relatively short times the motion most easily occurs in such a way as to convert work to heat, not the other way around. For long times, in which a steady state is achieved, work *must* be converted into heat. The contrary motion is not a possible steady solution of the equations of motion.

From the mathematical standpoint, the long-time steady-state solutions correspond to distribution functions diverging exponentially in the elapsed time. The significance of these formal divergences was unclear until computer simulation revealed that the corresponding steady-state phase-space distributions are zero-measure fractal objects, occupying subspaces of their original equilibrium phase spaces. Figures 10.5 and 11.4 show examples. In the latter Figure successive phase-space cross sections, called Poincaré sections, are shown for an ensemble of mass points falling through a

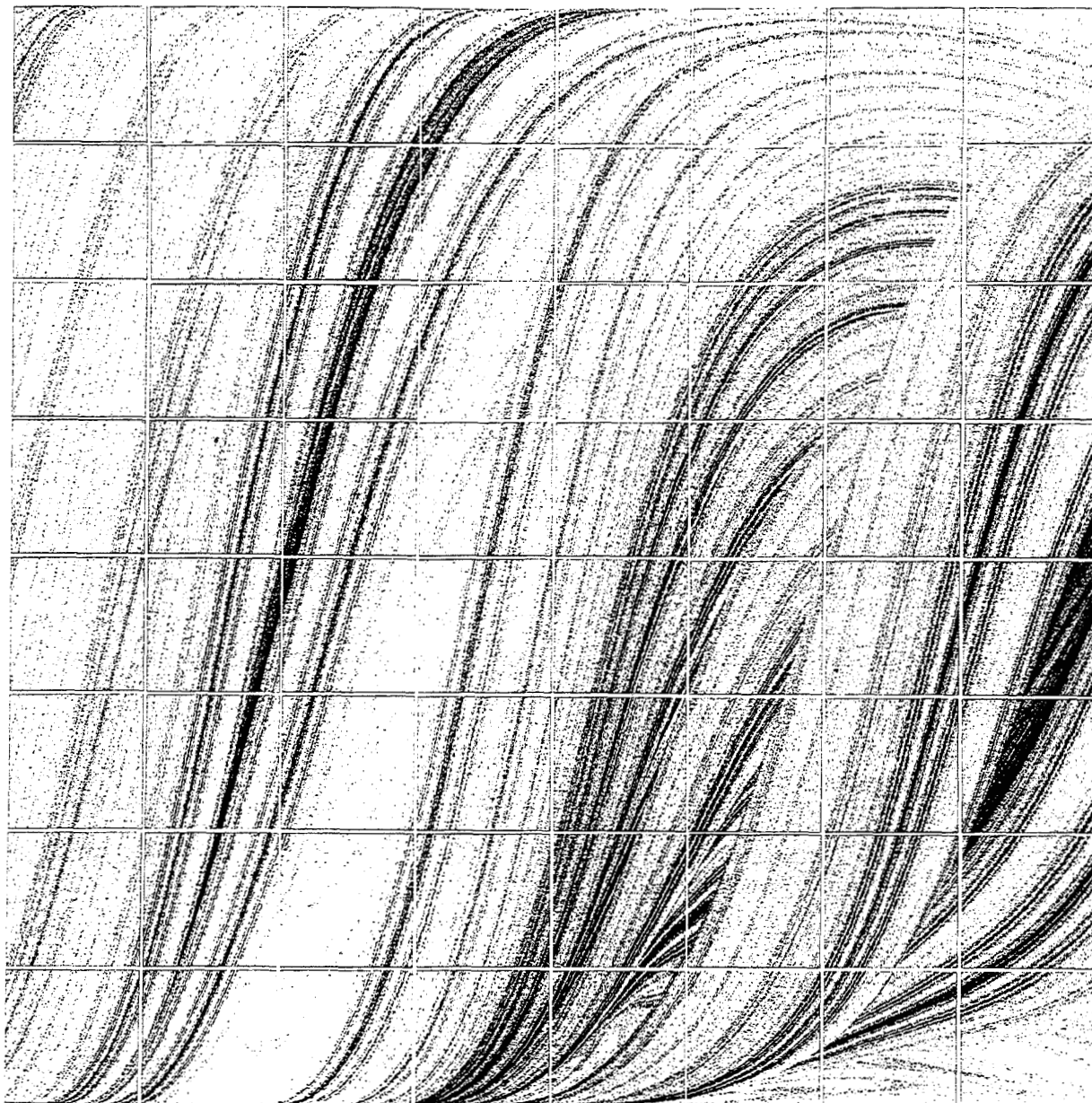


**Figure 10.5.** Poincaré section of phase space for the Galton Board with field strength equal to  $3p^2/m\sigma$ . The information dimension of this multifractal object is about 1.6. The dynamical *approach* to this structure is shown in Figure 11.4.

Pachinko-Parlor game's periodic triangular lattice of scatterers at fixed kinetic energy. The phase-space density description of the motion spreads out, reflecting Lyapunov instability, while simultaneously shrinking to a zero-volume fractal object.

At equilibrium such fractal states are not observable because their measure is negligible but away from equilibrium *only* these rare states can correspond to nonequilibrium steady states. The change from equilibrium to nonequilibrium is therefore not a simple one that can be described by perturbation theory. The phase-space geometry is fundamentally changed in a way which frustrates traditional analyses based on Taylor's-Series expansions.

## 10.6 Fractal Distributions

Because all nonequilibrium steady states lead to fractal phase-space structures we must discuss these objects. They are an integral part of nonequilibrium statistical mechanics. What is a fractal? To begin, "Fractal" distributions have a self-similar structure on all scales of observation, no matter how small. The distribution of points never becomes a continuous differentiable density function describable by the usual probability density. A classic example, based on the Cantor set, is the Sierpinski sponge shown in Figure 10.6. The sponge is constructed by first removing  $7/27$  of a unit cube by cutting three intersecting holes of square cross section normal to the cube faces. Next a second set of three square holes is centered in each of the remaining 20 smaller cubes. The process is then repeated on ever-smaller scales. Each succeeding set of holes reduces the remaining mass of solid material by a factor  $20/27$  so that the limiting mass of the sponge is zero.

In the zero-mass limiting case any enlarged version of any portion of the sponge reveals a corresponding infinite sequence of smaller-scale geometrically-similar models. If, for example, we choose a pair of the "ternary points" (see Problem 2 below) definitely in the sponge and separated by a vector  $r$  these two points correspond to 20 pairs of geometrically similar points separated by parallel vectors in cubes three times smaller and to 400 similar pairs in cubes nine times smaller in width than the originals. Had the sponge been a solid three-dimensional object rather than a fractal one, the number of such corresponding pairs would instead have been 27 and  $729 = 27^2$ .

Because this same scaling construction is valid for *every* pair of included points the number of pairs of such points lying within a distance range  $dr$  about  $r$  must vary as the  $\ln 20 / \ln 3 = 2.727$  power of  $r$ . That is, for small  $r_0$ , an increase in the scale of observation from  $r_0$  to  $3r_0$  reveals precisely 20 times as many pairs of points in the structure, so that  $d \ln N_2(r) / d \ln r$  is  $\ln 20 / \ln 3 = 2.727$ . Because this scaling relation holds at *all* sufficiently small scales the Sierpinski sponge is said to have a "fractal dimensionality" of  $D_2 = 2.727$ . For the sponge example we could instead consider

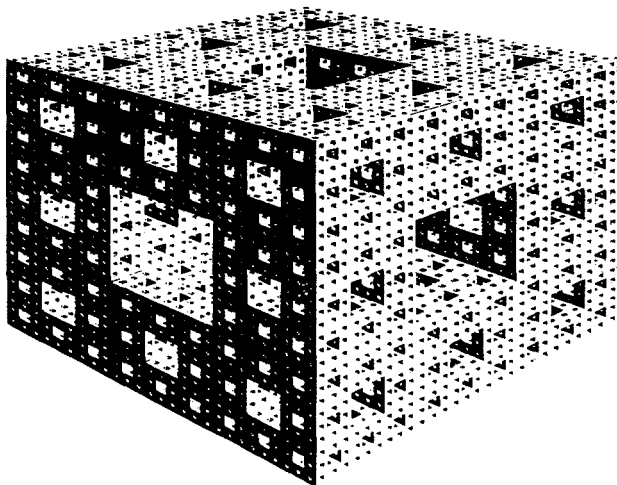


**Figure 10.6.** Sierpinski Sponge constructed by repeatedly boring square holes in a unit cube. The width of the  $n$ th generation of holes is  $(1/3)^n$ .

individual points, triples of points, quadruples, and so on, and exactly the same scaling relation, with the number varying as the 2.727 power of the scale, would apply. For any set of points in the sponge at one scale there are exactly 20 similar copies on a three-fold smaller scale. This simple scaling doesn't occur in the fractal objects generated in phase-space flows describing mechanical systems. In phase space the numbers of pairs, triples, quadruples, ... typically scale with different powers of  $r$  and the resulting distributions are said to be "multifractal." The corresponding set of fractal dimensions,  $\{D_1, D_2, D_3, D_4, \dots\}$ , depends on the number of points used to define it.

Figure 10.5 shows a typical cross section of a "multifractal phase-space object" generated by the steady-state field-driven Galton-Board flow described in Section 2 of Chapter 11. For this object the fractal dimensionality varies:  $D_1 = 1.81, D_2 = 1.58, \dots$ , down to zero, depending upon the number of points used to characterize it. The fractal nature of Lyapunov-unstable phase-space flows is a ubiquitous feature of nonequilibrium systems and furnishes the link between Lyapunov-unstable microscopic mechanics and the irreversibility characterizing phenomenological macroscopic thermodynamics. We discuss irreversibility in the following Section.

### Problems:

1. In constructing the Sierpinski sponge how does the *surface area* of the sponge depend on the number of holes cut?
2. Suppose that all locations in the unit cube are described in "base-3" form, so that the midpoint of the cube, for instance, is  $(0.111\dots, 0.111\dots, 0.111\dots)$  where  $0.111\dots$ , base-3, corresponds in decimal notation, to  $1/3 + 1/9 + 1/27 + \dots = 1/2$ . Show that points *in* the Sierpinski sponge must have  $x, y,$  and  $z$  coordinates with at most a single 1 in the  $d$ th digit of their expansion. That is, the base-3 point  $(0.21, 0.22, 0.20)$  is "in" the sponge but  $(0.21, 0.21, 0.20)$  is not.
3. Compute the fractal dimensionality of the Sierpinski carpet, the two-dimensional analog of the sponge shown in Figure 10.6.
4. Generate one hundred thousand pairs of "acceptable" randomly chosen points in the unit square. Acceptable points have at most a single 1 in the  $d$ th digit of their ternary expansions, as described in Problem 2 above. Plot the logarithm of the number of such pairs of points which lie within a distance  $r$  of each other as a function of the logarithm of  $r$ , using periodic boundary conditions for points near the "boundary" of the square. Is the fractal dimensionality consistent with that computed in Problem 3?
5. Consider two periodic Cantor-like sets, with each constructed by repeatedly removing the "middle third" and intersecting the other at an angle  $\theta$ , as shown in Figure 10.7. If each set has fractal dimensionality  $1 + (\ln 2 / \ln 3)$ , compute the fractal dimensionality of the intersection and union sets.

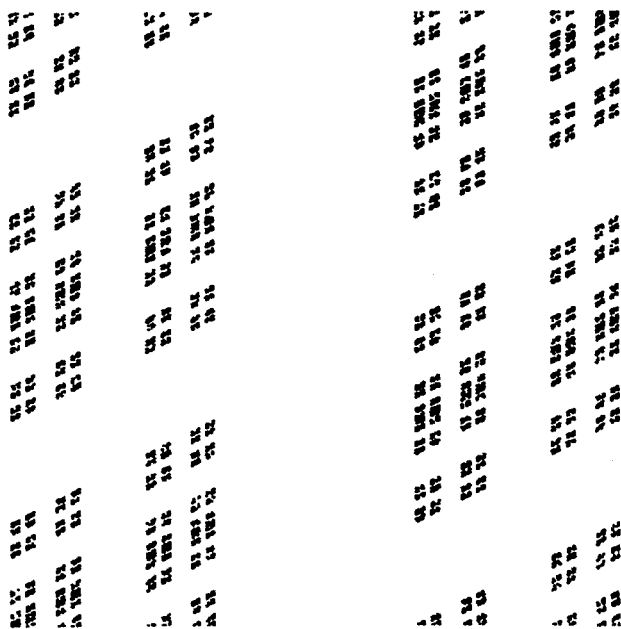


Figure 10.7. Two periodic Cantor sets crossing at an angle of  $\pi/3$ .

### 10.7 Irreversibility and the Second Law of Thermodynamics

The Second Law of Thermodynamics inexorably emerges from all steady-state nonequilibrium molecular dynamics simulations in a simple geometrical way, without the necessity for making any statistical approximations. *Only those dynamical evolutions which convert work into heat can be present in nonequilibrium steady states.* The common geometric characteristic of all these states is phase-space volume shrinkage in the comoving Lagrangian frame, leading ultimately to chaotic zero-volume strange attractors. This microscopic geometric property provides exactly the same thermodynamic predictions as does the macroscopic Second Law of Thermodynamics, to which it is equivalent.

Let us show the link between the equations of motion and thermodynamics in detail for the simplest possible case. Consider a system linked to two Nosé-Hoover heat reservoirs maintained at two different temperatures  $T_L < T_H$ . In the steady state the total heat transfer between the system and these reservoirs must vanish:

$$\langle -\Sigma \dot{Q} \rangle = \langle \Sigma \zeta(p^2/m) \rangle = 0 \Rightarrow$$

$$\langle \Sigma \zeta_H(p^2/m)_H \rangle + \langle \Sigma \zeta_C(p^2/m)_C \rangle = \langle \#_H \zeta_H(p^2/m)_H \rangle + \langle \#_C \zeta_C(p^2/m)_C \rangle = 0.$$

where the last two sums correspond to the time-averaged rates of heat transfer from the system to the hot and cold reservoirs. We use the abbreviations  $\#_H$  and  $\#_C$  to indicate the number of reservoir degrees of freedom. For either temperature, the Nosé-Hoover equations of motion for reservoir degrees of freedom,

$$\dot{\zeta}_T = \Sigma[(p^2/mkT) - 1]/\tau^2,$$

when multiplied by  $\zeta_T$  and time averaged, show that the average value of the product,  $\langle \sum \zeta_T (p^2/m)_T \rangle$ , can be replaced by the product of the averages:

$$\langle \zeta_T \dot{\zeta}_T \rangle = \langle (1/2)(d/dt)(\zeta_T^2) \rangle = 0 \Rightarrow$$

$$\langle \sum \zeta_C (p^2/m)_C \rangle = \langle \sum \zeta_C \rangle \langle (p^2/m)_C \rangle = \langle \sum \zeta_C \rangle kT_C = \#_C kT_C \langle \zeta_C \rangle ;$$

$$\langle \sum \zeta_H (p^2/m)_H \rangle = \langle \sum \zeta_H \rangle \langle (p^2/m)_H \rangle = \langle \sum \zeta_H \rangle kT_H = \#_H kT_H \langle \zeta_H \rangle .$$

Thus the steady-state condition for energy balance can be rewritten:

$$\langle kT_H \sum \zeta_H \rangle + \langle kT_C \sum \zeta_C \rangle = \#_H kT_H \langle \zeta_H \rangle + \#_C kT_C \langle \zeta_C \rangle = 0 .$$

At the same time, the geometric requirement that the occupied steady-state phase-space volume not diverge requires that the unweighted friction coefficient sum be positive,  $\#_H \langle \zeta_H \rangle + \#_C \langle \zeta_C \rangle > 0$ . The two simultaneous restrictions on the friction coefficients,

$$\#_H kT_H \langle \zeta_H \rangle + \#_C kT_C \langle \zeta_C \rangle = 0 ; \#_H \langle \zeta_H \rangle + \#_C \langle \zeta_C \rangle > 0 ,$$

taken together, can only be satisfied if the cold-reservoir coefficient  $\zeta_C$  is positive, and larger in magnitude than  $\zeta_H$ . In turn this requirement establishes that heat flows *out* of the system at the cold boundary and *in* at the hot, in agreement with Fourier's Law and with the Second Law of Thermodynamics. Similar demonstrations can be carried through for diffusive or viscous flows.

### Problem:

Show how to extend this microscopic demonstration of the macroscopic Second Law of Thermodynamics to nonequilibrium processes which are *periodic* in time rather than stationary.

For any nonequilibrium steady state including diffusion, viscous flow, or heat conduction, the motion inexorably develops in such a way that the probability collapses onto a (multi)fractal strange attractor obeying the Second Law of Thermodynamics and converting work into heat. This exact microscopic mechanical version of the Second Law of Thermodynamics applies to liquids and solids just as well as to gases. The only assumption is the use of a particularly-convenient form of heat reservoir, based on Gauss' or Nosé-Hoover equations of motion. It is clear that the nonlinear effects in systems with homogeneous thermostating forces depend on the details of the thermostats. On the other hand there is no evidence that properties of steady-state nonequilibrium systems with boundary thermostats depend significantly on the type of

thermostat used. This independence of bulk properties to surface effects is in fact what makes hydrodynamics a useful and reproducible description of nature. In elasticity theory, the corresponding observation that bulk elastic effects are (usually) independent of surface details is called "Saint Venant's Principle."

The microscopic equations of motion for a nonequilibrium system describe a phase-space flow linking together two topologically-similar but dynamically-dissimilar strange geometric objects, a phase-space "source," the repellor, and a phase-space "sink," the strange attractor. The existence of these nonequilibrium-steady-state strange attractors and repellors resolves Loschmidt's reversibility paradox discussed in Section 7 of Chapter 9. Although, as Loschmidt insisted, there are indeed states in the phase space which could violate the Second Law of Thermodynamics (states corresponding to time-reversed trajectories obeying that law) these states occupy a zero-measure fractal object, the "Strange Repellor," so that the possibility of finding such a state is not just small; it is exactly zero.

It is hard to visualize the complex topological structure of these objects in a many-dimensional phase space. Here we can only provide weak analogies with two-dimensional pictures or three-dimensional stereo views. To suggest the phase-space flow from a repellor to an attractor, consider the streamlines shown in Figure 10.8. The corresponding two-dimensional flow describes the progress of a one-dimensional particle with unit mass, moving along the  $x$  axis with momentum  $p$ . There is a constant accelerating field, of unit strength, and a Nosé-Hoover thermostating force. The corresponding equations of motion are these:

$$\dot{x} = p; \dot{p} = 1 - \zeta p; \dot{\zeta} = p^2 - 1.$$

The unstable fixed point at  $(p, \zeta) = (-1, -1)$  is the analog of a phase-space repellor, the *source* of the streamlines along which the motion occurs. Flow terminates at the analog of a phase-space attractor, the *sink* at  $(p, \zeta) = (+1, +1)$ . In many-body phase space, nonequilibrium flows originate in unstable multifractal repellor objects with dimensionalities of the same order as the dimensionality of the embedding space and then terminate on topologically similar attractors in which the momenta and friction coefficients have reversed signs. This last feature is shared by the two-dimensional example just outlined. Chaotic phase-space flows differ from this two-dimensional example in that they have no fixed points.

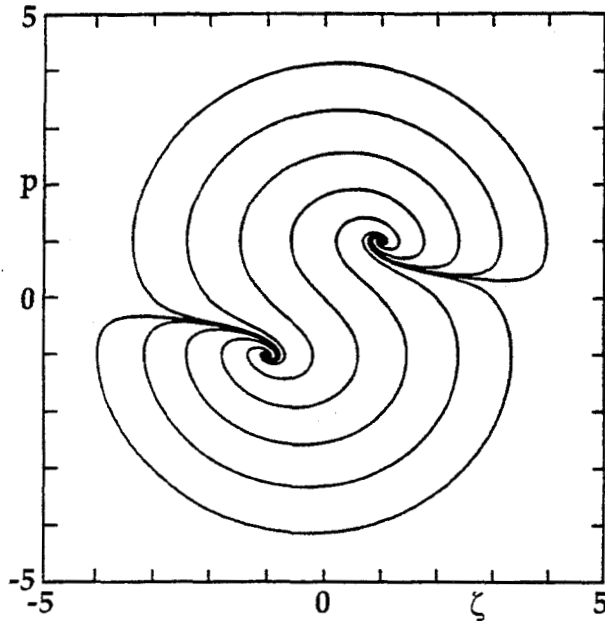


**Figure 10.8.** Streamlines in  $(p, \zeta)$  space for the differential equations:

$$\{ \dot{p} = 1 - \zeta p ; \dot{\zeta} = p^2 - 1 \}.$$

The flow links the repeller source at  $(-1, -1)$  to the attractor sink at  $(+1, +1)$ .

**Problem:**

For both fixed points of the set of equations  $\{ \dot{p} = 1 - \zeta p ; \dot{\zeta} = p^2 - 1 \}$ ,  $(-1, -1)$  and  $(+1, +1)$ , introduce new variables  $\Delta p$  and  $\Delta \zeta$ , where these new variables give the offset of a nearby point  $(p, \zeta)$  from the fixed point. Next linearize the differential equations in  $\Delta p$  and  $\Delta \zeta$ , ignoring terms of the second order in these offset variables. Finally, eliminate either  $\Delta p$  or  $\Delta \zeta$  from the equations to obtain a linear second-order equation for the remaining variable. Discuss the form of this equation in the vicinity of each of the two fixed points.

The strange attractor, to which steady nonequilibrium phase-space motions must collapse in obeying the Second Law, is aptly named. On it the Lyapunov exponents which describe the stability of the flow have a negative sum signifying compression of the flow. Nevertheless nearby trajectories separate exponentially fast from one another. It is this simultaneous collapse and divergence which makes these objects "strange". In the time-reversed repeller the signs of these exponents are reversed. Trajectories still separate, but the flow *expands*. The repeller is accordingly dynamically less stable than the attractor. That is, phase-space points close to it are generally repelled. It is these phase-space objects, the zero-measure strange attractor and corresponding repeller which provide reversible microscopic analogs for the irreversibility described by the macroscopic Second Law of Thermodynamics. By adopting a mechanical definition of heat reservoir based on the ideal-gas temperature scale we have derived the irreversible Second Law of Thermodynamics directly from time-reversible microscopic mechanics.

## 10.8 Summary and References

Nonequilibrium molecular dynamics typically includes atomistic, boundary, constraint, and driving forces. The extra forces make it possible to simulate diffusive, viscous, and heat flows with external fields, heat reservoirs, and time-dependent boundary conditions. The Green-Kubo theory of the transport coefficients is an exact formal analysis of the linearization of these simulations, and is valid for sufficiently small mass, momentum, and energy currents. The phase-space continuity equation,  $d\ln f/dt = \Sigma \zeta = -\Sigma \dot{Q}/kT$ , expresses the connection between the heat transfers maintaining a steady state and the changing size of a comoving phase space hypervolume: the product  $f(\Gamma)\Delta\Gamma$ , where  $\Delta\Gamma$  is a comoving phase-space volume element, is conserved by the equations of motion. In nonequilibrium steady states  $f$  diverges and  $\Delta\Gamma$  approaches zero. The corresponding steady-state limit is a zero-volume phase-space object, a (multi)fractal strange attractor. Time-reversed "repellor" states, which would violate the Second Law of Thermodynamics, can never be observed, because these repellor states are dynamically unstable and of zero measure. The microscopic mechanical basis of the Second Law of Thermodynamics is the Lyapunov-unstable strange-attractor dynamics of nonequilibrium steady states.

For an early review "Nonequilibrium Molecular Dynamics" see W. T. Ashurst and W. G. Hoover, *Advances in Theoretical Chemistry* 1, 1 (1975). See also my *Molecular Dynamics* (Springer-Verlag, Berlin, 1985). The paper by D. Farmer, E. Ott, and J. A. Yorke, "The Dimension of Chaotic Attractors," *Physica* 7D, 153 (1983) contains interesting examples and careful definitions of two of the many fractal dimensions. Applications of A. Chhabra and R. V. Jensen's method, described in "Direct Determination of the  $f(\alpha)$  Singularity Spectrum," *Physical Review Letters* 62, 1327 (1989), can be found in W. G. Hoover and B. Moran, "Phase-Space Singularities in Atomistic Planar Diffusive Flows," *Physical Review A* 40, 5319 (1989). The Sierpinski Sponge drawing is taken from B. B. Mandelbrot's *The Fractal Geometry of Nature* (W. H. Freeman, San Francisco, 1982). For a simple one-dimensional model with a fractal nonequilibrium distribution function see W. G. Hoover, H. A. Posch, B. L. Holian, M. J. Gillan, M. Mareschal, and C. Massobrio, "Dissipative Irreversibility from Nosé's Reversible Mechanics," *Molecular Simulations* 1, 79 (1987). The Galton Board multifractal attractors can be found in B. Moran, W. G. Hoover, and S. Bestiale, "Diffusion in a Periodic Lorentz Gas," *Journal of Statistical Physics* 48, 709 (1987). The connection of fractal phase-space distributions to the Second Law of Thermodynamics is discussed in B. L. Holian, W. G. Hoover, and H. A. Posch, "Resolution of Loschmidt's Paradox: The Origin of Irreversible Behavior in Reversible Atomistic Dynamics," *Physical Review Letters* 59, 10 (1987). This paper, with a different title and with the authors' names permuted, was twice rejected by Editor Basbas. See also W. G. Hoover, "Reversible Mechanics and Time's Arrow," *Physical Review A* 37, 252 (1988). This paper was rejected by Editor Lebowitz of the *Journal of Statistical Physics*.

# 11. Applications of Nonequilibrium Molecular Dynamics

*1 Introduction; 2 Diffusion; 3 Shear Viscosity and Yield Strength; 4 Heat Conduction; 5 Shockwave Structure; 6 Vibrational Relaxation; 7 Lyapunov Spectra; 8 Phase-Space Dimensionality Loss; 9 Summary and References*

## 11.1 Introduction

In this Chapter we describe applications of nonequilibrium molecular dynamics to simulations of mass, momentum, and energy flow in order to illustrate the basic techniques with examples. Because determining the structure of strong steady shockwaves is probably the simplest highly-nonlinear nonequilibrium fluid-flow problem with relatively simple boundary conditions, we choose to describe the corresponding simulations in detail. We also illustrate the application of nonequilibrium molecular dynamics to the calculation of molecular relaxation rates and describe a related method for the quantitative characterization of many-body phase-space flows through an accurate determination of the spectrum of Lyapunov exponents.

In choosing these examples for discussion we include many-body results together with the simplest possible illustrative few-body cases. This is not at all to suggest that small systems with one- or two-parameter pairwise-additive force laws are sufficiently complex to reproduce the quantitative properties of real materials. It is rather to emphasize that prior understanding of the behavior of small systems simplifies the simulation of the larger ones while saving both computer time and time spent analyzing results.

## 11.2 Diffusion

We have seen that the diffusion coefficient  $D$  in Fick's Second Law,  $\partial\rho/\partial t = D\nabla^2\rho$ , can be calculated in either of two equivalent ways: by measuring the equilibrium displacement history or by storing and integrating the corresponding equilibrium velocity autocorrelation function discussed in Section 9.14:

$$D = \langle x^2 \rangle_{\text{eq}} / 2t = \int ds \langle v_x(0)v_x(s) \rangle_{\text{eq}} .$$

In either case the sampling time  $t$  has to be long relative to the collision time responsible for destroying correlations by scattering. Qualitatively, velocity correlations decay in a time of order the collision time  $\tau$ :

$$\langle v_x(0)v_x(s) \rangle_{\text{eq}} \approx (kT/m)\exp(-s/\tau) ,$$

but this simple exponential form is an oversimplification. The correlation function must be *even* in the time and is not necessarily monotonic. In the solid phase, for which the diffusion coefficient is nearly zero, the negative and positive oscillations in the correlation function nearly cancel. The autocorrelation data are typically

unreliable beyond the time  $L/c$  at which  $\langle x^2 \rangle$  is perturbed by boundary soundwave reflections. Generally periodic boundaries are used in all spatial directions, but for some applications in materials science it is instead desirable to analyze diffusion on surfaces and interfaces.

The diffusion coefficient is usually measured by straightforward Newtonian molecular dynamics by averaging total particle displacements as a function of time, or, equivalently, by accumulating binned values of the velocity autocorrelation function  $\langle v(t)v(t+ndt) \rangle$ . For most calculations, the periodic boundaries discussed in Section 5.3 are used. If the displacements are to be measured it is simplest to ignore the periodic boundaries, allowing the particle coordinates to grow beyond the size of the box length  $L$ . In computing the forces from these wide-ranging coordinates the apparent distance component  $x_{ij} = x(i) - x(j)$  for a potentially-interacting pair of particles  $i$  and  $j$  needs first to be brought into the nearest-image range from  $-L/2$  to  $+L/2$ :

$$XIJ = XIJ + 100.0 * L - L * INT((XIJ + 100.5L) / L) ,$$

before the corresponding force is calculated. Because only *single-particle* coordinate changes are required the diffusion coefficient converges more rapidly than does either the viscosity or heat conductivity, which both reflect fluctuations in intrinsically many-particle properties.

The equilibrium diffusion calculation can be connected to nonequilibrium molecular dynamics through the Green-Kubo linear-response theory. That theory provides an exact link between the equilibrium position fluctuations  $\langle x^2 \rangle_{eq}$  and the nonequilibrium current  $\langle \dot{x} \rangle_{neq}$  induced by an infinitesimal external field  $E_J$  parallel to the  $x$  axis. Such an external field also provides a strictly-nonequilibrium method for defining and measuring the same coefficient outside the linear regime.

To see the connection between the current and the diffusion coefficient, imagine a field of strength  $E_J$  which accelerates half the particles in the positive direction and half in the negative direction, with  $F_D = \pm E_J$ , so as not to affect the center-of-mass velocity. We imagine that the field is turned on at time 0. After a time  $t$  has passed the field-independent internal energy of the system,  $E = \Sigma \phi + K$ , has changed (usually the change is an increase) by  $\Delta E = \Sigma \pm E_J \Delta x$ , where  $\Delta x$  is the distance moved in the field direction during the time interval  $\{0 \rightarrow t\}$ . As discussed in Section 10.4, Liouville's Theorem *still* applies to the motion, because the external force is velocity-independent, so that the system phase-space probability still has the original zero-time equilibrium value,  $f_0$ . But during the time interval  $t$  external work has changed the internal energy  $E = \Phi + K$  from  $E_0$  to  $E_0 + \Delta E$ . Thus the *nonequilibrium* probability density in phase space,  $f_{neq}(t) = f_{eq}(0) \propto \exp(-E_0/kT)$  exceeds the equilibrium value corresponding to the energy at time  $t$  by a multiplicative factor  $\exp(+\Delta E/kT)$ :

$$f_{neq}(t) = f_{eq}(0) = f_{eq}(t) \exp(+\Delta E/kT) ; \Delta E(t) = \Sigma \pm E_J \int ds v_x(s) .$$

The simple structure of this relation conceals the need to connect the phase-space coordinates at time  $t$  (upon which  $f_{\text{neq}}$  depends) to the phase-space coordinates at time zero (for which the equilibrium distribution  $f_{\text{eq}}$  is known to apply). This relation linking the phase-space densities at two different places and times is *exact* because the known equilibrium probability density depends only on energy. The phase-space location reached at time  $t$  depends not only on the initial phase-space coordinates but also on the strength of the external field  $E_J$ . We can use this exact *nonequilibrium* distribution to express the current at time  $t$  in terms of a nonlinear average over the equilibrium distribution function:

$$\langle J_x(t)V \rangle_{\text{neq}} = \langle \sum \pm m v_x(t) \rangle_{\text{neq}} = \int dq \int dp \left[ \sum \pm m v_x(t) f_0 \exp(+\Delta E/kT) \right] = \langle [J_x(t)V \exp(+\Delta E/kT)] \rangle_{\text{eq}},$$

where, in each of these four expressions, the dynamics leading to an energy increase  $\Delta E$  between times 0 and  $t$  is calculated *with the influence of the field  $E_J$  included*. If we then expand the exponential  $\exp(+\Delta E/kT)$  to find the linear part of the response we find directly the Green-Kubo autocorrelation form:

$$\langle J_x(t)V \rangle_{\text{neq}} = (1/kT) \sum \pm E_J \int ds v_x(s) m v_x(t) \rangle_{\text{eq}} \rightarrow [N^2/(N-1)] (m/kT) \sum E_J \int dt \langle v(0)v(t) \rangle_{\text{eq}},$$

so that the current is proportional to the *same* velocity autocorrelation integral  $\int dt \langle v(0)v(t) \rangle_{\text{eq}}$  that appears in the diffusion coefficient.

The factor of  $N^2/(N-1)$  is the final result of summing the positive and negative correlations from the equilibrium product of  $\sum \pm v_x(0)$  and  $\sum \pm v_x(t)$ . This two-time correlation of the current with itself involves  $N$  autocorrelation terms of the form  $v_{x1}(0)v_{x1}(t)$ . Of the remaining  $N(N-1)$  terms of the form  $v_{x1}(0)v_{x2}(t)$ ,  $N^2/2$  are multiplied by  $-1$  and  $(N^2/2) - N$  are multiplied by  $+1$ , contributing a net value for the linear current of:

$$N[v_{x1}(0)v_{x1}(t) - v_{x1}(0)v_{x2}(t)] = [N^2/(N-1)]v_{x1}(0)v_{x1}(t).$$

The two types of velocity correlations can be combined because the average value of  $v_{x2}$  is  $-v_{x1}/(N-1)$ , by conservation of total momentum.

Thus, the final result linking the linear conductivity  $\sigma$  to the diffusion coefficient  $D$  is:

$$\sigma = (J_x/E_J) = [N^2/(N-1)][Dm/kTV].$$

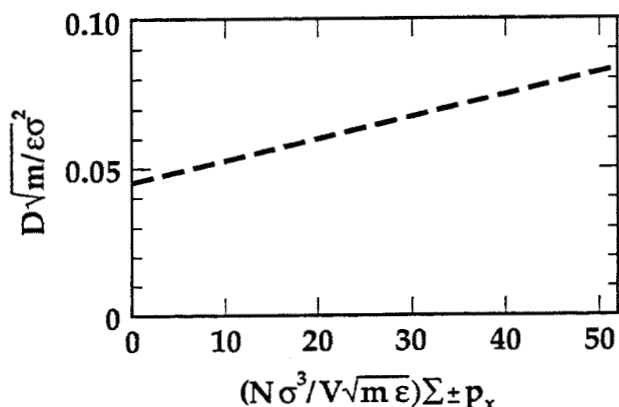


**Figure 11.1.** Nonequilibrium simulations of mass flow for a dense Lennard-Jones fluid at  $N\sigma^3/V = 0.85$  and  $kT/\epsilon = 1.08$ . The Green-Kubo theory gives the zero-field intercept exactly.

Figure 11.1 shows the result of a series of nonequilibrium simulations for a dense fluid of 108 Lennard-Jones atoms at relatively large fields. The small-field intercept gives the expected agreement with an independent Green-Kubo calculation, in agreement with the analysis just outlined.

To generate a nonequilibrium *steady state* it is only necessary that the energy from the field be extracted by using Nosé-Hoover thermostating forces:

$$\dot{p}_x = F_x \pm E_J - \zeta p_x; \dot{\zeta} = [(K/K_0) - 1]/\tau^2.$$

In three-dimensional problems the thermostat can be applied to one, two, or all three spatial directions and separate thermostats can be used for the positive and negative contributions to the mass current. Because the heating varies as the *square* of the current, all of these choices have no bearing on the linear response but each affects the definition and the numerical value of the nonlinear conductivity. Notice that the equations of motion are *time reversible*, with  $p$  and  $\zeta$  both changing sign on a reversed trajectory while the coordinates, field, forces, and energies are all unchanged.

Although the internal energy is no longer a constant of the motion in the presence of thermostats it is always possible to define an analogous potential which is a constant of the motion. This furnishes a useful check of the computer simulation. For the one-dimensional equations of motion just given the time derivative of  $[\Phi + K + (\#kT/2)(\tau\zeta)^2 + \int ds(\#kT\zeta(s) - (E_J/m)V_{J_x}(s))]$  is identically zero. This follows from the equations of motion:

$$(d/dt)[\Phi + K + (\#kT/2)(\tau\zeta)^2 + \int ds(\#kT\zeta(s) - (E_J/m)V_{J_x}(s))] =$$

$$\Sigma - F(p/m) + \Sigma(p/m)(F \pm E_J - \zeta p) + \#kT(\tau^2\dot{\zeta})[(K/K_0) - 1]/\tau^2 + \#kT\dot{\zeta}(t) - (E_J/m)V_{J_x}(t) = 0.$$

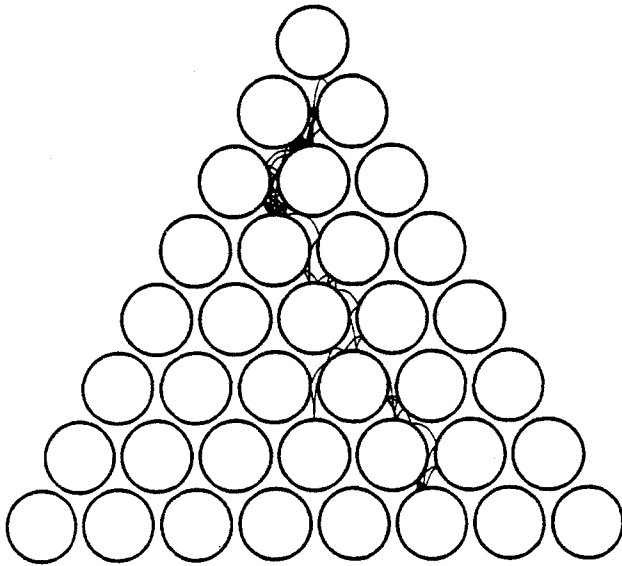


**Figure 11.2.** Portion of a Galton Board illustrating a sequence of 99 collisions for a field strength of  $E_J = 4(p^2/m\sigma)$ . The kinetic energy of the falling particle,  $p^2/2m$ , is maintained constant by using a Gaussian thermostat. The scatterer density is  $4/5$  the close-packed density.

If the Runge-Kutta method is being used to integrate the equations of motion the two integrands  $\{\#kT\zeta(s)$  and  $-(E_J/m)V_{J_x}(s)\}$  can simply be added to the list of differential equations being integrated.

The differential equations for this field-driven flow obey the Second Law of Thermodynamics in the way outlined in Chapter 10. That is, the phase-space representation of the dissipative many-body dynamics, in the process of converting work (from the field) into heat (extracted by the frictional reservoir forces) collapses to occupy a multifractal strange attractor in phase space. In order to visualize such a phase-space flow it is useful to study a much smaller problem, the isokinetic Galton Board shown in Figure 11.2. A related shear-flow example is discussed in Section 11.3.

The fractal nature of the distribution function for a diffusive flow can be seen explicitly in the Galton Board phase space. In that problem a single mass point travels through a fixed array of elastic hard-disk scatterers. If the equations of motion are chosen to keep the kinetic energy fixed, with the field  $E_J$  in the  $x$  direction, the equation of motion for the momentum can conveniently be written in terms of the polar angle  $\theta$  giving the *direction* of motion relative to the field direction. With the *magnitude* of the momentum fixed and equal to  $p$ , this polar-coordinate *isokinetic* equation of motion is:

$$\dot{\theta} = -(E_J/p)\sin(\theta) + (\partial\theta/\partial t)_c,$$

where  $(\partial\theta/\partial t)_c$  describes the impulsive change of the moving mass point's momentum associated with the elastic hard-disk scatterer collisions.

### **Problems:**

1. Show that *between* collisions the Galton Board equation of motion,  $\dot{\theta} = -(E_J/p)\sin(\theta)$  results if the Cartesian isokinetic equations of motion:

- $\dot{p}_x = E_J - \zeta p_x$ ;  $\dot{p}_y = -\zeta p_y$ ;  $\zeta = E_J p_x / p^2$ , are rewritten in *polar* velocity coordinates, with  $p_x = p \cos(\theta)$  and  $p_y = p \sin(\theta)$ .
2. Relate the solution of these equations of motion to the solution of a slightly-different but equivalent problem, the acceleration of two similar hard disks in opposite directions in a system with periodic boundary conditions, zero center-of-mass velocity, and a fixed kinetic energy.
  3. Derive the *spherical* polar-coordinate equations of motion for the three-dimensional analog of the Galton Board. Choose the field direction parallel to the direction  $\phi = 0$ .

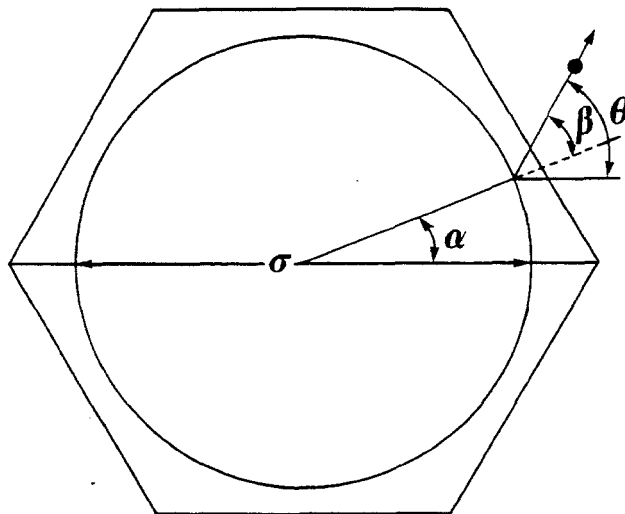
The equation of motion between collisions can be integrated analytically to find the trajectories:

$$\Delta x = - (p^2 / m E_J) \ln[\sin(\theta) / \sin(\theta_0)] ; \Delta y = - (p^2 / m E_J) (\theta - \theta_0) ;$$

$$\Delta t = - (p / E_J) \ln[\tan(\theta/2) / \tan(\theta_0/2)] ,$$

where the vector describing the distance traveled during the time interval  $\Delta t$  between successive hard-disk collisions has components  $\Delta x$  and  $\Delta y$  while the velocity direction changes from  $\theta_0$  to  $\theta$ . The intersection of the analytic trajectory with the force field of the succeeding scatterer can then be found by a rapidly-converging iterative process. Figure 11.2 shows a sequence of 99 collisions constructed in this way. Successive Galton-Board collisions can be calculated at the rate of about  $10^7$ /hour on a CRAY-1 computer and used to produce phase-space strange-attractor cross sections such as those shown in Figure 10.5 for a field strength of  $E_J = 3(p^2 / m\sigma)$ . (See Sections 10.5 and 10.6). The coordinate system describing each collision is based on two angles,  $\alpha$  and  $\beta$ . The location of each collision relative to the field direction is specified by  $\alpha$ ; the direction of motion following each collision, relative to the normal, is given by an angle  $\beta$ . See Figure 11.3.

**Figure 11.3.** Definitions of the configurational angle  $\alpha$  and the exit velocity angle  $\beta$  for a Galton Board collision. The direction of the particle velocity relative to the external field is described by the angle  $\theta$ .



Analysis of such patterns of successive collisions, measuring the number of pairs of attractor points separated by a distance less than  $r$ , provided the first clear evidence for the *fractal* nature of nonequilibrium phase-space distributions. In the attractor approached in Figure 11.4 the number of pairs of attractor points lying within a range  $r$  of each other varies as  $r^{1.6}$ . For field strengths up to that used in generating Figures 11.2 and 11.4,  $E = 3p^2/m\sigma$ , numerical work indicates that, despite the reduced dimensionality of the strange attractor, *all* parts of phase space are included in the fractal strange attractor. The equivalent zero-field two-disk system is known to be ergodic in its equilibrium configuration space. Evidently this ergodicity holds also in the nonequilibrium steady state generated by small-to-moderate fields. For somewhat higher field strengths the motion is no longer ergodic.

**Problem:**

Consider a Galton Board problem with a field strength  $E_j = 4(p^2/m\sigma)$  parallel to the  $x$  axis. The area of the scatterer lattice is expanded 25% from the the minimum (close-packed) area. There is a *stable* limit cycle in which a moving mass-point particle can bounce periodically between two neighboring scatterers of diameter  $\sigma$ . Show this surprising result by considering two scatterers, with  $x$  coordinate  $(3/4)^{1/2}(5/4)^{1/2}\sigma$  and  $y$  coordinates  $\pm(1/2)(5/4)^{1/2}\sigma$ . Find the corresponding values of the angles  $\alpha$  and  $\beta$  to an accuracy of 0.01 by developing a "shooting technique," with the mass point initially located on the positive  $x$  axis and moving in the  $y$  direction with speed  $p/m$ .

**11.3 Shear Viscosity and Yield Strength**

Green-Kubo linear response theory expresses the shear viscosity  $\eta$  in terms of an equilibrium pressure-tensor autocorrelation function:

$$\eta = (V/kT) \int dt \langle P_{xy}(0)P_{xy}(t) \rangle_{eq}.$$

In Section 10.2 we saw that this same expression is the exact linear approximation to the results of nonequilibrium molecular dynamics simulations in which the boundary conditions impose a steady shearing motion, with the systematic motion in the  $x$  direction proportional to the  $y$  coordinate,  $\langle v_x \rangle = \dot{\epsilon}y$ . The corresponding periodic shear can be viewed either in terms of sliding rectangular cells or as a homogeneous oblique shear. The first of these two alternatives is the simpler to program because it avoids the nuisance of defining time-varying oblique coordinates and periodically resetting them. See Figure 11.5.

In the simpler Cartesian case the equations of motion in a fixed laboratory frame describing the motion in the central rectangular cell are:

$$\dot{x} = (p_x/m) + \dot{\epsilon}y ; \dot{y} = (p_y/m) ; \dot{p}_x = F_x - \dot{\epsilon}p_y ; \dot{p}_y = F_y,$$

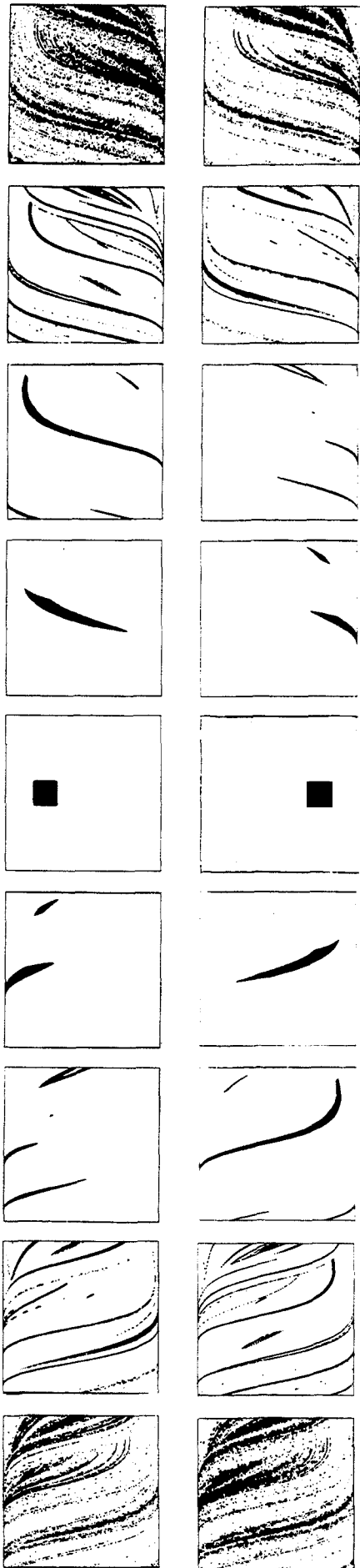
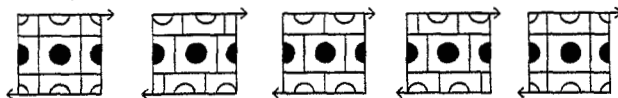
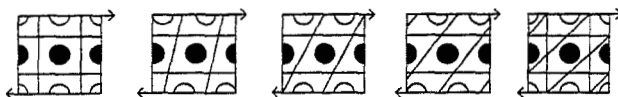


Figure 11.4. Evolution of two Galton Board ensembles toward the strange attractor for a field strength  $E = 3(p^2/m\sigma)$ . The initial ensembles, shown at the center, are displayed again after  $\pm 1, \pm 2, \pm 4,$  and  $\pm 8$  collisions. The Poincaré sections going *upward* from the center correspond to progressing *forward* in time. The sequence of sections eventually converges the steady-state multifractal "strange attractor." Going backward in time (*downward* in the Figure) the two ensembles approach instead the multifractal *repellor* which is the (time-reversed) mirror image of the attractor. In the same Figure we include the *time-reversed*  $\{\alpha, \beta\}$  trajectories for both ensembles of points. Each trajectory has been followed *backward* in time for 1, 2, 4, and 8 collisions. A comparison of this reversed evolution with the forward development verifies the reversibility of the underlying equations of motion. The reversibility of the equations corresponds to reversing the sign of the momentum. For any initial distribution symmetric about the  $\sin\beta$  axis [the horizontal axis in this view of the Poincaré sections] the development backward in time would provide an exact mirror-image of the forward development. For the asymmetric distributions shown in the Figure the symmetry is lost, but, as the Figure suggests, the longtime limiting solution is nevertheless the same, a set of "strange attractor" points in the forward direction, and a corresponding mirror-image set of "strange repellor" points in the backward direction of time.

In the *nonlinear* case shown here the distribution function  $f$  diverges, exponentially fast, as the integrated current strength,  $f/f_0 \equiv \exp[\langle \zeta \rangle t] = \exp[\int dt J_x(t) V(E_f/mkT)]$ , so that the comoving phase-space volume shrinks rapidly to zero despite the reversibility of the equations of motion. This Figure illustrates the development of two distinct sets of 10,000 separate initial conditions toward the strange attractor cross-section characterizing the steady state. In both cases the average current associated with the last picture lies within a percent of the steady-state value.



**Figure 11.5.** Two equivalent methods for describing a periodic shear flow. The Cartesian description is the simpler of the two.



where  $F_x$  and  $F_y$  are the usual components of the Newtonian atomistic forces due to collisions. The shearing periodic boundaries imply that vertically-displaced periodic images of each particle at  $y \pm L$  move with a strain-rate and coordinate-dependent horizontal velocity component,  $(p_x(y)/m) \pm L\dot{\epsilon}$ . If we define the internal energy  $E$  as the comoving Lagrangian energy, that part of the energy which is independent of the boundary motion,  $E = \Phi(\mathbf{r}) + K(\mathbf{p})$ , then the internal energy change with time  $\dot{E}$  has the form expected from the First Law of Thermodynamics,  $\dot{E} = -\dot{W}$ . This conclusion follows directly from the equations of motion:

$$\begin{aligned} \dot{E} &= \dot{\Phi} + \dot{K} = -\Sigma \mathbf{F} \cdot \dot{\mathbf{r}} + \Sigma (\mathbf{p}/m) \cdot \dot{\mathbf{p}} = \\ &-\Sigma [\mathbf{F} \cdot (\mathbf{p}/m) + F_x \dot{\epsilon} y] + \Sigma [(\mathbf{p}/m) \cdot \mathbf{F} - (p_x/m) \dot{\epsilon} p_y] = -\dot{\epsilon} P_{xy} V = -\dot{W}. \end{aligned}$$

We have used the microscopic representation of the pressure tensor from Section 5.6 to introduce  $P_{xy}$ . Although this microscopic energy change can have either sign, positive or negative, the corresponding energy change is *always* an increase for a macroscopic flow described by a Newtonian viscosity  $\eta$ , whether the sign of the strain rate is positive or negative:

$$\dot{E}_{\text{Newton}} = -\dot{\epsilon} V P_{xy} = +\eta \dot{\epsilon}^2 > 0.$$

Because, for the equations of motion describing this shear flow,  $(\partial \dot{q} / \partial q)$  and  $(\partial \dot{p} / \partial p)$  both vanish, so must the weighted sum,  $\Sigma f [(\partial \dot{q} / \partial q) + (\partial \dot{p} / \partial p)] = 0 \equiv -d \ln f / dt$ ; again Liouville's Theorem guarantees that the Lagrangian time derivative of the distribution function  $\dot{f}$  vanishes so that  $f$  propagates unchanged. During this propagation the internal energy has increased from its initial value by an amount  $\int \dot{E} ds = -\dot{\epsilon} V \int P_{xy} ds = \Delta E$ , giving an exact relation linking the nonequilibrium distribution function at time  $t$  to the equilibrium distribution at time zero:

$$f_{\text{neq}}(t) = f_{\text{eq}}(0) = f_{\text{eq}}(t) \exp[\Delta E / kT] = f_{\text{eq}}(t) \exp[-\dot{\epsilon} (V/kT) \int P_{xy}(s) ds].$$

From this nonequilibrium distribution function the usual Green-Kubo result follows by linearization. Just as in the case of diffusion it needs to be emphasized that the coordinates at time  $t$  are linked to the coordinates at time zero through the strain-rate-dependent dynamics, so that the simple notation conceals the need for solving the underlying many-body problem. This link between the nonequilibrium and equilibrium distribution functions is called a "Kawasaki relation." It follows directly from Liouville's Theorem for the phase-space flow.

When the Green-Kubo expressions for the transport coefficients were first applied to a "large-scale" (864 particles and  $10^5$  time steps) liquid-phase simulation, in a pioneering attempt to reproduce the experimental values of the diffusion coefficient, bulk and shear viscosities, and heat conductivity for liquid argon at its triple point, both the shear viscosity and the heat conductivity that resulted were in poor agreement with the experimental data. The direct nonequilibrium methods provided a welcome alternative computational method. A nonequilibrium shear viscosity simulation can be based on the same equations of motion used to derive the Green-Kubo results,

$$\dot{x} = (p_x/m) + \dot{\epsilon}y; \dot{y} = (p_y/m);$$

$$\dot{p}_x = F_x - \dot{\epsilon}p_y - \zeta p_x; \dot{p}_y = F_y - \zeta p_y,$$

but with the addition of a time-varying friction coefficient designed to achieve a nonequilibrium steady state. The friction coefficient  $\zeta$  regulates the *comoving kinetic temperature*, the temperature measured relative to the stream motion:  $K_0/N = (DkT/2)$  in  $D$  dimensions. In two dimensions, for instance, the mean value of the comoving kinetic energy per particle,

$$kT = \langle (m/2)[(\dot{x} - y\dot{\epsilon})^2 + \dot{y}^2] \rangle = \langle (1/2Nm)\Sigma[p_x^2 + p_y^2] \rangle,$$

can be controlled by using the Nosé-Hoover friction coefficient:

$$\dot{\zeta}_{NH} = [(K/K_0) - 1]/\tau^2.$$

Alternatively, either the comoving kinetic energy or the comoving internal energy can be made a constant of the motion by using a friction coefficient based on Gauss' Principle of Least Constraint.

**Problem:**

Use Gauss' Principle of Least Constraint to find both the isokinetic and isoenergetic forms of the thermostatted shear-flow equations of motion for a two-dimensional periodic system.

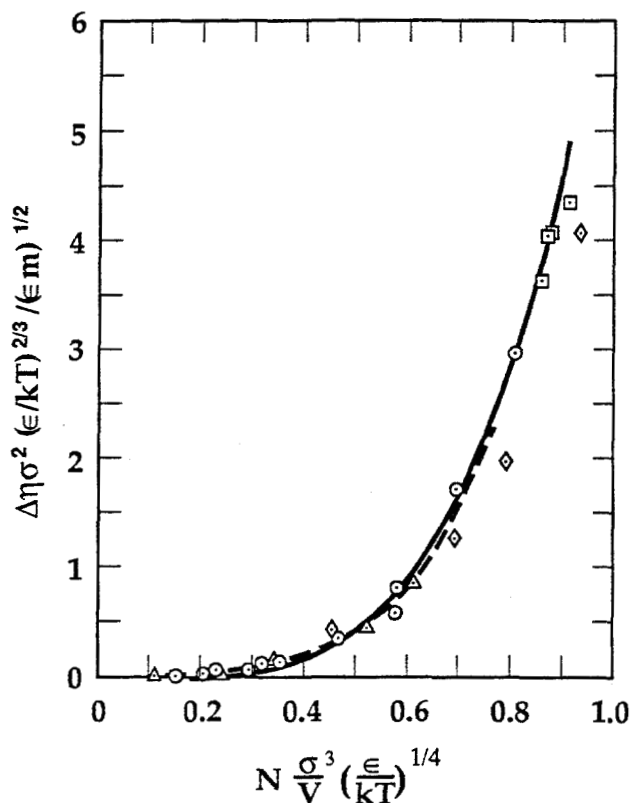
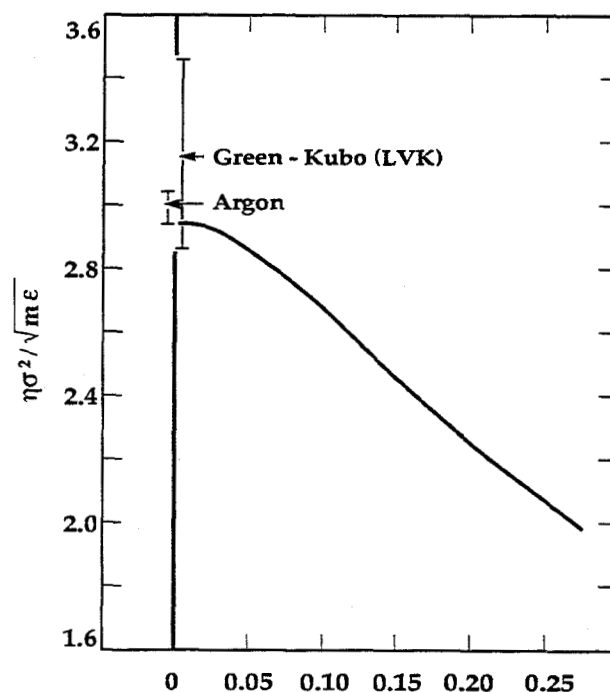


**Figure 11.6.** Excess shear viscosity (relative to the zero-density kinetic-theory value computed for this same temperature) for Lennard-Jones fluids covering a wide range of temperature and density. All the data can be roughly described as following a quartic dependence on the reduced density.

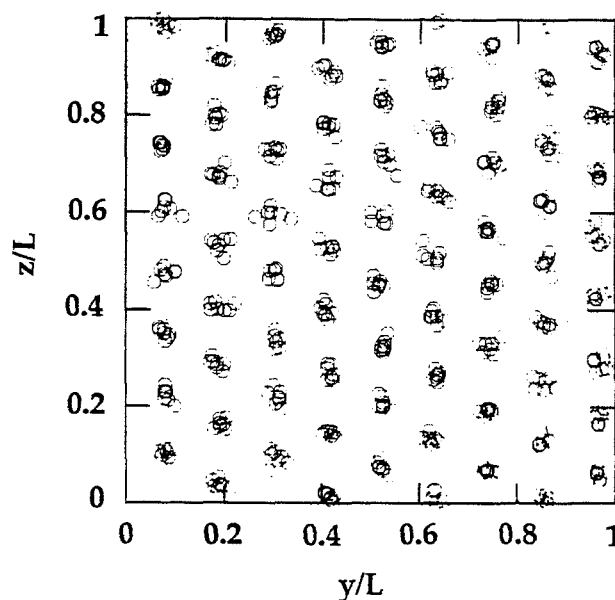
**Figure 11.7.** Strain-rate dependence for a three-dimensional Lennard-Jones liquid in periodic plane Couette flow at the triple-point density and temperature. The strain rate is  $du_x/dy$ . The corresponding experimental data for argon and the equilibrium Green-Kubo viscosity are indicated. The abscissa is the strain rate, in units  $(\epsilon/m\sigma^2)^{1/2}$ .



Computer simulations based on both the equilibrium Green-Kubo equations and the thermostatted nonequilibrium equations of motion have by now been carried out for a wide range of fluid thermodynamic states. For the Lennard-Jones potential the sampling of results shown in Figure 11.6 reproduces quite well both the *decrease* of viscosity with increasing temperature seen in real liquids and the *increase* typical of real gases. Except at high densities these results are insensitive to strain rate. Near the phase-diagram “melting” or “freezing” line linking the liquid and solid phases the dense fluid viscosity varies roughly as the square root of the strain rate, but at strain rates much too high for routine laboratory measurements. See Figure 11.7.

The nonequilibrium simulations, when applied to fluids at very high strain rates, reveal two kinds of reproducible nonlinear behavior which are most interesting. At sufficiently high rates of shear the particles tend to order into one-dimensional chains or two-dimensional sheets, as shown in Figure 11.8. This behavior, first seen in computer experiments, was later verified with laboratory experiments on the shear of micron-sized spheres. Such a "large" sphere size, relative to atoms, had to be used because the strain rates required to achieve these shear-induced phase transformations with simple molecules are of order  $10^{12}$  hertz, too high to achieve except with shockwaves.

**Figure 11.8.** Ordering of 500 hard spheres, 60% expanded from close-packing, by a rapid shear flow, taken from J. J. Erpenbeck, *Physical Review Letters* 52, 1333 (1984).



The nonequilibrium simulation of shear can just as well be applied to solids as to fluids, without any change in the equations of motion. The response of macroscopic isotropic solids to shear is conventionally called "plastic yielding" rather than viscous flow because simple metals tend to deform at a relatively-constant shear stress which varies only slowly with strain rate. This shear stress is an effective "yield stress," which would correspond, for a fluid, to the product of a viscosity coefficient and the strain rate:

$$\sigma_{xy} = -P_{xy} = Y = \eta \dot{\epsilon}.$$

Conventional laboratory measurements explore strain rates up to about a megahertz while computer simulations are most easily carried out at much higher rates. But the gap between laboratory and computer experiments is narrowing rapidly from both sides. The "highest" of the experimental shear rates just overlap the low-rate limit of what can be done with periodic computer simulations.

To see this, consider the minimum possible computational plastic strain rate, attained by following the shear of a periodic crystal containing a single pair of

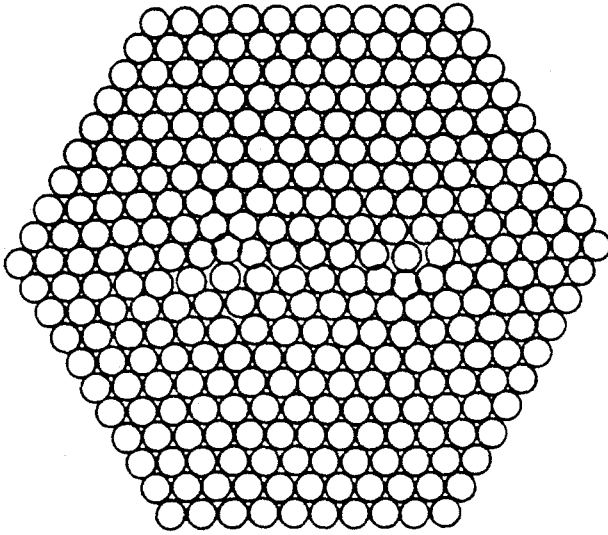


**Figure 11.9.** A pair of edge dislocations in a two-dimensional triangular-lattice crystal.

dislocations. (See Figure 11.9.) Consider a two-dimensional crystal containing  $10^5$  atoms with a unit cell area of  $10^{-10}$  square centimeters. If the two dislocations move at a speed of  $10^4$  cm/sec and the spacing between adjacent atomic rows is  $2 \times 10^{-8}$  cm, the corresponding "plastic" strain rate, the product of dislocation density, speed, and the interatomic spacing is:

$$\dot{\epsilon} = (2/10^{-10})(10^4)(2 \times 10^{-8}) = 4 \times 10^6 \text{ hertz.}$$

By increasing the strain rate, and the corresponding dislocation density, computer simulations of the shear of solids can reach strain rates of up to  $10^{12}$  hertz, corresponding to the relative motion of neighboring atoms at the sound speed. Under these maximally-extreme conditions the data shown in Figure 11.10 establish that the shear stress reaches about 10% of the shear modulus. At lower rates the stress varies as a temperature-dependent power of the strainrate,  $\sigma \propto \dot{\epsilon}^P$ . Although the exponent  $P$  is lower at low temperature the rate-dependence shown in Figure 11.10 is much stronger than that observed experimentally at lower rates.

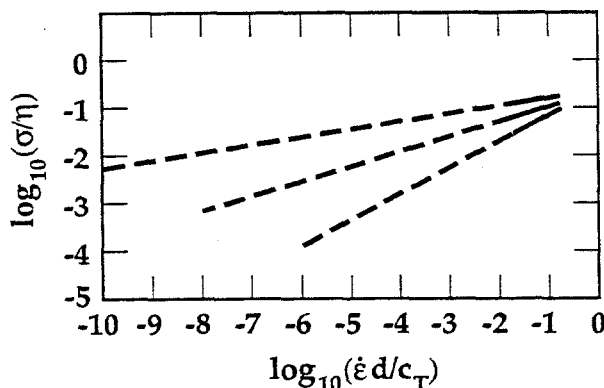


**Figure 11.10.** Dependence of the plastic shear stress  $\sigma$  on strain rate  $\dot{\epsilon}$  for solids undergoing steady plastic flow. The isotherms correspond to temperatures of 0.3, 0.6, and 0.9 relative to melting. At high strain rates all the isotherms converge to the maximum strength, about one-tenth the shear modulus. The extrapolations of the computer data, indicated by dashes, are in fair agreement with experimental data.

Just as the Galton Board served as the prototypical one-particle model for field-driven mass currents, there is a small-system caricature of nonequilibrium shear flow, the shearing "Lorentz Gas," in which two particles (hard disks, for instance) obey the isokinetic periodic shearing equations of motion. These equations can be solved by following the same ideas used to describe the closely-related mass-flow problem in the Galton Board. In polar coordinates the two-particle shear-flow equations of motion reduce to the simple form:

$$\dot{\theta} = \dot{\epsilon} \sin^2 \theta + (\partial \theta / \partial t)_{\text{Collisions}} .$$

Between collisions the velocity direction defined by  $\theta$  rotates counterclockwise toward "fixed points" where  $\dot{\theta}$  is zero. These occur at  $\theta = \pi$  for upward-moving disks and  $\theta = 2\pi$  for downward-moving disks. Analytic expressions for the motion between collisions can then be found by integrating twice with respect to time.

The resulting collision distribution resembles that found in the mass-current case. A sequence of 10,000 successive collisions is shown in the stereo Figure 11.11. Just as in the Galton Board case successive collisions can be characterized by two angles  $\alpha$  and  $\beta$  giving the location of the collision relative to the  $x$  axis and the direction of the velocity after collision. In addition a phase angle  $\gamma$  with  $0 < \gamma < 2\pi$  is required to describe the collision time relative to the boundary shear at the instant of collision. Thus collisions in a periodic two-body shear flow require the three-dimensional space of the stereo

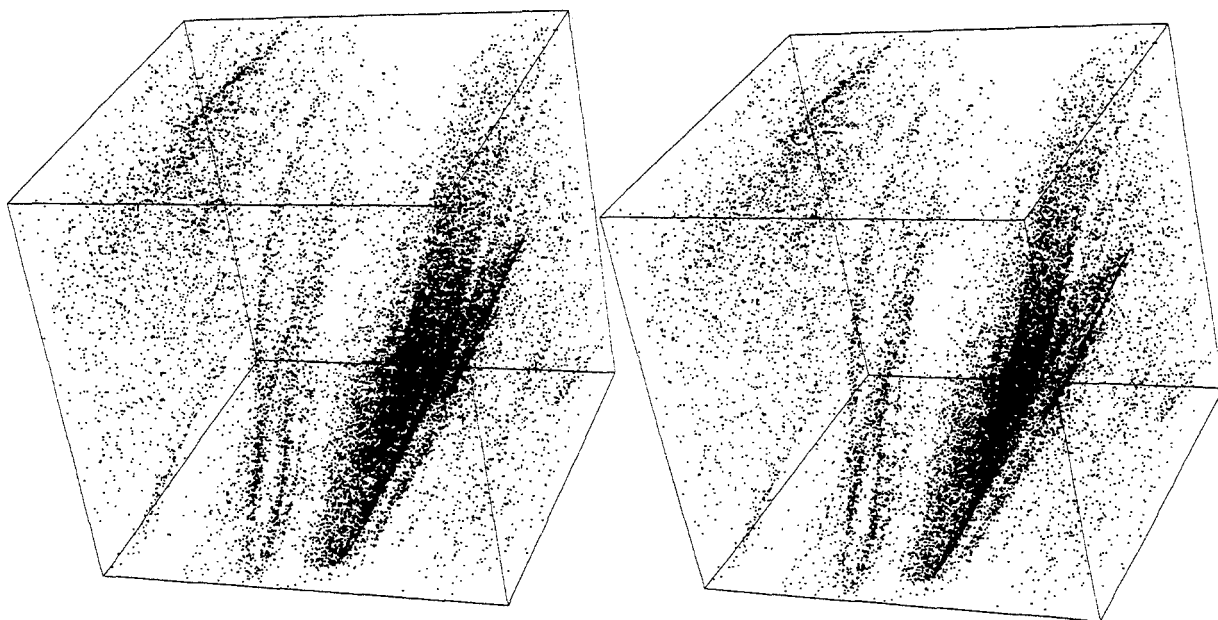


**Figure 11.11.** Stereo view of a three-dimensional phase-space attractor describing 10,000 successive collisions in the periodic shear flow of two hard disks. The collision variables  $0 < \alpha < 2\pi$  and  $-1 < \sin \beta < +1$  are the horizontal and vertical coordinates. The third dimension is the *phase* of the periodic boundary condition.

Figure for their description. The distribution of collision points in this three-dimensional space is *multifractal*, with an appearance reminiscent of the two-dimensional Galton-Board attractor. Figure 11.12 shows the dependence of the included number of pairs of points on distance in the three-dimensional phase space. The corresponding "correlation dimension" is  $D_2 = 2.3$ .

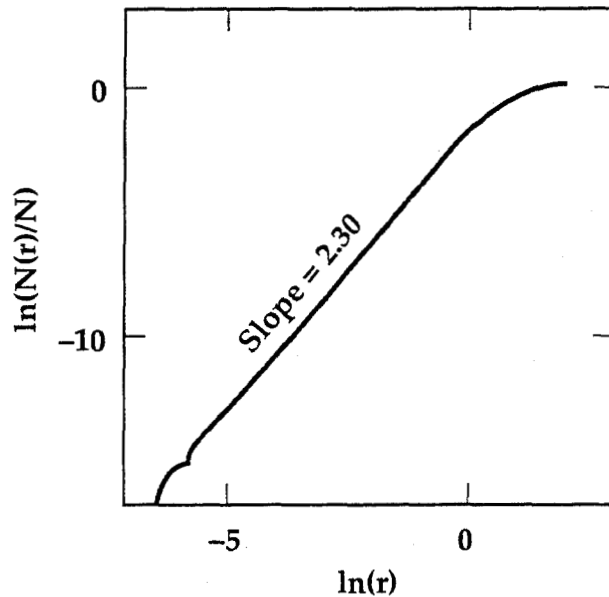


**Figure 11.12.** The ratio of the number of pairs of points lying within a distance  $r$  to the total number of such pairs for the strange attractor fractal object shown in Figure 11.11. The slope gives the corresponding correlation dimension,  $D_2 = 2.3$ .

#### 11.4 Heat Conduction

Dense-fluid heat conduction is an intrinsically more complicated phenomenon than diffusion or viscous flow. Heat flow requires a minimum of three particles for its simulation, not just two. In Chapters 5 and 7, we showed that each spatial component of the heat flux vector  $Q$  could be written as a sum of two terms, "kinetic" and "potential" respectively:

$$Q_x = Q_x^k + Q_x^\phi;$$

$$Q_x^k = (1/V)\sum v_x [(p^2/2m) + \phi]; \quad Q_x^\phi = (1/V)\sum_{ij} [F_{ij} \cdot (p_i + p_j)/2].$$

In a system containing only two identical particles and with a fixed center-of-mass both  $(p_1 + p_2)$  and  $\sum v_x$  vanish, and so also must the heat flux vector  $Q = (Q_x, Q_y)$ . In the two-dimensional three-particle case the constraints of fixed center of mass, fixed

#### Problem:

In fluid *mixtures* involving two or more separate components mass and heat diffusion are generally coupled. Diffusion of one species relative to another generally induces a (Dufour effect) heat flow. Likewise, heat flow in a mixture generally induces a corresponding (Soret effect) relative diffusion current. Discuss the simplest possible periodic atomistic system needed to simulate these effects.

momentum, fixed current and fixed temperature are a total of  $2 + 2 + 2 + 1 = 7$  constraints, leaving relatively unwieldy four-dimensional collision-space and five-dimensional phase-space objects for analysis.

Nonequilibrium many-body simulations of heat flow have been carried out in three different ways. The most direct of these approaches is to follow the dynamics of a Newtonian system coupled to two separate heat-reservoir regions, maintained at different temperatures, and to measure the heat flow from one reservoir to the other through the intermediate Newtonian system. See Figure 11.13. A related but less-direct approach is to measure the *curvature* of the steady-state temperature profile,  $d^2T/dx^2$ , or, equivalently, the boundary heat flux in a shear flow driven by thermostatted boundaries. In a uniform shear flow the viscous work acts as a heat source spread throughout the fluid, and the conductivity can be determined by measuring the rate at which the resulting heat current reaches the boundary. An even more indirect but very effective approach avoids reservoirs, and their influence, altogether, using instead Gillan and Evans' artificial field, sensitive to individual particle's contributions to the instantaneous energy and pressure tensor, and chosen to provide exact consistency with the Green-Kubo relation.

The equations of motion for this last approach apply to a homogeneous system with periodic boundaries. The additional driving forces  $\{F_D\}$  for each particle have components both in the flux direction and in the transverse direction(s). The components depend upon each particle's contributions to the energy and the potential part of the pressure tensor. Here we use the inverse length  $1/\lambda$  as a measure of the field strength used to induce a heat flux, indicate each particle's energy relative to the instantaneous average  $\langle E \rangle$  by  $\delta E = E - \langle E \rangle$ , and similarly indicate each particle's relative contributions to the pressure-tensor components by  $\delta P_{ij}$ . Then the two-dimensional equations of motion necessary to drive a nonequilibrium steady-state heat current in the  $x$  direction have the form:

$$\dot{p}_x = F_x + (1/\lambda)[\delta E + V\delta P_{xx}^\phi] - \zeta p_x; \dot{p}_y = F_y + (1/\lambda)[V\delta P_{xy}^\phi] - \zeta p_y.$$

This artificial field performs exactly the same work, for a given heat current, as would be dissipated at thermal heat reservoirs. It is straightforward to show that the work done by the extra force proportional to  $(1/\lambda)$  is also proportional to the microscopic heat flux:

$$m\dot{W}_\lambda = (1/\lambda)\sum[\delta E p_x + V\delta P_{xx}^\phi p_x + V\delta P_{xy}^\phi p_y]$$

$$\dot{W}_\lambda = (1/\lambda)\{\sum_{v_x}[(p^2/2m) + \phi] + \sum_{ij}[F_{ij}(p_i + p_j)/(2m)]\} = (1/\lambda)Q_x V.$$

It is unnecessary to subtract the mean flux contribution  $\{v_x \langle E/N \rangle\}$  from the sum,  $\sum_{v_x}[(p^2/2m) + \phi]$ , because these contributions necessarily sum to zero.

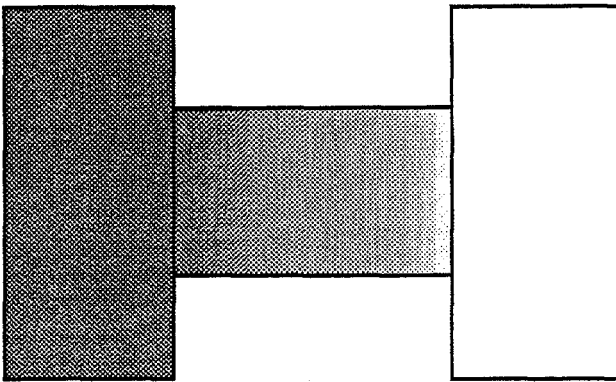


**Figure 11.13.** Steady conduction through a bar linking two heat reservoirs. The shading indicates temperature. The left hot reservoir is shaded and the right cold reservoir is white.

For small field strengths ( $1/\lambda$ ) the dissipation of this work into heat varies as  $(1/\lambda)^2$  and must approach that calculated from linear irreversible thermodynamics which can in turn be calculated from the thought experiment shown in Figure 11.13. Imagine the steady flow of heat in a homogeneous bar to be driven by a temperature difference  $\Delta T \ll T$ . Let us attempt to estimate the *rate* at which the entropy *in* the bar changes with time. The change from the constant heat flux  $Q_x$  through a cross section  $A$  is evidently

$$\dot{S} = Q_x A \{ [T + (\Delta T/2)]^{-1} - [T - (\Delta T/2)]^{-1} \}; Q_x > 0; \Delta T > 0.$$

There is clearly an *increase* in entropy at the hot end, where heat enters and a somewhat *larger decrease* at the cold end. This mismatch in the two entropy changes, with the loss outweighing the gain is embarrassing, because any reasonable "entropy" in a nonequilibrium *steady* state can obviously neither increase nor decrease. This contradiction is the macroscopic manifestation of the microscopic collapse to a strange attractor discussed in Section 10.5. In the microscopic case there is no way to rescue the equilibrium Gibbs-Boltzmann entropy,  $S = -k \langle \ln f \rangle$ , in discussing a nonequilibrium steady state because  $\langle \ln f \rangle$  *diverges*.

In the macroscopic case it is traditional to imagine a vaguely-defined nonequilibrium entropy and to make it constant in nonequilibrium steady states by the bald expedient of adding a phenomenological "entropy production,"  $\dot{S}_{\text{Source}}$ :

$$\dot{S} \equiv Q_x A \{ [T + (\Delta T/2)]^{-1} - [T - (\Delta T/2)]^{-1} \} + \dot{S}_{\text{Source}} \equiv 0,$$

forcing the total change of the "entropy" of the bar to vanish. Thus,

$$\dot{S}_{\text{Source}} \approx Q_x V (+\Delta T/T^2 L_x) \approx Q_x^2 V / \kappa T^2 \approx (1/\lambda) Q_x V / T,$$

where the  $\{\approx\}$  indicate relations which hold if the temperature gradient is so small that terms of order  $\Delta T^3$  as well as the temperature variation of the conductivity can be ignored. Then the heat conductivity can be expressed in terms of the work done by the external field, and the induced heat flux  $Q$  :

$$\kappa T = \lambda Q_x .$$

All three of the purely-nonequilibrium steady-state approaches just outlined provide limiting conductivities consistent with those from equilibrium calculations based on the Green-Kubo conductivity formula:

$$\kappa = (V/kT^2) \int dt \langle Q_x(0) Q_x(t) \rangle_{eq} .$$

The results obtained from these simulations illustrate an interesting corresponding-states relation for dense-fluid transport coefficients. This scaling relationship is, like van der Waals' equation of state, a semiquantitative model, rather than a theory. But it is nevertheless quite useful for practical applications. To develop the model we picture the liquid as composed of particles at a sufficiently high density that their motion can be described as vibrational.

The conductivity can then be crudely estimated by imagining that a vibrating particle transports energy from its hotter to its cooler neighbors at the Einstein frequency through an area  $d^2$ , where  $d$  is the interparticle spacing. Leaving aside multiplicative factors of order 1, so that the heat capacity  $C_P$  can be replaced by  $k$ , the corresponding conductivity  $\kappa$  has the form:

$$\kappa d^2 / (k^3 T / m)^{1/2} \propto v_{Einstein} d (m / k T)^{1/2} ;$$

At the same time, the thermodynamic *entropy* from the Einstein model, measured relative to an ideal gas, has a related form:

$$\exp(-S_{Excess} / Nk) \propto [v_{Einstein} d (m / k T)^{1/2}]^{3/2} ,$$

suggesting that conductivity data can be correlated with the thermodynamic entropy.

A similar approximate relation should also hold for the shear viscosity. To estimate the viscosity, imagine again the vibrations of a typical fluid particle. These transport a momentum of order  $-(mkT)^{1/2} d \dot{\epsilon}$  from neighbors below to neighbors above. This vibrational momentum flows through an area of order  $d^2$  at the Einstein frequency. The corresponding reduced shear viscosity coefficient is the same as the

reduced conductivity:

$$\eta d^2 / (mkT)^{1/2} \approx \kappa d^2 / (k^3 T / m)^{1/2} \propto v_{\text{Einstein}} d (m/kT)^{1/2}.$$

These scaling relations for viscosity and conductivity suggest defining *reduced* transport coefficients, multiplying  $\eta$  and  $\kappa$  by  $(V/N)^{2/3} \propto d^2$  and dividing by  $T^{1/2}$ , proportional to the thermal velocity. Thus logarithmic plots of the reduced viscosity and conductivity should both vary linearly with the excess entropy. Figure 11.14 shows that this rough approximation is an adequate semiquantitative description of transport in dense fluids. It does not work for gases, for which the vibrational description makes no sense so that the predicted transport coefficients are undefined.

This same vibrational approach can also be applied to heat conduction in solids, but with considerable difficulty at low temperatures where the scattering length for sound waves exceeds the system size. At the lowest temperatures the scattering from crystal defects is the dominant mechanism for scattering. The scattering varies as the thermal cross section CS swept out by the atoms, which can be estimated from the vibrational spectrum,

$$CS = \pi \delta^2 = \pi (DkT/m) \langle \omega^{-2} \rangle.$$

In solids this same method has been used successfully to measure the thermal conductivity and to compare that conductivity with the predictions of a solid-phase free path theory based on phonon transport.

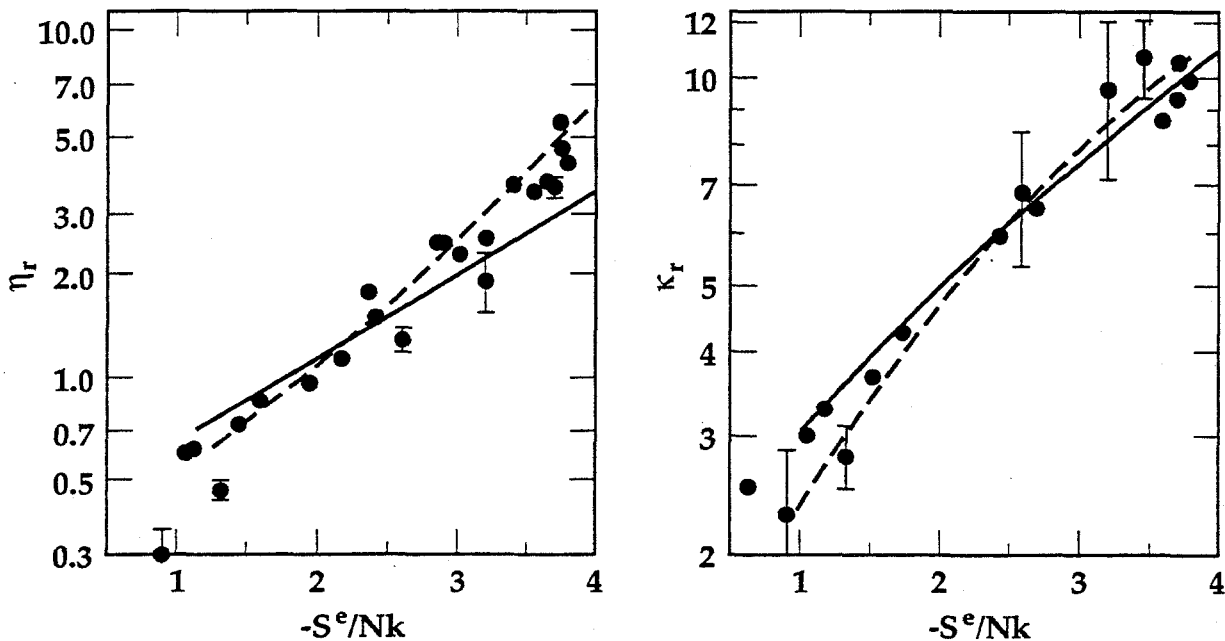


**Figure 11.14.** Corresponding states plot of reduced fluid-phase viscosity (left) and heat conductivity (right). The data span a wide range of computer simulations including plasmas, hard spheres, soft spheres, and the Lennard-Jones potential. The abscissa give the entropy relative to an ideal gas at the same density and temperature.

### 11.5 Shockwave Structure

Strong fluid shockwaves contain particularly interesting far-from-equilibrium states. They occupy a small rapidly-moving transition region in space which links together two equilibrium states of matter. It is this link with equilibrium properties which makes shockwaves an important source of equation-of-state information under extreme conditions. Shockwaves link a relatively cold low-pressure region to a relatively hot high-pressure region. Figure 11.15 shows the structure of a typical *strong* shockwave, representing the compression of liquid argon from the triple point to a temperature of 12,000 kelvins at a pressure of nearly half a megabar. Figure 11.16 illustrates three separate coordinate frames in which the shockwave can be observed. The spatial extent of the transition region, the "shock width" is small, typically of order the mean free path and here about equal to one atomic diameter; in the laboratory frame the transition region moves at the "shock speed,"  $u_s$ , somewhat greater than the speed of sound. In the simpler comoving frame the shock is fixed, cold material

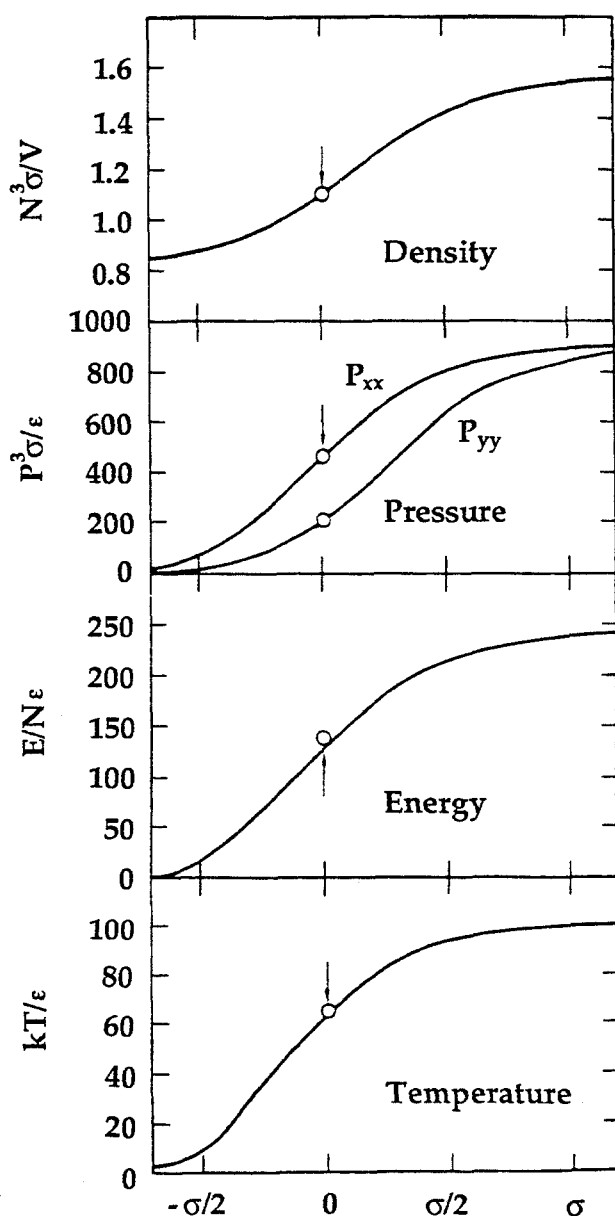
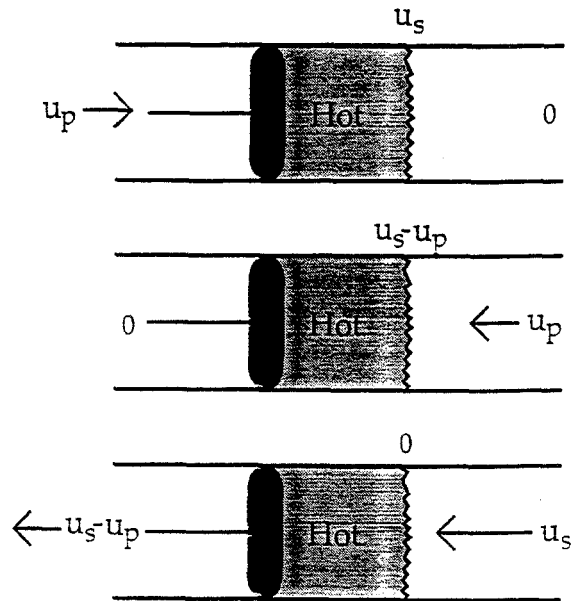


**Figure 11.15.** Variation of density, pressure tensor, internal energy, and temperature for a steady strong Lennard-Jones shockwave starting near the triple point. The number density increases from  $N\sigma^3/V = 0.844$  to 1.571; the pressure from  $P\sigma^3/\epsilon = 0$  to 917; the internal energy from  $E/N\epsilon = -5$  to 246; and the temperature from  $kT/\epsilon = 0.722$  to 100. The corresponding final temperature for argon is about 12,000 kelvins, a bit more than one electron volt. The full curves were calculated by solving the Navier-Stokes equations, using local values of the transport coefficients. The corresponding results from molecular dynamics are indicated by circles.

**Figure 11.16.** Shockwave motion as seen in three coordinate frames: the *laboratory frame*, with piston speed  $u_p$  and shockwave speed  $u_s$ ; the *stagnation frame*, in which cold fluid moving at  $u_p$  is brought to rest by a rigid wall; the *shockwave frame*, fixed on the wave, in which cold fluid enters at speed  $u_s$  and exits at speed  $u_s - u_p$ .



flowing toward the front from the right at speed  $u_s$ , and hot material exiting toward the left at speed  $u_s - u_p$ .

Shockwaves are a typical feature of rapid compression processes. This is because sound velocity is typically an increasing function of density. Thus a pressure wave in which the density gradually increases tends to steepen as the denser hotter high-pressure portion of the wave overtakes the low-pressure portion. Only the presence of viscosity (and to a lesser extent, heat conductivity) prevents such a propagating one-dimensional wave from becoming infinitely steep. As the concentrating effect of nonlinearity causes the wave to become steeper, the longitudinal strain rate  $du_x/dx$  increases in magnitude until the resulting viscous stress just offsets the concentrating effect of nonlinearity. When the two effects balance, a steady one-dimensional shockwave can result. At least locally a well-defined transition region between cold unshocked fluid and hot shocked fluid can be seen.

Such a shockwave simultaneously displays longitudinal gradients in density, velocity, and energy. Both the pressure and the temperature are anisotropic, with  $P_{xx} \neq P_{yy}$  and  $T_{xx} \neq T_{yy}$ . In strong shocks the longitudinal and transverse stresses and temperatures can differ by as much as a factor of two. Viscosity and conductivity act to smooth out these gradients. Because the problem is a one-dimensional steady one, it is relatively easy to solve the corresponding continuum hydrodynamic equations and to simulate the atomistic flow with molecular dynamics. If we consider the flow of mass, momentum, and energy in the coordinate system shown at the bottom of Figure 11.16 as centered *on* the shockwave, then the mass, momentum, and energy fluxes are necessarily constant throughout the shockwave. We arbitrarily choose the  $x$  axis to parallel the direction of shock propagation and use the notation  $\rho u_x$  for mass flux,  $P_{xx} + \rho u_x^2$  for the  $xx$  component of the momentum flux, and  $\rho u_x [e + (P_{xx}/\rho) + (u_x^2/2)] + Q_x$  for the  $x$  component of the energy flux. The heat flux vector contribution,  $Q_x$ , is the conductive flow of heat over and above that carried by the motion of the fluid. When

these fluxes are evaluated in the cold material, which moves toward the shock front at speed  $u_s$ , and hot material, which moves away from the shock front at speed  $(u_s - u_p)$  we obtain three equations linking together the thermodynamic properties of the cold and hot equilibrium states, the shock speed  $u_s$ , and the particle or piston speed  $u_p$ :

$$\rho u_x = \rho_I u_s = \rho_F (u_s - u_p) ;$$

$$P_{xx} + \rho u_x^2 = P_I + \rho_I u_s^2 = P_F + \rho_F (u_s - u_p)^2 ;$$

$$\rho u_x [e + (P_{xx}/\rho) + (u_x^2/2)] + Q_x =$$

$$\rho_I u_s [e_I + (P_I/\rho_I) + (u_s^2/2)] = \rho_F (u_s - u_p) [e_F + (P_F/\rho_F) + ((u_s - u_p)^2/2)] .$$

Notice that the longitudinal heat flux component  $Q_x$  vanishes away from the shock front and that because the material is a *fluid* the longitudinal and transverse pressure-tensor components  $P_{xx}$  and  $P_{yy}$  become equal to the equilibrium pressure,  $P(\rho, E)$ , as the tensor becomes isotropic. By eliminating the two speeds from the three equations the Hugoniot relation for the work done in compression results:

$$\Delta E_{\text{Shock}} = (P_I + P_F)(V_I - V_F)/2 .$$

Thus the strength of the shockwave can be described by specifying *either* of the two speeds  $u_s$  and  $u_p$ , *or* any of the variables identifying the final thermodynamic state:  $P_F$ ,  $V_F$ ,  $E_F$ . From the equation of state the rate at which a shockwave travels can then be calculated, just as we did for an ideal gas in Section 7 of Chapter 2.

Shockwaves have been simulated, using molecular dynamics, in two different ways, both different from that suggested in Section 2.7. A transient method is indicated in Figure 11.17. It incorporates time-dependent boundary conditions. Imagine that the original  $x$  coordinates for all particles in the system lie in the range from  $-L(0)/2$  to  $+L(0)/2$ :

$$-L(0)/2 < \{x\} < +L(0)/2 .$$

Then consider a molecular dynamics simulation in which the periodic images of all those particles, necessary for calculating the forces on particles near either end of the periodic box, are located as usual at  $x = \pm L$ , but with  $L(t)$  a decreasing function of time:

$$L(t) = L(0) - tu_p ;$$

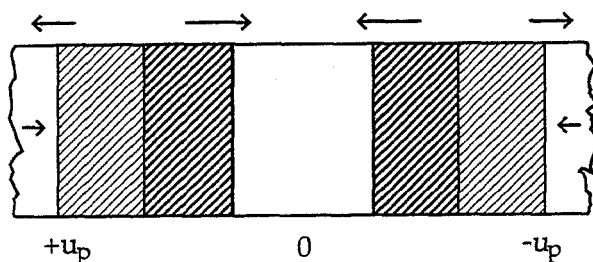


**Figure 11.17.** Special boundary conditions which produce two symmetric shockwaves at each boundary linking the system to a periodic images. Shock velocities are shown at the top in the laboratory frame. Laboratory frame velocities are shown at the base. Hot shocked regions are shaded.

The effect of such a boundary condition is to compress the periodic system simultaneously from both sides, using "pistons" which are replicas of the system itself. Two similar shockwaves then move from the box boundaries at  $x = \pm L(t)/2$  toward the center of the box at the "shock speed"  $u_s$ . The calculation is completed when the two shockwaves reach the center, at  $t = L(0)/(2u_s)$ . During the period of steady propagation the binning of coordinates, velocities, and the fluxes in frames centered on the moving shockwaves generates a statistical description of the shockwave profile. In the binning process it is advisable to smooth the data over one bin width by distributing each particle's contributions into two adjacent histogram bins with weights that change continuously in time and space. By further subdivision of the data in each spatial bin into local velocity bins it is quite possible to determine the deviation of the velocity distribution from the Maxwell-Boltzmann form. Figure 11.18 shows the variation of the fourth moment of the velocity distribution relative to the square of the second moment. All the data shown were generated with a 4800 particle simulation, initially made up by linking 150 periodic cubes containing 32 particles each.

An alternative to the transient simulation just described is a steady flow, in which particles enter the problem at one boundary and leave at the opposite boundary, gaining or losing an additional thermal velocity component when crossing the boundary between a "skin" region, having a width equal to the range of the forces, and bulk material. Within the two skin regions the particles move at a steady speed. Both this approach and the transient method have been used successfully.

The measured atomistic profiles can then be used to test the predictions of the Navier-Stokes equations, the solution of the flow equations for mass, momentum, and energy, making Newton's and Fourier's constitutive assumptions as described in Chapter 7:

$$P = (P_{eq} - \lambda \nabla \cdot u)I - \eta(\nabla u + \nabla u^t); Q = -\kappa \nabla T.$$

To solve the conservation equations for the mass, momentum, and energy flux is a four-step process:

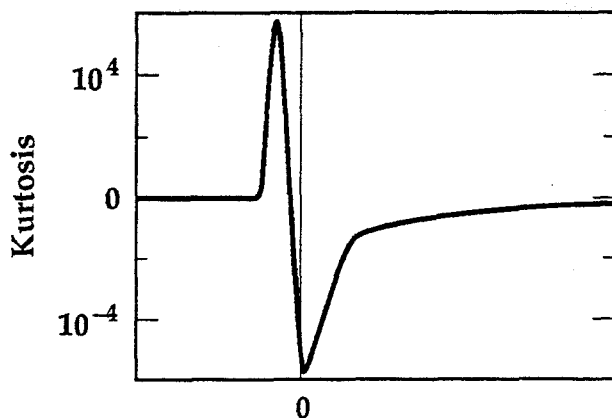


**Figure 11.18.** Deviation of the fourth velocity moment  $\langle v_x^4 \rangle$  from the equilibrium value,  $3\langle v_x^2 \rangle^2$ , in a dense-fluid shockwave profile. The abscissa spans a distance of  $25\sigma$ .

1. Start with the general conservation equations:  $\rho u_x = A$  ;  $P_{xx} + \rho u_x^2 = B$  ;  $\rho u_x[(E/m) + (P_{xx}/\rho) + (u_x^2/2)] + Q_x = C$  , where A, B, and C are constants satisfying the Hugoniot relations describing mass, momentum, and energy conservation, using the first of these equations to eliminate the variable  $u_x$  in favor of  $\rho$ .

2. Introduce the Newtonian and Fourier constitutive relations to obtain two coupled ordinary differential equations linear in  $dp/dx$  and  $dT/dx$ .

3. Integrate the corresponding equation for  $dp/dT = [(dp/dx)/(dT/dx)]$  to find the thermodynamic states through the shockwave.

4. Use the values of  $T(\rho)$  from Step 3 to integrate the profile equations from Step 2 to find  $\rho(x)$  and  $T(x)$ .

In order to carry out the calculation it is necessary to have an analytic or tabular equilibrium equation of state including the dependence of the transport coefficients  $\{\lambda = \eta_v - (2/D)\eta, \eta, \kappa\}$  on thermodynamic state. The Navier-Stokes calculation just outlined is numerically *unstable* if the integration begins in the cold state but converges easily if carried out from the hot state to the cold state. The thermodynamic profiles computed in this way are again compared to the corresponding molecular dynamics simulation in Figure 11.19. The good agreement between the Navier-Stokes linear-transport predictions and the dynamical simulation is amazing. The atomistic profiles shown were generated using the transient method to generate two symmetric shockwaves. Such a shock process is typical of what can be achieved experimentally with strong shockwaves. Shockwaves are a convenient way of measuring thermodynamic data under extreme conditions, at pressures too great for confinement in static experiments. In experimental shockwave research shockwaves are generated by using an energy source to drive a steady profile through a sufficiently long sample to reach and record steady-state conditions. Typically the two velocities  $u_s$  and  $u_p$  are measured. From these the hot-state density, pressure, and energy can all be calculated. Compressed gas, conventional explosives, and thermonuclear explosives have all been used as energy sources for the waves.

From the shockwave profiles generated during molecular dynamics simulations, the transport coefficients can be calculated by dividing the measured fluxes by the corresponding gradients. The measured viscosity and heat conductivity lie within 30% of their small-gradient values. Both transport coefficients are effectively somewhat

larger than the Navier-Stokes values. These increases reflect the disordered structure of the dense shocked fluid, which promotes more-rapid propagation of momentum and energy than the more-ordered equilibrium structure. Theoretical estimates of the effects of finite wavelength and frequency on transport coefficients typically predict reduced, rather than enhanced, values.

### 11.6 Vibrational Relaxation

Nonequilibrium molecular dynamics is by no means restricted to constitutive problems. It can be applied also to a variety of kinetic problems, both transient and steady. One of the most interesting, with potential applications to the study of chemical reaction rates in condensed matter as well as the interaction of laser radiation with matter is the determination of energy relaxation rates.

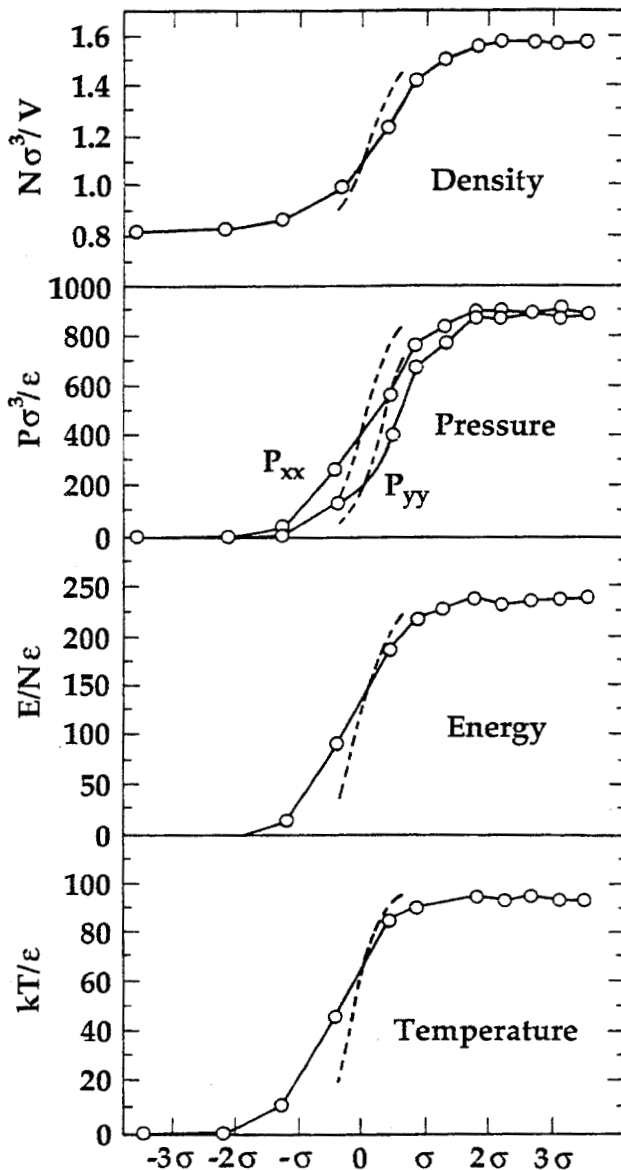


**Figure 11.19.** The points shown are the measured molecular dynamics shockwave profiles for the same shockwave shown in Figure 11.15. Here the Navier-Stokes results are shown dashed. The dynamic simulation and the Navier-Stokes approximation have exactly the same fluxes of mass, momentum, and energy. The difference in the slopes according to the two approaches is about 30% near the shockwave center, indicating that the effective transport coefficients are 30% larger than the small-gradient Newtonian and Fourier values. In the Navier-Stokes continuum calculations it is *assumed* that the fluid exhibits Newtonian viscosity and Fourier heat conduction.

Holian studied the vibrational relaxation of a realistic model of dense nitrogen, compressed to twice normal density. The thermodynamic state studied is typical of chemical detonations, with moderate compression and temperatures of a few thousand kelvins. By separating the energy of each molecule into translational, rotational, and vibrational parts, three separate temperatures can be defined for such a system:

$$3NkT_T/2 = \sum mv^2; NkT_R = (1/4)\sum mr^2\omega^2; NkT_V = (1/4)\sum mv^2,$$

where the notation indicates the division of the total kinetic energy into parts. The atomic mass, rotational frequency, and vibrational-mode velocity are respectively  $m$ ,  $\omega$ , and  $v$ . In such a system under shockwave conditions energy flows first into the translational motion, then to the rotational motion, and finally, to the vibrational motion. This last step can be very slow because the vibrational force constant is considerably larger than the effective force constant governing a collision between molecules.

**Problem:**

Consider a linear chain of three identical unit masses joined together by two Hooke's-Law springs with force constants of 1 and 100. Solve the equations of motion and find the maximum potential energy transfer from the righthand spring to the lefthand spring. Take the initial state motionless, but with displacements  $+\delta$ ,  $+\delta$ , and  $-2\delta$ . Why is it that the potential energy initially stored in one spring is not eventually transferred to the other spring?

A straightforward approach to the measurement of energy relaxation is to observe the three temperatures as functions of time and to fit the results to a set of linear relaxation equations:

$$\dot{T}_V = (T_T - T_V)(1/\tau_{VT}) + (T_R - T_V)(1/\tau_{VR});$$

$$\dot{T}_R = (T_V - T_R)(1/\tau_{VR}) + (T_T - T_R)(1/\tau_{RT});$$

$$\dot{T}_T = (T_R - T_T)(1/\tau_{RT}) + (T_V - T_T)(1/\tau_{VT}).$$

In the case of vibrational relaxation the relaxation times  $\tau_{VT}$  and  $\tau_{VR}$  are considerably longer than  $\tau_{RT}$  so that the rotational and translational temperatures reach a common equilibrium long before the vibrational modes are excited. Thus a single relaxation relation results:

$$\dot{T}_V = (T - T_V)(1/\tau_V),$$

where the relaxation is to the common temperature  $T$  which represents both translational and rotational modes. A difficulty with this approach is that the initial rate of change of the vibrational temperature depends fairly strongly on the exact  $\{q,p,\zeta\}$  phase of the initial conditions, necessitating a large number of independent calculations.

Holian invented a simpler more-effective nonequilibrium method. He studied the *virtual* decay rate by measuring the friction coefficients required to *maintain* a fixed nonequilibrium steady-state temperature difference:

$$\dot{p}_T = F_T - \zeta_T p_T; \dot{\zeta}_T = [(T/T_T) - 1]/\tau^2;$$

$$\dot{p}_R = F_R - \zeta_R p_R; \dot{\zeta}_R = [(T/T_R) - 1]/\tau^2;$$

$$\dot{p}_V = F_V - \zeta_V p_V; \dot{\zeta}_V = [(T/T_V) - 1]/\tau^2;$$

Holian maintained a tenfold difference between hot *translational and rotational* degrees of freedom at 4000 kelvins and cold *vibrational* degrees of freedom at 400 kelvins. The measured rate of heat transfer required to maintain this temperature difference is a direct measure of the kinetic rate.

The atomistic description of a dense fluid of diatomic nitrogen molecules was based on an interaction between nonbonded nitrogen atoms given by the exponential-six form:

$$\phi(r) = Ae^{-Br} - Cr^{-6},$$

and with the interactions between the two atoms in each molecule described by a Morse vibrational potential function:

$$\phi(r) = De^{-Er}(e^{-Er} - F).$$

Calculations were carried out in order to determine their sensitivity to the relaxation time  $\tau$  which determines the Nosé-Hoover friction coefficient  $\zeta$ . For a wide range of  $\zeta$  values the rate constant was essentially unchanged, indicating a characteristic relaxation time of 11 nanoseconds. On the other hand, when instead Gauss' Principle was used to keep the kinetic energy of the translational and rotational degrees of freedom *constant*, rather than allowing fluctuations, the result was a somewhat different, and apparently incorrect, relaxation time of about 13 nanoseconds. This is a second example of the failure of Gauss' Principle of Least Constraint to provide correct answers to nonequilibrium problems. The first was discussed in Section 10.2.

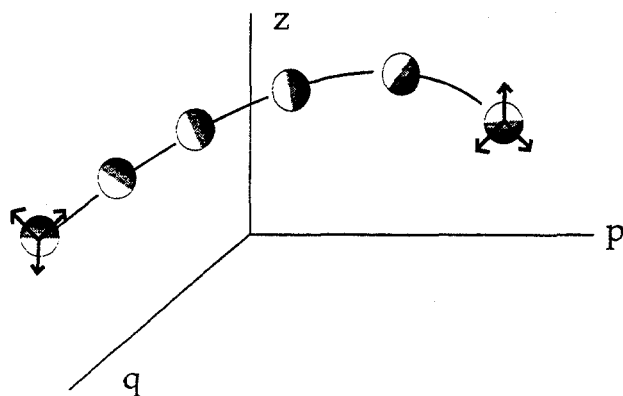


**Figure 11.20.** Motion of a comoving phase-space hypersphere centered on a trajectory. Satellite trajectory vectors  $\{\delta\}$ , indicated by arrows, are constrained to remain orthonormal while otherwise following the motion. The required constraints yield the Lyapunov spectrum and can be imposed by using Lagrange multipliers.

### 11.7 Lyapunov Spectra

The analysis of nonequilibrium phase-space flows shows very clearly that Lyapunov instability is responsible for the irreversible behavior summarized by the Second Law of Thermodynamics. To follow the details of phase-space distortion it is necessary to follow more than a single phase-space trajectory. This can be done by following the motion of one or more neighboring "satellite" trajectories in the vicinity of an unperturbed "reference" trajectory. See Figure 11.20.

Consider the unconstrained motion of a *satellite* trajectory separated by a phase-space offset vector  $\delta = (\delta q, \delta p)$  from the *reference* trajectory. Provided that the equations of motion are sufficiently differentiable, the motion of the offset vector  $\delta$  describing the motion of the satellite trajectory relative to the reference trajectory can be linearized:

$$\delta \dot{q} = (\partial \dot{q} / \partial q) \delta q + (\partial \dot{q} / \partial p) \delta p ; \delta \dot{p} = (\partial \dot{p} / \partial q) \delta q + (\partial \dot{p} / \partial p) \delta p .$$

In the case of a "separable" Hamiltonian,  $H = \Sigma p^2/2m + \Phi(q)$ , the equations simplify:

$$\delta \dot{q} = (1/m) \delta p ; \delta \dot{p} = (\partial F / \partial q) \delta q .$$

In the typical Lyapunov-unstable case the satellite trajectory has a tendency to separate, exponentially fast, leading to an exponential growth of the separation vector  $\delta = (\delta q, \delta p)$ . This growth can be prevented by using a Lagrange multiplier  $\lambda(t)$ , with the new equations of motion:

$$\delta \dot{q} = (1/m) \delta p - \lambda \delta q ; \delta \dot{p} = (\partial F / \partial q) \cdot \delta q - \lambda \delta p ; \dot{\delta} = D \cdot \delta - \lambda \delta ; \lambda = \delta^t \cdot D \cdot \delta / \delta^t \cdot \delta .$$

$D$  is used here as an abbreviation for the matrix giving the equations of motion of the offset vector  $\delta$ . This approach is not restricted to Hamiltonian systems. It can be applied generally, as suggested in the Figure. If, for instance, we consider the equations of motion of a thermostatted oscillator with mass, force constant, and thermostat relaxation time all set equal to unity:

$$\dot{q} = p ; \dot{p} = -q - \zeta p ; \dot{\zeta} = p^2 - 1 ,$$

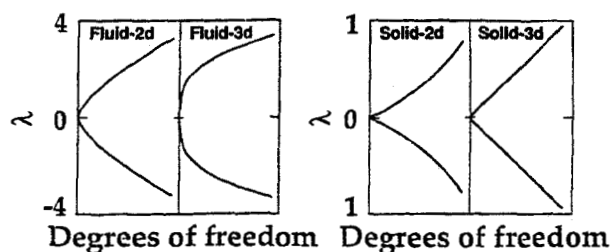


**Figure 11.21.** Equilibrium Lyapunov spectra for two- and three-dimensional dense fluids and solids determined by molecular dynamics simulation. The number of exponent pairs is twice the number of degrees of freedom.

the vector  $\delta$  is  $(\delta q, \delta p, \delta \zeta)$ , and the nonzero components of the  $3 \times 3$  matrix  $D$  are as follows:

$$D_{qp} = 1; D_{pq} = -1; D_{pp} = -\zeta; D_{p\zeta} = -p; D_{\zeta p} = 2p.$$

The superscript  $t$  indicates the *transposed* vector. It is easy to verify that the dot product  $\delta^t \cdot \delta$  is a constant of the constrained motion. Because the equation of motion for  $\delta$  is *linear* in the offset vector  $\delta$  the time average of the required "force,"  $-\lambda \delta$ , must exactly balance the unconstrained divergence rate,  $+\lambda_1 \delta$ , where  $\lambda_1$  is the largest of the Lyapunov exponents:

$$\lambda_1 \equiv \langle \lambda \rangle = \langle \delta^t \cdot D \cdot \delta \rangle / \delta^t \cdot \delta.$$

Again because the equations for the propagation of the offset vectors are linear, the Lyapunov spectrum is independent of the vectors' magnitude. The single-exponent process just outlined can be systematically extended to find the entire Lyapunov spectrum. In so doing, it is convenient to choose the vectors such that  $\delta^t \cdot \delta$  is equal to unity. If a third satellite trajectory is chosen close to the first two, but with an offset vector orthogonal to the vector linking them that required force is the second-largest Lyapunov exponent. By continuing this process the entire spectrum can be evaluated. Typical spectra are shown in Figure 11.21 for solids and fluids in two and three dimensions. The maximum Lyapunov exponent corresponds, roughly, to an effective collision rate. That in the fluid is greater than the solid collision rate because the fluid structure is more disordered.

The interpretation of the Lyapunov exponents is simplified by the reversible nature of the equations of motion. Reversibility suggests that any phase-space direction associated with growth corresponds to decay in the time-reversed solution of the equations of motion and *vice versa*. At equilibrium the forward and reversed trajectories are equally likely so that this symmetry argument is correct. The equilibrium spectra show the predicted symmetry with pairs of positive and negative exponents with equal magnitudes. The *shapes* of the spectra are reminiscent of the crude Debye models discussed in Section 8 of Chapter 4 as approximations to solid-phase vibrational spectra.

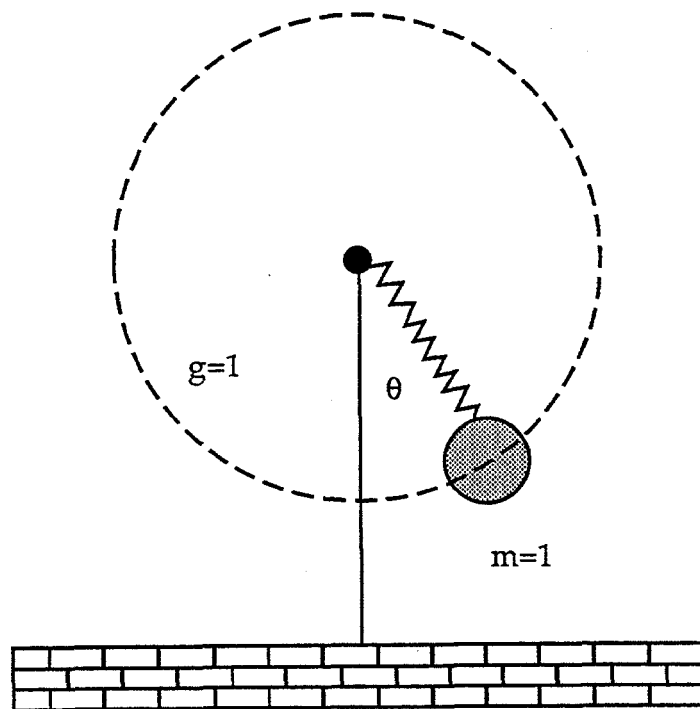


**Figure 11.22.** Hooke's-Law pendulum. When released from the high-energy vertical position, the motion is chaotic.

**Problem:**

Consider the Hooke's-Law pendulum shown in Figure 11.22, with mass 1 and spring constant 4, in a vertical gravitational field of unit strength, and with minimum spring potential energy at a length of unity. The Hamiltonian for this system is  $H(x, y, p_x, p_y) = \phi(r) + mgh + [p^2/2m] = 2(r - 1)^2 + y + (1/2)[p_x^2 + p_y^2]$ , where the pendulum length is  $r = (x^2 + y^2)^{1/2}$  and the  $y$  coordinate corresponds to the height  $h$ . Use the Lagrange-multiplier method to show that a reference trajectory with initial condition  $[x = 0.00001, y = 1]$  is chaotic, with a maximum Lyapunov exponent equal to 0.13. Use the Runge-Kutta method to integrate nine first-order differential equations, one for each member of the set  $\{x, y, p_x, p_y, \delta x, \delta y, \delta p_x, \delta p_y, I\}$ , where  $\delta$  is an infinitesimal offset vector of constant length, linking a nearby satellite trajectory to the reference trajectory, and  $I$  is the integral of the instantaneous Lagrange multiplier with respect to time:  $\langle \lambda \rangle_\tau = I(t)/\tau$ ;  $\dot{I} \equiv \lambda(t)$ .

Exactly these same ideas can be applied to nonequilibrium systems. If the phase space is extended by the inclusion of friction coefficients or strain rates then the satellite vectors acquire extra components and the dynamical matrix  $D$  which propagates the vectors becomes more complicated. Corresponding determinations of Lyapunov spectra have been carried out for nonequilibrium flows of mass, momentum, and energy. Because the equations of motion are time-reversible, even in the nonequilibrium case, it might be thought that the Lyapunov spectrum would retain the symmetry seen in equilibrium simulations. But, just as is required by the Second Law of Thermodynamics, the shrinking of phase-space hypervolume in the nonequilibrium steady state is accurately mirrored by a shift of Lyapunov exponents to more negative values. See Figure 11.23. The shifted exponents can be used to estimate

the fractal dimensionality of the nonequilibrium steady-state distribution function. The most extensive investigations have analyzed periodic mass-current simulations and shear viscosity simulations, both periodic and boundary-driven. There is a relation, discussed in the next Section, between the phase-space dimensionality of the nonequilibrium distribution function and the Lyapunov spectrum. In the problems just mentioned it was found that at relatively high fields the fractal dimensionality  $D_1$  of the corresponding nonequilibrium phase-space flow could be reduced by about 10%.

Results for *boundary driven* shear flows indicated relatively smaller losses of dimensionality. We can anticipate that more powerful computers and perhaps better methods for characterizing fractal geometry will enhance our knowledge of the multifractal objects which are the microscopic mechanical analogs of the macroscopic Second Law of Thermodynamics.

### 11.8 Phase-Space Dimensionality Loss

The *qualitative* mechanical basis of the irreversibility described by the Second Law of Thermodynamics was discussed in Section 10.7. We established there that the phase-space distribution corresponding to a nonequilibrium steady state shrinks to occupy a zero-volume fractal object called a "strange attractor." The corresponding time-reversed repeller, which would violate the Second Law of Thermodynamics, is intrinsically unstable—repelling rather than attracting—but likewise has zero phase-space volume. We can now make this general nonequilibrium qualitative analysis *quantitative* by expressing the consequences of irreversible behavior in terms of the Lyapunov Spectrum discussed in the last Section. In any steady nonequilibrium situation we use driving forces, Gaussian constraint forces, Nosé-Hoover thermostating forces, or a combination of these to impose any required mechanical and thermal boundary conditions. In the Nosé-Hoover case the dimensionality of the corresponding phase space is increased by the inclusion of these friction coefficients  $\{\zeta\}$  or strain rates  $\{\dot{\epsilon}\}$ . In such a case the satellite vectors  $\{\delta\} = \{(\delta q, \delta p, \delta \zeta, \delta \dot{\epsilon})\}$  describing the separations of pairs of phase-space trajectories acquire extra components and the dynamical matrix  $D$  which propagates the vectors becomes correspondingly more complicated.

In every case, just as is required by the Second Law of Thermodynamics, the relentless shrinking of phase-space hypervolume in the nonequilibrium steady state is accurately mirrored by a shift of Lyapunov exponents away from zero, with the sum of each exponent pair shifting downward from zero.

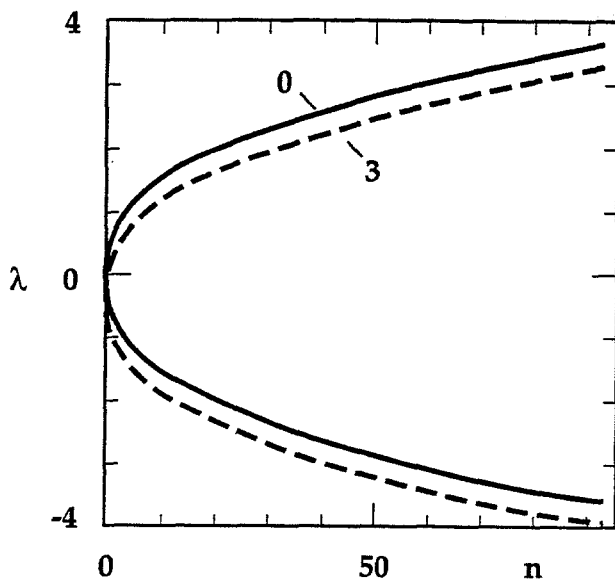


**Figure 11.23.** Comparison of equilibrium and nonequilibrium Lyapunov spectra for a 32-particle three-dimensional dense fluid, showing the nonequilibrium shift of the exponents to more negative values. An external field drives half the particles to the left and half to the right. The equilibrium phase-space dimensionality is 192. The dimensionality is reduced by about 16 by a driving field of strength  $3\epsilon/\sigma$ , where  $\epsilon$  and  $\sigma$  correspond to the well depth and the collision diameter.

Detailed calculations have been carried out for a variety of diffusive, viscous, and heat-conducting flows. Figure 11.23 shows the measured exponent pairs for a periodic three-dimensional dense fluid with half the particles driven to the right, and half to the left, by an external field. If we think about the geometric significance of the Lyapunov exponents we can easily estimate the dimensionality of the phase-space attractor occupied by the nonequilibrium steady-state distribution function. The largest exponent describes the growth rate of a one-dimensional *line* in phase space, the rate at which *pairs* of trajectories depart from one another:

$$\dot{\delta} = \lambda_1 \delta.$$

The sum of the largest two exponents gives the divergence rate for a two-dimensional *area* in phase space:

$$\dot{A} = (\lambda_1 + \lambda_2)A.$$

The sum of the largest *three* exponents gives the divergence rate for a *three*-dimensional volume in phase space, and so on. For *any* chaotic system at least  $\lambda_1$  must be positive. But, for a stable phase-space flow, the sum of *all* the Lyapunov exponents,  $\Sigma\lambda = -\Sigma\zeta = -\dot{S}$ , *must* be negative, with the entropy production  $\dot{S}$  positive. There *must* therefore be a critical dimensionality beyond which the exponent sum becomes negative. Kaplan and Yorke suggested that this critical dimension  $D_{KY}$  of a phase-space object which neither grows nor shrinks with time be identified with the "information dimension" of the corresponding attractor. Any phase-space object with a larger dimensionality would have to shrink with time and could therefore not represent the steady-state distribution function. Any phase-space object with a smaller dimensionality would have to expand with time and could likewise not represent a steady state.

**Problems:**

1. Consider a cubic centimeter of liquid water sheared at a strain rate of 1 hertz. Assume a Lyapunov-exponent distribution:  $\text{prob}(\lambda) \propto \lambda^{1/3}$ , and estimate the loss of dimensionality of the corresponding phase-space strange attractor.
2. Show that, for small departures from equilibrium, the phase-space dimensionality loss  $\Delta D$  for a *dilute-gas* N-particle system is of order  $\Delta D/N \approx (\lambda/c)^2(\nabla u)^2$  for a steady shear flow or  $(\lambda/T)^2(\nabla T)^2$ , for a steady heat flow, where here  $\lambda$  is the mean free path, *not* a Lyapunov exponent.
3. Show that, for small departures from equilibrium, the phase-space dimensionality loss  $\Delta D$  for a *dense-fluid* N-particle system is of order  $\Delta D/N \approx (\sigma/c)^2(\nabla u)^2$  for a steady shear flow or  $(\sigma/T)^2(\nabla T)^2$ , for a steady heat flow, where  $\sigma$  is the "collision diameter," approximately equal to the nearest-neighbor spacing in the fluid.

Numerical work shows that at relatively high fields the fractal dimensionality  $D_{KY} = D_1$  of homogeneously-driven nonequilibrium phase-space flows can easily be reduced from the equilibrium dimensionality by 10%. See again Figure 11.23 for an example. Geometric symmetry typically implies that the fractal dimension must be an *even* function of the driving field, equal for positive or negative fields of the same magnitude. The numerical simulations verified this expectation and showed that the low-field reduction in dimensionality was quadratic in field strength. Very similar results have been found for the dependence of other fractal dimensions for simple one- or two-particle systems. The finding that nonequilibrium phase-space distributions are fractal, with zero (hyper)volume relative to the equilibrium phase space provides a geometric interpretation of the Second Law of Thermodynamics: *phase-space states violating the Second Law cannot be observed* because first, *their measure is zero* in the equilibrium phase space, and second, *the phase space region occupied by such states is mechanically unstable*, repelling nearby trajectories.

**11.9 Summary and References**

Nonequilibrium flow simulations agree well with experimental data in the linear range. Simulations of viscosity and thermal conductivity are currently accurate within about a percent. The resulting viscosities and conductivities follow rough corresponding-states relations analogous to van der Waals' equilibrium equation of state. Strong shockwaves provide an opportunity to study nonlinear transport free of boundary influences. The nonequilibrium simulations can also be applied to energy-transfer problems in vibrational relaxation. The ideas underlying constrained dynamics make it possible to characterize both few-body and many-body phase-space flows of equilibrium and nonequilibrium systems through the corresponding Lyapunov spectra and to quantify the fractal nature of the Lyapunov-unstable phase-space distributions underlying the macroscopic Second Law of Thermodynamics.

Applications of Nonequilibrium Molecular Dynamics can be found in profusion in the *Physical Review*, *The Journal of Chemical Physics*, *Molecular Physics*, and the *Journal of Statistical Physics*. For a fairly recent summary see also the *Proceedings of the Enrico Fermi Summer School Course 97*, "Molecular-Dynamics Simulation of Statistical-Mechanical Systems" (North-Holland, Amsterdam, 1986) mentioned in Chapter 5. Examples with some historical interest include "Shear Viscosity of the Lennard-Jones Fluid Near the Triple Point: Green-Kubo Results," by J. J. Erpenbeck, *Physical Review A* **38**, 6255 (1988) and "On the Number Dependence of Viscosity in Three Dimensional Fluids," by D. J. Evans, G. P. Morriss, and L. M. Hood, *Molecular Physics* **68**, 637 (1989). See "Shockwave Structure *via* Nonequilibrium Molecular Dynamics and Navier-Stokes Continuum Mechanics," by B. L. Holian, W. G. Hoover, B. Moran, and G. K. Straub, *Physical Review A* **22**, 2798 (1980) and "Lennard-Jones Triple-Point Bulk and Shear Viscosities. Green-Kubo Theory, Hamiltonian Mechanics, and Nonequilibrium Molecular Dynamics," W. G. Hoover, D. J. Evans, R. B. Hickman, A. J. C. Ladd, W. T. Ashurst, and B. Moran, *Physical Review A* **22**, 1690 (1980). The simple few-body viscosity model is described in "Lorentz Gas Shear Viscosity *via* Nonequilibrium Molecular Dynamics and Boltzmann's Equation," by A. J. C. Ladd and W. G. Hoover, *Journal of Statistical Physics* **38**, 973 (1985). For descriptions of the homogeneous heat-flow method see M. J. Gillan and M. Dixon, "Calculation of Thermal Conductivities by Perturbed Molecular Dynamics Simulations," *Journal of Physics C* **16**, 869 (1983) and D. J. Evans, "Homogeneous Algorithm for Thermal Conductivity," *Physics Letters A* **91**, 458 (1982), as well as W. G. Hoover, B. Moran, and J. M. Haile, "Homogeneous Periodic Heat Flow *via* Nonequilibrium Molecular Dynamics," *Journal of Statistical Physics* **37**, 109 (1984) and "Corresponding States for Thermal Conductivities *via* Nonequilibrium Molecular Dynamics," R. Grover, W. G. Hoover, and B. Moran, *Journal of Chemical Physics* **83**, 1255 (1985).

References dealing with nonequilibrium relaxation are "Simulations of Vibrational Relaxation in Dense Molecular Fluids," B. L. Holian, *Journal of Chemical Physics* **84**, 3138 (1986) and S. Baratham, I. L'Heureux, and R. Kapral, "Reactive Dynamics in a Deterministic Heat Bath," *Journal of Chemical Physics* **91**, 5602(1989).

The standard method for determination of Lyapunov exponents, due to G. Benettin, L. Galgani, and J. M. Strelcyn, has been improved. See H. A. Posch and W. G. Hoover, "Lyapunov Instability of Dense Lennard-Jones Fluids," *Physical Review A* **38**, 473 (1988) for instance. See also H. A. Posch, W. G. Hoover, and B. L. Holian, "Time-Reversible Molecular Motion and Macroscopic Irreversibility," *Berichte der Bunsengesellschaft fuer Physikalische Chemie* **94**, 250 (1990).

## 12. Summary

The conceptual basis of macroscopic thermodynamics and microscopic statistical mechanics is the ideal gas. This simple model makes it possible to give quantitative definitions of pressure and temperature, to calculate the classical and quantum partition functions, and to link these two approaches through Bohr's Correspondence Principle. The simplicity of the macroscopic thermodynamic states described by the First, Second, and Third Laws of Thermodynamics, with one mechanical and one thermal variable specifying the thermodynamic state, corresponds microscopically to phase-space mixing, with all accessible regions of phase space equally likely to be occupied. The dissipation described by the Second Law of Thermodynamics, with work necessarily converted to heat, corresponds microscopically to Lyapunov instability. The Third Law of Thermodynamics affirms that statistical calculations are consistent with experience.

Computational statistical mechanics is a powerful tool for relating microscopic interaction models to macroscopic properties. Gibbs showed that equilibrium properties can be worked out as phase-space averages rather than as time averages. Except in problems involving quantum effects, such as the ideal-gas reactions which require spectroscopic information, it is hardly more complicated to work out the time averages using molecular dynamics than it is to work out the corresponding phase averages using a Monte Carlo method. On the other hand, over the past 15 years perturbation theory has been improved to the point that equilibrium properties can often be calculated relatively easily without the need for either time averages or phase-space sampling.

It is in dealing with nonequilibrium problems for which there is still no useful theory, that computational statistical mechanics has the most to offer. By using Nosé-Hoover thermostats to define the temperature of nonequilibrium systems, the mechanical basis of the Second Law of Thermodynamics has been identified. The equations of motion show directly that for *any* cyclic microscopic process the summed reservoir heat-flow contributions satisfy an inequality equivalent to the Second Law:

$$\Delta S_{\text{total}} = \Delta S_{\text{reservoirs}} = \sum (Q_{\text{reservoir}}/T) \geq 0.$$

This remarkable link between microscopic mechanics and thermodynamics makes it possible to analyze the phase-space description of nonequilibrium systems. Interesting far-from-equilibrium simulations can be carried out. At the state of the art today, simulations with billions of degrees of freedom are feasible and simulations with millions of degrees of freedom are well within the research budgets of colleges and universities.

The lack of an operational predictive nonequilibrium theory, despite tremendous effort and some good ideas makes the imaginative analysis of nonequilibrium

simulations a promising subject for research work. The influence of nonlinear dynamical systems study on statistical mechanics has already led to closer ties between the equilibrium formulation of Gibbs and Boltzmann and computer simulation. It is possible that a nonlinear theory may emerge to remove the present need for simulating each special case. But the prevalence of chaos in these Lyapunov-unstable problems guarantees that the information in a long-time solution exceeds the information we might provide. The nonlinearity of the same problems suggests that general principles will be ineffective, so that the need for computer simulation will not diminish. On the contrary.

I am convinced that the most rapid progress can be made if the problems studied are as simple as possible. As computer power expands it is increasingly necessary to apply Occam's Razor, looking for the simplest possible special cases that illustrate general principles rather than using more complex models. Experiments are beginning to record atomistic features, usually on a relatively long time scale and unfortunately with the underlying forces largely unknown. But the new observations suggest that with the fundamentals of simulation under control, there is promise of contributing to real problems using massively-parallel computing.

References:

"The Teraflop Supercomputer," G. Fox, *Computers in Physics*, 112 (January-February, 1990). For a recent million-atom simulation see "Large-Scale Elastic-Plastic Indentation Simulations via Nonequilibrium Molecular Dynamics," W. G. Hoover, A. J. De Groot, C. G. Hoover, I. Stowers, T. Kawai, B. L. Holian, T. Boku, S. Ihara, and J. Belak, *Physical Review A* (December, 1990).

### 13. Useful Information

Tolman's book provides a perceptive approximation to  $\pi \approx 3.14159265358979$ :  
 ("Yes, I want a drink, alcoholic of course, after the heavy sessions involving quantum mechanics.")

Age of the Universe:  $3 \times 10^{17}$  seconds

Avogadro's Number:  $6.02 \times 10^{23}$

Boltzmann's Constant:  $1.38 \times 10^{-23}$  joules/kelvin

Bulk Moduli: 6 Mbar (Diamond); 0.4 Mbar (Lead)

Bulk Sound Speed: 0.34 km/sec (Air); 1.5 km/sec (Water)

Debye Temperatures: 1900 K (Diamond) 420 K (Iron); 90 K (Lead)

Density: 19 gm/cm<sup>3</sup> (Gold); 2.7 gm/cm<sup>3</sup> (Aluminum)

Earth Mass:  $6.0 \times 10^{27}$  grams

Earth's Gravitational Field: 9.8 meters/sec<sup>2</sup>

Electronic Charge:  $4.8 \times 10^{-10}$  esu

Electronic Mass:  $9.1 \times 10^{-28}$  gm

Longitudinal Sound Velocities: 6 km/sec (Iron); 2 km/sec (Lead)

Pachinko Ball Mass: 5.45 gm

Planck's Constant:  $6.626 \times 10^{-34}$  jouleseconds

Proton Mass:  $1.7 \times 10^{-24}$  gm

Speed of Light:  $3.0 \times 10^{10}$  cm/sec

Thermal Conductivity (Room-Temperature): 1 cal/cmsecK (Silver)

Viscosity: 0.00018 poise (Air); 0.02 poise (Water)

Yen Coin Mass: 1.000 gram

Yen Coin Radius: 1.000 cm

$R = Nk = 83\text{cm}^3\text{atm/moleK} = 2.0 \text{ cal/moleK}$

"Electron Volt" = 11,400 K

Watt = Joule/sec =  $10^7$  erg/sec

Stirling's Approximation:  $N! \approx (2\pi N)^{1/2}(N/e)^N \exp(1/12N)$

Integrals from  $-\infty$  to  $+\infty$ :

$$\int \exp(-\alpha x^2) dx = (\pi/\alpha)^{1/2}; \int |x| \exp(-\alpha x^2) dx = (1/\alpha); \int x^2 \exp(-\alpha x^2) dx = (\pi/4\alpha^3)^{1/2};$$

$$\int |x^3| \exp(-\alpha x^2) dx = (1/\alpha)^2; \int x^4 \exp(-\alpha x^2) dx = (3/4)(\pi\alpha^5)^{1/2}.$$

## Index

- Atomistic forces
  - embedded-atom, 140
  - Lennard-Jones, 137
  - Lennard-Jones spline, 151
  - soft spheres, 136
- Boltzmann's equation, 235
- Brillouin zone, 109
- Bulk modulus, 187
- Bulk viscosity, 193
- Canonical ensemble
  - derivation, 73
  - heat capacity, 77
- Carnot cycle, 45
- Central limit theorem, 36
- Chemical potential, 167
- Chemical reactions, 115
- Constraints
  - holonomic, 20
  - nonholonomic, 21
- Compressibility factor, 57
- Continuity equation, 184
- Correlation dimension, 288
- Correspondence principle, 67, 95
- Corresponding states, 172, 292
- Couette flow, 201
- Courant condition, 220
- Critical point, 58
- Critical temperature, 58
- Crystal vacancies, 179
- Cubane, 98
- Cyclopropane, 98
- Degenerate states, 76
- Degrees of freedom, 2
- Diffusion equation, 9
- Distinguishability, 95, 115
- Double pendulum, 17
- Einstein model, 110
- Elastic constants
  - notation, 139
  - adiabatic and isothermal, 178
- Elastic equations, 195
- Electronic heat capacity, 120
- Energy equation, 197
- Enskog transport model, 249
- Enthalpy, 60
- Entropy
  - definition, 47, 50
  - ideal gas, 94
  - production, 290
  - Sackuer-Tetrode formula, 94
- Equation of motion, 191
- Equation of state
  - elastic solids, 178
  - ideal gas, 38
  - many parameter, 177
  - one parameter, 171
  - Newtonian viscous fluid, 193
  - two parameter, 176
  - van der Waals, 56
- Equilibrium constant, 116
- Equipartition theorem, 92
- Ergodic theory, 133
- Eulerian and Lagrangian coordinates, 183
- Euler's equations of motion, 99
- Feedback
  - differential (Gauss), 32
  - integral (Nosé-Hoover), 32, 85
- First law of thermodynamics, 42
- Fick's laws, 222, 244
- Fourier's law, 196, 222
- Fractals
  - correlation dimension, 288
  - definition, 266
  - information dimension, 305
- Free path distribution, 229
- Free-path transport theory, 232
- Galton board, 258, 278
- Gaussian integrals, 104
- Gauss' principle, 21
- Gibbs' free energy, 61
- Global error, 11
- Grand canonical ensemble, 86, 117, 120
- Green-Kubo theory, 250, 259
- H theorem, 238
- Hamiltonian mechanics, 24
- Hard disk thermodynamics, 161
- Hard sphere collision rate, 225
- Hard sphere thermodynamics, 169, 174
- Harmonic chain, 103
- Harmonic oscillator, 67, 100
- Heat capacity
  - electrons in metals, 120
  - fluctuation formula, 77
  - oscillator, 102
  - phonons and photons, 119
- Heat flux, 142, 288
- Heat reservoirs, 40, 75, 261
- Heat theorem, 141

- Helmholtz' free energy, 60  
 Hugoniot relations, 55  
 Hypersphere volume, 70  
 Hydrodynamics, 181, 200  
 Ideal gas temperature, 29  
 Impact parameter, 231  
 Integration errors, 11  
 Irreversibility, 239, 269  
 Joule-Thomson experiment, 52  
 Kawasaki relation, 283  
 Kepler's laws, 4  
 Kinematic viscosity, 202, 209  
 Kinetic theory, 222  
 Kolmogorov length, 209  
 Krook-Boltzmann equation, 243  
 Lagrange multipliers  
     canonical ensemble, 73  
     Gauss' principle, 22  
     Lagrangian constraints, 20, 32  
 Lagrangian mechanics, 16  
 Lamé constants, 195  
 Least action principle, 19  
 Lennard-Jones spline potential, 151  
 Lennard-Jones thermodynamics, 127, 176  
 Lennard-Jones transport properties, 284  
 Lindemann's melting model, 173, 175  
 Liouville's theorem, 26, 262  
 Local error, 11  
 Longitudinal wave, 108  
 Lorenz attractor, 212  
 Loschmidt's paradox, 239  
 Lyapunov instability, 6, 155, 301  
 Lyapunov spectra, 301, 305  
 Maxwell-Boltzmann distribution, 79, 238  
 Maxwell's equal-area rule, 58  
 Maxwell mean free path, 227  
 Maxwell relaxation time, 194  
 Maxwell relations, 61  
 Mayers' virial expansion, 121  
 Microcanonical ensemble, 70  
 Molecular dynamics  
     boundary conditions, 134  
     equilibrium, 130  
     fluid walls, 135  
     hard spheres, 157  
     isoenergetic, 142  
     isothermal (Gauss'), 145  
     isothermal (Nosé-Hoover), 146  
     isothermal-isobaric, 147  
     nonequilibrium, 255  
     number dependence, 162  
 Moments of inertia, 99  
 Monte-Carlo method, 80, 241  
 Navier-Stokes equations, 192  
 Nearest-image interactions, 137, 275  
 Newtonian viscosity, 193  
 Nonequilibrium systems  
     constant of the motion, 277  
     forces, 257  
     Galton board, 278  
     heat flow, 288  
     mass flow, 276  
     probability density, 275, 282  
     steady state, 264  
     thermostats, 261  
     velocity distribution, 247, 297  
     viscous flow, 282  
 Normal modes, 105  
 Nosé-Hoover mechanics, 84, 146, 262  
 Nosé-Hoover oscillator, 12  
 Nosé mechanics, 83  
 Numerical hydrodynamics, 218  
 One-dimensional hard-rod gas, 88  
 Pair distribution function, 164, 177  
 Parallel computing, 156, 256  
 Partition function  
     definition, 77  
     hard rod gas, 88  
     harmonic chain, 103  
     harmonic oscillator, 100  
     ideal gas, 93  
     quantum mechanical, 95, 97, 100  
     rigid bodies, 98  
     rigid rotors, 96  
     thermodynamic derivatives, 77  
 Periodic boundaries, 66, 134  
 Perpetual motion machines, 42, 45  
 Phase diagrams, 39  
 Phase equilibria, 166  
 Phase-space dimensionality loss, 304  
 Phase-space shrinkage, 263  
 Phonons and photons, 117  
 Plastic flow, 216, 285  
 Poincaré recurrence, 239  
 Poiseuille flow, 203  
 Poisson's ratio, 188  
 Polyatomic molecules, 113, 177  
 Pressure tensor, 186, 189, 193  
 Quasiharmonic crystals, 106  
 Random numbers, 81  
 Rayleigh-Bénard flow, 210  
 Rayleigh number, 211

- Rayleigh waves, 109
- Reciprocal space, 109
- Reversibility, 8, 33
- Reynolds number, 209
- Rigid rotor, 96
- Rotational temperature, 96
- Runge-Kutta computer program, 14
- Runge-Kutta integration, 10
- Satellite trajectories, 301
- Scattering angle, 231
- Schrodinger's equation, 67
- Second law of thermodynamics
  - macroscopic statement, 48
  - microscopic proof, 269
- Second virial coefficient, 137
- Shear modulus, 187
- Shear viscosity, 193, 280
- Shockwave compression, 53
- Shockwave structure, 293
- Sierpinski sponge, 267
- Single-occupancy properties, 170
- Soft sphere thermodynamics, 174
- SPRINT computer, 216, 256
- Stability
  - Lyapunov, 6
  - mechanical, 57
  - thermodynamic, 58
  - trajectory, 6
- Star graphs, 123
- Stoermer Hamiltonian, 25
- Stoermer integration, 10
- Stoermer computer program, 13
- Stokes' flow, 205
- Strange attractor, 212, 266, 281, 287
- Strange repeller, 271, 281
- Stress tensor, 178, 187
- Symmetry number, 98
- Thermodynamic perturbation theory, 126
- Thermodynamic potentials, 60
- Third law of thermodynamics, 50
- Transport coefficients
  - Diffusion, 222, 251, 277
  - Shear viscosity, 193, 222, 251, 292
  - Heat conductivity, 222, 251, 292
- Transverse wave, 108
- Triple point, 166
- Turbulence, 208
- van der Waals' equation, 56
- van der Waals loop for hard disks, 161
- Vibrational relaxation, 298
- Vibrational temperature, 96
- Virial series approximation, 125
- Virial theorem, 5, 140
- Wave function symmetry, 95
- Wigner-Kirkwood series, 101
- Yield strength, 280
- Young's modulus, 188
- Zermelo's paradox, 239
- Zero point energy, 102
- Zeroth law of thermodynamics, 41



William Graham Hoover was born in Boston on 18 April 1936. With a 1958 AB from Oberlin College, he completed his doctoral studies with Andrew De Rocco in Physical Chemistry at the University of Michigan in 1961. After a year of postdoctoral work with Jacques Poirier, at Duke University, he became a staff physicist at the Lawrence Radiation Laboratory in Livermore, California. Since 1972 he has held a joint appointment in the Department of Applied Science, University of California at Davis, while carrying out sabbatical research at the Australian National University (1977–1978), the University of Vienna (1984), and Keio University (1989–1990). Professor Hoover has climbed more than 250 separate peaks in California's Sierra Nevada. He has published about 150 research papers, including the monograph *Molecular Dynamics*, published by Springer Verlag. He lives with his wife and former student, Carol Griswold Hoover, on a ranch in Stanislaus County, California. His daughter, Frances Hoover Waid, works for the Sierra Club in Oakland, California; his son, Nathan Edgar Hoover, works for Teradyne in Tokyo. The photograph of the Hoovers was taken on the summit of Mount Langley in July of 1990.